THE JOURNAL OF
PHYSICAL CHEMISTRY

Volume 74, Number 22 October 29, 1970

NOTES

COMMUNICATIONS TO THE EDITOR

AUTHOR INDEX

THE JOURNAL OF
PHYSICAL CHEMISTRY

VOLUME 74, NUMBER 22 OCTOBER 29, 1970

Directed Transport of Monomer–Single Polymer Systems. A Comparison of the Countercurrent Analog and Asymptotic Approaches[1a]

by J. L. Bethune[1b]

Biophysics Research Laboratory, Department of Biological Chemistry, Harvard Medical School, and the Division of Medical Biology, Peter Bent Brigham Hospital, Boston, Massachusetts *(Received January 20, 1970)*

Theory for directed transport of rapidly reequilibrating polymerizing systems has been developed generally without reference to diffusion. A comparison is presented between results obtained using the countercurrent distribution analog, which includes (analog) diffusion, with those from the relevant asymptotic equations for dimerization and trimerization reactions. When diffusion is included, all concentration levels in a boundary, except that at 60% of the plateau concentration, undergo acceleration, leading to time-dependent velocities. As a result, equilibrium constants calculated from area distributions may be affected.

Theory for the effect of rapidly reequilibrating polymerization reactions of macromolecules subjected to directed transport has been developed generally without reference to the possible effects of transport due to diffusion upon the results obtained.[2-7] Diffusional effects, however, may be incorporated either by direct numerical solution of the relevant continuity equations[8] or through the countercurrent distribution analog.[9,10] While calculations have been reported for sedimentation of monomer–single polymer systems,[8b] no critical comparison of the results obtained from calculations incorporating diffusion have been made with those from the asymptotic theory, although the latter has been applied in the calculations of, *e.g.*, equilibrium constants.[2a,11]

This paper presents the results of such a comparison for monomer–single polymer systems using the countercurrent distribution analog to incorporate the effects of diffusion. The equations of Gilbert[2a] have been used in this direct comparison, both approaches thus applying to a rectangular liquid column in a uniform field. The equations of Fujita[4] for sedimentation analysis which incorporate the effects of radial dilution and a varying field have not been used, since it was desired to isolate the effects of diffusion in the simplest possible manner.

Theory

The general differential equation describing the total concentration distribution of a component undergoing the reaction nm $\rightleftharpoons$ p is

$$\frac{\partial}{\partial t}(C_m + C_p) = -\frac{\partial}{\partial x}(V_m C_m + V_p C_p) + \frac{\partial^2}{\partial x^2}(D_m C_m + D_p C_p) \quad (1)$$

(1) (a) This work was supported by Grant-in-Aid GM-15003 from the National Institutes of Health of the Department of Health, Education, and Welfare. (b) Research Career Development Awardee of the National Institutes of Health of the Department of Health, Education, and Welfare, U. S. Public Health Service.

(2) (a) G. A. Gilbert, *Discussions Faraday Soc.*, **20**, 68 (1955); (b) G. A. Gilbert, *Proc. Roy. Soc., Ser. A*, **250**, 377 (1959).

(3) M. S. N. Rao and G. Kegeles, *J. Amer. Chem. Soc.*, **80**, 5724 (1958).

(4) H. Fujita, "Mathematical Theory of Sedimentation Analysis," Academic Press, New York, N. Y., 1962.

(5) J. L. Bethune and P. J. Grillo, *Biochemistry*, **6**, 796 (1967).

(6) R. C. Makino and E. Rogers, *Arch. Biochem. Biophys.*, **109**, 499 (1965).

(7) G. G. Belford and R. L. Belford, *J. Chem. Phys.*, **37**, 1926 (1962).

(8) (a) J. R. Cann and W. B. Goad, *J. Biol. Chem.*, **240**, 148 (1965); (b) D. J. Cox, *Arch. Biochem. Biophys.*, **129**, 106 (1969).

(9) J. L. Bethune and G. Kegeles, *J. Phys. Chem.*, **65**, 1761 (1961).

where m and p represent monomer and polymer, C_m and C_p, V_m and V_p, and D_m and D_p the mass concentrations, velocities, and diffusion coefficients of monomer and polymer, respectively.[2b] x is the space axis along which transport is directed and t is time. V and D are assumed to be constants. In the asymptotic approach[2b] the differential eq 1 is simplified by dropping the diffusional terms. If an association constant is defined as

$$K_n' = C_p/C_m^n \tag{1a}$$

the simplified equation becomes

$$\frac{\partial C_m}{\partial t} + \frac{V_m + nK_n'V_pC_m^{n-1}}{1 + nK_n'C_m^{n-1}}\frac{\partial C_m}{\partial x} = 0 \tag{1b}$$

The characteristic equation describing curves along which C_m is a constant for this quasi-linear partial differential equation is[12]

$$\frac{dx}{dt} = \frac{V_m + nK_n'V_pC_m^{n-1}}{1 + nK_n'C_m^{n-1}} \tag{1c}$$

which is immediately integrated to

$$x = \frac{V_m + nK_n'V_pC_m^{n-1}}{1 + nK_n'C_m^{n-1}}t + X_0 \tag{1d}$$

where $X_0 = x$ at $t = 0$. Given the initial values prescribing a sharp boundary

$$C_m = 0,\ x \leq 0,\ t = 0$$

$$C_m = \text{constant},\ x > 0,\ t = 0$$

the value of X_0 is zero and the equation becomes

$$x/t = \frac{V_m + nK_n'V_pC_m^{n-1}}{1 + nK_n'C_m^{n-1}},\ 0 \leq C_m \leq \text{constant} \tag{1e}$$

Use of a dimensionless parameter

$$\delta = \frac{x/t - V_m}{V_p - V_m} \tag{1f}$$

allows eq 1e to be written as

$$C_m = \left(\frac{\delta}{nK_n'(1 - \delta)}\right)^{1/(n-1)}$$

and the total concentration as

$$C = C_m + C_p = \left(\frac{1}{nK_n'}\frac{\delta}{1 - \delta}\right)^{1/(n-1)}\left(1 + \frac{1}{n}\frac{\delta}{1 - \delta}\right) \tag{2}$$

The gradient of the total concentration then is

$$\frac{\partial C}{\partial \delta} = \frac{1}{n - 1}\left(\frac{1}{nK_n'}\right)^{1/(n-1)} \times \delta^{(2-n)/(n-1)}\left(\frac{1}{1 - \delta}\right)^{2(n-1)/(n-1)} \tag{3}$$

From these equations two relations can be derived.[2b] First, the position of any minimum in the total gradient pattern along the δ axis is related only to the degree of polymerization by

$$\delta_{min} = \frac{n - 2}{3(n - 1)} \tag{4}$$

Second, the equilibrium constant for the reaction is described by

$$K_n' = \left(\frac{2(n^2 - 1)}{\Delta_s}\right)^{n-1}\frac{n - 2}{\{n(2n - 1)\}^n} \tag{5}$$

where Δ_s is the concentration at the minimum (or, equivalently, the integral of the gradient curve up to that position). Thus, given n and K_n', the system is completely described.

In the countercurrent distribution analog, a slightly restricted form of eq 1 is integrated numerically. The relevant differential equation is

$$\frac{\partial}{\partial n}\{C_m + C_p\} = \frac{\partial^2}{\partial r^2}\{f(K_m)C_m + f(K_p)C_p\} - \frac{\partial}{\partial r}\{g(K_m)C_m + g(K_p)C_p\} \tag{6}$$

where K_z represents the partition coefficient of species z, and

$$f(K_z) = \frac{K_z}{2(K_z + 1)^2} \tag{7}$$

$$g(K_z) = \frac{K_z}{K_z + 1} \tag{8}$$

r is the number of the equilibrium stage and n the number of solvent transfers accomplished.

It has been shown[9] that $f(K_z)$ is analogous to a diffusion coefficient, governing the extent of spreading of a given species in a countercurrent distribution train, while $|g(K_z)|$ is the analog of velocity, governing the rate of movement of the species z along the distribution train. Thus, while in eq 1 both V and D are independent variables, this is not so in eq 6, both analogs being functions of K and, once K is chosen, both f and g are fixed. However, as detailed in methods of computation, *infra*, imposition of this restriction allows use of a superbly trouble-free method of integration.

Consideration of the distribution of a single, nonreacting solute can demonstrate the pertinence of eq 6. If such a solute is introduced once in the first tube of a countercurrent distribution train, at a concentration C_0, then

(10) D. F. Oberhauser, J. L. Bethune, and G. Kegeles, *Biochemistry*, **4**, 1878 (1965).

(11) L. W. Nichol, J. L. Bethune, G. Kegeles, and E. L. Hess, *Proteins*, **2**, 305 (1964).

(12) R. Courant and D. Hilbert, "Methods of Mathematical Physics," Vol. II, Interscience Publishers, New York, N. Y., 1962.

$$\frac{C(r,n)}{C_0} = \frac{1}{\sqrt{\frac{2\pi nK}{(K+1)^2}}} e^{-[(r-nK/K+1)^2/(2nK/(K+1)^2)]} \quad (9)$$

where $C(r,n)$ is the concentration in the rth equilibrium stage after n solvent transfers and K is the relevent partition coefficient.[13] This relation is immediately seen to be a solution of the differential equation

$$\frac{\partial C}{\partial n} = \frac{K}{2(K+1)^2}\frac{\partial^2 C}{\partial r^2} - \frac{K}{K+1}\frac{\partial C}{\partial r} \quad (10)$$

Using the analogies

$$\begin{aligned} n &\equiv t \\ r &\equiv x \\ \frac{K}{2(K+1)^2} &\equiv D \\ \frac{K}{K+1} &\equiv V \end{aligned} \quad (11)$$

where $\equiv$ symbolizes "analogous to," eq 10 becomes

$$\frac{\partial C}{\partial t} = D\frac{\partial^2 C}{\partial x^2} - V\frac{\partial C}{\partial x} \quad (12)$$

which, when applied to the reacting system yields eq 1, eq 10 similarly yielding eq 6. When the relations 11 are applied to eq 9, there results

$$\frac{C(x,t)}{C_0} = \frac{1}{2\sqrt{\pi Dt}} e^{-[(x-Vt)^2/4Dt]} \quad (13)$$

which is the equation for the concentration distribution of an ideal species, in a zone, undergoing transport and diffusion.[9]

While in eq 1 there are four parameters to be allocated (two diffusion coefficients and two velocities), in eq 6 there are only two, the partition coefficients. Since the velocity term is the more important (the diffusional process varying as $t^{1/2}$), this will be considered first.

There exist three cases to be considered

$$V_m > V_p$$
$$V_m < V_p$$
$$V_m = V_p$$

which since

$$V_z \equiv \frac{K_z}{K_z + 1}$$

may be represented by

$$K_m > K_p$$
$$K_m < K_p$$
$$K_m = K_p{}^{14}$$

Once the partition coefficients are selected, then the (analog) diffusion coefficients are fixed. It is not immediately apparent, however, that there exist in countercurrent distribution two domains in which ordering of the velocities, *i.e.*, the partition coefficients, imposes a quite different ordering upon the (analog) diffusion coefficients. These domains are $0 \leq K \leq 1$ and $1 \leq K \leq \infty$.

This differentiation may be illuminated by consideration of the ideal case. An increase in spreading, due to (analog) diffusion, may be equated to an increase the distance, in terms of the parameter r, between the position of the maximum value of C/C_0, *i.e.*, $(C/C_0)_{max}$ and that at which C/C_0 has fallen to $(C/C_0)_{max}/e$ at a fixed value of n. Then if

$$\Delta r = r - \frac{nK}{K+1}$$

$$(C/C_0)/(C/C_0)_{max} = \frac{1}{e} = e^{-\Delta r^2/(2nK/(K+1)^2)}$$

since $(C/C_0)_{max}$ obtains at $\Delta r = 0$. Then

$$(\Delta r)^2 = \frac{2nK}{(K+1)^2}$$

$$\frac{\partial(\Delta r)}{\partial K} = \sqrt{\frac{n}{2K}}\frac{1-K}{(K+1)^2}$$

and, at $\partial(\Delta r)/\partial K = 0$, $K = 1$. Since the second derivative at this point is negative, Δr is maximized at $K = 1$, and for greater or lesser values of K spreading decreases symmetrically. Therefore, if $K_M < K_P$ and $K_M = 1$, then $D_M > D_P$. If, however, $K_P = 1$, then $D_P > D_M$. If $K_M = K_P$, then $D_M = D_P$, an improbable result. It is of interest to obtain a rough idea of the magnitude of the error in this latter case. Assuming globular monomer and n-mer, then

$$f \propto r$$

where f if the frictional coefficient and r the molecular radius. Since

$$f \propto M^{1/3}$$

where M is the molecular weight and $D \propto 1/f$, then

$$\frac{D_M}{D_P} = n^{1/3}$$

and the error introduced, in this exceptional case, is of this order. If, however, the velocities are different, it is possible to select partition coefficients to satisfy almost any ratios of diffusion coefficient and of velocities. Thus, in the system nm $\rightleftharpoons$ p where m represents

(13) L. C. Craig and D. Craig, *Tech. Org. Chem.*, **3**, 171 (1950).

(14) Calculations here are performed only for situations in which $V_m \leq V_p$, migration occurring in the direction solvent $\rightarrow$ solution. For other situations, hypersharp boundaries are predicted: L. W. Nichol, A. G. Ogston, and A. Rescigno, *Proc. Roy. Soc., Ser. A*, **317**, 153 (1970).

monomer and p polymer, let the velocity and diffusion coefficient ratios be

$$V_m/V_p = \alpha$$

$$D_m/D_p = \beta$$

where, for sedimentation analysis

$$\alpha < 1 < \beta$$

Then

$$\frac{K_m}{K_m + 1} \cdot \frac{K_p + 1}{K_p} = \alpha$$

and

$$\frac{K_m}{(K_m + 1)^2} \cdot \frac{(K_p + 1)^2}{K_p} = \beta$$

Solving these simultaneous equations

$$K_m = \frac{\alpha}{\beta} \cdot \frac{\alpha - \beta}{\alpha - 1}$$

$$K_p = \frac{1}{\alpha} \cdot \frac{\alpha - \beta}{\alpha - 1}$$

The only restriction is that the partition coefficients be positive. This is determined by

$$\frac{\alpha - \beta}{\alpha - 1} > 0$$

For sedimentation analysis, in the simple case of ideal spherical molecules

$$\alpha = n^{-2/3}$$

$$\beta = n^{1/3}$$

and

$$\frac{\alpha - \beta}{\alpha - 1} = \frac{1 - n}{1 - n^{2/3}} > 0, \text{ if } n > 1$$

Thus, although it has been asserted[8b] that use of the countercurrent distribution analog requires that the solute component with the lowest velocity (*i.e.*, monomer) must have the lowest (analog) diffusion coefficient, this defect can be readily overcome and, generally, it is possible to assign values to fit all experimental situations of this type. Thus, considering spherical molecules, if the reaction is

$$6 \text{ monomer} \rightleftharpoons \text{hexamer}$$

Then

$$\alpha = 6^{-2/3}$$

$$\beta = 6^{1/3}$$

If

$$K_m = 0.362$$

$$K_p = 7.172$$

these relations are satisfied. In general, if $\alpha > \beta$ *and* $\alpha > 1$ or $\alpha < \beta$ *and* $\alpha < 1$, the partition coefficients can be selected to satisfy the required relationship.

Methods for Numerical Calculations

The relevant equations were programmed either for an SDS 940 time sharing computer, using the SDS version of Fortran II or for an SDS Sigma-7 using Fortran IV-H.

The asymptotic equations (eq 2 and 3) were programmed directly to provide the relevant values of C and $\partial C/\partial\delta$ at fixed increments of δ.

The countercurrent distribution analog program was structured as follows.

(1) A fixed concentration (C_0) of solute was assigned as T_r to n storage locations, representing tubes in a countercurrent distribution train.

(2) The relevant mass balance equation of the form

$$K_n'C_m^n + C_m - C_0 = 0$$

was solved for the first storage location, yielding the concentration of monomer at that location.

(3) The equilibrium concentration of polymer was then calculated from

$$C_p = K_n'C_m^n$$

(4) Using the assigned partition coefficients, the concentrations of monomer and polymer in the upper phase were calculated as

$$C_{m,u} = \frac{K_m}{K_m + 1} C_m$$

$$C_{p,u} = \frac{K_p}{K_p + 1} C_p$$

and stored.

(5) A transfer was accomplished by substracting $C_{m,u}$ and $C_{p,u}$ at this location from, and adding the similar amounts from the immediately preceding location to T_0 and substituting the result as the new value of T_0.

(6) Steps 2, 3, and 4 were repeated for the first two storage locations, the first with the new value of T_0 and the second with $T_1 = C_0$.

(7) Step 5 was accomplished for the first two locations, yielding new values of T_0 and T_1.

(8) Steps 6 and 7 were repeated until solute had been transferred n times.

(9) First differences were taken between adjacent total storage locations to give $\Delta C/\Delta r$.

(10) Locations, $\Delta C/\Delta r$, and T were printed.

The only limitation on accuracy is in the solution of the mass balance equation (step 2).

Quadratic equations were solved using the appropriate analytical solution, while cubic equations were solved using Newton–Rapheson iteration. The criterion for convergence was

$$\left|\frac{x_i - x_{i+1}}{x_i}\right| \leq 1.0 \times 10^{-8}$$

where | | denotes absolute value and x_i the ith approximation to the root.

Account was kept of the total mass balance, the error in which never exceeded 5 parts in 10^6. All programs were checked by allowing K_n' to equal zero or $K_m = K_p$. In both cases a single boundary resulted which was identical with that predicted for a single ideal solute.[9]

There remains only the problem of scaling, *i.e.*, translation of any results obtained from the countercurrent distribution analog, where C is a function of r and n, to an experimental situation in, *e.g.*, sedimentation or electrophoresis, where C is a function of x and t. Such translation may be accomplished as follows. Define ϕ as the factor which will convert a distance measured in tube numbers, into a distance measured in centimeters. Then, if the total distance traveled in the countercurrent train is d_{CCD}

$$d_{CCD} = \frac{nK}{K+1}$$

In another transport process, however, along an x axis

$$d_x = Vt$$

Then

$$\frac{nK}{K+1}\phi = Vt$$

or

$$t = \frac{nK}{K+1}\frac{\phi}{V}$$

But, in addition, from eq 9 and 13, after normalization

$$\frac{(r - r_{max})^2(K+1)^2}{2nK} = \frac{(x - x_{max})^2}{4Dt}$$

$$\left(\frac{x - x_{max}}{r - r_{max}}\right)^2 = \phi^2 = \frac{2Dt(K+1)^2}{nK}$$

Substituting the expression for t results in

$$\phi = \frac{2D(K+1)}{V} \qquad (14)$$

Thus, in conversion of a given countercurrent pattern, calculated with a given value of K, the resultant conversion ratio decreases with increasing V and/or decreasing D. Since this ratio is independent of time or the number of transfers (*i.e.*, the analog of time), increasing the number of transfers for a given system does not affect the point-to-point resolution in the analogous pattern. Indeed, all that is increased is the analog distance traveled, as may be seen from an example. Given a molecule with an s of $3S$, D of 9×10^{-7} cm^2/sec, and a partition coefficient of 0.4268, then $\phi = 0.0338$ cm/tube in an average field of 2.5×10^8 cm/sec^2.

If one performs 100 transfers

$$r_{max} = \frac{100 \times 0.4268}{1.4268} = 30$$

and the distance represented by 30 tubes, the r value at which the maximum is found, is 1.014 cm.

If s were $1.5S$, and $D = 1.8 \times 10^{-7}$ cm^2/sec, then $\phi = 0.134$ cm/tube and the analog distance covered is 4.056 cm.

Equation 14 also illuminates the existence of the two domains (*vide supra*) from which partition coefficients may be chosen to allow allocation of the extent of (analog) diffusional spreading, *i.e.*, $0 \leq K \leq 1$ or $1 \leq K \leq \infty$. If the partition coefficient is chosen in the first domain, the point-to-point resolution (when the results are used to explicate the results from another type of transport experiment) is better than if chosen in the second domain. Indeed, if $0 \leq K_1 \leq 1$ and $1 \leq K_2 \leq \infty$, then, for the extent of spreading to be identical in the two cases

$$K_1 \cdot K_2 = 1$$

and

$$\frac{\phi_1}{\phi_2} = K_1$$

Thus, since $K_1 < 1$, the point-to-point resolution in the first domain is better than in the second.

In this manner any of the computed patterns may be referred to a given experimental situation, or, conversely, from a given experimental situation, values of K and n may be selected to represent this situation in the analog patterns.

Graphics

The axis in many of the figures is $\partial C/\partial\delta$ and δ or $\partial C/\partial\delta_{rel}$ and δ. While the asymptotic patterns are calculated directly as functions of δ, the countercurrent distribution results have been scaled through the relation

$$\delta = \frac{r - \dfrac{nK_m}{K_m + 1}}{n\left(\dfrac{K_p}{K_p + 1} - \dfrac{K_m}{K_m + 1}\right)}$$

Where patterns resulting from both approaches are included in a single figure, each is normalized separately to its own maximum value. As a result, the areas under comparable patterns are not the same, the maximum value of $\partial C/\partial\delta$ predicted by the asymptotic approach differing from that obtained by the countercurrent distribution analog.

Results and Discussion

Two types of rapidly reequilibrating systems have been investigated for various values of the relevant parameters. These are monomer–dimer and monomer–trimer.

Monomer–Dimer. For the system $2M \rightleftharpoons D$ the asymptotic eq 2 and 3 become

$$C = \frac{\delta(2 - \delta)}{4K_2'(1 - \delta)^2}$$

and

$$\frac{\partial C}{\partial \delta} = \frac{1}{2K_2'(1 - \delta)^3}$$

The maximum value δ can attain, for a given total concentration, C_0, is calculated from

$$\delta_{max} = \frac{\sqrt{1 + 4K_2'C_0} - 1}{\sqrt{1 + 4K_2'C_0}} \quad (15)$$

Since only one boundary can occur the values of $\partial C/\partial\delta$ are readily normalized as

$$\frac{\partial C}{\partial \delta_{rel}} = \partial C/\partial\delta \Big/ \left(\frac{\partial C}{\partial \delta}\right)_{\delta = \delta_{max}}$$

moreover

$$\lim_{\delta \to 0} \frac{\partial C}{\partial \delta} = \frac{1}{2K}$$

Comparison of the patterns calculated with and without diffusion (Figure 1), reveals that, as a function of total concentration, only one boundary is found, as predicted by eq 4.[2a,8b] The patterns of Figure 1 are calculated for $K_m = 0.8$, $K_D = 2.75$, and $n = 90$. If applied to sedimentation, in an infinite rectangular cell in a uniform field of 2.5×10^8 cm/sec^2, of a monomer of molecular weight 95,000 undergoing a dimerization reaction

$$\phi = 0.01515 \text{ cm/tube}$$

and, the maximum for the dimer after 90 transfers will occur in tube 66, equivalent to a distance of 1 cm traveled. Then, if s is 9.5S, 4400 sec will have elapsed since the start of the experiment. However, in Figure 1a, $r_{max} = 42.5$, and this situation could be applied to a monomer molecular weight of 62,000 with $\phi = 0.023$ cm/tube. The inclusion of diffusion, however, causes the maximum in the curve to occur at a lower value of δ than that predicted by the asymptotic equations under the conditions used here. At low concentrations where monomer is the predominant species, the maximum is found at $\delta = 0$ and, at high concentrations, it is found at $\delta = 1$. The deviation in position of the maximum in the computed curve from that predicted by eq 15 attains its greatest value around a δ_{max} of 0.5 (Figure 2). At the two extremes of the curve, where KC_0 is either so low that effectively only monomer is present, or so high that dimer forms the major component, the values computed from the countercurrent distribution analog are identical with those predicted by eq 15. However, in those concentration ranges in which both monomer and dimer are present in significant amounts in the plateau region, the δ value by the maximum in the computed curve falls significantly behind that predicted by eq 15 for distances attainable in present experimental techniques. However, since eq

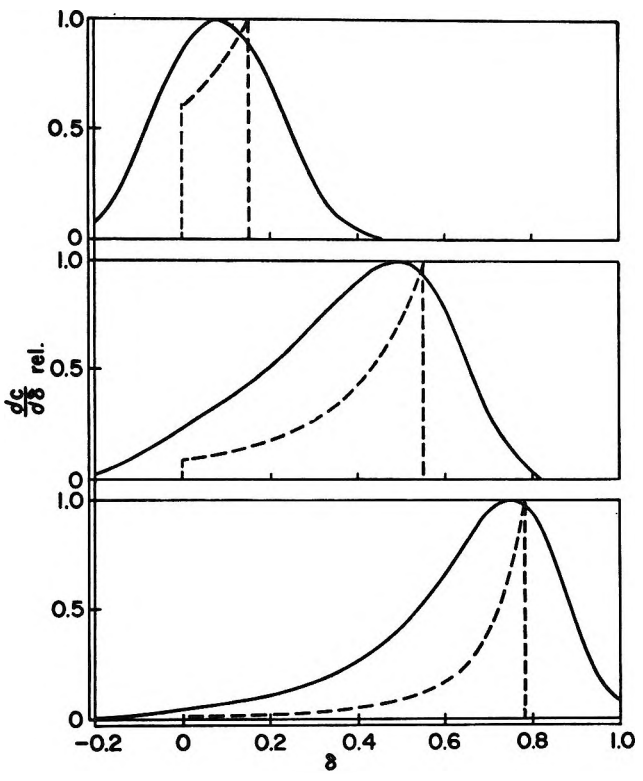

Figure 1. Countercurrent distribution (—) and asymptotic (---) patterns for monomer-dimer; $K_M = 0.8$; $K_D = 2.75$; $n = 90$; (top) $K_2'C_0 = 10^{-1}$; (center) $K_2'C_0 = 1.0$; (bottom) $K_2'C_0 = 5.0$.

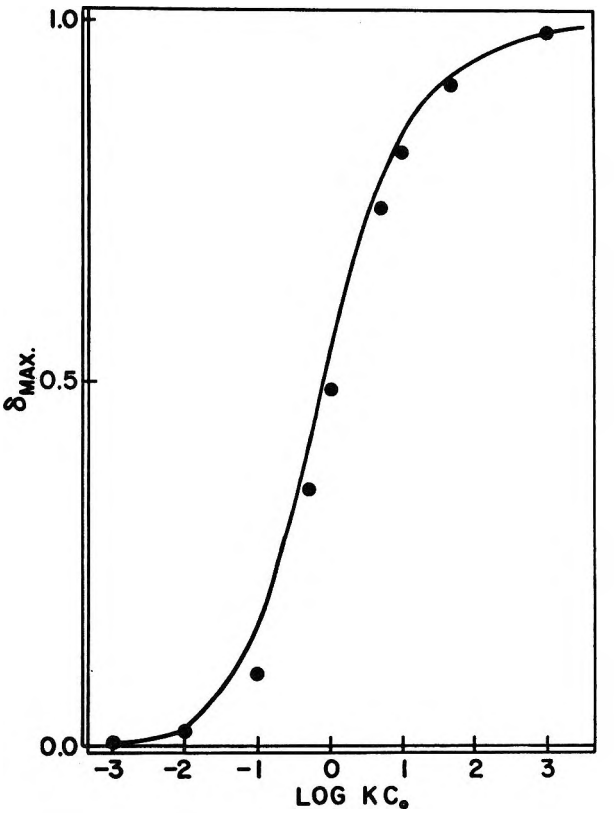

Figure 2. δ_{max} as predicted by the asymptotic equation (—) and as found by the countercurrent distribution analog (●). Conditions as in Figure 1.

15 predicts the position attainable at (essentially) infinite time, an increase in the distance over which transport occurs, *i.e.*, an increase in the time over which the field is applied, should yield a pattern the maximum of which is closer to the value predicted by eq 15. This indeed occurs (Table I). As n increases the r/n value at

Table I:[a] Variation in Position of the Maximum (r_{max}) As a Function of the Number of Transfers (n)

n	r_{max} Found	r_{max} Predicted[b]	r_{max}/n	Concn at $r_{max} \times 10^2$
50	23	...	0.46	0.300 ± 0.034
100	47	46	0.47	0.318 ± 0.020
200	95	92	0.475	0.333 ± 0.012
400	192	184	0.48	0.350 ± 0.007
800	388	368	0.485	0.370 ± 0.004

[a] $K_2 = 100$ l.²/g², $C_0 = 10^{-3}$ g/l., $K_M = 0.4286$, $K_D = 4$. [b] From $r_{max} = n \times (23/50)$.

which the maximum occurs is not a constant, as it would be if the velocity at which the maximum travels were constant. Thus, the incorporation of diffusional effects demonstrates that for monomer–dimer systems, the velocity of the single boundary measured as the position of the maximum in the gradient curve, is time dependent, a new criterion for the identification of such systems. The effect is dramatically illustrated in Table I, in which the second column shows the position of the maximum as a function of n, and the third column, the values that would be found if the rate of movement of the maximum found at $n = 50$ prevailed at higher numbers of transfer. At 800 transfers the difference between the position found and that predicted is 20 tubes. This may be translated to a positional difference, on an x axis, of 0.6 mm, if the total distance traveled along the x axis were 1 cm at a point-to-point resolution of 0.08 cm/tube. Moreover, the concentration at r_{max} increases with the number of transfers (Table I, column 5).

The definition of δ, however, implies that a given concentration level travels with a constant velocity, at least in the absence of diffusional terms. Figure 3 illustrates that if diffusion is present this holds only at a concentration level of $0.6C_0$. Here the δ value for a given concentration is calculated from

$$\delta_c = \frac{r_c/n - \dfrac{K_m}{K_m + 1}}{\dfrac{K_D}{K_D + 1} - \dfrac{K_m}{K_m + 1}}$$

where subscript c denotes a given concentration level, and normalized to the δ value calculated for that concentration by the asymptotic equation (15), to yield $\delta_{C,rel}$. While calculations have been performed over

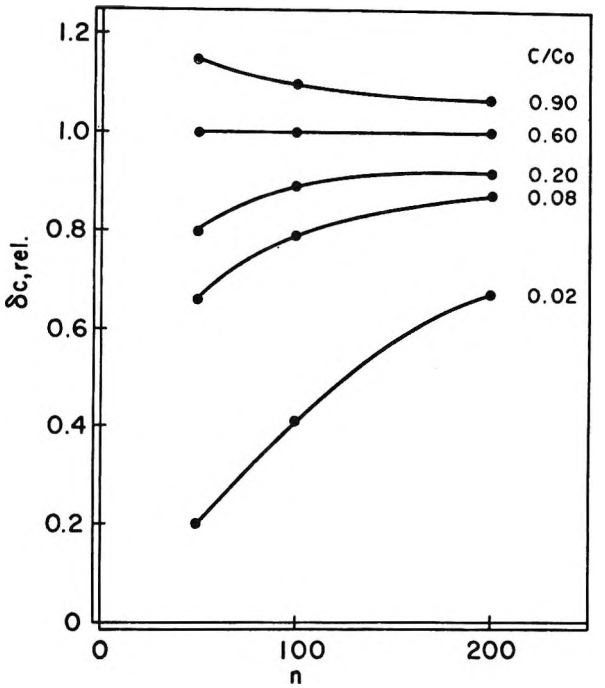

Figure 3. Velocity of various relative concentration levels (C/C_0) as a function of the number of transfers (n). The velocity is expressed as $\delta_{C,rel}$ where C refers to the given concentration and the value of δ found in the countercurrent distribution patterns is expressed as a fraction of the δ value predicted for that concentration level by the asymptotic equation. $K_2'C_0 = 5.0$; $K_M = 0.43$; $K_D = 4.0$.

only a limited range of equilibrium constants and partition coefficients, in all cases examined the only concentration level to move at a constant velocity is at $0.6C_0$. All concentration levels below this value exhibit an acceleration while those above a deceleration, with increasing values of n (*i.e.*, time).

Thus, for the system monomer–dimer, only one concentration level in the boundary moves with a constant velocity, and the shape of the boundary and the velocity of the single inflection point are functions of time. Therefore, mobility determination should involve measurement of the rate of movement of definite concentration levels rather than that of an inflection point of the boundary curve.

Monomer–Trimer. For the monomer–trimer system a single pattern, calculated by the countercurrent distribution analog for only one set of values of the relevant parameters, has been reported.[9] The calculation was performed only to determine the number of boundaries expected under the given conditions, with no critical comparison of the results from the two different approaches. Similar comparisons on the basis of concentration dependent sedimentation and diffusion coefficients have also been largely qualitative.[8b] The present investigation has expanded on this to include the effects of varying numbers of transfers, concentrations, and partition coefficients, in the countercurrent distribution analog and compares the results obtained with

those of asymptotic approach. In the latter case the relevant equations for the monomer–trimer system are

$$C = \left(\frac{1}{3K_3'}\frac{\delta}{1-\delta}\right)^{1/3}\left(1+\frac{1}{3}\frac{\delta}{1-\delta}\right)$$
$$\frac{\partial C}{\partial \delta} = \frac{1}{2}\left(\frac{1}{3K_3'\delta}\right)^{1/2}\left(\frac{1}{1-\delta}\right)^{5/2} \quad (16)$$

with

$$\delta = \frac{3K_3'C_m^2}{1+3K_3'C_m^2} \quad (17)$$

and

$$\lim_{\delta\to 0}\frac{\partial C}{\partial \delta} = \infty \quad (18)$$

For this system a minimum is predicted at a δ value of $^1/_6$, and, if the plateau concentration is such that $\delta_{max} > \delta_{min}$, where δ_{max} is the value of δ corresponding to the plateau monomer concentration, two boundaries should be apparent.

The effect of increasing total concentration, as calculated by the two approaches, is illustrated in Figure 4. The countercurrent distribution patterns are calculated for

$$\alpha = 3^{-2/3}$$
$$\beta = 3^{1/3}$$

i.e., for a spherical monomer and trimer. For a molecule with $D = 6 \times 10^{-7}$ cm²/sec and $V = 2.05 \times 10^{-4}$ cm/sec, the corresponding value of $\phi = 0.014$ cm/tube. At $n = 90$ the maximum for pure trimer would be in tube 71, corresponding to a physical distance, under these conditions, of 1 cm. The corresponding time is then 5000 sec. The value of V corresponds, *e.g.*, to a molecule with a mobility of 5×10^{-5} cm²/V-sec in an electric field of 4 V/cm. Under these conditions no resolution of a separate boundary is detected (Figure 4), only a shoulder appearing at the position of monomer. Additionally, as in the dimerization system, the position of the maximum lags behind that predicted by the asymptotic equations. Since these patterns are normalized, it is not apparent that the absolute area, up to any given value of δ, shifts with increasing concentration. This effect is illustrated in Figure 5, where absolute values are plotted. The values of $\partial C/\partial\delta$ at any given value of increase with total concentration, although eq 17 is single valued. At a concentration of 0.2754 g/l., under these conditions, the maximum value of δ attainable is $^1/_6$, *i.e.*, the value at which the minimum occurs. At higher concentrations eq 17 predicts no increase in area in this portion of the pattern with in-

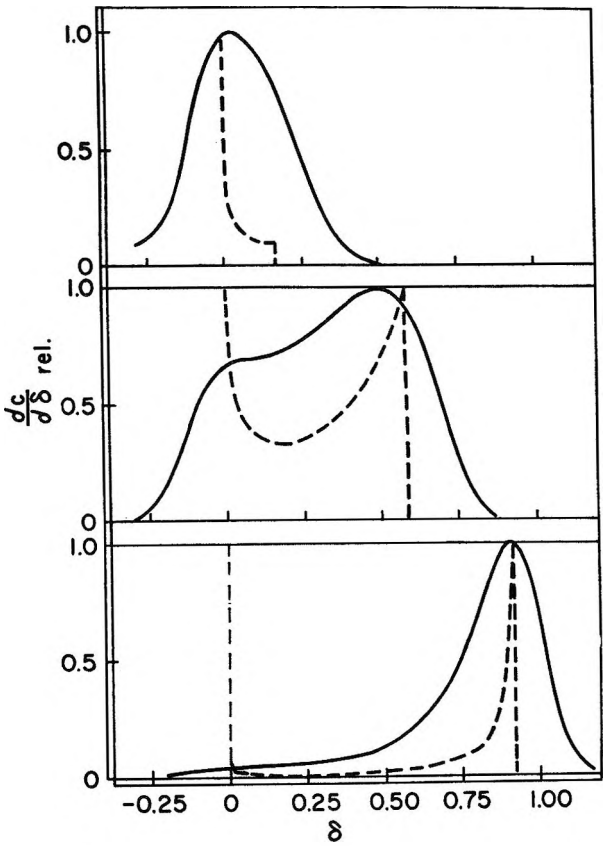

Figure 4. Countercurrent distribution (—) and asymptotic (- - -) patterns for monomer–trimer; $K_3' = 1$ l.²/g²; $K_M = 0.61$; $K_T = 3.7$; $n = 90$; (top) $C_0 = 1 \times 10^{-2}$ g/l.; (center) $C_0 = 1$ g/l.; (bottom) $C_0 = 10$ g/l.

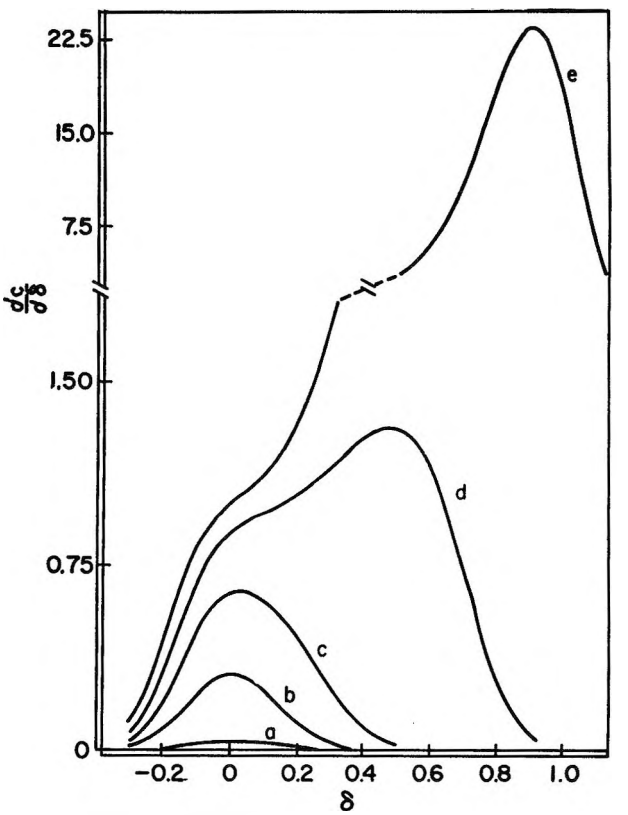

Figure 5. Countercurrent distribution patterns for the system of Figure 4. C_0 for the various patterns is (a) 10^{-2} g/l.; (b) 10^{-1} g/l.; (c) 2.754×10^{-1} g/l.; (d) 1 g/l.; (e) 10 g/l.

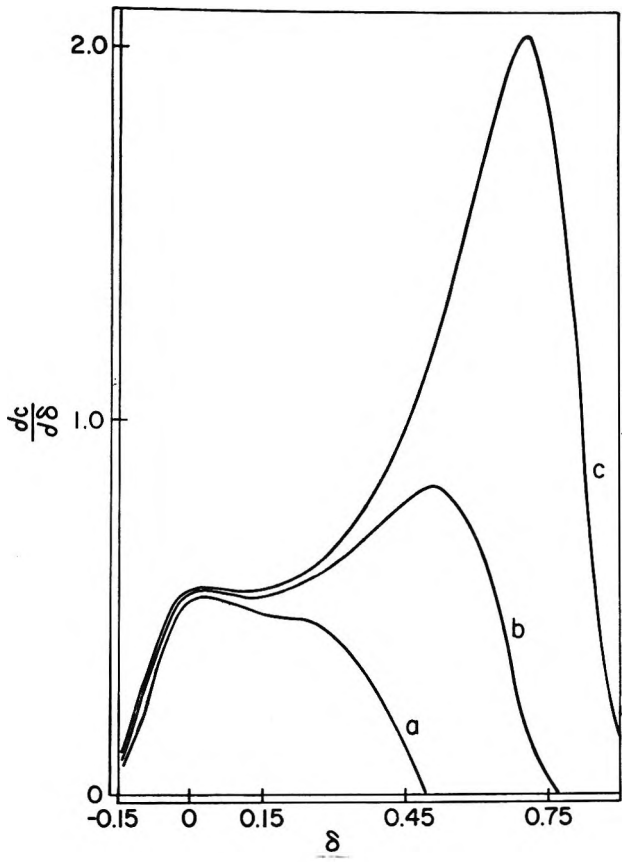

Figure 6. Countercurrent distribution patterns for the system system of Figure 4 at $n = 320$. C_0 for the various patterns is (a) 0.5 g/l.; (b) 1 g/l.; (c) 2 g/l.

creasing concentration. However, under these conditions, where resolution is limited both by diffusion and the distance over which separation occurs, this conclusion no longer holds.

If, however, the number of transfers is increased, *i.e.*, if the distance over which transport occurs is increased, then resolution into two boundaries may be accomplished (Figure 6). Here $n = 320$, equivalent to a distance traveled by trimer of 3.6 cm under the above assumptions. Remarkably, however, curve a, corresponding to a concentration of 0.5 g/l., almost twice that required for the appearance of a minimum, does not exhibit one, only one distorted boundary being present. A similar loss of definition, when diffusion is included, has been defined in sedimentation analysis.[8b] A minimum is clearly present at a concentration of 1 g/l. and is not obliterated at 2 g/l. From the concentrations at the minimum, in the two cases in which one is present, equilibrium constants may be calculated by eq 5 (Table II). The assigned value of K_3' is 1; the error therefore is of the order of 25% and becomes worse at the higher concentration. These changes suggest that, as in the case of dimerization, velocities of a given concentration level are not constant, but change with, *e.g.*, increasing numbers of transfers. This is indeed the case, and, as before, the only level to move with a constant velocity is $0.6C_0$.

Table II: Calculation of Equilibrium Constants by Eq 5

C_0, g/l.	C_{min}, g/l.	K_3', l.²/g²
1	0.253 ± 0.008	1.2 ± 0.1
2	0.243 ± 0.008	1.3 ± 0.1

Thus, the general conclusions of the overall appearance of a boundary in a dimerizing system apply to the trimerizing system, and, additionally, the overall acceleration which occurs should lead to time-dependent velocities, which should be especially apparent in electrophoresis, since here the separation path is longer than in sedimentation analysis.

Directed Transport of Monomer–Dimer–Trimer Systems. Comparison of the Asymptotic and Countercurrent Distribution Approaches[1a]

by B. J. McNeil,[1b] L. W. Nichol, and J. L. Bethune[1c]

Biophysics Research Laboratory, Department of Biological Chemistry, Harvard Medical School, and the Division of Medical Biology, Peter Bent Brigham Hospital, Boston, Massachusetts, and The Russell Grimwade School of Biochemistry, University of Melbourne, Parkville, Victoria, Australia
(Received January 20, 1970)

A numerical investigation of the equations governing the asymptotic transport behavior of a model system involving rapid equilibration between monomer, dimer, and trimer predicts that maximally only two boundaries may be found. The position of the minimum is a function of the equilibrium constants governing the reaction. For certain of the combinations of the relevant parameters for which the asymptotic equations predict the presence of two boundaries, the inclusion of diffusional effects indicate that such resolution is difficult to achieve in customary transport experiments. In all cases, when diffusion is present, only the 0.6C concentration level moves with a constant velocity, all other levels moving with time-dependent velocities.

The theory of the behavior of polymerizing macromolecular systems in directed transport has generally neglected the effects of diffusion upon the results obtained. A recent paper[2] has delineated a comparison of the theoretical results obtained from the asymptotic equations[3] and the countercurrent distribution analog,[4] which includes the effects of diffusion, for the systems monomer–dimer and monomer–trimer. This paper extends the comparison to a more complex system, monomer–dimer–trimer, which has been examined previously for only one set of relevant parameters.[4,5]

Chymotrypsin, under certain experimental conditions, appears to be an example of a monomer–dimer–trimer system, and patterns have been calculated previously by both approaches for one set of relevant parameters. For this system the asymptotic approach[5] predicted two boundaries and the countercurrent distribution analog approach the presence of one asymmetric boundary.[4]

Theory

If diffusion is neglected, the following equation describes this system in directed transport in a rectangular cell with a constant field[6]

$$\frac{\partial(C_M + C_D + C_T)}{\partial t} = -V_M \frac{\partial C_M}{\partial x} - V_D \frac{\partial C_D}{\partial x} - V_T \frac{\partial C_T}{\partial x} \quad (1)$$

where C_M, C_D, and C_T represent the concentrations of monomer, dimer, and trimer, respectively, V_M, V_D, and V_T their respective constant velocities along the x axis, and t is time.

Definition of two dissociation constants, $K_D = C_M^2/C_D$ and $K_T = C_M^3/C_T$, allows transformation of eq 1 into

$$\frac{\partial C_M}{\partial t} + \frac{V_M + 2V_D C_M/K_D + 3V_T C_M^2/K_T}{1 + 2C_M/K_D + 3C_M^2/K_T} \frac{\partial C_M}{\partial x} = 0 \quad (1a)$$

Using the method of characteristics,[2] this equation may be immediately integrated to

$$x = \frac{V_M + 2V_D C_M/K_D + 3V_T C_M^2/K_T}{1 + 2C_M/K_D + 3C_M^2/K_T} t + x_0 \quad (1b)$$

Using the initial values describing a sharp boundary

$$C_M = 0, x \leq 0, t = 0$$

$$C_M = \text{constant}, x > 0, t = 0$$

yields

$$x/t = \frac{V_M + 2V_D C_M/K_D + 3V_T C_M^2/K_T}{1 + 2C_M/K_D + 3C_M^2/K_T}, \quad 0 \leq C_M \leq \text{constant} \quad (1c)$$

(1) (a) This work was supported by Grant-in-Aid GM-15,003 from the National Institutes of Health of the Department of Health, Education and Welfare. (b) Postdoctoral Fellow of the National Institutes of Health, of the Department of Health, Education and Welfare. (c) Research Career Development Awardee of the National Institutes of Health of the Department of Health, Education and Welfare. To whom correspondence should be addressed.

(2) J. L. Bethune, *J. Phys. Chem.*, **74**, 3837 (1970).

(3) G. A. Gilbert, *Proc. Roy. Soc., Ser. A*, **250**, 377 (1959).

(4) J. L. Bethune and G. Kegeles, *J. Phys. Chem.*, **65**, 1761 (1961).

(5) M. S. N. Rao and G. Kegeles, *J. Amer. Chem. Soc.*, **80**, 5724 (1958).

(6) (a) The asymptotic equations pertaining to this situation have been utilized rather than those elaborated by Fujita, which pertain to a sector-shaped cell and a radial field in sedimentation analysis, to allow facile detection of the effect of diffusion on the patterns obtained. H. Fujita, "Mathematical Theory of Sedimentation Analysis," Academic Press, New York, N. Y., 1962. (b) Calculations were performed only for situations in which $V_M \leq V_D \leq V_T$, migration in the applied field occurring in the direction solvent → solution. For other situations, hypersharp boundaries are predicted: L. W. Nichol, A. G. Ogston, and A. Rescigno, *Proc. Roy. Soc., Ser. A*, **317**, 153 (1970).

Use of the dimensionless parameters

$$\delta = \frac{x/t - V_M}{V_T - V_M} \tag{1d}$$

$$R = \frac{V_D'}{V_T'} = \frac{V_D - V_M}{V_T - V_M}$$

converts eq 1c to

$$\delta = \frac{2RC_M/K_D + 3C_M^2/K_T}{1 + 2C_M/K_D + 3C_M^2/K_T} \tag{1e}$$

Since the total concentration, C, may be written as

$$C = C_M + C_M^2/K_D + C_M^3/K_T$$

the gradient of the total concentration becomes

$$\frac{\partial C}{\partial \delta} = \frac{\partial C_m}{\partial \delta}(1 + 2C_m/K_D + 3C_m^2/K_T) \tag{1f}$$

Differentiation of eq 1e yields $\partial C_m/\partial\delta$ and solution of the quadratic equation (1e) yields C_m, and use of these two expressions in eq 1f yields

$$\frac{\partial C}{\partial \delta} = \frac{K_T^2\left(\frac{R-\delta}{K_D} - D\right)^2\left(\frac{2R\delta - R - \delta}{K_D} - D\right)^2}{18\delta^2(1-\delta)^4 D} \tag{2}$$

$$D = \left[\left(\frac{R-\delta}{K_D}\right)^2 + \frac{3\delta(1-\delta)}{K_T}\right]^{1/2}$$

The limiting value of the gradient is[5]

$$\lim_{\delta \to 0} \frac{\partial C}{\partial \delta} = K_D/2R$$

Since eq 2 describes the gradient of total concentration along the δ axis, it may be differentiated once and the resultant equation equated to zero to isolate any minima. The equation obtained, however, is of the eighth order in δ, and therefore no analytical solution is possible. Since numerical solution of an eighth-order equation can be time consuming, it was decided to scan eq 2 for 100 values of δ given values of the parameter R, K_T, and K_D and to elaborate criteria for direct detection of any minima.[7] In a few cases the results from eq 2 were checked by confirming that the value at which a minimum was found by this procedure was indeed a root of the equation

$$\frac{\partial^2 C}{\partial \delta^2} = 2\psi \frac{\partial \psi}{\partial \delta} = 0 \tag{3}$$

where

$$\psi = \frac{K_T\left(\frac{R-\delta}{K_D} - D\right)\left(\frac{2R\delta - R - \delta}{K_D} - D\right)}{18^{1/2}\delta(1-\delta)^2 D^{1/2}}$$

Concentration gradients of the individual species were also calculated. The gradient of monomer concentration was calculated from

$$\frac{\partial C_M}{\partial \delta} = \frac{1 + \frac{2C_M}{K_D} + \frac{3C_M^2}{K_T}}{\frac{2}{K_D}(R - \delta) + \frac{6C_M}{K_T}(1 - \delta)} \tag{4}$$

where

$$C_M = \frac{\frac{R-\delta}{K_D} - D}{3\left(\frac{\delta - 1}{K_T}\right)}$$

Gradients of dimer and trimer were obtained from the expressions defining the dissociations constants, *i.e.*

$$\frac{\partial C_D}{\partial \delta} = \frac{2C_M}{K_D} \cdot \frac{\partial C_M}{\partial \delta}$$

$$\frac{\partial C_T}{\partial \delta} = \frac{3C_M^2}{K_T} \cdot \frac{\partial C_M}{\partial \delta} \tag{5}$$

The countercurrent distribution analog[2,4] was used to determine the additional effects of diffusion.

All calculations were programmed for an IBM 7094 computer in Fortran IV utilizing a Newtonian approximation to obtain the single positive root of the mass conservation equation.[7] Recalculation of the total concentration as the sum of monomer, dimer, and trimer concentrations found gave results that never differed from the amount initially present by more than 3 parts in 10^8. The total concentration gradients determined from eq 2 agreed with the sum of the gradients of the individual species to 5 parts in 10^5. The computer results were checked for a few values of the relevant parameters by hand calculations for both the asymptotic and countercurrent approaches. These were carried out to only three significant figures and agreed at this level with the computer results.

Results and Discussion

Asymptotic Approach. Since the existence of multiple minima in the polymerizing system monomer–trimer–nonomer has been established,[6] an extensive survey over a wide range of the relevant parameters was conducted to determine the characteristics of the present system. In a previous investigation,[4] a single minimum was found for one set of the relevant parameters (*i.e.*, K_D and K_T, the dimer and trimer dissociation constants, and R, the reduced velocity ratio). Patterns resulting from dissociation constants between 10^{-7} and 10^4 (g/l. for K_D and $g^2/l.^2$ for K_T) at intervals of 0.01 were calculated; a few values outside this range were examined also. The reduced velocity ratios employed were 0.54 (that expected for spherical molecules in sedimentation), and 0.0, 0.15, 0.25, 0.45, 0.75, and 0.90, any of which could be applicable, *e.g.*, in electrophoresis.

(7) J. L. Bethune and P. J. Grillo, *Biochemistry*, **6**, 796 (1967).

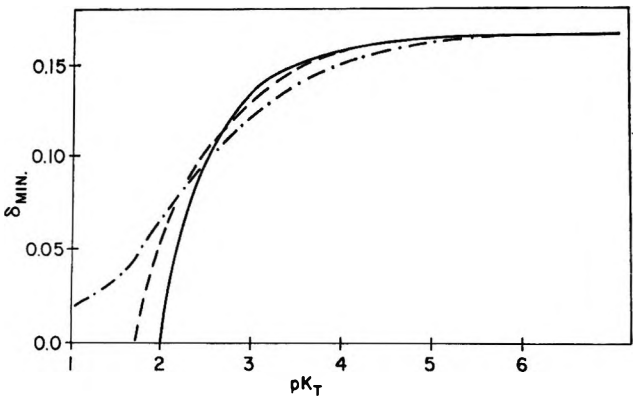

Figure 1. Dependence of the location of δ_{min} on pK_T for constant $pK_D = 1$: $R = 0.54$ (—); $R = 0.25$ (- - -); $R = 0.0$ (-·-·-).

In all cases examined, either a single minimum or no minimum was found. Remarkably, however, the δ value at which a minimum occurs is not a constant as in monomer–single polymer systems, where its location on the δ scale is a function only of the degree of polymerization.[3] Figure 1 illustrates the correlation found for δ_{min} and pK_T at a given pK_D, for various values of R. Here $pK_D = 1.0$, but the results can be transposed to other values of pK_D by fixing the origin of the pK_T axis at $2pK_D - 1.0$. At $R = 0$, *i.e.*, if $V_D = V_M$ or if V_T is much larger than V_D and V_M, then $0 < \delta_{min} \leq 0.166$. However, as R is increased, the range diminishes until for $R \geq 0.54$ no minimum was found for $pK_T \leq 2pK_D$. The overall variation in δ_{min} as a function of pK_T is a reflection of the weight-average degree of polymerization in the plateau, and, indeed, increasing concentrations of dimer are associated with the lower values of δ at which the minimum appears. The discovery that the position of the minimum is not a function of the degree of polymerization only, raises the disconcerting possibility that the presence of such a system could lead, without ancillary data, to an incorrect interpretation of the reality underlying experimental results. Thus, such a system could mimic a monomer–single polymer system exactly in all relevant characteristics. The calculation of equilibrium constants from the area under the slow boundary,[3] however, could lead to erroneous results, as would any attempt to calculate the velocity of the polymeric species,[8] since here the minimum position is not fixed by the degree of polymerization. The dependence of the value of δ_{min} on the equilibrium constants again raises the possibility of temperature dependent patterns, if the enthalpies of the two reactions differ.

The magnitude of some possible errors is indicated in Table I where the actual values of the concentration at the minimum, (C_{min}), for various values of K_D and K_T, have been used to calculate equilibrium constants on the assumption that only a monomer–trimer system is present. When δ_{min} is near 0.166, the expected value for

Table I: Calculation of K_T from C_{min}, Assuming a Monomer–Trimer System

δ_{min}	C_{min}	K_D, g/l.	K_T, g²/l.² Taken	K_T, g²/l.² Found[a]
0.166	2.7×10^{-3}	1.0	1.0×10^{-4}	1.0×10^{-4}
0.166	2.6×10^{-4}	1.0×10^{-1}	1.0×10^{-6}	0.9×10^{-6}
0.156	2.6×10^{-3}	1.0×10^{-1}	1.0×10^{-4}	0.9×10^{-4}
0.128	7.3×10^{-3}	1.0×10^{-1}	1.0×10^{-3}	0.7×10^{-3}
0.059	1.0×10^{-2}	1.0×10^{-1}	1.0×10^{-2}	1.3×10^{-3}

[a] Calculated from $1/K_T = (1/C_{min}^2)[2(n^2 - 1)]^{n-1}[n - 2]/[n(2n - 1)]^n$.

a monomer–trimer system, the amount of dimer present is insignificant (*i.e.*, K_D is large) and agreement is excellent. However, as the amount of dimer increases and δ_{min} drops to lower values, agreement becomes much poorer; in the last line, indeed, the difference amounts to one order of magnitude.

These changes in position of δ_{min} reflect certain relations between the gradient of total concentration and those of the individual species. These may be developed as follows. Since

$$C = C_M + C_D + C_T \tag{6}$$

then

$$\frac{\partial^2 C}{\partial \delta^2} = \frac{\partial^2 C_M}{\partial \delta^2} + \frac{\partial^2 C_D}{\partial \delta^2} + \frac{\partial^2 C_T}{\partial \delta^2} \tag{7}$$

From the definition of the dissociation constants, it follows that

$$\frac{\partial^2 C_D}{\partial \delta^2} = \frac{2}{K_D}\left(\frac{\partial C_M}{\partial \delta}\right)^2 + \frac{2C_M}{K_D} \cdot \frac{\partial^2 C_M}{\partial \delta^2} \tag{8a}$$

$$\frac{\partial^2 C_T}{\partial \delta^2} = \frac{6C_M}{K_T}\left(\frac{\partial C_M}{\partial \delta}\right)^2 + \frac{3C_M^2}{K_T} \cdot \frac{\partial^2 C_M}{\partial \delta^2} \tag{8b}$$

or

$$\frac{\partial^2 C}{\partial \delta^2} = A\frac{\partial^2 C_M}{\partial \delta^2} + B\left(\frac{\partial C_M}{\partial \delta}\right)^2 \tag{9}$$

where

$$A = \frac{2C_M}{K_D} + \frac{3C_M^2}{K_T}$$

$$B = \frac{2}{K_D} + \frac{6C_M}{K_T}$$

Therefore, a minimum in the gradient of total concentration can occur if, and only if

$$\frac{\partial^2 C_M}{\partial \delta^2} + \frac{B}{A}\left(\frac{\partial C_M}{\partial \delta}\right)^2 = 0 \tag{10}$$

Since a minimum in the gradient of monomer is present only if $\partial^2 C_M/\partial \delta^2 = 0$, the location of a minimum

(8) L. W. Nichol and J. L. Bethune, *Nature*, 198, 880 (1963).

in the gradient of total concentration, if one is present, can never coincide with that in the monomer gradient since $(B/A)(\partial C_M/\partial\delta)^2$ is always positive in the boundary region. Moreover, since $(B/A)(\partial C_M/\partial\delta)^2$ is positive, the left-hand side of eq 10 can vanish for large negative $\partial^2 C_M/\partial\delta^2$; hence, there can be a minimum in the total gradient with none in the monomer, dimer, or trimer gradients. Conversely, if $\partial^2 C_M/\partial\delta^2$ never attains negative values greater than $(B/A)\cdot(\partial C_M/\partial\delta)^2$, no minimum can exist in the total gradient even if one is present in the monomer gradient. The gradients of dimer and trimer can never be negative (eq 5).

Examples of all three possibilities have been found in the survey. Variations in the location of the minimum in the monomer and in the total concentration gradient are illustrated in Figure 2, and systems in which a minimum occurs either in the monomer or in the total concentration gradient, but not in both, are illustrated in Figure 3.

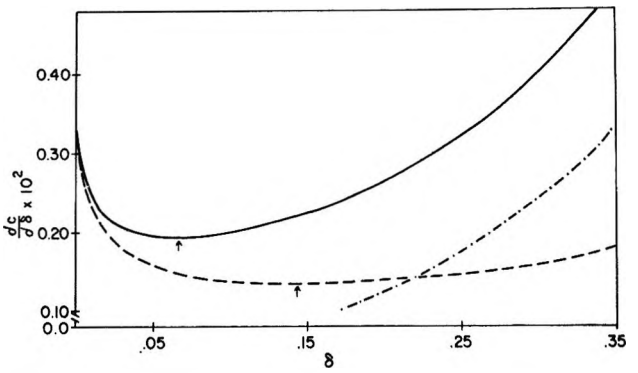

Figure 2. Asymptotic gradient patterns illustrating noncoincidence in the location of a minimum in the gradient of total concentration with that of monomer. Gradient of monomer concentration (---), of total concentration (—), and of the sum of dimer and trimer concentrations (-·-·-). The arrows indicate the position of the minima; $K_D = 10^{-3}$ g/l., $K_T = 10^{-6}$ g²/l.², $R = 0.15$.

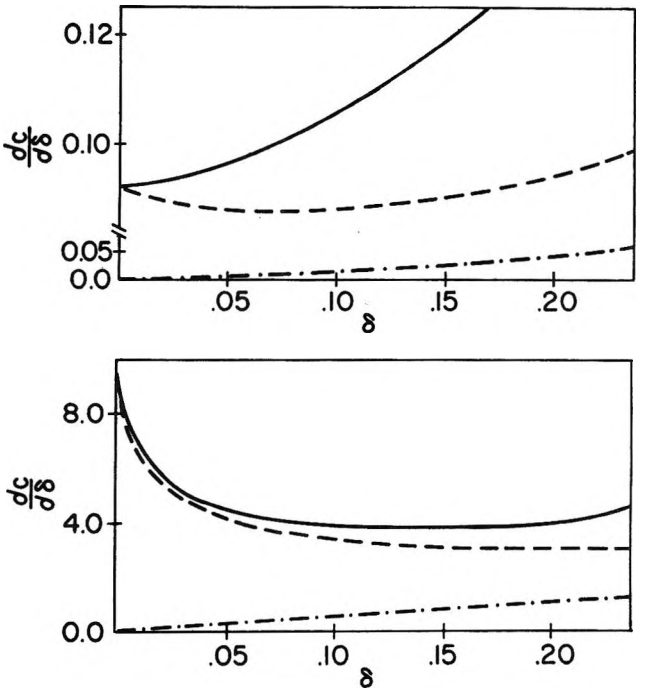

Figure 3. Asymptotic gradient patterns illustrating, in the upper section, a minimum in the gradient of monomer (---) but not in that of the total concentration (—). In the lower section one occurs in the gradient of total concentration but not in those of the individual species. Sum of the gradients of dimer and trimer concentrations (-·-·-). Upper: $K_D = 0.1$ g/l., $K_T = 0.01$ g²/l.², $R = 0.54$; lower: $K_D = 10$ g/l., $K_T = 10$ g²/l.², $R = 0.54$.

Countercurrent Distribution Analog Approach. In addition to dimer and trimer dissociation constants, total concentration, C, and partition coefficients for the three species are included explicitly as parameters in the countercurrent analog formulation.[2,4] Analogies of certain functions of the partition coefficients to diffusion coefficients and velocities pertaining in other transport methods have been explicated.[2,4]

Thus, the partition coefficient P_X, for a species X, is related to the velocity, V_X, of the maximum in the gradient pattern in a countercurrent distribution train by

$$V_X = \frac{P_X}{P_X + 1}$$

The corresponding reduced velocity for such a system, analogous to that defined above for the asymptotic case, is therefore

$$R = \frac{\dfrac{P_D}{P_D + 1} - \dfrac{P_M}{P_M + 1}}{\dfrac{P_T}{P_T + 1} - \dfrac{P_M}{P_M + 1}} \tag{11}$$

Thus, given R alone, an infinite number of sets of P_M, P_D, and P_T can be chosen.

However, in the limiting case of three spherical molecules, applicable to sedimentation analysis

$$\frac{V_M}{V_N} = \frac{s_M}{s_N} = \left(\frac{M_M}{M_N}\right)^{2/3} = \frac{1}{N^{2/3}}$$

then

$$\frac{P_M}{P_M + 1}\cdot\frac{P_D + 1}{P_D} = \frac{1}{2^{2/3}} = 0.63 \tag{12a}$$

and

$$\frac{P_M}{P_M + 1}\cdot\frac{P_T + 1}{P_T} = \frac{1}{3^{2/3}} = 0.48 \tag{12b}$$

where N denotes the degree of polymerization and where s_M, M_M, s_N, and M_N are sedimentation coefficients and molecular weights of the monomer and polymer, respectively. As has been shown,[4] spreading

due to free diffusion is analogous to the spreading of a boundary in a countercurrent distribution train, the relation being

$$D \rightarrow \frac{P}{(P+1)^2}$$

Since $D_M/D_N = N^{1/3}$, two further relations among the partition coefficients may be elaborated

$$\frac{P_M}{(P_M+1)^2}\cdot\frac{(P_D+1)^2}{P_D} = 2^{1/3}$$

$$\frac{P_M}{(P_M+1)^2}\cdot\frac{(P_T+1)^2}{P_T} = 3^{1/3}$$

Thus, there exist four relations among three unknowns, and it is, in general, impossible to fulfill them all exactly. The velocity relations were retained as well as the (analog) diffusion relation between monomer and trimer. The resulting set of partition coefficients ($P_M = 0.6$, $P_D = 1.5$, and $P_T = 3.8$) gave a ratio of the (analog) diffusion coefficient of monomer to that of dimer approximately equal to one. With these partition coefficients, countercurrent distribution patterns were calculated over a range of dissociation constants, for $n = 100$.[9] No minimum was observed, in agreement with similar calculations for the systems monomer–dimer and monomer–trimer,[2] and the single calculation for monomer–dimer–trimer performed previously.[4] Therefore, if the velocity ratios are those predicted for spherical molecules in sedimentation analysis, no resolution is expected under normal experimental conditions.

To examine a situation in which a minimum could occur, the partition coefficients of monomer and trimer were set at 0.2 and 9. The partition coefficient of dimer (1.29) was then calculated using eq 11 with an R value of 0.54. At low concentrations (10^{-3} g/l.) the entire system moves with a velocity characteristic of monomer; no effect of diffusion on peak location is observed (Figure 4). At 10^{-2} g/l. a minimum appears, but at a smaller value of δ than that predicted by the asymptotic relations, which apply in the absence of diffusion. At 10^{-1} g/l. the slow boundary is relatively small, and now the rapid boundary is nearer the position predicted by the asymptotic equation, consistent with the results obtained on simpler systems.[2]

An assessment of the role of dimer on such patterns was obtained by altering K_D over three orders of magnitude at fixed values of K_T and C. The concentrations in the plateau region of the three species, as K_D is varied, are given in Table II and the associated patterns in Figure 5. At lower values of K_D, where dimer constitutes a large proportion of the total, no minimum is seen. At higher K_D's, however, a minimum is clearly detectable, shifting from a δ value of 0.14 at $K_D = 0.1$ g/l. to 0.15 at $K_D = 1.0$ g/l. All of these values are lower than those predicted from the asymptotic equations alone (0.160 for $K_D = 0.1$ g/l. and 0.166 for $K_D = 10$ g/l.). Thus, an increase in the dimer concentration may be associated with a minimum occurring at values of δ below 0.166, in agreement with the conclusion reached from Figure 1.

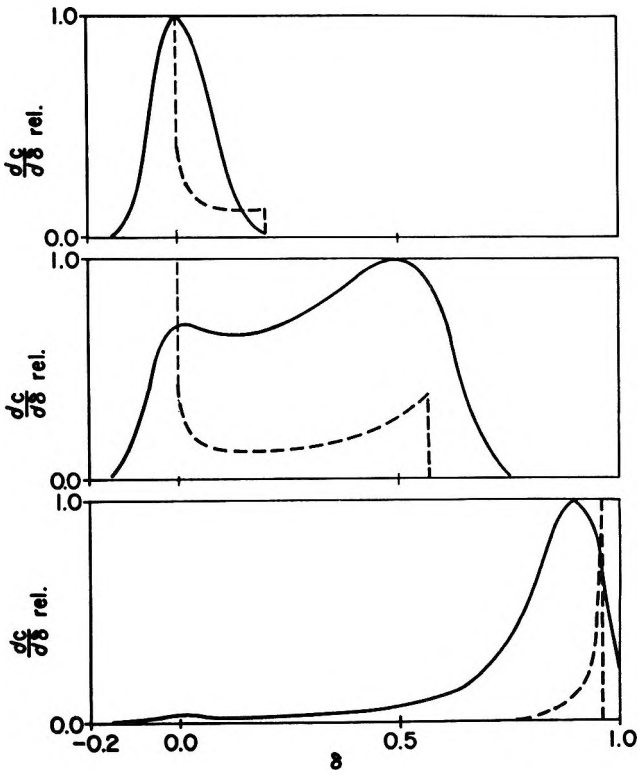

Figure 4. The effect of concentration on transport patterns calculated by the asymptotic (- - -) and the countercurrent distribution (—) approaches at $K_D = 0.1$ g/l., $K_T = 10^{-4}$ g²/l.², and $R = 0.54$ for 100 transfers. $P_M = 0.2$, $P_D = 1.29$, $P_T = 9.0$. Upper: $C = 10^{-3}$ g/l.; middle: $C = 10^{-2}$ g/l.; lower: $C = 10^{-1}$ g/l. Each pattern has been normalized independently to its maximum value.

Table II: Variation in the Plateau Concentrations of Monomer, Dimer, and Trimer As a Function of K_D[a]

K_D	c_M[b]	c_D[b]	c_T[b]
1.0×10^{-2}	54	30	16
1.0×10^{-1}	66	5	29
1.0[c]	68	1	31

[a] $K_T = 10^{-4}$ g²/l.², $C = 10^{-2}$ g/l. [b] As per cent of C. [c] For larger values of K_D little further change is found.

Several other values of partition coefficients and reduced velocities, where the asymptotic equations predict the existence of minima at δ values less than 0.16 (*i.e.*, at increased dimer concentrations) were examined by the countercurrent distribution analog. Minima

(9) C was chosen to place the maximum in gradient curve at a δ value of approximately 0.5. An analogous sedimentation experiment would involve a system in which monomer has a sedimentation coefficient of 4S and a diffusion coefficient of 5×10^{-7} cm²/sec, the maximum having moved approximately 1 cm (*vide infra*).

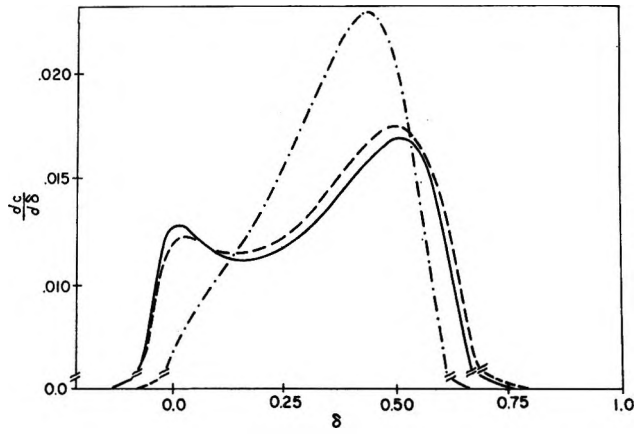

Figure 5. Effect of variation of K_D on countercurrent distribution patterns for $K_T = 10^{-4}$ g²/l.², $C = 10^{-2}$ g/l., $R = 0.54$, 100 transfers. $P_M = 0.2$, $P_D = 1.29$, $P_T = 9.0$, $K_D = 0.01$ g/l. (·····), $K_D = 0.1$ g/l. (- - -), $K_D = 1.0$ g/l. (—).

between 0.13 and 0.16 on the δ scale were approximately reproduced after 100 transfers and hence may be experimentally accessible (*vide infra*). One system ($K_D = 0.1$ g/l., $K_T = 10^{-2}$ g²/l.², $C = 10^{-1}$ g/l., $R = 0.25$) for which the asymptotic equations predicted a minimum at a δ value of 0.06 was examined up to 1500 transfers. For all transfers from 50 to 1500, the patterns exhibited one peak with a shoulder on the trailing

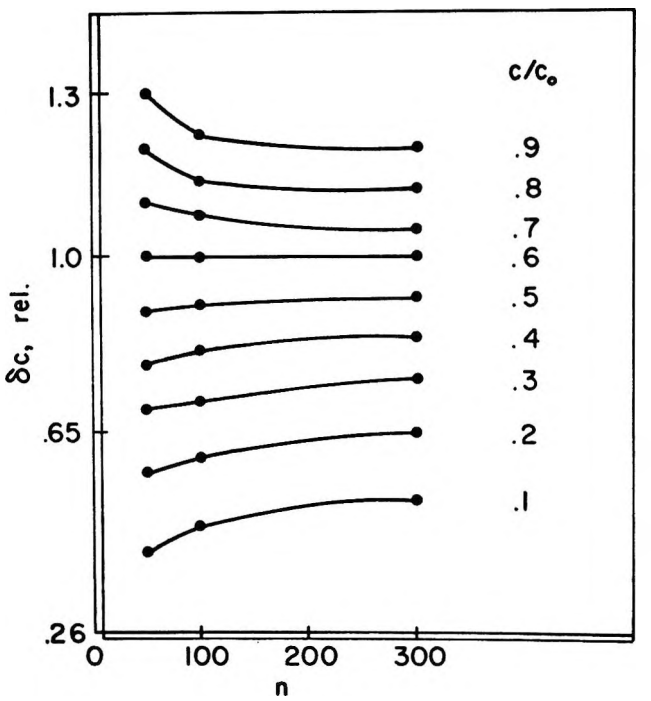

Figure 6. Velocity of various relative concentrations (C/C_0) as a function of the number of transfers (n). The velocity is expressed as $\delta_{C,rel}$ where C refers to a given concentration level. The value of δ for that concentration level found in the countercurrent distribution pattern is expressed as a fraction of the value predicted for that concentration by the asymptotic equation. $K_D = 10^{-1}$ g/l., $K_T = 10^{-2}$ g²/l.², $C = 10^{-1}$ g/l., $P_M = 0.2$, $P_D = 0.536$, $P_T = 9.0$.

Table III: Correlation of Peak Position (δ_{max}^{CCD}) with Number of Transfers (n)[a]

Number of transfers	δ_{max}^{CCD}	% deviation from δ_{max}^{asy} [b]	d,[c] cm
50	0.3188	17.6	0.12
100	0.3324	14.1	0.24
300	0.3415	11.7	0.75
500	0.3460	10.6	1.26
700	0.3480	10.0	1.77
1000	0.3501	9.5	2.54
1500	0.3515	9.1	3.82

[a] $K_D = 10^{-1}$ g/l., $K_T = 10^{-2}$ g²/l.², $C = 10^{-1}$ g/l., $P_M = 0.2$, $P_D = 0.536$, $P_T = 9.0$. [b] Calculated from[5] $\delta_{max} = [(2RC_M/K_D) + (3C_M^2/K_T)]/[1 + (2C_M/K_D) + (3C_M^2/K_T)]$. [c] Calculated from $d = r_{max}\phi$, $\phi = 0.006$ cm/tube.

edge, but no evidence of separation (*i.e.*, no minimum) appeared even at 1500 transfers. However, as is the case in the monomer–single polymer systems,[2] the velocity of the maximum in the gradient curve was dependent upon the number of transfers (Table III). Moreover, the velocities of all concentration levels, except that at $0.6C$, exhibit a similar dependence (Figure 6). This is again reminiscent of the monomer–single

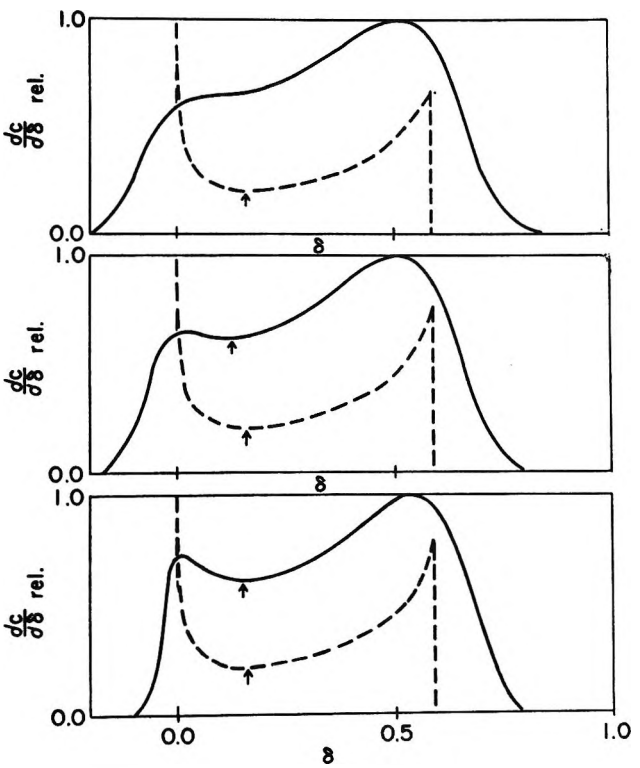

Figure 7. Effect of variation in ratio of monomer to trimer velocities for $K_D = 10^{-1}$ g/l., $K_T = 10^{-4}$ g²/l.², $C = 10^{-2}$ g/l., 100 transfers. The arrows indicate the position of minima. Upper: $P_M = 0.34$, $P_D = 4.4$, $P_T = 5.4$; middle: $P_M = 0.21$, $P_D = 6.5$, $P_T = 7.8$; lower: $P_M = 0.10$, $P_D = 12.8$, $P_T = 14.9$. Each pattern has been normalized independently to its maximum value.

polymer systems, where only the $0.6C$ concentration level moved at a fixed velocity,[2] which was equal to that predicted by the asymptotic equation[3] for that concentration level.

Also included in Table III is one example of conversion of the distance traveled in the countercurrent distribution train into that which would obtain in, *e.g.*, electrophoresis. Here it is assumed that $D_M = 5 \times 10^{-7}$ cm^2/sec, $V_M = 2 \times 10^{-4}$ cm/sec. Conversion is accomplished through

$$\phi = \frac{2D_M(P_M + 1)}{V_M} = 0.006 \text{ cm/tube}$$

where ϕ is the factor which scales distances in the train to distances along an x axis, *i.e.*, its units are centimeters/tube.[2] If the velocity were constant, the distance traveled after 1500 transfers should be 30 times that traveled after 50 transfers, *i.e.*, 3.60 cm. The actual calculated distance is 3.82 cm, a difference of 0.22 cm.

A further set of calculations were performed for values of the reduced velocities between 0.99 and 0.95, *i.e.*, where the velocity of dimer approaches that of trimer for $n = 100$. Although this situation is unlikely in sedimentation in the absence of large variations in frictional coefficients, it is not improbable in moving boundary electrophoresis. Since an infinite number of sets of partition coefficients exist for a given R, a further restriction was imposed; the (analog) diffusion coefficients were restricted to the ratios pertaining to spheres (*vide supra*). Relative velocity ratios of monomer to trimer of 0.1, 0.2, and 0.3 were utilized together with several combinations of dimer and trimer dissociation constants and total concentration. Figure 7 shows typical transport patterns obtained as the velocity ratio changes. The relevant symptotic patterns are also included. If the relative velocity ratio is above 0.2, no minimum is seen, under these conditions, in the countercurrent distribution pattern. However, for a ratio of 0.1 or 0.2 a minimum is found. In all cases, since the value of R is almost constant, the asymptotic patterns are nearly identical, predicting a minimum in all cases. If the countercurrent calculation is carried out for very large numbers of transfers, equivalent to a long separation distance, a minimum can be detected at a ratio of 0.3. Thus, the detection of a minimum depends on the resolving power of the experimental technique employed.

Mathematical Analysis of Isotope Exchange Reactions

by P. L. Corio[1]

Mobil Research & Development Corporation, Central Research Division Laboratory, Princeton, New Jersey 08540
(Received March 19, 1970)

A mathematical analysis of the rate equations for the single-step redistribution of hydrogen and deuterium atoms among the deuterium isomers of a parent molecule containing N chemically equivalent exchangeable hydrogen atoms is presented. Assuming complete degeneracy in the specific rate constants for all exchanges, the explicit solution of the rate equations is obtained for arbitrary N in terms of a system of orthogonal polynomials. The properties of these polynomials are used to deduce important properties of the redistribution kinetics. In particular, their orthogonality may be used to transform experimental data to a representation in which the exponential decays are uncoupled. The application of the uncoupled representation to the analysis of experimental data is illustrated for the exchange among the deuterioethylenes on nickel wire, and the exchange among the deuteriobenzenes over a rare-earth-exchanged zeolite. The rate equations are also solved for the case where all hydrogenations are described by the specific rate constant k_H and all deuterations by the specific rate constant k_D. The isomer distributions obtained in this circumstance are formally identical with those obtained in the absence of an isotope effect. The observed rate constant is equal to an atom-fraction weighted average of the rate constants for hydrogenation and deuteration. The ratio k_H/k_D can, in principle, be determined from the observed equilibrium distribution. The analysis is strictly applicable to homogeneous reactions, but it is also applicable to heterogeneous catalytic systems for which the contact time between molecules and catalyst is long enough to ensure the establishment of isotopic equilibrium in reasonable time periods, but short enough to preclude the necessity for considering diffusion and multistep kinetics.

1. Introduction

The catalyzed exchange of hydrogen and deuterium atoms among the deuterio isomers of hydrocarbon molecules has been observed over a number of metal catalysts.[2] Many of these reactions apparently conform to a kinetic model in which the insertion of hydrogen and deuterium atoms occurs in a stepwise manner without an appreciable isotope effect.[3] The rate equations for this model predict a binomial distribution of isomers at equilibrium, and experimentally observed equilibrium distributions are frequently of binomial form.[3,4] Nonequilibrium solutions of the rate equations have been obtained only for special initial conditions,[4] so that detailed experimental investigations of the model and its implications have not been undertaken. The solution of the rate equations for arbitrary initial conditions will be derived in this paper for the special case of an exchange reaction in which hydrogen and deuterium atoms are redistributed among the $N + 1$ deuterio isomers of a parent molecule containing N chemically equivalent exchangeable hydrogen atoms. If $D(x)$, $x = 0, 1, 2, \ldots, N$, denotes the isomer containing x deuterium atoms and $N - x$ hydrogen atoms, the reaction sequence may be schematically written

$$D(x-1) \underset{k}{\overset{k}{\rightleftharpoons}} D(x) \underset{k}{\overset{k}{\rightleftharpoons}} D(x+1) \qquad (I)$$

where k denotes the specific rate constant, measured in reciprocal time units, characterizing all exchanges.[5] The complete reaction sequence commences with the parent molecule $D(0)$ and terminates with the perdeuterio isomer $D(N)$. However, as the single-step mechanism is assumed to be operative in each exchange, only three contiguous elements of the reaction sequence are explicitly indicated. It should not be inferred, however, that $D(x)$ exchanges hydrogenlike atoms only with its nearest neighbors; $D(x)$ may acquire a hydrogen or deuterium atom at the expense of any isomer containing one or the other of these atoms.

The special case $N = 4$ is illustrated by methane, and it will be observed that the insertion of one or two deuterium atoms into the methane molecule does not remove the full chemical equivalence of the remaining protons. The significance of this observation is that the statistical factor for the introduction of a deuterium atom into a given isomer is always equal to the number of hydrogen atoms in the isomer. This is to be con-

(1) Address where correspondence should be sent: Department of Chemistry, University of Kentucky, Lexington, Ky. 40506.

(2) The subject has been reviewed by (a) T. I. Taylor in "Catalysis," Vol. V, P. H. Emmett, Ed., Reinhold, New York, N. Y., 1957, p 257; (b) C. Kemball in "Advances in Catalysis," Vol. XI, D. D. Eley, P. W. Selwood, and P. B. Weisz, Ed., Academic Press, New York, N. Y., 1959, p 263.

(3) (a) C. D. Wagner, J. D. Wilson, J. W. Otvos, and D. P. Stevenson, *J. Chem. Phys.*, **20**, 338 (1952); (b) C. Kemball, *Trans. Faraday Soc.*, **50**, 1344 (1954); (c) H. Kloosterziel in "Chemisorption," W. E. Garner, Ed., Academic Press, New York, N. Y., 1956, p 76; (d) G. Pass, A. B. Littlewood, and R. L. Burwell, Jr., *J. Amer. Chem. Soc.*, **82**, 6281 (1960); ref 2b, pp 226–230.

(4) (a) G. Dallinga, A. A. Stuart Verrijn, P. J. Smit, and E. L. Mackor, *Z. Elektrochem.*, **61**, 1019 (1957); (b) R. J. Mikovsky and J. Wei, *Chem. Eng. Sci.*, **18**, 253 (1963); (c) H. Bolder, G. Dallinga, and H. Kloosterziel, *J. Catal.*, **3**, 312 (1964).

(5) Some consequences of an isotope effect will be considered in section 5.

trasted with the case of benzene where the statistical factor is six for the insertion of the first deuterium atom, but may be 1 or 2 for a second such insertion, depending on the ring position taken by the entering deuterium atom. To the extent that the equality of all rate constants is a reasonable first approximation for systems of the benzene type, the following analysis may be applied by considering all isomers containing a fixed number of deuterium atoms as a single entity whose mole fraction is equal to the sum of the mole fractions of the individual isomers.

The exchange will be supposed to occur in a closed reaction system maintained at a fixed temperature. The rate of reaction will be assumed to be first order with respect to each reacting species, and otherwise governed by statistical factors reflecting the numbers of hydrogen and deuterium atoms in the reactants. This limits the analysis to homogeneous systems, but it can also be applied to heterogeneous catalytic systems for which the contact time between molecules and catalyst is long enough to ensure the establishment of isotopic equilibrium in reasonable time periods, but short enough to preclude the necessity for considering molecular diffusion and multistep kinetics.[6]

The closure assumption requires the conservation of mass, the number of deuterium atoms, and the number hydrogen atoms. If $D(x,t)$ denotes the mole fraction of $D(x)$ at time t, the conservation conditions may be written in the form

$$\sum_{x=0}^{N} D(x,t) = 1 \tag{1.1}$$

$$\sum_{x=0}^{N} xD(x,t) = Np \tag{1.2}$$

$$\sum_{x=0}^{N} (N - x)D(x, t) = Nq \tag{1.3}$$

where p and q are positive constants satisfying

$$p + q = 1 \tag{1.4}$$

From the definitions (1.2) and (1.3), it is evident that p and q are the atom fractions of deuterium and hydrogen, respectively. The quantity Np may be interpreted as the mean value of the discrete variable x.

2. Integration of the Rate Equations

The preceding kinetic assumptions yield the following expression for the rate of production of $D(x)$

$$\lambda^{-1}\dot{D}(x,t) = q(x + 1)D(x + 1,t) - [(q - p)x + Np]D(x,t) + p(N - x + 1)D(x - 1,t) \tag{2.1}$$

where

$$\lambda = Nk \tag{2.2}$$

and the dot over $D(x,t)$ denotes differentiation with respect to time.

The function $D(x,t)$ is defined to be zero for all integers not included in the closed interval $[0,N]$. For $x = 0, 1, 2, \ldots, N$, eq 2.1 defines a system of $N + 1$ first-order linear differential equations with constant coefficients. The solution of this system for small values of N can be obtained by standard mathematical techniques, but the computational labor increases rapidly with increasing N. The solution for arbitrary N will be obtained by a less familiar procedure that is considerably more expeditious and not without formal elegance.[7]

Let n be a nonnegative integer not exceeding N, and assume a particular solution of the form

$$D_n(x,t) = w(x)K_n(x)e^{-n\lambda t} \tag{2.3}$$

where

$$w(x) = \binom{N}{x} p^x q^{N-x} \tag{2.4}$$

and $K_n(x)$ is independent of t. Substituting (2.3) into (2.1) one obtains, after some algebraic reductions

$$p(N - x)K_n(x + 1) - [(q - p)x + pN - n]K_n(x) + qxK_n(x - 1) = 0 \tag{2.5}$$

Equation 2.5 is the second-order linear difference equation satisfied by the Krawtchouk polynomial of degree n in the discrete variable x. These polynomials[8,9] satisfy the following sets of orthogonality relations

$$\sum_{x=0}^{N} w(x)K_n(x)K_m(x) = (pq)_n \binom{N}{n} \delta_{nm} \tag{2.6}$$

$$\sum_{n=0}^{N} \left\{(pq)^n \binom{N}{n}\right\}^{-1} K_n(x)K_n(y) = [w(x)]^{-1}\delta_{xy} \tag{2.7}$$

where $\delta_{rs} = 0$, for $r \neq s$, $\delta_{rs} = 1$, for $r = s$.

(6) For a discussion of multistep kinetics see J. R. Anderson and C. Kemball, *Proc. Roy. Soc., Ser. A*, 223, 361 (1954). Multiple exchange reactions have also been discussed by Bolder, Dallinga, and Kloosterziel, ref 3c. The effect of diffusion has been considered by F. G. Dwyer, L. C. Eagleton, J. Wei, and J. C. Zahner, *ibid.*, 302, 253 (1968).

(7) The determination of the general solution of (2.1) and the specification of its properties—especially the explicit form of the orthogonality relations—by matrix methods, the Laplace transform, or the generating function technique, would seem to be a problem of considerable difficulty. An equation of the form (2.1) occurs in the stochastic model of the reaction A ⇄ B and McQuarrie [*J. Chem. Phys.*, 38, 433 (1963)] has given a particular solution. In the present context the general solution is essential, and in section 4 the utility of the orthogonality relations in the analysis of experimental data is demonstrated.

(8) For a discussion of Krawtchouk's polynomials, see (a) G. Szegö, "Orthogonal Polynomials," American Mathematical Society, New York, N. Y., 1959, pp 35–37; (b) Bateman Manuscript Project, "Higer Transcendental Functions," Vol. 2, A. Erdelyi, Ed., McGraw-Hill, New York, N. Y., 1953, pp 224, 225. For a more detailed discussion, see P. L. Corio, *Intern. J. Quantum. Chem.*, to be published.

(9) The orthogonality property may be realized for any set of reversible first-order reactions conforming to the principle of detailed balance. For a discussion see W. Jost, *Z. Naturforsch.*, 2a, 159 (1947); J. Z. Hearon, *Ann. N. Y. Acad. Sci.*, 108, 36 (1963); J. Wei and C. D. Prater, "Advances in Catalysis," Vol. 13, D. D. Eley, P. W. Selwood, and P. B. Weisz, Ed., Academic Press, New York, N. Y., 1962, p 203.

The Krawtchouk polynomials are generated by the function

$$(1 - ps)^{N-x}(1 + qs)^x = \sum_n K_n(x)s^n \qquad (2.8)$$

and are given explicitly by the formula

$$K_n(x) = \sum_{\nu=0}^{n} (-1)^{n-\nu}\binom{x}{\nu}\binom{N-x}{n-\nu}p^{n-\nu}q^\nu \qquad (2.9)$$

In particular

$$K_0(x) = 1 \qquad (2.10)$$

$$K_1(x) = x - Np \qquad (2.11)$$

$$K_2(x) = {}^1/_2[x(x-1) - 2(N-1)px + N(N-1)p^2] \qquad (2.12)$$

The orthogonality relations (2.6) imply that the $N + 1$ particular solutions $D_0(x,t)$, $D_1(x,t)$, ..., $D_N(x,t)$ are linearly independent, so that the general solution of (2.1) is

$$D(x,t) = \sum_{n=0}^{N} a_n w(x) K_n(x) e^{-n\lambda t} \qquad (2.13)$$

The a_n are independent of t and x and may be expressed in terms of the initial distribution by setting $t = 0$, multiplying by $K_m(x)$, and then summing over x. This computation gives, by virtue of (2.6)

$$a_n = \left\{(pq)^n\binom{N}{n}\right\}^{-1} \sum_{x=0}^{N} K_n(x)D(x,0) \qquad (2.14)$$

In particular

$$a_0 = \sum_x D(x,0) = 1 \qquad (2.15)$$

$$a_1 = (Npq)^{-1}\sum_x (x - Np)D(x,0) = 0 \qquad (2.16)$$

Equation 2.16 follows from the fact that Np is the average value of x; hence, a_1, being proportional to the first moment about the mean, must vanish identically.

The orthogonality relations 2.6 and 2.7 may also be used to show that the solution (eq 2.13) satisfies (1.1), (1.2), and the initial conditions. For example, (1.1) may be verified by summing both members of (2.13) over x, noting that $K_0(x) = 1$

$$\sum_{x=0}^{N} D(x,t) = \sum_{n=0}^{N} a_n e^{-n\lambda t} \sum_{x=0}^{N} w(x)K_n(x)K_0(x) = 1$$

A similar application of (2.6) may be used to establish (1.2), upon noting that $x = K_1(x) + NpK_0(x)$, and that $a_1 = 0$. The verification that (2.13) satisfies the initial conditions is obtained by replacing the summation index in (2.14) with y, and introducing the resulting expression into the right member of (2.13). The desired result then follows on setting $t = 0$ and applying (2.7).

The reduction of the preceding formulas to special cases of interest presents no difficulties. For $N = 2$ one obtains[10]

$$D(0,t) = q^2 + \{p^2D(0,0) - pqD(1,0) + q^2D(2,0)\}e^{-4kt} \qquad (2.17)$$

$$D(1,t) = 2pq - 2\{p^2D(0,0) - pqD(1,0) + q^2D(2,0)\}e^{-4\lambda t} \qquad (2.18)$$

$$D(2,t) = p^2 + \{p^2D(0,0) - pqD(1,0) + q^2D(2,0)\}e^{-4kt} \qquad (2.19)$$

3. Properties of the Solution

An examination of the general solution (2.13) shows that as $t \to \infty$, the isomer distribution approaches the binomial distribution

$$D(x,\infty) = \binom{N}{x}p^xq^{N-x} \qquad (3.1)$$

If the initial distribution of isomers is binomial, that is, if at time $t = 0$, $D(x,0) = w(x)$, then the distribution is binomial for all t. Indeed, setting $D(x,0) = w(x)$ in (2.14), it follows, by virtue of (2.6), that every a_n vanishes except $a_0 = 1$; hence, (2.13) reduces to $D(x,t) = w(x)$.

The binomial distribution is the only distribution satisfying the condition $D(x,t) = D(x,0)$. For upon setting the time derivative of $D(x,t)$ equal to zero, (2.1) yields a system of $N + 1$ homogeneous linear equations for the $D(x,0)$, whose solution, subject to the condition (1.1), is $D(x,0) = w(x)$.

If the initial distribution is not binomial, the distribution at any finite value of t will not be binomial. Consider, for example, an initial distribution consisting of equal fractions of the parent molecule and its perdeuterio isomer

$$D(0,0) = D(N,0) = {}^1/_2; \quad D(x,0) = 0,\ 0 < x < N \qquad (3.2)$$

For this distribution, $p = q = {}^1/_2$

$$a_n = 2^{n-1}[1 + (-1)^n] \qquad (3.3)$$

and (2.13) may be written

$$D(x,t) = 2^{-N}\binom{N}{x}\sum_{r=0}^{[{}^1/_2N]} 2^{2r}K_{2r}(x;{}^1/_2)e^{-2r\lambda t} \qquad (3.4)$$

where

$$[{}^1/_2N] = \begin{cases} {}^1/_2N \text{ if } N \text{ is even} \\ {}^1/_2(N-1) \text{ if } N \text{ is odd} \end{cases}$$

The sum in (3.4) may be evaluated explicitly with the help of the generating function for the Krawtchouk polynomials. Indeed, for any p,q

$$\sum_{r=0}^{[{}^1/_2N]} K_{2r}(x)s^{2r} = {}^1/_2\{(1 - ps)^{N-x}(1 + qs)^x + (1 + ps)^{N-x}(1 - qs)^x\} \qquad (3.5)$$

(10) The results for $N = 2$ apply to the reaction $H_2 + D_2 \rightleftarrows 2HD$ only at high temperatures.

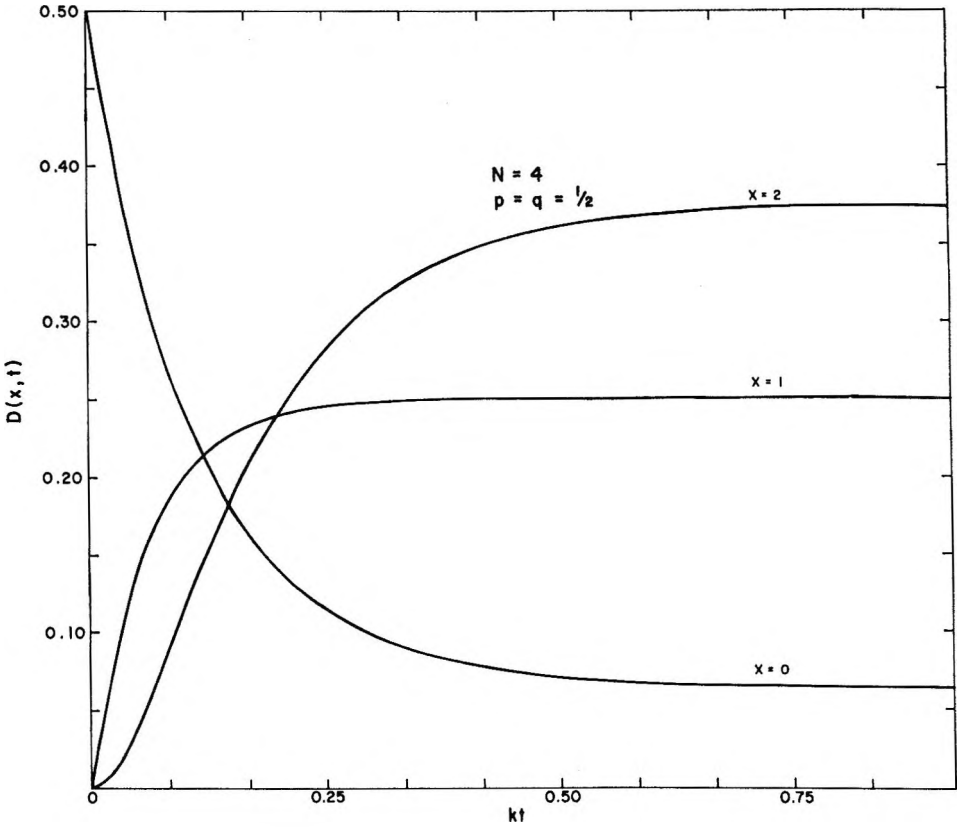

Figure 1. Graphs of D(x,t), as defined by eq 3.6, for $N = 4$.

It follows that

$$\mathrm{D}(x,t) = 2^{-N-1}\binom{N}{x}\{(1 - e^{-\lambda t})^{N-x}(1 + e^{-\lambda t})^{x} + (1 + e^{-\lambda t})^{N-x}(1 - e^{-\lambda t})^{x}\} \quad (3.6)$$

Graphs of eq 3.6 are shown in Figures 1 through 4 for several values of N. For each N, only the curves corresponding to $x = 0, 1, \ldots, [1/2N]$ are plotted, since (3.6) shows that $\mathrm{D}(x,t) = \mathrm{D}(N - x,t)$.

The symmetry of (3.6) with respect to an interchange of x and $N - x$ is a special case of a general symmetry property realized whenever the initial conditions are such that $\mathrm{D}(x,0) = \mathrm{D}(N - x,0)$ for all x. To establish this property, let the dependence of $\mathrm{D}(x,t)$ on p be denoted $\mathrm{D}(x,t;p)$. From (2.9) one may derive the following symmetry property of the Krawtchouk polynomials: $K_n(N - x;q) = (-1)^n K_n(x;p)$. This property, applied to (2.13) and (2.14), shows that

$$\mathrm{D}(N - x,t;q) \equiv \mathrm{D}(x,t;p) \quad (3.7)$$

Thus the function $\mathrm{D}(N - x,t;p)$ is obtained from $\mathrm{D}(x,t;q)$ by replacing x and p with $N - x$ and q. This is readily verified in the special case $N = 2$, described by eq 2.17, 2.18, and 2.19. Now $D(N - x,t;p)$ will not, in general, be equal to $\mathrm{D}(x,t;p)$; but the identity just established shows that these functions are equal when $p = q$. It can also be shown that if $p = q$, and $\mathrm{D}(x,0) = \mathrm{D}(N - x,0)$ for all x, then all $a_{2n+1} = 0$.

A somewhat more general initial distribution for which $p = q$ is the uniform distribution

$$\mathrm{D}(x,0) = \frac{1}{N + 1}, \text{ for all } x \quad (3.8)$$

It can be shown that

$$\sum_{x=0}^{N} K_n(x) = (-1)^n\binom{N + 1}{n + 1}p^{n+1}\left\{1 + (-1)^n\left(\frac{q}{p}\right)^{n+1}\right\} \quad (3.9)$$

so that

$$a_n = \frac{2^{n-1}}{n + 1}[1 + (-1)^n] \quad (3.10)$$

$$\mathrm{D}(x,t) = 2^{-N}\binom{N}{x}\sum_{r=0}^{[1/2N]}\frac{2^{2r}}{2r + 1}K_{2r}(x;1/2)e^{-2r\lambda t} \quad (3.11)$$

when $x = N$, the sum may be evaluated to give

$$\mathrm{D}(N,t) = \frac{e^{\lambda t}}{2^{N+1}(N + 1)}(1 + e^{-\lambda t})^{N+1} - (1 - e^{-\lambda t})^{N+1}\} \quad (3.12)$$

4. The Uncoupled Representation

The determination of $\lambda = Nk$ by direct applications of (2.13) to experimental data would require tedious

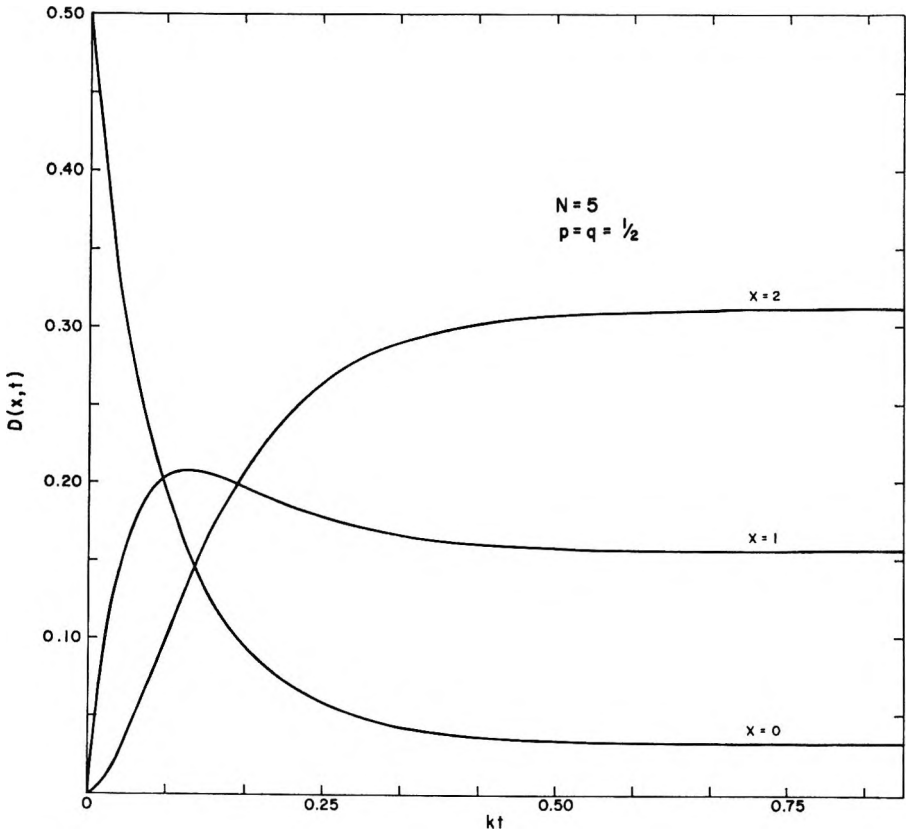

Figure 2. Graphs of $D(x,t)$, as defined by eq 3.6, for $N = 5$.

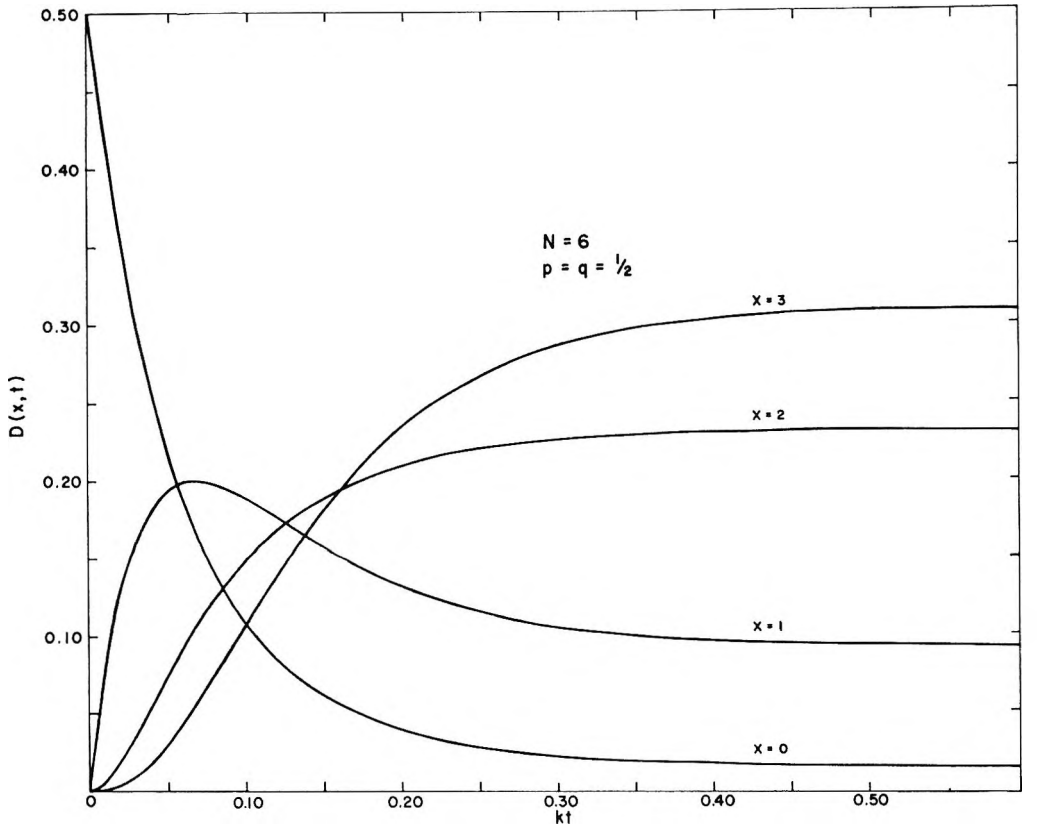

Figure 3. Graphs of $D(x,t)$, as defined by eq 3.6, for $N = 6$.

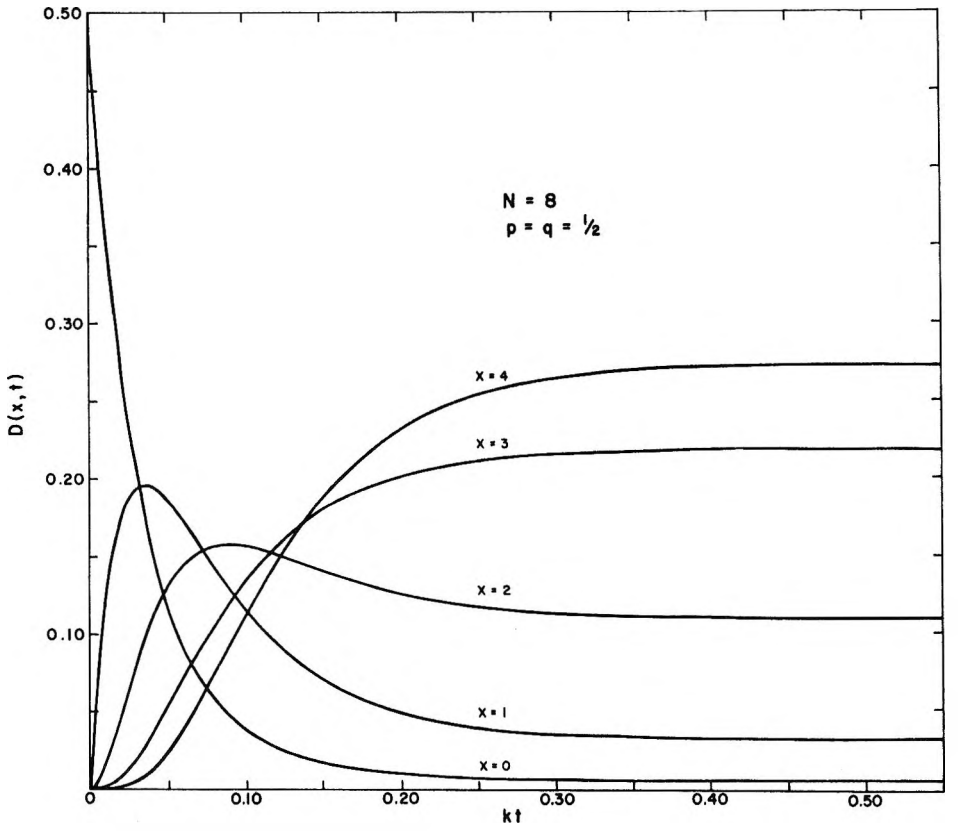

Figure 4. Graphs of $D(x,t)$, as defined by eq 3.6, for $N = 8$.

curve fitting. The experimental evaluation of λ is considerably facilitated by transforming the $D(x,t)$ to a representation in which the exponential decays are uncoupled.

Let the function $E(m,t)$, $m = 0, 1, 2, \ldots, N$, be defined by

$$E(m,t) = \sum_{x=0}^{N} K_m(x)D(x,t) \tag{4.1}$$

The $D(x,t)$ are experimentally measurable, and the polynominals $K_m(x)$ depend on the integers m, x, N, and the probability p, the latter being given in terms of the initial distribution by

$$p = N^{-1} \sum_{x=0}^{N} xD(x,0) \tag{4.2}$$

The $E(m,t)$ are, therefore, defined in terms of measurable and calculable quantities.

The theoretical significance of the $E(m,t)$ may be deduced by explicit evaluation of the summation indicated in (4.1). Multiplying (2.13) by $K_m(x)$ and summing over x one obtains, by virtue of (2.6)

$$E(m,t) = E(m,0)e^{-m\lambda t} \tag{4.3}$$

where

$$E(m,0) = \sum_{x=0}^{N} K_m(x)D(x,0) \tag{4.4}$$

Thus the $E(m,t)$ are the $D(x,t)$ in the uncoupled representation.[9]

From (4.3), it follows that a graph of ln $E(m,t)$ as a function of kt will be a straight line of slope $-mN$. The intercept on the logarithmic axis is ln $E(m,0)$, whose numerical value may be calculated from (4.4). Since

$$E(0,0) = 1, E(1,0) = 0 \tag{4.5}$$

for any initial distribution, nontrivial graphical representations are obtained only for $m \geq 2$. The analysis of experimental data in the uncoupled representation should provide a convenient test of the several kinetic assumptions.

For the initial distribution (3.2)

$$E(m,0) = \frac{1}{2^{m+1}} \binom{N}{m} [1 + (-1)^m] \tag{4.6}$$

so that all $E(m,t)$ with m odd are zero, whereas

$$E(m,t) = \frac{1}{2^m} \binom{N}{m} e^{-m\lambda t}, \; m = 0, 2, 4, \ldots \tag{4.7}$$

Graphs of the natural logarithm of the left member of (4.7) *vs.* kt are given in Figure 5 for $m = 2$ and $m = 4$. The plotted points were obtained from experimental data on hydrogen–deuterium exchange among the deuterioethylenes on nickel wire[11] at 153°, adapted to the

(11) T. B. Flanagan and B. S. Rabinovitch, *J. Phys. Chem.*, **60**, 730 (1956).

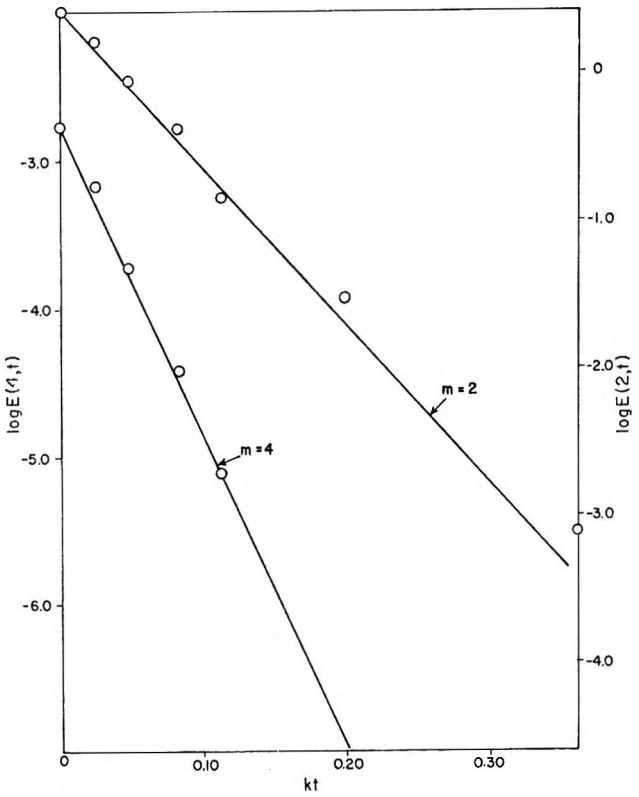

Figure 5. Graphs of ln $E(m,t)$ against kt for an equimolar mixture of ethylene and ethylene-d_6. The experimental data were obtained from the work of Flanagan and Rabinovitch.[11]

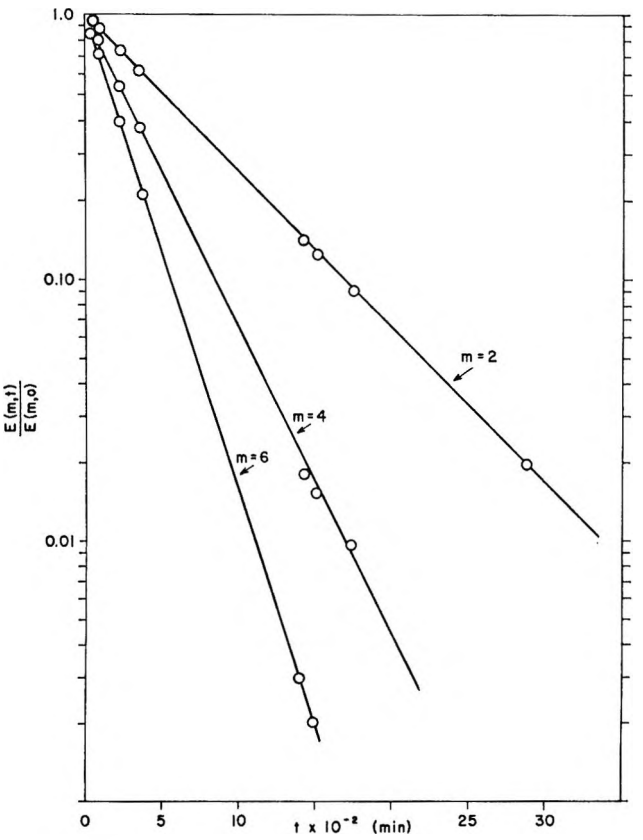

Figure 6. Semilogarithmic plots of $E(m,t)/E(0,t)$ against t for an equimolar mixture of benzene and its perdeuterio isomer. The experimental points are taken from the work of Lago and Haag.[12]

kinetic assumptions described in section 1. The deviation of $E(2,t)$ from linearity for $kt \geq 0.2$ probably results from a poisoning of the catalyst.

Figure 6 shows semilogarithmic plots of $E(m,t)/E(m,0)$ against time for the equilibration of an equimolar mixture of benzene and its perdeuterio isomer.[12] The exchange was carried out over a rare-earth-exchanged zeolite of the Y type at room temperature. These curves are all consistent with $k = 7.45 \times 10^{-6}$ sec^{-1}/g of catalyst.

The explicit form assumed by $E(m,t)$ for the initial distribution (3.8) is

$$E(m,t) = \frac{1}{2^m(m+1)}\binom{N}{m}e^{-m\lambda t},\ m = 0, 2, 4, \ldots \quad (4.8)$$

Thus a change of initial distribution from (3.2) to (3.8) merely effects a decrease in the vertical intercept on a rectilinear or logarithmic plot.

5. Isotope Effect

The most general redistribution reaction conforming to the single-step mechanism may be schematically written

$$\mathrm{D}(x-1) \underset{k_x^{(\mathrm{H})}}{\overset{k_{x-1}^{(\mathrm{D})}}{\rightleftharpoons}} \mathrm{D}(x) \underset{k_{x+1}^{(\mathrm{H})}}{\overset{k_x^{(\mathrm{D})}}{\rightleftharpoons}} \mathrm{D}(x+1) \quad \text{(II)}$$

where $k_x^{(\mathrm{H})}$ and $k_x^{(\mathrm{D})}$ denote the specific rate constants for the insertion of hydrogen and deuterium atoms into a molecule containing x deuterium atoms. The rate of production of D(x) in this reaction scheme is

$$N^{-1}\dot{\mathrm{D}}(x,t) = k_{x+1}^{(\mathrm{H})}q(x+1)\mathrm{D}(x+1,t) - [(k_x^{(\mathrm{H})}q - k_x^{(\mathrm{D})}p)x + Npk_x^{(\mathrm{D})}]\mathrm{D}(x,t) + k_{x-1}^{(\mathrm{D})}(N-x+1)p\mathrm{D}(x-1,t) \quad (5.1)$$

Explicit, closed form solutions of (5.1) may be obtained by assuming particular functional relations among the rate constants, but the solution of (5.1) will be considered here only for the special case defined by the equations

$$k_1^{(\mathrm{H})} = k_2^{(\mathrm{H})} = \ldots k_N^{(\mathrm{H})} \equiv k_{\mathrm{H}} \quad (5.2)$$

$$k_0^{(\mathrm{D})} = k_1^{(\mathrm{D})} = \ldots k_{N-1}^{(\mathrm{D})} \equiv k_{\mathrm{D}} \quad (5.3)$$

These equations, (5.2) and (5.3), together with the constants k, P, and Q, defined by

$$k = pk_{\mathrm{D}} + qk_{\mathrm{H}} \quad (5.4)$$

$$P = pk_{\mathrm{D}}/k,\ Q = qk_{\mathrm{H}}/k \quad (5.5)$$

$$P + Q = 1 \quad (5.6)$$

(12) R. M. Lago and W. O. Haag, private communication.

transform (5.1) to the precise form of (2.1). Thus, all of the results established in the preceding sections are valid for the present case with k given by (5.4), and p,q replaced with P,Q. In particular, the equilibrium distribution is

$$D(x,\infty) = \binom{N}{x} P^x Q^{N-x} \tag{5.7}$$

The formal similarity between the present solution and that obtained above shows that one ought not be too hasty in concluding the absence of an isotope effect. The discrimination between the two cases requires experimental data of sufficient precision to distinguish the stoichiometric p and q, defined by the initial composition, from the kinetic P and Q, defined by (5.5).

It should also be observed that, in the present case, the transformation of experimental data into the uncoupled representation cannot be accomplished without knowledge of P or Q. To effect the transformation, P or Q must be obtained from the observed equilibrium distribution. The evaluation of k, then, provides two relations for the determinations of k_H and k_D.

6. Approximate and Asymptotic Solutions

There are two limiting cases of the binomial distribution that may be useful in special cases, namely, the Poisson and Gaussian distributions.[10]

When $N \gg 1$ and $p \ll 1$, but their product $\mu = Np$ is of the order of unity, the binomial distribution may be approximated by the Poisson distribution

$$w(x;\mu) = \frac{\mu^x e^{-\mu}}{x!} \tag{6.1}$$

Evidently, this approximation may be used for molecules containing a large number of chemically equivalent exchangeable hydrogen atoms, but the initial distribution includes comparatively few deuterated molecules. In this case, the Krawtchouk polynomials may be approximated by the Poisson–Charlier polynomials.[8]

When N, x, and $N - x$ all tend to infinity in such a way that $(x - Np)^3/N^2 \to 0$, the binomial distribution tends asymptotically to the Gaussian distribution

$$w(x) \simeq (2\pi Npq)^{-1/2} \exp[-(2Npq)^{-1}(x - Np)] \tag{6.2}$$

In this limit, the Krawtchouk polynomials are asymptotically equal to the Hermite polynomials

$$K_n(x) \simeq (2^n n!)^{-1} H_n[(2Npq)^{-1}(x - Np)] \tag{6.3}$$

The normal approximation (6.2) is remarkably good,[13] even for moderate values of N (≈ 10).

Acknowledgments. The author wishes to express his appreciation to Dr. R. J. Mikovsky for arousing his interest in isotope exchange reactions, and to Dr. W. O. Haag and Mr. R. M. Lago for permission to incorporate their data on the C_6H_6–C_6D_6 system.

(13) W. Feller, "Probability Theory and Its Applications," Vol. 1, Wiley, New York, N. Y., 1950, pp 110, 111, 133–136.

A Dielectric Study of the Dimerization of N-Methylaniline in Cyclohexane and Benzene[1]

by Herbert R. Ellison[2a] and Barbara W. Meyer[2b]

Department of Chemistry, Wheaton College, Norton, Massachusetts 02766 *(Received April 6, 1970)*

A dielectric method based upon Onsager's theory of the dielectric constants of dilute solutions of polar molecules in nonpolar solvents has been devised to determine simultaneously dipole moments and formation constants of weak hydrogen-bonded complexes. The dimerization of N-methylaniline (NMA) in cyclohexane and in benzene was chosen as a test because data obtained by infrared techniques are available for these systems. The dimerization constant for NMA in cyclohexane at 25° was found to be 0.424 l. mol^{-1}, very close to the ir value of 0.434 l. mol^{-1}. The dipole moments of NMA and dimer are 1.66 and 2.75 D, respectively. Our data and literature data for NMA in benzene at 25° yield a dipole moment of 1.80 D and a formation constant of 0.135 l. mol^{-1} (ir value is 0.14 l. mol^{-1}) for the complex formed by NMA and benzene. Suggestions about possible structures of the NMA dimer and NMA–benzene complex are discussed.

Introduction

Formation constants and thermodynamic data for H-bonded complexes of amines and amides have been obtained by a variety of procedures. A common technique involves measuring complex formation induced frequency shifts in infrared spectra[3-8] or proton magnetic resonance spectra.[9-11] Vapor–liquid equilibrium studies[12,13] have also been employed to obtain thermodynamic data and in some instances have been used along with dielectric measurements[14,15] to give the dipole moments of H-bonded complexes. Relatively few workers have attempted to use dielectric methods to obtain information about both the dipole moment of the complex and the extent of complex formation. Few and Smith[16] have developed a procedure based on measurement of the apparent change in the value of the molecular polarization at infinite dilution of a solute A when it is the only solute in a solution and when another solute B is also present in the solution. They and others have used this method to obtain results which agree reasonably well with data produced by ir and pmr techniques.[17,18] This procedure is limited, however, because it is applicable only to systems with relatively large formation constants.[19]

This paper presents another dielectric method which also yields dipole moments and values for formation constants but which is applicable to systems which have small formation constants. It is based on Onsager's theory of the dielectric constant of dilute solutions of polar molecules in nonpolar solvents.[20] The system of N-methylaniline and various ketones and ethers in cyclohexane was chosen to test this procedure since it has been extensively studied by ir and pmr techniques.[3,4] Results on the autoassociation of N-methylaniline in cyclohexane and benzene are presented in this paper; complex formation between N-methylaniline and various ketones will appear in a subsequent paper.

Experimental Section

Equipment and Materials. Dielectric constants were determined with the Kahl Scientific Instruments Corp. Model DM 01 Dipolmeter which operates on the superposition (beat) method at 2.0 MHz. A DFL-1 cell (range $\epsilon = 1.8$ to 3.4) with a capacity of 30 ml was used for all measurements. Temperature was controlled to ±0.05° by circulating water from a constant temperature bath through the cell jacket. Refractive indices were measured with an Abbe refractometer equipped with jacketed prisms.

(1) This research was supported in part by the National Science Foundation under Grants GY 4354 and GY 6007.

(2) (a) To whom correspondence should be addressed. (b) Participant, National Science Foundation Undergraduate Research Participation Program, Summers 1968 and 1969.

(3) J. H. Lady and K. B. Whetsel, *J. Phys. Chem.*, **71**, 1421 (1967).

(4) S. Nishimura and N. C. Li, *ibid.*, **72**, 2908 (1968).

(5) K. B. Whetsel and J. H. Lady, *ibid.*, **69**, 1596 (1965).

(6) J. H. Lady and K. B. Whetsel, *ibid.*, **68**, 1001 (1964).

(7) K. B. Whetsel and J. H. Lady, *ibid.*, **68**, 1010 (1964).

(8) I. Motoyama and C. H. Jarboe, *ibid.*, **71**, 2723 (1967).

(9) M. Nakano, N. I. Nakano, and T. Higuchi, *ibid.*, **71**, 3954 (1967).

(10) R. A. Murphy and J. C. Davis, Jr., *ibid.*, **72**, 3111 (1968).

(11) B. B. Howard, C. F. Jumper, and M. T. Emerson, *J. Mol. Spectrosc.*, **10**, 117 (1963); W. C. Meyer and J. T. K. Woo, *J. Phys. Chem.*, **73**, 2989 (1969); W. Lin and S. Tsay, *ibid.*, **74**, 1037 (1970).

(12) G. Pannetier and L. Abello, *Bull. Soc. Chim. Fr.*, 1645 (1966).

(13) R. L. Denyer, A. Gilchrist, J. A. Pegg, J. Smith, T. E. Tomlinson, and L. E. Sutton, *J. Chem. Soc.*, 3889 (1955).

(14) M. D. Gregory, H. E. Affsprung, and S. D. Christian, *J. Phys. Chem.*, **72**, 1748 (1968).

(15) J. R. Hulet, J. A. Pegg, and L. E. Sutton, *J. Chem. Soc.*, 3901 (1955).

(16) A. V. Few and J. W. Smith, *ibid.*, 2781 (1949).

(17) R. J. Bishop and L. E. Sutton, *ibid.*, 6100 (1964).

(18) A. H. Boud and J. W. Smith, *ibid.*, 4507 (1956); D. Cleverdon G. B. Collins, and J. W. Smith, *ibid.*, 4499 (1956).

(19) M. E. Bauer, D. A. Horsma, C. M. Knobler, and P. Perez, *J. Phys. Chem.*, **73**, 641 (1969).

(20) L. Onsager, *J. Amer. Chem. Soc.*, **58**, 1486 (1936).

Table I: Dielectric Constants of Calibrating Liquids

Substance	ϵ, 20°	Tolerance	$\Delta\epsilon/\Delta t$	Reference
Cyclohexane	2.0228	$\pm 2 \times 10^{-4}$	-1.6×10^{-3}	*a*
Carbon tetrachloride	2.2363	$\pm 1 \times 10^{-5}$	-2.0×10^{-3}	*b*
Benzene	2.2825	$\pm 2 \times 10^{-4}$	-1.96×10^{-3}	*b*

[a] K. Rosswog, dissertation, Freiburg, 1953. [b] R. Mecke and K. Rosswog, Z. *Elektrochem.*, **60**, 47 (1956).

The *N*-methylaniline (NMA) was purified by at least two fractional distillations under reduced pressure. Fresh samples of the cut boiling at 57–61° (4.5–5 mm, n^{25}D 1.5687) were used in preparation of solutions. Research grade cyclohexane and benzene (Fisher or Matheson Coleman and Bell) were employed as solvents and were used without further purification. Fisher Spectrograde cyclohexane, benzene, and carbon tetrachloride, whose purities were checked by vapor phase chromatography, were used for calibration of the Dipolmeter.

Sample Preparation and Measurement. Solutions of NMA in cyclohexane or in benzene were prepared by carefully weighing the NMA and the solvent into calibrated 100-ml volumetric flasks. Six to nine solutions, with NMA concentrations ranging between 0.07 and 0.9 *M*, were used in each run. All solutions were equilibrated for at least 24 hr at the temperature of the run.

Dielectric measurements of the NMA solutions were made after calibrating the instrument with the Spectrograde solvents whose dielectric constants as a function of temperature are listed in Table I. Once a series of measurements was started care was taken not to move the cell as this would introduce error. After the dielectric constant of each solution was measured, the cell was drained and dried with a stream of dry air. It was then thoroughly rinsed with the next sample and carefully filled in such a manner that no air bubbles became entrapped. It is estimated that errors in dielectric constants do not exceed ± 0.0005 ϵ unit.

Dimerization Constants. Infrared studies by Lady and Whetsel[3,7] have shown that in solutions of NMA in cyclohexane the only significant reaction is the formation of a dimer. The system can be described by the equation

$$A + A \rightleftharpoons D \qquad K_D = \frac{C_D}{C_A^2} \tag{1}$$

where K_D is the formation constant of the NMA dimer and C_A and C_D are the equilibrium molar concentrations of monomer and dimer, respectively. Letting C_A° represent the initial concentration of NMA allows us to write the mass balance equation as

$$C_A^\circ = C_A + 2C_D \tag{2}$$

Theoretical considerations by Onsager[20] and much experimental evidence[14,21] have shown that the dielectric constant, ϵ, of a solution containing a polar molecule in a nonpolar solvent is linearly dependent on the concentration of the solute, C_s.

$$\epsilon = \text{constant} + \alpha_s C_s \tag{3}$$

The proportionality constant α_s is defined by

$$\alpha_s = \frac{4\pi N_0 \times 10^{-3}}{27kT} (n_m^2 + 2)^2 \mu_s^2 \tag{4}$$

N_0 is Avogadro's number, k is the Boltzmann constant, n_m is the refractive index of the solvent, and μ_s is the dipole moment of the solute. The constant in eq 3 is a function of the squares of the refractive indices of both solvent and solute but can effectively be taken as the dielectric constant of the pure solvent, ϵ_0.

Making the assumption that eq 3 can be applied to solutions with more than one solute permits us to write the Onsager equation for our system

$$\epsilon = \epsilon_0 + \alpha_A C_A + \alpha_D C_D \tag{5}$$

where α_A and α_D are the Onsager constants for NMA and dimer, respectively. Substituting eq 2 into eq 5 gives

$$C_D = \frac{\epsilon - \epsilon_0 - \alpha_A C_A^\circ}{\alpha_D - 2\alpha_A} \tag{6}$$

If the values of α_A and α_D were known, then C_D could be readily evaluated and K_D might be obtained using eq 2 and 1. However, the two Onsager constants cannot be determined independently since it is impossible to have a solution of either pure monomer or pure dimer.

The procedure we have followed was to write a FORTRAN program for use on an IBM System 360 computer in which the values of α_A and α_D were Systematically varied and the value of K_D calculated for each solution in the run. The average K_D, the standard deviation of the dimerization constants, s_{K_D}, and the relative standard deviation, rel $s_{K_D} = s_{K_D}/\text{av } K_D$, were all computed. The set of α_A and α_D that produced the smallest rel s_{K_D} was then chosen as the correct one for these parameters. It was also found necessary to vary the value of ϵ_0 to minimize rel s_{K_D}.

This procedure however, did not work when applied to solutions of NMA in benzene. Whetsel and Lady[5] have shown that NMA also forms a weak complex with benzene as well as dimerizing. Thus an additional equilibrium must be considered in benzene solutions.

$$A + B \rightleftharpoons C \qquad K_C = \frac{C_C}{C_A C_B} \tag{7}$$

Here C_A, C_B, and C_C represent the equilibrium molar concentrations of NMA, benzene, and NMA–benzene

(21) Unpublished data of B. W. Meyer.

Table II: *N*-Methylaniline in Cyclohexane at 25°

Wt NMA	Wt cyclohexane	ϵ	$C_A°$, M	Equil concn		K_D, l. mol^{-1}
				C_A, M	C_D, M	
1.0825	76.4071	2.0472	0.1010	0.0936	0.0037	0.424
2.1601	75.6028	2.0799	0.2016	0.1752	0.0132	0.430
3.2585	74.6140	2.1142	0.3041	0.2477	0.0282	0.460
4.3898	73.8416	2.1493	0.4097	0.3248	0.0424	0.402
5.4558	73.0664	2.1835	0.5092	0.3851	0.0620	0.418
6.5696	72.2053	2.2192	0.6131	0.4484	0.0824	0.410
7.6980	71.2122	2.2564	0.7185	0.5012	0.1086	0.433
8.7655	70.3670	2.2917	0.8181	0.5499	0.1341	0.444
9.8862	69.6476	2.3280	0.9227	0.6094	0.1566	0.422

All volumes = 100.0 ml
$\epsilon_0 = 2.0154$, $\alpha_A = 0.3081\ M^{-1}$, $\alpha_D = 0.797\ M^{-1}$
Av $K_D = 0.428\ M^{-1}$, $s_{K_D} = 0.0175$, rel $s_{K_D} = 0.0408$

complex, respectively. The equation for mass balance of NMA now becomes

$$C_A° = C_A + C_C + 2C_D \quad (8)$$

and the Onsager equation can be written as

$$\epsilon = \epsilon_0 + \alpha_A C_A + \alpha_C C_C + \alpha_D C_D \quad (9)$$

Using eq 1, 7, and 8 and noting that the concentration of benzene remains essentially constant so that C_B can be replaced by $C_B°$, the initial concentration of benzene, allows eq 9 to be rewritten as

$$K_D(\alpha_D - 2\alpha_C)C_A^2 + (\alpha_A - \alpha_C)C_A - (\epsilon - \epsilon_0 - \alpha_C C_A°) = 0 \quad (10)$$

Equation 10 may be solved for C_A only if the values of K_D, α_A, α_C, and α_D are known. The procedure we have followed was to assume that K_D remained the same in benzene as in cyclohexane and that the dipole moments of NMA and the dimer also remained the same in the two solvents. The weakest of these assumptions is the supposition that K_D is the same in both solvents even though there is a substantial difference in their solvating abilities. Then α_A and α_D were calculated using eq 4 with experimental values of the index of refraction of benzene. A computer program was written to vary the value of α_C and solve eq 10 for C_A for each solution in a run. Equations 1, 8, and 7 were employed to evaluate each K_C, the average K_C, and the relative standard deviation of K_C for every value of α_C. Once again it became necessary to vary ϵ_0 to minimize rel s_{K_C}.

Results

Table II presents data from a representative run of NMA in cyclohexane. A plot of the observed dielectric constant *vs.* the initial concentration of NMA appears linear, but calculation of the slopes ($\Delta\epsilon/\Delta C_A°$) between each pair of points reveals that the line curves upward. This is in contrast with data from solutes that do not undergo reaction and which do produce straight lines.[14,21] The plot of ϵ *vs.* $C_A°$ was useful however, for the intercept at zero $C_A°$ was used as the initial choice for ϵ_0 in the computer program which handled these data. This value was usually slightly higher than ϵ for the pure solvent since the usual methods of handling exposed the solutions to air longer than the solvent and so more water vapor may have been absorbed by the solutions than by the solvent.[22]

Figure 1 illustrates the behavior of the relative stan-

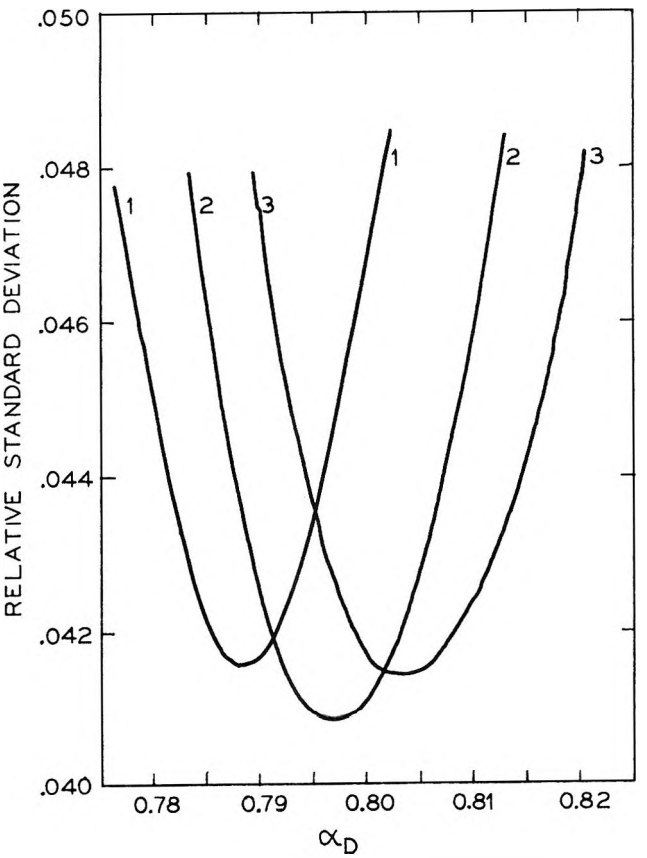

Figure 1. Relative standard deviation of the dimerization constant *vs.* α_D at constant α_A: 1, α_A = 0.3076 l. mol^{-1}; 2, α_A = 0.3081 l. mol^{-1}; 3, α_A = 0.0384 l. mol^{-1}.

(22) See I. F. Halverstadt and W. D. Kumler, *J. Amer. Chem. Soc.*, 64, 2988 (1942), for a more complete discussion of this point.

Table III: *N*-Methylaniline in Cyclohexane

Run no.	Temp, °C	No. of solns	ϵ_0	α_A, l. mol^{-1}	α_D, l. mol^{-1}	Av K_D, l. mol^{-1}	Rel s_{K_D}
9	20	9	2.0265	0.3006	0.827	0.514	0.0413
10	20	7	2.0264	0.2985	0.856	0.443	0.0200
1	25	9	2.0154	0.3081	0.797	0.428	0.0408
2	25	7	2.0165	0.3003	0.856	0.321	0.0307
3	25	7	2.0168	0.3015	0.830	0.403	0.0331
4	25	7	2.0166	0.2986	0.813	0.505	0.0334
5	25	6	2.0160	0.3039	0.859	0.319	0.0145
6	25	6	2.0164	0.2997	0.802	0.519	0.0024
7	25	7	2.0166	0.3004	0.848	0.389	0.0455
8	25	6	2.0155	0.3089	0.796	0.491	0.0314
11	30	7	2.0096	0.2980	0.822	0.380	0.0445
12	30	7	2.0095	0.2980	0.814	0.405	0.0383

dard deviation of the dimerization constants under various choices of α_A and α_D. The values of these parameters which produced the smallest rel s_{K_D} were then used to evaluate the equilibrium concentrations of NMA and dimer and finally, the dimerization constant K_D. Values of C_A, C_D, and K_D calculated in this fashion are also presented in Table II. Results with all of the sets of NMA solutions in cyclohexane are presented in Table III. A summary of these data along with resulting thermodynamic quantities is presented in Table IV.

Table IV: Summary of NMA–Cyclohexane Results

Temp, °C	ϵ_0	α_A, l. mol^{-1}	α_D, l. mol^{-1}	K_D, l. mol^{-1}	K_D, ref 3[a]
20	2.0264	0.2996	0.842	0.478	0.464
25	2.0162	0.3027	0.825	0.422	0.434
30	2.0095	0.2980	0.818	0.392	0.407

	This work	Reference 3
$\Delta H°_{298}$ (kcal mol^{-1})	−3.56	−2.45
$\Delta G°_{298}$ (kcal mol^{-1})	+0.51	+0.50
$\Delta S°_{298}$ (cal mol^{-1} °K^{-1})	−13.6	−9.9

[a] Pannetier and Abello[12] using a vapor–liquid equilibrium method found $K_D = 0.18 \pm 0.01$ l. mol^{-1} at 25° in carbon tetrachloride.

As mentioned previously, the solutions of NMA in benzene were treated by making the assumption that the values of the dipole moments of NMA and dimer were the same in benzene as in cyclohexane. It then becomes possible to calculate α_A and α_D in the benzene solutions using the results from the cyclohexane solutions. This is done by rewriting eq 4 as

$$\alpha_s = \alpha' \mu_s^2 \tag{11}$$

where

$$\alpha' = \frac{4\pi N_0 \times 10^{-3}}{27kT} (n_m^2 + 2)^2 \tag{12}$$

α' is thus seen to be a parameter which is a function of the temperature and the refractive index of the solvent and is independent of the solute. Experimental indices of refraction and calculated values of α' are shown in Table V. Using these data the values of α_A and α_D in benzene at 25° are calculated as 0.3365 and 0.917 l. mol^{-1}, respectively. Results with three sets of NMA solutions in benzene are given in Table VI. Also included in this table are results obtained by applying this method of calculation and the same values of K_D, α_A, and α_D to data obtained by Few and Smith,[23] Barclay, LeFèvre, and Smythe,[24] and Cumper and Singleton.[25]

Table V: Refractive Indices and Calculated α' Values

Solvent	Temp, °C	n_m	α'
Cyclohexane	20	1.4259	0.1126
Cyclohexane	25	1.4233	0.1104
Cyclohexane	30	1.4207	0.1081
Benzene	25	1.4979	0.1226

Discussion

The method of calculation employed with the systems of *N*-methylaniline in cyclohexane and benzene depends on selection of the Onsager constants that best fit the data. Initially the standard deviation of the dimerization constants (actually the "estimated" standard deviation, *s*) was used in an attempt to decide which set of α values would be most suitable for a set of solutions. In the case of NMA in cyclohexane it was quickly found, however, that the standard deviation steadily decreased as α_D was increased at constant α_A.

(23) A. V. Few and J. W. Smith, *J. Chem. Soc.*, 753 (1949).

(24) G. A. Barclay, R. J. W. LeFèvre, and B. M. Smythe, *Trans. Faraday Soc.*, **47**, 357 (1951).

(25) C. W. N. Cumper and A. Singleton, *J. Chem. Soc.*, Sect. C. 1096 (1967).

FIRST CLASS
PERMIT No. 1411-R
WASHINGTON, D. C.

BUSINESS REPLY MAIL
No Postage Stamp Necessary if Mailed in the United States

— POSTAGE WILL BE PAID BY —

AMERICAN CHEMICAL SOCIETY
1155 Sixteenth Street, N.W.
Washington, D.C. 20036

ATTN. H. C. SPENCER

Table VI: *N*-Methylaniline in Benzene at 25°[a]

Source	No. of solns	ϵ_0	α_C, l. mol^{-1}	Av K_C,[b] l. mol^{-1}	Rel s_{K_C}
This work	7	2.2738	0.4004	0.158	0.0526
This work	8	2.2727	0.3980	0.147	0.0413
This work	6	2.2736	0.3993	0.127	0.0602
Reference 23	8	2.2725	0.3963	0.113	0.0414
Reference 24	9	2.2725	0.3947	0.128	0.0303
Reference 25	6	2.2741	0.3953	0.135	0.0497
Average		2.2732	0.3973 ± 0.0023[c]	0.135 ± 0.016[c]	0.0459

[a] Assumed that K_D = 0.422 l. mol^{-1}, α_A = 0.3363 l. mol^{-1} and α_D = 0.917 l. mol^{-1}. [b] Whetsel and Lady[5] have found K_C = 0.14 l. mol^{-1} at 25° using ir spectroscopy. [c] Estimated standard deviation.

The reason for this is that K_D is very sensitive to α_D, as examination of eq 6 and 1 reveals, and so increasing α_D leads to a decrease in K_D. On the other hand, when the relative standard deviation was computed, it was found that this parameter passed through a distinct minimum as α_D was increased at constant α_A (see Figure 1) or if α_A was increased at constant α_D. Similar behavior of rel s_{K_C} was found in the case of the NMA solutions in benzene; increasing α_C produced a minimum in the relative standard deviations of the formation constants.

The validity of this method of evaluating formation constants of weak complexes by using the Onsager equation with dielectric data appears to be confirmed by the agreement of our calculated results with those found by Lady and Whetsel using an infrared procedure (see Table IV). Also presented in this table are data produced by Pannetier and Abello,[12] who carried out a vapor–liquid equilibrium study using carbon tetrachloride as the solvent. Both our results and those of Lady and Whetsel differ by approximately a factor of 2 from their value of K_D. Whether the reason for this lies in their theory or in their data is not clear. On the other hand, the differences in our dimerization constants from those of Lady and Whetsel appear to be due entirely to experimental errors. We estimate that the uncertainty in our dielectric constants is approximately ±0.0005 ϵ unit, or about ±0.02%. Calculations have shown that varying ϵ_0 by this amount from the optimum value selected by the computer leads to changes in K_D by as much as 25–30% and increases in rel s_{K_D} of about 20–25%. Errors in dielectric constants of individual solutions were reflected in the observation that in some instances rel s_{K_D} remained rather large, no matter what choice of ϵ_0, α_A, or α_D was made. Close examination of a plot of $C_A°$ *vs.* ϵ then usually revealed that one or more solutions deviated by more than 0.0010 ϵ unit from the curve. Discarding these solutions always resulted in lower rel s_{K_D}. Our estimate is that our values of K_D are probably accurate within ±15–20%.

The system of NMA in benzene offered a somewhat more rigorous test of this procedure in that here there are two competing equilibria. The results shown in Table VI represent application of this method to three sets of data produced by us and to three sets of data found in the literature.[23–25] The agreement in both the values of α_C and K_C among these various sets is remarkably good considering the different instrumentation used to produce the data. Furthermore, the average value for the formation constant, 0.135 l. mol^{-1}, is essentially the same as the value found by Lady and Whetsel[5] using infrared spectroscopy. The conformity of these formation constants then appears to justify our assumption that the dipole moments of monomeric and dimeric NMA do not change in going from cyclohexane to benzene. This can be shown quite readily upon calculation of the effects of changing either α_A or α_D. For example, a 10% decrease in α_D results in only a slight change in α_C but a 45% decrease in K_C. Our assumption that K_D is the same in both solvents is not verified as clearly, for a 10% decrease in K_D produces only an 8% decrease in K_C.

One advantage of our method of evaluating formation constants and dipole moments of H-bonded complexes is that it does not require extrapolation of either dielectric constants or densities to infinite dilution. The procedure developed by Few and Smith[16] is based on determination of the change in the molecular polarization at infinite dilution, P, of a solute A when it is the only solute in a solution and when another solute B is present in the solution. As Bauer, *et al.*,[19] have pointed out, the value of P varies linearly with mole fraction when the solute is a stable polar molecule, but when an equilibrium involving that solute is present P varies in a nonlinear fashion with mole fraction. Thus to reduce errors it becomes necessary to work with very dilute solutions to obtain reasonably accurate values of P at infinite dilution. This in turn requires that formation constants of complexes be fairly large so that significant changes in P might be observed. An additional factor which reinforces the need to work with dilute solutions is that most extrapolation procedures, and in particular the forms based on Hedestrand's

method,[26] require extrapolation of both the dielectric constant and the density to infinite dilution. Both of these parameters vary in a nonlinear fashion with mole fraction when the solution contains an equilibrium system, thus increasing the problem of obtaining accurate results for slopes and intercepts. These limitations on accuracy thus appear to limit Few and Smith's procedure to those systems in which the change in P is relatively large as a result of equilibrium constants of about 10–100 or larger.

The dipole moments found in this investigation are summarized in Table VII. The only one that has been

Table VII: Dipole Moments Obtained from α Values

Solution	Temp, °C	μ_{NMA}, D	μ_{dimer}, D	$\mu_{complex}$, D
NMA–cyclohexane	20	1.63	2.73	...
NMA–cyclohexane	25	1.66	2.75	...
NMA–cyclohexane	30	1.66	2.75	...
NMA–benzene	25	1.66[a]	2.75[a]	1.80

[a] Values taken from NMA–cyclohexane results and used in evaluation of NMA–benzene data.

determined previously is that for NMA; our result of 1.66 D at 25° compares favorably with the value of 1.67 D recommended by McClellan,[27] offering further proof of the validity of this procedure. Table VIII contains the results of applying the Hedestrand method[26] of calculating dipole moments to all of our data and the results obtained by three other investigators using similar extrapolation procedures. The slightly larger moments found in benzene solutions offers further evidence that NMA is reacting with this solvent.

The dipole moments of the dimer and the NMA–benzene complex can be used to make suggestions about the possible structures of these complexes. On the basis of a study of the dipole moments of various substituted aniline compounds in benzene solution Smith[28] concluded that the angle at which the resultant dipole moment in NMA is inclined to the N–C bond is 38.5°, as shown in Figure 2. For this calculation Smith assumed that the four groups attached to the nitrogen (E represents the lone pair of electrons) are all at angles of 109° to each other. Data from various methylamines suggest that this is reasonable within ±3°.[29] Dipole moments for different configurations of the NMA dimer were calculated using Smith's angles and our value of 1.66 D for the dipole moment of NMA. The structure that produces a dipole moment closest to the experimental value of 2.75 D is shown in Figure 3. In this configuration θ, the angle between the two phenyl groups as seen by looking down the N···H–N axis in Figure 3a, is 67° and the calculated moment is 2.74 D. If, instead of using 109° as the angle at which groups are attached to the nitrogen, we use a Ph–N–H angle

Table VIII: Dipole Moments of N-Methylaniline Obtained with the Hedestrand Procedure

Run no.	ϵ_0	P_2°, cm³	P_{2D}°, cm³	$P_{2\mu}^\circ$, cm³	μ, D
		Cyclohexane at 20°[a]			
9	2.0199	91.68	35.67	56.01	1.642
10	2.0184	92.25	35.67	56.58	1.650
		Cyclohexane at 25°[b]			
1	2.0107	91.88	35.71	56.17	1.656
2	2.0111	91.11	35.71	55.40	1.647
3	2.0084	91.63	35.71	55.92	1.654
4	2.0115	90.27	35.71	54.56	1.634
5	2.0100	90.65	35.71	54.94	1.640
6	2.0100	92.70	35.71	56.99	1.668
7	2.0091	92.82	35.71	57.11	1.670
8	2.0081	92.50	35.71	56.79	1.666
		Cyclohexane at 30°[c]			
11	2.0009	90.32	35.75	55.47	1.648
12	2.0047	94.19	35.75	58.44	1.705
		Benzene at 25°[b]			
13	2.2738	94.21	35.71	58.50	1.691
14	2.2726	94.11	35.71	58.40	1.689
15	2.2731	94.10	35.71	58.39	1.689
		Benzene at 25°			
Reference 23	2.2725	93.20	35.81	55.20	1.643
Reference 24	2.2725	93.13	35.68	57.45	1.67
Reference 25	2.2741	...	36.30	57.70	1.68

[a] Used $n^{20}D$ 1.5708 and d^{20} 0.9867 g ml^{-1} for NMA. [b] Used $n^{25}D$ 1.5687 and d^{25} 0.9826 g ml^{-1} for NMA. [c] Used $n^{30}D$ 1.5667 and d^{30} 0.9787 g ml^{-1} for NMA.

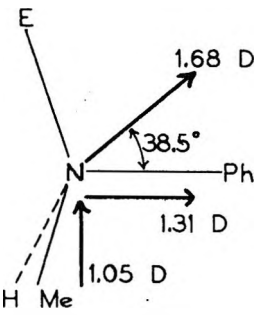

Figure 2. Moments in N-methylaniline; after Smith.[28]

of 107° and a Ph–N–E angle of 112° (suggested from data in ref 29), we calculate that θ has a value of 58° to give a calculated dipole moment of 2.75 D for the dimer. In either case the calculations are insensitive to the

(26) G. Hedestrand, *Z. Phys. Chem.*, B2, 428 (1929).

(27) A. L. McClellan, "Tables of Experimental Dipole Moments," W. H. Freeman and Co., San Francisco, Calif., 1963, p 259. This value was recommended by McClellan after he had used the procedure outlined on p 581 to recalculate the data reported in six other papers.

(28) J. W. Smith, *J. Chem. Soc.*, 81 (1961).

(29) "Handbook of Chemistry and Physics," 50th ed, Chemical Rubber Co., Cleveland, Ohio, 1969, p F 157.

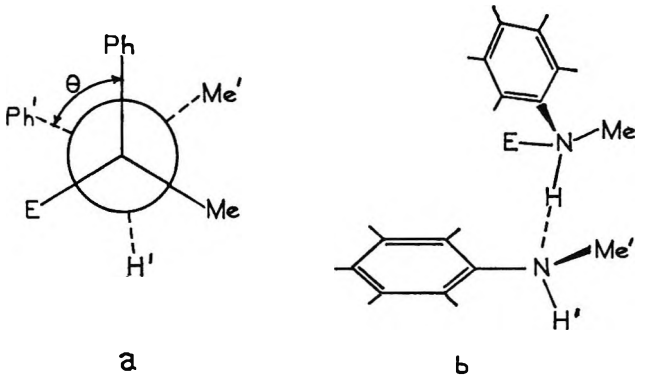

Figure 3. Structure of the NMA dimer.

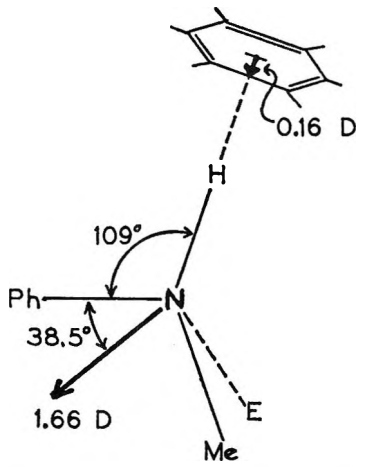

Figure 4. Structure of the NMA–benzene complex.

value of the angle at which the dipole moment is inclined to the N–C bond in monomeric NMA; this will not be so, however, when NMA forms a complex with benzene or other substances.

It should be noted, however, that a structure such as that shown in Figure 3 can only be viewed as an approximation. The calculations assume that the moment of the NMA moieties remains the same in the dimer as in the monomer, but there is no apparent way of being certain of this. Several workers[14,30] have recently pointed out that the interaction of two species causes a polarization which changes both dipole moments by an unknown amount, so that the moments of the two molecules in the complex are unknown. Although there does not appear to be any way to determine the amount of "enhancement" due to such an interaction, it is possible to calculate the change in the geometry of the dimer if such an induced dipole effect were present. If the measured dipole moment included an enhancement of 0.1 D, then θ in Figure 3 would be 73°, a difference of 6° from the situation with no enhancement. An enhancement of 0.2 D results in a θ of 78°, an increase of 11°. Thus Figure 3 offers a reasonably accurate view of the dimer's structure only if we assume that there is little or no enhancement of the dipole moments of two NMA monomers as they come together to form the dimer.

Interpretation of the observed dipole moment of 1.80 D for the NMA–benzene complex must rely heavily on this concept of enhancement of moments due to polarization. Assuming that the moment of NMA remains unchanged we calculate that a moment of 0.16 D is induced in the benzene molecule and that it is directed towards the H–N axis. This calculation furthermore assumes that the proton approaches the center of the benzene ring (see Figure 4) and interacts with the full sextet of π electrons. This configuration can also be used to explain the small formation constant for this complex. If the proton approaches other parts of the benzene ring, it can only interact with a small fraction of the π-electron density and so no bond is formed. Thus the small formation constant of the complex is reflected in the low probability of approaching the center of the ring.

The Onsager equation for the dielectric constant of a solution has been used previously with equilibrium constants determined by other methods to give dipole moments of complexes.[14,30,31] The results presented here clearly indicate that the Onsager equation can also be used to determine formation constants as well as dipole moments of weak hydrogen-bonded complexes. The two equilibrium constants obtained in this investigation agree reasonably well with those obtained by infrared spectroscopy, and the dipole moment of NMA is also in agreement with values obtained using different evaluation procedures. The mathematical formulation of the method is relatively simple; however, the calculations do require the use of a computer because of the many computations involved. A subsequent paper will deal with the application of this procedure to cyclohexane solutions of NMA and various ketones and ethers.

(30) C. F. Jumper and B. B. Howard, *J. Phys. Chem.*, **70**, 588 (1966).

(31) T. F. Lin, S. D. Christian, and H. E. Affsprung, *ibid.*, **71**, 1133 (1967).

Polarization Spectra in Stretched Polymer Sheets. II.[1] Separation of $\pi-\pi^*$ Absorption of Symmetrical Molecules into Components

by E. W. Thulstrup, J. Michl, and J. H. Eggers

Department of Chemistry, Aarhus University, Aarhus, Denmark *(Received November 13, 1969)*

A detailed description is presented of a simple method for quantitative evaluation of dichroic absorption spectra due to $\pi-\pi^*$ transitions in planar molecules belonging to point symmetry groups in which x, y, z each transforms according to a different irreducible representation, such as C_{2v} or D_{2h}. Importance of the resulting information for further development of spectral theories for π-electron systems is pointed out. In the way of examples, the long-axis and short-axis polarized components in regions of strong absorption of phenanthrene, pyrene, perylene, and benzoperylene are derived and compared with data obtained by other methods and with results of calculations.

Introduction

Quantum mechanical methods for large conjugated molecules have made tremendous advances in the last 20 years from the first attempts to explain the main observed bands in aromatic hydrocarbons by the perimeter model[2] to the present variety of modifications of the Pariser–Parr–Pople (PPP) and other models (for leading references, see ref 3–8). Unfortunately, studies of $\pi-\pi^*$ excited states in aromatic molecules seldom go beyond a rough comparison of the calculated transition energies and oscillator strengths with the shape of the absorption curve in solution, or with sometimes randomly chosen peaks in the spectrum. This was perhaps satisfactory in the past, but now the calculations have reached a level such that any further improvement requires checking against more complete experimental data. Accurate analyses of vapor phase spectra[9] are at present rarely possible for large conjugated molecules, and then usually for a limited number of states. Thus, other techniques for band assignments, detection of hidden weak transitions, and distinguishing between vibrational fine structure and distinct electronic transitions are needed. Some that have been used are the study of minor perturbations of the chromophore (such as solvent, temperature, pressure, and substituent shifts[10,11]), which usually shift band origins measurably and have less effect on the vibrational fine structure, electron-impact spectroscopy,[12] fluorescence lifetime studies,[13] and investigations of the mirror-image relationship between absorption and emission.[14] Particularly powerful are methods using polarized light,[15,16] which also provide information on transition moment directions and the vibronic fine structure. They require an at least partially oriented assembly of molecules, produced using, *e.g.*, pure or mixed crystals,[16,17] strong electric fields,[16,18] solutions in nematic liquid crystals[19] and in stretched polymers,[15,16] or the principle of photoselection[15,16,20,21] (magnetophotoselection[22]). Each of these methods has some limitations, such as providing only relative transition moment directions or requiring elaborate instrumentation. Moreover, as pointed out by Albrecht,[20] it is customary to extract much less information from the data obtained than is actually possible. For example, only a change of some

(1) Part I: E. W. Thulstrup and J. H. Eggers, *Chem. Phys. Lett.*, **1**, 690 (1968).

(2) J. R. Platt, *J. Chem. Phys.*, **17**, 484 (1949).

(3) R. G. Parr, "Quantum Theory of Molecular Electronic Structure," W. A. Benjamin, New York, N. Y., 1963; K. Jug, *Theoret. Chim. Acta*, **14**, 91 (1969); H. Yamaguchi, T. Nakajima, and T. L. Kunii, *ibid.*, **12**, 349 (1968); K. D. Warren and J. R. Yandle, *ibid.*, **12**, 279 (1968); G. Leroy and S. Jaspers, *J. Chim. Phys.*, **64**, 455 (1967); A. Julg and P. Francois, *Theoret. Chim. Acta*, **8**, 249 (1967); N. L. Allinger, J. C. Tai, and T. W. Stuart, *ibid.*, **8**, 101 (1967); E. Heilbronner and J. N. Murrell, *Mol. Phys.*, **6**, 1 (1963); B. Roos and P. N. Skancke, *Acta Chem. Scand.*, **21**, 233 (1967); H. D. Försterling and H. Kuhn, *Int. J. Quant. Chem.*, **2**, 413 (1968).

(4) R. L. Hummel and K. Ruedenberg, *J. Phys. Chem.*, **66**, 2334 (1962).

(5) J. E. Bloor, B. R. Gilson, and N. Brearley, *Theoret. Chim. Acta*, **8**, 35 (1967).

(6) K. Nishimoto and L. S. Forster, *ibid.*, **3**, 407 (1965).

(7) E. Weltin, J. P. Weber, and E. Heilbronner, *ibid.*, **2**, 114 (1964).

(8) P. N. Skancke, *Acta Chem. Scand.*, **19**, 401 (1965).

(9) G. Herzberg, "Molecular Spectra and Molecular Structure, III. Electronic Spectra and Electronic Structure of Polyatomic Molecules," D. Van Nostrand Co., Inc., Princeton, N. J., 1966; for recent examples see K. K. Innes, H. D. McSwiney, Jr., J. D. Simmons, and S. G. Tilford, *J. Mol. Spectrosc.*, **31**, 76 (1969); A. Mani and J. R. Lombardi, *ibid.*, **31**, 308 (1969); K.-T. Huang and J. R. Lombardi, *J. Chem. Phys.*, **51**, 1228 (1969); J. M. Hollas and R. A. Wright, *Spectrochim. Acta*, **25A**, 1211 (1969).

(10) R. S. Becker, I. S. Singh, and E. A. Jackson, *J. Chem. Phys.*, **38**, 2144 (1963).

(11) W. W. Robertson, O. E. Weigang, Jr., and F. A. Matsen, *J. Mol. Spectrosc.*, **1**, 1 (1957); W. W. Robertson and A. D. King, Jr., *J. Chem. Phys.*, **34**, 2190 (1961); E. Clar, *Spectrochim. Acta*, **4**, 116 (1950); O. E. Weigang, Jr., *J. Chem. Phys.*, **33**, 892 (1960); O. E. Weigang, Jr., and D. D. Wild, *ibid.*, **37**, 1180 (1962).

(12) E. N. Lassettre, A. Skerbele, M. A. Dillon, K. J. Ross, *ibid.*, **48**, 5066 (1968); R. S. Berry, *Ann. Rev. Phys. Chem.*, **20**, 357 (1969).

(13) I. B. Berlman, H. O. Wirth, and O. J. Steingraber, *J. Amer. Chem. Soc.*, **90**, 566 (1968); E. Vander Donckt, J. Nasielski, J. R. Greenleaf, and J. B. Birks, *Chem. Phys. Lett.*, **2**, 409 (1968).

(14) H. Baba and S. Suzuki, *Bull. Chem. Soc. Jap.*, **35**, 683 (1962); S. Suzuki and H. Baba, *ibid.*, **37**, 519 (1964).

dichroism-dependent parameter with light frequency is reported. Hidden weak bands then easily escape detection and most of the information on vibronic fine structure is lost. It seems crucial to obtain the separate ("reduced") absorption curves for transitions along the individual principal axes in symmetrical molecules. Among the above methods, measurements of dichroism of solid solutions in stretched polymer sheets attracted our attention because of their simplicity and wide applicability. At present, the method is not considered absolute, since too little is known about the relations between molecular shape and orientation. In special cases, absolute orientations can be determined from simultaneous investigation of dichroism in the infrared region.[23,24] Such observations and also comparison with results of absolute methods have led to general agreement that in the absence of special interactions solute molecules are likely to prefer the orientation in which their longest dimension is parallel to the stretching direction.[16,24,25]

Most of the pioneering work[26] was done on dyestuffs of rather complicated structures. In 1957–1959, Tanizaki, *et al.*, developed the first model for quantitative evaluation[27,28] assuming a specific orientation distribution as a function of the degree of stretching. The orientation was described by one angle only and the method is thus applicable only to rod-shaped molecules. Indeed, some of the reported "reduced" absorption curves show disturbing features, such as strongly mixed polarization also for the 0–0 component of the transition into the lowest ("L_b") excited state of 2,3-dihydroxynaphthalene.[28] Very recently, a different method based on a simplified model for orientation was described in a preliminary communication.[29] It seems subject to similar limitations as the model of Tanizaki. In 1965–1968, two of us[1,30] reported a simple method for determination of the reduced curves for molecules of C_{2v} or D_{2h} symmetry, which avoids assumptions about the molecular orientation distribution function or the shape of the molecule (rod-like or otherwise), and is experimentally easy, since no measurement of the degree of stretching is needed. In the present paper the procedure is described in detail and illustrated on examples. In the immediately following paper, formulas are derived for the determination of transition moment directions in molecules of lower symmetry. Following papers shall present applications of our method to numerous aromatic molecules.

Experimental Section

A polarizer and a spectrophotometer are the only equipment really needed for the method. We have done successful experiments using polyethylene from sandwich bags stretched by hand. To obtain more reproducible results, we use a simple device (Figure 1) which allows *ca.* 600% stretching of commercial polyethylene sheet clamped between brass bars lined with Teflon spacers. This sheet-holder fits into an adapted sample compartment of the Cary 14 recording spectrophotometer in two possible positions, with stretching direction vertical or horizontal. In either case, the sheets are perpendicular to the light beam. The sample compartment also contains a calcite Glan prism in both the sample and the reference beams. They transmit plane polarized light with the electric vector vertical. Sheets can be easily removed undamaged from the sheet-holder after the sliding rod is moved back a little.

Before use, the sheets are thoroughly extracted with chloroform and air-dried. They are subsequently saturated with the compound to be measured by dipping into its fairly concentrated solution in chloroform. Another possibility, which requires much less material but leads to less uniform distribution, is smearing mounted sheets with a piece of cotton wool soaked in a chloroform solution of the compound. Before measurements, the sheets are thoroughly washed with methanol to remove crystals from the surface.

(15) F. Dörr and M. Held, *Angew. Chem.*, **72**, 287 (1960).

(16) F. Dörr, *ibid.*, **78**, 457 (1966).

(17) For reviews see D. S. McClure, *Solid State Phys.*, **8**, 1 (1959); H. C. Wolf, *ibid.*, **9**, 1 (1959); D. P. Craig and S. H. Walmsley, "Physics and Chemistry of the Organic Solid State," D. Fox, M. M. Labes, and A. Weissberger, Ed., Vol. I, Interscience Publishers, New York, N. Y., 1963, Chapter 10; A. S. Davydov, *Sov. Phys.-Usp.* (English transl.), **7**, 145 (1964); B. G. Anex, *Mol. Cryst.*, **1**, 1 (1966). For a recent example, see A. Bree, C. Y. Fan, and R. A. Kydd, *Spectrochim. Acta*, **25A**, 1375 (1969), who confirm the low-energy transition in acenaphthylene to be long-axis polarized as deduced from our measurements by the stretched-sheet method.[30]

(18) For reviews, see W. Liptay in "Modern Quantum Chemistry," O. Sinanoglu, Ed., Part III, Academic Press, New York, N. Y., 1965, p 45; H. Labhart, *Advan. Chem. Phys.*, **13**, 179 (1967); W. Liptay, *Angew. Chem.*, **81**, 195 (1969).

(19) E. Sackmann, *J. Amer. Chem. Soc.*, **90**, 3569 (1968); *Chem. Phys. Lett.*, **3**, 253 (1969); E. Sackmann and P. Krebs, *ibid.*, **4**, 65 (1969); G. P. Ceasar and H. B. Gray, *J. Amer. Chem. Soc.*, **91**, 191 (1969).

(20) A. C. Albrecht, *J. Mol. Spectrosc.*, **6**, 84 (1961).

(21) For theory, see P. P. Feofilov, "The Physical Basis of Polarized Emission," Consultants Bureau, New York, N. Y., 1961; W. Liptay in "Modern Quantum Chemistry," O. Sinanoglu, Ed., Part III, Academic Press, New York, N. Y., 1965, p 81; Y.-N. Chiu, *J. Chem. Phys.*, **48**, 5702 (1968); for a recent elaborate application, see P. M. Johnson and A. C. Albrecht, *ibid.*, **48**, 851 (1968).

(22) For references see G. P. Rabold and J. M. Gaidis, *J. Phys. Chem.*, **74**, 227 (1970).

(23) J. Kern, *Z. Naturforsch.*, **17a**, 271 (1962).

(24) H. Jakobi, A. Novak, and H. Kuhn, *Z. Elektrochem.*, **66**, 863 (1962), and references therein.

(25) G. Scheibe, J. Kern, and F. Dörr, *ibid.*, **63**, 117 (1959).

(26) H. Ambronn, *Ann. Phys.*, **34**, 340 (1888); A. Jablonski, *Acta Phys. Polonica*, **4**, 371 (1935); P. Pringsheim, *ibid.*, **4**, 331 (1935).

(27) Y. Tanizaki and N. Ando, *J. Chem. Soc. Japan, Pure Chem. Sec.*, **78**, 542 (1957); Y. Tanizaki, *Bull. Chem. Soc. Jap.*, **32**, 75 (1959); Y. Tanizaki, T. Kobayashi, and N. Ando, *ibid.*, **32**, 1362 (1959); Y. Tanizaki, *ibid.*, **33**, 979 (1960); Y. Tanizaki and H. Ono, *ibid.*, **33**, 1207 (1960); Y. Tanizaki, *ibid.*, **38**, 1798 (1965); Y. Tanizaki, H. Inoué and N. Ando, *J. Mol. Spectrosc.*, **17**, 156 (1965).

(28) Y. Tanizaki and S.-I. Kubodera, *ibid.*, **24**, 1 (1967).

(29) A. Yogev, L. Margulies, D. Amar, and Y. Mazur, *J. Amer. Chem. Soc.*, **91**, 4558 (1969); A. Yogev, J. Ribold, J. Marero, and Y. Mazur, *ibid.*, **91**, 4559 (1969).

(30) J. H. Eggers, E. W. Thulstrup, and collaborators, Lectures at the 8th European Congress on Molecular Spectroscopy, Copenhagen, 1965.

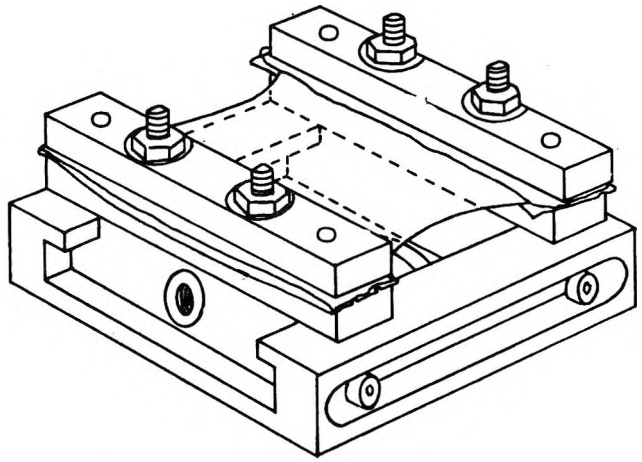

Figure 1. Holder with a stretched sheet.

Absorption of the set of stretched sheets is recorded both for the electric vector parallel ($E_{||}^{B}$) and perpendicular ($E_{\perp}^{B}$) to the stretching direction. The solute is then washed out with chloroform and the base lines are recorded for both orientations, yielding $B_{||}$ and $B_{\perp}$, respectively. This procedure involves more work but gives more reproducible results than recording the base line before the compound is applied. Figure 2 gives an example of such results. The dichroic curves obtained after correction for the base lines shall be called

$$E_{||}(\lambda) = E_{||}^{B}(\lambda) - B_{||}(\lambda)$$

and

$$E_{\perp}(\lambda) = E_{\perp}^{B}(\lambda) - B_{\perp}(\lambda)$$

Since the cross-section of the light beam in the Cary 14 is rectangular, it passes through only partially overlapping portions of the sheet in the two orientations of the holder. If the solute happens to be distributed nonuniformly, the number of solute molecules in the light path is different for the two orientations, which may be undesirable. To reduce the difference, several measurements are averaged. In our experimental setup, each measurement can be repeated three times with the light passing in turn through three roughly adjacent sections of the sheet adding in total to an approximately square-shaped area. Within mechanical error, the same area is used after the holder is rotated. In this manner, nearly the same number of molecules is used in the measurements in light of both polarizations. The arrangement is not perfect because of varying width and nonuniform intensity distribution in the light beam. In applications where perfection is required, a correction factor is derived from comparison with dichroic ratios obtained for one or several suitably chosen wavelengths using a circular mask in the light beam. Measurements with this mask are unfortunately not generally advisable because of sharply reduced light intensity.

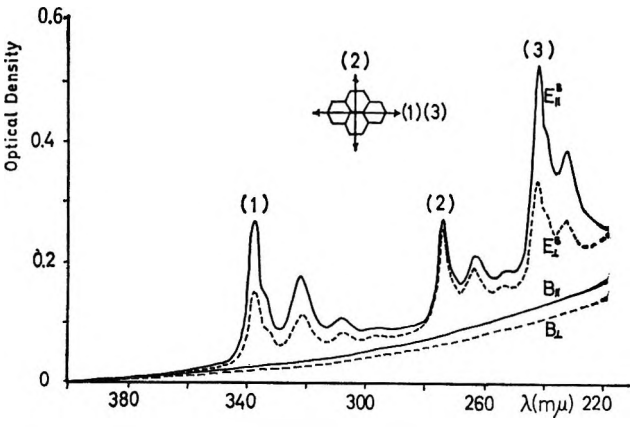

Figure 2. The electronic spectrum of pyrene. The observed optical densities $E_{||}^{B}(\lambda)$, $E_{\perp}^{B}(\lambda)$, $B_{||}(\lambda)$, and $B_{\perp}(\lambda)$ are shown. The solid and the dotted lines indicate $||$ and $\perp$, respectively.

The spectrophotometer is operated in the double-beam mode. When more than three polyethylene sheets are used in a measurement, it is usually necessary to cut down the intensity of the reference beam by a suitable neutral filter. Absorption curves are recorded in digital form and fed to a computer which subtracts base lines, averages the three measurements, and plots results in the desired form (sets of reduced curves; see below). We wish to stress, however, that while convenient, the use of a computer is not essential for symmetrical molecules. During the first several years of our work, we evaluated all data by hand. It is also not necessary to average results of three measurements unless one is interested in deriving orientation factors for the purpose of comparing these for molecules of different shapes.

Alternatively, one could keep the position of the sheets unchanged and rotate the Glan prism to obtain $E_{||}(\lambda)$ and $E_{\perp}(\lambda)$. This involves certain other problems, such as changing light intensity.

It is preferable to use as small a number of sheets in each measurement as possible, for two reasons. First, the accuracy is higher because of smaller base line corrections, and second, we have observed occasionally that the degree of dichroism was slightly lower when a larger number of sheets was used.

A series of measurements on the strong bands of pyrene showed that the results are the same if the solute is introduced into the sheet before stretching or after stretching. For convenience, we usually introduce it after stretching and then remount the sheet and stretch again to the desired degree. Chloroform seems the solvent of choice for introducing solutes into polyethylene. Other solvents which swell polyethylene can be used, *e.g.*, benzene, xylene, and chlorobenzene. Generally, only solvents with Hildebrand solubility parameter δ quite close to that for polyethylene[31] (*ca.* 8) can

(31) J. H. Hildebrand and R. L. Scott, "The Solubility of Nonelectrolytes," 3rd ed, Dover Publications, Inc., New York, N. Y., 1964, p 393.

be used. Solvents which do not swell the sheet (*e.g.*, methanol) do not wash out solutes present in the sheet even if these are otherwise quite soluble.

Even at the highest concentrations used, the solute seems to be dispersed monomolecularly. At least, pyrene emission spectra taken on sheets which contained much more compound than needed for absorption measurements showed only monomer emission. The degree of dichroism is independent of the concentration of the solute within the experimental uncertainty.

In general, the bands observed in sheet spectra are sharper than those recorded in solution at the same temperature. There are sometimes small differences in the wavelengths of peak maxima in $E_{||}(\lambda)$ and $E_{\perp}(\lambda)$, possibly connected to the birefringence of the stretched sheet. We have not yet investigated these phenomena in detail.

Orientation Model

It is generally agreed that practically all the solute is dissolved in the amorphous parts of the polyethylene sheet. This is in accord with our observation that polyethylene of high crystallinity absorbs fewer solute molecules. According to the present state of knowledge,[32,33] amorphous parts of stretched polyethylene consist of rubber-like highly strained elastic paraffinic chains which are predominantly in the all-trans zig-zag confirmation. Optical measurements indicate that these chains are partially aligned with the stretching direction. For small stretching ratios the degree of alignment, as determined *e.g.*, from dichroism in the infrared region, increases with further stretching. It levels off at a certain elongation and then remains virtually constant. We have observed the same behavior on the samples of polyethylene used for our experiments; the levelling off occurred at a stretching factor of about 4. The dichroic ratios $E_{||}/E_{\perp}$ for anthracene at 3785 Å and for pyrene at 3400 Å in polyethylene were also investigated as a function of the degree of stretching and gave a very similar result: the dichroic ratio grows with the degree of stretching up to a factor of about 4 and then remains approximately constant for factors between 4 and 7. This indicates strongly that the solute molecules are embedded fairly rigidly in cavities between the polymer chains. As various originally not mutually oriented regions in the polymer become partially aligned on stretching, solute molecules (or cavities, or potential cavities actually formed only on swelling) in all these regions acquire similar partial orientation with respect to the stretching direction. Further stretching hardly aligns the polymer chains in the amorphous regions any more; it is reasonable that it does not affect the orientation of the cavities or the solute molecules if these are rigidly embedded.

For a constant degree of stretching, the dichroic ratios $E_{\perp}/E_{||}$ for the short-axis polarized L_a band decrease in the order anthracene, 9-methylanthracene, 9,10-dimethylanthracene, *i.e.*, in the order of increasing width of the solute molecule. The length and thickness are approximately constant along the series. Again for a constant degree of stretching, the dichroic ratios $E_{||}/E_{\perp}$ for the long-axis polarized B_b band increase in the order naphthalene, anthracene, and tetracene. There, the length is increasing in the given order, while width and thickness are constant. 2,3-Dimethylnaphthalene shows a similar but stronger dichroism than naphthalene itself. 1,2,3,6,7,8-Hexahydropyrene, containing the same chromophore and having a very similar spectrum, shows strong dichroism of the opposite sense. 1,3-Dibromoazulene shows dichroism reversed with respect to azulene itself; an examination of molecular models shows that the smallest molecular cross section is perpendicular to the C_1–C_3 axis in the former and to the C_2–C_6 axis in the latter. Similar observations were made on about three dozen other molecules and shall be published in detail later.

All these results confirm the validity of the old notion[16,24–29] according to which both the preferred direction and the degree of orientation in the nonpolar polyethylene depend primarily on molecular shape. A planar molecule tends to orientate with its smallest cross section perpendicular to the stretching direction. Our results indicate that the degree of orientation grows with the difference between the length and width of the molecule.

This is in good agreement with expectations based on a simple evaluation of the intermolecular forces involved in the orientation of solute molecules dispersed in the amorphous parts of stretched polyethylene. The elastic polymer chains are highly strained and should quite effectively resist any further extension necessary for embedding a solute molecule. The interaction forces are dispersion (London) forces counteracted by short-range repulsive forces. Thus, in the vicinity of the solute molecule most of dispersion stabilization between the chains is lost and the strain of the single chains is increased. On the other hand, new dispersion stabilization between the chains and the polarizable π-electron cloud of the solute is gained. The energy balance shall determine the average molecular orientation. It is seen that all forces involved work in the same direction: losses should be least and gains largest if the solute molecules expose as small a cross section as possible perpendicular to the stretching direction, just as deduced from experimental data. Obviously, this

(32) Y. Nishijima, Y. Onogi, and T. Asai, *J. Polym. Sci. C*, **15**, 237 (1966); C. R. Desper and I. Kimura, *J. Appl. Phys.*, **38**, 4225 (1967); M. Takayanagi, K. Imada, and T. Kajiyama, *J. Polym. Sci. C*, **15**, 263 (1966); A. Peterlin, *ibid.*, **15**, 427 (1966); A. Peterlin and H. G. Olf, *J. Polym. Sci. A-2*, **4**, 587 (1966); I. L. Hay, T. Kawai, and A. Keller, *J. Polym. Sci. C*, **16**, 2721 (1967).

(33) R. S. Stein and B. E. Read, *J. Appl. Polym. Sci., Appl. Polym. Symp.*, **8**, 255 (1969).

model for the orientation mechanism is only a rough first approximation. Nevertheless, since all forces involved, although of unknown magnitudes, act in the same direction, a fair degree of confidence can be placed in its predictions.

Let us now define the concept of *effective orientation axis* for a given molecular orientation distribution: if the molecule had a transition polarized along this particular direction, its dichroic ratio $E_{||}/E_{\perp}$ would be larger than that of transitions polarized along any other direction in the molecule. To actually find the effective orientation axis of a planar molecule of general shape, we first locate all of its smallest cross section on a molecular model. Let us call directions perpendicular to these the *preferred molecular orientation axes*. If there is only one such axis, the effective orientation axis will coincide with it in symmetrical molecules. In unsymmetrical molecules, it need not coincide with it exactly, but it will usually be quite close. Our model then allows only approximate determination of the effective orientation axis from consideration of the size of cross sections perpendicular to directions close to the preferred molecular orientation axis. However, in practice this has never been a real difficulty since determination of transition moment directions in such molecules involves additional assumptions and is typically subject to errors as large as $\pm 15°$. If there are several preferred orientation axes in a symmetrical molecule, they are usually related by its symmetry operations. The effective orientation axis is then either easily found from symmetry considerations (*e.g.*, in dibenzo[*a*,*c*]-anthracene (I) the dashed lines are preferred orientation axes and the solid line is the effective orientation axis), or it is not unambiguously defined (*e.g.*, in molecules with a threefold symmetry axis) and the π–π^* absorption of the molecule cannot be profitably studied by the stretched sheet method.

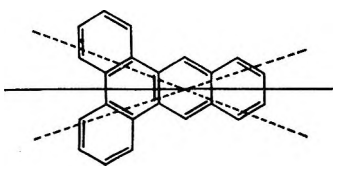

I

Separation of Spectra into Components

Let us introduce a sheet-fixed rectangular coordinate system X, Y, Z, such that Z coincides with the stretching direction and the beam of plane-polarized monochromatic light used passes along the X axis (perpendicular to the sheet). According to our previous definitions, the absorption curve recorded with the electric vector along Z is $E_{||}(\lambda)$, that for electric vector along Y is $E_{\perp}(\lambda)$.

In the following we limit our attention to planar molecules of arbitrary shape with negligible out-of-plane polarized absorption. Most aromatic molecules fall into this category (nonplanar substituents such as *tert*-butyl may be present as long as the chromophore itself remains planar). Let us introduce a molecule-fixed rectangular coordinate system x, y, z, such that x is perpendicular to the molecular plane. For the moment, the direction of z can be chosen arbitrarily. Consider the ith transition in the molecule, with electric dipole transition moment lying in the yz plane, and oriented at an angle ϕ_i with respect to the z axis. If all N molecules in the light path were perfectly aligned with this particular direction along the electric light vector, the observed optical density due to this transition would be $A_i(\lambda)$. For a given orientation distribution of the molecular assembly, the values of $E_{||}(\lambda)$ and $E_{\perp}(\lambda)$ can be obtained as a sum of contributions from all transitions

$$\begin{pmatrix} E_{||}(\lambda) \\ E_{\perp}(\lambda) \end{pmatrix} = \begin{pmatrix} K_1 & K_2 \\ K_3 & K_4 \end{pmatrix} \sum_i \begin{pmatrix} \cos^2 \phi_i \\ \sin^2 \phi_i \end{pmatrix} A_i(\lambda) \qquad (1)$$

In reality, while the measurement of $E_{\perp}$ is carried out on N molecules, the number of molecules in the light path during the measurement of $E_{||}$ may be slightly different because of experimental uncertainties, say $f \cdot N$. Then K_1 and K_2 have to be replaced by $f \cdot K_1$ and $f \cdot K_2$, respectively, and corresponding changes have to be made in all formulas. The positive numbers K_1 through K_4 shall be called orientation factors since they describe the degree of orientation of the solute in the polymer sheet; they are independent of λ (and of N, which is very large). Their physical significance will be discussed in detail in part III.

Now we shall supplement the specification of the molecular coordinate system by identifying z axis with the effective orientation axis. From the definition of the effective orientation axis and from eq 1, for this choice K_1/K_3 has the maximum possible value ($K_1/K_3 \geq 1$). This specification is incomplete in that it does not define the absolute orientation of the axes with respect to the molecular framework. As mentioned above, this can be found approximately from the molecular shape.

In the rest of this paper, we concentrate on the particularly simple case of planar molecules belonging to symmetry groups in which x, y, and z each transform according to a different irreducible representation, such as groups C_{2v} or D_{2h}. In such molecules, the effective orientation axis z can only lie in one of two mutually perpendicular in-plane directions dictated by symmetry. As discussed above, choice between the two possibilities can be made from the consideration of the two cross sections. Electric dipole transition moments of in-plane transitions (π–π^* transitions belong in this category) can only be directed along the z ($\phi_i = 0°$) or y ($\phi_i = 90°$) axis. We shall use the notation $A_z(\lambda) = \sum_{i(\phi=0°)} A_i(\lambda)$, $A_y(\lambda) = \sum_{i(\phi=90°)} A_i(\lambda)$. Thus, $A_z(\lambda)$ represents the sum total of light absorption due to "long-

axis polarized" transitions, and $A_y(\lambda)$ that due to to "short-axis polarized" transitions. Equation 1 now becomes

$$\begin{pmatrix} E_{||}(\lambda) \\ E_{\perp}(\lambda) \end{pmatrix} = \begin{pmatrix} K_1 & K_2 \\ K_3 & K_4 \end{pmatrix} \begin{pmatrix} A_z(\lambda) \\ A_y(\lambda) \end{pmatrix} \tag{2}$$

or, in matrix form

$$\mathbf{E} = \mathbf{KA} \tag{3}$$

If the ratio $E_{||}(\lambda)/E_{\perp}(\lambda)$ is constant for all λ within experimental error, the orientation of the molecular assembly is unsuitable ($K_1/K_3 = K_2/K_4$ and $\mathbf{K}^{-1}$ does not exist) or the π–π^* absorption is isotropic in the molecular plane, or both. The former happens when the breadth and length of the solute molecule differ too little (pyridine, fluorobenzene). However, we find that the method is already applicable to molecules such as acenaphthylene or benzo[*ghi*]fluoranthene although there the two cross sections do not differ very much. Previous belief[15] that the stretched sheet method is only applicable to very elongated molecules was mistaken.

If $\mathbf{K}^{-1}$ exists, $\mathbf{A} = \mathbf{K}^{-1} \cdot \mathbf{E}$, where

$$\mathbf{K}^{-1} = \frac{1}{(K_1K_4 - K_2K_3)} \begin{pmatrix} K_4 & -K_2 \\ -K_3 & K_1 \end{pmatrix} \tag{4}$$

Thus, the solutions are

$$\begin{aligned} A_z'(\lambda) &= A_z(\lambda) \cdot (K_1K_4 - K_2K_3)/K_4 = \\ &\qquad E_{||}(\lambda) - d_{||}{}^0 E_{\perp}(\lambda) \\ A_y'(\lambda) &= A_y(\lambda) \cdot (K_1K_4 - K_2K_3)/K_1 = \\ &\qquad E_{\perp}(\lambda) - d_{\perp}{}^0 E_{||}(\lambda) \end{aligned} \tag{5}$$

where $d_{||}{}^0 = K_2/K_4$ and $d_{\perp}{}^0 = K_3/K_1$ shall be called reduction factors (both are positive and independent of λ). $A_z'(\lambda)$ and $A_y'(\lambda)$ shall be called (unnormalized) reduced absorption curves. They are proportional to the previously defined $A_z(\lambda)$ and $A_y(\lambda)$; the proportionality factors are not the same. For most purposes, knowledge of the $A'(\lambda)$'s is sufficient.

For most molecules of the symmetry assumed here the reduction factors can be determined fairly easily. In the simplest case, the spectrum contains at least one peak due to purely long-axis polarized transition (large $E_{||}/E_{\perp}$) and at least one due to a purely short-axis polarized transition (small $E_{||}/E_{\perp}$), *i.e.*, for some values of λ, say λ_a, A_z is negligible; for others, say λ_b, A_y is negligible. Then, from equations 5, $d_{||}{}^0 = E_{||}(\lambda_a)/E_{\perp}(\lambda_a)$, $d_{\perp}{}^0 = E_{\perp}(\lambda_b)/E_{||}(\lambda_b)$. If band overlapping prevents the use of this procedure, we find the d's by trial and error. It is best to plot a series of curves $E_{||} - E_{\perp} \cdot d_{||}$ and $E_{\perp} - E_{||} \cdot d_{\perp}$ for $d_{||}$ and $d_{\perp}$ ranging from 0 to 1 in steps of, say, 0.1 ("stepwise reduction"). From eq 1, we have the following basic equations of our method ("reduction equations")

$$\begin{aligned} E_{||} - d_{||}E_{\perp} &= A_z(K_1 - d_{||}K_3) + A_y(K_2 - d_{||}K_4) \\ E_{\perp} - d_{\perp}E_{||} &= A_z(K_3 - d_{\perp}K_1) + A_y(K_4 - d_{\perp}K_2) \end{aligned} \tag{5a}$$

Thus, each curve in both plots is a linear combination of A_z and A_y and one can determine by inspection for which values of $d_{||}$ and $d_{\perp}$ spectral features due to "short-axis polarized" absorption A_y and "long-axis polarized" absorption A_z just disappear from the plotted curve. For values of $d_{||}$ and $d_{\perp}$ slightly larger or smaller than these, the spectral features appear again as negative or positive peaks. A suitable choice of $d_{||}$ can usually be found which eliminates the contribution of A_y; this is the desired $d_{||}{}^0 = K_2/K_4$. Similarly, the value of $d_{\perp}$ which eliminates A_z is equal to $d_{\perp}{}^0 = K_3/K_1$. If it happens that the contribution of A_z is just cancelled in one of the curves $E_{||} - d_{||} \cdot E_{\perp}$, say for $d_{||} = a$, then $d_{\perp}{}^0 = 1/a$, and finally if A_y is eliminated in one of the curves $E_{\perp} - d_{\perp} \cdot E_{||}$, say for $d_{\perp} = b$, then $d_{||}{}^0 = 1/b$. Obviously, the particular two curves for which features due to A_z or A_y are absent are just the sought reduced absorption curves A_y' and A_z' (*cf.* eq 5).

Examples of this procedure are given below. For spectra with sharp peaks usual for aromatic hydrocarbons and their simple derivatives, the d^0's can be usually determined with an accuracy ± 0.05. Molecules with broad featureless spectra are the only ones that present difficulties. Only approximate estimates of the d^0's may be possible, using the fact that A_z' and A_y' must be non-negative ($d_{\perp}{}^0 \leq [E_{\perp}(\lambda)/E_{||}(\lambda)]_{\min}$, $d_{||}{}^0 \leq [E_{||}(\lambda)/E_{\perp}(\lambda)]_{\min}$). Even in such unfavorable cases, the method gives rough information about the number of bands present and their polarizations.[34]

However, the procedure requires a computer and a plotter. If they are not available, an indirect approach is often possible for cases of substantial band overlap. A wavelength region a near a peak with a large $E_{||}/E_{\perp}$ ratio, and thus a relatively large contribution from A_z, and a similar region b near a peak with a small $E_{||}/E_{\perp}$ ratio, and thus a relatively large contribution from A_y, are selected in the spectrum. The assumption is made that the variations of $E_{||}$ and $E_{\perp}$ in such regions are only due to changes in the strong contributions from A_z and A_y, respectively. Differentiating eq 5, and neglecting $(dA_z/d\lambda)_{\lambda_b}$ and $(dA_y/d\lambda)_{\lambda_a}$,

(34) A referee has pointed out that even in molecules of C_{2v} or D_{2h} symmetry the 0–0 components of transitions may have, or appear to have, weak components polarized along the two axes other than the polarization axis of the transition. This would be possible if perturbations due to anisotropic environment were strong enough to destroy the symmetry of the chromophore, or, more likely, if the observed "0–0 band" contained unresolved vibronic components due to nonsymmetrical vibrations of very low frequency. If present, such contributions would typically be only very small, as suggested, *e.g.*, by the high polarization ratios observed in careful studies of polarized emission. In typical instances, the error introduced into our procedure would be smaller than the inherent error in reading off the d^0's. In particularly bad cases, it would increase the error in the d^0's. It is seen in Figure 3 that our conclusions concerning the number and polarization of bands are very little sensitive to errors in the d^0's, the intensities of "pure" reduced spectra being somewhat more sensitive.

where λ_b and λ_a lie in the regions b and a, respectively, we have

$$d_{||}^0 = (dE_{||}/d\lambda)_{\lambda_b}/(dE_\perp/d\lambda)_{\lambda_b}$$
$$d_\perp^0 = (dE_\perp/d\lambda)_{\lambda_a}/(dE_{||}/d\lambda)_{\lambda_a} \quad (6)$$

These equations are used to evaluate the d^0's for several values of λ_a and λ_b. If the assumptions are correct, the resulting d^0's are independent of the particular choice of λ_a and λ_b, and can be used to obtain the $A_z'(\lambda)$ and $A_y'(\lambda)$ curves. This is usually the case if strong sharp peaks are used for the evaluation, unless it so happens that both A_z and A_y contain a peak at almost the same wavelength. Then, one can often select a different peak in the spectrum for this procedure.

Ideally, one would like to obtain the curves $A_z(\lambda)$ and $A_y(\lambda)$ relating to a measurement on 1 mole of the solute in the light path, $A_z^0(\lambda)$ and $A_y^0(\lambda)$. So far, we have described a procedure which provides $A_z'(\lambda) = k \cdot A_z^0(\lambda)$ and $A_y'(\lambda) = k' \cdot A_y^0(\lambda)$, where $k \neq k'$. The actual values of k and k' cannot be obtained without the knowledge of the number of molecules in the light path N. This could be estimated using the assumption that the spectrum measured on a solution of known concentration in a nonpolar solvent is the same as that in unstretched polyethylene. More important, it is possible to obtain a "normalization factor" n_0 such that $n_0 A_y'(\lambda) = k \cdot A_y^0(\lambda)$. Then, $n_0 A_y'(\lambda)$ and $A_z'(\lambda)$ are related to $A_y^0(\lambda)$ and $A_z^0(\lambda)$ with the same proportionality factor k.

From eq 5, $n_0 = K_1/K_4$. The evaluation can be performed if the absorption curve of the solute in unstretched polyethylene sheet $E_0(\lambda)$ is measured. The number of molecules in the light path used for this measurement N' is unimportant but accuracy suffers if it differs too much from N. The solution in unstretched sheet does not show observable dichroism (the sheet itself is optically isotropic[33]). Then

$$E_0(\lambda) = K_0 A_z(\lambda) + K_0 A_y(\lambda) \quad (7)$$

Because $E_0(\lambda)$, $E_{||}(\lambda)$, and $E_\perp(\lambda)$ are linear combinations of the same two functions, $A_z^0(\lambda)$ and $A_y^0(\lambda)$, it is easy to see that one has

$$c_{||} E_{||}(\lambda) + c_\perp E_\perp(\lambda) = E_0(\lambda) \quad (8)$$

where the c's can be uniquely defined if $E_{||}(\lambda)$ and $E_\perp(\lambda)$ are not proportional.

From (2), (7), and (8), one has

$$c_{||} K_1 A_z(\lambda) + c_\perp K_3 A_z(\lambda) = K_0 A_z(\lambda)$$
$$c_{||} K_2 A_y(\lambda) + c_\perp K_4 A_y(\lambda) = K_0 A_y(\lambda)$$

which gives

$$c_{||} K_1 + c_\perp K_3 = K_0 = c_{||} K_2 + c_\perp K_4$$

or

$$K_1(c_{||} + c_\perp d_\perp^0) = K_4(c_{||} d_{||}^0 + c_\perp)$$

from this equation n_0 can be found

$$n_0 = \frac{K_1}{K_4} = \frac{c_{||} d_{||}^0 + c_\perp}{c_{||} + c_\perp d_\perp^0} \quad (9)$$

Since K_0 cancels, its value is immaterial. Using procedures similar to those described in part III, it can be shown that it is equal to $N'/3N$.

In part III of this series it is shown that if all directions perpendicular to the stretching direction in the bulk of the polymer sheet are equivalent (uniaxial stretching), the following relation holds

$$n_0 = \frac{2 + d_{||}^0}{2d_\perp^0 + 1} \quad (10)$$

Thus, if the number of molecules N was the same in the measurement of $E_{||}$ and $E_\perp$, one can obtain the normalization factor n_0 without any additional work with unstretched sheets. Relation 10 holds quite well in the cases which we have checked but its validity perhaps should not be assumed for polyethylene of different provenance, which might stretch less regularly.

Examples of Application

An example of the use of the differentiation technique for the determination of $d_\perp^0$ and $d_{||}^0$ has already been given elsewhere.[1] In the following, we give one example of reduction by hand, using the assumption of "pure transition regions" (perylene) and three examples of the "stepwise reduction" performed by a computer (phenanthrene, pyrene, benzo [*ghi*] perylene). In the case of pyrene, which has essentially pure transitions in both principal directions, reduction by hand is also easily possible. Preliminary results on these compounds have been reported.[30]

Pyrene. Williams,[35] using a simple fluorescence polarization technique, found that the three bands at 370, 340, and 280 mμ were polarized parallel to each other. By a better technique, Zimmerman and Joop[36] showed that though their fluorescence polarization curve does not change sign in the spectral region, its variation indicates that the 340- and 240-mμ transitions are polarized perpendicular to the 370- and 280-mμ transitions. Lyons and Morris[37] found by a crystal method that the 370-mμ band is polarized parallel to the short axis while the 340-mμ band is long-axis polarized. By measurements on mixed crystals Hochstrasser[38] concluded that both these transitions are short-axis polarized. New measurements by Bree and Vilkos,[39] however, have reaffirmed the results of Lyons and Morris. Hoijtink and Zandstra[40] found by means of an inge-

(35) R. Williams, *J. Chem. Phys.*, 26, 1186 (1957).
(36) H. Zimmermann and N. Joop, *Z. Elektrochem.*, 65, 66, 138 (1961).
(37) L. E. Lyons and G. C. Morris, *J. Chem. Soc.*, 3661 (1957).
(38) R. M. Hochstrasser, *J. Chem. Phys.*, 33, 459 (1960).
(39) A. Bree and V. V. B. Vilkos, *ibid.*, 40, 3125 (1964).
(40) G. J. Hoijtink and P. J. Zandstra, *Mol. Phys.*, 3, 371 (1960).

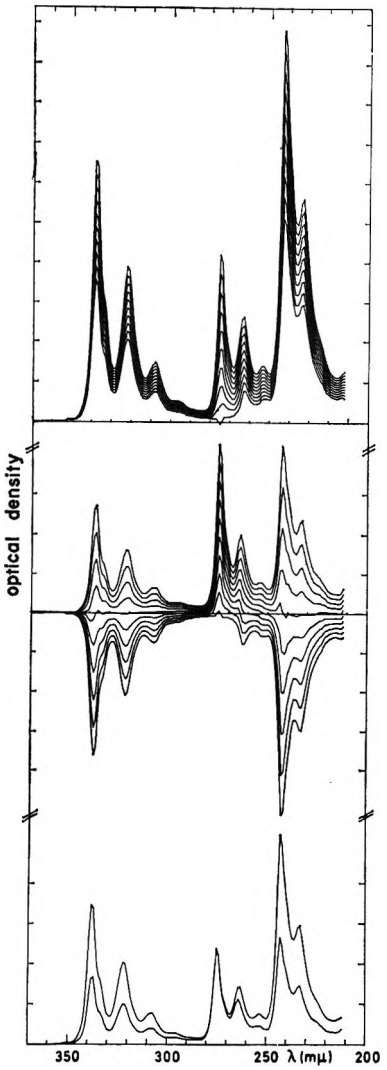

Figure 3. The electronic spectrum of pyrene (optical density in arbitrary units). From the bottom: (1) $E_{\parallel}(\lambda)$ and $E_{\perp}(\lambda)$ (with $E_{\parallel}(\lambda) \geq E_{\perp}(\lambda)$); (2) $2(E_{\perp}(\lambda) - d_{\perp}E_{\parallel}(\lambda))$; (3) $2(E_{\parallel}(\lambda) - d_{\parallel}E_{\perp}(\lambda))$; $d_{\parallel}$ and $d_{\perp}$ go from 0.1 to 1.0. It is seen that the peaks at 340 and 280 mμ disappear in (2) and (3), respectively, for $d_{\perp} = 0.5$ and $0.9 < d_{\parallel} < 1.0$.

nious photoselection technique that the 370- and 280-mμ transitions are polarized parallel to each other and perpendicular to the 340-mμ transition.

The experimental stretched film spectra (Figure 2) indicate two long-axis polarized transitions (1) and (3) and a single short-axis polarized one (2). For determination of the reduction factors the stepwise reduction method was used. Figure 3 shows $E_{||}$ and $E_{\perp}$, the absorption after subtraction of the base lines, and the two combinations $E_{||}-d_{||}E_{\perp}$ and $E_{\perp}-d_{\perp}E_{||}$ for different values of the d's. The reduction factors $d_{||}^{0}$ and $d_{\perp}^{0}$ can now be determined by inspection of the 340- and 280-mμ peaks. To remove the first of these from $E_{\perp}-d_{\perp}E_{||}$, $d_{\perp}$ must be put equal to 0.50, while the second disappears from $E_{||}-d_{||}E_{\perp}$ for $d_{||} = 0.95$. The results are shown in Figure 4, and as in Figure 2 it is obvious that there are two strong long-axis polarized transitions at

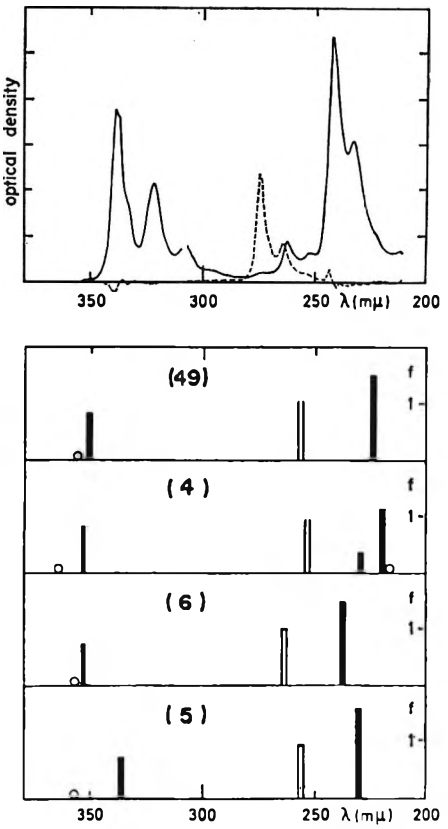

Figure 4. The "reduced" spectra A_z' and A_y' of pyrene ($d_{\parallel}^{0} = 0.55$, $d_{\perp}^{0} = 0.50$, $n_0 = 1.37$). The solid and the dotted lines indicate long- and short-axis polarized absorbance (arbitrary units), respectively. Below are shown the results of four different calculations, characterized by their reference numbers (TBM approximation of ref 4 and NM approximation of ref 6 were chosen). Black (white) bars: long (short) axis polarization. Circles: zero oscillator strength (or too small to be plotted).

340 and 240 mμ, while there is a single strong short-axis polarized transition near 280 mμ. In addition there is long-axis polarized absorption near 260 mμ. This might be due to vibronic coupling of the 280-mμ with the 240-mμ band. The shape indicates that it is probably due to a separate electronic transition, but no such transition was detected in a detailed study of substituent effects on (unpolarized) spectra by Becker, *et al.*[10]

Spectra obtained by the use of a large number (about 20) of sheets show that the weak band starting at 370 mμ has a short-axis polarized 0–0 transition, while in the following vibronic series the long-axis polarized transitions dominate.[41] In this case the same reduction factors were used as in Figure 4.

Perylene. Earlier measurements by a simple fluorescence polarization technique by Williams[35] indicated that the bands at 440 mμ and 250 mμ are polarized perpendicular to each other. This result was reaffirmed by Zimmerman and Joop,[36] who in addition obtained

(41) E. W. Thulstrup, Dissertation, Aarhus, 1967.

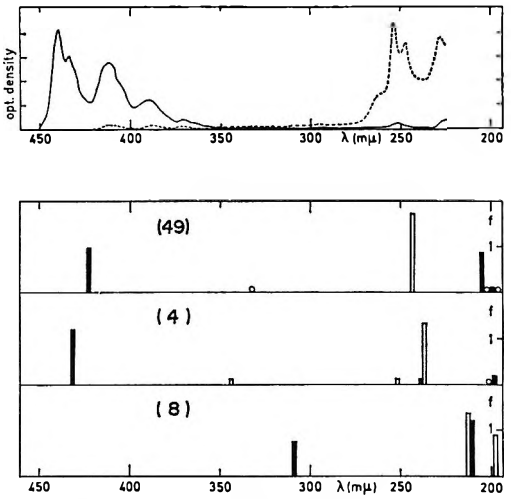

Figure 5. The "reduced" electronic spectra A_z' and A_y' of perylene ($d_\parallel^0 = 0.55$, $d_\perp^0 = 0.25$, $n_0 = 1.66$). The nomenclature of Figure 4 is used.

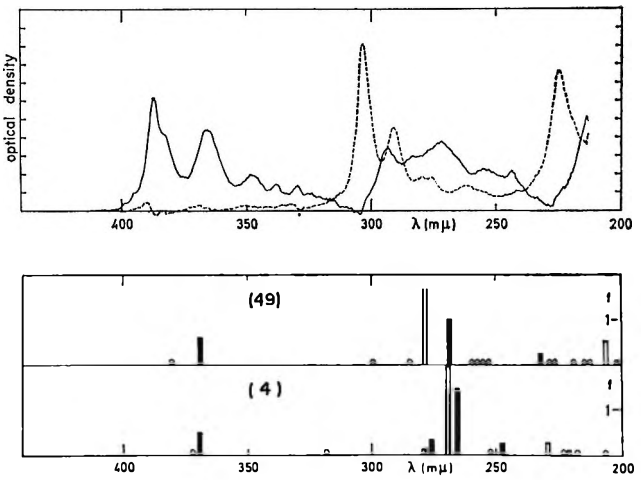

Figure 6. The "reduced" spectra A_z' and A_y' of benzo[*ghi*]perylene ($d_\parallel^0 = 0.90$, $d_\perp^0 = 0.50$, $n_0 = 1.41$). The nomenclature of Figure 4 is used.

some information about the polarization of the two weak bands near 330 and 290 mμ, which seem to be polarized perpendicular and parallel, respectively, to the 440-mμ band.

In the experimental film spectra $E_\parallel/E_\perp$ varies from about 4 (near 440 mμ) to 0.5 (near 250 mμ). This shows that these two transitions are long- and short-axis polarized, respectively, and from the assumption of "pure transitions" the reduction factors can be found. The final result is shown in Figure 5 and it is in perfect agreement with the results mentioned above. The two 330- and 290-mμ bands have not been studied in stretched films, because of low intensity.

Benzo[ghi]perylene. Crystal measurements by Ganguly and Mukherjee[42] indicate that the first transition near 410 mμ is short-axis polarized. This weak transition has not been investigated in detail by the stretched film method, but the following series of strong bands in the region down to 220 mμ has been studied carefully. From the experimental spectrum it is clear that the strong transition near 390 mμ is long-axis polarized ($E_\parallel/E_\perp = 2$) while the strong, sharp peak at 300 mμ seems to be short-axis polarized ($E_\parallel/E_\perp = 0.9$). From these assumptions the reduction factors can be determined by using stepwise reduction. The result is shown in Figure 6, and it is seen that a wealth of information is contained in the reduced spectra. Strong long-axis polarized absorption is found in the region 390 to 350 mμ, apparently due to a single electronic transition, and in the region below 290 mμ. From the shape of the $A_z(\lambda)$ curve it is likely that there are at least three separate electronic transitions in this region, at about 290, 270 and 220 mμ. The $A_y(\lambda)$ curve clearly shows two strong transitions near 305 and 230 mμ. Besides the strong transitions both A_z and A_y seem to have components due to weaker transitions in the regions outside the strong bands.

Phenanthrene. Measurements by several authors on single and mixed crystals[43] showed that the first transition near 340 mμ is short-axis polarized. By fluorescence polarization Zimmerman and Joop[36] found that the 290-mμ band is polarized perpendicular to the 340-mμ band, and two maxima in the fluorescence polarization curve, near 280 and 260 mμ, were assigned to two separate electronic transitions (polarized parallel to the 340-mμ transition). Azumi and McGlynn[44] and Dörr, *et al.*,[45] found similar results, but suggest that vibronic coupling may be the reason for one or both of the maxima. In addition to earlier results Gallivan and Brinen[46] have found, also by fluorescence polarization, that the 250-mμ transition is polarized perpendicular to the 340-mμ band.

The orientation factors for the stretched film spectra have been determined by inspection of two sets of reduced curves; $d_\perp^0$ and $d_\parallel^0$ are chosen so that the sharp peaks near 290 and 220 mμ disappear in the curves $A_y(\lambda)$ and $A_z(\lambda)$, respectively. Figure 7 shows the result: long-axis polarized transitions at 290, 250, and near 210 mμ, and short-axis polarized ones at 280, 260, and 220 mμ. While the long-axis polarized transitions seem to be due to separate electronic transitions, like the short-axis polarized one at 220 mμ, the assignment of the 280- and 260-mμ bands is not so clear. However, the position and shape of the 260-mμ band indicate that it is due to a separate electronic transition, while the 280-mμ band may be explained as a result of vibronic coupling,

(42) S. C. Ganguly and B. C. Mukherjee, *Proc. Phys. Soc.*, **79**, 220 (1962); B. C. Mukherjee and S. C. Ganguly, *ibid.*, **83**, 93 (1964).

(43) D. S. McClure, *J. Chem. Phys.*, **22**, 1256 (1954); **25**, 481 (1956); D. P. Craig and R. D. Gordon, *Proc. Roy. Soc. Sect. A*, **288**, 69 (1965); R. M. Hochstrasser and G. J. Small, *J. Chem. Phys.*, **45**, 2270 (1966).

(44) T. Azumi and S. P. McGlynn, *ibid.*, **37**, 2413 (1962).

(45) F. Dörr and H. Gropper, *Ber. Bunsenges. Phys. Chem.*, **67**, 193 (1963); F. Dörr, G. Hohlneicher, and S. Schneider, *ibid.*, **70**, 803 (1966).

(46) J. B. Gallivan and J. S. Brinen, *J. Chem. Phys.*, **50**, 1590 (1969).

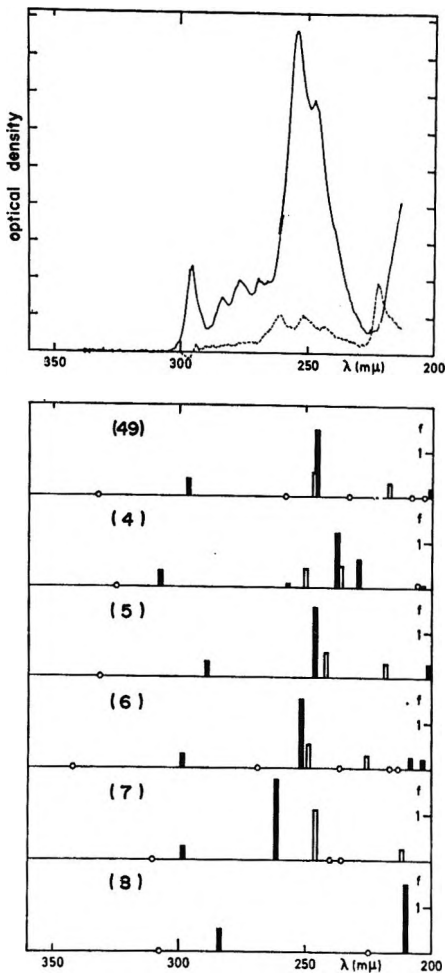

Figure 7. The "reduced" electronic spectra A_z' and A_y' of phenanthrene ($d_\parallel^0 = 0.70$, $d_\perp^0 = 0.45$, $n_0 = 1.31$). The nomenclature of Figure 4 is used.

in agreement with tentative conclusions of Dörr, *et al.*,[45] and with investigations of substituent effects.[47]

As in the case of pyrene, the first weak band (near 340 mμ) has been studied using a large number of sheets.[41] These measurements showed that the first peak in the vibronic series is short-axis polarized, while long-axis polarized components become more important at shorter wavelengths.

Comparison with Theory. In addition to the reduced spectra, several examples of calculations are shown. An assignment of electronic spectra can be considered as a mapping of a set of observed transitions into a set of calculated ones.[48] The mapping is determined from a series of criteria, such as transition energy, moment direction, and oscillator strength. The calculations shown all give information about these three properties, and it is remarkable how useful the moment direction criterium is.

Our own calculations[49] using the simple version of PPP method (variation of resonance integral β with bond length according to ref 50 led to similar results) and those of Hummel and Ruedenberg[4] have been carried out for all four compounds. The results are quite similar and in relatively good agreement with experiment. In the case of pyrene it is noteworthy that only Hummel and Ruedenberg's TBM calculation predicts a long axis polarized transition between the strong short- and long axis transitions (Figure 4). This prediction seems to be in agreement with the observations.

The methods of Bloor, Gilson, and Brearley[5] and of Nishimoto and Forster,[6] which include a variation of β with bond length, show good agreement with each other and with experiment in the cases of phenanthrene (Figure 7) and pyrene (Figure 4).

The method of Weltin, Weber, and Heilbronner[7] shows a fairly good agreement with experiment in the case of phenanthrene (Figure 7). These calculations include only nine configurations and use a simplified set of parameters. On the other hand, the method of Skancke[8] predicts all transition energies too high, both in the case of phenanthrene and perylene (Figure 5).

It is of interest that a complete assignment of all observed relatively strong transitions is possible for most theoretical models discussed here. This assignment can only be made with such a confidence by means of the polarization data, which provides separation of the transitions into two classes, thereby lowering the requirements for other criteria. Also for weak transition, in usual spectra often hidden by stronger bands of different polarization, the film spectra give some possibilities for assignments, or at least for checking the approximate positions of calculated weak transitions (*e.g.*, Figure 6).

Conclusions

The stretched sheet method described in this paper is the simplest and possibly the most universally applicable of presently available methods for separation of π–π^* absorption of planar molecules of C_{2v} or D_{2h} symmetry into components. Absolute direction assignments are possible with a reasonable degree of confidence. It is probable that even in high-resolution studies of vapors or crystals a simple preliminary experiment of the nature described here would provide valuable clues and should be considered.

The results are of importance for excited state symmetry assignments, detection of hidden bands, investigations of vibronic interactions, and differentiation between vibrational fine structure and separate electronic transitions. They should provide a better background for testing of π-electron theories.

(47) R. N. Jones and E. Spinner, *Spectrochim. Acta*, **16**, 1060 (1960).

(48) E. W. Thulstrup, *Int. J. Quant. Chem., Symp. Vol.*, **3S**, 641 (1970).

(49) PPP calculations by the authors using self-consistent molecular orbitals and parameters from: J. Koutecký, J. Paldus, and R. Zahradník, *J. Chem. Phys.*, **36**, 3129 (1962).

(50) P. Hochmann, R. Zahradník, and V. Kvasnička, *Coll. Czech. Chem. Commun.*, **33**, 3478 (1968).

The main limitation of the method is its inapplicability to molecules of equal width and length. However, this is much less serious than previously assumed[15] and good results have been obtained, *e.g.*, for acenaphthylene, benzo[*ghi*]perylene, and benzo[*ghi*]fluoranthene.

A second limitation is the small solubility of some compounds in polyethylene and similar polymers, which makes observation of weak transitions difficult or impossible. This is not very serious with solutes of low molecular weight. For example, we have recently determined[51] even the polarization of the first transition in fluoranthene which is seen as a shoulder of log ϵ *ca.* 2 in the absorption spectrum. Very much larger molecules present difficulties. Polar molecules are usually insoluble in polyethylene. They can be studied in polyvinyl alcohol, which, however, does not orientate solutes as well.

The third main limitation is inherent to our method of quantitative evaluation: the method is difficult to apply to molecules whose spectra consist only of diffuse featureless overlapping bands and to molecules whose spectra do not contain any region without substantial contribution from out-of-plane polarized transitions. Some help might be obtained using estimates of orientation factors from molecular shape.

Finally, accuracy is fairly low for weak bands buried under much stronger bands of opposite polarization. This is unfortunately true of most methods.

Acknowledgments. The authors wish to thank Dr. Lis Hansen, Dr. Bent Have, Dr. Finn Rasmussen, Per Strand, Else Hommelgaard, Jonna Have, and Lise Flindt Pedersen, who have worked with this method for several years and have contributed considerably to its development. We also want to thank Statens Almindelige Videnskabsfond for a grant which made it possible to buy a digital attachment for our spectrophotometer.

(51) J. Michl, *Theoret. Chim. Acta*, 15, 315 (1969).

Polarization Spectra in Stretched Polymer Sheets. III.[1] Physical Significance of the Orientation Factors and Determination of π–π^* Transition Moment Directions in Molecules of Low Symmetry

by J. Michl, E. W. Thulstrup, and J. H. Eggers

Department of Chemistry, Aarhus University, Aarhus, Denmark *(Received November 13, 1969)*

Orientation factors of planar molecules in stretched polymer sheets are discussed in relation to molecular shape and orientation distribution. Normalization factors n_0 determined from measurements in unstretched polyethylene agree with those calculated from results of stretched sheet measurements assuming axial symmetry around the stretching direction. Methods are described for the determination of the angles between transition moment directions in planar molecules of arbitrary shape and the effective orientation axis of dichroism in a stretched polyethylene sheet. The necessary information about the orientation distribution could be obtained from measurements on molecules of C_{2v} or D_{2h} symmetry and related shape in the manner described in part II.[1] It could also be obtained from measurements on less symmetrical molecules of related shape, for which directions of two of the transitions are already known, such as alkyl derivatives of hydrocarbons of C_{2v} or D_{2h} symmetry. As an example, results for 10a,4a-borazarophenanthrene are presented, using phenanthrene to obtain orientation factors.

Introduction

In part II[1] we have discussed ways in which those characteristics of the orientation distribution of solute molecules in stretched polyethylene which determine dichroic properties can be found from absorption measurements on stretched and unstretched sheets. The procedure was limited to planar molecules of D_{2h} or C_{2v} symmetry with negligible out-of-plane absorption. For our purposes the orientation distribution is sufficiently described by the ratios of the orientation factors K_1–K_4.

(1) Part II: E. W. Thulstrup, J. Michl, and J. H. Eggers, *J. Phys. Chem.*, **74**, 3868 (1970).

In this paper, we first examine the physical significance of the factors K_1–K_4. Then, we investigate the use of our approach for the determination of the angles ϕ between electric dipole transition moment directions in planar molecules of low symmetry and the effective orientation axis. Such molecules constitute a large majority of molecules of interest; the π–π^* transition moment directions may lie anywhere in the molecular plane. Out-of-plane polarized absorption is again assumed to be negligible. In the general case it is not possible to derive the necessary ratios of orientation factors K_1–K_4 from the observed dichroic spectra. Then, only the order of the $|\phi|$'s can be determined from the spectra alone.

If the conclusion of part II that the ratios of K_1–K_4 are primarily determined by molecular shape is accepted, it becomes possible to estimate these ratios for molecules of low symmetry from values which had been derived for those of D_{2h} or C_{2v} symmetry. Such an assumption is highly plausible on the basis of the orientation model discussed in part II, which quite successfully accounts for all experimental observations available.

At present, it is not possible to measure these ratios with high accuracy, mostly because for the symmetrical molecules themselves the reproducibility is low (typical uncertainty $\pm 10\%$). We hope that this can be improved in the future. Nevertheless, it is already possible to estimate reasonable limits. In the following, we derive formulas for $|\phi|$ and discuss several cases of practical importance where good estimates of orientation factor ratios should be possible already at present. Orientation of transitions in 10a,4a-borazarophenanthrene is discussed as an example; other applications will be described in forthcoming papers. We believe that our method for analysis of stretched sheet data offers significant advantages over other existing methods,[2,3] both in experimental simplicity and in that it makes far fewer assumptions.

Physical Significance of the Orientation Factors K_1–K_4

We shall use the three Euler angles α, β, γ, as defined in ref 4 (Figure 1) to express the orientation of the molecule-fixed coordinate system x, y, z with respect to the sheet-fixed system X, Y, Z, which are defined as in part II. Thus, β is the angle between the effective orientation axis z and the stretching direction Z, γ describes the rotation of the molecule-fixed coordinate system around the molecular z axis, and the angle α corresponds to rotation of the z axis around Z.

The orientation factors K_1–K_4 introduced in part II can then be expressed[4] in terms of α, β, γ (*cf.* ref 5 for similar treatments orientated toward investigation of the polymer itself)

$$K_1 = \frac{1}{N}\sum_{j=1}^{N} \cos^2 \beta_j \qquad (1)$$

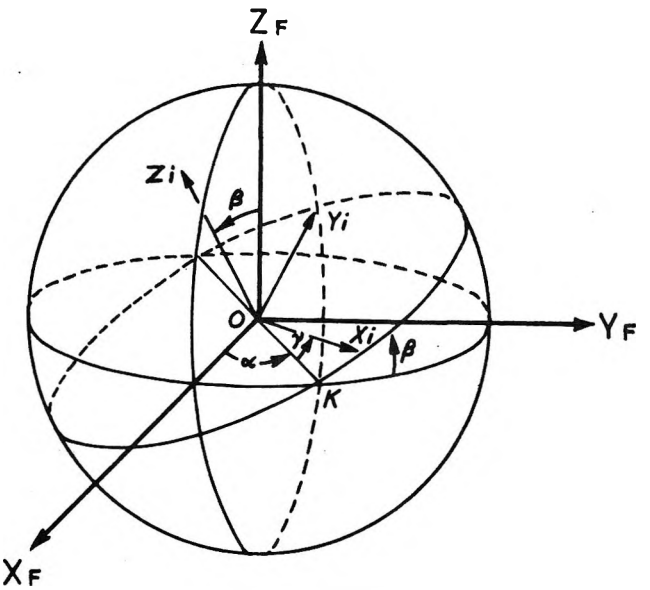

Figure 1. The sheet-fixed (X_F, Y_F, Z_F) and the molecule-fixed (x_i, y_i, z_i) coordinate systems and the three Euler angles (α, β, γ).

$$K_2 = \frac{1}{N}\sum_{j=1}^{N} \sin^2 \beta_j \cdot \cos^2 \gamma_j \qquad (2)$$

$$K_3 = \frac{1}{N}\sum_{j=1}^{N} \cos^2 \alpha_j \cdot \sin^2 \beta_j \qquad (3)$$

$$K_4 = \frac{1}{N}\sum_{j=1}^{N} (\cos \alpha_j \cdot \cos \beta_j \cdot \cos \gamma_j - \sin \alpha_j \cdot \sin \gamma_j)^2 \qquad (4)$$

Clearly, K_1–K_4 lie between 0 and 1. If the α distribution is independent of the β and γ distributions and symmetrical with respect to reflection in the YZ and XZ planes, as is considered highly likely for uniformly stretched sheets,[5] K_4 can be simplified

$$K_4 = \frac{1}{N}\sum_{j} (\cos^2 \alpha_j \cdot \cos^2 \beta_j \cdot \cos^2 \gamma_j + \sin^2 \alpha_j \cdot \sin^2 \gamma_j) \qquad (5)$$

The expressions for K_1–K_4 simplify considerably if one assumes that the α distribution is uniform, $\langle \cos^2 \alpha \rangle_{av} = 1/2$. This assumption (uniaxial stretching) seems reasonable but cannot be made automatically since in stretching the width of the sheet decreases by only 20% or less, while its thickness decreases 4 times or more.

(2) Y. Tanizaki and S.-I. Kubodera, *J. Mol. Spectrosc.*, **24**, 1 (1967), and references therein.

(3) A. Yogev, L. Margulies, D. Amar, and Y. Mazur, *J. Amer. Chem. Soc.*, **91**, 4558 (1969).

(4) H. Margenau and G. M. Murphy, "The Mathematics of Physics and Chemistry," 2nd ed, D. Van Nostrand Co., Princeton, N. J., 1956, p 286.

(5) R. Zbinden, "Infrared Spectroscopy of High Polymers," Academic Press, New York, N. Y., 1964; S. Nomura, H. Kawai, I. Kimura, and M. Kagiyama, *J. Polym. Sci. A-2*, **5**, 479 (1967); I. Kimura, M. Kagiyama, S. Nomura, and H. Kawai, *ibid.*, **7**, 709 (1969).

Table I: Reduction and Normalization Factors

Compound	Reduction factors $d_{\|\|}^0$	$d_\perp^0$	The K's and n_0 calculated from the assumption $\langle\cos^2\alpha\rangle_{av} = 1/2$ K_1	K_2	K_3	K_4	n_0	n_0 found from $E_{\|\|}(\lambda)$, $E_\perp(\lambda)$, and $E_0(\lambda)$ n_0
Fluoranthene	0.80	0.40	0.56	0.29	0.22	0.36	1.56	1.70
Phenanthrene	0.70	0.45	0.52	0.26	0.23	0.37	1.41	1.31
Acridine	0.55	0.40	0.55	0.22	0.22	0.39	1.41	1.39
Benzo[*ghi*]perylene	0.90	0.50	0.50	0.31	0.25	0.35	1.43	1.41
Pyrene	0.95	0.50	0.50	0.32	0.25	0.34	1.48	1.37
Anthracene	0.50	0.33	0.59	0.20	0.20	0.40	1.48	1.46
Perylene	0.55	0.25	0.67	0.21	0.17	0.39	1.72	1.66

Some information about the detailed structure of stretched polyethylene under our experimental conditions can be obtained from X-ray diffraction photographs taken on our stretched sheets. While the diffraction pattern changes when the direction of the incident X-ray beam is moved in the XZ plane, it stays unchanged when the beam is directed along various directions in the XY plane. This strongly indicates that the "α distribution" of the crystallites is uniform so that it is very likely that the amorphous part also is uniaxial. Another way to verify this would be a study of polarized fluorescence[6] which we have not yet undertaken.

If the α distribution is uniform, eq 1–3 and 5 can be combined to give

$$K_3 = (1 - K_1)/2 \tag{6}$$

and

$$K_4 = (1 - K_2)/2 \tag{7}$$

so that, using the notation of part II, the quantities characterizing the β and γ distributions can be expressed in terms of observables $d_\perp^0$ and $d_{||}^0$

$$\langle\cos^2\beta\rangle_{av} = K_1 = 1/(2d_\perp^0 + 1) \tag{8}$$

$$\langle\sin^2\beta\cdot\cos^2\gamma\rangle_{av} = K_2 = d_{||}^0/(2 + d_{||}^0) \tag{9}$$

The usual orientation function for the z axis then becomes $(3\langle\cos^2\beta\rangle_{av} - 1)/2 = (1 + d_\perp^0)/(1 + 2d_\perp^0)$ as it should in this special case (*e.g.*, ref 7).

At the same time, the following relation should hold

$$n_0 = K_1/K_4 = (2 + d_{||}^0)/(2d_\perp^0 + 1) \tag{10}$$

This relation provides another way to check the correctness of the assumption $\langle\cos^2\alpha\rangle_{av} = 1/2$, since n_0, $d_{||}^0$ and $d_\perp^0$ can all be measured.

Table I gives results of an attempt to determine how well relation 10 is satisfied under our experimental conditions (assuming the same number of molecules in the light path during measurement of $E_{||}$ and $E_\perp$; these results are averages of three measurements; for details see part II). It should be remembered that n_0, $d_\perp^0$, and $d_{||}^0$ themselves are read off with relatively large errors (up to 10%). The deviation of the n_0 values calculated from the assumption of uniform α distribution from those measured is always less than 10%. The accuracy of the data is not sufficient to detect reliably any deviation of $\langle\cos^2\alpha\rangle_{av}$ from 0.5. Therefore, in the following discussions of β and γ distributions, we shall assume that the α distribution is uniform. This result is also important as a labor-saving device; since n_0 can be obtained from $d_\perp^0$ and $d_{||}^0$, extra measurements on unstretched sheets are not needed.

Equation 8 allows the formal definition of the direction of the effective orientation axis in a planar molecule to be expressed in terms of the orientation distribution: it is that choice of the z axis for which $K_1 = \langle\cos^2\beta\rangle_{av}$ acquires maximum value. One could expect $\langle\cos^2\beta\rangle_{av}$ to be simply related to the ratio of the width and length of the molecule. Our results indicate that this is only approximately true since factors such as "filling of the corners" also play a role (compare pyrene and perylene in Table I). Actually, the ratio of the diagonal to the width is the best shape describing factor that we have found so far. An increase in thickness, for instance *t*-butyl substitution, decreases the value of $\langle\cos^2\beta\rangle_{av}$ remarkably. A study of relations between molecular shape and $\langle\cos^2\beta\rangle_{av}$ is being continued.

While the results given so far characterize the β distribution directly by the value $K_1 = \langle\cos^2\beta\rangle_{av}$, the γ distribution is only characterized indirectly from $K_2 = \langle\sin^2\beta\cdot\cos^2\gamma\rangle_{av}$. It is not possible to derive the value of $\langle\cos^2\gamma\rangle_{av}$ from the measurements without assuming some special form of the γ distribution such as its being independent of the β distribution. This assumption is not *a priori* justifiable for planar molecules of arbitrary shape (it is made both in the model of Tanizaki and collaborators[2] and the recent model of Yogev, Muzur, and collaborators[3]). Using our orientation model to estimate what the possible γ distributions could be, it is seen that one extreme is a completely uniform distribution, to be expected for rod-shaped molecules; the other (hypothetical) extreme is $\gamma = 0°$ or 180° for all molecules, which might be approached for very large

(6) Y. Nishijima, Y. Onogi, and T. Asai, *J. Polymer Sci., C*, 15, 237 (1966); C. R. Desper and I. Kimura, *J. Appl. Phys.*, 38, 4225 (1967).

(7) R. S. Stein and B. E. Read, *J. Appl. Polymer Sci., Appl. Polym. Symp.*, 8, 255 (1969).

sheet-shaped molecules (in reality, that fraction of molecules for which β is close to 0° will always have a nearly uniform γ distribution). On the other hand, it is unlikely that the values of γ near 90° would be preferred. Thus, our hypothesis about the orientation mechanism gives $^1/_2 \leq \langle\cos^2\gamma\rangle_{av} < 1$. In both extreme cases, the γ distribution is independent of the β distribution and we may write from (1) and (2)

$$K_2 = \langle\cos^2\gamma\rangle_{av}(1 - K_1) \tag{11}$$

From (8), (9), (11)

$$1/d_{||}^0 = [1 + 1/(2d_\perp^0)]/2\langle\cos^2\gamma\rangle_{av} - {}^1/_2 \tag{12}$$

and from (2), (3)

$$K_2 = 2\langle\cos^2\gamma\rangle_{av}\cdot K_3 \tag{13}$$

For uniform γ distribution (rod-shaped molecules) $K_2 = K_3$ and further $1/d_{||}^0 = {}^1/_2 d_\perp^0 + {}^1/_2$, $K_4/K_2 = K_1/2K_3 + {}^1/_2$; for the other limiting case $\langle\cos^2\gamma\rangle_{av} = 1$, $K_2 = 2K_3$, and $1/d_{||}^0 = {}^1/_4 d_\perp^0$, $K_4/K_2 = K_1/4K_3$. Our experimental data agree qualitatively with these expectations. A detailed study is in progress.

Determination of In-Plane Transition Moment Directions in Molecules of Low Symmetry

The starting point is the same as for molecules of D_{2h} and C_{2v} symmetry

$$\begin{pmatrix} E_{||}(\lambda) \\ E_\perp(\lambda) \end{pmatrix} = \begin{pmatrix} K_1 & K_2 \\ K_3 & K_4 \end{pmatrix} \sum_i \begin{pmatrix} \cos^2\phi_i \\ \sin^2\phi_i \end{pmatrix} A_i(\lambda) \tag{14}$$

using notation of part II.

If the structuring of the observed spectra is sufficient, features contributed by a transition can be recognized as peaks and shoulders; the contribution of the jth transition to the curves $E_{||}$ and $E_\perp$ will be labeled $[E_{||}]_j$ and $[E_\perp]_j$. For spectra consisting entirely of broad strongly overlapping bands such features may be impossible to recognize and our method will be of little use.

Let us construct a series of curves $E_{||}(\lambda) - b\cdot E_\perp(\lambda)$ for suitable positive values of b, until for each transition we find such a value of b (say b_j for the jth transition), for which the spectral features due to that transition are just absent in the curve, so that $[E_{||}(\lambda)]_j - b_j[E_\perp(\lambda)]_j = 0$. In practice, we use the same computer program as for symmetrical molecules;[1] if the contribution of the jth transition just disappears in one of the curves $E_{||}(\lambda) - d_{||}E_\perp(\lambda)$, then obviously $b = d_{||}$; if this happens in one of the curves $E_\perp(\lambda) - d_\perp E_{||}(\lambda)$, then $b = 1/d_\perp$. It is usually sufficient to plot the curves for both $d_{||}$ and $d_\perp$ varying between 0 and 1 in steps of 0.1.

From eq 14, for the jth transition

$$K_1\cdot\cos^2\phi_j + K_2\cdot\sin^2\phi_j - b_j(K_3\cos^2\phi_j + K_4\sin^2\phi_j) = 0 \tag{15}$$

Thus

$$\tan^2\phi_j = (K_1 - b_jK_3)/(b_jK_4 - K_2) \tag{16}$$

For a transition which happens to lie in the effective orientation axis ($\phi_j = 0^0$), $b_j = K_1/K_3$, while for a transition perpendicular to this axis ($\phi = 90^0$), $b_j = K_2/K_4$. For molecules of C_{2v} and D_{2h} symmetries treated in part II, such relationships could be used for the actual determination of the quotients $K_1/K_3 = 1/d_\perp^0$ and $K_2/K_4 = d_{||}^0$ since for any transition either $\phi = 0^0$ or $\phi = 90^0$. Obviously, such a straightforward procedure is not generally possible for molecules of lower symmetry.

Certain limits can nevertheless be obtained, using the condition $\tan^2\phi \geq 0$ and the fact that for all molecules investigated so far, $K_1/K_3 > K_2/K_4$.

The condition $\tan^2\phi \geq 0$ and eq 16 give for all b_j

$$K_2/K_4 \leq b_j \leq K_1/K_3 \tag{17}$$

Differentiation of eq 16, using $K_1/K_3 > K_2/K_4$, shows that $\tan^2\phi$ is a monotonously decreasing function of b. Therefore, the order of decreasing values of b is the order in which the transition moments deviate from the effective orientation axis, the transition with smallest b deviating the most. The sense of the deviation cannot be determined; if two transitions deviate by the same angle they may be parallel or lie at a mutual angle of 2ϕ.

This is an important result since the determination can be easily carried out even in cases of strong band overlap. Since transitions with differing polarization usually have different b values, an inspection of the change in the $E_{||}(\lambda) - bE_\perp(\lambda)$ curve as a function of b may help to distinguish between vibrational structure and distinct electronic transitions as well as help to find hidden bands. Great caution is required, however, since in these molecules the individual vibronic components of a given electronic transition may in principle have quite arbitrary transition moment directions in the yz plane, particularly for weak transitions. It should be helpful to investigate the effect of some weakly interacting substituents as well, or to find correlations with a related and more symmetrical molecule.

To calculate the values of $|\phi|$, we rewrite eq 16

$$\tan^2\phi_j = (K_3/K_4)(K_1/K_3 - b_j)/(b_j - K_2/K_4) \tag{18}$$

In part II, we have mentioned the existence of relations between the orientation factors K_1–K_4 and molecular shape. Although more and better data are needed before such relations can be used for reliable *a priori* estimates, a certain amount of interpolation is already possible.

In the absence of any information on the orientation ratios, one could obtain some idea of the relative values of $|\phi|$ for the various transitions in the molecule by assuming that the transition which deviates least from the effective orientation axis (largest b) actually lies in it and that the one which deviates most from this axis (smallest b) is perpendicular to it. Thus, in such an unfavorable case, we set $K_1/K_3 = b_{max}$, $K_2/K_4 = b_{min}$,

where the b's are determined from the set of curves $E_{||}(\lambda) - bE_{\perp}(\lambda)$. One must keep in mind that the differences in the absolute magnitudes of the finally calculated angles $|\phi|$ may be exaggerated; only relative values of the differences between the calculated values are meaningful. The third needed ratio, K_2/K_3, which is a measure of the deviation of the molecular shape from a perfect rod, only varies between 1 and 2 and in practice only between 1.0 and 1.4; use of both limiting values will provide information about a range for the $|\phi|$'s. Alternatively, K_2/K_3 can be derived from K_1/K_3 and K_2/K_4 assuming that the stretched polymer sheet is uniaxial.

Fortunately, usually a suitable similarly shaped molecule of C_{2v} or D_{2h} symmetry can be measured and somewhat more reliable values of K_1/K_3 and K_2/K_4 derived. A comparison of values for anthracene and acridine (Table I) makes it clear that even for molecules of quite similar shape the orientation ratios can differ somewhat. A further investigation of this point shall hopefully lead to an improvement in the estimates. A specific example of the errors in $|\phi|$ resulting from such uncertainties is presented below.

If the stretched polymer can be considered uniaxial, a certain simplification is possible: eq 16 can be rewritten in terms of the basic orientation factors K_1 and K_2 as

$$\tan^2 \phi_j = [K_1 - b_j/(b_j + 2)]/[b_j/(b_j + 2) - K_2] \quad (19)$$

Now, K_1 and K_2 must be obtained from measurements on symmetrical molecules of similar shape. The factor $b/(b + 2)$ can acquire values between K_1 (for $\phi = 0°$) and K_2 (for $\phi = 90°$). Since K_1 and K_2 for symmetrical molecules are experimentally obtained from measured $d_{||}^0 = K_2/K_4$ and $(1/d_{\perp}^0) = K_1/K_3$, it is useful to rewrite eq 19 in a more direct way

$$\tan^2 \phi_j = \frac{(1/d_{\perp}^0) - b_j}{b_j - d_{||}^0} \frac{2 + d_{||}^0}{2 + (1/d_{\perp}^0)} \quad (20)$$

The procedure described so far is particularly suitable for molecules of approximately symmetrical shape, for instance aza analogs of hydrocarbons which themselves are of C_{2v} or D_{2h} symmetry.[8] Although aza substitution may destroy the symmetry of the chromophore, it barely affects the symmetry of the shape. A comparison of orientation factors for the parent hydrocarbon and suitable symmetrical polyaza analogs may allow a fairly accurate bracketing of the values for the less symmetrical aza analogs. This case seems to be of considerable theoretical interest.[9]

Another case of importance for theoretical work[9,10] is the effect of substituents on polarization of transitions in symmetrical hydrocarbons. Here the shape is usually unsymmetrical and it is not possible to find a symmetrical molecule of quite such a close shape as the derivative in question. One may of course make approximate estimates even from orientation factors of molecules whose shape differs somewhat more, but these may be less reliable.

A possible solution to the problem consists in finding a substituent of similar shape to that under investigation, which, however, interacts so weakly with the parent C_{2v} or D_{2h} chromophore that it does not affect polarization of transitions (for example, alkyl). This can be checked in some cases using polarized emission measurements. In principle, it is sufficient if polarizations of at least two bands remain unaffected by the substituent and their intensities are comparable so that they can both be recorded accurately in one spectrum. Let the deviations of these transitions from the effective orientation axis be ϕ_1 and ϕ_2; we assume that the position of the effective orientation axis can be estimated so that ϕ_1 and ϕ_2 are known. In the simplest case of a very weakly perturbed inherently symmetrical hydrocarbon all transitions are polarized at either ϕ_1 or ϕ_2 and these two directions are mutually perpendicular. Let the b values of the transitions polarized at ϕ_1 and ϕ_2 be b_1 and b_2, respectively. To determine the three ratios $K_1:K_2:K_3:K_4$, three independent equations are needed. Two are obtained from eq 15 by putting $j = 1$ and $j = 2$.

If uniaxial stretching can be assumed, relations 6 and 7 provide enough information to calculate not only the ratios but K_1 and K_2 themselves. From eq 19 for ϕ_1 and ϕ_2, and assuming $|\phi_1| \neq |\phi_2|$ and thus $b_1 \neq b_2$

$$K_1 = [b_1 \sin^2 \phi_2/(b_1 + 2) - b_2 \sin^2 \phi_1/(b_2 + 2)]/(\sin^2 \phi_2 - \sin^2 \phi_1)$$

$$K_2 = [b_1 \cos^2 \phi_2/(b_1 + 2) - b_2 \cos^2 \phi_1/(b_2 + 2)]/(\cos^2 \phi_2 - \cos^2 \phi_1) \quad (21)$$

Obviously, the results are very inaccurate when $|\phi_1|$ is close to $|\phi_2|$.

If it is not possible to assume that the stretching is uniaxial, or if an independent check is desired, the third equation may be obtained from measurements using unstretched sheet by a procedure similar to that described in part II.

Application to 10a,4a-Borazarophenanthrene

As an example of an application of our method we present data on a borazaro analog of phenanthrene (I).[11] The experimental dichroic curves were obtained by a low-temperature (77°K) modification of the technique described in part II; they are shown in Figure 2, together with sets of their linear combinations $E_{\perp}(\lambda) - d_{\perp}E_{||}(\lambda)$ and $E_{||}(\lambda) - d_{||}E_{\perp}(\lambda)$. For each of the

(8) J. Michl, *Theoret. Chim. Acta*, 15, 315 (1969).

(9) J. Koutecký, *J. Chem. Phys.*, 47, 1501 (1967).

(10) K. Nishimoto and R. Fujishiro, *Bull. Chem. Soc. Jap.*, 37, 1660 (1964); K. Nishimoto, *ibid.*, 39, 645 (1966).

(11) The origin of the sample and additional spectral measurements are described elsewhere: J. Michl and R. Jones, *Coll. Czech. Chem. Commun.*, in press.

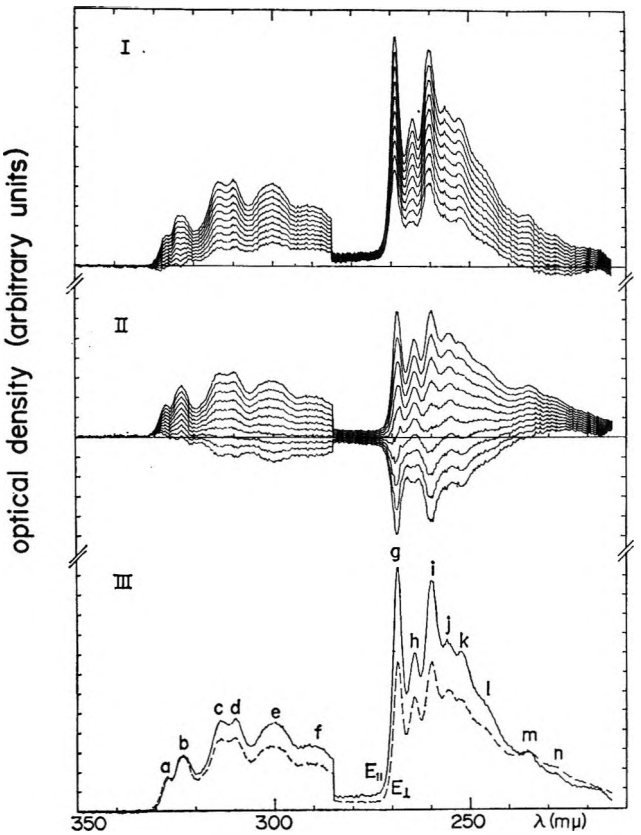

Figure 2. Dichroic spectra $E_{\perp}(\lambda)$, $E_{\parallel}(\lambda)$ of 10a,4a-borazarophenanthrene in stretched polyethylene (III) and sets of curves $E_{\perp}(\lambda) - d_{\perp}E_{\parallel}(\lambda)$ (II) and $E_{\parallel}(\lambda) - d_{\parallel}E_{\perp}(\lambda)$ (I) for $d_{\perp}$ and $d_{\parallel}$ varying from 0.1 to 1.0 in steps of 0.1. Three sheets were used in the long-wavelength part, one in the short-wavelength part.

peaks a–n the value of $d_{\perp}$ or $d_{||}$ is found for which the peak is just absent in the linear combination. These values and estimated errors are collected in Table II. The shape of peak b is different in $E_{\perp}(\lambda)$ and $E_{||}(\lambda)$, indicating that it is a composite. The resolution is insufficient to treat its components separately, however, and therefore only very crude estimates are possible. A better resolved unpolarized absorption spectrum in 3-methylpentane[11] actually shows clearly that b is a superposition of at least two peaks.

The following order is obtained for the values of $|\phi|$

$$|\phi_a| > |\phi_j| \doteq |\phi_l| > |\phi_m| = |\phi_n| > |\phi_h| > |\phi_c| = |\phi_d| > |\phi_e| = |\phi_f| > |\phi_k| \doteq |\phi_g| = |\phi_i|$$

To obtain numerical estimates for the ϕ's, assumptions about orientation ratios must now be made. The values of b shown in Table II, used in formulas 18 or 19, give results presented in columns 1–5, depending on the assumptions about orientation ratios. In columns 1 and 2, they are assumed to be the same as in phenanthrene. Since the assumption of uniaxial stretching is justified, columns 1 and 2 differ very little. In columns 3 and 4, I is assumed to orient somewhat better and somewhat worse than phenanthrene, respectively. In column 5, peaks g, i, and k are assumed to be polarized parallel to the effective orientation axis, peak a perpendicular to it.

It is seen that small uncertainties in the estimates of orientation ratios are not critical. Accuracy is worst for transitions with ϕ close to 0 or 90°. To relate the calculated angles to the molecular framework, one must make an additional assumption concerning the position of the effective orientation axis. As discussed in detail earlier,[1] it should be quite close to the z axis in formula I.

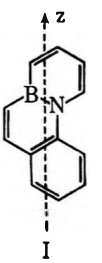

I

Table II: Deviation of Transition Moment Directions in 10a,4a-Borazarophenanthrene (I) from the Orientation Axis

Band[a]	$d_{||}(= b)$[a]	$d_{\perp}(= 1/b)$[a]	$\|\phi\|$, deg 1[b]	2[c]	3[d]	4[e]	5[f]
a	0.9 ± 0.05		60–67	61–68	66–73	54–61	(90)
b	(1.0)[g]	(1.0)[g]	(57)[g]	(58)[g]	(63)[g]	(51)[g]	(66)[g]
j	1.0 ± 0.1	1.0 ± 0.1	51–63	52–63	57–68	46–57	55–83
l	1.0 ± 0.2	1.0 ± 0.2	46–68	46–69	51–74	40–62	44–90
m, n		0.9 ± 0.1	46–57	46–58	51–63	40–51	44–66
h		0.78 ± 0.05	41–47	41–48	47–53	35–42	35–47
c, d		0.75 ± 0.05	39–46	39–46	45–51	32–40	30–44
e, f		0.70 ± 0.05	35–42	35–43	41–48	28–36	21–37
k		0.60 ± 0.05	25–35	25–35	32–41	16–28	(0)
g, i		0.60 ± 0.03	27–33	27–33	34–40	19–26	(0)

[a] See Figure 2. [b] Assuming $K_3/K_1 = 0.45$, $K_2/K_4 = 0.70$, $K_1/K_4 = 1.31$, as in phenanthrene (obtained from $E_{||}$, $E_{\perp}$, and E_0) and using eq 18. [c] Assuming $K_3/K_1 = 0.45$, $K_2/K_4 = 0.70$ as in phenanthrene, and uniaxial stretching ($K_1 = 0.52$, $K_2 = 0.26$), using eq 19. [d] Assuming $K_3/K_1 = 0.40$, $K_2/K_4 = 0.75$, but keeping $K_2/K_3 = 1.19$ as in phenanthrene, and using eq 18. [e] Assuming $K_3/K_1 = 0.50$, $K_2/K_4 = 0.65$, but keeping $K_2/K_3 = 1.19$ as in phenanthrene, and using eq 18. [f] Assuming that band a is polarized perpendicular and bands g,i,k parallel to the effective orientation axis: $K_3/K_1 = 0.6$, $K_2/K_4 = 0.9$, with $K_2/K_3 = 1.19$ as in phenanthrene, and using eq 18. [g] Uncertain values; see text.

Conclusions

The stretched sheet method allows a determination of the deviations of individual transition moments of planar molecules from the effective orientation axis, if the molecule is not round-shaped and if an estimate of the ratio of orientation factors can be made. The most favorable cases are those of molecules with an essentially symmetrical shape and an unsymmetrical chromophore, and of simple derivatives of symmetrical hydrocarbons. As more data on the relation between shape and orientation distribution of various symmetrical molecules are accumulated, applications to planar molecules of arbitrary shape should give more accurate results. At present, the errors are as much as $\pm 15°$, the major obstacle to more accurate determination of angles being the relatively low reproducibility of the orientation factors even for symmetrical hydrocarbons. In most cases this will overshadow the errors in the estimates of the exact position of the effective orientation axis.

Acknowledgments. We wish to thank Professor S. E. Rasmussen, who has kindly taken X-ray diffraction photographs of our stretched sheets, and Statens Almindelige Videnskabsfond who has given valuable economic support. We are further indebted to Dr. A. Berg and Dr. E. Clar for kind gifts of samples.

A Further Investigation of the Osmotic Properties of Hydrogen and Sodium Polystyrenesulfonates[1]

by M. Reddy and J. A. Marinsky*

Department of Chemistry, State University of New York at Buffalo, Buffalo, New York 14214 *(Received March 9, 1970)*

The instability of polystyrenesulfonic acid (HPSS) and the marked effect of its degradation, as a consequence of this instability, on osmotic measurement reliability have been carefully examined. Criteria for sample purity and appropriate methods for storage and handling of HPSS to assure such purity for meaningful osmotic study have been developed. The osmotic properties of HPSS and its sodium salt that have been measured over a large concentration range extending from approximately 0.01 to 7.5 *m* (monomer basis) by using two experimental methods, vapor pressure osmometry and isopiestic equilibration, are believed to be more reliable than previously published measurements because of this careful attention to sample purity. Although there is reasonable accord between the data compiled here and in some of the earlier studies, the osmotic properties appear to be insensitive to molecular weight to contradict the results of an earlier investigation. In addition there is almost quantitative agreement between the data compiled in this research program with many of the data that have been obtained in earlier studies for their counterpart low cross-linked gels.

Introduction

The osmotic properties of H^+ and Na^+ ion forms of polystyrenesulfonate (PSS) have been investigated over an extended concentration range by vapor pressure osmometry and by the standard isopiestic method. The objectives of this research have been (1) to provide a reexamination of earlier studies effected in this laboratory by differential osmometry[2a] and (2) to extend the concentration range of study for appropriate comparison with similar data obtained for a 0.5% cross-linked PSS gel.[2b] The sharp disagreement between the earlier measurements reported from this laboratory[2a] and those due to Ise and Okubo[3] needed to be resolved and provided reason for pursuit of the first objective. The employment of experimental procedures different from those utilized in the earlier research[2a] sought to eliminate experimental bias. Attainment of the second objective of this research program was expected to provide a meaningful consideration of the validity of the suggestion that relationships describing the physical-chemical behavior of ionized macromolecular systems are generally applicable to the corresponding cross-linked systems (ion-exchange gels) as well.[4] It has been claimed that the cross-linking of an ionized macromole-

* To whom correspondence should be addressed c/o Dr. Leo Yaffe, Chemistry Department, McGill University, Montreal, Quebec, Canada.

(1) This paper is based on a portion of a dissertation submitted by M. Reddy in partial fulfillment of the requirements of the degree of Doctor of Philosophy.

(2) (a) P. Chu and J. A. Marinsky, *J. Phys. Chem.*, 71, 4352 (1967); (b) B. Soldano and Q. V. Larson, *J. Amer. Chem. Soc.*, 77, 1331 (1955).

(3) N. Ise and T. Okubo, *J. Phys. Chem.*, 72, 1361 (1968).

(4) J. A. Marinsky in "Ion Exchange," Vol. 1, J. A. Marinsky, Ed., Marcel Dekker, New York, N. Y., 1966, Chapter 9.

cule does not alter the thermodynamic properties of the polymer unit, with some experimental verification.[5-7]

HPSS is not stable under ambient conditions and may undergo several reactions such as: chain scission,[8] desulfonation,[9] and autoxidation,[10] cross-linking, and sulfone formation.[11] The degradation of HPSS is thus as much a potential source of error to this projected program as the presence of simple electrolyte.

The presence of simple electrolyte would be expected to yield too high a value for the osmotic coefficient of a given sample, the distortion of the measurement upward being quite sensitive to the presence of simple electrolyte. The presence of such impurity in samples from a common source would be expected to mask somewhat the relative change in osmotic coefficient of the polyelectrolyte with concentration as well.

Degradation of HPSS by oxidation with the production of low molecular weight polymer fragments and the consequent lowering of the charge density of the polyelectrolyte would also be expected to produce too high an experimental osmotic coefficient. The effect of this source of impurity on the variation of osmotic property with concentration is less predictable.

Since sample degradation by slow oxidation was believed to be the major potential source of experimental difficulty in this investigation, the removal of simple electrolyte impurity having been assured by the purification techniques employed in this study, a method to preserve sample integrity in the course of the measurement program was sought successfully to facilitate the objectives of this program.

Experimental Section

Sodium polystyrenesulfonates, average molecular weight ~40,000 (Lot Number CP 522-13-118), and average molecular weight ~500,000 (Lot Number ST 475-4-87B) were kindly supplied by Dr. H. Volk and Dr. T. A. Brodof of the Dow Chemical Company, Midland, Michigan. Dialysis tubing was from Union Carbide. A Model 301 A vapor pressure osmometer (VPO) manufactured by Hewlett-Packard, Inc. and an isopiestic apparatus designed and constructed in this laboratory were employed for the osmotic coefficient measurements. A Beckman DU spectrophotometer with hydrogen lamp and photomultiplier tube and a Cary 15 spectrophotometer were used to examine the spectra of PSS samples in the uv region.

Preparation of PSS Samples. Sodium polystyrenesulfonate was first dialyzed for 24 hr to remove a large fraction of simple electrolyte impurities. Dialyzer tubing was treated[12] to remove preservatives usually contained by the tubing.[13] The polyelectrolyte solution, after dialysis, was concentrated at the ambient temperature, evaporation from the dialysis bag being facilitated by its exposure to a flow of air for 1 day. Concentration of PSS at elevated temperatures was avoided because of its instability. This product was then passed through two ion-exchange resin columns arranged in tandem to remove residual simple electrolyte and low molecular weight polyelectrolyte fragments. The first column contained Dowex-50 resin in the hydrogen form and the second column consisted of Dowex-1 resin in the hydroxide form. The HPSS product thus obtained was dialyzed for 1 week, was concentrated as before, and was frozen prior to storage.

An alternate procedure was developed for preparation of the more viscous higher molecular weight HPSS. In this method NaPSS, placed in a dialysis bag, was converted completely to HPSS during exchange dialysis with 0.1 *N* HCl. Exhaustive dialysis of this HCl–HPSS product with distilled deionized water until the diffusate was free of chloride ion produced HPSS free of simple electrolyte. The polymer solution after concentration was stored frozen.

The HPSS solutions were analyzed after preparation; HPSS (molecular weight ~40,000) had an equivalent weight of 185.4 g/equiv and extinction coefficients of 407 l. cm^{-1} $equiv^{-1}$ at 261 mμ and 10,180 l. cm^{-1} $equiv^{-1}$ at 224 mμ. HPSS (molecular weight ~500,000) had an equivalent weight of 186.5 g/equiv and extinction coefficients of 388 l. cm^{-1} $equiv^{-1}$ at 261 mμ and 10,210 l. cm^{-1} $equiv^{-1}$ at 224 mμ.

The exhaustive dialysis method was also used to prepare the NaPSS solutions. The NaPSS (molecular weight ~500,000) solution was analyzed after preparation and was found to have an equivalent weight of 210 g/equiv and extinction coefficients of 396 l. cm^{-1} $equiv^{-1}$ at 261 mμ and 9980 l. cm^{-1} $equiv^{-1}$ at 224 mμ. NaPSS (molecular weight ~40,000) had an equivalent weight of 206 g/equiv and extinction coefficients of 402 l. cm^{-1} $equiv^{-1}$ at 261 mμ and 9910 l. cm^{-1} $equiv^{-1}$ at 224 mμ.

The HPSS prepared by both methods was colorless. By storing it frozen, an HPSS inventory could be maintained for months without encountering any noticeable deterioration of the product. Its rather rapid deterioration, as evidenced by the appearance of amber color in the solution which progressively intensifies with standing at the ambient temperature, required prompt utilization of the HPSS in the osmotic studies once it was sampled for study. The NaPSS is a much more stable

(5) G. E. Boyd and B. Soldano, *Z. Elektrochem.*, **57**, 162 (1953).

(6) E. Glueckauf, *Proc. Roy. Soc., Ser. A*, **214**, 207 (1952).

(7) A. Chatterjee and J. A. Marinsky, *J. Phys. Chem.*, **67**, 41 (1963).

(8) R. B. Hodgdon, Jr., *J. Polym. Sci., Part A-1*, **6**, 171 (1968).

(9) H. Cerfontain, "Mechanistic Aspects in Aromatic Sulfonation and Desulfonation," Interscience, New York, N. Y., 1968, Chapter 12.

(10) T. A. Brodof, Dow Chemical Company, Midland, Mich., private communication, 1968.

(11) H. H. Roth, *Ind. Eng. Chem.*, **49**, 1820 (1957).

(12) D. S. Olander and A. Holtzer, *J. Amer. Chem. Soc.*, **90**, 4549 (1968).

(13) L. C. Craig in "Advances in Analytical Chemistry and Instrumentation," Vol. 4, C. N. Reilley, Ed., Interscience, New York, N. Y., 1965, p 41.

product and could be stored at 0 to 5° for an extended period prior to its utilization.

Sample Purity. Two principal absorption maxima in the ultraviolet region (224 and 261 mμ) characterize the PSS. The peak at 224 mμ is unaffected by degradation of the polyelectrolyte whereas the molar extinction coefficient of the absorption maximum at 261 mμ increases with sample deterioration. Spectroscopic examination of PSS using this criterion was employed periodically to substantiate sample purity. In the more dilute polyelectrolyte systems the amber color of degraded product is difficult to detect visually

Osmotic Coefficient Measurements. The Mechrolab VPO is a commercial model of the thermoelectric osmometer of Brady, Huff, and McBain.[14] A description of this instrument detailing the principles and mode of its operation and the scope of its utilization has been presented by Burge.[15]

Recently, Boyd,[16] *et al.*, have used a vapor pressure osmometer to determine osmotic coefficients of aqueous solutions of *p*-ethylbenzenesulfonic acid and its alkali metal salts.

In the experiments performed in this laboratory both KCl and sucrose were used as calibration standards. An all-glass syringe and a Kel-F stainless steel needle were eventually used to hold samples before measurement to eliminate the possibility of sample contamination arising from interaction of polyelectrolyte with the metal fittings of the standard syringe assembly provided with the instrument. The conveniently small sample volume (0.5 ml) of the glass syringe was an additional advantage.

The calibration constant of the instrument, K, determined by measuring the difference in resistance, ΔR, between two thermistor beads that originates from the difference in temperature arising from the unequal vapor pressure of solutions of known water activity placed on the thermistor beads was computed with eq 1

$$K = \Delta R/m\nu\phi \qquad (1)$$

where m is the molal concentration of the standard solution, ν is the number of particles produced when one molecule of the reference standard dissolves, and ϕ is the published practical osmotic coefficient corresponding to the experimental molality of the reference standard. Measurement of ΔR values effected by differences in vapor pressure between reference solution and the different polyelectrolyte samples for employment in eq 1 then yielded the practical osmotic coefficient of polyelectrolyte samples under investigation. In the case of polyelectrolyte m was expressed on a monomer basis to make ν correspond to unity. The precision of ΔR measurements was enhanced by repetitive measurements.

Use of the Mechrolab VPO was restricted to HPSS (molecular weight ~40,000) at concentrations no greater than 1.5 m. Higher concentration values could not be employed because of the sizeable viscosity of such samples. Osmotic study with this instrument of the higher molecular weight HPSS above a concentration value of 0.9 m was inpracticable for the same reason.

The essential requirements for a highly efficient isopiestic apparatus that have been listed by Scatchard[17] were incorporated into the system designed and constructed in this laboratory. The isopiestic chamber was a truncated 500-ml freeze dry flask. Its interior and the outer upper portion were silvered. An electrodeless nickel-plated copper disk (7.40 cm in diameter and 1.3 cm thick) with six 0.6-cm deep circular depressions symmetrically arranged to hold the gold-plated silver sample cups (1.7 cm in diameter and 2.0 cm deep) was machined to fit securely in the bottom of the chamber. The chamber, spring mounted on an electric vibrating motor with adjustable speeds, was placed in a water-tight Plexiglas compartment which was sealed to a second similar compartment that held the motor firmly secured to a steel plate base (Figures 1 and 2). The two compartments were submerged in a constant temperature bath fitted with a Plexiglas cover and insulated on all sides. Operation of the vibrating motor produced extremely efficient agitation of the samples. The complete assembly was in a temperature-controlled air-conditioned room. Compressed air used to agitate the bath water was released directly below a 125-W blade heater. The compressed air forced bath water first to contact the heater and then a proportional temperature controller probe manufactured by the Yellow Springs Instrument Company, Inc. (YS1-Model

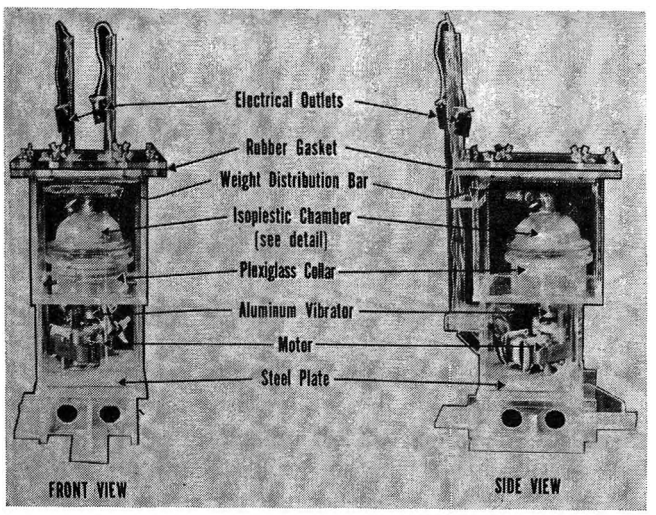

Figure 1. Isopiestic chamber and Plexiglas container.

(14) A. P. Brady, H. Huff, and J. W. McBain, *J. Phys. Colloid Chem.*, **55**, 304 (1951).

(15) D. E. Burge, *J. Phys. Chem.*, **67**, 2590 (1963).

(16) G. E. Boyd, F. Vaslow, A. Schwarz, and J. W. Chase, *ibid.*, **71**, 3879 (1967).

(17) G. Scatchard, W. J. Hamer, and S. E. Wood, *J. Amer. Chem. Soc.*, **60**, 3061 (1938).

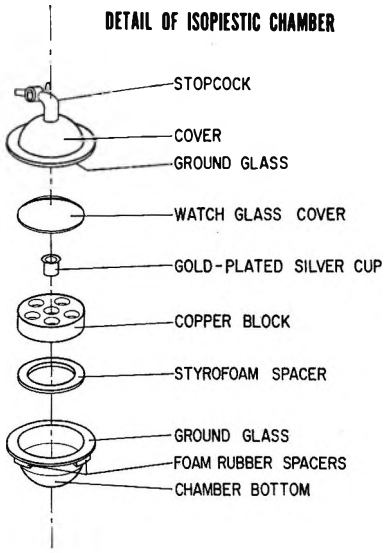

Figure 2. Isopiestic chamber.

72). This arrangement was shown to provide excellent temperature stability (±0.003°) by continuous monitoring with a quartz thermometer (Model 2801 A-Dymec) in connection with a digital to analog converter and a strip chart recorder. With this procedure the temperature of the bath was displayed as an absolute centigrade value to the nearest 10^{-4} deg over the operation interval.

Isopiestic equilibrations were performed using the procedures described by Robinson and Stokes.[18] In all experiments the reference isopiestic salt was reagent grade KCl dried at 110° and stored over P_2O_5. The polyelectrolyte solutions were brought to the starting concentration by freeze drying. At the beginning of an equilibration the isopiestic chamber was evacuated to the vapor pressure of water at 25°.

Isopiestic experiments were performed with reference solutions ranging from 0.2 *m* to saturated KCl. Equilibration attainment was verified by repeated experiments at fixed concentrations.

Results

Sample Purity. Degraded HPSS samples, prepared by allowing the solutions to become distinctly amber colored during storage in tightly capped bottles at various temperatures above their freezing point and in one instance by concentrating rapidly at ~100°, were studied spectroscopically for comparison with the highly purified colorless source material and *p*-toluenesulfonic acid. Representative results of this study are presented in Table I. There are two absorption peaks in the ultraviolet region which characterize the spectra of all the HPSS samples. They occur at very nearly the same wavelength at which maxima are observed for the *p*-toluenesulfonic acid. The absorption maxima at 224 and at 261 mμ correspond to the maxima observed with a concentrated effluent wash solution from cross-linked polystyrenesulfonate ion exchangers collected in this laboratory. The 224-mμ peak characterizing such wash effluent had been reported earlier.[19]

Table I: A Comparison of Uv Absorption Maxima and Extinction Coefficients for Toluenesulfonic Acid and Various Polystyrenesulfonic Acid Samples[a]

	Wavelength of absorption max	Extinction coefficient at absorption max	Wavelength of absorption max	Extinction coefficient at absorption max
Toluenesulfonic acid	260.5	377	221	10,700
Polystyrenesulfonic acid (PSSA) [B5 P80]	261	534	224	10,200
PSSA [B5 P82-M138]	261	442	224	10,150
PSSA [B5 P82-M142]	261	443	224	10,400
PSSA [B5 P84-M024]	261	427	224	10,000
PSSA [B5 P86 I]	261	509	224	10,250
PSSA [B5 P86 II]	261	552	224	10,130
PSSA [B5 P99]	261	432	224	10,120
PSSA [B6 P9]	261	506	224	9,900

[a] All measurements were made using a Beckman DU photometer with a hydrogen lamp and photomultiplier tube. The samples were contained in quartz cells (path lengths of 1.0 and 0.1 cm were used). The values given above are the average values obtained from a minimum of three measurements at different concentrations. Wavelength is given in mμ and extinction coefficient is expressed as l. cm^{-1} $equiv^{-1}$.

The extinction coefficient at 224 mμ is much less affected by HPSS degradation than at 261 mμ. The marked increase in its value at this wavelength is, we believe, an indication of HPSS deterioration. Evidence for HPSS deterioration has been presented in the literature[11,20,21] and may arise from sulfone formation,[11,20,21] chain scission,[8] or desulfonation.[9] Experimental results listed in Table I can be reasonably rationalized with the assumption that the increased absorption at 261 mμ reflects degradation of HPSS. The magnitude of the absorption coefficient at 261 mμ appears to be a good semiquantitative test for sample purity.

The effect of sample degradation on the osmotic properties of HPSS is very dramatically demonstrated in Figure 3 where a purified source sample (ϵ_{261} 407) (the lower curve) is compared with one of the degraded samples (ϵ_{261} 506). The osmotic coefficients are considerably elevated in the degraded sample over the entire concentration range studied. The change in osmotic coefficient with sample concentration is not, however, appreciably affected. Spectroscopic examinations

(18) R. A. Robinson and R. H. Stokes, "Electrolyte Solutions," 2nd ed, rev, Butterworths, London, 1959, pp 177–180.

(19) G. E. Boyd and K. Bunzl, *J. Amer. Chem. Soc.*, **89**, 1776 (1967).

(20) H. H. Roth, *Ind. Eng. Chem.*, **46**, 2435 (1954).

(21) J. A. V. Butler, A. B. Robins, and K. V. Shooter, *Proc. Roy. Soc., Ser. A*, **241**, 299 (1957).

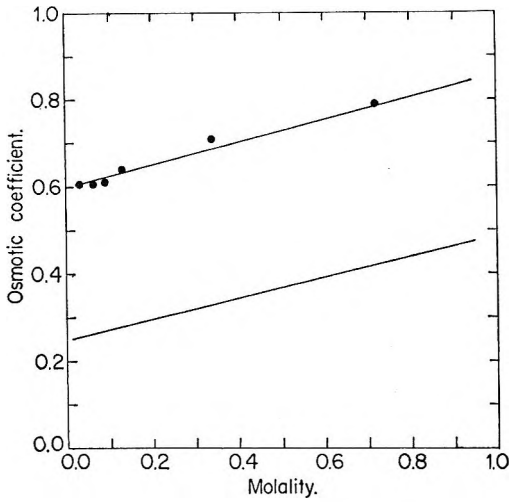

Figure 3. Concentration dependence of the molal osmotic coefficient, ϕ, for degraded (upper curve) and pure (lower curve) polystyrenesulfonic acid.

of HPSS samples thus provide a useful analytical criterion of sample purity for meaningful study of the osmotic properties of this polyelectrolyte. It was experimentally determined that HPSS samples could be stored frozen for months without noticeable degradation, thereby assuring the validity of the osmotic measurements performed in this experimental program.

Calibration of Vapor Pressure Osmometer. Representative data that were obtained with the Mechrolab VPO during its periodic calibration in the course of continuing osmotic studies are presented in Table II.

Osmotic Coefficient Data. The osmotic coefficient data obtained with vapor pressure osmometry for HPSS (mol wt 40,000 and 500,000) over the concentration range 0.01 to 1.4 m and for NaPSS (mol wt 40,000 and 500,000) over the concentration range 0.07 to 0.6 m are represented by eq 2.

$$\phi = 0.24m + 0.24 \qquad (2)$$

Table II: Determination of the Mechrolab Osmometer Calibration Constant K

A. Calibration with Sucrose

$\overline{\Delta R}$	m	$m\nu\phi$	K	
1.84	0.0259	0.0260	71.04	
5.08	0.0727	0.0731	69.88	
6.91	0.0983	0.0991	70.30	
				$\bar{K} = 70.41$

B. Calibration with Potassium Chloride

$\overline{\Delta R}$	m	$m\nu\phi$	K	
3.74	0.0273	0.0521	71.81	
4.73	0.0347	0.0658	71.90	
14.67	0.1155	0.216	68.64	
18.39	0.1431	0.264	69.76	
27.29	0.2125	0.388	70.37	$\bar{K} = 70.49$

Results of isopiestic measurements of HPSS and NaPSS osmotic coefficients are given in Tables III–VI. The osmotic coefficient data for both NaPSS and HPSS are in reasonable accord in the region of overlap for the two methods of measurement, thus indicating absence of experimental bias. In addition, the osmotic coefficients of HPSS and NaPSS appear to be insensitive to polyanion molecular weight and temperature within the precision of the measurement.

Discussion

The osmotic data presented in the preceding section for polystyrenesulfonate solutions extend over a larger useful concentration range than has been examined by earlier investigators. As a consequence, the objectives of this program, comparison of these results with (1)

Table III: Isopiestic Measurements of HPSS (Mol Wt 40,000) at 25°

m_{HPSS}, monomol/1000 g of H_2O	m_{KCl}, mol/1000 g of H_2O	ϕ_{HPSS}
0.959	0.224	0.43
0.983	0.229	0.42
1.503	0.504	0.60
1.504	0.495	0.59
2.89	1.501	0.94
3.56	2.018	1.03
4.29	2.66	1.15
4.33	2.74	1.18
4.37	2.84	1.21
4.88	3.49	1.36
5.01	3.59	1.37

Table IV: Isopiestic Measurements of HPSS (Mol Wt 500,000) at 25°

m_{HPSS}, monomol/1000 g of H_2O	m_{KCl}, mol/1000 g of H_2O	ϕ
1.020	0.224	0.40
1.042	0.229	0.40
1.516	0.504	0.60
1.524	0.495	0.58
2.90	1.501	0.93
3.01	1.442	0.88
3.03	1.453	0.89
3.08	1.480	0.90
3.58	2.02	1.03
3.99	2.43	1.12
4.02	2.46	1.10
4.29	2.66	1.15
4.34	2.74	1.17
4.39	2.84	1.20
4.88	3.49	1.36
5.02	3.51	1.34
5.05	3.59	1.36
5.51	4.03	1.41
5.53	4.07	1.42
5.58	4.12	1.43

Table V: Isopiestic Measurements of NaPSS (Mol Wt 40,000) at 25°

m_{NaPSS}, monomol/1000 g of H_2O	m_{KCl}, mol/1000 g of H_2O	ϕ_{NaPSS}
0.801	0.1749	0.40
1.264	0.328	0.47
1.630	0.470	0.52
2.047	0.643	0.56
2.637	0.888	0.60
3.070	1.074	0.63

Table VI: Isopiestic Measurements of NaPSS (Mol Wt 500,000) at 25°

m_{NaPSS}, monomol/1000 g of H_2O	m_{KCl}, mol/1000 g of H_2O	ϕ_{NaPSS}
0.799	0.1749	0.40
1.256	0.328	0.47
1.620	0.470	0.52
2.042	0.643	0.57
2.640	0.888	0.60
3.064	1.074	0.63
3.962	1.501	0.68
5.195	2.018	0.71
6.394	2.738	0.80
6.599	2.837	0.80
7.541	3.590	0.91

those of earlier studies of the linear polyelectrolyte and (2) its low cross-linked analog, has been facilitated. More attention is believed to have been given to sample preparation and purity than in earlier published studies as well to justify criticism of some of the earlier work.

Data that are available for HPSS and NaPSS from this study and the literature in the low and intermediate concentration range are presented graphically in Figures 4 and 5. The lowest lines in Figures 4 and 5 represent data compiled by Chu and Marinsky[2a] using differential osmometry. The next lowest curve in each figure is a representation of the data obtained in this research program while the third curve tangent to curve 2 in Figure 4 is based on data obtained from freezing point lowering measurements reported by Waxman, Sundheim, and Gregor.[22] The highest curves in Figures 4 and 5 are obtained from isopiestic studies of Ise and Okubo[3] and deviate remarkably from the others.

There is good agreement between this research and that of Waxman, *et al.* The increasing discrepancy between the data with increasing molality can be explained reasonably by a difference in charge density between the HPSS samples employed. If sulfonation of the Waxman, *et al.*, HPSS product was somewhat less than in the HPSS samples used in this research, one would expect the above result.

There is some discrepancy between the data obtained

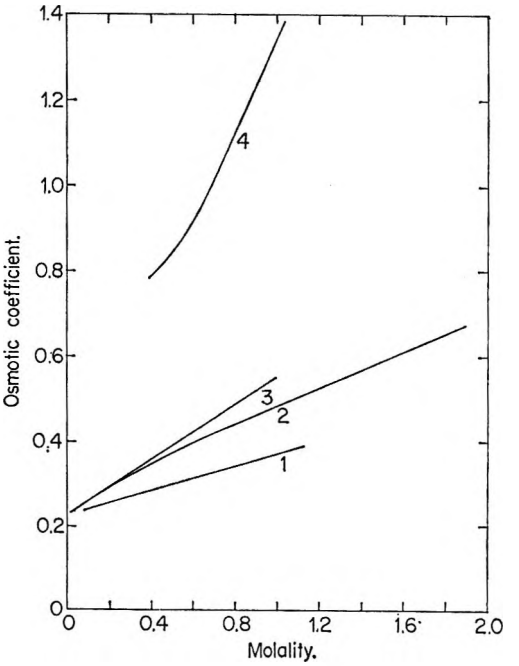

Figure 4. Comparison of the concentration dependence of the molal osmotic coefficient, ϕ, for polystyrenesulfonic acid at intermediate concentrations with published data (curve 1 ref 1, curve 2 this study, curve 3 ref 22, and curve 4 ref 3).

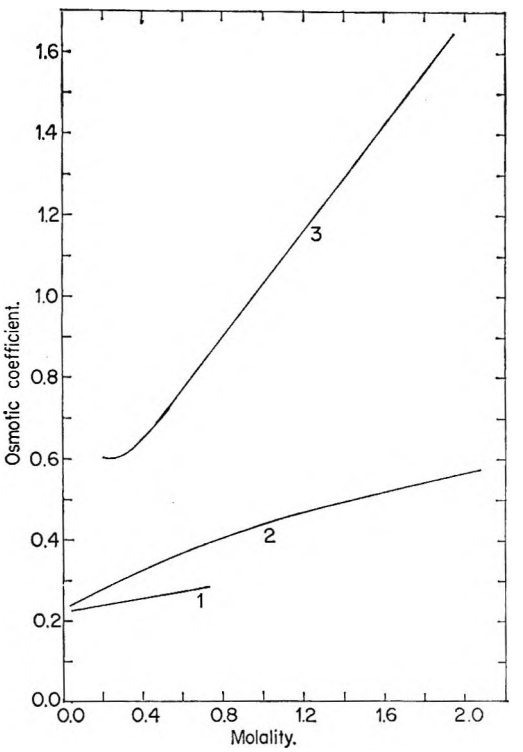

Figure 5. Comparison of the concentration dependence of the molal osmotic coefficient, ϕ, for sodium polystyrenesulfonate at intermediate concentrations with published data (curve 1 ref 1, curve 2 this study, and curve 3 ref 3).

(22) M. H. Waxman, B. R. Sundheim, and H. P. Gregor, *J. Phys. Chem.*, **57**, 969 (1953).

in this study and the data compiled by Chu and Marinsky using differential osmometry. Experiments were conducted to examine more closely the reliability of the differential osmometry method, and the slightly lower values of the earlier study were demonstrated to be an artifact of the method of measurement employed. The differential osmometry technique employed by these researchers, although based on fundamentally sound principles, yielded low results. This failure has been attributed to the small permeability of the membrane that was employed to the polyethylene glycol reference solution. This deviation from ideality of the membrane was expected by Chu and Marinsky to have a negligible influence on the measurement.

The anomalous behavior of Ise and Okubo's data may be attributable to improper attention having been given to the preparation of their HPSS samples. In the study of the effect of sample impurity on osmotic measurements that was conducted in this investigation it was shown that degraded samples yielded results similar to those reported by Ise and Okubo (see Figure 3) to strongly suggest this possibility as the source of their conflicting observations. Since all of the salt forms of the PSS employed by Ise and Okubo were converted from the H^+ form by neutralization with standard alkali, the osmotic data due to these investigators for the Na^+ and other salt forms of HPSS are believed to be in error as well and need to be disregarded.

A second compelling reason for strongly questioning their results originates in the osmotic data that are reported for barium polystyrenesulfonate over a concentration range, on a monomer basis, from 0.242 to 3.45 *m*.

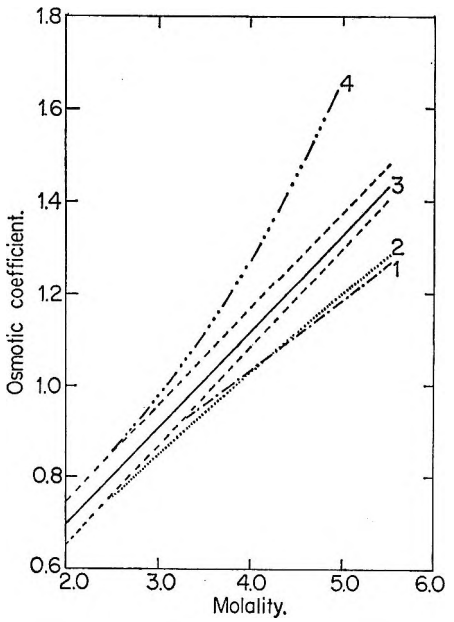

Figure 6. Comparison of the concentration dependence of the molal osmotic coefficient, ϕ, for polystyrenesulfonic acid at high concentrations with published data (curves 1 and 2 ref 23, curve 3 this study, the area within the dashed lines bordering curve 3 ref 23, 2, and 24, and curve 4 ref 25).

It is difficult to rationalize this with the solubility behavior of this salt form of HPSS at 25°. Barium polystyrenesulfonate has been reported to be insoluble.[22] Its solubility at 25° has been measured in this laboratory as well and it lies far below the concentration values reported for this salt by Ise and Okubo. The low charge density product of degraded PSS could account for the observed solubility of their $Ba(PSS)_2$.

The osmotic coefficient data available for HPSS and the corresponding low cross-linked (DVB) gels at more elevated concentrations are presented in Figure 6 together with the data (curve 3) that were obtained in this investigation. The data obtained by Bonner and Overton[23] for low molecular weight HPSS and the H^+ ion form of Dowex 50, by Soldano and Larson[2] for <0.5% cross-linked (DVB) HPSS, and by Sundheim, Waxman, and Gregor[24] for 0.4% cross-linked (DVB) HPSS lie within the two dashed lines on either side of curve 3 and are in closest agreement with the results of this study. The osmotic coefficients obtained for the higher molecular weight HPSS (curves 1 and 2) by Bonner and Overton[23] increase more slowly with concentration than those determined in this program, while the osmotic behavior of 0.5% cross-linked (DVB) HPSS observed by Myers and Boyd[25] (curve 4) indicate a more rapid increase of the osmotic coefficient with the concentration of the gel.

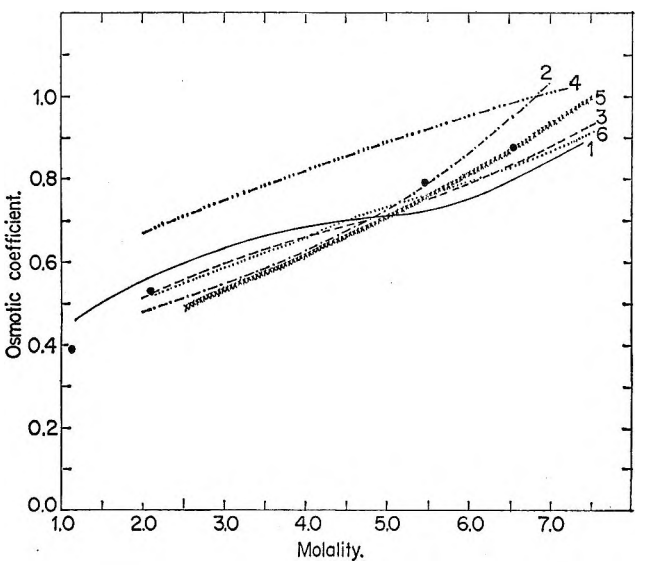

Figure 7. Comparison of the concentration dependence of the molal osmotic coefficient, ϕ, for sodium polystyrenesulfonate at high concentrations with published data using NaPSS with different molecular weights or cross-linkages (curve 1 mol wt 40,000 and 500,000 this study, curve 2 mol wt 10,000 ref 23, curve 3 mol wt 70,000 ref 23, curve 4 mol wt 400,000 ref 23, curve 5 Dowex 50 X-1 ref 23, curve 6 < 0.5% cross-linked (wt % DVB) ref 2, and ● 0.4% cross-linked (wt % DVB) ref 24.

(23) O. D. Bonner and J. R. Overton, *J. Phys. Chem.*, **67**, 1035 (1963).
(24) B. R. Sundheim, M. H. Waxman, and H. P. Gregor, *ibid.*, **57**, 974 (1953).
(25) G. E. Myers and G. E. Boyd, *ibid.*, **60**, 521 (1956).

A comparison of the data compiled for NaPSS in Figure 7 shows that the osmotic measurements with NaPSS (molecular weight ~70,000) and with the Na^+ ion form of Dowex-50 X-1 by Bonner and Overton (curves 3 and 5) and with the 0.4 and the < 0.5% cross-linked (DVB) NaPSS by Gregor, *et al.*,[24] and by Soldano and Larson[2] (circles and curve 6) are in closest agreement with the results obtained in this research program. The Bonner–Overton data do in the first instance yield an S-shaped curve similar to but less exaggerated than is obtained in this investigation.

The osmotic data obtained by Bonner and Overton[23] for HPSS (molecular weight 70,000 and 400,000) deviate from the results presented in this study, although these two sets of data are parallel. The sensitivity of osmotic properties to molecular weight observed by Bonner and Overton with other ion forms of PSS (Na^+ and Li^+) as well led to their conclusion that this eolligative property of polystyrenesulfonates was a function of molecular weight. This observation, however, is contrary to experimentally and theoretically based conclusions that have received general acceptance.[26]

The almost quantitative agreement between the osmotic coefficient data for HPSS that have been compiled in this investigation and a large proportion of the data obtained for their counterpart low cross-linked gels together with the observation that molecular weight is unimportant support the validity of the concept that relationships describing the physicochemical behavior of ionized linear macromolecular systems are generally applicable to their cross-linked ion-exchange gel analogs.

Acknowledgment. The authors wish to express their appreciation to Dr. H. Volk and Dr. T. A. Brodof of Dow Chemical Company for supplying sodium polystyrenesulfonate and to the United States Atomic Energy Commission for financial support through Contract No. AT(30-1)-2269.

(26) S. A. Rice and M. Nagasawa, "Polyelectrolyte Solutions," Academic Press, New York, N. Y., 1961.

Osmotic Properties of Divalent Metal Polystyrenesulfonates in Aqueous Solution[1]

by M. Reddy, J. A. Marinsky,* and A. Sarkar

Department of Chemistry, State University of New York at Buffalo, Buffalo, New York 14214 *(Received April 21, 1970)*

Molal osmotic coefficients of aqueous solutions of divalent polystyrenesulfonates have been measured over a large concentration range using two experimental methods: vapor pressure osmometry and isopiestic equilibration. The osmotic coefficients of the divalent polystyrenesulfonates (Mg^{2+}, Ca^{2+}, Sr^{2+}, Co^{2+}, Ni^{2+}, Zn^{2+}, and Cd^{2+}) were practically independent of concentration in the low concentration region (0.04 to 0.5 *m*); at higher concentrations the osmotic coefficients increased rapidly with concentration, eventually becoming greater than unity. The osmotic coefficient of zinc polystyrenesulfonate increased most rapidly with concentration while that for strontium polystyrenesulfonate increased most slowly. The osmotic coefficients at low concentrations are in agreement with theoretically based predictions. At high concentrations the osmotic behavior is remarkably similar to that exhibited by the divalent metal perchlorates over the same concentration range. A most interesting and important observation is the equivalent osmotic properties of the cross-linked polystyrenesulfonate ion-exchange resin and its linear polyelectrolyte analog.

Introduction

In this research program a systematic study of the osmotic coefficients of seven counterion forms of polystyrenesulfonate (Mg^{2+}, Ca^{2+}, Sr^{2+}, Co^{2+}, Ni^{2+}, Zn^{2+}, and Cd^{2+}) was undertaken to extend earlier studies of polyion–monovalent counterion interaction.[2] The aims of this program were threefold: (1) to determine the osmotic coefficients of polystyrenesulfonate as a function of divalent counterion identity and concentration; (2) to examine the validity of theoretically based predictions of the osmotic properties of divalent salts of

* To whom correspondence should be addressed c/o Dr. Leo Yaffe, Chemistry Department, McGill University, Montreal, Quebec, Canada.

(1) This paper is based on a portion of a dissertation submitted by M. Reddy in partial fulfillment of the requirements of the degree of Doctor of Philosophy.

polystyrenesulfonic acid; and (3) to test the hypothesis that linear divalent polystyrenesulfonates are suitable model compounds for their cross-linked polystyrenesulfonate ion-exchange resin counterparts in the divalent ion form.

Knowledge of the physical and chemical properties of polyelectrolyte solutions has evolved primarily from experimental and theoretical studies conducted during the past 20 years.[2-6] For example, Kern[7,8] Nagasawa, and coworkers,[4] and Alexandrowics[5,6] have measured the osmotic coefficients of several polyelectrolytes. Their results as well as those of others[3] indicate that the polyelectrolyte osmotic coefficient is one of the most useful parameters for describing the properties of polyelectrolyte solutions. Unfortunately, almost all osmotic coefficient measurements of polyelectrolytes have been obtained with their univalent counterion forms over a limited concentration range. Theoretical examination has been essentially confined, as a consequence, to these systems.

Katchalsky[3] has pointed out that for polyelectrolytes with monovalent counterions the osmotic coefficient of the polyelectrolyte does not seem to be sensitive either to the chemical nature of the polymeric charged group or to the counterion. Proton magnetic resonance[9] and Raman[10] investigations indicate that polystyrenesulfonic acid is completely dissociated in aqueous solution. Osmotic coefficient measurements and theoretical calculations have shown that the simple monovalent cations Li^+, Na^+, and K^+ behave similarly to H^+ in dilute polystyrenesulfonate solutions.[11] For polyelectrolytes with divalent counterions, the osmotic coefficient may be strongly influenced by the nature of the repeating functional unit of the polyelectrolyte. For example, weakly acidic functional units have been shown to complex divalent ions as a function of solution pH[12-16] and to give rise to divalent ion–polyanion precipitates.[17-20] Specific ion-binding, however, is not a general phenomenon in polyelectrolyte solutions and may be unimportant in many divalent polyelectrolyte solutions. Recent measurements have shown a smooth increase in volume changes (in the series Li^+, Na^+, K^+, Mg^{2+}, Ca^{2+}) accompanying the interactions between polyelectrolytes containing sulfonate groups and alkali and alkaline earth metal ions.[21] This suggests that specific ion-binding and ion-association of divalent counterions are not appreciable in polystyrenesulfonate solutions. Furthermore, the "single ion" activity coefficients of the salt-free solutions of divalent and univalent counterion forms of polyelectrolytes show a similar concentration dependence.[22,23]

Experimental Section

Distilled deionized water was used in all experiments. All chemicals, except where indicated, were reagent grade. Sodium polystyrenesulfonate of average molecular weight 40,000 (Lot CP 522-13-118) was kindly supplied by Dr. T. A. Brodof of the Dow Chemical Co., Midland, Mich. All polymer solutions were prepared and stored in polyethylene vessels.

Polystyrenesulfonic acid, used in the preparation of the divalent polystyrenesulfonates, was obtained by the methods described earlier.[24] Equivalent weight and uv extinction coefficients for this material have been reported.[24]

Magnesium, calcium, strontium, cobalt, and nickel polystyrenesulfonates were prepared by treating the freshly dialyzed, colorless polystyrenesulfonic acid with the appropriate divalent carbonate until the pH of the solution exceeded 5.0. Nonreacted carbonate was filtered from solution using a Millipore filter. The concentrations of the divalent salts were determined from the initial concentration of the polystyrenesulfonic acid used in their preparation. The concentrations were checked by complexometric titrations.[25] The exchange dialysis method[24] was used to prepare calcium, strontium, zinc, and cadmium polystyrenesulfonates and the concentrations of these salts were determined by complexometric titration.[25]

(2) S. A. Rice and M. Nagasawa, "Polyelectrolyte Solutions," Academic Press, New York, N. Y., 1961.

(3) A. Katchalsky, Z. Alexandrowicz, and O. Kedem in "Chemical Physics of Ionic Solutions," B. E. Conway and R. G. Barradas, Ed., Wiley, New York, N. Y., 1966, pp 295–346.

(4) (a) M. Nagasawa and I. Kagawa, *J. Polym. Sci.*, **25**, 61 (1957); (b) A. Takahashi, N. Kato, and M. Nagasawa, *J. Phys. Chem.*, **74**, 944 (1970).

(5) Z. Alexandrowicz, *J. Polym. Sci.*, **40**, 91 (1959).

(6) Z. Alexandrowicz, *ibid.*, **43**, 337 (1960).

(7) W. Kern, *Z. Phys. Chem., Abt.*, **181**, 249 (1938).

(8) W. Kern, *ibid.*, **184**, 197 (1939).

(9) L. Kotin and M. Nagasawa, *J. Amer. Chem. Soc.*, **83**, 1026 (1961).

(10) S. Lapanje and S. A. Rice, *ibid.*, **83**, 496 (1961).

(11) P. Chu and J. A. Marinsky, *J. Phys. Chem.*, **71**, 4352 (1967).

(12) H. P. Gregor, L. B. Luttinger, and E. M. Loebl, *ibid.*, **59**, 34 (1955).

(13) A. M. Kotliar and H. Morawetz, *J. Amer. Chem. Soc.*, **77**, 3692 (1955).

(14) M. Mandel and J. C. Leyte, *J. Polym. Sci.*, **56**, S23 (1962).

(15) J. C. Leyte, *Kolloid-Z. Z. Polym.*, **212**, 168 (1966).

(16) J. C. Leyte, L. H. Zuiderweg, and M. van Reisen, *J. Phys. Chem.*, **72**, 1127 (1968).

(17) L. Costantino, V. Crescenzi, F. Quadrifoglio, and V. Vitagliano, *J. Polym. Sci., Part A-2*, **5**, 771 (1967).

(18) M. Mandel and A. Jenard, *Trans. Faraday Soc.*, **59**, 2170 (1963).

(19) A. Ikegami and N. Imai, *J. Polym. Sci.*, **56**, 133 (1962).

(20) A. Shatkay and I. Michaeli, *J. Polym. Sci., Part A-2*, **5**, 1055 (1967).

(21) U. P. Strauss and Y. P. Leung, *J. Amer. Chem. Soc.*, **87**, 1476 (1965).

(22) J. W. Lyons and L. Kotin, *ibid.*, **87**, 1670 (1965).

(23) S. Oman and D. Dolar, *Z. Phys. Chem. (Frankfurt am Main)*, **56**, 13 (1967).

(24) M. M. Reddy and J. A. Marinsky, *J. Phys. Chem.*, **74**, 3884 (1970).

(25) G. Schwarzenbach, "Complexometric Titrations," H. Irving, Ed., Interscience, New York, N. Y., 1957.

Table I: Osmotic Coefficients of Divalent Polystyrenesulfonates for Interpolated Molalities

	ϕ						
m	$Mg(PSS)_2$	$Ca(PSS)_2$	$Sr(PSS)_2$	$Co(PSS)_2$	$Ni(PSS)_2$	$Zn(PSS)_2$	$Cd(PPS)_2$
0.05		0.11	0.11	0.15	0.17	0.12	0.12
0.10		0.11	0.11	0.15	0.17	0.12	0.12
0.20		0.11	0.11	0.16	0.17	0.12	0.12
0.30	0.17	0.12	0.11	0.17	0.18	0.12	0.13
0.40	0.18	0.12	0.11	0.19	0.19	0.14	0.14
0.50	0.19	0.14	0.11	0.22	0.21	0.16	0.15
0.60	0.20	0.16	0.11	0.26	0.24	0.20	0.18
0.70		0.18	0.12	0.31	0.28	0.24	0.21
0.80		0.21	0.14	0.37	0.34	0.29	0.26
0.90		0.24	0.16	0.43	0.40	0.35	0.31
1.00		0.28	0.18	0.50	0.46	0.42	0.37
1.20		0.35	0.24	0.66	0.62	0.57	0.50
1.40		0.45	0.31	0.83	0.78	0.74	0.64
1.60		0.55	0.40	1.02	0.96	0.92	0.77
1.80		0.66	0.48	1.21	1.15	1.10	0.90
2.00		0.78	0.57	1.41	1.35	1.29	1.04
2.50		1.06	0.88	1.76	1.87	1.74	1.42
3.00		1.34	1.00			2.34	1.81
3.50		1.62	1.22			2.94	2.20
4.00		1.88	1.44			3.60	2.59
4.50		2.14	1.66			4.32	3.06
5.00		2.40	1.86				3.35
5.50		2.66	2.07				3.68
6.00		2.92	2.27				4.05
6.50		3.18	2.48				
7.00			2.69				

Osmotic coefficient measurements were obtained using two techniques: vapor pressure osmometry and isopiestic equilibration. The deviation of individual osmotic coefficient measurements from a best fit curve of the experimental data was usually less than 3%. At low concentrations the deviation increased to 10%. A description of the experimental procedure employed in this study has been given elsewhere.[24]

Results

Osmotic coefficients for seven divalent polystyrenesulfonates, obtained using vapor pressure osmometry (at 37°) and isopiestic equilibration (at 25°), are listed in Table I. Values of the osmotic coefficients at rounded concentrations were determined by interpolation from experimental data. Potassium chloride, the reference solute in vapor pressure osmometry and most isopiestic experiments, could not be used as reference solute in experiments at the highest polyelectrolyte concentrations because of its limited solubility. Lithium chloride served as reference solute for isopiestic experiments in these cases.

The osmotic coefficients in Table I are shown to be constant at low concentration and increase rapidly at high concentration. This behavior is depicted in Figure 1 for the osmotic coefficients of HPSS, $Sr(PSS)_2$, $Ca(PSS)_2$, $Zn(PSS)_2$, and $Cd(PSS)_2$. The osmotic coefficients of $Co(PSS)_2$ and $Ni(PSS)_2$ are practically the same as those for $Zn(PSS)_2$.

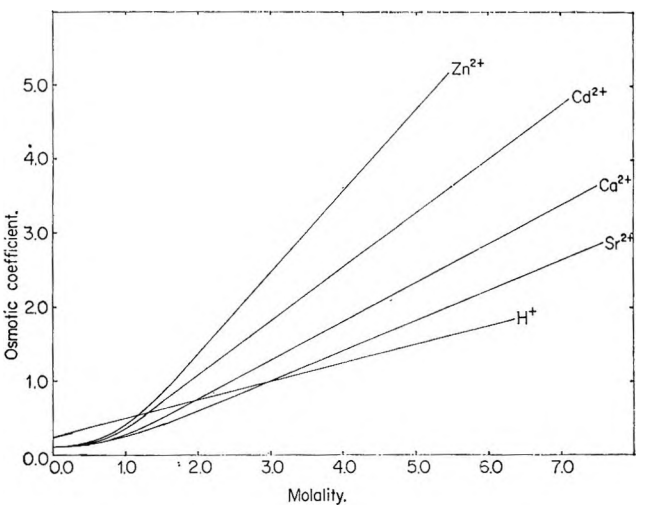

Figure 1. Concentration dependence of the molal osmotic coefficient, ϕ, for polystyrenesulfonic acid and several of its metal salts in aqueous solution.

Discussion

As was mentioned earlier, the osmotic coefficients of divalent polystyrenesulfonates have not been studied previously in any detail. Ise and Okubo[26] have reported osmotic coefficients for $Ba(PSS)_2$ and $Ca(PSS)_2$ which are questionable.[24] For example, the barium

(26) N. Ise and T. Okubo, *J. Phys. Chem.*, **72**, 1361 (1968).

Table II: Osmotic Coefficients of Divalent Metal Perchlorates at 25° in Aqueous Solution

	ϕ					
m	$Mg(ClO_4)_2$	$Ca(ClO_4)_2$	$Sr(ClO_4)_2$	$CO(ClO_4)_2$	$Ni(ClO_4)_2$	$Zn(ClO_4)_2$
1.0	1.323	1.219	1.170	1.340	1.337	1.328
2.0	1.945	1.710	1.577	1.996	1.990	1.986
3.0	2.667	2.261	2.008	2.755	2.762	2.739

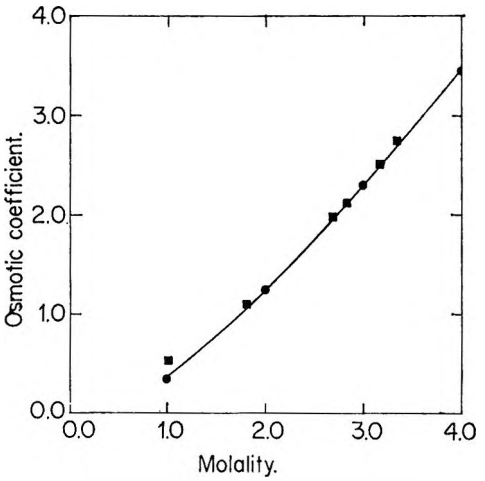

Figure 2. Concentration dependence of the molal osmotic coefficient, ϕ, for zinc polystyrenesulfonate (■, this study; ●, ref 28).

form of polystyrenesulfonate is insoluble at 25°[27] in the molecular weight range of polymer employed by them, yet they report osmotic coefficient data for $Ba(PSS)_2$ at 25° over a concentration range of 0.24 to 3.45 m. Their $Ca(PSS)_2$ osmotic data which do not agree with the results reported here for this divalent salt form of polystyrenesulfonic acid must also be suspect as a consequence.

Osmotic coefficient data reported at high concentrations for $Zn(PSS)_2$ (low cross-linked ion-exchange resin) by Soldano and Larson[28] are presented in Figure 2 together with the results of this research. These data, expressed on a molality scale, are in excellent agreement. This agreement supports further the contention that the physicochemical properties of a cross-linked ion-exchanger and its polyelectrolyte analog should be identical provided the gel is homogeneous.

Water adsorption measurements for several low cross-linked (DVE) polystyrenesulfonates have been determined by Glueckauf and Kitt[29] at low water activities. Their data show that the order of decreasing osmotic coefficient at a fixed polyelectrolyte concentration is: $Mg^{2+} > Ca^{2+} > Sr^{2+}$. This is the same order found in this study for the polystyrenesulfonate osmotic coefficients.

Insight with regard to the nature of interactions regulating the osmotic behavior of the divalent polystyrenesulfonates can be obtained by comparing the experimental results in Table I with the recently reported data of Libus and Sadowska[30] and with the data given by Robinson and Stokes.[31] Libus and Sadowska report the osmotic coefficients of $Ni(ClO_4)_2$ and $Co(ClO_4)_2$ while Robinson and Stokes list the osmotic coefficients of $Mg(ClO_4)_2$, $Ca(ClO_3)_2$, $Sr(ClO_4)_2$, and $Zn(ClO_4)_2$. Data from these references (in Table II) demonstrate that the osmotic coefficients of $Co(ClO_4)_2$, $Ni(ClO_4)_2$, and $Zn(ClO_4)_2$ are equal within experimental error and that the magnitude of the osmotic coefficient is: $Sr^{2+} < Ca^{2+} < Mg^{2+} < Co^{2+} = Ni^{2+} = Zn^{2+}$. These trends are equivalent to those observed in the osmotic coefficient measurements obtained for the divalent polystyrenesulfonates at high concentration as shown in Figure 1. Differences between cobalt, nickel, and zinc polystyrenesulfonate osmotic coefficients are slightly greater than experimental error.

Similarities between osmotic coefficients in divalent polystyrenesulfonate solutions and divalent perchlorate solutions beyond the dilute concentration region suggest that in both systems at high concentrations corresponding divalent ion–solvent interactions become important.

Quantitative interpretation of the increase in osmotic coefficient of simple divalent halides at high concentration has been attempted by Robinson and Stokes[32] and by Glueckauf[33] by assuming that each ion in solution removes a certain number of water molecules from the bulk solvent to form a hydration sphere. By combining Bjerrum's[34] thermodynamic treatment of ion–solvent interactions with the Debye–Hückel treatment of ion–ion interactions an equation was obtained which permitted evaluation of the hydration number of the ionic species. Glueckauf's approach was different from Robinson and Stokes' by the substitution of "volume fraction statistics" for "mole fraction statistics." Glueckauf[29] also used water absorption measurements of lightly cross-linked polystyrenesulfonate ion-exchange resins to attempt quantitative evaluation of the

(27) M. H. Waxman, B. R. Sundheim, and H. P. Gregor, *J. Phys. Chem.*, **57**, 969 (1953).

(28) B. Soldano and Q. V. Larson, *J. Amer. Chem. Soc.*, **77**, 1331 (1955).

(29) E. Glueckauf and G. P. Kitt, *Proc. Roy. Soc., Ser. A*, **228**, 322 (1955).

(30) Z. Libus and T. Sadowska, *J. Phys. Chem.*, **73**, 3229 (1969).

(31) R. A. Robinson and R. H. Stokes, "Electrolyte Solutions," 2nd ed rev, Butterworths, London, 1965, Appendix 8.10, Tables 4 and 5, pp 486–487.

(32) Reference 31, Chapter 9.

(33) E. Glueckauf, *Trans. Faraday Soc.*, **51**, 1235 (1955).

(34) N. Bjerrum, *Z. Anorg. Allgem. Chem.*, **109**, 275 (1920).

number of water molecules associated with a divalent cation in solution.

Libus and Sadowska,[30] influenced by the above, concluded that the behavior of Co^{2+}, Ni^{2+}, and Zn^{2+} perchlorates reflects only the presence of the hydrated divalent cation in solution. This interpretation implies that ionic species such as $\{[M(H_2O)_6](H_2O)_n\}^{2+}$ exist over a large perchlorate concentration range and are independent of the nature of the metal ion (*i.e.*, Co^{2+}, Ni^{2+}, or Zn^{2+}) in solution. In the case of Mg^{2+}, Ca^{2+}, and Sr^{2+} perchlorates the hydrated ionic species $\{[M(H_2O)_6](H_2O)_n\}^{2+}$ exist over a large concentration range as well. However, the value of n is not independent of divalent ion and is less than that for the Co^{2+}, Ni^{2+}, and Zn^{2+} ions.

This interpretation of the osmotic coefficient behavior of divalent perchlorate solutions at high concentration may be applicable to the osmotic coefficient behavior of divalent polystyrenesulfonate solutions. If this is the case the increase of the osmotic coefficient in the divalent polystyrenesulfonate solutions at high concentrations originates from divalent ion–solvent interactions. These interactions can be represented by the existence of a hydrated ionic species $\{[M(H_2O)_6](H_2O)_n\}^{2+}$ in these solutions. A similar interpretation of cation hydration in monovalent polyelectrolyte systems has been presented by Marinsky.[35]

Valid interpretation of the osmotic properties of uni-univalent polyelectrolytes at low concentration has been reasonably well achieved with the theoretical model of Fuoss, Katchalsky, and Lifson.[36] Additional insight has come from modification and extension of this model by several authors.[11,37] It has been shown in the case of polystyrenesulfonate that the variation of osmotic coefficient with concentration in the dilute region can be anticipated from the computation of the change in free energy of the polyelectrolyte with volume, other factors being equal.[37]

Recently, Manning[38] has presented a limiting law for the osmotic coefficient of polyelectrolyte solutions. A different interpretation of ion-binding evolves as a result but does not alter in any way the statements that are made above. In fact, the assumption of a flexible cylindrical rod model is stated to be scheduled for study by Manning.

Since it is felt that the variation of ϕ with concentration is well understood from the flexible cylindrical rod model, concern is with the relative ϕ values of uni-divalent forms of PSS. The equations proposed by Manning are useful for examination of this aspect. The equation given by Manning for the osmotic coefficient of a highly charged linear polyelectrolyte in solution at infinite dilution is

$$\phi = \frac{DkTb}{2e^2Z_M + A} \quad (1)$$

where e is the protonic charge, $Z_M + A$ the charge of the counterion, D the dielectric constant of the solvent, b the total contour length of the polystyrenesulfonate anion divided by the total number of charged groups on the polyanion, and k and T have their usual meanings. This equation showing an inverse dependence of the osmotic coefficient on counterion charge, though pertaining to the situation approaching infinite dilution, describes well the osmotic behavior of a dilute polyelectrolyte solution. This equation is not valid for real polyelectrolyte solutions at very low concentration (less than 10^{-5} N) since it has been assumed in its derivation that the length of the polyion rod is much greater than the distance between strands. Using the osmotic coefficient of HPSS,[24] extrapolated to zero concentration with eq 1, the osmotic coefficient for the divalent polystyrenesulfonates may be calculated. Table III shows the results of such a calculation and the osmotic coefficients of the divalent polystyrenesulfonates extrapolated to infinite dilution. The results of this analysis indicate that an electrostatic model is appropriate for the interpretation of the osmotic coefficients of the divalent polystyrenesulfonates at low concentration.

Table III: Calculated and Experimental Values of the Divalent Polystyrenesulfonate Osmotic Coefficient at Low Concentration

Calcd	Experimental						
$\phi H^+/2$	ϕMg^{2+}	ϕCa^{2+}	ϕSr^{2+}	ϕCo^{2+}	ϕNi^{2+}	ϕZn^{2+}	ϕCd^{2+}
0.12	0.14	0.11	0.11	0.15	0.17	0.12	0.12

Experimental results in the present study as well as data in the literature[19–24,39–41] clearly indicate that the osmotic coefficients of the divalent polystyrenesulfonates can best be interpreted in terms of divalent ion-polyanion and divalent ion–solvent interactions. Divalent ion–polyanion interactions dominate the osmotic coefficient behavior at low concentrations while divalent ion–solvent interactions appear to dominate at high concentrations.

Acknowledgment. The authors wish to express their appreciation to T. A. Brodof of Dow Chemical Company for supplying sodium polystyrenesulfonate and to the United States Atomic Energy Commission for financial support through Contract No. Act (30-1)-2269.

(35) J. A. Marinsky, *J. Phys. Chem.*, 71, 1572 (1967).

(36) R. M. Fuoss, A. Katchalsky, and S. Lifson, *Proc. Nat. Acad. Sci.*, 37, 579 (1951).

(37) J. Farewell, Ph.D. Thesis, The State University of New York at Buffalo, Buffalo, N. Y., 1968.

(38) G. S. Manning, *Polym. Prepr.*, 10(2), 850 (1969).

(39) R. F. Prini and A. E. Lagos, *J. Polym. Sci., Part A*, 2, 2917 (1964).

(40) J. C. Leyte, L. H. Zuiderweg, and H. J. Vledder, *Spectrochim. Acta*, 23A, 1397 (1967).

(41) J. Skerjanc, D. Dolar, and D. Leskovesk, *Z. Phys. Chem. (Frankfurt am Main)*, 56, 218 (1967).

The Solubilities of Calcium in Liquid Calcium Chloride in Equilibrium with Calcium–Copper Alloys[1a]

by Ram A. Sharma[1b]

Chemical Engineering Division, Argonne National Laboratory, Argonne, Illinois 60439 *(Received June 10, 1970)*

The solubilities of calcium in liquid calcium chloride in equilibrium with liquid Ca–Cu alloys were measured by determining the calcium content of the chloride in the temperature range 800–925°. Relative partial molar enthalpy and excess partial molar entropy of solution of calcium in liquid calcium chloride were found to be about 10 kcal mol^{-1} and 1.5 cal deg^{-1} mol^{-1}, respectively. From the activities of calcium in Ca–Cu alloys that were calculated from the solubilities of calcium in $CaCl_2$ and compared with the activities of calcium in Ca–Zn alloys and of magnesium in Mg–Zn and Mg–Cu alloys, it appears that calcium dissolves either by the reaction $Ca + Ca^{2+} \rightleftarrows 2Ca^{+}$ or $Ca \rightleftarrows Ca^{2+} + 2e^{-}$. The calcium activities so calculated were used to derive the activities of copper in liquid Ca–Cu alloys at 1150°K. The relative partial molar and integral molar free energies of mixing for liquid Ca–Cu alloys were also calculated at this temperature.

Introduction

In the past decade, extensive effort has been made to understand the nature of metals dissolved in their molten salts. Most of the work has been done with alkali metal–metal halide and alkaline earth metal–metal halide systems.[2,3] The studies include: temperature–composition equilibria;[2] electrical conductivity,[2,4,5] magnetic susceptibility;[6] polarographic,[7] spectroscopic,[8,9] and chronopotentiometric measurements;[10] and metal alloy–metal halide equilibria.[11,12]

In the present investigation, the solubilities of calcium in liquid calcium chloride in equilibrium with liquid Ca–Cu alloys in the temperature range 800–925° have been measured. The solubility data were required in studying the kinetics of UO_2 reduction by calcium dissolved in liquid calcium chloride. The equilibrium phase diagram of Ca–$CaCl_2$ systems has been investigated by Staffanson.[13] The solubilities of calcium in liquid calcium chloride in equilibrium with pure calcium have been reported by Peterson and Hinkebein,[14] Dworkin, Bronstein, and Bredig,[4] Feschotte-Oestertag,[3] Emons and Hellmold,[3] and Wade and Wolf.[15] The vapor pressures of calcium over Ca–$CaCl_2$ have been determined by Johnson,[16] and Van Westenburg.[17] The electrical conductivity measurements have been reported by Dworkin, Bronstein, and Bredig.[4,5]

Experimental Section

Materials. Anhydrous calcium chloride, in the granular form, was purified by a method similar to that described for the purification of $MgCl_2$ by Laitinen, *et al.*[18] In this method hydrogen chloride gas was passed through the solid and liquid $CaCl_2$ for several hours. The HCl gas was then removed by passing dry helium gas through the chloride for about 1 hr. The chloride was then filtered through a silica frit into a silica capsule which was later sealed. Calcium metal (Mg 0.5%, Fe + Al + Mn + Co + N_2 < 0.05%) was distilled in all tantalum equipment before use. Elec-

(1) (a) Work performed under the auspices of the U. S. Atomic Energy Commission. (b) Correspondence should be addressed to the author at General Motors Research Laboratories, Warren, Mich. 48090.

(2) (a) E. A. Ukshe and N. G. Bukun, *Russ. Chem. Rev.*, **30**, 90 (1961); (b) M. A. Bredig, "Mixture of Metals with Molten Salts," in "Molten Salt Chemistry," M. Blander, Ed., Interscience, New York, N. Y., 1964, p 364.

(3) J. D. Corbett, "The Solution of Metals in Their Molten Salts," in "Fused Salts," Benson Ross Sundheim, Ed., McGraw-Hill, New York, N. Y., 1964, p 341.

(4) A. S. Dworkin, H. R. Bronstein, and M. A. Bredig, *Discuss. Faraday Soc.*, **32**, 188 (1961); M. A. Bredig, *ibid.*, **32**, 257 (1961).

(5) A. S. Dworkin, H. R. Bronstein, and M. A. Bredig, *J. Phys. Chem.*, **70**, 2384 (1966).

(6) (a) N. H. Nachtrieb, *ibid.*, **66**, 1163 (1962); (b) M. Bettman, *J. Chem. Phys.*, **44**, 3254 (1966).

(7) J. J. Egan, *J. Phys. Chem.*, **65**, 2222 (1961).

(8) C. R. Boston and G. P. Smith, *ibid.*, **66**, 1178 (1962).

(9) D. M. Gruen, M. Krumpelt, and I. Johnson, "Molten Salts: Characterization and Analysis," G. Mamantov, Ed., Marcel Dekker, New York, N. Y., 1969.

(10) J. D. Van Norman and J. J. Egan, *J. Phys. Chem.*, **67**, 2460 (1963).

(11) P. S. Rogers, J. W. Tomlinson, and F. D. Richardson, "Physical Chemistry of Process Metallurgy," Interscience, New York, N. Y., 1961, p 909.

(12) M. Krumpelt, J. Fischer, and I. Johnson, *J. Phys. Chem.*, **72**, 506 (1968).

(13) L. I. Staffanson, "The Physical Chemistry of Metals in their Molten Halides," Ph.D. Thesis, London University, Dec 1959.

(14) D. T. Peterson and J. A. Hinkebein, *J. Phys. Chem.*, **63**, 1360 (1959).

(15) W. Z. Wade and T. Wolf, Lawrence Radiation Lab., University of California, California, UCRL 50403 (1968).

(16) E. W. Johnson, M.S. Thesis, Iowa State University, Ames, Iowa, 1960.

(17) J. A. Van Westenburg, Ph.D. Thesis, Iowa State University, Ames, Iowa, 1964.

(18) H. A. Laitinen, W. S. Ferguson, and R. A. Osteryoung, *J. Electrochem. Soc.*, **104**, 516 (1957).

trolytic copper was used in the preparation of Ca–Cu alloys.

Apparatus. The apparatus has been described in detail by Krumpelt, *et al.*,[12] in their studies of Mg–Mg-Cl_2 solutions. The Kanthal-wound tubular furnace suitable for use up to 1000° had three separate heating elements. The stainless steel furnace well that fitted in the furnace tube was attached by a flange to the bottom of a helium-atmosphere drybox. A tantalum liner was placed into the furnace well. By manipulating the input voltage to the furnace heating elements, a uniform (±1°) heating zone 6 in. long was obtained.

The tantalum melt container, 1.9 in. in diameter by 5 in. in depth, was covered with a tantalum lid to minimize loss of metal or salt by evaporation. It was placed inside another tantalum vessel (2.5-in. diameter, 8-in. height). In addition, two tantalum shields were mounted above the latter container. The lid of the container and the radiation shields had about 10-mm diameter central holes for insertion of the sampling tube. In each radiation shield a hole was also made for a thermocouple protection tube. The thermocouple protection tube was inserted into the annulus between the two containers. The temperature was measured by the chromel–alumel thermocouple that was placed in this tube and was found to be equal to the temperature measured by another thermocouple that was immersed in the salt. It was calibrated against a National Bureau of Standards standard Pt—Pt–10% Rh thermocouple.

Procedure. In each experiment a calcium–copper alloy (30–40 g) of known composition was melted, homogenized, and subsequently quenched in a tantalum container. The composition of the alloy was checked by chemical analysis of the samples which were taken by sampling tubes from the liquid alloy. Calcium chloride (150 g) was added to the alloy in the container. The container was placed inside the furnace at a definite temperature for 3 to 24 hr for equilibration. The tantalum sampling tube with a tantalum frit was gradually lowered into the furnace over a period of 20 min so that it would come to temperature prior to introduction into the chloride. The sampling tube was also kept immersed in the chloride for another 20 min to allow the system to attain the equilibrium that might have been disturbed during immersion of the sampling tube. A pressure of 2 atm of helium was applied for about 3 min over the calcium chloride in which the sampling tube was still immersed. The sampling tube was raised under pressure to the upper and cooler part of the furnace to solidify the sample. The system was then restored to atmospheric pressure. Three samples were taken at intervals of 2 hr after the initial equilibrium period, which was observed to be about 3 hr. The same procedure was adopted for each of the compositions of the alloy studied. The equilibrium between calcium chloride and the alloy at different temperatures was approached only by proceeding from lower to higher temperatures. This was necessary because the calcium metal which dissolved in the calcium chloride was not observed to precipitate out into the alloy phase on lowering the temperature.

Analysis. The outside of each of the tubes that were used for sampling the chloride was mechanically cleaned. The upper part of the tube and the frit at the lower end were cut off. The part of the tube containing the salt sample was weighed and placed in a glass hydrolysis vessel inside the helium atmosphere drybox. The hydrolysis apparatus consisted of a bulb for HCl solution, an argon reservoir, a calibrated gas container, a (Toepler) pump, a mercury gauge, a manometer, and equipment to evacuate the entire apparatus. The hydrolysis vessel was incorporated into the hydrolysis apparatus, evacuated, and then cooled with a mixture of Dry Ice and trichloroethylene. The (1 *N*) HCl solution which had been twice degassed was admitted into the hydrolysis vessel, which was then filled with argon to about 90 mm pressure. The hydrolysis vessel was warmed, and the salt sample dissolved in the acid solution with the evolution of hydrogen. After the evolution of hydrogen ceased, the acid solution was frozen with a mixture of Dry Ice and trichloroethylene, and the Ar–H_2 gas mixture was pumped by the Toepler pump into the calibrated gas container. A measured fraction of this gas mixture was analyzed chromatographically for its hydrogen content. The accuracy of the gas chromatographic analysis was observed to be ±5%, and was further checked by wet analysis of duplicate salt samples. In the wet analysis, the sample was dissolved in a known amount of 0.05 *N* HCl solution, the excess of which was back titrated with 0.05 *N* NaOH solution using Brom Cresol Green as indicator. The results of the wet analysis for calcium in the salt sample were found to be in agreement (±6%) with those obtained chromatographically. The copper contents of salt samples equilibrated with Ca–Cu alloy were observed to be below the limits of spectroscopic determination, and therefore, calcium–copper intermetallics in the salt phase were assumed to be absent.

Results and Discussion

The calcium solubilities in liquid $CaCl_2$ in equilibrium with liquid Ca–Cu alloys at different temperatures are given in Table I. Each alloy composition has been calculated for the average of the equilibrium concentrations of calcium in the chloride. The mole per cent of calcium in solution with $CaCl_2$ at 850° and 925° are plotted against the atom per cent of calium in Ca–Cu alloys in Figure 1. The calcium solubilities in $CaCl_2$ in equilibrium with pure calcium are in good agreement with those of Dworkin, Bronstein, and Bredig[4] (2.2 at 785° and 2.95 ± 0.2 mol % Ca at 855°) and in fair agreement with those of Peterson and Hinkebein[14] (3.8 at 900° and 4.2 mol % Ca at 950°). However,

Table I: Solubilities of Calcium in Liquid $CaCl_2$ in Equilibrium with Liquid Ca–Cu Alloys

Calcium atom, fraction in Ca–Cu alloys	Mol % calcium in $CaCl_2$ at temp, °C			
	800	850	900	925
0.30	0.263	0.335		0.473
0.43	0.576	0.624	0.668	0.690
0.55	0.820	1.078		1.647
0.63	1.660	1.926		2.330
0.70	1.737	2.061		2.435
0.76	1.796	2.322		2.801
1.00	2.142 (2.45 at 830°)	2.748	3.257	3.466 (3.598 at 940°)

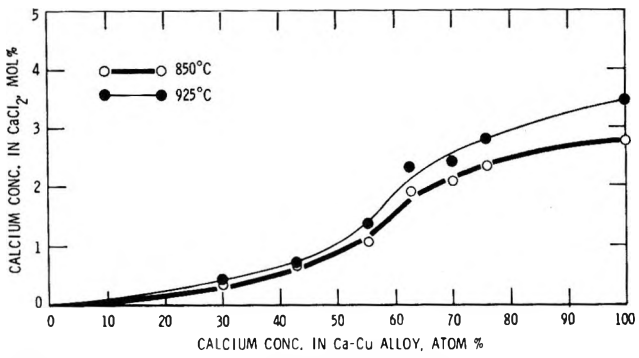

Figure 1. Solubilities of calcium in liquid $CaCl_2$ as a function of calcium concentration in Ca–Cu alloys.

the calcium solubilities are too low to be in agreement with those that have been reported by Staffanson[13] (3.3 mol % Ca at 763°), Emmons and Hellmold,[3] Feschotte-Oestertag[3] (12.5 mol % Ca at 1000°), and Wade and Wolf.[15] This disagreement might be a result of segregation during quenching[13] or the presence of impurities, especially water and CaO in the $CaCl_2$[14] used by these investigators. The plot between the logarithm of mole fraction of calcium in $CaCl_2$ in equilibrium with pure calcium and the reciprocal of absolute temperature was observed to be a straight line. The relative partial molar enthalpy and the excess partial molar entropy of solution of calcium in liquid calcium chloride that were calculated from the slope and the intercept of the plot were found to be about 10 kcal mol^{-1} and 1.5 cal deg^{-1} mol^{-1}, respectively.

At the present time, three modes of dissolution of metals in their molten salts have been proposed in the literature.[2b,3] In the case of dissolution of calcium in $CaCl_2$, they may be represented by the following reactions

$$Ca \rightleftharpoons Ca^0 \quad (1)$$

i.e., calcium dissolves in $CaCl_2$ as a neutral atom

$$Ca + Ca^{2+} \rightleftharpoons 2Ca^+ \quad (2a)$$

$$Ca + Ca^{2+} \rightleftharpoons (Ca_2)^{2+} \quad (2b)$$

i.e., calcium dissolves in $CaCl_2$ forming a monomeric (2a) or dimeric (2b) subchloride

$$Ca \rightleftharpoons Ca^{2+} + 2e^- \quad (3)$$

i.e., calcium dissolves in $CaCl_2$, dissociating into a calcium ion and two electrons. The electrons are assumed to be like F-centers and to behave thermodynamically like the other anions.

The possibility of reaction 1 has been discounted because of its inconsistency with the depression of the melting point of $CaCl_2$ by the addition of calcium.[2] Johnson[16] measured the vapor pressures of calcium over Ca–$CaCl_2$ solutions at 1255°K by the carrier-gas method. He found that the calcium vapor pressures were proportional to the square of the mole fractions of calcium in the $CaCl_2$ and thus obeyed Henry's law in a modified form, $P_{Ca} = CX_{Ca}^2$, which takes into account complete dissociation (3) or reaction with the Ca^{2+} (2a) of the solute Ca to form two particles, even up to the saturation solubility of calcium in $CaCl_2$. This observation was confirmed by Van Westenburg,[17] who measured the calcium vapor pressures over Ca–$CaCl_2$ solutions at 1133.5°K by the Knudsen effusion method. In other words, the activity coefficient of calcium when accordingly defined as $\gamma_{Ca} = a_{Ca}/X_{Ca}^2$ is independent of its mole fraction, X_{Ca}, in the calcium chloride.

In the case of the present studies of the solubilities of calcium in liquid calcium chloride in equilibrium with Ca–Cu alloy, X_{Ca} would be proportional to the square root of calcium activity in Ca–Cu alloy for the dissolution reactions 2a or 3 if the modified Henry's law is obeyed, and to the activity of calcium in the alloy for the dissolution reaction 2b on the application of the usual Henry's law. This means that the activity of calcium in Ca–Cu alloy would be equal to $(X_{Ca}/X_{Ca}^\circ)^2$ for reactions 2a or 3 and to (X_{Ca}/X_{Ca}°) for reaction 2b, where X_{Ca}° is the mole fraction of calcium in $CaCl_2$ in equilibrium with pure calcium. The activities of calcium in Ca–Cu alloys with reference to pure liquid calcium, a_{Ca}, which were calculated on the basis of reactions 2a or 3, and also on the basis of reaction 2b are shown in Figure 2. The activities of calcium in Ca–Zn[19] and the activities of magnesium in Mg–Zn[20] and Mg–Cu[21] alloys are also shown in this figure for comparison.

The activities of calcium in Ca–Cu alloys that were calculated on the basis of reactions 2a or 3 are observed to fall in the right order with respect to the calcium activities in Ca–Zn alloys and to the magnesium activities in Mg–Zn and Mg–Cu alloys (assuming the relation between Ca–Zn and Ca–Cu similar to that be-

(19) P. Chiotti and R. J. Hecht, *Trans. Met. Soc. AIME*, 239, 536 (1967).

(20) P. Chiotti and E. R. Stevens, *Trans. AIME*, 233, 198 (1965).

(21) R. Hultgren, R. L. Orr, P. D. Anderson, and K. K. Kelley, "Selected Values of Thermodynamic Properties of Metals and Alloys," Wiley, New York, N. Y., 1963, p 677.

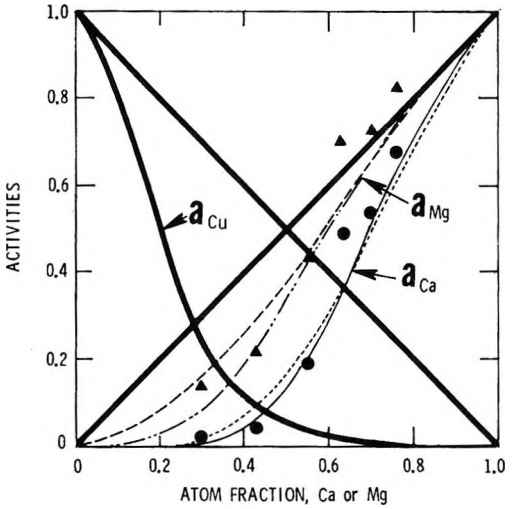

Figure 2. Activities of Ca in Ca–Cu and Ca–Zn and of Mg in Mg–Cu and Mg–Zn at 1150°K as a function of atomic fraction of calcium or magnesium (supercooled liquid in the regions of solidification below 0.2 atom fraction Ca): dashed curve, Mg–Zn; dash-dot-dot curve, Mg–Cu; dotted curve, Ca–Zn; smooth curve, Ca–Cu; ▲, $a_{Ca} = X_{Ca}/X_{Ca}^0$; ●, $a_{Ca} = (X_{Ca}/X_{Ca}^0)^2$.

tween Mg–Zn and Mg–Cu). The activities of calcium in Ca–Cu alloys that were calculated on the basis of reaction 2b are not only misplaced with respect to the activities of calcium in Ca–Zn alloys and the activities of magnesium in Mg–Zn and Mg–Cu alloys, but have also positive deviations above 0.6 mole fraction (Figure 2) which is most unlikely for the activities of calcium in Ca–Cu alloys. They are also observed to have no agreement with the activities of calcium in Ca–Cu alloys with reference to pure liquid calcium that were computed on the assumption that, at a given mole fraction, the ratio of the activity coefficients of calcium in Ca–Cu and Ca–Zn alloys is equal to the ratio of the activity coefficients of magnesium in Mg–Cu and Mg–Zn alloys (Figure 2). The activities of calcium in Ca–Cu alloys that were calculated on the basis of reactions 2a or 3 are observed to have agreement with the calcium activities that were computed from the derived calcium activity coefficients (Figure 2). This indicates that calcium most probably dissolves in calcium chloride by reactions 2a or 3. This inference is in agreement with the observation by Johnson,[16] as well as Van Westenburg,[17] that the calcium vapor pressures over Ca–$CaCl_2$ solutions show a dependence on composition which is consistent with a two-particle solute. Dworkin, Bronstein, and Bredig[4,5] have reported a cryoscopic number of 2 from the analysis of the depression of freezing point of $CaCl_2$. This is again consistent with the dissolution of calcium in $CaCl_2$ by reactions 2a or 3.

From the results of the present study, it is not possible to distinguish whether calcium dissolves in $CaCl_2$ by reactions 2a or 3. Dworkin, Bronstein, and Bredig[4,5] observed an increase in specific conductivity in $CaCl_2$ with the addition of calcium and proposed the dissolution of calcium by reaction 3. However, the increase in specific conductivity in $CaCl_2$ has been reported to be only 17% up to the saturation solubility of calcium, and the rate of increase in the specific conductivity and the equivalent conductance of calcium in the $CaCl_2$ was observed to decrease with increasing calcium concentration. The decrease in the equivalent conductance of calcium in $CaCl_2$ was attributed to the trapping of the mobile electrons by the reaction $2e^- + 2Ca^{2+} = (Ca_2)^{2+}$. The cryoscopic data and the results of measurements of calcium vapor pressures over Ca–$CaCl_2$ solutions do not indicate the extent of this reaction to be large, even though it seems to be much larger in the $CaBr_2$–Ca system.[5] The slightly greater values of the experimentally derived activities of calcium than those

Table II: Computed Activities and Free Energies for Liquid Ca–Cu Alloys at 1150°K

Calcium atom fraction	a_{Ca}	a_{Cu}	$-\Delta\bar{G}_{Ca}$, kcal/g atom	$-\Delta\bar{G}_{Cu}$, kcal/g atom	$-\Delta G$, kcal/g atom
0.1	0.00007	0.78	22.8	0.6	2.8
0.2	0.0012	0.48	16.0	1.8	4.6
0.3	0.010	0.23	11.0	3.4	5.7
0.4	0.047	0.10	7.3	5.4	6.2
0.5	0.14	0.04	4.7	7.6	6.1
0.6	0.30	0.017	2.9	9.8	5.6
0.7	0.50	0.006	1.7	12.0	4.8
0.8	0.70	0.0024	0.9	14.4	3.6
0.9	0.87	0.0007	0.3	17.4	2.0

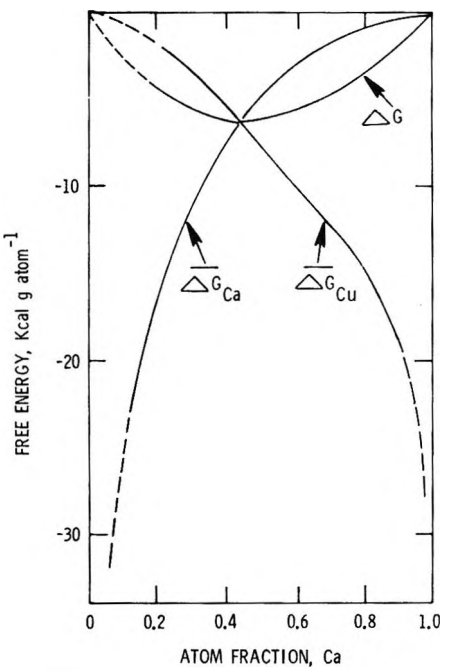

Figure 3. Relative partial molar and integral molar free energies of mixing for liquid Ca–Cu alloys at 1150°K. Dashed curve supercooled liquid region.

of the computed activities in Ca–Cu alloys in the region of higher concentration of calcium (Figure 2) may indicate the above reaction proposed for trapping the mobile electrons.

Thermodynamic data on calcium-based alloys, with the exception of Ca–Zn[19] and Ca–Mg[22] systems, are nonexistent in the literature.[21] The calcium activities of the present investigation that have been calculated on the basis of reactions 2a or 3 have been used to derive the activities of copper in liquid Ca–Cu alloys with respect to pure solid copper, a_{Cu}, at 1150°K by the Gibbs–Duhem relation and are given in Table II. The relative partial molar free energies of mixing of calcium ($\Delta\bar{G}_{Ca}$) and copper ($\Delta\bar{G}_{Cu}$) and integral molar free energies of mixing, ΔG, for liquid Ca–Cu system were also calculated and are given in Table II and Figure 3. The data below 0.2 atom fraction of calcium, in the ranges of solidification, are for supercooled liquids. Large negative deviations from ideal solution behavior are apparent in this system.

Acknowledgment. The author wishes to thank Dr. Irving Johnson for helpful discussions and Dr. R. K. Steunenberg for his encouragement during the investigation. The author also wishes to thank A. Panek for gas chromatographic analyses and T. Lekberg for assistance with the experimental work.

(22) V. P. Mashovets and L. V. Puchkov, *Zh. Prikl. Khim.*, **38**, No 5, 1009 (1965).

Enthalpies of Alkylammonium Ions in Water, Heavy Water, Propylene Carbonate, and Dimethyl Sulfoxide[1]

by C. V. Krishnan and Harold L. Friedman

Department of Chemistry, State University of New York at Stony Brook, Stony Brook, New York 11790
(Received May 28, 1970)

The enthalpies of solution at infinite dilution of alkylammonium salts have been measured in several solvents. Salts of R_3NH^+, $R_2NH_2^+$, RNH_3^+, and NH_4^+ have been studied, with R a normal alkyl chain ranging from methyl to amyl and, in some cases, to octyl. The regularities previously reported for the behavior of alkyl chains in aprotic solvents (*J. Phys. Chem.*, **73**, 1572, 3934 (1969)) are also found here in the enthalpies of transfer to PC (propylene carbonate) from DMSO. In addition, evidence is found for the strong mutual interference of the N–H···O hydrogen bonds involving a single nitrogen. For example, the enthalpy of transfer to PC from DMSO, after extrapolating to zero length of the R chains, is 1.64 kcal/mol for R_3NH^+ and 1.16 kcal/mol for $^1/_3RNH_3^+$. The enthalpies of transfer of the alkylammonium ions to DMSO from H_2O show a relatively complex dependence on the length and number of R chains. This has been interpreted in terms of two effects in the aqueous solutions: interference of the R chains with the N–H···O hydrogen bonds and mutual interference of the N–H···O hydrogen bonds. The latter effect is so great that the enthalpy of NH_4^+ is 5 kcal/mol higher in water than in PC. The enthalpies of transfer of RNH_3^+ to D_2O from H_2O, when analyzed as in the earlier studies of ROH and R_4N^+ solutions, tend to confirm the estimate that the structural or hydrophobic effect of alkyl groups in aqueous media is 5% larger in D_2O than in H_2O. The previously reported saturation of the structural effect is not found here.

1. Introduction

Studies of the enthalpies of transfer of normal alcohols[2] and tetraalkylammonium ions[3,4] to propylene carbonate (PC) from water (W), to PC from dimethyl sulfoxide (DMSO), and to W from D_2O(D), have led to a measure of the enthalpy associated with the structural effect (sometimes called "icebergs") produced by these species in water. In a qualitative way these results fit in quite well with other measures of the same phenomenon, for example, heat capacities[5–7] and mobilities.[8] These studies also have led to a simple picture of the solvation of the hydrocarbon chains in PC and DMSO.

(1) Grateful acknowledgment is made of the support of this work by the National Institutes of Health.

(2) C. V. Krishnan and H. L. Friedman, *J. Phys. Chem.*, **73**, 1572 (1969).

(3) C. V. Krishnan and H. L. Friedman, *ibid.*, **73**, 3934 (1969).

(4) C. V. Krishnan and H. L. Friedman, *ibid.*, **74**, 2356 (1970).

(5) E. M. Arnett, W. B. Kover, and J. V. Carter, *J. Amer. Chem. Soc.*, **91**, 4028 (1969).

It seems of great interest to extend these results to primary, secondary, and tertiary alkylammonium ions, both to test the interpretation made of the R_4N^+ behavior and because of the great biological importance of some of the less alkylated species. As reported below, the new results are complicated by the appearance of a sizable contribution from the hydrogen bonding of the alkylammonium ions to the solvent. This contribution is found to be quite sensitive to the nature and number of alkyl chains attached to the nitrogen. A corresponding complication would no doubt appear in the study of the alcohols if a wider range of alcohols were studied.

Properties of these incompletely alkylated ammonium ions as solute species have not previously been systematically investigated, with the following notable exceptions: the partial molal volumes, viscosities, and conductivities of aqueous solutions of the primary ammonium salts,[9-11] the acid ionization constants,[12,13] and partial molar volumes[14,15] of some secondary and tertiary ammonium salts in aqueous solution.

2. Experimental Section and Results

The instrumental aspects have already been described.[16] The alkylamine hydrochlorides were commercially available. All other salts were prepared from the corresponding amines and trifluoroacetic acid (HTFA) or mineral acid. The salts were purified by crystallizing from alcohols, acetone, or ether. Each salt was dried under vacuum, ground, and dried under vacuum again. Me_2NH_2TFA, a liquid at room temperature, was crystallized at low temperature. The purity of the halide salts was checked by estimation of the halide and found to be better than 99.7%. The agreement with the heats of transfer of the cations obtained from the halide salts was used as the criterion of purity for the trifluoroacetates except for NH_4TFA and $(C_5H_{11})_2NH_2TFA$. In these cases the purity, found to be better than 99.9 and 99.7%, respectively, was estimated by passing a known amount of salt through a sulfonic acid exchanger and titrating the liberated acid.

The purification of the solvents used has been described elsewhere.[2,3,16,17]

The dissolution and mixing processes were practically complete within 2–10 min except as follows: Bu_2NH_2TFA in water, $MeNH_3TFA$, $PrNH_3TFA$, $HexNH_3TFA$, $HeptNH_3TFA$, Bu_2NH_2Cl, Me_3NHBr in DMSO, all salts except tetraalkylammonium halides in PC, 15–35 min. The heat of solution of NH_4TFA in PC could not be satisfactorily obtained because of the slow rate of dissolution and the uncertainty is as high as ±0.5 kcal/mol.

All the measurements were made at 25.0°. The results are given in Table I. The values given are averages of two or more measurements agreeing within 0.05 kcal/mol except as noted. In the case of heats of solution in H_2O and D_2O the agreement is within 0.03 kcal/mol.

Table I: Enthalpies of Solutions of Pure Substances at 25° (Values in kcal/mol)

Solute	Solvent: H_2O	D_2O	DMSO	PC
CH_3NH_2HCl	1.42	1.40	−0.93	
$C_2H_5NH_2HCl$	2.08	2.03	0.78	
$C_3H_7NH_2HCl$	0.33	0.22	−0.49	
$C_4H_9NH_2HCl$	−0.64	−0.80	−1.20	
$C_5H_{11}NH_2HCl$	−0.23	−0.43	−0.73	
$C_6H_{13}NH_2HCl$	0.28	0.04	−0.18	
$C_7H_{15}NH_2HCl$	0.90	0.63	0.50	
$C_8H_{17}NH_2HCl$	3.04	2.75	2.57	
CH_3NH_2HTFA	1.77		1.93	6.12
$C_2H_5NH_2HTFA$	0.51		1.69	5.80
$C_3H_7NH_2HTFA$	1.06		2.75	6.76
$C_4H_9NH_2HTFA$	0.42		2.33	6.27
$C_5H_{11}NH_2HTFA$	1.93		3.87	7.93
$C_6H_{13}NH_2HTFA$	2.33		4.24	7.95
$C_7H_{15}NH_2HTFA$	3.48		5.45	9.03
$C_8H_{17}NH_2HTFA$	4.41		6.50	10.21
$(CH_3)_2NHHCl$	0.47		0.46	
$(CH_3)_2NHHTFA$	−2.61		−0.37	3.45
$(C_2H_5)_2NHHBr$	1.93		0.65	
$(C_2H_5)_2NHHTFA$	−0.52		4.28	7.87
$(C_3H_7)_2NHHBr$	−0.42		−0.78	
$(C_3H_7)_2NHHTFA$	−0.39		5.47	8.95
$(C_4H_9)_2NHHCl$	−1.61		2.37	
$(C_4H_9)_2NHHTFA$	−0.85		5.49	8.72
$(C_5H_{11})_2NHHTFA$	0.02		6.28	9.41
$(CH_3)_3NHCl$	0.83		2.02	
$(CH_3)_3NHBr$	4.59		2.14	5.80
$(CH_3)_3NHTFA$	−0.50		3.22	5.16
$(C_2H_5)_3NHBr$	2.83		3.36	6.86
$(C_3H_7)_3NHBr$	−0.97		1.48	4.64
$(C_4H_9)_3NHBr$	0.24		3.83	6.63
$(C_2H_5)_3CH_3NI$	4.78		1.80	3.30
$(C_2H_5)_3C_3H_7NI$	4.45		3.25	4.48
$(C_4H_9)_3CH_3NI$	2.32		3.05	3.93
$(C_4H_9)_3C_3H_7NI$	−0.66		1.94	2.70
NH_4TFA	3.92		1.08	6.60

For the trifluoroacetates of dialkylammonium ions

(6) E. M. Arnett and J. J. Campion, to be published.

(7) T. S. Sarma, R. K. Mohanty, and J. C. Ahluwalia, *Trans. Faraday Soc.*, **65**, 2333 (1969).

(8) R. L. Kay and D. F. Evans, *J. Phys. Chem.*, **69**, 4216 (1965).

(9) J. E. Desnoyers and C. Jolicoeur, "Modern Aspects of Electrochemistry," Vol. 5, J. O'M. Bockris and B. E. Conway, Ed., Butterworths, London, 1968.

(10) J. E. Desnoyers and M. Arel, *Can. J. Chem.*, **45**, 359 (1967).

(11) J. E. Desnoyers, M. Arel, and P. A. Leduc, *ibid.*, **47**, 547 (1969).

(12) E. Grunwald, *J. Phys. Chem.*, **71**, 1846 (1967).

(13) E. Grunwald and E. K. Ralph, *J. Amer. Chem. Soc.*, **89**, 4405 (1967).

(14) B. E. Conway and R. E. Verrall, *J. Phys. Chem.*, **70**, 3952 (1966).

(15) B. E. Conway and R. E. Verrall, *ibid.*, **70**, 3961 (1966).

(16) H. L. Friedman and Y. C. Wu, *Rev. Sci. Instrum.*, **36**, 1236 (1965).

(17) Y. C. Wu and H. L. Friedman, *J. Phys. Chem.*, **70**, 501 (1966).

and Me_3NH^+, the heats of solution in propylene carbonate were found to be strongly concentration dependent. This suggests an ion association process with a substantial heat effect contributing to the heat of solution. Since the concentration dependence was not linear, heat values were fitted by the equation

$$\Delta H_m = \Delta H_0 + Am + Bm^2$$

where m is the molal concentration, ΔH_m is the heat of solution at molality m, ΔH_0 is the value at infinite dilution, and A and B are constants. The ΔH_0 values (± 0.2 kcal/mol) obtained from the least-squares solution of this equation are given in Table I for the above-mentioned salts.

The ionic enthalpies of transfer in Table II provide an extension, made possible by the new data, of similar tables given earlier.[3] They depend on the convention[3] that the enthalpies of transfer of Ph_4As^+ and Ph_4B^- are equal. In the body of this table the figures are "best values" while the individual experimental values are given in the footnotes when there are data for the cation with more than one anion.

Table II: Ionic Enthalpies of Transfer at 25° (Values in kcal/mol[a])

Ion	DMSO ← H_2O	PC ← H_2O	D_2O ← H_2O
$CH_3NH_3^+$	−6.82[c]	−3.44[m]	0.03[n]
$C_2H_5NH_3^+$	−5.79[c]	−2.50[m]	0.00[n]
$C_3H_7NH_3^+$	−5.30[c]	−2.09[m]	−0.06[n]
$C_4H_9NH_3^+$	−5.05[c]	−1.94[m]	−0.11[n]
$C_5H_{11}NH_3^+$	−5.01[c]	−1.79[m]	−0.15[n]
$C_6H_{13}NH_3^+$	−5.00[e]	−2.17[m]	−0.19[n]
$C_7H_{15}NH_3^+$	−4.95[f]	−2.24[m]	−0.22[n]
$C_8H_{17}NH_3^+$	−4.92[g]	−1.99[m]	−0.24[n]
$(CH_3)_2NH_2^+$	−4.61[h]	−1.73[m]	
$(C_2H_5)_2NH_2^+$	−2.14[d]	0.60[m]	
$(C_3H_7)_2NH_2^+$	−1.15[d]	1.55[m]	
$(C_4H_9)_2NH_2^+$	−0.57[i]	1.78[m]	
$(C_5H_{11})_2NH_2^+$	−0.71[m]	1.64[m]	
$(CH_3)_3NH^+$	−3.28[b]	−2.08[j]	
$(C_2H_5)_3NH^+$	−0.30[k]	0.79[k]	
$(C_3H_7)_3NH^+$	1.62[k]	2.37[k]	
$(C_4H_9)_3NH^+$	2.76[k]	3.15[k]	
NH_4^+	−9.81[m]	−5.11[m]	
$(C_2H_5)_3CH_3N^+$	0.07[l]	−0.70[l]	
$(C_2H_5)_3C_3H_7N^+$	1.85[l]	0.81[l]	
$(C_4H_9)_3CH_3N^+$	3.78[l]	2.39[l]	
$(C_4H_9)_3C_3H_7N^+$	5.65[l]	4.14[l]	

[a] For each solvent pair the ionic enthalpies of transfer depend on the convention that Ph_4As^+ and Ph_4B^- have the same enthalpy of transfer. For further details see ref 3 and 4 from which some of the data used in the construction of this table were taken. [b] Data for Cl^-, Br^-, and TFA^- salts agree within 0.06 kcal/mol. [c] Data for Cl^- and TFA^- salts agree within 0.06 kcal/mol. [d] Data for Br^- and TFA^- salts agree within 0.06 kcal/mol. [e] From Cl^-, −4.95; from TFA^-, −5.06. [f] From Cl^-, −4.89; from TFA^-, −5.00. [g] From Cl^-, −4.96; from TFA^-, −4.88. [h] From Cl^-, −4.50; from TFA^-, −4.73. [i] From Cl^-, −0.51; from TFA^-, −0.63. [j] From Br^-, −2.13; from TFA^-, −2.03. [k] From Br^- alone. [l] From I^- alone. [m] From TFA^- alone. [n] From Cl^- alone.

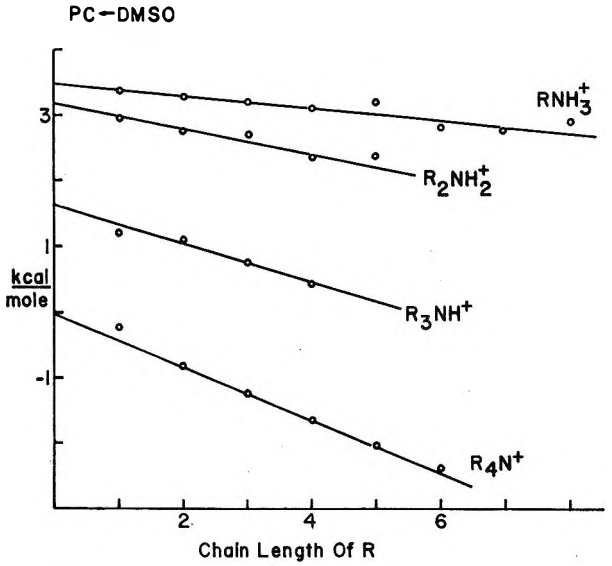

Figure 1. Ionic enthalpies of transfer to PC from DMSO based on the data in Table II. These depend on the convention that the enthalpy of transfer is the same for Ph_4As^+ and Ph_4B^-. The R_4N^+ data are from an earlier report.[3] The slope of the straight line through these data is −0.40. The other lines are drawn with the slopes RNH_3^+, −0.10; $R_2NH_2^+$, −0.20; R_3NH^+, −0.30. Thus these lines are drawn on the assumption that in every case there is a constant increment per CH_2 group and this increment is −0.10, the same as for normal alcohols.[2]

3. Transfers to PC from DMSO

The enthalpy data for this process are plotted as a function of the length of the alkyl chains in Figure 1. The lines are drawn on the assumption that[18]

$$(CH_2)_{PC \leftarrow DMSO} = -0.10 \text{ kcal/mol} \qquad (3.1)$$

as determined already from the studies of the normal alcohols[2] and the tetraalkylammonium ions.[3] Apparently the constancy of this group contribution to the enthalpy of transfer holds equally well for the incompletely alkylated ammonium ions. Of course, it would be paradoxical if it turned out otherwise since the degree of interaction between the alkyl chains must be minimal for the normal alcohols as well as for the RNH_3^+ ions. As noted previously, the constancy of this group contribution and the magnitude observed are to be expected if the dominant contribution is either the interaction[2] $-\mu^2\alpha/r^6$ of the dipole μ of the solvent with the polarizability α of the methylene group at a distance r from the dipole, or the van der Waals interaction[3] treated in the approximate framework of the solubility parameter theory of Hildebrand and Scott.[19]

(18) In this notation, which was introduced earlier,[2] $(x)_{b \leftarrow a}$ is the standard enthalpy of transfer of solute species x to solvent b from solvent a. In eq 3.1 the solute species is just the methylene group. The linearity of the plots in Figure 1 makes it possible to identify a methylene group contribution.[2]

(19) J. H. Hildebrand and R. L. Scott, "Solubility of Non-Electrolytes," 3rd ed, Reinhold, New York, N. Y., 1950.

Table III: Enthalpy of Transfer of Hydrogen-Bond Donors to PC from DMSO, Extrapolated to Zero Alkyl Substituent in Figure 1

Type	R_3N-H^+	$R_2NH_2^+$ [a]	RNH_3^+
kcal/mol per H bond	1.64	1.59	1.16
Type	NH_4^+ [a]	ROH [b]	H_2O [b]
kcal/mol per H bond	1.18	1.93	1.64

[a] Because of the difficulties described in section 2 the error limits on this datum are ±0.15 kcal/mol rather than 0.05 kcal/mol as for the others. [b] From ref 2.

The intercepts at $N = 0$ in Figure 1 are dominated by the difference in strengths of the hydrogen bonds to the solvent in DMSO and in PC. Adopting the general formula

$$(C_NH_{2N+1})_{4-L}NH_L^+ \qquad (3.2)$$

for these ions, the intercept in Figure 1 divided by L is the average value of the enthalpy of transfer of a hydrogen bond

$$(NH\cdots solvent)_{PC\leftarrow DMSO}$$

for each type of ammonium ion. These results are given in Table III together with some relevant earlier results. They are consistent with the usual view that NH···O hydrogen bonding is weaker than OH···O hydrogen bonding[20] if we assume that the stronger bonds distinguish more sharply between PC and DMSO as acceptors. In the case of the ROH, H_2O comparison this assumption may be checked because these species are known in the gas phase so one knows the enthalpy of solvation in each solvent as well as the enthalpy of transfer; in that case it is correct. That is, both liquid DMSO and liquid PC, as hydrogen bond acceptors, react more energetically with ROH (extrapolated to zero length of the R chain) than with $^1/_2H_2O$, and the difference is 0.5 kcal/mol larger for DMSO which forms stronger hydrogen bonds than PC by about 2 kcal/mol.[2]

The other conclusion which may be drawn from Table III is that multiple hydrogen bonds from a given donor molecule interfere with each other, at least judging from the enthalpy criterion. Of course the interaction of several hydrogen bonds connected to a given molecule may be different in other cases in which the molecule functions both as a hydrogen bond donor and hydrogen bond acceptor (*e.g.*, water) or in which the molecule offers widely separated sites for hydrogen bonding.

4. Transfers to DMSO from Water

In the earlier studies with other solutes[2,3] the data were organized to focus the discussion on transfers to PC from other solvents for the reason that PC provides the weakest solvation, judging by all the criteria except methylene group transfers, and therefore is most appropriate for use as a reference solvent.[2] However, in the present case the data are less complete in PC than in DMSO because of experimental difficulties with $R_2NH_2^+$ and NH_4^+ salts, so it seems advantageous to discuss DMSO ← W transfers rather than PC ← W.

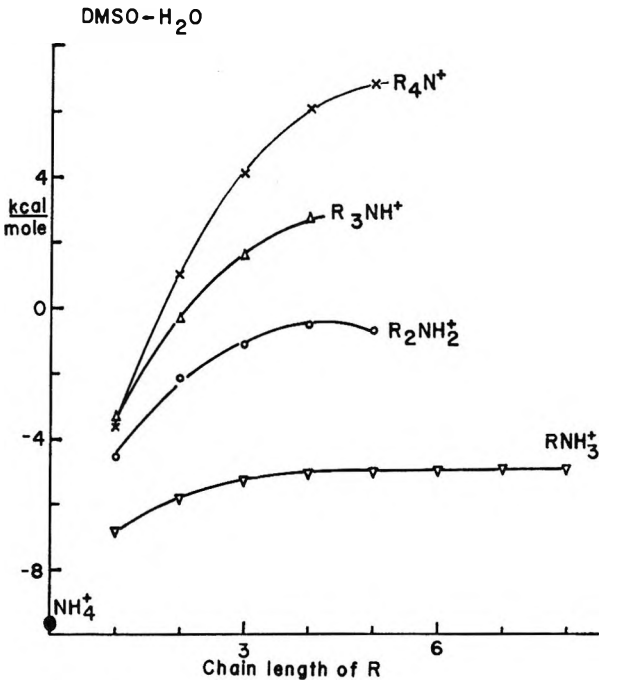

Figure 2. Ionic enthalpies of transfer to DMSO from water based on the data in Table II.

We may think of the enthalpy of transfer

$$H_t(N,L) \equiv ([C_NH_{2N+1}]_{4-L}NH_L^+)_{DMSO\leftarrow W} \qquad (4.1)$$

as a surface depending on the independent variables N and L. The corresponding surface for PC ← DMSO transfers (Figure 1) has a very simple shape which indicates that the CH_2 groups in the chains act independently. For the present case the projection of the H_t surface on the H_t,N plane (Figure 2) and on the L,N plane (Figure 3) reveals much more complicated behavior. This was to be anticipated because it was reported earlier that, for PC ← W transfers, the methylene groups in normal alcohols[2] or in R_4N^+[3] (also included in Figure 2 and 3) do not act independently.

While the projection in Figure 2 is the familiar way to represent such data, Figure 3 shows an important feature which is clear neither in Figure 2 nor in Table II, where of course there are only entries for integral N and L so it is hard to visualize the surface. Variation along the dashed line in Figure 3 shows that the enthalpy of transfer increases as the hydrocarbon content is increased; this much is apparent in Figure 2. Next, examine the tangent to the intersection of a contour and the dashed line, such as the dotted line in Figure 3. This shows that as one increases N while

(20) Presumably the difference is larger in cases in which -NH hydrogen-bond donors are uncharged.

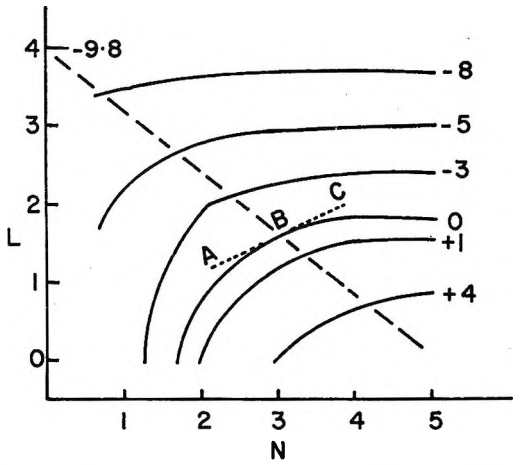

Figure 3. Lines of constant H_t projected on the LN plane. The lines are labeled with H_t in kcal/mol.

changing L so as to keep the total hydrocarbon content nearly constant, the enthalpy of transfer first increases (AB) and then decreases (BC). This enthalpy effect is about as large as that along the dashed line, which makes it abundantly clear that the hydrophobic effect of a given amount of hydrocarbon can depend very strongly on how it is distributed in a molecule.

It is interesting to see what happens if it is assumed that the $H_t(N,L)$ surface results from independent action of the alkyl *chains*. The function

$$H_t'(N,L) \equiv H_t(N,L) - \frac{4-L}{4}H_t(N,0) \quad (4.2)$$

would be just the hydrogen-bond contribution to the enthalpy of transfer to DMSO from water if $H_t(N,L)$ were the sum of $4 - L$ chain terms and a term for the net effect of the L hydrogen bonds. It is plotted as a function of L for various N values in Figure 4. The simplest picture of the underlying phenomena would have all the data falling on line I or II which would represent the additive contribution of the L hydrogen bonds to the enthalpy of transfer, with the hydrogen bonds having lower enthalpy (stronger H bonds) in DMSO than in water. Although the data do not lie on the line II, it certainly represents the dominant effect in H_t'. Four minor effects may be distinguished.

Chain–Chain Interactions. Evidence that the enthalpy effect of chain–chain interactions is small is given in Table IV.

In terms of eq 4.2 these data are all for $L = 0$, tetraalkylammonium ions, but the various chains have different carbon numbers N. Clearly, eq 4.2 can be generalized to include this case. The difference between the second and third columns in Table IV is H_t' for the PC ← water transfer in cases in which there is no hydrogen bonding from the ions to the solvent. These H_t' values are indeed very small compared to those in Table III. To test these ideas further, the same comparison was made for the PC ← DMSO transfer where the enthalpies do comprise additive contributions from the methylene groups; the H_t' quantities have magnitudes as large as 0.1 kcal/mol. Therefore, H_t' values of this order for the DMSO ← water transfers in Table IV cannot be taken as evidence for "hydrophobic" contributions to the enthalpy of chain–chain interaction in water.

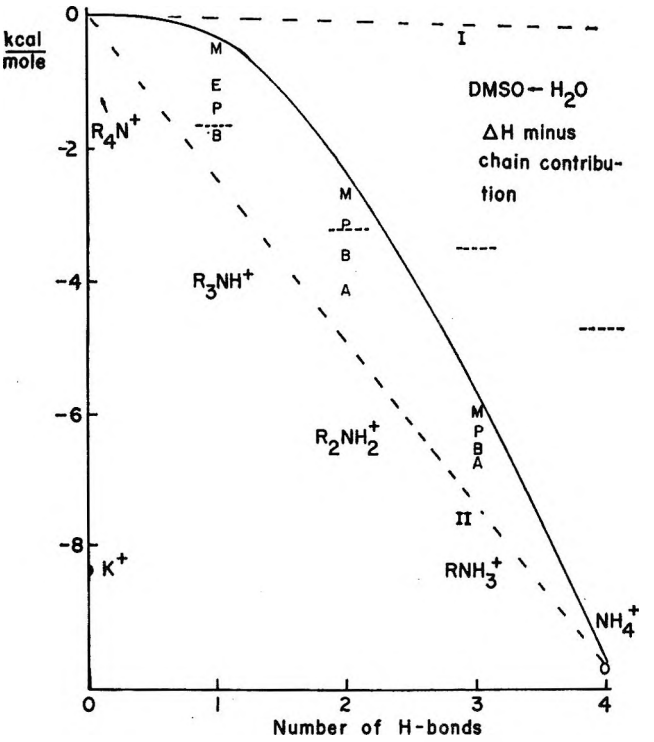

Figure 4. H_t', ionic enthalpies of transfer to DMSO from water reduced on the assumption that the alkyl chains make independent contributions. Data points: M = methyl, E = ethyl, P = propyl, B = butyl, A = amyl; —, rough extrapolation to zero chain length. I, data would fall on this line if H bonds were independent of each other and of R groups, with H-bond strength given by R_3NH^+ data. II, same as I but with H-bond strength given by NH_4^+ datum; ····, DMSO ← PC transfers extrapolated to zero chain length.

Table IV: Enthalpies of Transfer in kcal/mol

Ion	PC ← H_2O		PC ← DMSO	
	Obsd[a]	Add.[b]	Obsd[a]	Add.[b]
Et_3MeN^+	−0.70	−0.85	−0.77	−0.69
Et_3PrN^+	0.81	0.83	−1.04	−0.94
Bu_3MeN^+	2.39	2.32	−1.39	−1.30
Bu_3PrN^+	4.14	3.99	−1.51	−1.55

[a] Observed enthalpy of transfer, Tables I and II. [b] Enthalpy of transfer calculated from data for symmetrical tetraalkylammonium ions[3] assuming additive contributions of alkyl chains.

Interaction of the Alkyl Chain with the Hydrogen Bonds. This interaction is manifested by the spread of data points for various N but fixed L in Figure 4. Two kinds of interaction may be distinguished, an inductive effect and a steric effect. We assume the inductive

effect is roughly constant from methyl to amyl so it does not contribute to the spread of the data points. The steric effect would be expected to be largest when $L = 1$, as observed, and to change uniformly with chain length. Most of the data are consistent with this too. However, looking at changes at fixed L it is also apparent that increasing steric effect (*i.e.*, increasing N) either strengthens the N–H···O hydrogen bonds to DMSO more than those to water or weakens the hydrogen bonds to water more than those to DMSO. This seems surprising; we would have expected the steric interference to weaken the hydrogen bonds in either solvent and to weaken those in DMSO more because they are stronger to begin with. The observations imply that the peculiar "structural" properties of water play a dominant role here.

For example, one might suppose that the steric interference with a hydrogen bond by a given alkyl group is larger in water than in DMSO because of the conflicting requirements of the solvent–solvent hydrogen bonds in the vicinity of the alkyl groups and the N–H···O hydrogen bonds. In this case the steric effect mainly weakens the N–H···O hydrogen bonds in water. This is consistent with the data for the PC ← DMSO transfers while an interpretation requiring a larger steric effect (leading to strengthening of the H bonds) in DMSO than in water would lead one to expect that the steric effect would be reflected in the data for the PC ← DMSO transfers.

Mutual Interference of the Hydrogen Bonds. The $N = 0$ curve in Figure 4 is a rough extrapolation of the $H_t'(N,L)$ data to $N = 0$ at fixed L. Assuming that the mutual interaction of the hydrogen bonds to a given ammonium ion is destructive rather than cooperative, it follows from the relation of the $N = 0$ curve to line I that the mutual interaction is more destructive in water as solvent than in DMSO. Since this occurs in spite of the large size of a molecule of DMSO relative to H_2O, one may be tempted to also characterize this as a "structural" effect in the water, but in this case it would seem desirable to seek a more detailed explanation in terms of models for the distribution of charge and polarizability in each of the solvent molecules; maybe the dominant effect here is the mutual electrical repulsion of water molecules participating in N–H···O hydrogen bonds to the same nitrogen atom.

It is interesting to note that the $N = 0$ curve in Figure 4 passes through -0.3 kcal/mol at $L = 1$. This may be compared with the corresponding extrapolation for the normal alcohols which may be deduced from Table IV of ref 2, which is -0.4 kcal/mol. This comparison seems reasonable in view of the corresponding comparison in Table III, which was much more simply arrived at. The new comparison tends to support the rather tentative conclusion reached earlier[2] that when an ROH molecule is added to water there is a net gain of one hydrogen bond.

The enormous magnitude of the mutual interference of the hydrogen bonds in water is shown by considering the dotted lines in Figure 4. These represent the data in Table III for the PC ← DMSO transfers after extrapolation to zero chain length. They have been multiplied by $-L$ to correspond to the ordinate scale of Figure 4. Comparing with the $N = 0$ line we see the four hydrogen bonds from NH_4^+ to water are weaker than to PC by 5 kcal/mol and the three hydrogen bonds from $-NH_3^+$ to water are weaker than to PC by 2 kcal/mol while for $\equiv NH^+$ the comparison shows that the hydrogen bond to water is 1.4 kcal stronger than to PC. If the interference effect were negligible in PC these data would average out to an interference in the enthalpy of about 2 kcal/mol per hydrogen bond. It seems important to note that interference effects of this order have been found for three water molecules hydrogen-bonded in the parallel topology

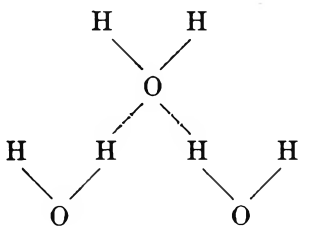

in recent quantum-mechanical calculations.[21] This also suggests that the H-bond interference effects may be understood without recourse to the study of large assemblies of water molecules.

Effect of the Residual Charge in H_t'. It must be noted that the charge does not balance in eq 4.2 in the sense that there is a complete cancellation of the charge when $L = 0$ and no cancellation when $L = 4$. Therefore line II in Figure 4 may be misleading if interpreted as suggested above because it must also incorporate the effect of the changing charge. One may take the enthalpy of transfer $(K^+)_{DMSO \leftarrow W}$ shown in Figure 4 as representative of where the $L = 0$ point on the line II might be if the charge it represents were constant at $+1$. It is not known how to estimate this effect in interpreting the other data in Figure 4. Its neglect in the preceding discussion presumably makes a contribution to what has been identified as the effect of the mutual interference of the hydrogen bonds.

5. D_2O from H_2O Transfers

The new data for enthalpies of transfer to D_2O from H_2O are shown in Figure 5 as a function of the chain length and compared with similar data for other solute types. It is striking that the new data show less leveling-off at large N than the ROH data.[22] In the case of RNH_3^+ much longer chain lengths are accessible to

(21) D. Hankins, J. W. Moskowitz, and F. H. Stillinger, *Chem. Phys. Lett.*, 4, 527 (1970).

(22) G. C. Kresheck, H. Schneider, and H. A. Scheraga, *J. Phys. Chem.*, 69, 3132 (1965).

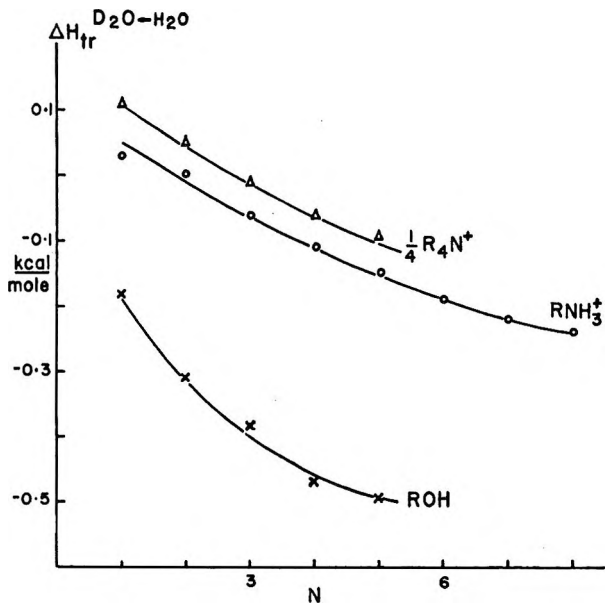

Figure 5. Enthalpies of transfer to D_2O from H_2O based on the data in Table I in the case of RNH_3^+, ref 3 in the case of R_4N^+, and ref 22 in the case of ROH.

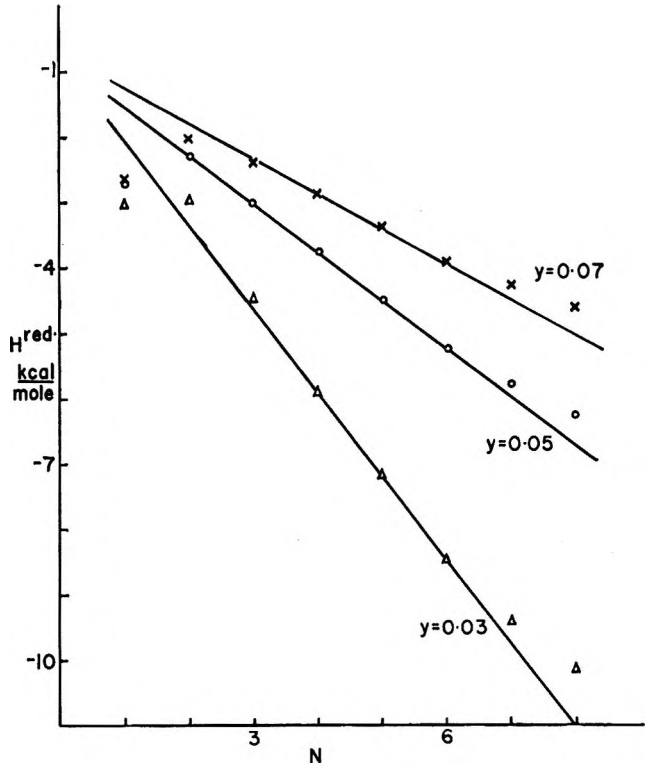

Figure 6. Test of the assumption that the structural effect in aqueous solutions of RNH_3^+ is a fixed percentage larger in D_2O than in H_2O.

determination of calorimetric heats of solution than for the other solutes in Figure 5 because of the more favorable rates of solution.

On the assumption that the structural effect is a fixed percentage larger in D_2O than in H_2O solutions[2] one can reduce the D_2O–H_2O transfer data in terms of enthalpies of transfer to an aprotic solvent from water, as shown earlier.[23] The corresponding plot for the present data is shown in Figure 6. While the treatment of the data in this way is rather difficult here because the enthalpies of the $D_2O \leftarrow H_2O$ transfer are so small for the alkylammonium ions, still reasonably good linearity of the reduced enthalpy plot is obtained for $y = 0.05$, corresponding to the structural effect being 5% larger in D_2O than in H_2O, the same as in the systems studied earlier.[2-4] If the underlying assumptions were correct, one could estimate the slope of the $y = 0.05$ line from the alcohol data[2] and the slopes of the PC $\leftarrow$ DMSO transfers in Figure 1. The estimate obtained in this way, using $y = 0.05$ for the alcohols as well, is -1.12 while the actual slope of the $y = 0.05$ line in Figure 6 is -0.74. A similar calculation can be made for the adjacent y values in the figure, and it is found that the agreement is best for $y = 0.05$. It seems likely that the difference between -1.12 and -0.74 mostly reflects the chain–hydrogen bond interaction in aqueous solutions of RNH_3^+ which was already deduced from the DMSO $\leftarrow$ H_2O transfers in section 4. This also may account for the lack of saturation in the $D_2O \leftarrow H_2O$ transfers of the alkylammonium ions.

The near parallelism of the curves for RNH_3^+ and $^1/_4R_4N^+$ in Figure 5 suggests that the difference, -0.05 kcal/mol, is the enthalpy of transfer of an $-NH_3^+$ group to D_2O from H_2O, although this can be only an approximate figure in view of the evidence previously cited as supporting a substantial chain–H-bond interaction in these solutions. It is of interest to consider how much of the enthalpy of transfer of $-NH_3^+$ might be due to the transfer without exchange and how much due to the establishment of the isotope exchange equilibrium between $-NH_3^+$ and the D_2O medium. While it is hard to investigate this here, it is found that in the case of the alcohols it can be established that the exchange is the dominant effect in the heats of transfer of the –OH group to D_2O from H_2O.

To see this, consider the following sequence of reactions and their heats.

$$CH_3OH(g) + D_2O(g) \longrightarrow CH_3OD(g) + HOD(g) \qquad \Delta H = -0.20 \text{ kcal/mol} \qquad (A)^{24}$$

$$CH_3OD(g) + CH_3OH(L) \longrightarrow CH_3OD(L) + CH_3OH(g) \qquad -0.13 \qquad (B)^{25}$$

(23) See eq 10 and Figure 3 of ref 2, and Figure 3 of ref 3. In those studies the aprotic solvent used was PC while here the reduction is made with DMSO because of the complications due to low rate of dissolution in PC (section 2).

(24) The ΔH for this process was computed from the differences in the zero point energies of the reactants and products. The vibrational frequencies used for calculating these for CH_3OH and CH_3OD are taken from M. Falk and E. Whalley, *J. Chem. Phys.*, **34**, 1554 (1961), and that of HDO and D_2O from the tabulated data given by H. C. Urey, *J. Chem. Soc.*, 562 (1947).

(25) The ΔH for this process has been quoted by L. Benjamin and G. C. Benson, *J. Phys. Chem.*, **67**, 858 (1963).

$D_2O(D) + HOD(g) \longrightarrow$		(C)[26]
$D_2O(g) + HOD(D)$	0.19	
$CH_3OD(L) + CH_3OH(W) \longrightarrow$		(D)[27]
$CH_3OD(D) + CH_3OH(L)$	−0.14	
$CH_3OH(W) + D_2O(D) \longrightarrow$		(E)
$CH_3OD(D) + HOD(D)$	−0.28, −0.18, −0.23	

The final reaction is the sum of the others, and the first value given for its ΔH is obtained by summing the data for the other reactions. The second figure is that determined by Kresheck, Schneider, and Scheraga,[22] and the third is the result obtained by Arnett and McKelvey.[28] The good agreement of the sum with the more directly observed values is gratifying. Moreover, the comparison of the simple exchange reaction (A) with the overall transfer reaction (E) shows that the enthalpy of the exchange reaction is a dominant contribution in the enthalpy of transfer. A similar conclusion can be reached on the basis of a similar treatment for the data for C_2H_5OH assuming that the reaction corresponding to (A) has the same ΔH as (A) itself.

6. Comparison with Other Studies

Here brief mention is made of earlier studies which seem especially relevant to the conclusions reached here.

The rate constant k_H for breaking the N–H···O hydrogen bond in aqueous ammonium salts decreases in the sequence RNH_3^+, $R_2NH_2^+$, R_3NH^+, as is consistent with the present finding that the NH···O hydrogen bond gets stronger in this order.

The partial molal volumes at infinite dilution in alkylammonium salts change with increasing substitution in a way which has been interpreted in terms of decreasing hydration at the N^+ center as one substitutes H by R groups.[15] The effect is qualitatively like the chain–H-bond interaction discussed here.

The nmr relaxation of $^{79}Br^-$ in aqueous solutions of alkylammonium bromides also give evidence for chain–hydrogen-bond interference.[29] The alkylammonium ions all promote the relaxation to a larger extent than predicted from the solution viscosities alone. The extra relaxation produced by an R group is larger when it is in R_4N^+ than in less alkylated ammonium ions.

The effect of the alkylammonium ions in salting-in or salting-out of benzene in aqueous solution[30] also shows that an R group is more effective in tetraalkylammonium ions than in the ions with NH···O hydrogen bonds.

(26) This is the difference in heats of vaporization of D_2O and HDO, the values for which are obtained from "Selected Values of Chemical Thermodynamic Properties," Circular of the National Bureau of Standards, 500, 1952. The heat of mixing of HDO with D_2O or H_2O in the liquid state seems to be negligible, judging from the calorimetric data of E. Lange and E. Doehlemann, *Z. Elektrochem.*, **41**, 539 (1935), for the reaction $H_2O(W) + D_2O(D) \rightarrow 2HOD$ (in mixtures of W and D).

(27) L. Benjamin and G. C. Benson, *J. Phys. Chem.*, **67**, 858 (1963).

(28) E. M. Arnett and D. R. McKelvey in "Solute-Solvent Interactions," J. F. Coetzee and C. D. Ritchie, Ed., Marcel Dekker, New York, N. Y., 1969.

(29) B. Lindman, H. Wennerstrom, and S. Forsen, *J. Phys. Chem.*, **74**, 754 (1970).

(30) J. E. Desnoyers, G. E. Pelletier, and C. Jolicoeur, *Can. J. Chem.*, **43**, 3232 (1965).

Ionization Constants for Water in Aqueous Organic Mixtures

by Earl M. Woolley, Donald G. Hurkot, and Loren G. Hepler*

Department of Chemistry, The University of Lethbridge, Lethbridge, Alberta, Canada *(Received May 14, 1970)*

A potentiometric method is described for determining the equilibrium constants for ionization of water in various aqueous organic mixed solvent systems. The method has been applied to determination of ionization constants for water in binary mixtures of water with ethanol, 1-propanol, 2-propanol, 2-methyl-2-propanol, ethylene glycol, acetone, and *p*-dioxane at 25°. In general, pK_w values increase with increasing organic concentration, but the opposite is observed for glycol solutions and is discussed in relation to enthalpies and entropies of ionization.

Introduction

The ionization of water has been investigated[1] by a variety of methods that have led to reasonably accurate equilibrium constants over a wide range of temperature and pressure and a considerable range of dissolved salt concentration. In spite of evidence[2] of a small error in the temperature dependence of these K_w values, it must be accepted that there are several satisfactory methods for determination of K_w in purely aqueous solvent systems. Similar methods have been applied with considerable success to determination of ionization constants for various weak acids in aqueous solution.

The status of measurements leading to ionization constants for water and various weak acids in aqueous organic mixed solvent systems is not nearly so satisfactory, in spite of excellent work by Harned, Grunwald, Bates, and others.[1,3-5] Experimental methods are difficult and those methods that make use of the hydrogen electrode can only be applied to systems in which there is no complication due to reduction at the hydrogen electrode.

Our measurements were undertaken to provide data on the ionization of water in a variety of aqueous organic mixed solvent systems and to establish a convenient and rapid method for determination of ionization constants of various weak acids in these same solvent systems.

Method and Calculations

We describe the ionization of water in solvent S by[1,6,7]

$$H_2O(S) = H^+(S) + OH^-(S) \qquad (1)$$

Various equilibrium expressions for (1) can be defined on the basis of several reasonable choices of standard states for the various species. One such choice leads to quantities that should be called equilibrium quotients rather than equilibrium constants. In these expressions we use molar concentrations of H^+ and OH^- and set the activity of water to be unity in all solutions so that we have

$$Q_{c/1} = C_H C_{OH} \qquad (2)$$

in which the subscript $c/1$ indicates molar concentrations in the numerator and unit activity in the denominator. We also define an equilibrium constant with activities on the molar scale for H^+ and OH^- and with the activity of water again taken to be unity as

$$K_{a/1} = C_H C_{OH}(y_\pm)^2 = Q_{c/1}(y_\pm)^2 \qquad (3)$$

in which $y_\pm$ is the mean activity coefficient for the solute ions. Still another useful equilibrium expression can be defined with molar activities in the numerator and the activity of water in the denominator set equal to the molarity of water in the solution (subscript a/c so that we have

$$K_{a/c} = C_H C_{OH}(y_\pm)^2/C_w = (K_{a/1})C_w \qquad (4)$$

Our last equilibrium constant is one in which we use activities for all species as indicated by

$$K_{a/a} = C_H C_{OH}(y_\pm)^2/a_w = (K_{a/1})/a_w \qquad (5)$$

In principle we have a wide choice of standard states for the activity of water denoted by a_w, but in practice the only choice that appears to be useful and for which we have the necessary vapor pressure data for a wide variety of systems is the choice based on Raoult's law—that is, the activity of pure water is taken to be unity.

Our investigations of the ionization of water in var-

* To whom correspondence should be addressed.

(1) H. S. Harned and B. B. Owen, "The Physical Chemistry of Electrolyte Solutions," 3rd ed, Reinhold Publishing Corp., New York, N. Y., 1958.

(2) J. W. Larson and L. G. Hepler in "Solute–Solvent Interactions," J. F. Coetzee and C. D. Ritchie, Ed., Marcel Dekker, Inc., New York, N. Y., 1969.

(3) H. S. Harned and L. D. Fallon, *J. Amer. Chem. Soc.*, **61**, 2374 (1939).

(4) B. Gutbezahl and E. Grunwald, *ibid.*, **75**, 565 (1953).

(5) R. G. Bates, "Determination of pH: Theory and Practice," Wiley, New York, N. Y., 1964.

(6) H. S. Harned and B. B. Owen, *Chem. Rev.*, **25**, 31 (1939).

(7) E. J. King, "Acid–Base Equilibria," Pergamon Press, Inc., Oxford, England, 1965.

ious aqueous organic mixed solvent systems are based on the potentials of cells represented by

glass electrode|soln A: $HCl(C_1)$,

$KNO_3(C_2)$, in solvent S|AgCl,Ag (A)

and

glass electrode|soln B: $NaOH(C_3)$,

$NaCl(C_4)$, in solvent S|AgCl,Ag (B)

A general equation for the potentials of these cells is

$$E = k_1 + k_2 \log (a_H a_{Cl}) \quad (6)$$

and a specific equation for cell A is

$$E_A = k_1 + k_2 \log (C_1)^2 + k_2 \log (y_\pm)_A^2 \quad (7)$$

A similar specific equation for cell B containing known concentration of hydroxide ion can be given in terms of an equilibrium expression for the ionization of water. It is convenient to do this in terms of $Q_{c/1}$ defined by eq 2, which leads to

$$E_B = k_1 + k_2 \log (Q_{c/1} C_4/C_3) + k_2 \log (y_\pm)_B^2 \quad (8)$$

Since solvent compositions are the same and ionic strengths in solutions A and B are low and nearly identical for each pair of measurements, junction potentials, asymmetry potentials, glass electrode responses, and mean activity coefficients may be taken to be equal. Thus we combine (7) and (8) to obtain

$$E_A - E_B = k_2 \log (C_1^2 C_3/C_4 Q_{c/1}) \quad (9)$$

Equation 9 leads directly to

$$p(Q_{c/1}) = \frac{E_A - E_B}{k_2} + \log (C_4/C_3 C_1^2) \quad (10)$$

Thus we can calculate $Q_{c/1}$ from the two potentials and known concentrations represented by C_1, C_3, and C_4. This procedure, in which we make use of the difference in two potentials, thereby eliminating the (often unknown) standard potential (k_1) from our calculations, was used by Harned and coworkers[1,6,8] in determining ionization constants for water in aqueous electrolyte systems.

For solvent of any particular composition it is possible to determine the equilibrium constant denoted by $K_{a/1}$ by extrapolating values of $Q_{c/1}$ derived from eq 10 to zero ionic strength, or we can calculate the mean activity coefficient represented by $y_\pm$ by making use of some equation based on the Debye–Hückel theory and then obtain $K_{a/1}$ from eq 3. In general, we have found that $p(K_{a/1})$ values obtained in these two ways differ by less than 0.03 and we have therefore treated most of our data with the equation[1,7]

$$\log (y_\pm)^2 = -\frac{709.0[\rho(S)/\epsilon^3(S)]^{1/2} I^{1/2}}{1 + 8.876[\rho(S)/\epsilon(S)]^{1/2} I^{1/2}} \quad (11)$$

In this equation ρ (S) and ϵ (S) are used to represent the density and dielectric constant of solvent mixture S and I represents the ionic strength, which typically varied from about 0.004 to about 0.015 M. Density and dielectric data were obtained from Timmermans,[9] with additional dielectric data for aqueous 2-methyl-2-propanol from Brown and Ives.[10]

The value of k_2 to be used in eq 10 for each series of measurements was evaluated by setting $pK_{a/1} = 14.00$[1] for the entirely aqueous solvent systems. These k_2 values ranged from 58.3 to 58.9 mV, as compared to $2.303RT/F = 59.16$ mV.

Calculation of $K_{a/c}$ from $K_{a/1}$ only requires knowledge of the molarity of water in the solution and is easily done from knowledge of solvent composition.

Carrying these calculations on to $K_{a/a}$ requires activities of water obtained from

$$a_w = P_w/P_w^0 \quad (12)$$

in which P_w and P_w^0 represent vapor pressures of water over solution S and over pure water, respectively. Vapor pressure data for aqueous 2-methyl-2-propanol solutions have been taken from Brown and Ives.[10] Data for aqueous dioxane are from Goates and Sullivan[11] and data for all other systems are from Timmermans.[9]

Experimental Section

Potential measurements were made both with an Orion Model 801 digital pH meter and with a Corning Model 12 research pH meter. Glass electrodes used with these meters were the Beckman 39004 pH 0–14 electrode, the Coleman 3-472 pH 0–14 electrode, and the Fisher 13-639-1 pH 0–14 electrode. The AgCl,Ag electrode was prepared from a Beckman 39261 Silver Billet Electrode by electrolysis in chloride solution.[5]

Most of our measurements began with cell A containing a known volume of purely aqueous solution of HCl and KNO_3 of known concentrations represented by C_1 and C_2. After E_A was measured, a known amount of pure organic solvent was added and the new potential measured. This procedure was continued until the solvent composition reached 50–60 wt % organic component. The same procedure was then followed with cell B that initially contained the same known volume of purely aqueous solution with appropriate concentrations of NaOH and NaCl such that $C_1 + C_2 = C_3 + C_4$. These C values ranged between 0.0005 and 0.01 M in the initial solutions and decreased in known fashion as the solutions in the cells were diluted with organic solvent.

(8) H. S. Harned and W. J. Hamer, *J. Amer. Chem. Soc.*, 55, 2194 (1933).

(9) J. Timmermans, "The Physico-chemical Constants of Binary Systems in Condensed Solutions," Vol. 4, Interscience Publishers, Inc., New York, N. Y., 1960.

(10) A. C. Brown and D. J. G. Ives, *J. Chem. Soc.*, 1608 (1962).

(11) J. R. Goates and R. J. Sullivan, *J. Phys. Chem.*, 62, 188 (1958).

Table I: Data from a Typical Series of Measurements with Water–Ethanol Mixtures[a]

Wt % EtOH	ϵ	ρ	$-\log (P_w/P_w^0)$	ΔE, mV	$pQ_{c/1}$	$pK_{a/1}$	$pK_{a'a}$	$pK_{a/c}$
0.00	78.5	0.9971	0.000	545.8	13.91	14.00	14.00	15.74
3.77	76.4	0.9902	0.006	547.7	13.99	14.08	14.07	15.80
7.27	74.3	0.9845	0.012	550.1	14.06	14.16	14.15	15.86
10.5	72.5	0.9796	0.017	552.1	14.13	14.23	14.21	15.92
13.5	70.7	0.9754	0.024	553.2	14.19	14.29	14.27	15.96
16.4	69.1	0.9715	0.031	554.1	14.24	14.34	14.31	15.99
21.5	66.7	0.9642	0.038	555.3	14.32	14.42	14.38	16.04
26.0	63.4	0.9573	0.046	556.2	14.38	14.48	14.43	16.07
30.1	61.0	0.9506	0.053	556.3	14.44	14.54	14.49	16.11
33.7	58.8	0.9440	0.058	556.1	14.49	14.60	14.54	16.14
36.9	56.9	0.9377	0.063	555.7	14.52	14.63	14.57	16.14
39.9	55.0	0.9317	0.067	555.2	14.58	14.69	14.62	16.18
42.6	53.4	0.9261	0.071	554.5	14.62	14.74	14.67	16.21
45.1	51.9	0.9208	0.075	553.9	14.65	14.77	14.69	16.22
47.3	50.5	0.9159	0.079	553.1	14.68	14.80	14.72	16.23
49.3	49.3	0.9113	0.082	552.5	14.70	14.83	14.75	16.24
51.3	48.2	0.9069	0.085	551.2	14.74	14.87	14.78	16.26

[a] 20.00 ml of solution in each cell, with $C_1 = 0.005075\ M$, $C_2 = 0.004805\ M$, $C_3 = 0.004880\ M$, and $C_4 = 0.005000\ M$; $k_2 = 58.56$ mV.

In all cases the cells were maintained at 25.0 (± 0.1)° and the potential readings were recorded when they became constant to ±0.1 mV, which was usually within 2 min after each addition of the organic component to the solution in the cell. Measurements were repeated at least three times, using different combinations of pH meters and electrodes. Average deviations in $pQ_{c/1}$ and $pK_{a/1}$ values derived from these independent measurements were always less than 0.06 except for water–dioxane solutions containing more than 40 wt % dioxane, for which some average deviations were as large as 0.13.

Results and Discussion

Data for a typical series of measurements are given in Table I, in which we have also included the auxiliary data used in our calculations and the results of the calculations.

Results of all our pK determinations in mixtures of water with seven organic cosolvents are shown in Tables II–VIII. Each pK value reported is the mean result of three to five series of measurements.

Gutbezahl and Grunwald[4] have reported $pK_{a/1}$ values for mixtures of water with 20.0, 35.0, and 50.0 wt % ethanol. Their results are in excellent agreement with our $pK_{a/1}$ values at the same solvent compositions obtained by interpolation in Table II, with differences of 0.06, 0.05, and 0.02. Harned and Fallon[3] have reported pK values (molality standard state) that lead to $pK_{a/1}$ values for mixtures of water with 20.0 and 45.0

Table II: Ionization Constants of Water in Aqueous Ethanol

Wt % EtOH	$pK_{a/1}$	$pK_{a/a}$	$pK_{a/c}$
0.00	14.00	14.00	15.74
3.77	14.10	14.09	15.82
7.27	14.17	14.16	15.87
10.5	14.23	14.21	15.92
13.5	14.29	14.27	15.96
16.4	14.35	14.32	16.00
21.5	14.43	14.39	16.05
26.2	14.49	14.44	16.08
30.1	14.54	14.49	16.11
33.7	14.61	14.55	16.15
36.9	14.65	14.59	16.16
39.9	14.70	14.63	16.19
42.6	14.75	14.68	16.22
45.1	14.79	14.71	16.24
47.3	14.82	14.74	16.25
49.3	14.85	14.77	16.26
51.3	14.89	14.80	16.28

Table III: Ionization Constants of Water in Aqueous Dioxane

Wt % dioxane	$pK_{a/1}$	$pK_{a/a}$	$pK_{a/c}$
0.00	14.00	14.00	15.74
4.90	14.14	14.14	15.86
9.35	14.27	14.26	15.95
13.4	14.38	14.37	16.07
17.1	14.49	14.47	16.16
20.5	14.60	14.58	16.25
26.5	14.79	14.76	16.41
31.7	14.97	14.94	16.56
36.2	15.14	15.10	16.70
40.1	15.31	15.26	16.84
43.2	15.45	15.40	16.96
46.7	15.60	15.54	17.08
49.5	15.76	15.70	17.22
52 0	15.83	15.76	17.27
54 3	15.93	15.86	17.35
56.3	16.01	15.94	17.41

Table IV: Ionization Constants of Water in Aqueous Ethylene Glycol

Wt % glycol	$pK_{a/1}$	$pK_{a/a}$	$pK_{a/c}$
0.00	14.00	14.00	15.74
5.27	13.93	13.92	15.65
10.0	13.88	13.85	15.58
14.3	13.82	13.78	15.50
18.2	13.78	13.71	15.44
21.8	13.73	13.66	15.38
28.0	13.69	13.60	15.30
33.4	13.65	13.55	15.23
38.0	13.61	13.50	15.16
42.0	13.59	13.47	15.12
45.5	13.57	13.44	15.07
48.6	13.55	13.41	15.03
51.4	13.54	13.38	15 00
53.9	12.54	13.37	14.98
56.1	13.54	13.36	14.95
58.2	13.54	13.35	14.93

Table V: Ionization Constants of Water in Aqueous 1-Propanol

Wt % 1-PrOH	$pK_{a/1}$	$pK_{a/a}$	$pK_{a/c}$
0.00	14.00	14.00	15.74
3.86	14.08	14.08	15.80
7.43	14.17	14.17	15.88
10.7	14.24	14.24	15.93
13.8	14.29	14.29	15.96
16.7	14.35	14.35	15.98
21.9	14.42	14.42	16.04
26.5	14.49	14.48	16.08
30.6	14.55	14.54	16.11
34.3	14.62	14.61	16.16
37.6	14.66	14.65	16.17
40.6	14.73	14.72	16.22
43.3	14.78	14.77	16.24
45.7	14.83	14.81	16.27
48.0	14.87	14.86	16.29
50.1	14.92	14.91	16.32

Table VI: Ionization Constants of Water in Aqueous 2-Propanol

Wt % 2-PrOH	$pK_{a/1}$	$pK_{a/a}$	$pK_{a/c}$
0.00	14.00	14.00	15.74
3.77	14.11	14.11	15.83
7.26	14.20	14.19	15.90
10.5	14.30	14.29	15.97
13.5	14.38	14.36	16.03
16.4	14.46	14.44	16.09
21.5	14.58	14.56	16.18
26.1	14.67	14.64	16.23
30.1	14.76	14.73	16.29
33.7	14.84	14.81	16.35
37.0	14.91	14.87	16.39
40.0	14.98	14.94	16.44
42.7	15.04	15.00	16.47
45.1	15.10	15.05	16.51
47.4	15.15	15.10	16.54
49.5	15.22	15.17	16.59

Table VII: Ionization Constants of Water in Aqueous 2-Methyl-2-Propanol

Wt % *t*-BuOH	$pK_{a/1}$	$pK_{a/a}$	$pK_{a/c}$
0.00	14.00	14.00	15.74
3.76	14.12	14.11	15.84
7.26	14.23	14.21	15.93
10.5	14.32	14.30	16.01
13.5	14.40	14.38	16.07
16.4	14.46	14.44	16.11
21.5	14.61	14.59	16.23
26.0	14.70	14.68	16.29
30.1	14.77	14.74	16.33
33.7	14.86	14.83	16.40
37.0	14.95	14.92	16.46
39.9	15.01	14.98	16.50
42.7	15.09	15.06	16.55
45.1	15.16	15.13	16.60
47.4	15.22	15.19	16.64
49.4	15.29	15.26	16.69

wt % dioxane that differ by 0.03 and 0.14 from the values we obtain at the same solvent compositions by interpolation in Table III. For solutions that are 10.0, 30.0, and 50.0 wt % ethylene glycol we have pK values (molality standard state) and thence $pK_{a/1}$ values from Banerjee, Kundu, and Das[12] that differ by 0.03, 0.00, and 0.02 from the values we obtain at the same concentrations by interpolation in Table IV.

All of the earlier pK values cited above[3,4,12] were derived from measurements with the hydrogen electrode. The good agreement of those results with our results confirms that the glass electrode responds to the same H^+ (S) species in these aqueous organic solvent systems as does the hydrogen electrode.

Results of our pK determinations are displayed graphically in Figures 1, 2, and 3. A simple treatment in which the solvent is regarded as a continuous dielectric medium suggests that a plot of pK *vs.* $1/\epsilon$(S) should be linear with positive slope.[1,5,7] Figure 1 demonstrates once again the well known inadequacies of this approach, especially for water–glycol mixtures for which the slope is negative. Figure 2 was suggested by Marshall's[13] treatment of "complete" equilibrium constants in relation to "traditional" constants. According to this treatment, which was intended to apply only in the case of "inert" cosolvents such as dioxane, the slopes of the lines provide evidence about the difference between "hydration numbers" of H^+(S) + OH^-(S)

(12) S. K. Banerjee, K. K. Kundu, and M. N. Das, *J. Chem. Soc., A*, 166 (1967).

(13) W. L. Marshall, *J. Phys. Chem.*, **74**, 346 (1970).

Table VIII: Ionization Constants of Water in Aqueous Acetone

Wt % acetone	$pK_{a/1}$	$pK_{a/a}$	$pK_{a/c}$
0.00	14.00	14.00	15.74
3.79	14.11	14.11	15.84
7.30	14.21	14.20	15.92
10.6	14.30	14.29	15.99
13.6	14.42	14.40	16.09
16.5	14.51	14.48	16.17
21.6	14.68	14.64	16.31
26.2	14.84	14.79	16.44
30.2	15.00	14.94	16.57
33.9	15.12	15.05	16.66
37.1	15.24	15.16	16.75
40.1	15.36	15.27	16.85
42.8	15.48	15.38	16.95
45.3	15.58	15.47	17.03
47.5	15.69	15.57	17.12
49.6	15.78	15.66	17.19

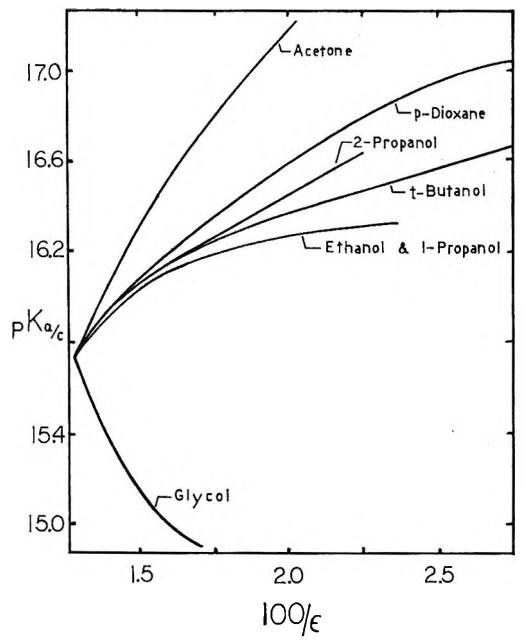

Figure 1. Plots of $pK_{a/c}$ *vs.* $1/\epsilon$ as suggested by the Born theory.

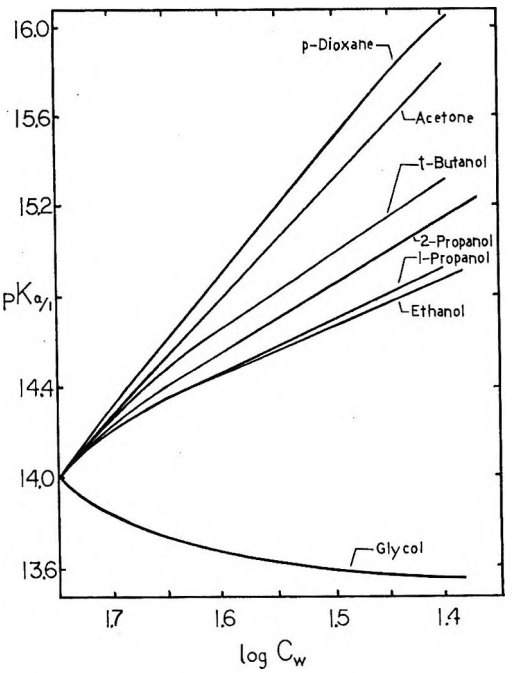

Figure 2. Plots of $pK_{a/1}$ *vs.* log C_w as suggested by Marshall's treatment.[13]

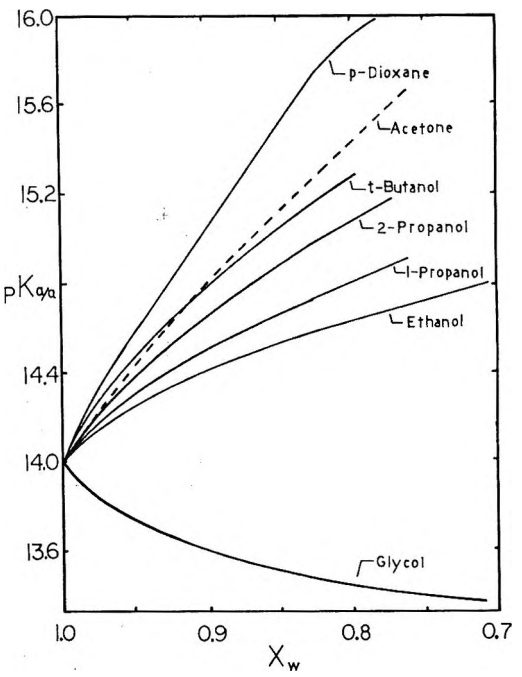

Figure 3. Plot of $pK_{a/a}$ *vs.* mole fraction of water in the solvent.

and $H_2O(S)$. The initial slopes of these lines are about -3, $+5$, $+5$, $+5$, $+6$, $+6$, and $+7$ for mixtures of water with ethylene glycol, ethanol, 1-propanol, 2-propanol, 2-methyl-2-propanol, acetone, and dioxane, respectively. Comparison of Figures 1–3 shows the importance of careful consideration of standard states and the basis for classifying or describing solvent composition. For example, in Figure 1 we have pK for water in aqueous acetone always greater than pK for water in aqueous dioxane, whereas just the reverse order is observed in Figures 2 and 3.

Possibly the most striking feature of all our results is the qualitative difference between pK values for ionization of water in aqueous ethylene glycol and in all of the other systems. The increasing values of pK with increasing organic content in the solvent system is to be expected on the basis of the decreasing dielectric constant of the medium and has been observed before for aqueous ethanol and dioxane,[3,4] in good agreement with our results. Further, the "unexpected" decrease in pK for ionization of water in aqueous ethylene glycol has

also been observed before,[12] again in good agreement with our results. It thus appears that neither the "normal" behavior of water in most of the systems nor the "abnormal" behavior in aqueous ethylene glycol can be attributed to experimental error.

Banerjee, Kundu, and Das[12] have previously discussed the decrease in pK for ionization of water in aqueous ethylene glycol in terms of the idea that ethylene glycol is more acidic and less basic than water. Since further understanding along this line requires more data about the acid–base properties of the organic solvents that appear to lead to "normal" behavior of water in their aqueous mixtures, we presently turn to another approach.

Earlier calorimetric measurements[14] have led to ΔH° values for reaction 1 in aqueous ethanol mixtures. We also have ΔH° values for reaction 1 in aqueous ethylene glycol from the pK values at several temperatures as calculated by Banerjee, Kundu, and Das.[12] Both sets of positive ΔH° values decrease with increasing organic content, which corresponds to decreasing (positive) ΔG° of ionization and thence to decreasing pK values as observed for water in ethylene glycol, but opposite to the observed trend for ionization of water in aqueous ethanol. It is therefore required that the trend in $T\Delta S^\circ$ with increasing organic content must be dominant in determining the trend in pK for ionization of water in aqueous ethanol.

As previously noted, the choice of standard states can have important bearing on conclusions drawn from comparisons of equilibrium constants, and also on ΔG° and ΔS° values derived from these equilibrium constants. For present purposes it appears to be most useful to calculate ΔG° from p$K_{a/c}$ values and then to combine these ΔG° values with the ΔH° values cited above to obtain $T\Delta S^\circ$ values. In order to display the results of these calculations in convenient form, we define the quantity $\delta\Delta G^\circ$ in terms of the difference between pK values in solvent S and for pure water as

$$\delta\Delta G^\circ = 2.303RT(\mathrm{p}K_{a/c}^{s} - \mathrm{p}K_{a/c}^{w}) \qquad (13)$$

in which superscripts s and w indicate pK values referring to solvent system S and to pure water. We similarly define $\delta\Delta H^\circ$ as

$$\delta\Delta H^\circ = \Delta H_s^\circ - \Delta H_w^\circ \qquad (14)$$

in which subscripts s and w indicate ΔH° of ionization values referring to solvent system S and to pure water. We also have

$$T\delta\Delta S^\circ = \delta\Delta H^\circ - \delta\Delta G^\circ \qquad (15)$$

Values of $\delta\Delta G^\circ$, $\delta\Delta H^\circ$, and $T\delta\Delta S^\circ$ for ionization of water in aqueous ethanol and in aqueous ethylene glycol are displayed in Figure 4. We see that there is partial compensation of $\delta\Delta H^\circ$ values by $T\delta\Delta S^\circ$ values so that changes in $\delta\Delta G^\circ$ values are smaller than the increments in either enthalpy or entropy with changes in the chemical system under consideration. This sort of compensation has been observed many times before[2,7] for other ionization reactions and also for other reactions in solution. The magnitude of $\delta\Delta H^\circ$ for ionization of water in aqueous ethylene glycol is always larger than the corresponding $T\delta\Delta S^\circ$ value and thus establishes the trend in $\delta\Delta G^\circ$ that accounts for the "unusual" decrease in pK with increasing glycol concentration. Except at very small ethanol concentration, the situation is just the reverse for aqueous ethanol, where the magnitude of $T\delta\Delta S^\circ$ is greater than that of the corresponding $\delta\Delta H^\circ$. It is therefore $T\delta\Delta S^\circ$ that largely accounts for the "normal" trend in $\delta\Delta G^\circ$ for ionization of water in aqueous ethanol, and we might expect to find the same situation for other "normal" solutions. Further data are necessary to determine whether $T\delta\Delta S^\circ$ values are in fact larger than $\delta\Delta H^\circ$ values for these other systems.

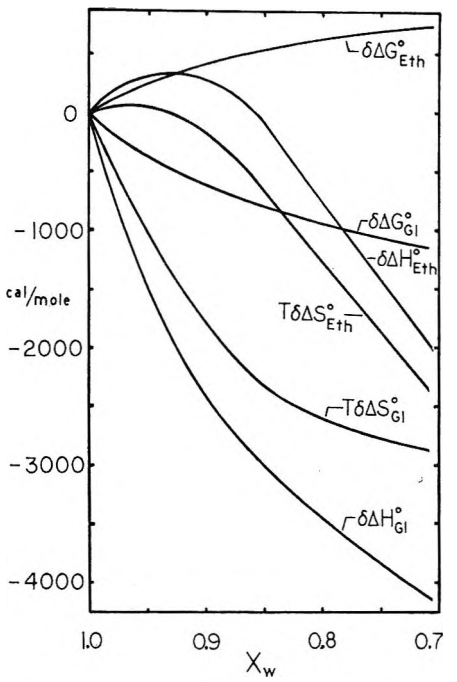

Figure 4. Thermodynamics of ionization of water in aqueous ethanol and ethylene glycol.

Acknowledgment. We are grateful to the National Research Council of Canada for support of this research.

(14) G. L. Bertrand, F. J. Millero, C. H. Wu, and L. G. Hepler, *J. Phys. Chem.*, **70**, 699 (1966).

Evidence for Very Early Effects in the Radiolysis of Water

by Takeshi Sawai and William H. Hamill*

Department of Chemistry and the Radiation Laboratory,[1] University of Notre Dame, Notre Dame, Indiana 46556
(Received February 4, 1970)

This investigation is based on the working hypothesis that very early electronic effects in aqueous systems (*i.e.*, those which precede dipole relaxation) are susceptible to observation. As a possible example, high concentrations of neutral Cl^- produce large yields of Cl_2^- and an increase in $G(e_{aq}^-)$ which can be attributed to hole trapping. Extensive studies of charged species in the radiolysis of liquid and solid alkanes provide a partial guide to the physical and chemical effects to be expected in water prior to relaxation. Relative scavenging efficiencies of solutes for mobile electrons in CH_3OH–H_2O glasses at 77°K do not correlate consistently with the rate constants $k(e_{aq}^- + S)$ in water. The effects of phenol, acetone, Cd^{2+}, HCl, and NO_3^- on G_{H_2} in aqueous solutions correlate better with results for glassy CH_3OH–H_2O than with conventional rate constants. In aqueous solutions results for scavenging dry electrons and holes (by hypothesis) are described by a trial function algebraically equivalent to a conventional kinetic competition between first-order decay and second-order scavenging. Relative efficiencies of scavengers and primary yields of precursors appear as parameters, and internal consistency provides a test of the probably over-simplified model. Hole scavenging by anions appears to be a general phenomenon and OH^- does not occupy a unique position. Results in very acid solutions may be complicated by this anion effect. High yields of oxidized species, *e.g.*, Cl_2^- and I_2^-, and an increase in $G(e_{aq}^-)$ at high concentrations of OH^-, Cl^-, and F^- support the dry electron model.

Introduction

The following reactions are generally considered to contribute to G_{H_2}, the yield of "molecular" hydrogen in water, according to the spur diffusion model[2]

$$e_{aq}^- + e_{aq}^- \longrightarrow H_2 \quad (1)$$

$$e_{aq}^- + H \longrightarrow H_2 \quad (2)$$

$$H + H \longrightarrow H_2 \quad (3)$$

Mahlman and Sworski[3] have pointed out that competition between N_2O and H^+ and between NO_3^- and H^+ for e_{aq}^- gives results which seem to be inconsistent with known rate constants.[4] The substantial constancy of G_{H_2} over the range pH 0.89 to 12.6 was taken as evidence that e_{aq}^- in the spur is not a precursor of H_2. These and other possible difficulties have been reviewed by Anbar.[5]

Schwarz[6] has recently reported the results of quantitative calculations, using the spur diffusion model, for several aqueous systems which had been claimed to be anomalous. He has shown that the spur diffusion model "is adequate to explain the major portion of the molecular yields of hydrogen and hydrogen peroxide."[6] This model assumes that at a time between 10^{-11} and 10^{-10} sec after the primary event the radiolysis of water can be described in terms of the entities e_{aq}^-, H, H_2, H_3O^+, and OH, with e_{aq}^- on the average 23 Å from the center of the spur.[6]

An attempt has been made by Hamill[7] to describe the radiolysis of water in terms of a somewhat different model with the emphasis on very early events. It is an implicit consequence of the spur diffusion model that the electron encounters not less than $\sim 10^2$ molecules prior to hydration, and some prompt recombination cannot be excluded. Very early events in water would resemble those in an alkane because the high-frequency dielectric constant is ~2, and such dry electrons should be scavengable as they are in alkanes. The efficiency of scavenging dry electrons in water will be less than it is in alkanes because hydration competes with recombination of the dry charge pair. There are only three features of the dry electron model which need be considered here. (1) Some charge recombination occurs before hydration and is responsible for the molecular products, H_2 and H_2O_2. (2) Prior to dipole relaxation the "dry" hole H_3O^+ (or H_2O^+) and dry electron e^- can be trapped by suitable reagents. (3) The chemical behavior of the dry electron is to be inferred from the reactions of the "mobile electron" e_m in polar solids, or of the electron in liquid and solid alkanes.[8] One concludes by these criteria that dry electrons, unlike e_{aq}^-, react efficiently with phenol and very inefficiently with $H_3O_{aq}^+$. It should be noted that the dry electron

* To whom correspondence should be addressed.

(1) The Radiation Laboratory of the University of Notre Dame is operated under contract with the U. S. Atomic Energy Commission. This is AEC document No. COO-38-690.

(2) "Fifth Informal Conference on the Radiation Chemistry of Water," Radiation Laboratory, University of Notre Dame, 1966, COO-38-519 (1967).

(3) "The Chemistry of Ionization and Excitation," G. R. A. Johnson and G. Scholes, Ed., Taylor and Francis Ltd., London, 1967, p 259.

(4) M. Anbar and P. Neta, *Int. J. Appl. Radiat. Isotopes*, **18**, 493 (1967).

(5) M. Anbar in "Fundamental Processes in Radiation Chemistry," P. Ausloos, Ed., Wiley, New York, N. Y., 1968, Chapter 10.

(6) H. A. Schwarz, *J. Phys. Chem.*, **73**, 1928 (1969).

(7) W. H. Hamill, *ibid.*, **73**, 1341 (1969).

(8) W. H. Hamill in "Radical Ions," E. T. Kaiser and L. Kevan, Ed., Wiley-Interscience, New York, N. Y., 1968.

model is concerned only with electronic processes, *i.e.*, events prior to solvation. Molecular motions and conventional kinetics can be neglected. Electronic events probably terminate at $\sim 10^{-12}$ sec and therefore do not overlap the range covered by the spur diffusion model. Consequently, the studies reported here may bear on apparent difficulties of the spur diffusion model, but not on those which are real (if there any).

Recently reported experiments[9] provide evidence that e_m^- in methanol–water glassy solids at 77°K reacts efficiently with C_6H_6, C_6H_5OH, Cd^{2+}, and NO_3^- and that HCl suppresses the yield of Cd^+ but not the reduction products C_6H_7 and C_6H_6OH from C_6H_6 and C_6H_5OH, while NO_3^- suppresses all these reduced products quite efficiently.

The present preliminary study considers principally the effects of scavengers for H atoms, for e_{aq}^- and e^-, and for H_2O^+ or H_3O^+ (the dry hole), on the yield of molecular hydrogen. By way of illustration, allyl alcohol is selective for H atoms with $k(H + C_3H_5OH) = 2.3 \times 10^9\ M^{-1}\ sec^{-1}$; there is no measurable reaction with electrons.[4] Strong acid is specific for e_{aq}^-, according to the evidence cited. Phenol is a comparatively efficient reagent for e^- in 3-methylpentane or methanol at 77°K while $k(e_{aq}^- + C_6H_5OH) = 1.8 \times 10^7\ M^{-1}\ sec^{-1}$ and $k(H + C_6H_5OH) = 4.2 \times 10^9\ M^{-1}\ sec^{-1}$, with the H adduct formed in both instances.[4,10]

The scavenging of dry charge species involves competition with prompt recombination and with hydration. These are first-order and second-order processes in a limited sense because conventional kinetics is not applicable. It will be assumed that the relative probabilities of scavenging and first-order removal can be fitted by $\sigma_1[S]/\sigma_2$, where [S] is the concentration of scavenger and the σ's are appropriate parameters, *e.g.*, cross sections. The corresponding trial function is given by

$$G(\text{product}) = G_1^\circ(\text{product}) \pm \frac{G_2^\circ(\text{precursor})\sigma_1[S]}{\sigma_1[S] + \sigma_2} \quad (A)$$

In some systems G_1° may be zero, in others it may equal G_2°. When $G_1^\circ = G_2^\circ$, the dependence of G^{-1} *vs.* [S] is linear and such a plot is preferred when it is permitted. When $G_1^\circ \neq G_2^\circ$, then G_1° becomes a fitted parameter and $(G - G_1^\circ)^{-1}$ *vs.* $[S]^{-1}$ is linear. It should be noted that G_2° is the total yield of scavengable precursor when $G_1^\circ = 0$. When $G_1^\circ \neq 0$, G_2° represents only the partial yield of precursor which gives rise to the product being measured and not necessarily to all of the latter. It will be convenient to use, *e.g.*, $G_2^\circ(H_2)$ to represent that part of the primary yield of the product which is susceptible to suppression by scavenging of a precursor.

Experimental Section

Water was triply distilled. Allyl alcohol was purified by distillation and passed through a column of activated alumina. Acetone-d_6 and acetic acid-d_4 were 99.7 atom % isotopic purity. Inorganic chemicals were Baker's analytical grade.

Samples of 5 ml of aqueous solutions were purged with N_2 and outgassed by repeated freeze–pump–thaw cycles, then sealed in Pyrex cells with break-seals. Irradiation with ^{60}Co γ rays was conducted at 1.36×10^{18} eV g^{-1} min^{-1}, determined by Fricke dosimetry. The results for $G_{H_2O_2}$ and $G(NO_2^-)$ with Cl^- as scavenger, which have been published in part,[11] were performed at the Tokyo Metropolitan Isotope Center. For these experiments the dose was 7.8×10^{17} eV/g. The yields for all aqueous solutions were measured in the linear region of yield–dose dependence. For measurements of G_{H_2} the solutions contained $5 \times 10^{-2}\ M$ allyl alcohol (to scavenge H and OH) except for solutions of phenol. Gaseous products were recovered by Toepler pumping and analyzed using a CEC 21-102 mass spectrometer. The experimental procedures for methanolic glasses have been described.[9]

Results

Electrons in Aqueous Glass. The effects of several solutes on the 560-nm absorption of e_{solv}^- in glassy 38% CH_3OH–62% H_2O at 77°K were surveyed to allow comparison of scavenging efficiencies for e_m^- (which is presumed to be dry) with e_{aq}^-. They are also to be compared with results for electron scavenging in water at high solute concentrations. The results appear in Figure 1 and values of σ_1/σ_2 are summarized in Table I.

H Atom Scavenging. Small concentrations of allyl alcohol depress G_{H_2} by ~ 0.05, with G_{H_2} in acid solutions greater than in neutral solutions. The results, summarized in Table II, show a very slow decrease in G_{H_2} for $[C_3H_5OH] > 0.1\ M$, which may be due in part to simple dilution.

The α-hydrogen of allyl alcohol is rather reactive and at low pH $G(H)$ is much larger than G_{H_2}. As a result the contribution to $G(H_2)$ from $G(H)k_4/(k_4 + k_5)$ must be considered according to reactions 4 and 5. An esti-

$$C_3H_5OH + H \longrightarrow C_3H_4OH + H_2 \quad (4)$$

$$C_3H_5OH + H \longrightarrow C_3H_6OH \quad (5)$$

mate of this contribution to G(hydrogen) was made using solutions of allyl alcohol in D_2O with the results shown in Table I. $\Delta G_{HD} = 0.053$ and 0.050 in D_2O when $G_{e_{aq}^-} \cong 2.3$ is converted into $G(D) = 2.3$ by acid, from which one obtains $k_4/k_5 = 0.022$. At $10^{-2}\ M$ allyl alcohol in H_2O, results for neutral and 0.1 M acid solutions give $k_4/k_5 = 0.021$. Similarly with 1 M alyl alcohol, $k_4/k_5 = 0.019$. If one adopts $G_H^\circ = 0.62$ which Schwartz has used,[6] then reaction 4 contributes

(9) T. Sawai and W. H. Hamill, *J. Phys. Chem.*, 73, 2750 (1969).
(10) E. J. Land and M. Ebert, *Trans. Faraday Soc.*, 62, 1181 (1967).
(11) T. Sawai and W. H. Hamill, *J. Chem. Phys.*, 52, 2843 (1970).

Table I: Relative Efficiencies for Scavenging e_m^- in Methanol–Water at 77°K, e^- and e_{aq}^- in Water

Primary solute	Secondary solutes	(a) σ_1/σ_2 soln	(b) σ_1/σ_2 glass[a]	(c) $k_{e^-} \times 10^{-10}$ [b]	(a)/(c)[c]	(a)/(b) × 10^2
Cd^{2+}	0.1 *N* H^+	1.7	13	5.2	1.6	13
Cu^{2+}		8.4	60	3.5	12	14
NO_2^-		1.5	22	0.6	1.3	7
NO_3^-	1 *N* H^+	2.6	40	1.0	1.3	6
H_2O_2		0.94	18	1.2	0.8	5
CH_3NO_2		21	60	0.5	42	35
$(CH_3)_2CO$	10^{-2} *N* H^+	0.9	19	0.6	1.5	5
C_6H_5OH		0.6	1.2	0.002	300	50

[a] No second solute. [b] From ref 4. [c] The rate constants for Cd^{2+} and Cu^{2+} have been multiplied by 0.2, those for NO_3^- and NO_2^- by 2 as a rough adjustment for ionic strength effects.

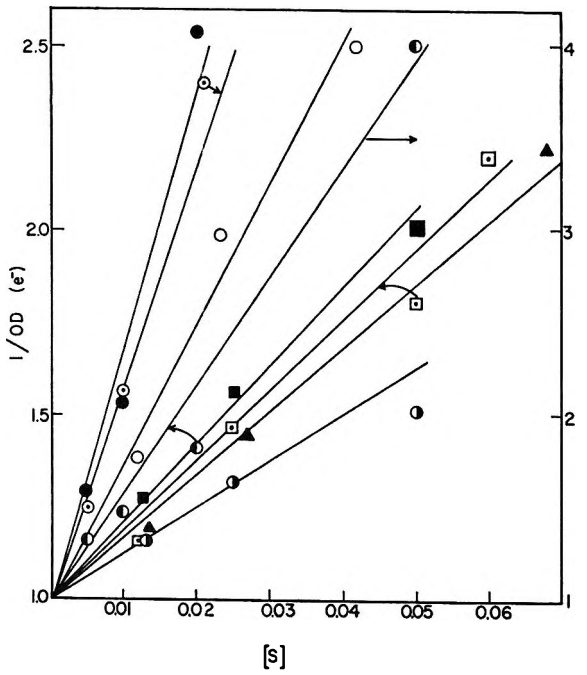

Figure 1. The relative efficiencies of several solutes for decreasing $OD(e_{solv}^-)$ in 38 mol % CH_3OH–62 mol % H_2O at 77°K and 10^{19} eV g^{-1} in a cell 2 mm thick. The curves, reading clockwise, describe results for Cu^{2+}, CH_3NO_2, phenol ($3 \times \Delta OD^{-1} - 2$), acrylonitrile (right-hand scale), NO_2^-, acetone, H_2O_2, and Cd^{2+}.

Table II: Effect of Allyl Alcohol on Hydrogen Yields in H_2O and in D_2O[a]

Allyl alcohol, *M*	HCl, *M*	$G(H_2)$	$G(D_2)$	$G(HD)$
0.01	1	0.447		
0.05	1	0.413		
0.10	1	0.423		
0.50	1	0.410		
1.0	1	0.410		
0.01	0.1	0.437		
0.05	0.1	0.443		
0.10	0.1	0.405		
0.50	0.1	0.398		
1.0	0.1	0.393		
1.5	0.1	0.388		
0.01	0	0.381		
0.2	0	0.382		
1.0	0	0.358		
0.2	0	0.005	0.240	0.039[b]
1.0	0	0.027	0.166	0.069
0.2	0.01	0.011	0.195	0.092
1.0	0.01	0.019	0.154	0.119

[a] Dose = 1.3×10^{19} eV g^{-1}. [b] In neutral 0.02 *M* NO_3^-, $G_{HD} = 0.0060$, $G_{D_2} = 0.244$; for 0.1 *M* NO_3^-, $G_{HD} = 0.0048$, $G_{D_2} = 0.182$.

$\Delta G(H_2) \cong 0.012$ in neutral 1 *M* allyl alcohol. The corrected G_{H_2} becomes $0.358 - 0.012 = 0.346$ and $\Delta G_{H_2} \cong 0.44 - 0.346 = 0.09$ for the combined contributions of reactions 2 and 3 to G_{H_2}.

Electron Scavenging. Several scavengers have been used in this work, both in neutral and acid (HCl) solutions. Acid solutions also contained 0.05 *M* allyl alcohol to remove H and OH. The systems have been selected with the purpose of testing the dry electron model, *e.g.*, dry electrons do not react with acid.

Acetone-d_6 was used to examine the effect of electron scavenging on G_H. For the combined yields $G_{H_2} + G_H$, 0.1 *M* isopropyl alcohol in neutral solution was used. For measurements of G_{H_2}, solutions contained 0.05 *M* allyl alcohol and 0.01 *M* HCl. The results, which appear in Figure 2, show that the yield of hydrogen from acetone cannot be neglected. The yield of H atoms, $G_H = G(H_2) - G_{H_2}$, would be substantially constant at 0.2 *M* acetone-d_6 if a small correction for dilution were to be applied.

The effect of NO_3^- on G_{H_2} with 10^{-2} *M* and 1 *M* HCl and 0.05 *M* allyl alcohol appears in Figure 3 and Table III. Scavenging of H atoms occurs almost entirely by 0.05 *M* allyl alcohol, even at 0.5 *M* NO_3^-. If e_{aq}^- is the principal precursor of molecular hydrogen, then in 1 *M* HCl conversion into H atoms will be considerable with appreciable scavenging by allyl alcohol. There is no evidence for such an effect. If the dry electron is an

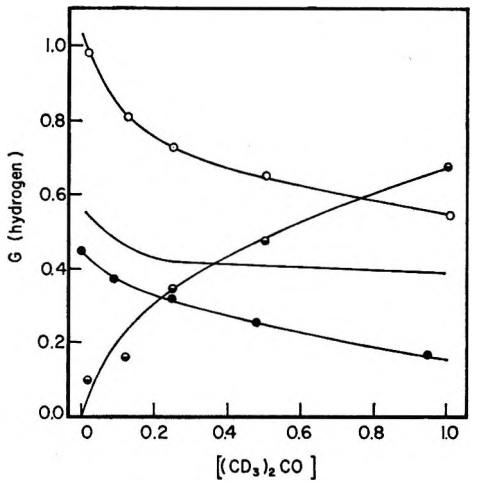

Figure 2. The yield of H_2 for solutions of acetone-d_6 with 0.1 M isopropyl alcohol (○); G_{H_2} (●) and 10 × G(HD) (◒) for 0.05 M allyl alcohol and 0.01 M HCl. The difference curve is attributed to G_H.

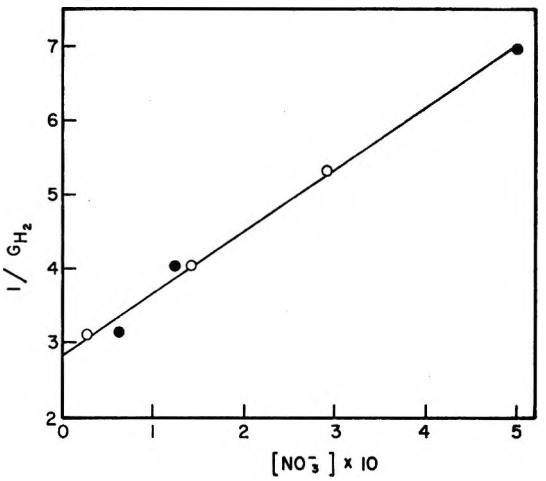

Figure 3. The yield of molecular hydrogen with 10^{-2} M HCl (○) and 1 M HCl (●), as functions of NO_3^- concentration. Both systems contain 0.05 M allyl alcohol.

important precursor of H_2, acid would not compete with NO_3^-.

For $G(H) = 3.3$ and $k_4/k_5 = 0.02$, allyl alcohol will produce $\Delta G(H_2) \cong 0.07$ at low pH and for $[NO_3^-] = 0$, but this will decrease as $[NO_3^-]$ increases. This changing contribution from $\Delta G(H_2)$ has been subtracted from the observed $G(H_2)$. The value $G_1^\circ = 0.35$ is less than the value for water, ~0.45, due to 0.02 M allyl alcohol. Equations formally equivalent to A have been used by Sworski[12] for the effects of scavengers on G_{H_2}. His values of σ_1/σ_2 for NO_3^- in other systems agree approximately with ours and are included in Table III.

The results of Hayon[13] for $G(NO_2^-)$ in aerated 0.005 M ethanol and NO_3^- appear in Figure 4. Values of σ_1/σ_2 for these two systems are roughly equal, 2.9 and 1.9, which is to be expected if $\Delta G(H_2)$ and $\Delta G(NO_2^-)$

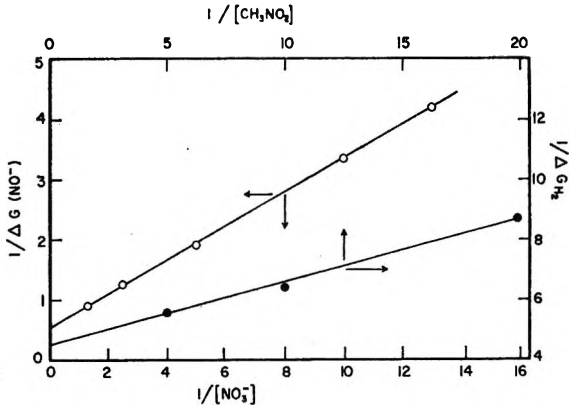

Figure 4. G_{H_2} as a function of $[CH_3NO_2]$ (●); $G(NO_2^-)$ as a function of $[NO_3^-]$, from Hayon's results[13] (○).

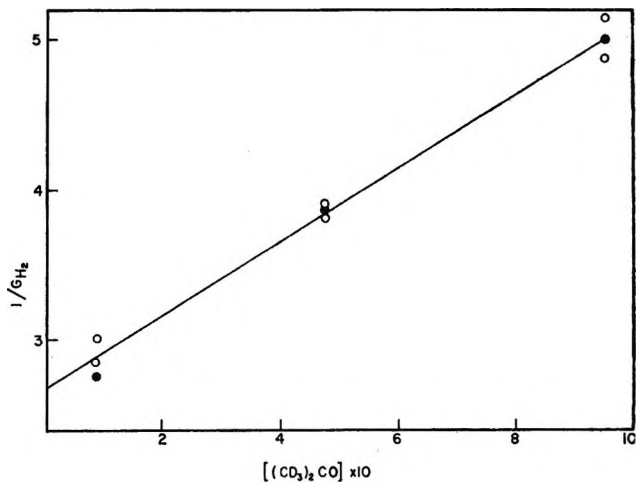

Figure 5. The yield of molecular hydrogen as a function of acetone-d_6 concentration with 10^{-2} (●), 10^{-1} (○), and 1 M HCl (⊙).

are due to a common precursor. The combined yield is $G_1^\circ(NO_2^-) + G_2(NO_2^-) = 3.9$. This value will be shown to be typical for G°(electrons), but the reaction scheme in this system cannot be stated with confidence.

Both G_H and G_{H_2} were measured by Appleby[14] using acetone but use of this reagent involves some ambiguity which can be avoided by using acetone-d_6. As an example, at [acetone-d_6] = 1 M, G(HD) was 0.07 in neutral solution. Results for $G(H_2)$ in solutions containing 0.05 M allyl alcohol and 10^{-2}, 10^{-1}, or 1 M HCl appear in Figure 5 and Table III. They have been corrected for $\Delta G(H_2)$ from allyl alcohol. The precursors of molecular hydrogen not suppressed by allyl alcohol appear to be completely scavengable by acetone, and they are substantially indifferent to as much as 1 M HCl. Again, G_1° is smaller than G_{H_2} because of added allyl alcohol.

(12) T. J. Sworski in "The Solvated Electron," Advances in Chemistry Series, American Chemical Society, Washington, D. C., 1965, p 263.

(13) E. Hayon, *Trans. Faraday Soc.*, **61**, 723 (1965).

(14) A. Appleby, ref 3, p 269.

Table III: Summary of Results for Scavenging Electrons and Holes in Water

Primary solute	Secondary solute or condition	Product measured	$G_1°$ product	$G_2°$ precursor	σ_1/σ_2	$G°(e^-)$ or $G°(H_3O^+)$	Reference
NO_3^-	1 M HCl[d]	H_2	0.35	0.35	2.9		This work
NO_3^-	Ce^{4+}, H_2SO_4	Ce^{3+}	7.92	5.4	2.3		12
NO_3^-		H_2		0.34	2.57		12
NO_3^-	Reactor radiation	H_2		0.67	2.35		12
NO_3^-	O_2 ethanol, NO_3^-	NO_2^-	2.1	1.8	1.9	3.9[a]	13
OH^-	HCO_2^-, NO_3^-	NO_2^-	~2.5	~1.1	3.5	~3.8[b]	13
OH^-		OH	2.1	1.5	3.4	3.6[a] 4.2[c]	13
OH^-		H_2O_2	0.75	0.40	3.0		13
NO_2^-		H_2		0.354	1.48		12
Cl^-	NO_3^-, propanol	NO_2^-	2.76	0.72	0.41	3.4[b]	This work
Cl^-	O_2, i-PrOH	H_2O_2	3.5	3.7	0.43		15
Cl^-		Cl_2^-		3.8	0.38	3.8	17
Cl^-		H_2O_2	0.64	0.83	0.43		This work
I^-	Aerated	I_2^-	(2.7)	2.0	0.60		15
C_6H_5OH		H_2	0.41	0.20	0.61		This work
C_6H_5OH	0.1 N HCl	H_2	0.40	0.20	0.91		This work
C_6H_5OH	1 N HCl	H_2	0.46	0.20	2.6		This work
CH_3NO_2	1 N HCl[d]	H_2	0.38	0.22	21		This work
$(CD_3)_2CO$	10^{-2} N HCl[d]	H_2	0.37	0.37	0.90		This work
$(CD_3)_2CO$	10^{-1} N HCl[d]	H_2	0.37	0.37	0.90		This work
$(CD_3)_2CO$	1 N HCl[d]	H_2	0.37	0.37	0.90		This work
H_2O_2		H_2		0.345	0.94		12
H_2O_2	19 MeV D^+	H_2		0.475	0.98		12
$H_2^{16,16}O_2$	$H_2^{18}O$	$H_2^{18,18}O_2$	0.745	0.53	0.46		16
Cu^{2+}		H_2		0.325	8.40		12
Cd^{2+}	10^{-1} N HCl	H_2	0.42	0.18	1.7		This work
Cd^{2+}	1 N HCl[d]	H_2	0.37	0.15	6.5		This work
Cd^{2+}	Aerated	Cd^+	(2.7)	1.26	1.6	4.0[a]	15
CH_3Cl	Cyclohexane	CH_3		2.9	15	2.9	21
C_2H_5OD	Cyclohexane	HD		4.0	2.0	4.0	20

[a] $G_1° + G_2°$. [b] $G_{e_{aq}^-} + G_2°$. [c] $G_{OH} + G_2°$. [d] Solutions also contain 0.5 M allyl alcohol.

For Cd^{2+}, unlike acetone, $G_2°(H_2) \cong 0.5G_{H_2}$ (Figure 6 and Table III) while HCl greatly increases σ_1/σ_2. Bevan's[15] results from pulse radiolysis for $G(Cd^+)$ in neutral solution give a value of σ_1/σ_2 almost equal to the preceding at 10^{-1} M HCl, with $G_2°$(precursor) = 1.3. From the same work, $G_1°(Cd^+) = G_1°(e_{aq}^-) = 2.7$ and $G_2°(Cd^+) = 1.3$ which combine to give $G°(e^-) = 4.0$. Results for G_{H_2} using nitromethane as scavenger with 1 M HCl and 0.05 M allyl alcohol are included in Figure 4, for which $G_2° = 0.22$. The value of $G_1°(H_2)$ is consistent with other systems which contain allyl alcohol. The value $\sigma_1/\sigma_2 = 21$ is remarkably large.

Solutions of phenol contained no allyl alcohol. The results for these solutions, which appear in Figure 7, give $G_2°(H_2) = 0.20$ in both neutral and acid solutions while σ_1/σ_2 increases strongly with increasing [HCl]. Phenol is a very inefficient scavenger for e_{aq}^- while Cd^{2+} is nearly the best. Their relative efficiencies in suppressing G_{H_2}, both in neutral and in acid solutions, are rather similar. Phenol is an efficient H atom scavenger ($k = 4 \times 10^9$ M^{-1} sec^{-1}), but allyl alcohol is nearly as efficient ($k = 2 \times 10^{9}$ ^{-1}M sec^{-1})[4] and its efficiency was not appreciably affected by acid.

The effect of hydrogen peroxide as scavenger for a precursor of molecular hydrogen[16] has been interpreted by Sworski[12] and the values of his parameters appear in Table III. He has called attention to the invariance of scavenging efficiency with LET, the only change being exhibited in $G_2°$. The same LET effects on G_{H_2} were found for NO_3^- (Table III).[12] The value of σ_1/σ_2 for $H_2^{16,16}O_2$ to suppress the molecular yield of $H_2^{18,18}O_2$ in $H_2^{18}O$ has been evaluated from the results of Anbar, *et al.*[17] The efficiency is only half that for suppression of G_{H_2}, and the precursors are probably different.

Hole Scavenging. Anions provide the most obvious reagents which can be expected to scavenge dry holes

(15) P. L. T. Bevan and W. H. Hamill, *Trans. Faraday Soc.*, in press.

(16) A. R. Anderson and E. J. Hart, *J. Phys. Chem.*, **65**, 804 (1961).

(17) M. Anbar, I. Pecht, and G. Stein, *J. Chem. Phys.*, **44**, 3635 (1966).

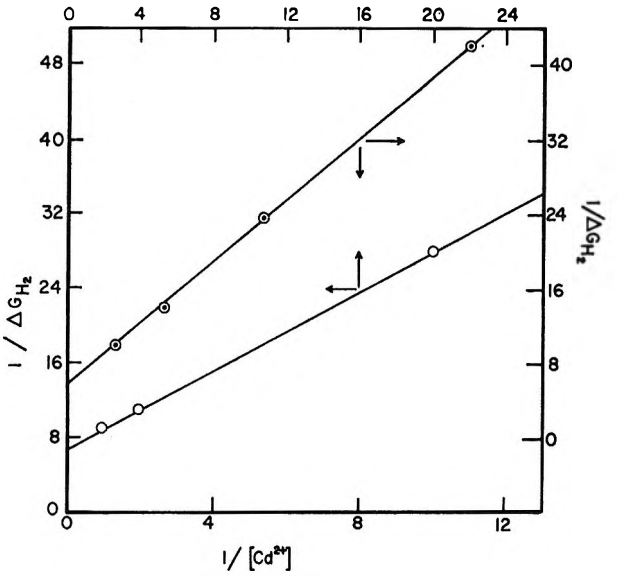

Figure 6. The yield of molecular hydrogen as functions of $[CH_3NO_2]$ (●) and of $[Cd^{2+}]$ with 10^{-1} (⊙) and 1 M HCl (○).

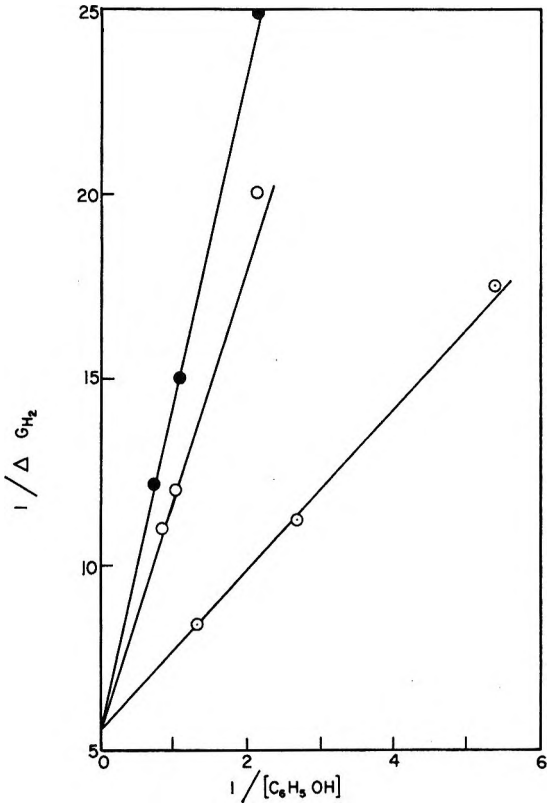

Figure 7. The yield of molecular hydrogen as functions of the concentration of phenol and 0 (●), 10^{-1} (○), or 1 M HCl (⊙).

and acetate ion was selected first because the reactions which can plausibly occur are

$$H_2O^+ + CH_3CO_2^- \longrightarrow H_2O + CH_3CO_2 \quad (6)$$

or possibly the proton transfer reaction 7. Reaction 6

$$H_3O^+ + CH_3CO_2^- \longrightarrow H_2O + CH_3CO_2H \quad (7)$$

would be followed by the very fast reaction[18] 8 and methyl radicals are converted into methane by reaction 9. In this work only G(hydrogen) and G(methane)

$$CH_3CO_2 \longrightarrow CH_3 + CO_2 \quad (8)$$

$$RH + CH_3 \longrightarrow R + CH_4 \quad (9)$$

were measured, using CH_3CO_2H or CD_3CO_2D at pH ~8. Results for the latter reagent (Table IV) show $G(H_2) + G(HD)$ = constant, with $G(D_2)$ negligible. The combined $G(CD_4)$ and $G(CD_3H)$ increased linearly, but not strongly, with $[CD_3CO_2^-]$. The rather small G(methane) in solutions of 1 M $CD_3CO_2^-$ may be due to interference from reaction 7. The results provide no evidence for hole trapping by electron transfer, and G(methane) is probably due to direct effect.

Table IV: Product Yields from $CH_3CO_2^-$ and $CD_3CO_2^-$

[acetate]	Other solutes, M	$G(H_2)$	$G(CH_4)$	$G(CD_3H)$	$G(HD)$
0.1[a]	0.02 *i*-PrOH 0.003 $NaNO_3$	0.795	0.005		
0.5[a]	0.02 *i*-PrOH 0.003 $NaNO_3$	0.760	0.035		
1.0[a]	0.02 *i*-PrOH 0.003 $NaNO_3$	0.734	0.073		
0.1[b]	0.002 $NaNO_3$	0.397		0.009	0.009
0.5[b]		0.383		0.027	0.025
1.0[b]		0.368		0.057	0.042
0.1	0.02 *i*-PrOH 1.0 NaOH	0.583		0.023	0.00
1.0	0.02 *i*-PrOH 1.0 NaOH	0.442		0.100	0.014

[a] $CH_3CO_2^-$. [b] $CD_3CO_2^-$.

The fact that Cl^- can be oxidized radiolytically in neutral and even in alkaline solutions[19] indicated the use of this reagent. If the mechanism is written as

$$(H_2O^+, e^-) + Cl_{aq}^- \longrightarrow H_2O + e_{aq}^- + Cl \quad (10)$$

it is expected that an increased yield of e_{aq}^- will be observed since the hole has been annihilated and some prompt charge pair recombination has been prevented. With 0.002 M NO_3^- and 0.02 M isopropyl alcohol, $G(H_2)$ is unchanged at 1 M Cl^-, and G_{H_2} is nearly unchanged at 2 M Cl^-.

In deaerated neutral solutions containing 10^{-2} M NO_3^-, 10^{-4} M $FeSO_4$, and 5×10^{-2} M isopropyl alcohol $G(NO_2^-)$ increased with $[Cl^-]$. The extinction coefficient of NO_2^- was unaffected by the highest concentrations of Cl^-. From Figure 8, $G_1^\circ[NO_2^-] = 2.76$ and $G_2^\circ[NO_2^-] = 0.72$. The value $\sigma_1/\sigma_2 = 0.41$ is typical for Cl^- hole scavenging.

(18) J. R. Nash, W. H. Hamill, and R. R. Williams, *J. Phys. Chem.*, **60**, 823 (1956).

(19) M. Anbar and J. K. Thomas, *ibid.*, **68**, 3829 (1964).

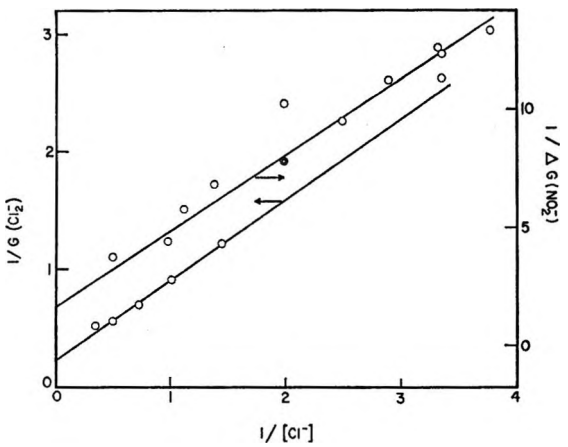

Figure 8. $\Delta G(NO_2^-)$ from 10^{-2} M KNO_3 measures $\Delta G(e_{aq}^-)$ from hole trapping by Cl^-; $G(Cl_2^-)$ is a direct measure of hole trapping (data from ref 17).

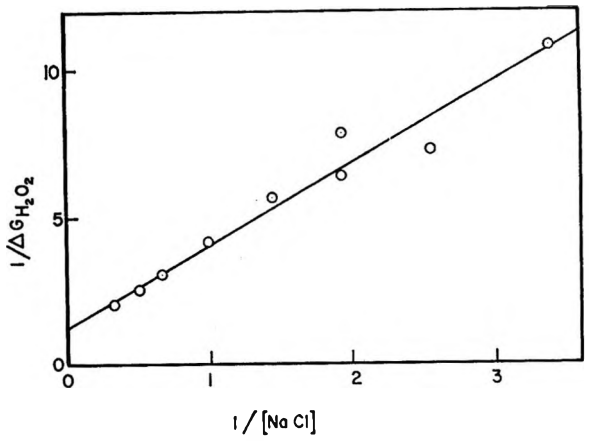

Figure 9. The yield of molecular hydrogen peroxide as a function of $[Cl^-]$.

The results of Anbar and Thomas[19] for Cl_2^- in neutral solutions as a function of $[Cl^-]$ also appear in Figure 8. Their measurements extended to 3 M Cl^-, and all data at high concentrations have been included although there must be appreciable contributions to $G(Cl_2^-)$ from a direct effect. There will be a partial compensation since energy absorbed by NaCl diminishes $G(H_2O^+)$. The intercept in Figure 8 gives $G_2^\circ = 3.9$ which is interpreted as $G_2^\circ(H_2O^+) = 3.9$. The efficiency, $\sigma_1/\sigma_2 = 0.38$, compares with that for aerated solutions of 0.3 M isopropyl alcohol at various $[Cl^-]$. The parameters appear in Table III.

Fluoride ion reacts very slowly with H atoms,[4] but

$$F^- + H \longrightarrow HF + e_{aq}^-; \qquad k = 1.4 \times 10^4\ M^{-1}\ \text{sec}^{-1} \quad (11)$$

this reaction was repressed in another series of experiments by adding 0.1 M isopropyl alcohol to 0.01 M NO_3^- which show $\Delta G(NO_2^-) \cong -\Delta G(H_2) \cong 0.15$ at 1 M F^- and 0.25 at 5 M F^-. The efficiency of F^-, which cannot be oxidized by OH, compares with Cl^- for which $\Delta G(NO_2^-) = 0.22$ at $[Cl^-] = 1$ M. For the same reaction system, $G(H_2)$ decreased from 0.960 at $[F^-] = 0$ to 0.780 and 0.688 in 1 and 5 M solutions of F^-, while $G(NO_2^-)$ increased from 2.52 to 2.66 and 2.74. A small change in the extinction coefficient of NO_2^- has been allowed for. The necessity of adding isopropyl alcohol as a scavenger for H precluded measuring G_{H_2} in solutions of F^-. In related experiments the solutions contained 10^{-2} M NO_3^- and 1.5×10^{-3} M allyl alcohol. G_{H_2} was 0.375 at $[F^-] = 0$ and 0.345 at $[F^-] = 1$ M. This is much less than the change in $G(H_2)$ for solutions containing isopropyl alcohol and indicates that $\Delta G(H_2)$ arises chiefly from ΔG_H. Parallel experiments measuring $G(H_2)$ and G_{H_2} in solutions with Cl^- with and without isopropyl alcohol showed changes of these yields did not exceed ~3% for $G(H_2)$ while G_{H_2} increased from 0.445 to 0.464 and 0.483 in 1 and 2 M Cl^-.

For measurements of $G_{H_2O_2}$ with Cl^- as hole scavenger the neutral, deaerated solutions contained 5×10^{-2} M isopropyl alcohol and 10^{-2} M NO_3^-. The results appear in Figure 9 and Table III.

Results for $G(I_2^-)$ in aerated solutions of iodide ion from the work of Bevan[15] are summarized in Table III.

High concentrations of OH^- would be expected to produce effects comparable to other anions. The results of Hayon[20] for $G(NO_2^-)$ to pH 14 in solutions containing 5×10^{-3} M HCO_2^- and 10^{-3} M NO_3^- are summarized in Table III. It should be noted that for the same system $\Delta G_{H_2} = -0.04$ at 1 M OH^-, somewhat comparable to the result for 1 M F^-. The results for G_{OH} and $G_{H_2O_2}$ appear in Figure 10. The oxidation of OH^- to OH is predictable from the formation of Cl_2^- and quite analogous. All values of σ_1/σ_2 for OH^- lie between 3.0 and 3.5, while $G_2^\circ(OH) = 1.5$ depends

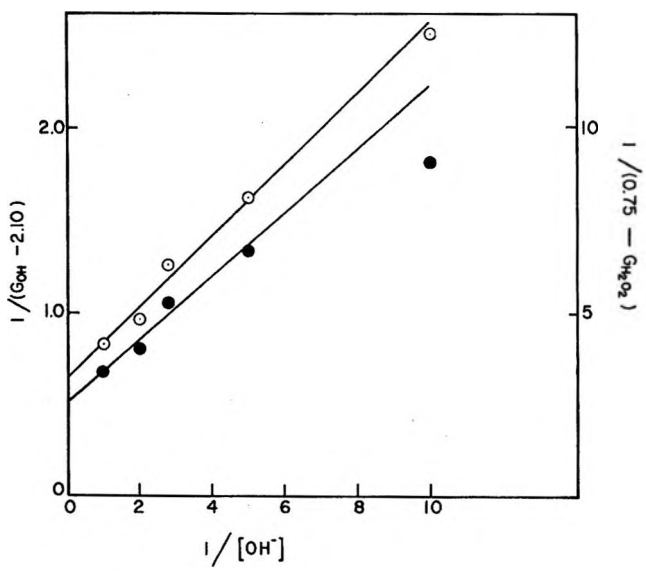

Figure 10. The yields of molecular H_2O_2 (●) and primary OH (○) as functions of $[OH^-]$ (from Hayon's results[20]).

(20) E. Hayon, *Trans. Faraday Soc.*, **61**, 734 (1965).

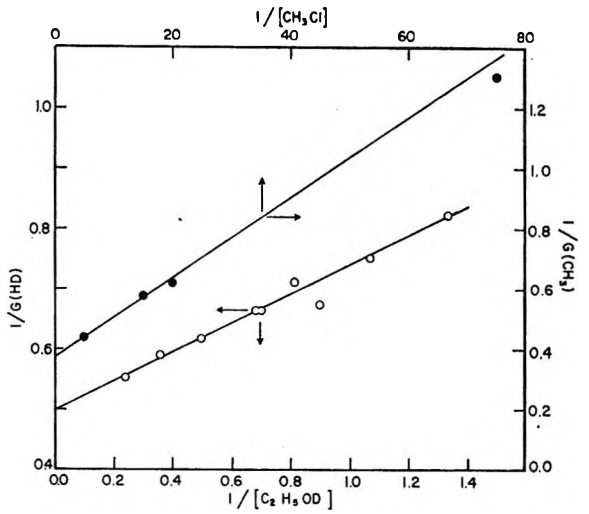

Figure 11. The yields of HD (○) as a function of $[C_2H_5OD]$ and of CH_3 (●) as a function of $[CH_3Cl]$, both in cyclohexane (from ref 21 and 22).

partly on this oxidation and partly on suppression of molecular hydrogen peroxide.

Hole scavenging by C_2H_5OD in cyclohexane, reported by Buchanan and Williams,[21] and electron scavenging by CH_3Cl in cyclohexane by Warman, *et al.*,[22] have been included in this presentation (Figure 11). The high-frequency dielectric constant of water approximates that of an alkane and comparisons are desirable.

Discussion

A revised estimate of k_4/k_5 is required by the increase in $G(e_{aq}^-)$ due to hole scavenging at high [HCl]. At 10^{-2} *M* allyl alcohol for 0 and 1 *M* HCl, $\Delta G_{H_2} = 0.066$ and $\Delta G(H) = 2.7 + 0.4$ (Table III and eq A) to give $k_4/k_5 = 0.021$. Similarly for 10^{-2} *M* allyl alcohol and 0 and 0.1 *M* HCl, $\Delta G_{H_2} = 0.056$, $\Delta G(H) = 2.7$ from which $k_4/k_5 = 0.021$. With 1 *M* allyl alcohol and 0 and 1 *M* HCl, $k_4/k_5 = 0.017$ while 0 or 0.1 *M* HCl gives $k_4/k_5 = 0.013$. The average k_4/k_5 is 0.018. At various [HCl], $\Delta G(H_2)$ for 10^{-2} and 1 *M* solutions of allyl alcohol is 0.038, 0.040, and 0.037 at 0, 0.1, and 1 *M* HCl, respectively. There is no trend with [HCl] and no definite evidence that HCl converts e_{aq}^- into H "in the spur." The results for D_2O show $\Delta G(HD) \cong 0.03$ as [allyl alcohol] increases from 0.2 to 1.0 *M* which indicates $\Delta G(D) \cong 0.03/0.018 \gtrsim 1.6$ which would otherwise be lost through geminate recombination. The result $G(HD) = 0.069$ in neutral D_2O with 1 *M* allyl alcohol requires that $G(H_2)$ in neutral H_2O with 1 *M* allyl alcohol should be corrected downward by a comparable amount, and $\Delta G^\circ_{H_2}$ may be $\sim$0.11 due to H-atom scavenging. This approximates the combined contributions of reactions 2 and 3 in neutral solutions according to the calculations of Schwarz.[6]

The interpretation of other results from this work, as well as results from the literature, depends principally on the adequacy of the trial function A to describe the facts consistently. This model was suggested by the familiar expressions commonly used for competition kinetics but, when dry charge species are being scavenged, conventional kinetics are not predictably applicable. These expressions are comparable with those used by Sworski[12] except that he employed rate constants, *i.e.*, $k_1[S]/k_2$, and attributed the first-order process to the unimolecular decomposition of "excited water" to form molecular hydrogen. For eq A to apply, it is sufficient that $\sigma_1[S]/\sigma_2$ account for the relative probabilities of the competing processes, *i.e.*, that σ_1/σ_2 remain constant for a useful range of [S], or of time. This is not known *a priori*, but must be established by experience. The introduction of an adjustable parameter G_1° is unfortunate but inherently required by many reaction systems for internal consistency. On the other hand, there are usually narrow bounds for fitting this parameter, *i.e.*, the range of acceptable values of G_{H_2}, $G_{e_{aq}^-}$, and the like, and these uncertainties are not peculiar to the trial function.

For 50% scavenging, or $\sigma_1[S]/\sigma_2 = 1$, the results in Table III show that $[S]_{1/2}$ usually lies between 0.5 and 2 *M*, and this regime of scavenging effectively terminates at 10^{-2} or 10^{-1} *M*. The typical range for the spur diffusion model extends to $\sim 10^{-1}$ *M*, and the two models may prove to be complementary and not mutually exclusive. One is designed to describe very early effects; the other is for late effects. It is trivial to observe that if $e^- \rightarrow e_{aq}^-$ and $e_{aq}^- \rightarrow H_2$, then $e^- \rightarrow H_2$, where H_2 is molecular hydrogen. Consequently, if scavenging dry electrons suppresses molecular hydrogen, the precursor has been only partially identified. It would be difficult to demonstrate by a qualitative experiment (rather than by kinetic analysis) that e_{aq}^- is the immediate precursor of molecular hydrogen. The present work only attempts to determine how the dry charge species can be scavenged and to what extent each of them is an ultimate precursor of the final products.

This requires being able to distinguish between H_2O^+ (or H_3O^+) and OH as oxidants, or between e_{aq}^- and e^- as reductants. To illustrate, there are two possible mechanisms for oxidizing Cl^-, one being a conventional reaction possible in the very acid spur. If the exclusive mechanism is (12), then $G_2^\circ(H_2O^+) = 3.9$, and this is interpreted as being due entirely to scavenging prior to hydration and geminate charge pair recombination. This reaction system possesses unique signifi-

$$H_2O^+ + Cl_{aq}^- \longrightarrow H_2O + Cl \qquad (12)$$

$$H_3O_{aq}^+ + OH + Cl_{aq}^- \longrightarrow 2H_2O + Cl \qquad (13)$$

(21) J. W. Buchanan and F. Williams, *J. Chem. Phys.*, **44**, 4377 (1966).

(22) J. M. Warman, K. D. Asmus, and R. H. Schuler, *J. Phys. Chem.*, **73**, 931 (1969).

cance because it is the only one considered which must occur either with a dry charge species or entirely within the spur. (It should be clear that the model for scavenging dry charge species does not invoke spurlike processes, each entity being assumed to originate from a single ionization. Reactions "in the spur" will be considered only with reference to the conventional description.)

If the exclusive mechanism is (13), then $G_2°(OH) \gtrsim 3.9$ and $G(H_3O^+) \gtrsim 3.9$ in the spur, with substantially complete reaction required. If such large yields of Cl were produced in the spur, with little or no escape of OH and H_{aq}^+, then there must also be efficient conversion of Cl into Cl_2 and Cl_3^- which absorb very weakly in the region of $\lambda_{max}(Cl_2^-)$. For this reason G(oxidation) > 3.9 if trapping occurs partly in the spur. It is concluded that reaction 12 must contribute to $G(Cl_2^-)$, *i.e.*, H_2O^+ or H_3O^+ can be scavenged. Consequently, a new model is required to deal with very early effects. Also, the spur diffusion model should not be applied to solutions containing more than ~0.1 *M* charge scavenger because of intervention in very early ionic processes.

The preceding argument rests on the large value of $G(Cl_2^-)$ which, if real, cannot be explained conventionally. It has been noted that a direct effect to produce Cl must contribute to some extent. This effect cannot exceed $\Delta G(e_{aq}^-)$ from ionization of Cl^- and hole trapping combined, which is given by $G_2°(NO_2^-) = 0.72$ from dilute NO_3^- with Cl^- scavenging. It is probably much less than this because recent pulse radiolysis measurements by Khorana[23] have shown that 2 *M* Na_2SO_4 increases $OD(e_{aq}^-)$ by only 5.6%.

With I^- as scavenger, $G_1°(I_2^-) = 2.7$ at small $[I^-]$ from homogeneously distributed OH. With increasing $[I^-]$ the same population $G_{OH} = 2.7$ will react at much earlier times but will not be distinguishable since it has already been counted. As $[I^-]$ continues to increase, dry H_3O^+ may contribute to $G_2°(I_2^-)$ and if H_2O^+ is inaccessible we expect $G_1°(I_2^-) + G_2°(I_2^-) = G_{OH} + G_2°(OH) + G_2°(H_3O^+) \gtrsim 7.8$. Alternatively, if H_2O^+ is scavengable, then the major source of OH will be suppressed at high $[I^-]$ and the total $G(I_2^-)$ will exceed $G_2°(H_2O^+) = 3.9$ only by the geminate (H, OH) nonionic yield of OH. Since $G_1°(I_2^-) + G_2°(I_2^-) = 4.7$ it appears that H_2O^+ is scavengable. The nonionic component of OH amounts to $G_1°(I_2^-) + G_2°(I_2^-) - G_2°(H_2O^+) = 4.7 - 3.9 = 0.8$, roughly the same as G_H.

The large value $G_2°(OH) = 1.5$ at high $[OH^-]$ can be accounted for in part by reaction 14 which is totally analogous to reaction 12. The increased yield of e_{aq}^-

$$(H_2O^+, e^-) + OH_{aq}^- \longrightarrow H_2O + OH + e_{aq}^- \quad (14)$$

is indicated by $G_2°(NO_2^-) = 1.1$ with NO_3^- at high pH. Although the mechanism is not quite certain, $G_2°(NO_2^-) = 1.1$ is too great to attribute to $H + OH^- \rightarrow e_{aq}^-$ alone. The large value of $G_2°(OH)$ is not accounted for by the conventional appeal to pH effect; *i.e.*, base neutralizes acid in the spur which would increase $G(e_{aq}^-)$, since this would also decrease G(OH) by forming OH^- in the spur. Alternatively, if reaction 14 gives $G_2°$(oxidation) $\cong 3.9$ and the oxidant and reductant from the decomposition of water cancel, then $G_1°(OH) + G_2°(OH) = 2.1 + 1.5 = 3.6$, somewhat less than the value of G assumed for reaction 14, but $G_{OH} + G_2°(OH) = 2.7 + 1.5 = 4.2$ agrees better.

The reliability of results for the radiolysis of very alkaline solutions is difficult to evaluate. In support of the data employed here it should be observed that σ_1/σ_2 for OH^- is substantially constant for three different systems. It is also to be observed that $G_1° + G_2°$ approximates 3.8 for scavenging electrons and for scavenging holes, in good agreement with other results. The value for $G_2°(H_2O_2) = 0.40$ is not evidently unacceptable. Also, using the parameters for NO_2^- formation we calculate $\Delta G_{e_{aq}^-} = 0.38$ at pH 13, which compares with $\Delta G_{e_{aq}^-} = 0.40$ from the work of Fielden and Hart.[24] The results for G(OH) may be inaccurate, but they provide evidence for appreciable increases in yield at high pH which agree qualitatively with the observations of increased $G(e_{aq}^-)$ from hole scavenging and for oxidation of OH^-. Czapski[25] has recalculated the data of Fielden and Hart to obtain $G_{OH} = 3.2$ at pH 13, which is higher than Hayon's result. Measurements by Khorana[23] of $G(I_2^-)$ with 10^{-2} *M* I^- in very alkaline solutions by pulse radiolysis give values of $G(I_2^-)$ which agree well with Hayon's G_{OH} in the range of high pH.

The change in $G_2°(H_2)$ with solute is somewhat complicated and this is also indicated by the fact that the spur diffusion model requires four precursors to describe G_{H_2}. The systems examined by Sworski consistently lead to $G_2°(H_2) \cong 0.34$ at low LET, although e^-, e_{aq}^-, and H are scavenged by H_2O_2, NO_2^-, and Cu^{2+} while NO_3^- scavenges H_2O^+ (since it is an anion)[26,27] as well as e^- and e_{aq}^-, but not H.

Acetone-d_6, at each of three concentrations of HCl, produced significant yields of HD although k(H + allyl)[allyl alcohol] $\gg k$(H + acetone)[acetone] and $G_2°$(HD) was uniformly about 0.1. The origin of HD is therefore not hydrogen abstraction nor is it plausibly direct effect since $G(D_2) = 0.003$ in 1 *M* solution. A source of HD is suggested by the fact that acetone is a strong base in H_2SO_4 and therefore can act as a proton acceptor with H_2O^+. Subsequent neutralization may lead to decomposition with evolution of hydrogen.

The spur diffusion model can account for the inde-

(23) Work in progress in this laboratory.

(24) E. M. Fielden and E. J. Hart, *Radiat. Res.*, **32**, 564 (1967).

(25) G. Czapski, Advances in Chemistry Series, No. 81, American Chemical Society, Washington, D. C., 1968, p 106.

(26) The anion effect can account for $\Delta(G_{e_{aq}^-} + G_H)$ in acid solutions.

(27) The prompt yield of NO_3 in pulse-irradiated solutions of NO_3^- (attributable to hole trapping) obeys eq A with $\sigma_1/\sigma_2 = 0.80$ and $G_1° = 0$ according to M. Daniels, *J. Phys. Chem.*, **73**, 3710 (1969).

pendence of $\sigma_1[NO_3^-]/\sigma_2$ with high acidity,[6] but the efficiency of Cd^{2+} was markedly increased by acid without appreciably changing $G_2°(H_2)$. Because $k(Cd^{2+} + H) < 10^5$, the effect of acid cannot be attributed to $e_{aq}^- + H_{aq}^+ \rightarrow H$, while $k(Cd^{2+} + e_{aq}^-) = 5.2 \times 10^{10}\ M^{-1}\ sec^{-1}$ at pH 7, and the rate cannot be increased fourfold to $\sim 20 \times 10^{10}\ M^{-1}\ sec^{-1}$.

A possible explanation of the effect of acid on $G_2°(H_2)$ with Cd^{2+} is capture of e^- by Cd^{2+} to give an energetic transient Cd^{+*} which may ionize to Cd^{2+} and e_{aq}^-, while capture of e_{aq}^- occurs adiabatically. Thus two successive captures (*i.e.*, low efficiency) would be required to completely remove the precursor of molecular hydrogen if both e^- and e_{aq}^- contribute to G_{H_2}. The effect of acid would then be to provide an efficient route to convert Cd^{+*} to Cd^{2+} and H.

If the effect of phenol, for which $G_2°(H_2) = 0.20$ from pH 0 to 7, is attributed exclusively to H-atom scavenging, then it exceeds the estimate of $\Delta G(H_2)$ caused by allyl alcohol. It also exceeds the combined yields from reactions 2 and 3 according to spur-diffusion theory, which is 0.145 at pH 7.[6] If phenol scavenges both H and e_{aq}^-, but not e^-, then $G_2°(H_2)$ should be 0.281 at pH 7 and 0.323 at pH 0.7 according to Schwarz.[6] Since phenol scavenges H about 10^3 times faster than e_{aq}^-, adding 1 M HCl should have a larger effect than was observed if e_{aq}^- is the principal precursor of molecular hydrogen.[28] We attribute the effect of phenol on G_{H_2} principally to scavenging H and e^- so that $G_2°(H_2) = G_2°(e^-) + G_2°(H)$. The marked increase in σ_1/σ_2 as [HCl] increases from 0 to 1 M with $\Delta G_2°(H_2) = 0$ is entirely similar to the effect observed with Cd^{2+} and is similarly explained by reactions 15 to 19.

$$\phi OH + e^- \longrightarrow \phi OH^- \qquad (15)$$

$$\phi OH^- \longrightarrow \phi OH + e_{aq}^- \quad \text{fast} \qquad (16)$$

$$\phi OH^- \longrightarrow \phi OH_{aq}^- \quad \text{fast} \qquad (17)$$

$$\phi OH^- + H_2O \longrightarrow \phi HOH + OH_{aq}^- \quad \text{slow} \qquad (18)$$

$$\phi OH^- + H_{aq}^+ \longrightarrow \phi HOH \quad \text{fast} \qquad (19)$$

There is some regularity in the several values of $G_2°(H_2)$ if it is assumed that each of three precursors contribute as follows: $G_2°(e^-) \cong G_2°(e_{aq}^-) = G_2°(H) \cong 0.1$ with an unidentified $G_2°(?) \cong 0.1$ which will be quite tentatively attributed to $H_2O(^3B_1)$.[29] Scavengers of $H_2O(^3B_1)$ are considered to be NO_3^-, NO_2^-, $(CD_3)_2CO$, and ϕOH which are known to have low-lying triplet states. We add H_2O_2 to this list since its lowest triplet should lie under the first singlet, and H_2O_2 absorbs to <4 eV. We also include, qualitatively, OH^- which suppresses G_{H_2} weakly, since there is some evidence that it has a low-lying triplet state, $^3B_1$.[30]

The scavengers, and precursors of molecular hydrogen scavenged, are summarized: $NO_3^-(e^-, e_{aq}^-, {}^3B_1, H)$; $NO_2^-(e^-, e_{aq}^-, {}^3B_1, H)$; $\phi OH(e^-, {}^3B_1, H)$; $CH_3NO_2(e^-, e_{aq}^-)$; $(CD_3)_2CO(e^-, e_{aq}^-, {}^3B_1)$; $H_2O_2(e^-, e_{aq}^-, {}^3B_1)$; $Cu^{2+}(e^-, e_{aq}^-, H)$; $Cd^{2+}(e^-, e_{aq}^-)$. For scavenging in n channels we expect $G_2°(H_2) \cong 0.1\ n$. The values of $G_2°$ are in adequate agreement with expectation in all instances except NO_2^- and ϕOH, the observed value of $G_2°(H_2)$ being smaller than expected by ~ 0.1. Scavenging precursors of molecular hydrogen in three channels can only be described fortuitously by eq A. Since each of three different values of $G_2°$ are about the same, the function ΔG^{-1} *vs.* $[S]^{-1}$ still applies only if the values of σ_1/σ_2 are about the same for each precursor.

Scavenging dry charge species in water should bear some resemblance to the corresponding processes in alkanes, the dielectric constants being roughly equal. For alkanes one may expect σ_2 to refer to charge recombination. The results for electron scavenging by CH_3Cl and hole scavenging by C_2H_5OD, both in cyclohexane, appear in Table III. The value $\sigma_1/\sigma_2 = 15$ for CH_3Cl (a relatively poor scavenger) is rather larger than the corresponding efficiencies for the neutral scavengers phenol (0.6), acetone (1.1), and nitromethane (1.6) in water. These results can be explained in terms of the $\sim 70\%$ interference of hydration with recombination of the dry charge pair. Since hydration is incomplete, it must be more probable for charge pairs with greater than average separations. To scavenge a given fraction of the remainder, which have shorter than average lifetimes for recombination, will require correspondingly larger concentrations of scavenger than would be required if dielectric relaxation were "turned off."

The results in Table II for electron scavenging in CH_3OH–H_2O glass strongly favor correlations with values of σ_1/σ_2 from Table III in preference to rate constants. The average deviations from constancy are 80 and 133% for the ratios in columns 7 and 6, even excluding from the second group the result for phenol. For a decisive test one requires a reagent which reacts very slowly with e_{aq}^- and which would therefore be expected to take advantage of the much higher energy of the dry electron.[31] Of the solutes tested, only phenol reacts with e_{aq}^- at a rate considerably less than diffusion controlled while its value of σ_1/σ_2 is almost normal for aqueous solutions.

From the quantitative aspect, the model as expressed by eq A is useful in providing linear functions which yield two important parameters. The consistency of the description can be tested (i) by requiring σ_1/σ_2 to

(28) In a private communication, H. A. Schwarz reports good agreement for calculated G_{H_2} and the yields found here in neutral phenol solutions.

(29) D. Lewis and W. H. Hamill, *J. Chem. Phys.*, **51**, 456 (1969).

(30) H. J. Maria and S. P. McGlynn, *ibid.*, **52**, 3402 (1970).

(31) An example of this effect was claimed by M. Haissinsky and M. Duflo, *J. Chim. Phys.*, **52**, 955 (1959), for $[U^{4+}] > 0.05\ M$. Reduction by e_{aq}^- is thermodynamically unfavorable.

be constant for a given scavenger when the effect is observed in several channels and (ii) by requiring $G_2°$ to be constant in one channel for several scavengers. The first requirement is fairly well satisfied for six systems with S = NO_3^-, three with S = OH^-, three (possibly four) with S = Cl^-, and two (of three) with S = Cd^{2+}. For seven systems one can deduce $\Sigma G° \cong 4$ for H_2O^+, e^-, or OH.

Acknowledgment. The authors are grateful to Dr. A. Mozumder and Dr. H. A. Schwarz for detailed comments on the manuscript which have greatly improved the presentation.

The Effect of Ion and Radical Scavengers on the Cyclohexyl Radical Yield in the Radiolysis of Cyclohexane[1]

by Krishan M. Bansal and Robert H. Schuler

Mellon Institute Radiation Research Laboratories and Department of Chemistry, Carnegie-Mellon University, Pittsburgh, Pennsylvania 15213 *(Received May 27, 1970)*

Scavenging studies with iodine indicate that the yield of cyclohexyl radicals produced in the radiolysis of pure cyclohexane is ~5.7. Iodine concentrations in the range of 10^{-2} *M*, however, reduce the observed yield to ~4.2. This decrease is interpreted as being produced both by hydrogen atom and by positive ion scavenging reactions of iodine. The effect of a number of other solutes on the production of cyclohexyl radicals has also been examined. Cyclopropane reduces the yield by an amount approximately equal to the yield of the positive ion reactions. Ethylene has a similar effect with a superimposed reduction which results from hydrogen atom scavenging. The various electron scavengers examined (CH_3Br, CH_3I, CH_3Cl, SF_6, N_2O, and CO_2) have differing effects which depend on the relative importance of secondary abstraction reactions. The comparison of CH_3Br and CH_3Cl is particularly interesting because the first solute causes a reduction approximately equal to the yield of electron capture while the second has essentially no effect. Nitrous oxide is unique in that an increase is observed in $G(C_6H_{11}\cdot)$ which is equal to the yield of electrons captured by the N_2O. The quantitative aspects of the various effects can be correlated quite well by expressions derived from a description of the concentration dependence of ionic processes in these systems if it is assumed that on the average one cyclohexyl radical is produced for each neutralization that occurs between a positive ion–electron geminate pair. The interpretation of the data is, however, more complex than in the case of hydrogen production because certain processes produce several cyclohexyl radicals while others produce none.

Various radical and ion scavengers are known to depress the yield of hydrogen produced in the radiolysis of hydrocarbons, and in the case of cyclohexane it has been possible to describe the effects of a number of solutes quantitatively and with considerable accuracy in terms of their known scavenging properties.[2] At this point it becomes of particular interest to examine the effects of these same solutes on radical production to see if effects are observed that can be related to changes produced by interference with the neutralization processes. The present study has been carried out on cyclohexane because studies of the effects of various ion scavengers indicate that in pure cyclohexane neutralization leads to the formation of (very nearly) one molecule of hydrogen. Thus one might expect a simple relationship between the yields of the scavenging reactions and their effects on the radical yield. Experimentally this system is relatively simple because ~90% or better of the radicals produced in the primary reactions are expected to be cyclohexyl.[3] Thus for the present purposes one needs to examine only a single product species. Cyclohexane has, of course, been studied extensively in many laboratories,[4] and related results of the effect of scavengers on the production of

(1) Supported in part by the U. S. Atomic Energy Commission.

(2) K.-D. Asmus, J. M. Warman, and R. H. Schuler, *J. Phys. Chem.*, **74**, 246 (1970). Numerous references to the reduction in $G(H_2)$ produced by various solutes are included.

(3) The major dimer product is known to be cyclohexyl–cyclohexane with the principal other dimer being 6-cyclohexyl-1-hexene which is produced in about a 10% yield (P. J. Dyne and J. A. Stone, *Can. J. Chem.*, **39**, 2381 (1961)). In the related case of cyclopentane the radical sampling results reported by R. A. Holroyd and G. W. Klein, *J. Amer. Chem. Soc.*, **87**, 4983 (1965), show that 89% of the radicals are cyclopentyl.

(4) For a summary of the results of various studies on cyclohexane see Chapter IV by W. A. Cramer in "Aspects of Hydrocarbon Radiolysis," T. Gaümann and J. Hoigné, Ed., Academic Press, New York, N. Y., 1968.

dicyclohexyl and cyclohexene have been reported.[5-7] Results are reported here which show that various solutes affect the production of cyclohexyl radical in differing ways, with each solute reflecting the importance of secondary reactions particular to its individual case.

Experimental Section

Radicals were detected by scavenging with radioiodine ($^{131}I_2$) and the product alkyl iodides were separated gas chromatographically. Cyclohexyl iodide is high boiling and somewhat difficult to transfer quantitatively. It also is known that iodides of even lower volatility are formed in this type of system.[8] The radiochemical assay was, therefore, made directly on the chromatographic column. After irradiation the sample was extracted with aqueous sodium thiosulfate in order to remove the free iodine and any hydrogen iodide formed. An appropriate sample (usually 0.5 cc) was injected into a chromatographic column and the total relative activity determined by scanning the column past a 1-in. crystal scintillation detector on a constant velocity bench. The detector "saw" about 5 cm of the column. The column was scanned again after a partial elution sufficient to move the component of interest down the column. The development of the sample in this way is illustrated in Figure 1. A reference sample of known specific activity was similarly scanned so that absolute amounts of product were available from the activity measurements. Although the sensitivity of this type of counting is about an order of magnitude less than that in previous radioiodine chromatographic studies where the sample was trapped, the reproducibility is quite good. Five determinations of the cyclohexyl radical yield from cyclohexane containing ~0.5 mM I_2 gave yields of 5.16, 5.21, 5.18, 5.38, and 5.26 for a mean of 5.23 and a standard deviation of 0.08. In general, the individual determinations of G(R) appear to be accurate to ~0.1.

Known amounts of the solutes of interest (CH_3Br, CH_3Cl, CH_3I, SF_6, N_2O, CO_2, C_2H_4, c-C_3H_6) were added to the outgassed cyclohexane–iodine solution on a vacuum line in the conventional way. Irradiations were in a ^{60}Co source at an absorbed dose rate of 1×10^{17} eV/g min. Doses were from 5×10^{17} to 6×10^{18} eV/g with most experiments being carried out at a dose of 1.5×10^{18} eV/g. At an iodine concentration of 6×10^{-4} M this dose corresponds to reaction of 10% of the iodine. At lower concentrations, iodine of higher than normal specific activity was used and therefore the doses were correspondingly lower. Where tested, yield–dose plots were nicely linear (as is illustrated in Figure 2) and it is assumed in the following that there is no dose effect on the observed yields.

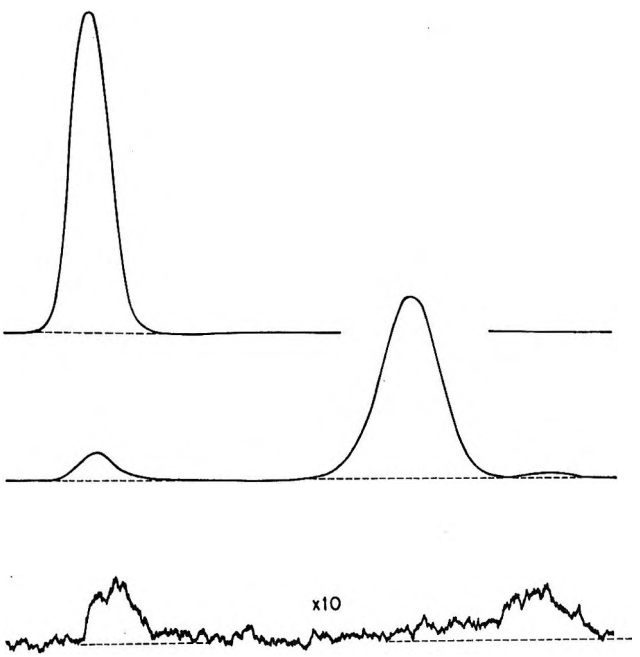

Figure 1. Development of chromatographic column. Top trace, initial scan with no elution. Column 110 cm long scanned in 16 min. Total activity in peak was 34,800 counts; background was 400 cpm. Center trace, scan after 70 min elution at ~100°. Activity in major (cyclohexyl iodide) peak 30,490 counts; 978 counts in the very small peak at the right and 2880 counts in the peak at the origin. Bottom trace, scan after further elution of 150 min at ~150° recorded at gain of 10×; 1250 counts in the peak at the right; 1210 counts at the origin.

Results and Discussion

At iodine concentrations below 10^{-3} M the yield of radioiodine incorporated as organic iodide was found

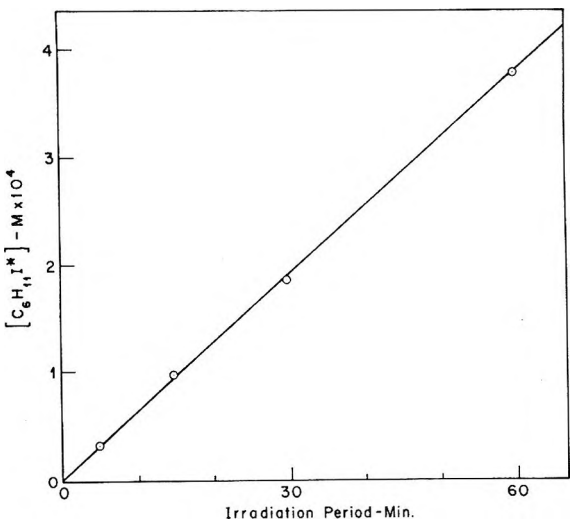

Figure 2. Yield–dose plot for cyclohexyl iodide formed in cyclohexane solutions 0.1 M in CH_3Cl. Iodine concentration was 0.6 mM; absorbed dose rate was 9.3×10^{16} eV g^{-1} min^{-1}.

(5) R. Blackburn and A. Charlesby, *Nature*, **210**, 1036 (1966); *Proc. Roy. Soc., Ser. A*, **293**, 51 (1966).

(6) L. S. Polak, N. Ya. Chernyak, and A. S. Shcherbakova, *Khim. Vys. Energ.*, **1**, 220 (1967).

(7) N. H. Sagert and A. S. Blair, *Can. J. Chem.*, **45**, 1351 (1967).

(8) C. E. McCauley and R. H. Schuler, *J. Amer. Chem. Soc.*, **79**, 4008 (1957).

to be 5.8. This value is slightly higher than that of 5.6 found previously in a similar experiment.[9] The organic radioiodine-containing products could be chromatographically separated into three principal components (see Figure 1). The retention time of the major component corresponds to that of cyclohexyl iodide. This product was preceded by a minor radioiodine-containing material with a retention time ~75% that of cyclohexyl iodide. It seems likely that this more volatile component is an unsaturated C_6 iodide formed by ring opening which occurs simultaneously with radical formation. Its yield, which was 0.14 for solution 6×10^{-4} M in iodine, was not affected in any obvious way by the addition of solutes. The scatter was $\sim \pm 0.05$ and in no case was a value higher than 0.22 recorded. Because this component amounts to only ~3% of the product, possible variations can have little effect on the overall interpretation of the effects of the solutes. The third component did not move down the column at all under the conditions used for resolving the cyclohexyl iodide. With prolonged elution it could be further split into 2 approximately equal peaks, one of which moved very little, but no detailed studies were carried out. The total yield in this component was found to be 0.57 at an iodine concentration of 6×10^{-4} M; however, as indicated in Figure 3, the yield increases appreciably with iodine concentration. It is affected in various ways by the addition of second solutes: decreasing to 0.39 upon the addition of 0.1 M CH_3Br and increasing to 0.98 upon the addition of 0.1 M SF_6.

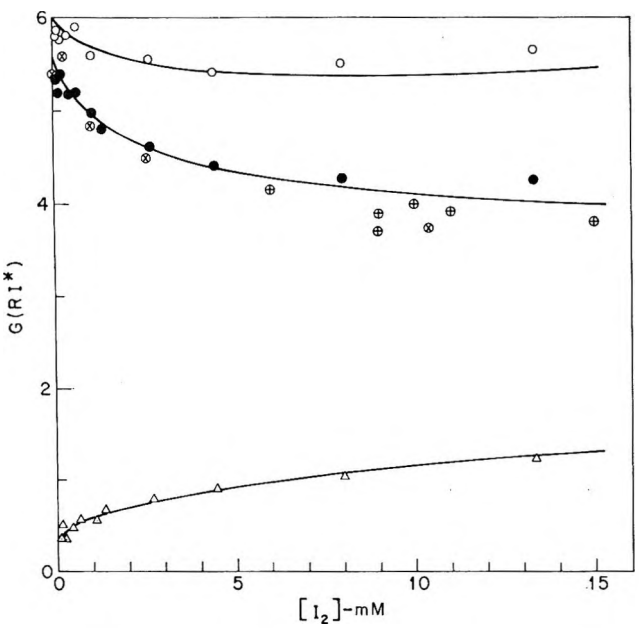

Figure 3. Yield of cyclohexyl radicals ●, total organic iodide ○, and high boiling component △, as a function of iodine concentration. Hydrogen yields from iodine solutions from ref 16 ⊗ and 17 ⊕ are also given. Curve through $G(C_6H_{11}I)$ calculated from eq III. Lower curves calculated as 2.5 times eq I; upper curve is the sum of the other two plus 0.14.

Cyclopropane, CH_3Cl, N_2O, and CO_2 have essentially no effect. Perhaps the most interesting result is that obtained with CH_3I where the yield monotonically decreases to 0.27 at 0.1 M and 0.24 at 0.3 M. It is believed that this component results, at least in part, from ionic reactions involving the radioiodine. If this is so then in the case of methyl iodide similar but competing reactions involving inactive iodine should reduce the observed yield. In one experiment in which 0.1 M CH_3I was added it was found that the peak which did not move on the column was reduced to <0.05, indicating that this peak is produced mainly by ionic processes, with the residual yield ~0.2 originating from some other source. In the region up to 10^{-2} M I_2 the total yield is for empirical purposes two and one-half times the ionic yield.

Effect of Iodine on Cyclohexyl Radical Production. The cyclohexyl radical yield was measured over the iodine concentration range of 10^{-4} to 10^{-2} M and found to decrease from 5.40 to 4.26. The observed data are given in Figure 3. Over this range the total organic iodide changes very little, as indicated by the uppermost curve in the figure. The decrease in the cyclohexyl radical yield is largely compensated by an increase in the yield of the third (high boiling) component. At still higher iodine concentrations ($I_2 > 10^{-2}$ M) the total organic iodide increases to a yield ~8 for iodine saturated solutions (0.05 M).[9] Presumably this increase reflects a further increase in this latter component. In the case of butane a similar increase in the yield of total organic iodide observed at high iodine concentrations was found to be attributable to an increase in the yield of high boiling iodides.[8]

Iodine will, of course, affect cyclohexyl radical production by scavenging hydrogen atoms and thus interfering with hydrogen atom abstraction processes

$$H\cdot + I_2 \xrightarrow{k_1} HI + I\cdot \qquad (1)$$

which otherwise result in the secondary production of cyclohexyl radicals.

$$H\cdot + c\text{-}C_6H_{12} \xrightarrow{k_2} H_2 + c\text{-}C_6H_{11}\cdot \qquad (2)$$

The rate constant for reaction 2 is sufficiently high that iodine can be added at a concentration (*i.e.*, 10^{-4} M) which will be sufficient to quantitatively scavenge cyclohexyl radicals[10] but which will still have little effect on the abstraction process. As one increases the iodine concentration reaction 1 will increase and thus decrease the importance of reaction 2. If no complications occur the cyclohexyl iodide yield is expected to decrease at high iodine concentrations by an amount equal to the yield of hydrogen atoms. This latter yield for pure cyclohexane ($G(H)_0$) has been estimated to be ~1.5.[2] At an iodine concentration equal to

(9) R. W. Fessenden and R. H. Schuler, *J. Amer. Chem. Soc.*, 79, 273 (1957).

(10) R. H. Schuler and R. R. Kuntz, *J. Phys. Chem.*, 67, 1004 (1963).

$k_2[RH]/k_1$ the yield will be reduced by one half of this and at an order of magnitude higher concentration by 91%. It is seen that the midpoint of such a change is observed in the region of a few millimolar so that $k_2[RH]/k_1 \sim 2$ to 3×10^{-3}. Two problems to a more detailed interpretation of the competition exist; the first is in knowing the exact value of the cyclohexyl radical yield at zero iodine concentration $G(C_6H_{11}\cdot)_0$ and the second in knowing to what extent the iodine interferes with the ion-neutralization processes and thus affects the primary yield of radicals $G(C_6H_{11}\cdot)_p$ produced directly from the solvent. Because the second effect is undoubtedly significant, any extrapolation of the data to zero iodine concentration is somewhat tenuous, but it is obvious from the data reported in Figure 3 that $G(C_6H_{11}\cdot)_0$ must be $\sim$5.5. These difficulties make it essentially impossible to obtain anything other than approximate estimates of $G(H)_0$ and k_2/k_1 solely from an examination of the effect of iodine on cyclohexyl radical formation.

We will now attempt to take into account the complicating effects ionic reactions have on cyclohexyl radical production. Iodine is known to interfere with the positive ion reactions of cyclopropane[11] although it seems to have little effect in competing with electron scavengers. For example the addition of 10^{-2} M I_2 to a solution 10^{-3} M in CH_3Br caused a reduction in $G(CH_3I)$ only from 0.57 to 0.55. Similarly, the addition of iodine to a 0.1 M N_2O solution has been shown to have little effect on $G(N_2)$.[12] Thus electron capture by iodine appears (surprisingly) to be inefficient and it will be assumed here that any effects of such capture will be masked by the other difficulties. By analogy with the effects of cyclopropane and ethylene reported below, it is expected that iodine will decrease the cyclohexyl radical yield from the primary process. This decrease should be proportional to the yield of positive ion reactions, the concentration dependence of which can be expressed by the relation

$$G(\text{ion}) = G_{fi} + G_{gi}\frac{\sqrt{\alpha_s S}}{1 + \sqrt{\alpha_s S}} \qquad \text{(I)}$$

where $G_{fi} = 0.12$, $G_{gi} = 3.8$, and $S = [I_2]$.[13] A value of 0.97 for the parameter α_{I_2} has been obtained by Rzad from an examination of the competing effect iodine has on the ionic reactions of cyclopropane.[11] The observed yield of cyclohexyl radical will be further affected by any reduction in the number of hydrogen atoms which undergo abstraction. If we assume that 23% of the neutralization processes lead to the formation of hydrogen atoms (as derived from the results of a study on ethylene solutions)[2] then the yield of hydrogen atoms for any given concentration of ion scavenger will be given by

$$G(H)_s = G(H)_0 - 0.23G(\text{ion}) \qquad \text{(II)}$$

Assuming simple competition between reactions 1 and 2 the fraction of the hydrogen atoms which react with iodine is $1/[1 + (k_2[RH]/k_1[I_2])]$ and the yield of cyclohexyl radicals produced by abstraction will, therefore, be

$$G(H)_s\{1 - 1/[1 + (k_2[RH]/k_1[I_2])]\}$$

The observed radical yield should be describable by

$$G(C_6H_{11}\cdot)_s = G(C_6H_{11})_p - \epsilon_R G(\text{ion}) + (G(H)_0 - 0.23\,G(\text{ion}))\left(1 - \frac{1}{1 + \dfrac{k_2[RH]}{k_1[I_2]}}\right) =$$

$$G(C_6H_{11}\cdot)_0 - (G(H)_0 - 0.23\,G(\text{ion}))\times \frac{1}{1 + \dfrac{k_2[RH]}{k_1[I_2]}} - (\epsilon_R + 0.23)G(\text{ion}) \qquad \text{(III)}$$

where ϵ_R is the efficiency with which cyclohexyl radicals are produced in the ion-recombination and presumably has a value somewhere between 0 and 2. In eq III $G(C_6H_{11}\cdot)_0$ is the cyclohexyl radical yield from pure cyclohexane and includes any secondary radicals produced by hydrogen atom abstraction processes, *i.e.*, $G(C_6H_{11}\cdot)_0 = G(C_6H_{11}\cdot)_p + G(H)_0$. From the results of the cyclopropane experiments reported below $\epsilon_R + 0.23 \sim 1.0$. If we take $G(H)_0$ as the value obtained in the work with ethylene (1.46),[2] $G(C_6H_{11}\cdot)_0$ can be estimated from the measured cyclohexyl radical yields provided k_2/k_1 is known. While k_2/k_1 is certainly in the region of a few times 10^{-4}, the exact value of this ratio is not determinable from presently available data. (The analogous ratio $k_{H + RH}/k_{H + HI}$ is known to be 5×10^{-4} in hexane.)[14] If we take $k_2[RH]/k_1$ as 0.002 then, as indicated in Table I, $G(C_6H_{11}\cdot)_0$ is constant at a value of 5.7. Decreasing $k_2[RH]/k_1$ to 0.001 will increase this quantity to 5.9 and increasing it to 0.004 will decrease the estimate of $G(C_6H_{11}\cdot)_0$ to 5.5.

If one examines the disappearance of iodine during the course of irradiation by following its optical absorption, a linear decrease with dose is observed at iodine concentrations below 0.5 mM. The slope of the decrease measured during the course of this work ($G(-{}^1/_2I_2) = 5.60$) agrees with that previously reported.[15] A slightly higher value (5.8) is given above for the yield of total organic iodide but the difference is of the magnitude of the errors involved in the measurements. It is important to note, as was commented on in the earlier study,[9] that the two measurements give essentially

(11) S. J. Rzad, Abstracts, 158th National Meeting of the American Chemical Society, New York, N. Y., Sept 1969.

(12) K.-D. Asmus, private communication.

(13) S. J. Rzad, R. H. Schuler, and A. Hummel, *J. Chem. Phys.*, **51**, 1369 (1969).

(14) D. Perner and R. H. Schuler, *J. Phys. Chem.*, **70**, 317 (1966).

(15) R. H. Schuler, *ibid.*, **63**, 925 (1959).

Table I: Effect of Iodine on Cyclohexyl Radical Production

$[I_2]$	$G(C_6H_{11}\cdot)$ observed	$\Delta G(C_6H_{11}\cdot)_H$[a]	G_{ion}[b]	$G(C_6H_{11}\cdot)_0$[c]
0.00010	5.35	0.07	0.16	5.58
0.00013	5.20	0.09	0.16	5.45
0.00022	5.40	0.14	0.17	5.71
0.00044	5.18	0.25	0.20	5.63
0.00064	5.20	0.34	0.21	5.75
0.00107	4.97	0.49	0.24	5.70
0.00133	4.80	0.56	0.25	5.61
0.00266	4.61	0.80	0.30	5.71
0.00443	4.41	0.95	0.35	5.71
0.0080	4.27	1.09	0.43	5.79
0.0133	4.26	1.16	0.51	5.93
			Mean	5.69

[a] Reduction in cyclohexyl radical production expected to result from hydrogen atom scavenging by the iodine. Calculated from second term in eq III assuming $G(H)_0 = 1.46$ and $k_2[RH]/k_1 = 0.002$. [b] Calculated from eq I. [c] Calculated from observed $G(C_6H_{11}\cdot)$ and eq III.

Table II: Effect of Cyclopropane and Ethylene on Cyclohexyl Radical Production

[S]	$G(C_6H_{11}\cdot)_{obsd}$[a]	$G(C_6H_{11}\cdot)_{calcd}$[b]
0	5.20	5.18
	Cyclopropane	
0.010	5.02	5.03
0.039	4.70	4.85
0.110	4.58	4.62
0.30	4.40	4.32
	Ethylene	
0.010	4.66	4.87
0.052	4.22	4.30
0.105	3.90	3.98
0.20	3.66	3.69
0.23	3.63	3.63

[a] At an iodine concentration of 0.6 mM. [b] Calculated in the case of cyclopropane from eq III with $\alpha = 0.40$ and the other parameters as described in text. For ethylene the yield was calculated from eq V with $\alpha = 0.43$, $k_2[RH]/k_3 = 0.044$ and $k_1/k_3 = 22$.

identical yields at $[I_2] \sim 0.5$ mM and leave little room for the formation of much HI at this iodine concentration. If $k_2[RH]/k_1$ is smaller than 0.002 then a difference greater than 0.3 should be observed at 0.5 mM iodine. Such a difference should be detectable. A value of at least 0.002 for $k_2[RH]/k_1$ is therefore indicated. For purposes of the remaining discussion, the results are compared on the basis of $G(C_6H_{11}\cdot)_0 = 5.7$ and $k_2[RH]/k_1 = 0.002$ which cannot be far from the correct values and should give internal consistency within the indicated comparisons.

According to the treatment previously given for the effect of scavengers on hydrogen production[2] the hydrogen yield from iodine-containing solutions should be given by

$$G(H_2)_s = G(H_2)_0 - \epsilon_{H_2}G(\text{ion}) - [G(H)_0 - 0.23\,G(\text{ion})]\frac{1}{1 + \dfrac{k_2[RH]}{k_1[I_2]}} \quad \text{(IV)}$$

Since $G(H_2)_0 \simeq G(C_6H_{11}\cdot)_0$ and $\epsilon_{H_2} \simeq \epsilon_R + 0.23 \simeq 1$ the right-hand sides of eq III and IV are essentially identical and the hydrogen yield and cyclohexyl radical yields should be very nearly equal at all iodine concentrations. Data from two early studies[16,17] are given in Figure 3. For I_2 concentrations below $\sim$10 mM the hydrogen yields fall on top of the cyclohexyl radical yields within the experimental error involved in the measurements of $G(H_2)$. In the region above 10 mM the yields of hydrogen tend to be slightly lower than those for cyclohexyl, indicating that some effects may be present which have not been quite properly taken into account. The differences are, however, small and the hydrogen data confirm the idea that electrons do not react efficiently with iodine since if such were the case the yield would be reduced to $\sim$3.0 at $[I_2] = 0.01$ M.[2] One should also comment here that the apparent agreement between the initial yields of cyclohexyl radicals and hydrogen is strictly accidental since one molecule of hydrogen is equivalent to two cyclohexyl radicals and other products are produced which satisfy the material balance requirements (see below).

Effects of Cyclopropane and Ethylene. The addition of either cyclopropane (Δ) or ethylene to cyclohexane causes a reduction in the observed yield of cyclohexyl radicals (Table II). In the case of cyclopropane part of the observed decrease results from a small decrease in the yield of hydrogen atoms (see eq II)[2] and the remainder from a much more important decrease in the yield of primary radicals produced in the neutralization. If the reactions involving cyclopropane are accompanied by a reduction in the efficiency for production of cyclohexyl radical to 0, as seems likely, then the concentration dependence should be describable by eq III with zero substituted for ϵ_R. The ionic yield can be calculated from eq I with a value for α_s of 0.40 M^{-1} as determined from measurements of the products from the cyclopropane.[13] The only undetermined parameter in eq III is ϵ_R. As is indicated in Table II, the observed data can be fit quite well if $(\epsilon_R + 0.23)$ is taken as 1.0. It should be pointed out that in the case of cyclopropane about 30% of the ionic processes yield propyl radicals.[18] There is no evidence here that there is a complementary yield of cyclohexyl radicals; therefore their production must involve some process other than simple proton transfer from a $C_6H_{12}^+$ ion. This observation is in

(16) R. H. Schuler, *J. Phys. Chem.*, 61, 1472 (1957).

(17) M. Burton, J. Chang, S. Lipsky, and M. P. Reddy, *Radiat. Res.*, 8, 203 (1958).

(18) S. J. Rzad and R. H. Schuler, *J. Phys. Chem.*, 72, 228 (1968).

accord with the suggestion of Ausloos, *et al.*, that in this system propyl radicals are predominantly formed by hydrogen atom transfer from the cyclohexane positive ion to cyclopropane.[19]

In the case of ethylene the reduction observed can be interpreted in terms of an effect analogous to the above, together with a superimposed effect involving the scavenging of hydrogen atoms by the ethylene.

$$H\cdot + C_2H_4 \xrightarrow{k_3} C_2H_5\cdot \qquad (3)$$

If we take into account the fact that both reactions 1 and 3 interfere with cyclohexyl radical production then

$$G(C_6H_{11}\cdot)_{C_2H_4} = G(C_6H_{11}\cdot)_0 - (\epsilon_R + 0.23)G(\text{ion}) - [G(H)_0 - 0.23\,G(\text{ion})]\,\frac{1}{1 + \dfrac{k_2[RH]}{k_3\left([C_2H_4] + \dfrac{k_1}{k_3}[I_2]\right)}} \qquad (V)$$

From studies of ethyl radical formation[2] $k_2[RH]/k_3$ has been estimated to be 0.044. From this and $k_2[RH]/k_1 = 0.002$, $k_1/k_3 = 22$, *i.e.*, iodine is taken at 22 times as efficient as C_2H_4 in the scavenging of hydrogen atoms. Equation V involves no undetermined parameters ($\alpha_{C_2H_4} = 0.43\ M^{-1}$ was determined by Rzad[11]). The excellent agreement between observed and calculated yields is indicated in Table II.

Material Balance Considerations. In principle one should be able to use information on the radical yield, along with auxiliary information on the yield of molecular products, to derive the yields of hydrocarbon products expected from the radiolysis of pure hydrocarbons. The principal products from cyclohexane are (in addition to hydrogen) cyclohexene and dicyclohexyl with the most significant minor products being 1-hexene, methylcyclopentane, and 6-cyclohexyl-1-hexene.[20] The first two of these minor products have no importance in the material balance considerations since they are isomeric with cyclohexane. Hydrogen has been measured many times and most investigators are now agreed that its initial yield is very close to 5.6.[4] Dyne and Stone carefully studied the dose dependence of the hydrogen formation and have given an initial yield of 5.55.[21] A recent determination in these laboratories, in which the observed yields are empirically corrected to zero dose, gave a slightly higher value of 5.67[2] but the difference cannot be regarded as significant. The hydrocarbon products have been studied to a lesser extent but the results of a fair number of measurements have now been reported in the literature.[4] Unfortunately, there is very poor agreement between the various results. More seriously there is extremely poor material balance within most of the individual sets of results and only in the work reported by Dyne and Stone[21] can the situation be regarded as satisfactory. They find initial yields for cyclohexene, dicyclohexyl, and 6-cyclohexyl-1-hexene of 3.27, 1.95, and 0.27. The total yield of hydrogen deficient products, 5.49, can be compared with their measured $G(H_2)$ of 5.55. In most other studies the reported values for the hydrogen deficient products are much lower and account for only 80–90% of the hydrogen observed.

In the following we will idealize the stoichiometry involved in the cyclohexane radiolysis by assuming that the only primary products are atomic and molecular hydrogen, cyclohexyl radicals, cyclohexene, and dicyclohexyl (note that 6-cyclohexyl-1-hexene is isomeric with and therefore stoichiometrically equivalent to dicyclohexyl). In the case of hydrogen production, the various sources have been broken down into the categories ionic and nonionic with each having components of molecular and atomic hydrogen.[2] We will use the estimates given in Table VI of reference 2 for each of these. The present study indicates that of the G of 5.7 observed for cyclohexyl radicals ~3.9 come from ionic processes and the remainder (~1.8) from nonionic processes. The following stoichiometric (but not necessarily mechanistic) equations can be written to account for the observations.

Ionic

	G =	
$C_6H_{12}^+ + e^- \xrightarrow{23\%} C_6H_{11}\cdot + H\cdot$	0.89	(4)
$C_6H_{12}^+ + e^- + C_6H_{12} \xrightarrow{27\%} 2C_6H_{11}\cdot + H_2$	1.06	(5)
$C_6H_{12}^+ + e^- \xrightarrow{40\%} C_6H_{10} + H_2$	1.55	(6)
$C_6H_{12}^+ + e^- + C_6H_{12} \xrightarrow{10\%} C_6H_{11}\text{–}C_6H_{11} + H_2$	0.40	(7)

Nonionic

$C_6H_{12} \longrightarrow C_6H_{10} + H_2$	0.87	(8)
$\longrightarrow C_6H_{11}\cdot + H\cdot$	0.57	(9)
$2C_6H_{12} \longrightarrow 2C_6H_{11}\cdot + H_2$	0.33	(10)

It is assumed that the hydrogen atoms produced in eq 4 and 9 go on to abstract a hydrogen atom from the solvent and produce hydrogen and a second cyclohexyl radical. The indicated yields have been assigned in the following manner. Of the ionic processes, hydrogen atoms are produced only in 4 and this is given the yield of 0.89 estimated for ionically produced atomic hydrogen.[2] Subtracting twice this value from the yield for ionically produced cyclohexyl radicals and dividing by 2 we obtain 1.06 for eq 5. These two processes account for only one-half the observed yield of 3.90 for ionically produced hydrogen so the other half must be balanced by the production of cyclohexene

(19) P. Ausloos, A. A. Scala, and S. G. Lias, *J. Amer. Chem. Soc.*, **89**, 3677 (1967).

(20) S. K. Ho and G. R. Freeman, *J. Phys. Chem.*, **68**, 2189 (1964).

(21) P. J. Dyne and J. A. Stone, *Can. J. Chem.*, **39**, 2381 (1961).

and dicyclohexyl. A yield of 0.40 is assigned to eq 7 since this yield must be slightly higher than the 0.31 observed for dicyclohexyl formation in the presence of 6 mM iodine.[22] The yield of 1.55 for eq 6 makes up the remaining hydrogen yield of 3.90. Of the yield of 1.46 given for atomic hydrogen, 0.57 is estimated[2] to be produced from nonionic processes and is assigned to eq 9. This accounts for 1.14 out of the 1.80 yield given above for cyclohexyl radicals produced by nonionic processes and leaves a yield of 0.33 for eq 10 to account for the remainder. Finally, eq 8 is assigned a value of 0.87 to account for the total observed yield of hydrogen. This breakdown is, at the moment, completely *ad hoc*. One needs independent determinations of the yields of cyclohexene and dicyclohexyl at low doses and as a function of scavenger concentration to overdetermine the situation and provide a measure of check. Measurements of cyclohexene production in the presence of oxygen[20] or 6 mM I_2[22] give a (molecular) yield $\sim$1.5 which indicates that the sum of eq 6 and 8 may be overestimated. These experiments were, however, carried out at considerably higher doses than those reported here and in the case of the work with I_2 the observed cyclohexene is insufficient to account for the sum of yields of hydrogen and the HI expected from reaction 1. Obviously one needs additional detailed measurements at low doses.

We can now use the information of eq 4–10 to estimate the initial cyclohexene and dicyclohexyl yields which should be observed in the absence of any scavenger. One needs additionally the disproportionation–combination ratio for reaction between two cyclohexyl radicals. Taking a value for this ratio of 1.1[23] a yield of 1.49 is given for the formation of cyclohexene from the cyclohexyl radicals. The total cyclohexene should be this plus the yields of eq 6 and 8 or 3.90. Similarly the yield of eq 7 must be added to a yield of 1.36 from the dimerization of cyclohexyl radicals for a total of 1.76 for dicyclohexyl. All reported yields for cyclohexene measured gas chromatographically are substantially lower than the above estimate although an optical measurement[18] gave an estimate of total unsaturation of 3.90. Probably the best measurements of cyclohexene formation are those of Dyne and Stone[21] and Ho and Freeman[20] which gave, respectively, yields of 3.27 and 3.2 at doses of $\sim 10^{19}$ eV/g where the yields should be only slightly less than at zero dose. The difference between the observed and estimated yields can, of course, always be accounted for in terms of the formation of other hydrogen deficient products but then the good material balance reported by Dyne and Stone would be illusionary. Perhaps a greater difficulty is the low value estimated for dicyclohexyl formation. Dyne and Stone[21] report yields of 1.95 for dicyclohexyl and 0.27 for 6-cyclohexyl-1-hexene for a total dimer yield of 2.22. Ho and Freeman[20] report respective values of 1.76 and 0.12 for a sum 1.88, in reasonable agreement with the present calculation. The latter are, however, unable to account for all of the observed hydrogen. If we accept as fact a disproportionation ratio no lower than 1.1 then the maximum value of G(dimer) that can be expected from the radicals is 1.36 (*i.e.*, 1/2 × 1.0/2.1 × 5.70). The yield of dimer observed in the presence of iodine is $\sim$0.3 so that the maximum yield of dimer that can be attributed to nonradical products appears to be of this order of magnitude. The total cannot, therefore, be much greater than 1.7. Clearly a reasonably important discrepancy exists and either there is some other source of dimer that is not properly taken in account in the series of equations written or the disproportionation–combination ratio is considerably less than has been reported. A ratio of 0.6 would account for the yields reported by Stone and Dyne.

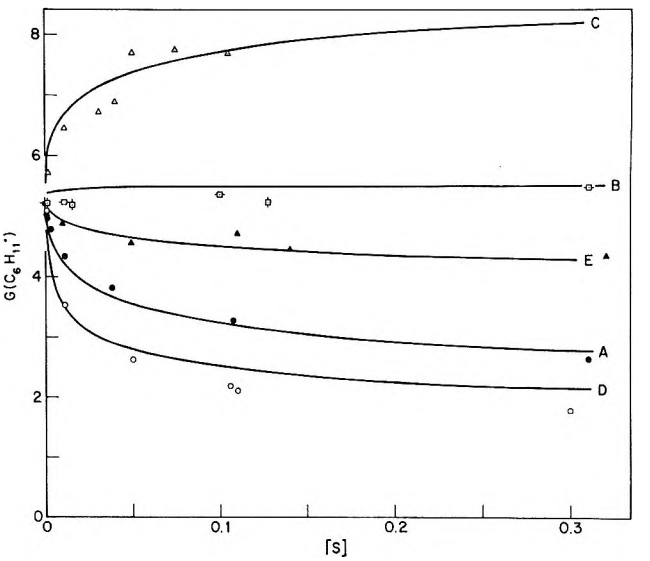

Figure 4. Effect of electron scavengers on cyclohexyl radical yield for cyclohexane solutions 0.6 mM in I_2; ●, CH_3Br; —□—, CH_3Cl; □, SF_6; △, N_2O; ○, CH_3I; and ▲, CO_2. Curves calculated from the sum of eq III and, respectively, for A, B, C, and E, 0, 1, 2, and 0.5 × G(ion) calculated from eq I with the parameters taken as described in the text. Curve D is calculated from eq III on the assumption that CH_3I and I_2 scavenge hydrogen atoms with the same efficiency.

Effect of Electron Scavengers. The effects of the electron scavengers CH_3Br, CH_3Cl, CH_3I, SF_6, N_2O, and CO_2 were studied and the results are reported in Figure 4. It is seen that the effects fall qualitatively into several different groups, in contrast to the common effect that all these solutes have in reducing the hydrogen yield.[2] It seems likely that different secondary reactions of the chemical intermediates produced by

(22) S. Z. Toma and W. H. Hamill, *J. Amer. Chem. Soc.*, **86**, 1478 (1964).

(23) W. A. Cramer, *J. Phys. Chem.*, **71**, 1171 (1967).

the neutralization are involved though it is possible that variations in the neutralization processes can be responsible. The simplest case seems to be CH_3Br where the reduction in cyclohexyl production is reasonably well described by eq III (see Figure 4) with α_{CH_3Br} taken as 16 M^{-1} from the observations on $CH_3\cdot$ production. Presumably electron scavenging by the CH_3Br results in the formation of bromide ion (since methyl radicals are an observed product).

$$e^- + CH_3Br \longrightarrow CH_3\cdot + Br^- \qquad (11)$$

In order to explain the lack of formation of cyclohexyl radical upon neutralization it must be assumed that reaction 12

$$RH^+ + Br^- \text{—//→} R\cdot + HBr \qquad (12)$$

does not occur. It would seem that any bromide ions formed must, when they are neutralized, form bromine atoms which, since they do not in turn abstract hydrogen, must react with the iodine present to form relatively unreactive IBr.

$$RH^+ + Br^- \longrightarrow RH + Br\cdot \qquad (13)$$

In contrast to the decrease observed with CH_3Br, the addition of CH_3Cl has essentially no effect on the cyclohexyl radical yield (yields of 5.21, 5.37, and 5.56 were observed at CH_3Cl concentrations of 0.01, 0.1, and 0.3 M) although large yields of methyl radicals are known to be produced from this solute.[24] Cyclohexyl radicals thus must result either directly from the neutralization

$$RH^+ + Cl^- \xrightarrow{?} R\cdot + HCl \qquad (14)$$

or from secondary abstraction reactions of chlorine atoms produced as intermediates. The efficiency of production of cyclohexyl radicals by the processes which occur subsequent to electron capture must be very close to unity. If this is so then a term equal to G(ion) must be added to eq III and the addition of CH_3Cl to a 0.6 mM solution of iodine in cyclohexane is expected to increase the yield of cyclohexyl radical slightly (~0.2 at 0.6 mM I_2) because the reduction caused by reaction of ions with iodine will effectively have been removed.

Three experiments with SF_6 also showed no effect on the cyclohexyl yield (observed G of 5.21, 5.18, and 5.22 at 0.001, 0.01, and 0.13 M). Again electron capture by the SF_6 is known to occur (as evidenced by the reduction in $G(H_2)$ produced by this solution and also its competitive effect on other electron scavengers) but it has no effect on the production of $C_6H_{11}\cdot$. The lack of effect of SF_6 on cyclohexyl iodide production reported here contrasts with the reduction in the yields of cyclohexene and dicyclohexyl reported by Sagert and Blair.[7] It would seem that in the absence of iodine complicating secondary effects involving the reaction of cyclohexyl radicals with the degradation products of SF_6 must be involved in determining the overall yields.

Nitrous oxide has a qualitatively different effect in that it is found to produce a marked increase in $G(C_6H_{11}\cdot)$. The data from the present experiments are reported in Figure 4. Previously it was noted that the addition of N_2O to cyclohexane resulted in an increase in the yield of dicyclohexyl,[5,6,7] cyclohexene,[7] and uptake of iodine.[5] The increase in the yields of dicyclohexyl and cyclohexene estimated by Sagert and Blair (~0.7 and 0.3, respectively, in the region of 0.1 M N_2O) corresponds to an increase ~2.0 in the cyclohexyl yield in agreement with the value found here. While the data from the nitrous oxide experiments scatter somewhat more than those obtained with the other solutes, they can be roughly described by assuming that the ionic component increases rather than decreases the yield, *i.e.*, that the sign of the third term in eq III is positive rather than negative. Indeed for 0.1 M N_2O and CH_3Br solutions the observed difference is 4.42 or almost identically equal to 2 G(ion). Additional radicals must obviously come from secondary reactions. This situation is perhaps not too surprising since ·OH radicals seem an intermediate likely to be produced from the N_2O and these would undoubtedly abstract hydrogen from the solvent.

Methyl iodide suppresses the cyclohexyl radical yield somewhat more than does methyl bromide. This is as expected since a very large yield of methyl radicals is observed from these solutions,[25] presumably because the methyl iodide is a reasonably efficient hydrogen atom scavenger. The addition of C_2H_4 to a CH_3I solution had no effect on the observed yield as indicated by the data reported in Table III, whereas it reduced the observed yields in the cases of CH_3Br and CH_3Cl. Curve D in Figure 4 was calculated from eq III, substituting for the iodine concentration the methyl iodide concentration. At the highest concentrations the observed yields of cyclohexyl radical are still somewhat lower than calculated. This additional decrease may conceivably result from further complications involving the positive ion component since methyl iodide is known to be a positive ion scavenger.[11]

With CO_2 a decrease in the cyclohexyl yield is observed but this decrease is less than expected from the

Table III: Effect of Ethylene on Cyclohexyl Radical Yield from Alkyl Halide Solutions

S	[S]	$G(C_6H_{11}\cdot)_{C_2H_4=0}$	$G(C_6H_{11}\cdot)_{C_2H_4=0.1}$
	0		3.90
CH_3I	0.108	2.11	2.07
CH_3Br	0.107	3.26	2.69
CH_3Cl	0.105	5.37	4.18

(24) J. M. Warman, K.-D. Asmus, and R. H. Schuler, *J. Phys. Chem.*, **73**, 931 (1969).

(25) J. L. McCrumb and R. H. Schuler, unpublished results.

ionic component calculated from eq I if α_{CO_2} is taken as the value of 8 indicated by the effect of CO_2 on hydrogen production.[2] It would appear from this that a fraction of the ionic events result in secondary reactions which produce cyclohexyl radicals. Curve E in Figure 4 was calculated by assuming that 50% of the ionic reactions ultimately result in the production of cyclohexyl radicals, *i.e.*, by adding 0.5 of the value of G(ion) calculated from eq I to $G(C_6H_{11}\cdot)$ calculated from eq III. It is not obvious to what mechanistic process this factor of 0.5 corresponds but one might speculate that neutralization of the positive ion by CO_2^- might eliminate the contribution from eq 5 but have no effect on that from eq 4 (or *vice versa*).

Mixed Solutes. Data on the effect of adding both cyclopropane and electron scavengers to the cyclohexane are given in Table IV. First it is noted that

Table IV: Effect of Electron Scavengers on the Cyclopropane Solutions

S	[S]	$G(C_6H_{11})_{\Delta=0}$	$G(C_6H_{11}\text{-R}\cdot)_{\Delta=0.1}$
		5.20	4.58
SF_6	0.33	5.22	4.57
CH_3Cl	0.10	5.37	4.52
CO_2	0.11	4.72	4.11
CO_2	0.32	4.33	3.55

adding 0.1 *M* cyclopropane to any given solution reduces $G(C_6H_{11}\cdot)$ by ~0.7. This reduction may be compared with that of 0.56 calculated for the effect of cyclopropane in the absence of electron scavenger. More importantly it is noted that the addition of either CH_3Cl or SF_6 to a cyclopropane containing solution causes no further reduction in $G(C_6H_{11}\cdot)$. Because the positive ion reactions of cyclopropane are increased upon addition of electron scavenger[13] the number of cyclohexyl radicals produced directly from the neutralization will be decreased. These results tend to rule out the importance of reaction 14 since somehow this decrease must be balanced by products produced indirectly from the electron scavenger. From this it is implied that the high yields observed in the CH_3Cl and SF_6 cases are associated with secondary chemical abstraction reactions. Abstraction of hydrogen by Cl and F atoms seem to be a likely prospect. It is in fact quite surprising that in the case of SF_6 an increase in $G(C_6H_{11}\cdot)$ is not observed to result from secondary reactions of intermediates which are produced as the SF_6 is degraded.

As already commented on, ethylene has little effect on the cyclohexyl radical yield from methyl iodide solutions because the methyl iodide scavenges both hydrogen atoms and the ionic intermediates. Data from CH_3Br and CH_3Cl solutions are recorded in Table III which indicate that in the case of CH_3Br the cyclohexyl radical yield is reduced by hydrogen atom scavenging and in the case of CH_3Cl by the sum of H· atom and ion scavenging.

In summary, it can be said that solutes added to cyclohexane change the radiation chemistry of the system by reaction with either the positive ions or electrons initially produced. In the former case such reaction clearly results in a decrease in the production of cyclohexyl radicals. In the latter case complicating secondary abstraction reactions occur which can, in fact, even increase the yield of cyclohexyl radicals. Superimposed are any effects of hydrogen atom scavenging by the solute which reduce the yield of cyclohexyl radicals. While the overall effects are complicated, they can be effectively correlated in terms of expressions developed to describe the ion scavenging processes on the assumption that on the average one cyclohexyl radical is produced for each ion pair formed in the radiolysis of the pure hydrocarbon.

Kinetics of γ-Induced Decomposition of Methyl Iodide in Air[1]

by I. N. Tang and A. W. Castleman, Jr.

Brookhaven National Laboratory, Upton, New York 11973 *(Received April 16, 1970)*

The ^{60}Co γ-ray induced decomposition of methyl iodide in air was investigated at 15° over an initial concentration range of 2.8×10^{-12} to 2.4×10^{-7} mol/cc. The decomposition reaction is pseudo-first order with respect to methyl iodide at concentrations below 2.4×10^{-10} mol/cc and is zero order at 2.4×10^{-7} mol/cc. At intermediate methyl iodide concentrations, however, the decomposition does not follow a simple reaction order. A mechanism is proposed which quantitatively accounts for the observed reaction kinetics.

Introduction

The photooxidation of gaseous methyl iodide in oxygen has been the subject of a number of extensive studies.[2-4] Although the detailed reaction mechanism is still not fully understood, the primary photochemical act and many of the important secondary reactions have been identified. In contrast, the radiation-induced oxidation of methyl iodide has received little attention.

This paper presents the results of a study on the ^{60}Co γ-ray induced decomposition of methyl iodide in air. While the emphasis was placed on the elucidation of the decomposition mechanism, the choice of air as the oxidizing environment was dictated by practical considerations. Methyl iodide has been shown to form *via* impurity reactions wherever tracer-level iodine is present.[5,6] The stability of this compound in a combined radiation and oxidizing environment is of great importance in making safety analyses of nuclear reactors.

Experimental Section

Mallinckrodt reagent grade CH_3I was used without further purification. Compressed air was dried before use by passing through a molecular sieve trap maintained at Dry Ice–acetone temperature. The apparatus for sample preparation consisted of a 3-l. gas reservoir connected to a sampler manifold and a high-vacuum system. Only Delmar-Urry greaseless stopcocks were used in the system. Before filling the reservoir, the system was thoroughly torched under vacuum and evacuated to better than 5×10^{-6} Torr. Two sizes of sample bulbs were employed. The smaller 25-ml bulbs were made of Pyrex and equipped with capillary break-seals. The 400-ml bulbs, each attached to a Nupro S. S. bellows valve, were constructed of either Pyrex, quartz, or Type 321 stainless steel. Before use, the glass bulbs were cleaned with chromic acid in an ultrasonic bath and the stainless steel bulbs with dilute nitric acid. They were rinsed thoroughly with distilled water, dried in an oven, and then outgassed at 500° *in vacuo* for 18 hr.

Mixtures of air and CH_3I were irradiated at 15° with ^{60}Co γ-ray sources having dose rates ranging from 3.5×10^4 to 1.2×10^6 rads/hr. A dual-column gas chromatograph equipped with an electron-capture detector and a flame-ionization detector was employed for sample analysis before and after irradiation. The columns were constructed of 0.125-in. nickel tubings, 10–20 ft in length. These were packed with 35% DC-200 silicone oil on 60–80 mesh HMDS treated Chromosorb W and were operated at 65° with a dry nitrogen carrier gas flowing at 50 cc/min. In some experiments, mass spectrometry was employed for identifying the radiolysis products.

Results

The change in CH_3I concentration due to γ-ray action was followed during an experiment. A typical semilogarithmic plot of the concentration change as a function of irradiation duration is shown in Figure 1. In this particular series of experiments, samples with initial CH_3I concentrations ranging from 1.6×10^{-11} to 2.4×10^{-10} mol/cc were irradiated at a dose rate of 3.48×10^5 rads/hr as measured by Fricke dosimetry. The parallel lines shown in Figure 1 indicate that the decomposition reaction is pseudo-first-order with respect to methyl iodide. Similar results were obtained with other dose rates, and the slopes of the straight lines varied in direct proportion to the dose rates employed.

A summary of the results from experiments covering the initial CH_3I concentration range from 2.8×10^{-12} to 2.4×10^{-10} mol/cc and the dose rate range from 3.6×10^4 to 1.2×10^6 rads/hr is shown in Figure 2.

(1) This work was performed under the auspices of the U. S. Atomic Energy Commission.

(2) (a) M. I. Christie, *Proc. Roy. Soc., Ser. A*, **244**, 411 (1958); (b) J. F. McKellar and R. G. W. Norrish, *ibid.*, **263**, 51 (1961).

(3) J. Heicklen and H. S. Johnston, *J. Amer. Chem. Soc.*, **84**, 4030 (1962).

(4) M. Barber, J. Farren, and J. W. Linnett, *Proc. Roy. Soc., Ser. A*, **274**, 306 (1963).

(5) A. E. J. Eggleton and D. H. F. Atkins, *Radiochim. Acta*, **3**, 151 (1964).

(6) A. W. Castleman, Jr., I. N. Tang, and H. R. Munkelwitz, *J. Inorg. Nucl. Chem.*, **30**, 5 (1968).

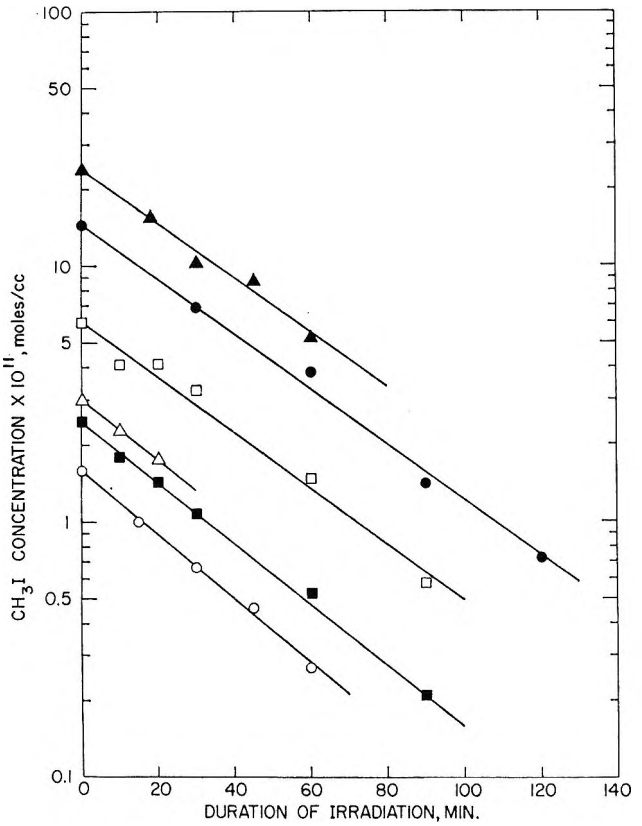

Figure 1. The time dependence of CH_3I concentration during irradiation with ^{60}Co γ rays at dose rate of 3.48×10^5 rads/hr; air density = 1.05×10^{-3} g/cc.

Here, all data are normalized to percentage of CH_3I remaining and plotted on semilogarithmic coordinates as a function of total absorbed dose in eV/g of air. A conversion factor of 5.62×10^{13} was used in the calculation to convert rads as measured by Fricke dosimetry into electron volts absorbed per gram of air. The density of air employed in these experiments is 1.05×10^{-3} g/cc. The straight line shown in the plot is a least-squares fit of all data points.

The results from experiments of high initial CH_3I concentration (2.4×10^{-7} mol/cc) and intermediate CH_3I concentration (4.8×10^{-8} mol/cc) are given in Figures 3 and 4, respectively. The air density employed in both series of experiments was 1.25×10^{-3} g/cc. While the data shown in Figure 3 are well represented by a least-squares straight line, suggesting a zeroth-order reaction for the oxidation of CH_3I at high concentrations, no simple reaction order was found to represent the results from the intermediate concentration experiments.

Most of the low CH_3I concentration experiments were carried out with Pyrex sample bulbs. However, no appreciable difference was noted when quartz sample bulbs were used. There was also no noticeable change in the CH_3I decomposition rate measured in sample bulbs which were opaque to light. In experiments carried out with higher CH_3I concentrations, both

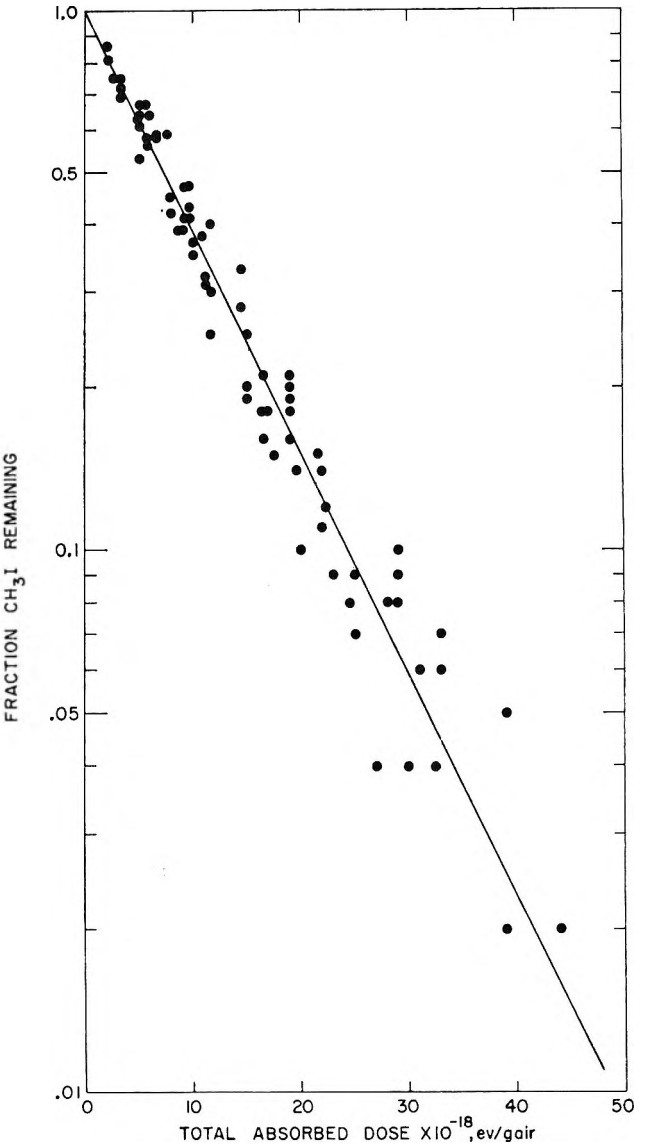

Figure 2. The decomposition of CH_3I as a function of total absorbed dose for the initial concentration range of 2.8×10^{-12} to 2.4×10^{-10} mol/cc; air density = 1.05×10^{-3} g/cc.

quartz and stainless steel sample bulbs were employed and again no effect of wall material was observed. The observation indicated that the size of the sample bulbs (55 mm in diameter) used in the experiments was large enough to ensure minimal contribution of the secondary electrons emitted from the walls[7] and that the container walls also did not contribute significantly to the recombination processes taking place during radiolysis.

In general, no postirradiation effect was observed, except in one run where the air was saturated with moisture at 0°. This was expected since in the latter case, appreciable amounts of nitric acid would undoubtedly form[8] and react with the remaining CH_3I even after the irradiation ceased.

(7) J. Weiss, A. O. Allen, and H. A. Schwarz, *Proc. Int. Conf. Peaceful Uses At. Energy*, **14**, 179 (1956).

(8) A. R. Jones, *Radiat. Res.*, **10**, 655 (1959).

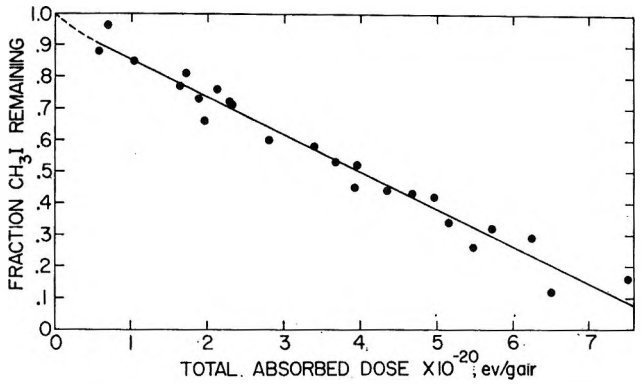

Figure 3. The decomposition of CH_3I as a function of total absorbed dose for the initial concentration of 2.4×10^{-7} mol/cc; air density = 1.25×10^{-3} g/cc.

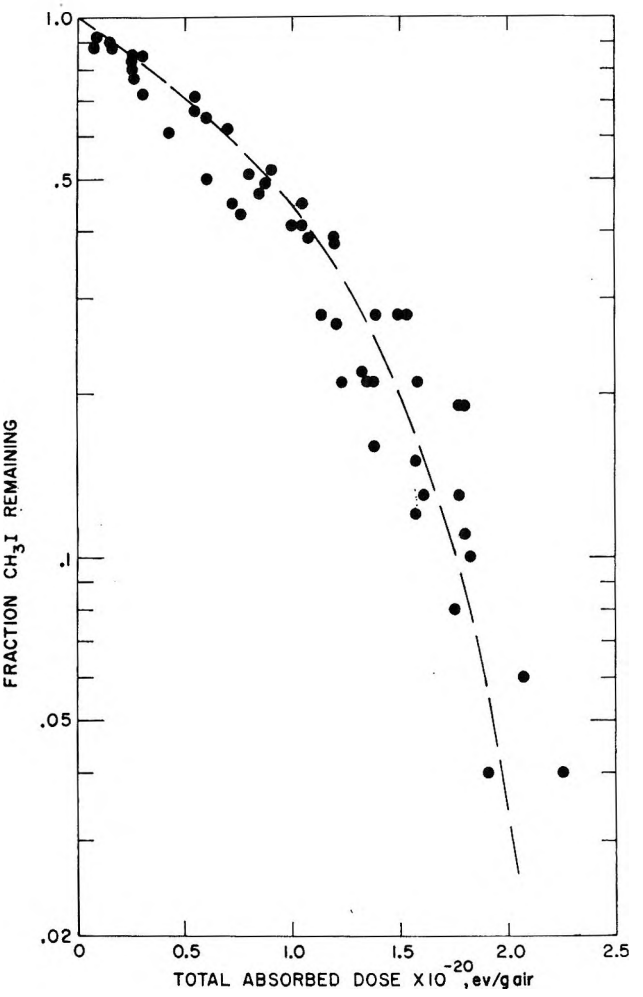

Figure 4. The decomposition of CH_3I as a function of total absorbed dose for the initial concentration of 4.8×10^{-8} mol/cc; air density = 1.25×10^{-3} g/cc.

The radiolysis products observed in the low concentration experiments were mainly methyl nitrate and methyl nitrite. An electron-capture detector was employed in the analysis of samples using gas chromatography. Since electron-capture detectors are known to be only sensitive to compounds of high electron affinity, the failure to detect species other than CH_3ONO_2 and CH_3ONO does not preclude the possibility of other radiolysis products. However, no other species were ever detected with a flame-ionization detector. In the high concentration experiments, both gas chromatographic and mass spectrometric analyses showed the presence of HCHO, CH_3OH, CH_4, C_2H_6, and some other higher molecular weight compounds. The presence of I_2 among the radiolysis products was also shown by mass spectrometry. The amounts of CH_3ONO_2 and CH_3ONO formed during radiolysis, on the contrary, were very small in this case.

It was noted that, in the low concentration experiments, the impurity level in the sample often interfered with the radiolytic decomposition of CH_3I. Thorough cleaning and outgassing procedures must be undertaken to obtain reproducible results. One of the possible interfering impurities was the adsorbed moisture that might be released from the container walls upon irradiation. Since it was difficult to determine the water vapor at very low concentration levels, its effect was demonstrated in a series of experiments in which appreciable amounts of water vapor were metered into the samples. The results from the experiments indicated that increasing the moisture level lowered the CH_3I decomposition rate expressed in terms of adsorbed doses.

Discussion

Decomposition Mechanism. Since the molar ratio of CH_3I to air even in the most concentrated samples used in this study is only 1:200, it is a reasonable assumption that the γ-ray energy is primarily absorbed by air to form active particles, M*, which in turn transfer energy to CH_3I molecules upon collision, *i.e.*

$$M \xrightarrow{\gamma\ k_1} M^* \qquad (1)$$

$$M^* \xrightarrow{k_1'} X \qquad (1a)$$

$$M^* + CH_3I \xrightarrow{k_2} CH_3\cdot + I\cdot + M \qquad (2)$$

Reaction 1a represents the decay of M* by processes other than reaction 2. The dissociation of CH_3I *via* reaction 2 is expected to occur since the carbon–iodine bond is by far the weakest in the molecule. The rupture of the C–I bond has been shown to constitute the primary act in the vapor phase photochemical oxidation of CH_3I,[2-4] in its vapor and liquid phase radiolysis[9] and even in the radiolysis of its dilute aqueous solutions.[10]

Reactions involved in the radiolysis of oxygen–nitrogen systems are rather complicated, and no general agreement has been reached even on the initial radio-

(9) L. H. Gevantman and R. R. Williams, Jr., *J. Phys. Chem.*, 56, 569 (1952).

(10) J. Shanker, K. V. S. Rama Rao, and L. V. Shastri, *ibid.*, 73, 52 (1969).

chemical steps in the formation of nitrogen oxides.[11] Harteck and Dondes[12a] believe that, initially, the dominant reactions are the dissociation of N_2 and O_2 as a result of both molecular excitation and neutralization of charged particles. Pshezhetsky and Dmitriev,[12b] however, have proposed a rather different mechanism involving sets of ion–molecule reactions. Since ion–molecule reactions, as well as charge neutralization, usually proceed at extremely fast rates compared to molecular or even free-radical reaction, it is likely that the M*'s postulated in the present study are excited N_2 and O_2 triplets both because of their chemical reactivity and relatively long lifetimes. The reaction of CH_3I with stray electrons in the system, namely

$$CH_3I + e^- \longrightarrow CH_3\cdot + I^- \qquad (2a)$$

may also contribute to its dissociation. No attempt was made in the study to identify the active energy-transfer species.

It is generally accepted that the reaction of methyl radicals with oxygen takes place *via* two routes, namely, termolecular reaction 3 leading to the formation of methyl peroxide radicals[2a,17] and bimolecular reaction 4 which gives rise to formaldehyde[2b]

$$CH_3\cdot + O_2 + M \xrightarrow{k_3} CH_3O_2\cdot + M \qquad (3)$$

$$CH_3\cdot + O_2 \xrightarrow{k_4} HCHO + OH\cdot \qquad (4)$$

The recombination of iodine atoms will occur according to reaction

$$I\cdot + I\cdot + M \xrightarrow{k_5} I_2 + M \qquad (5)$$

The methyl peroxide radicals produced from reaction 3 may undergo further reaction *via* one of the following three reactions, depending upon the given conditions

$$CH_3O_2\cdot + CH_3O_2\cdot \xrightarrow{k_6} CH_3OH + HCHO + O_2 \qquad (6)$$

$$CH_3O_2\cdot + NO_2 \xrightarrow{k_7} CH_3ONO_2 + O\cdot \qquad (7)$$

$$CH_3O_2\cdot + NO \xrightarrow{k_8} CH_3ONO + O\cdot \qquad (8)$$

where NO_2 and NO are being formed from air by γ radiolysis. Reactions involving methoxy radicals[13] have been adapted frequently, and often successfully at high peroxy radical concentrations, by many investigators to account for their observations. Consequently, a set of alternative reactions might also be proposed in place of reactions 6, 7, and 8 as

$$CH_3O_2\cdot + CH_3O_2\cdot \longrightarrow 2CH_3O\cdot + O_2 \qquad (6a)$$

$$CH_3O\cdot + CH_3O\cdot \longrightarrow CH_3OH + HCHO \qquad (6b)$$

$$CH_3O\cdot + NO_2 \longrightarrow CH_3ONO_2 \qquad (7a)$$

$$CH_3O\cdot + NO \longrightarrow CH_3ONO \qquad (8a)$$

However, based on the evidence presently available, it is not possible to favor one set of reactions over the other.

In experiments where the concentration of I_2 formed is appreciable, I_2 will compete with O_2 for the methyl radicals, thereby leading to the formation of CH_3I according to

$$CH_3\cdot + I_2 \xrightarrow{k_9} CH_3I + I\cdot \qquad (9)$$

The decomposition mechanism proposed here, although not a complete description of the radiolysis of CH_3I in air, includes all dominant reactions leading to the formation of important intermediates and major radiolysis products observed. As will be shown later, this mechanism also gives a quantitative account for the decomposition kinetics in agreement with the experimental data.

Decomposition Kinetics. In the following derivations, the quantity of a radical or molecular product formed directly from primary radiochemical acts is denoted by G with an appropriate subscript, while the actually observed yield of a substance is denoted by G followed by the formula of the substance in parentheses. A minus sign placed in parentheses before the formula represents the G value for decomposition of this substance. The reaction rate is denoted by R with an appropriate subscript. Thus, the rate of production of methyl radicals from reaction 2 may be expressed as

$$\mu G_{CH_3\cdot} = R_2 = \frac{d[CH_3\cdot]}{dt} = k_2[M^*][CH_3I] \qquad (10)$$

where G_{CH_3} = number of $CH_3\cdot$ formed per 100 eV absorbed, R = mol/(cc hr), μ = a conversion factor = $\rho I_M/100N$, ρ = air density in g/cc, I_M = dose rate in eV absorbed (g of air)$^{-1}$ hr^{-}, N = Avogadro's number.

In considering reactions 2 and 9, the following equation is obtained for the net rate of CH_3I decomposition

$$\mu G(-CH_3I) = R_2 - R_9 = k_2[CH_3I][M^*] - k_9[CH_3\cdot][I_2] \qquad (11)$$

Assuming stationary concentrations of M* and $CH_3\cdot$, we can equate their respective rates of formation and removal as

$$M^*: \quad \mu G_{M^*} = R_{1a} + R_2 \qquad (12)$$

$$CH_3: \quad \mu G_{CH_3\cdot} = R_3 + R_4 + R_9 = R_2 \qquad (13)$$

Therefore

$$[M^*] = \frac{\mu G_{M^*}}{k_1' + k_2[CH_3I]} \qquad (14)$$

(11) J. W. T. Spinkes and R. J. Wood, "An Introduction to Radiation Chemistry," Wiley, New York, N. Y., 1964, p 206.

(12) (a) P. Harteck and S. Dondes, *Proc. Second Int. Conf. Peaceful Uses At. Energy, United Nations, Geneva*, 29, 415 (1958); *J. Phys. Chem.*, 63, 956 (1959); (b) S. Ya. Pshezhetsky and M. T. Dmitriev, *Int. J. Appl. Radiat. Isotopes*, 5, 67 (1959).

(13) J. H. Raley, L. M. Porter, F. F. Rust, and W. E. Vaughan, *J. Amer. Chem. Soc.*, 73, 15 (1951).

$$[CH_3\cdot] = \frac{\mu G(-CH_3I)}{k_3[O_2][M] + k_4[O_2]} \quad (15)$$

Consequently, it can be shown by substituting eq 14 and 15 into eq 11 and rearranging, that

$$G(-CH_3I) = G_{M*}\left\{\frac{1 + \frac{k_3}{k_4}[M]}{1 + \frac{k_3}{k_4}[M] + \frac{k_9[I_2]}{k_4[O_2]}}\right\}\left\{\frac{[CH_3I]}{\frac{k_1'}{k_2} + [CH_3I]}\right\} \quad (16)$$

The above equation may be simplified in appearance by making the following substitutions

$$B = 1 + \frac{k_3}{k_4}[M]$$

$$\beta = \frac{k_9}{k_4[O_2]}$$

$$\lambda = \frac{k_1'}{k_2}$$

Therefore

$$G(-CH_3I) = G_{M*}\left(\frac{B}{B + \beta[I_2]}\right)\left(\frac{[CH_3I]}{\lambda + [CH_3I]}\right) \quad (16a)$$

It will be shown in the later sections that eq 16 is adequate to account for the observations, and that the unknown constants contained in the equation can be evaluated from the data obtained in this study.

Low CH_3I Concentration Experiments. It is obvious that reaction 9 may be ignored in cases where the concentration of I_2 produced is extremely small compared to the quantity of O_2 present in the system. This assumption is certainly justified in experiments carried out with initial CH_3I concentrations ranging from 2.8×10^{-12} to 2.4×10^{-10} mol/cc. For example, since the maximum I_2 concentration that could be produced in a run is half of the initial CH_3I concentration of the run, we take a value of 1.2×10^{-10} mol/cc to represent the highest I_2 concentration of this series. This is obviously small compared with the O_2 concentration employed, namely, 7.9×10^{-6} mol/cc.

Christie[2a] has given a value of 278 or k_9/k_4 at 20°. Referring to eq 16, we conclude that

$$\frac{k_9[I_2]}{k_4[O_2]} = 0.0042 \ll 1$$

and, therefore

$$G(-CH_3I) = G_{M*}\left\{\frac{[CH_3I]}{\lambda + [CH_3I]}\right\}$$

For $\lambda \gg [CH_3I]$, the above equation may further be reduced to

$$G(-CH_3I) = -\frac{1}{\mu}\frac{d[CH_3I]}{dt} = \frac{G_{M*}}{\lambda}[CH_3I] \quad (17)$$

After substituting for μ, rearranging and integrating, we find

$$\ln\frac{C}{C_0} = \ln f = -\left(\frac{\rho G_{M*}}{100N\lambda}\right)(I_M t) \quad (18)$$

where $C = [CH_3I]$, the subscript 0 referring to initial concentration, and $f = C/C_0$ = fraction of CH_3I remaining at time t corresponding to an absorbed dose $(I_M t)$.

Equation 18 represents a first-order reaction with respect to CH_3I, which is in complete agreement with the experimental observations as illustrated in Figures 1 and 2. The ratio of G_{M*}/λ may be evaluated from the slope of the line given in Figure 2, namely

$$\frac{G_{M*}}{\lambda} = 5.43 \times 10^9 \quad (19)$$

High CH_3I Concentration Experiments. When the initial CH_3I concentration in a sample is high enough, the iodine being produced by radiolysis will quickly reach a saturation concentration, $[I_2]°$, corresponding to the vapor pressure at the reaction temperature. At 15°, the vapor pressure of iodine is 0.137 Torr,[14] which leads to 0.76×10^{-8} mol/cc for $[I_2]°$. Therefore, starting with a CH_3I concentration of 2.4×10^{-7} mol/cc, the sample undergoing radiolysis will become saturated with I_2 in the gas phase at approximately 7% decomposition of CH_3I. Referring to eq 16a, we have for $[CH_3I] \gg \lambda$

$$G(-CH_3I) = G_{M*}\left(\frac{B}{B + \beta[I_2]°}\right) = A = \text{constant} \quad (20)$$

The assumption of small λ will be justified later.

Equation 20 essentially predicts a zeroth-order decomposition with respect to CH_3I. This is indeed in agreement with the experimental findings as evidenced in Figure 3 by the linearity of the data after the first few per cent decomposition. The slope of the straight line yields a value of 13.6 for $G(-CH_3I)$. The constant β, may be estimated using Christie's value of 278 for k_9/k_4 and the O_2 concentration of 9.05×10^{-6} mol/cc employed in the experiments

$$\beta = \frac{k_9}{k_4[O_2]} = 3.07 \times 10^7$$

and whence $\beta[I_2]° = 0.233$. By substitution and rearranging eq 20, we obtain

$$G_{M*} = 13.6\left(\frac{B + 0.233}{B}\right) \quad (21)$$

Although the precise value of G_{M*} cannot yet be obtained without a knowledge of B, eq 21 does provide

(14) A. N. Nesmeyanov, "Vapor Pressure of the Chemical Elements," R. Gray, Ed., Elsevier, Amsterdam, 1963, p 430.

a bracket for G_{M^*}. Recalling the definition of B, it is evident that B can never be less than unity and therefore, G_{M^*} will not exceed 16.8. On the other hand, should B be much larger than unity, G_{M^*} would approach 13.6 as the lower limit. In short, we conclude that $13.6 < G_{M^*} < 16.7$ and consequently, from eq 19, $2.5 \times 10^{-9} < \lambda < 3.1 \times 10^{-9}$. Therefore, it is seen that in the high concentration experiments, $CH_3I \gg \lambda$ as assumed. It will be shown in the following section that the limits given here for G_{M^*} and λ serve as a useful guide for estimating their respective best values.

Intermediate CH_3I Concentration Experiments. In this case, the iodine concentration is building up at the expense of CH_3I decomposition. The I_2 concentration can be expressed in terms of the CH_3I concentration through an iodine material balance

$$[I_2] = {}^1/_2(C_0 - C) \tag{22}$$

Substituting (22) into (16a) and integrating, we obtain a rather complex expression

$$-\lambda\left(\frac{B}{C_0} + \frac{\beta}{2}\right) \ln f - \frac{\beta C_0}{4}(1 - f^2) + \left(B + \frac{\beta C_0}{2} - \frac{\beta\lambda}{2}\right)(1 - f) = \frac{\rho B G_{M^*}}{100 N C_0}(I_M t) \tag{23}$$

It should be noted, however, that for the particular CH_3I concentration ($C_0 = 4.8 \times 10^{-8}$ mol/cc) employed in the present series of experiments, eq 23 is only valid up to 32% decomposition of CH_3I. This is due to the fact that the gas phase will become saturated with iodine at this point, *i.e.* $[I_2] = [I_2]^\circ = 0.76 \times 10^{-8}$ mol/cc at $f \leq 0.68$. Since the air density used here is the same as that in the high CH_3I concentration experiments, B and β should have the same values and remain constant. However, λ is not negligible with respect to C as it was in the high concentration experiments.

Equation 16a may then be rewritten as

$$G(-CH_3I) = A\left(\frac{C}{\lambda + C}\right) = -\frac{1}{\mu}\cdot\frac{dC}{dt} \tag{24}$$

where, according to eq 20

$$A = G_{M^*}\left(\frac{B}{B + \beta[I_2]^\circ}\right) = 13.6$$

Integrating eq 24 from $0.68C_0$ to any $C < 0.68C_0$ and rearranging in terms of f, we have for $f \leq 0.68$

$$-\lambda \ln \frac{f}{0.68} + C_0(0.68 - f) = \frac{\rho A}{100N}[(I_M t) - (I_M t)'] \tag{25}$$

where $(I_M t)'$ = total absorbed dose at $f = 0.68$.

A trial and error procedure may now be employed to evaluate the unknown constants λ, G_{M^*}, and B. This is accomplished by first estimating λ using its limits as a guide, calculating G_{M^*} from eq 19 and B from eq 21. Then f is computed as a function of $(I_M t)$ using eq 23 for the composition range down to a point where 32% of the CH_3I is decomposed. Equation 25 is used for calculating f as decomposition proceeds further. The broken curve shown in Figure 4 represents a best fit of the data and was computed using the following values: $\lambda = 2.80 \times 10^{-9}$; $G_{M^*} = 15.2$; $B = 1.98$.

Conclusions

The experimental results presented in this work clearly show that the radiochemical oxidation of methyl iodide in air proceeds at a rate determined by the initial CH_3I concentration. A mechanism is proposed which accounts satisfactorily for the CH_3I decomposition kinetics observed for the concentration range 2.8×10^{-12} to 2.4×10^{-7} mol/cc. The decomposition kinetics is governed primarily by the competition between the M* quenching processes 1a and 2, and by the competition between the subsequent methyl radical reactions 3 and 9. Reactions 5 through 8 account for the major radiolysis products observed in this work. At high CH_3I concentrations, reaction 6 is expected to predominate over reactions 7 and 8 because of the relatively high concentration of methyl peroxide radicals.

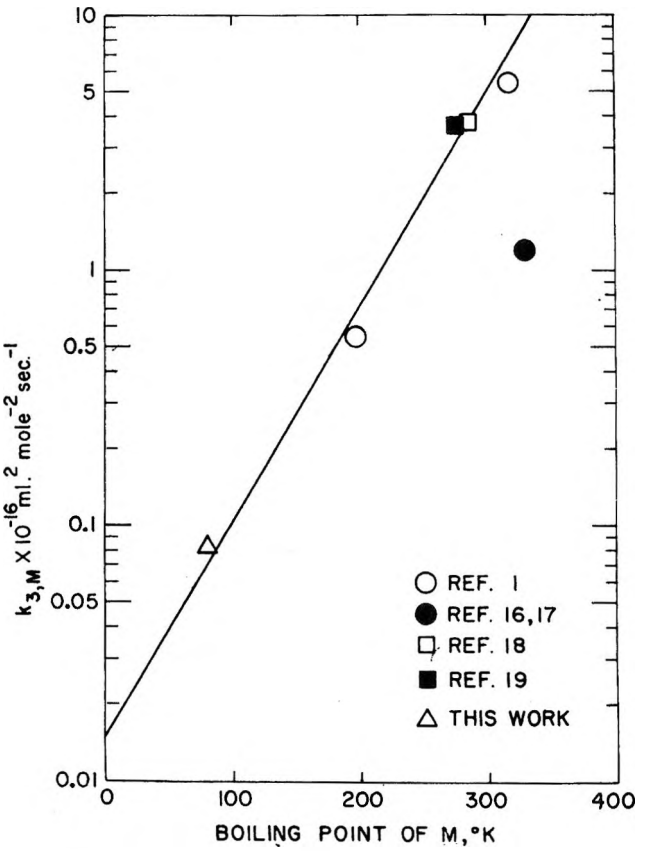

Figure 5. A summary of the experimental values for the rate constant k_3 as a function of the third body involved in the reaction.

In addition, CH_3ONO_2 and CH_3ONO, initially formed *via* reactions 7 and 8, will undergo decomposition by the prolonged irradiation normally employed in experiments with high CH_3I concentrations. At low CH_3I concentrations, reactions 6 and 9 become unimportant compared with reactions 7 and 8, resulting in the formation of methyl nitrate and nitrite in agreement with the observations.

No attempt was made to elucidate the nature of the active energy transfer species. However, it is interesting to note that the value of G_{M^*} obtained in the present study gives an average energy of 6.6 eV per each M*, which is just enough energy to raise either a nitrogen or an oxygen molecule from their ground state to their respective triplet state.

An estimate of the rate constant k_3 may also be obtained from the constant B. Taking the air density employed in this study (4.31×10^{-5} mol/cc) and Christie's value of 278 for k_9/k_4, we calculated from the definition of B that k_3/k_9, = 82. The activation energy for reaction 9 is generally considered to be very small. Golden, Walsh, and Benson[15] have estimated from the results of their thermochemical studies a value of 10^{13} cc/(mol sec) for k_9, which is in good agreement with Christie's value[2a] derived from photochemical reactions. Therefore, we have $k_3 = 8.2 \times 10^{14}$ (cc/mol)^2/sec.

Since reaction 3 is a termolecular reaction, the rate constant, k_3, depends on the type of third body present in the system. Some estimates of k_3 have been made by a number of investigators who used as a third body carbon dioxide,[2a] methyl iodide,[2a] acetone,[16,17] azomethane,[18] and neopentane (+ azomethane).[19] Russell and Simons[20] have shown that the rate constant of termolecular recombination of iodine atoms may be correlated to the boiling point of third body by a straight line plot on semilogarithmic coordinates. Assuming that the same rule applied to reaction 3, a similar plot was made for k_3 including the point found in this work (see Figure 5). In general, the data from the different sources appear to be consistent.

Acknowledgment. The authors acknowledge the invaluable assistance of Mr. George Hardman in performing the experiments. They are grateful to Dr. R. A. Mackay, Dr. Donald J. Metz, Dr. James Sutherland, and Dr. Jerome Weiss for helpful discussions.

(15) D. M. Golden, R. Walsh, and S. W. Benson, *J. Amer. Chem. Soc.*, **87**, 4053 (1965).

(16) F. B. Marcotte and W. A. Noyes, Jr., *Discussions Faraday Soc.*, **10**, 236 (1951).

(17) D. E. Hoare and A. D. Walsh, *Trans. Faraday Soc.*, **53**, 1102 (1957).

(18) G. R. Hoey and K. O. Kutschke, *Can. J. Chem.*, **33**, 496 (1953).

(19) W. C. Sleppy and J. G. Calvert, *J. Amer. Chem. Soc.*, **81**, 769 (1959).

(20) K. E. Russell and J. Simons, *Proc. Roy. Soc., Ser. A*, **217**, 271 (1953).

A Pulsed Mass Spectrometric Study of Penning Ionization in Helium–Argon Mixtures[1a]

by J. J. DeCorpo and F. W. Lampe[1b]

Whitmore Laboratory, Department of Chemistry, The Pennsylvania State University, University Park, Pennsylvania 16802
(Received November 3, 1969)

Pulsed mass spectrometric studies of argon ions formed by ionizing collisions in helium–argon mixtures show the contributions to these processes from direct excitation to the 2^3S and 2^1S metastable states of helium, from excitation to higher levels that populate the metastable levels by cascade processes, and apparently from charge exchange collisions with He^+. Studies of the time dependence of the argon ion intensity at 23 eV permit some conclusions to be drawn concerning the magnitude of the total excitation cross sections.

Introduction

The study of inelastic collision processes is of particular interest in chemistry, since the transfer of internal energy upon collision is often necessary for a chemical reaction to take place. The special case in which the excitation energy transformed from one atom exceeds the ionization potential of the struck atom has been studied in this work; if the struck atom is ionized the

(1) (a) Based on a thesis submitted by J. J. DeCorpo to The Pennsylvania State University in partial fulfillment of the requirements for the Ph.D. degree. (b) To whom correspondence should be addressed.

process is termed the Penning effect.[2] The excitation energies of the 2^3S and 2^1S helium metastable states,[3] namely 19.8 and 20.6 eV, are well above the 15.68-eV ionization potential of argon. Thus, bombardment of a mixture of argon and helium in an electron impact ion source at energies between 15.5 and 24.5 eV will result in argon ion formation *via* the following reactions[4]

$$Ar + e^- \longrightarrow Ar^+ + 2e^- \quad (1)$$

$$He^*(2^3S) + Ar \longrightarrow Ar^+ + He(1^1S) \quad (2)$$

$$He^*(2^1S) + Ar \longrightarrow Ar^+ + He(1^1S) \quad (3)$$

In (2) and (3) the excited helium atoms return to the ground state, since there are no intermediate states. This report describes pulsed mass spectrometric studies of reactions 1–3.

Experimental Section

Apparatus. Kinetic studies of Penning ionization reactions were carried out in a Bendix Model 14-101 time-of-flight mass spectrometer, the design of which has been described previously.[5,6] The instrument was modified by incorporating a closed ion source and an additional 6-in. mercury diffusion pump to provide an adequate pressure differential between the ion source and the source envelope. A 2-in. mercury diffusion pump and a flight tube baffle were also added at the electron multiplier to lend a degree of differential pumping in the detection region.

A variable time-delay circuit was installed as previously described.[7,8] This circuit allows a time delay, varying from 0 to 10 μsec, between the end of the electron beam and the onset of the draw-out pulse. During this time, the reaction zone is field free, thus emulating the conditions first used by Tal'roze and Frankevich[9] to study the purely thermal rates of ion–molecule reactions.

The back plate of the Bendix ion source was replaced with a 0.75-in. diameter etched Mo screen of 85% transmission. Other pertinent dimensions of the ion source have been cited in a previous publication.[7] The ion-source pressure was monitored directly with a McLeod gauge connected *via* 0.5-in. diameter tubing to the flange of the source housing. Measurements of the actual ion-source concentrations by total ionization measurements in argon, and by examination of the extent of D_3^+ formation from D_2, and CH_5^+ formation from CH_4 indicate that the McLeod gauge readings are higher than the actual source pressure by a factor of 6 ± 1.

A Nuclide 12-90G magnetic deflection mass spectrometer was employed to study ionization-efficiency curves utilizing the retarding-potential-difference technique (rpd).[10] The ion source of the instrument was closed as much as possible to obtain the high pressures required for studying the Penning effect or any other secondary process involving bimolecular collisions. The ion-source pressure was determined by studying the methane ion–molecule reactions at various reservoir pressures and leak openings.

Procedures. During the kinetic studies the electron-beam pulse of the time-of-flight instrument had a duration of 0.25 μsec and was pulsed at 10 kHz. The ion-drawout pulse, with an amplitude of −280 V and width of 3.5 μsec, was applied 0–2 μsec after the cutoff of the electron beam.

The length of the drawout pulse ensures the collection of all ions surviving in the volume sampled by the analyzing system. Owing to the thermal drift of the particles, however, the total ion current will diminish as the residence time of the ions is increased. This phenomenon is mass dependent, and a correction for it must be made, since the kinetic studies involve ratios of the ion intensities of Ar^+ and Ne^+. Essentially, the correction involves the calculation of the fraction of ions remaining in a fixed sampling volume at some time after the ionizing pulse of electrons.

Assuming that there is perfect Wiley focusing,[5] then any horizontal drift of the ions in the direction of the axis of the drift tube is negligible. Since the electron beam extends the entire width of the source, any horizontal motion in the axis of the beam may be considered irrelevant. Drift in the vertical direction, along the z axis, however, results in a loss, because the electron beam does not extend over the entire height of the source. The probability of an ion being collected at time t is expressed by

$$F(t) = 2\int_0^{z_0/t} P(V_z)\mathrm{d}V_z \quad (4)$$

where z_0 is the distance from the center to the edge of the ion-exit slit, and $P(V_z)$ is the one-dimensional Maxwell probability density in velocity space. Some of the ions which would be collected for an infinitely high draw-out pulse may have a sufficient velocity component in the z direction to result in a loss during the actual finite withdrawal time. Thus, the t in (4) is the sum of the delay time and the ion-withdrawal time.

Experimental correction curves for various masses [$I(t)/I(0)$ *vs.* t] were found to be of the same form as

(2) F. M. Penning, *Naturwissenschaften*, 15, 818 (1927).

(3) C. E. Moore, *Natl. Bur. Stand. Circ.*, No. 467 (1949).

(4) K. L. Bell, A. Dalgarno, and A. E. Kingston, *Proc. Phys. Soc., Ser. 2*, 1, 18 (1968).

(5) (a) F. W. Lampe and G. G. Hess, *J. Amer. Chem. Soc.*, 86, 2952 (1964); (b) W. C. Wiley and I. H. McLaren, *Rev. Sci. Instrum.*, 26, 1150 (1955).

(6) G. B. Kistiakowsky and P. H. Kydd, *J. Amer. Chem. Soc.*, 79, 4825 (1957).

(7) P. M. Becker and F. W. Lampe, *J. Chem. Phys.*, 42, 3857 (1965).

(8) C. W. Hand and H. Von Weyssenhoff, *Can. J. Chem.*, 42, 195 (1964).

(9) V. L. Tal'roze and E. L. Frankevich, *Zh. Fiz. Khim.*, 34, 2709 (1960).

(10) R. E. Fox, W. M. Hickman, D. J. Grove, and T. Kjeldaas, Jr., *Rev. Sci. Instrum.*, 26, 1101 (1955).

(4), differing only by a constant which was incorporated into the actual corrections. In the ionization-efficiency study this correction was not required, as only relative intensities at a constant delay time were measured.

In utilizing the retarding-potential-difference technique for the study of the ionization-efficiency curves, the electron beam in the Nuclide instrument was pulsed at 100 kHz. An electronic switch alternated the high and low levels of the retarding potential applied to the retarding grid as a square wave of 22 Hz. Because of the low intensities of the secondary peaks, the difference, ΔE_R, between these high and low rpd levels was required to be at least 0.1 eV. Under these conditions, the output of the electron multiplier appeared as a quasi-sine wave with the peak-to-peak amplitude of this wave form representing the change in intensity, ΔI, due to the ΔE_R on the retarding grid. This signal was fed into a Princeton Applied Research Model HR-8 lock-in amplifier which abstracts the peak-to-peak value, ΔI, from the signal, amplifies it, and transmits it as a dc signal to the ordinate of a Moseley Model 135AM X–Y recorder, so that continuous rpd curves were obtained.

The source temperature, 70°, was determined by using an alumel–chromel thermocouple. Samples of two or more gases were prepared by using a Saunders–Taylor apparatus, in which partial pressures could be accurately measured.

Results and Discussion

General Observations. The ionization-efficiency curve of Ar^+ in a 100:1 He–Ar mixture (3 μ total pressure) and for pseudomonergetic electrons with an energy spread of 0.1 eV is shown in Figure 1. The curve for

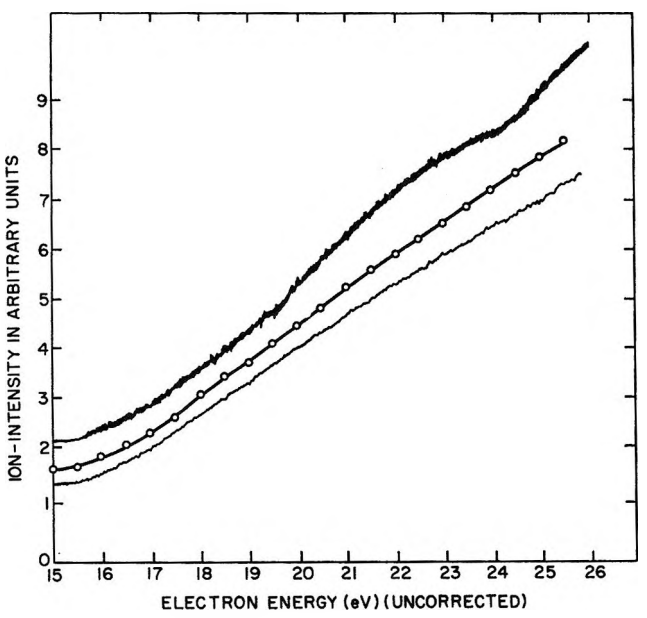

Figure 1. Ionization-efficiency curves of Ar^+. The uppermost curve is for a 100:1 He–Ar mixture; the lowest curve is for a 100:1 Kr–Ar mixture: O-O-O-, data of ref 11.

Ar^+ in He shows a definite upward break from a linear region near 19.5 eV (uncorrected) and a subsequent fall back to a linear region at about 24 eV. By contrast the ionization-efficiency curve of Ar^+ in a 100:1 Kr–Ar mixture at the same total pressure (also shown in Figure 1) shows no such features between 19.5 and 24 eV. Since in the Kr–Ar mixture Ar^+ cannot be formed by Penning ionization, we conclude the additional structure exhibited by Ar^+ in the He–Ar mixture to be due to Penning processes.

Also included in Figure 1 for comparison is a plot of the total electron-impact ionization cross section of argon as reported by Englander-Golden and Rapp.[11] Our ionization-efficiency curve for Ar^+ in the Kr–Ar mixture can be superimposed on the cross section data[12] quite nicely from onset to about 20 eV. Above this energy, deviations occur, but these deviations are monatonic with increasing energy and are probably due to a slowly varying effective electron current and/or transmission efficiency in our ionization chamber. These monatonic deviations from total cross-section data over a wide energy range are not unexpected and certainly do not in any way resemble the differences between our Ar^+ ionization efficiency curves in the He–Ar and Kr–Ar mixtures.

The initial portions of the two ionization-efficiency curves in Figure 1 (that is, the portions from onset to about 19 eV) are quite superimposable. If we make such a superposition, then, in principle, the difference between the two curves represents the ionization-efficiency curve for Penning ionization of argon by helium. Although the result is admittedly not very accurate, it is of interest to carry out such a procedure and compare this difference curve with the sum of the excitation functions to states of helium that can produce Penning ionization some 10^{-4} sec after electron impact.[13] This difference curve and its comparison with the sum of the excitation functions as given by Cermak[13] are shown in Figure 2.

The general agreement of the shapes of the two curves in Figure 2 lends credence to our conclusion that the structure in the Ar^+ ionization-efficiency curve in the He–Ar mixture is indeed due to Penning ionization. Both curves show the onsets at 19.8 and 20.6 eV of processes that produce Ar^+ by direct electron impact excitation of helium to the 2^3S and 2^1S states, respectively. As shown by Cermak,[13] the continuing rise of the curves in Figure 2 after about 21.5 eV (at which energy the maximum of the excitation curve of the 2^1S state occurs) is to be attributed to the formation of higher triplet states of helium which cascade rapidly to the 2^3S metastable. The onset energies of some of these states are also shown in Figure 2. Some population of

(11) P. Englander-Golden and D. Rapp, *J. Chem. Phys.*, 43, 1464 (1965).

(12) H. S. W. Massey, *Rept. Progr. Phys.*, 12, 248 (1949).

(13) V. Cermak, *J. Chem. Phys.*, 44, 3774 (1966).

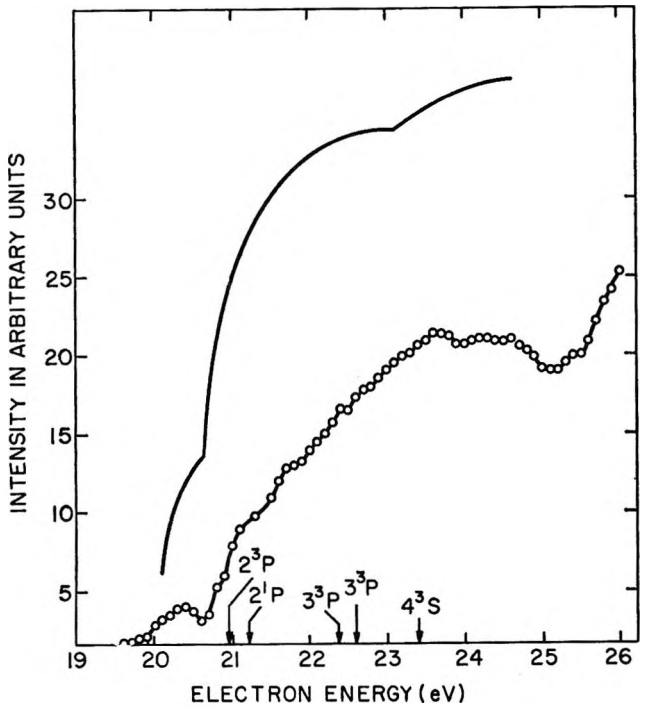

Figure 2. Excitation function for Penning ionization of Ar by He: —, ref 13: O-O-O-, this work.

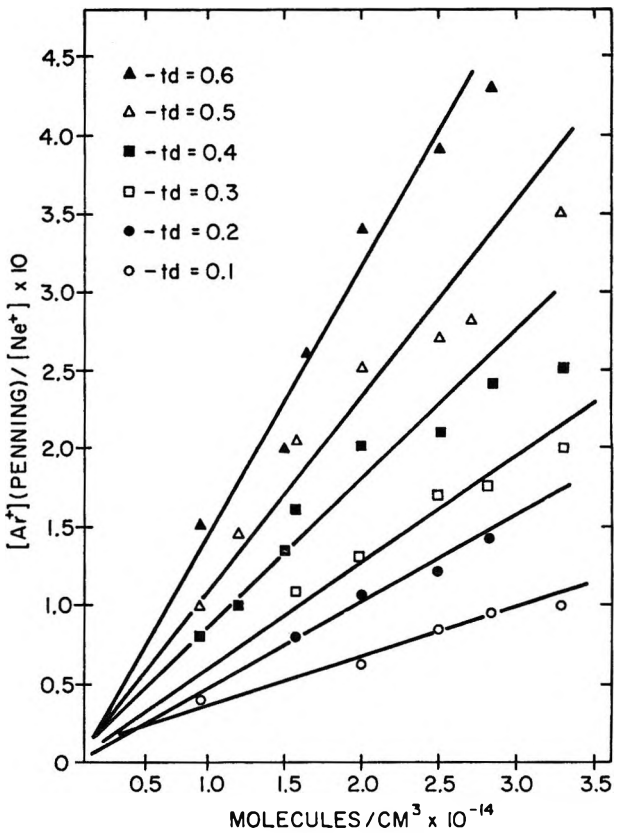

Figure 3. Plots of ion ratio (eq 8) as a function of He concentration for various delay times.

the 2^1S metastable state by transitions from the 2^1P may take place, but, since the 2^1P is optically connected directly to the ground state, the extent of this populating effect is very small; it has been reported by Gabriel and Heddle[14] that only 0.11% of the transitions of the 2^1P state are to the 2^1S state.

Our curve in Figure 2 suggests that there is an additional helium-collision process forming Ar^+ which has an onset at about 24.8 eV—that is, near the ionization potential of helium. Such a process could only be charge exchange from He^+, *viz.*

$$He^+ + Ar \longrightarrow Ar^+ + He \qquad (5)$$

but this reaction, as written, has a large energy defect of 8.8 eV and on the basis of the adiabatic criterion[12] would be expected to have a very small cross section for thermal energy ions. It is possible that (5) may be occurring in our system with a measureable cross section *via* a radiative charge transfer mechanism,[15] *viz.*

$$He^+ + Ar \longrightarrow (HeAr^+)^* \longrightarrow \begin{matrix} HeAr^+ + h\nu \\ \downarrow \\ He + Ar^+ \end{matrix} \qquad (5a)$$

An analogous mechanism has been invoked for the charge-transfer reaction

$$He^{2+} + H \longrightarrow He^+ + H^+ + h\nu \qquad (6)$$

and a rate coefficient of 1.6×10^{-13} cm³/sec has been calculated.[16] However, we should point out that the errors inherent in the curve subtraction process became greater as we consider energy regions more distant from the region of superposition. Thus we cannot rule out the possibility that the increase in Ar^+ intensity after 24.8 eV is an experimental artifact.

Kinetic Studies. The electron-impact excitation functions of the helium metastable states overlap each other[13,17,18] (Figure 3) making it virtually impossible to investigate mass spectrometrically the kinetics of reactions 2 and 3 separately. Thus, the results of any kinetic study by electron impact, which detects the product Ar^+, must be considered to be some average over the properties of both metastable states. As shown in Figure 2, the maximum in the sum of the excitation functions of states of helium that produce Penning ionization occurs near 24 eV. As a compromise between the objectives of maximum sensitivity and minimum probability of occurrence of (5), kinetic experiments were conducted at an electron energy of 23 eV.

(14) A. H. Gabriel and D. W. O. Heddle, *Proc. Roy. Soc., Ser. A*, **258**, 124 (1960).

(15) D. R. Bates and R. McCarroll, *Proc. Roy. Soc., Ser. A*, **245**, 175 (1958).

(16) A. M. Arthurs and J. Hyslop, *Proc. Phys. Soc.*, **A70**, 849 (1957).

(17) R. Marriott in "Atomic Collision Processes," M. R. C. McDowell, Ed., North-Holland Publishing Co., Amsterdam, 1964, p 122.

(18) L. S. Frost and A. V. Phelps, Westinghouse Research Report 6-94439-6-R3 (1957).

Since Ar^+ ions are produced by both Penning ionization, namely (2) and (3), and by direct electron-impact ionization (1), the extent of the latter must be determined and subtracted from the overall Ar^+ ion intensity. This was done by investigation of the extent of ionization of argon in mixtures in which helium was replaced by equal amounts of krypton, with all other conditions maintained constant.

At the pressure employed in this study, the time between collisions is of the order of 10^{-5} sec. According to the reported transition probabilities in helium,[14] in 10^{-5} sec nearly all excited states will have undergone transitions to either the ground state or to the two metastable levels. Therefore, we shall assume in our kinetic treatment that the states of helium actually undergoing the Penning ionization reaction are the 2^3S and 2^1S as written in (2) and (3). With this assumption we may write the overall intensity of argon ions as shown in (7a) and (7b), *viz.*

$$I_{Ar^+} = I_{\text{Penning}} + I_{\text{electron impact}} \tag{7a}$$

$$I_{Ar^+} = \alpha\{k_S[He][Ar]t_e t_d \sum_s \sigma_{e,s} + k_T[He][Ar]t_e t_d \sum_t \sigma_{e,t} + \sigma_i[Ar]t_e\} \tag{7b}$$

where k_S and k_T are the specific reaction rates of (3) and (2), respectively, $\Sigma\sigma_{e,s}$ is the sum of the cross sections of formation of singlet excited states of helium that ultimately are transformed by emission of radiation to the 2^1S state, $\Sigma\sigma_{e,t}$ is the analogous sum over the triplet states of helium, σ_i is the ionization cross section of argon by electron impact, t_e and t_d are the durations of the electron beam pulse and delay time, respectively, and σ is a proportionality constant. Subtracting from (7b) the last term, which is determined experimentally using Kr as described above, leads immediately to an equation describing the intensity of Ar^+ formed solely in the Penning ionization processes 2 and 3.

It is more convenient to study the ratio of the intensity of argon ions (from Penning ionization) to the intensity of ions of some "marker" gas, rather than absolute intensities. Neon was chosen for this purpose because the metastable states of helium cannot ionize it. It was added to the helium–argon system at a partial pressure equal to that of argon. It was observed that with increasing delay time, t_d, the Ne^+ ion intensity decreased while at the same time the Ar^+ ion intensity increased. Since states of helium above 21.6 eV can ionize neon, this observation confirms our conclusion that, at the pressure employed, the decay of higher states to the metastable levels will be complete within the average time between collisions.

Taking the ratio of the Ar^+ intensity due to the Penning processes to the Ne^+ intensity (neglecting charge transfer from Ne^+ to Ar and Penning ionization of argon by neon because the partial pressure of neon and argon are so small relative to helium) and recognizing that [Ne] = [Ar], we obtain

$$\frac{I(Ar^+)_{\text{Penning}}}{I(Ne^+)} = \left\{k_S \sum_s \sigma_{e,s} + k_T \sum_t \sigma_{e,t}\right\} \frac{[He]t_d}{\sigma_i^1} \tag{8}$$

where σ_i^1 is the electron impact ionization cross section of neon.

A plot of the intensity ratio in (8), corrected for thermal drift, *vs.* the helium concentration should yield a straight line with a slope λ of

$$\lambda = \left\{k_S \sum_s \sigma_{e,s} + k_T \sum_t \sigma_{e,t}\right\} \frac{t_d}{\sigma_i} \tag{9}$$

In agreement with (8), Figure 3 depicts a series of lines for various fixed delay times, t_d. In Figure 4, the slopes of the lines in Figure 3 are plotted *vs.* delay time and, as indicated by (9), yield a straight line; the slope of the line in Figure 4 leads to the result shown in (10), after incorporating the value of 2.5×10^{-18} cm^2 for the ionization cross section of neon[1] at 23 eV.

$$\left\{k_S \sum_s \sigma_{e,s} + k_T \sum_t \sigma_{e,t}\right\} = 5.85 \times 10^{-27} \text{ (cm}^3\text{/sec)(cm}^2\text{)} \tag{10}$$

Consideration of the energy levels in helium[19] lead at once to the conclusion that, with the thermal-energy

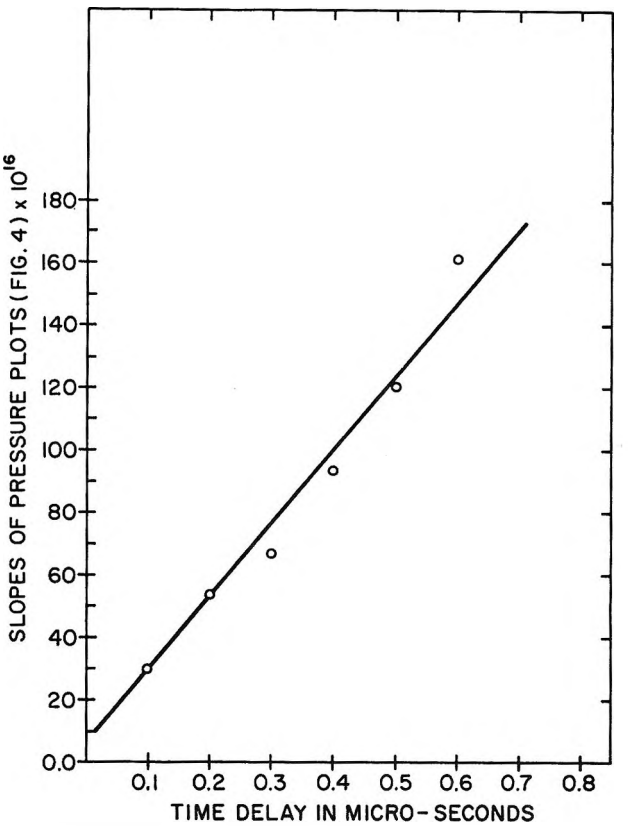

Figure 4. Slopes of ion ratio *vs.* concentration plots (eq 9) as a function of delay time.

(19) G. Herzberg, "Atomic Spectra and Atomic Structure," Dover Publications, New York, N. Y., 1944.

spread of our nominally 23-eV electron beam, direct excitation to all $n = 2$ and $n = 3$ levels, and perhaps even higher, is occurring. However, in view of the transition probabilities in helium,[14] it is probable that cascading into the 2^1S metastable state, at least from the n^1P family, is negligible. On the other hand, it is evident from our results in Figure 2, from the work of others,[13,20,21] and from the transition probabilities in helium,[14] that both excitation into the higher triplet levels and cascading from these levels to the 2^3S level are taking place. Therefore, the term $\sum_t \sigma_{e,t}$ is a sum, at the very least, of the excitation cross sections to the 2^3S, 2^3P, 3^3S, 3^3P, and 3^3D states of helium.

Experimental values of the cross sections for electron-impact excitation to the 2^1S, 2^3S, and 2^3P levels of helium at energies near 23 eV are available.[20,22,23] The values are in only fair agreement with theoretical calculations[17,24,25] and, moreover, are limited to the three states mentioned; therefore, it is not feasible to use (10) to obtain rate constant data or reaction cross sections for (2) and (3).

Some work has been reported concerning the reaction cross sections for (2) and (3). Benton, *et al.*,[26] have reported the cross sections for the destruction of helium metastable states in collisions with argon atoms to be 6.6 and 55 Å^2 for He(2^3S) and He(2^1S), respectively. However, they have mentioned that the latter value may be too high by a factor of 2 or 3. This has been substantiated by Schmeltekopf,[27] who finds the destruction cross sections in argon collisions to be 5.34 Å^2 for He(2^3S) and 16.4 Å^2 for He(2^1S). Cermak[13] has found that his measurements of the excitation functions of He(2^3S) and He(2^1S), using energy and intensity analysis of the electrons released in Penning ionization of argon, are consistent with the data of Holt and Krotkov[20] only if $\sigma_s > \sigma_t$. On the other hand, Sholette and Muschlitz[28] have studied the *total* ionization induced in argon by the helium metastables as a function of the energy of the impacting electrons that produce the metastables, and they conclude that $\sigma_s = \sigma_t = 7.6$ Å^2. MacLennan[29] has reported that $\sigma_s = \sigma_t = 9 \pm 3$ Å^2, in essential agreement with Sholette and Muschlitz.[26] In the most recent study Hotop, Niehaus, and Schmeltekopf[30] have separated the contributions made by the individual metastable levels and have, in addition, measured the contribution made by formation of $HeAr^+$ to the metastable loss processes and total ionization. They report[30]

$$\frac{\sigma_s(P)}{\sigma_t(P)} = 1.10; \qquad \frac{\sigma_s(\text{total})}{\sigma_t(\text{total})} = 1.15 \tag{11}$$

$$\frac{\sigma_s(a)}{\sigma_s(P)} = 0.212; \qquad \frac{\sigma_t(a)}{\sigma_t(P)} = 0.155 \text{ at } 320°K \tag{12}$$

where $\sigma_s(a)$ denotes the cross section for associative ionization of He(2^1S) with Ar, *e.g.*, the cross section for formation of $HeAr^+$ by He(2^1S).

There seems to be general agreement as to the value of σ_t for total ionization (or destruction); the four values,[26-29] quoted above, yield an average of σ_t(total) = 7.1 Å^2 with an average deviation of ±1.2 Å^2. The same cannot be said for σ_s, but we may use the above ratio determined by Hotop, Niehaus, and Schmeltekopf[30] to obtain σ_s(total) = 8.2 Å^2. Use of the ratios for associative to Penning ionization then lead to the following values for Penning ionization of argon by metastable helium at 320°K: $\sigma_2 = 6.0$ Å^2; $\sigma_3 = 6.5$ Å^2. Combination of the ratio[30] of 1.15 for σ_s(total)/σ_t(total) with Cermak's data[13] leads to the value (*cf.* eq 10)

$$\frac{\sum_s \sigma_{e,s}}{\sum_t \sigma_{e,t}} = 0.61 \tag{13}$$

Finally, using the simple hard-sphere relationship between reaction cross section and rate constant and making the assumption that the ratios, (12), of Hotop, Niehaus, and Schmeltekopf[30] are the same at 343° as at 320°K, we obtain from (10) the following results for the sum of the excitation cross sections at 23 eV to states of helium that lead to Penning ionization.

$$\sum_t \sigma_{e,t} = 4.2 \times 10^{-17} \text{ cm}^2 \tag{14}$$

$$\sum_s \sigma_{e,s} = 2.6 \times 10^{-17} \text{ cm}^2 \tag{15}$$

In general, the excitation cross sections in (14) and (15) at 23 eV are higher than expected from experimental reports.[20,22,23] Thus combination of the results of Fleming and Higginson[23] with those of Schulz[22] lead to a value of $\sim 4 \times 10^{-18}$ cm^2 for the cross section of total metastable production at 23 eV. A similar value was reported by Holt and Krotkov.[20] A possible reason for this discrepancy is the energy spread of our nominally 23-eV electron beam, which permits Penning ionization of argon by states of helium with $n > 3$, and our cross sections in (14) and (15) are sums over all states that contribute. It is of interest that our sums

(20) H. K. Holt and R. Krotkov, *Phys. Rev.*, **144**, 82 (1966).
(21) J. L. G. Dugan, H. L. Richards, and E. E. Muschlitz, Jr., *J. Chem. Phys.*, **46**, 346 (1967).
(22) G. J. Schulz and R. E. Fox, *Phys. Rev.*, **106**, 1179 (1957).
(23) R. J. Fleming and G. S. Higginson, *Proc. Phys. Soc.*, **84**, 531 (1964).
(24) H. S. W. Massey and B. L. Moiseiwitsch, *Proc. Roy. Soc., Ser. A*, **227**, 38 (1954).
(25) H. S. W. Massey and B. L. Moiseiwitsch, *ibid.*, **258**, 147 (1960).
(26) E. E. Benton, E. E. Ferguson, F. A. Matsen, and W. W. Robertson, *Phys. Rev.*, **128**, 206 (1962).
(27) A. L. Schmeltekopf, private communication, Oct 1969.
(28) W. P. Sholette and E. E. Muschlitz, Jr., *J. Chem. Phys.*, **36**, 3368 (1962).
(29) D. A. MacLennan, *Phys. Rev.*, **148**, 218 (1966).
(30) H. Hotop, A. Niehaus, and A. L. Schmeltekopf, *Z. Phys.*, **229**, 1 (1969).

of excitation cross sections are not inconsistent with theoretical calculations.[24,25] Thus Massey and Moiseiwitsch[24,25] have calculated values of $\sim 2 \times 10^{-18}$ cm^2 for $\sigma(2^3S)$ and $\sigma(2^1S)$ and 1.3×10^{-17} cm^2 for $\sigma(2^3P)$ at 23 eV. Their[24,25] value of 1.5×10^{-17} cm^2 for $\sigma(2^3S) + \sigma(2^3P)$ is to be compared with our value of 4.2×10^{-17} cm^2 for the sum, which may have to be taken over *all* triplet states in view of the width of our electron beam.

Acknowledgment. This work was supported by Grant GP-8065 from The National Science Foundation. We also wish to thank The National Science Foundation for supplying funds to assist in the original purchase of the mass spectrometers.

Preferential Solvation and the Thermal and Photochemical Racemization of Tris(oxalato)chromate(III) Ion[1]

by V. S. Sastri and C. H. Langford[2]

Department of Chemistry, Carleton University, Ottawa 1, Canada *(Received May 19, 1970)*

The nmr method for determining the composition of the solvation shell of a paramagnetic solute introduced by Frankel, Stengle, and Langford has been applied to the $[Cr(C_2O_4)_3]^{3-}$ complex in H_2O–DMSO mixtures. Thermal and photochemical racemization rates of *d*-$[Cr(C_2O_4)_3]^{3-}$ have been determined as a function of the solvation shell composition. Both thermal and photochemical rates were found to be acid-catalyzed with the former showing a first-order dependence on H^+ ion concentration in the pH range 1 to 3. The results could be explained in terms of a cooperative effect of the solvent molecules in the aquodechelation of the complex through hydrogen bonding. Quantum yields obtained at 4200 Å ($^4T_{1g}$) and their solvent dependence may be explained in terms of relaxation of the initial excited state to an intermediate which is substitution labile. The solvent dependence of quantum yields is regarded as arising in the relaxation process.

Introduction

Spees and Adamson[3] have proposed a substitutional mechanism for the thermal and photochemical racemization of $Cr(C_2O_4)_3^{3-}$ ion based on the mechanism for aquation and oxalate exchange proposed by Harris and coworkers.[4] The crucial step is an aquo-dechelation step

$$[Cr(C_2O_4)_3]^{3-} + H_2O \rightleftharpoons [Cr(C_2O_4)_2(OCOCO_2)(OH_2)]^{3-}$$

Although wavelength dependence, temperature dependence, and solvent dependence in alcohol–water mixtures can be consistently interpreted with this proposal, Spees and Adamson noted[3] that: "...In the absence of some independent means of determining the solvent cage composition, it is difficult to make any detailed treatment of our data...."

An independent nmr method for the determination of relative solvent shell composition in mixed solvents has been proposed by Frankel, Stengle, and Langford.[5] It has been possible to establish the correlation suggested by Adamson with respect to thermal substitution reactions of $[Cr(NH_3)_2(SCN)_4]^-$ in acetone–water mixtures,[6] acetonitrile–water mixtures,[7] and for $[Cr(NCS)_6]^{3-}$ in acetonitrile–water mixtures.[8]

However, the photochemical substitution reactions in acetonitrile–water mixtures[7,8] display a different solvent dependence. The results indicate that the entering water ligand need not be in encounter with the Cr complex in advance of excitation.

In this paper, a somewhat different kind of mixed solvent system is examined. The dechelation step which is assumed to be crucial for racemization of $[Cr(C_2O_4)_3]^{3-}$ is a substitution reaction, but unlike acet-

(1) Presented at the 157th National Meeting of the American Chemical Society, Minneapolis, Minn., April 13–18, 1969.

(2) All correspondence should be addressed to this author; Alfred P. Sloan Fellow, 1968–1970.

(3) S. T. Spees and A. W. Adamson, *Inorg. Chem.*, 1, 531 (1962).

(4) K. V. Krishnamurty and G. M. Harris, *J. Phys. Chem.*, 64, 346 (1960).

(5) L. S. Frankel, T. R. Stengle, and C. H. Langford, *Chem. Commun.*, 373 (1965).

(6) C. H. Langford and J. F. White, *Can. J. Chem.*, 45, 3049 (1967).

(7) V. S. Sastri, S. Behrendt, R. Henwood, and C. H. Langford, to be published.

(8) S. Behrendt, C. H. Langford, and L. S. Frankel, *J. Amer. Chem. Soc.*, 91, 2236 (1969).

onitrile, dimethyl sulfoxide (DMSO) which is here mixed with water is a good ligand for attack on Cr^{III}.[9] Despite this property the reaction in DMSO is much slower than the reaction in water. The reason for such a solvent effect on rates *must be sought in a factor other than the ability of one solvent to function as an entering ligand* in a substitution reaction. This point is clearly made in what follows by the fact that the rates are much more sensitive to bulk solvent composition than is the probability of occupancy of a particular site in the solvation shell (or "solvent cage" or "encounter complex"). In contrast to earlier examples,[6,7] the quantum yield for photochemical racemization is shown to be quite solvent sensitive.

The discussion in this paper will attempt to rationalize the solvent dependence of the thermal racemization of $[Cr(C_2O_4)_3]^{3-}$ and then proceed to a discussion of solvent effects in photochemical reactions by development of a "plausible" model (for photochemical substitution of Cr^{III} that lends itself to analysis in the framework for discussion of mechanistic photochemistry recently proposed by Hammond.[10]

Experimental Section

Materials. Crystalline $K_3Cr(C_2O_4)_3 \cdot 3H_2O$ was prepared according to the published procedure[11] and resolved according to the procedure given in the literature,[12] and the resulting complex d-$K_3Cr(C_2O_4)_3$ had a molar rotation of 7600°. Crystalline $K_3Fe(C_2O_4)_3 \cdot 3H_2O$ was prepared according to the standard procedure.[13] Reinecke's salt obtained from Alfa Inorganics was purified by recrystallization. Reagent grade strychnine sulfate (Mann Research Laboratory, New York, N. Y.) and Fisher certified buffer solutions were used as such. Spectranalyzed DMSO (Fisher Scientific Co.) and distilled water were used to make solvent mixtures.

Apparatus. (i) A 1000-W xenon–mercury source (Oriel Optics) was used as the light source and the beam collimated with the help of lenses of 7.5- and 5-cm focal length, and passed through a Jarrell-Ash monochromator (Model 82-410) for selecting the appropriate wavelength. A circular spectrophotometric cell of 5-cm path length thermostated at 25.0 ± 0.1° was used for irradiation. The light source was calibrated using Reinecke's salt[14] as well as potassium ferrioxalate[15] as standards for chemical actinometry. (ii) Optical activity was measured with a Perkin-Elmer spectropolarimeter (Model 141) to an accuracy of ±0.001°. (iii) Absorbance measurements in the course of chemical actinometric procedures were made with a Gilford spectrophotometer Model 240.

Reaction Studies. A weighed amount of the optically active complex was dissolved in the solvent mixture and thermostated at 25°. An aliquot of the solution was transferred into a cell and the optical rotation was recorded as a function of time. Thermal runs were carried out for 2 to 3 half-lives and good linear plots were obtained.

An aliquot (15 ml) was transferred into a 5-cm cell and irradiated for a definite period of time and the optical activity was determined after irradiation. Chemical actinometry before and after irradiation of the complex confirmed the constancy of the light intensity. A parallel dark run was conducted for correcting the photochemical rate of racemization.

Solvation Studies. Preferential solvation studies by nmr were carried out by recording solvent proton signals at 25.0° on a JEOL C-60 nmr spectrometer. Confirmation was obtained by observation of the solvent dependence of the ligand field bands of the complex recorded on a Cary 14 spectrophotometer.

Results

Preferential Solvation. The nmr studies were analyzed according to the previously described methods.[5-8] These are summarized in an Appendix to the present paper. Typical line broadenings are collected in Table I. These reflect two factors: (a) the probability that a solvent molecule is in the paramagnetic environment (solvation shell of Cr^{III} complexes) and (b) the relaxation time characteristic of that environment. Since the latter cannot be obtained absolutely, we evaluate *relative* solvation in the mixed solvent compared to pure solvent. The parameter reported is

Table I: Nmr Data on Excess Line Width of ^1H Signal of Water ($K_3Cr(C_2O_4)_3$ 0.025 M; Temp 25°)

Mole fraction of DMSO	Excess line width, $\Delta\nu_{1/2}$, Hz	Relative viscosity[16]	n/n_0
0.0	3.48	1.00	1.00
0.02	5.06	1.03	1.10
0.04	4.73	1.10	0.83
0.07	5.38	1.20	0.70
0.10	5.85	2.00	0.59
0.20	8.63	3.25	0.38
0.30	10.23	3.95	0.27
0.40	9.94	3.80	0.20
0.50	9.69	3.40	0.16
0.60	8.86	3.04	0.12
0.70	9.12	2.67	0.09
0.80	8.97	2.40	0.06
0.90	8.96	2.20	0.04

(9) L. S. Frankel, T. R. Stengle, and C. H. Langford, *Can. J. Chem.*, 46, 3183 (1968).

(10) G. S. Hammond, *Advan. Photochem.*, 7, 373 (1969).

(11) G. Croft, *Phil. Mag.*, 21, 197 (1842).

(12) G. K. Schweitzer and J. L. Rose, *J. Phys. Chem.*, 56, 428 (1952).

(13) J. C. Bailar, Jr., and E. M. Jones, *Inorg. Syn.*, 1, 36 (1939).

(14) E. E. Wegner and A. W. Adamson, *J. Amer. Chem. Soc.*, 88, 394 (1966).

(15) C. G. Hatchard and C. A. Parker, *Proc. Roy. Soc., Ser. A*, 235, 518 (1956).

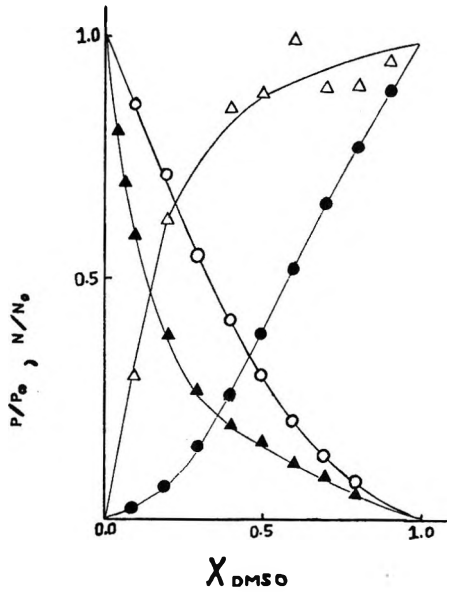

Figure 1. Activity of water (p/p_0) and nmr solvation data (n/n_0) *vs.* mole fraction of DMSO: △, n/n_0 for DMSO; ▲, n/n_0 for H_2O; ○, p/p_0 for H_2O; ●, p/p_0 for DMSO; $T = 25°$.

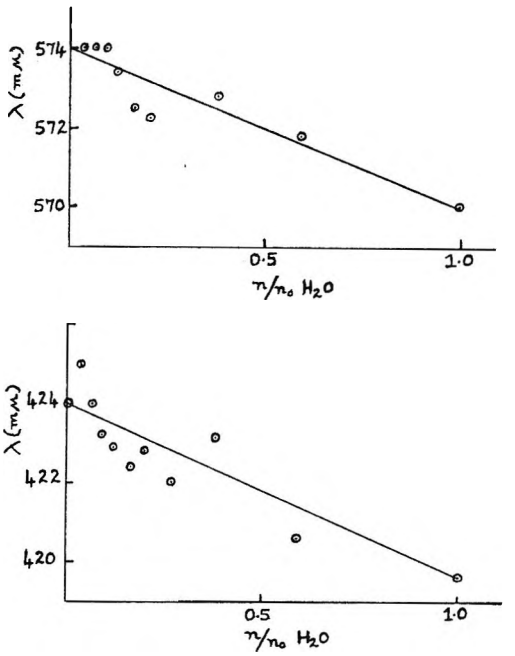

Figure 2. Position of $Cr(C_2O_4)_3^{3-}$ visible ligand field absorption band maxima (nm) *vs.* n/n_0 for water; $T = 25°$.

n/n_0 which represents the number of a particular type of solvent molecules solvating the complex in a mixed solvent compared to the number of the same solvent solvating in the pure solvent. The important assumption is that the relaxation time in the paramagnetic environment is either constant or varies only as a linear function of bulk viscosity as the composition of the solvent is changed.[9] The validity of the assumptions is checked by agreement between values obtained from analysis of protons of water and DMSO. The results are shown in Figure 1. The relaxation time in the paramagnetic environment has been assumed to be proportional to bulk solvent viscosity and the viscosity correction has been applied using Kruus' data[16] on DMSO–H_2O viscosities. A further check on the validity is supplied by the parallelism shown in Figure 2 between the nmr derived n/n_0 values and the (small) solvent dependence of ligand field bands of the Cr^{III} chromophore.

Table II gives the thermal rates and the photochemical quantum yields for racemization of d-$K_3Cr(C_2O_4)_3$ in DMSO–H_2O mixtures. Table III records the data on the hydrogen ion dependence of the thermal rates and quantum yields for the racemization reaction, and the n/n_0 values derived from the nmr data as a function of the mole fraction of DMSO are presented in Figure 3.

Table II: Thermal Rate Constants and Quantum Yields of Racemization of d-$K_3[Cr(C_2O_4)_3]$ at 25 ± 0.1°

Mole fraction of DMSO	k, sec^{-1}	ϕ, 4200 Å
0.00	5.55×10^{-4}	0.110
0.02	3.79×10^{-4}	0.103
0.04	2.72×10^{-4}	0.076
0.07	1.36×10^{-4}	0.069
0.10	8.62×10^{-5}	0.036
0.20	8.37×10^{-6}	0.0087
0.30	7.73×10^{-7}	0.0018
0.40	2.91×10^{-7}	0.0004 (?)
0.50	2.17×10^{-7}	0.0009 (?)
1.00	1.44×10^{-7}	0.0005 (?)

Discussion

Thermal Reaction. Although DMSO is probably a better ligand for coordination at a vacated position of Cr^{III} in a dechelation step than any of the several solvents in which racemization of $Cr(C_2O_4)_3^{3-}$ was examined by Schweitzer and Rose,[12] it retards racemization more effectively than any other solvent considered. The first interesting point is that this effect does not arise from changes in thermodynamic activity of water in the solvent mixtures. As the vapor pressure curve for water[17] in Figure 1 indicates, mixing of water with DMSO does not lead to lowering of water activity that differs significantly from the other solvents methanol, ethanol, propanol, dioxane, or acetone, which affect reactivity of this complex less strikingly.[3,12] We must look to something involving the metal complex itself and its immediate environment. Comparison of the vapor pressure curve (p/p_0)[17] in Figure 1 with the n/n_0 (H_2O) and measures of reactivity shown in Figure 3 is suggestive. We see that reactivity changes more rapidly than water activity and that n/n_0 decreases

(16) P. Kruus, private communication.

(17) B. G. Cox and P. T. McTigue, *Aust. J. Chem.*, **20**, 1815 (1967).

Table III: pH Dependence of Racemization Rate Constants and Quantum Yield of d-$K_3Cr(C_2O_4)_3$ at 25.0 ± 0.1°

pH	k, sec^{-1} [a]	ϕ, 4200 Å [b]
0.00	3.93×10^{-3}	
1.05	1.10×10^{-3}	
1.35	4.56×10^{-4}	
2.05	1.38×10^{-4}	0.0206
2.52	1.80×10^{-5}	
3.00	1.67×10^{-5}	0.0248
6.00	8.37×10^{-6}	0.0087

[a] In water. [b] In 0.2 M DMSO.

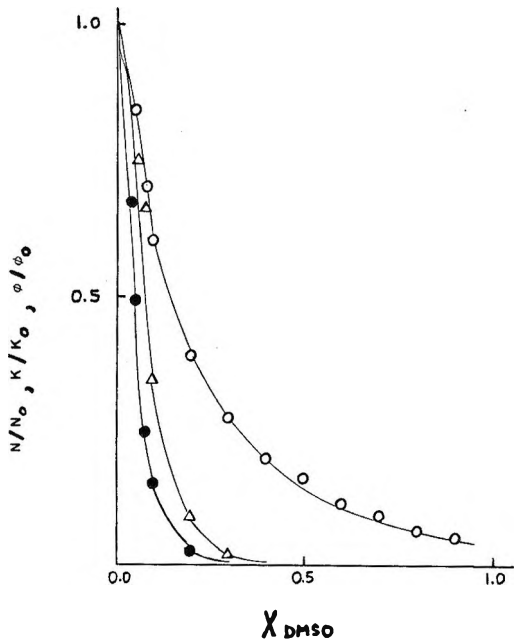

Figure 3. Relative thermal rates (●) and quantum yields (△) for racemization of $Cr(C_2O_4)_3^{3-}$ in DMSO-H_2O, and n/n_0 for water (○) *vs.* mole fraction of DMSO; T = 25°.

rapidly as DMSO is introduced. That is, DMSO replaces water in the solvation shell of $Cr(C_2O_4)_3^{3-}$ *preferentially*. However, the relationship of reactivity to n/n_0 is not simple. If the reaction rate were simply related to the probability of encounter between $Cr(C_2O_4)_3^{3-}$ and a water molecule in a suitable solvation site, one would predict proportionality of rate to n/n_0 as has been elsewhere observed.[8] That behavior would be what might be expected if water were simply functioning as a nucleophile in the dechelation step, but we have said that DMSO is a good nucleophile so we need to identify other roles for water.

In fact, there is a simple and plausible account of the role of water. It can solvate the *dissociating oxalate of the transition state of the dechelation step by hydrogen bonding*. Although DMSO appears to be a good competitor for solvation of $Cr(C_2O_4)_3^{3-}$ *in the ground state*, it is *not* so in the transition state. The transition state with a weakened Cr–O bond has a *requirement* for hydrogen bonding that may be imagined to involve all of the oxygens on the oxalate group which is undergoing dechelation. This will require several water molecules playing *nonequivalent* hydrogen bonding roles. Thus the rate is expected to depend on n/n_0 to a high and not necessarily integral power.

It would seem that this explanation of the solvent dependence of racemization rate is supported by the existence of an H^+ dependent term in the rate law. If hydrogen bonding can stabilize the transition state, protonation of the complex should also stabilize the transition state relative to the ground state. The two paths, one H^+ dependent and the other H_2O dependent, are probably mechanistically similar.

Photochemical Reactions. To make suggestions concerning the photochemistry of $Cr(C_2O_4)_3^{3-}$, it is useful to compare the results to those obtained for $Cr(NCS)_6^{3-}$ and $Cr(NH_3)_2(NCS)_4^-$, but first, some general suggestions must be recorded. Adamson[18] has emphasized that the wavelength dependence of a number of reactions of Cr^{III} complexes may be understood if reactions occur from the quartet excited states. He has also pointed out that these states are likely to be subject to substantial distortion from octahedral symmetry. In fact, the distortion is required if the lifetimes implied by the photochemical kinetics are to be understood.[19] An increase in the excited-state distortion can be expected to favor "relaxation" of that state to photochemical product rather than to the initial ground state if the distortion tends to make the excited state resemble product more than reactant. This point is cogently discussed by Hammond.[10]

Now the role of solvent may be considered. There is a parallel (but not an exact correspondence) between the solvent sensitivities in thermal and photochemical reactions for the three complexes we discuss. For both reaction types solvent sensitivity decreases in the order $Cr(C_2O_4)_3^{3-} > Cr(NH_3)_2(NCS)_4^- > Cr(NCS)_6^{3-}$. In the thermal reaction, this is to be understood in terms of the degree to which the hydrogen bonding of solvent waters aids the distortion of the complex required for heterolytic fission of a metal to ligand bond. Photochemically, it is to be understood in terms of the degree to which hydrogen bonding to water favors distortion of the excited state so that it resembles the primary photoproduct.

Now an interesting difference arises between thermal and photochemical pathways. The photochemical pathways are consistently *less* solvent sensitive. In the case of $Cr(NCS)_6^{3-}$ and $Cr(NH_3)_2(NCS)_4^-$, this difference is indicated to be one water molecule by the n/n_0 correlation. It is certainly tempting to suggest that the primary photochemical product is a reactive *inter-*

(18) A. W. Adamson, *J. Phys. Chem.*, **71**, 798 (1967).
(19) S. Chen and G. B. Porter, *J. Amer. Chem. Soc.*, **92**, 2189 (1970).

mediate with one ligand removed so that one water molecule which is present in the thermal transition state is not required. Of course, there are alternate accounts of the present limited information.

Acknowledgments. We thank the National Research Council of Canada for financial support.

Appendix. Solvation Analysis by Nmr[5-9]

The transverse relaxation time, T_2, of the proton on a solvent molecule will be greatly reduced by a paramagnetic solute. In cases of solvation in the outer coordination sphere, this effect depends on dipolar coupling between the paramagnetic elections and the proton under observation. This coupling enters relaxation time equations with an r^{-6} distance dependence. As a result of the short-range character of the interactions, it is a good approximation to partition the solution into a paramagnetic environment (solvation shell) and a diamagnetic environment (bulk solvent). Exchange between these environments is fast and McConnell's equation applies

$$\frac{1}{T_2} = \frac{P}{T_{2D}} + \frac{P}{T_{2M}}$$

T_2 is the observed relaxation time, P_D is the probability that a solvent molecule is in the diamagnetic environment (bulk), and P_M is the probability that a proton is in the paramagnetic environment (solvation shell). T_{2D} and T_{2M} are the relaxation times characteristic of the two environments, respectively. In a *dilute* solution of the paramagnetic solute, $P_D \simeq 1$ and the term $1/T_{2D}$ may be measured from study of solvents free of paramagnetic solute. Consequently, P_M/T_{2M} is experimentally accessible. It is related to the *excess* line width at half-height of the nmr absorption signal ($\Delta\nu$)

$$\pi\Delta\nu = \frac{P_M}{T_{2M}}$$

T_{2M} is difficult to evaluate accurately by either experiment or theory. If we may hope that $T_{2M} = T_{2M0}$ where T_{2M} is the paramagnetic environment relaxation time for protons of a particular component of a mixed solvent (say, DMSO) and T_{2M0} is the relaxation time in the paramagnetic environment for protons of the same component in *pure solvent* (*e.g.*, pure DMSO), we may write

$$\frac{\Delta\nu}{\Delta\nu_0} = \frac{P_M}{T_{2M}} \times \frac{T_{2M0}}{P_{M0}} = \frac{P_M}{P_{M0}}$$

where the subscript 0 designates *pure solvent* and unsubscripted variables denote mixtures. If the *bulk composition* of the solvent mixture is known, it is a straightforward matter to convert P_M/P_{M0} data into the fraction of the particular solvent (*e.g.*, DMSO) in the solvation shell of the complex in a mixed solvent. This fraction is called n/n_0.

Now, the "hope" that $T_{2M} = T_{2M0}$ is not always realized. One major reason for a failure is that T_{2M} may be dependent upon "tumbling" times which are proportional to solvent viscosity. Such a failure is easily corrected by normalizing all line width values to the same bulk viscosity.[9]

Vapor Pressure Studies of Complex Formation in Solution. II. Methanol and Benzophenone in Diphenylmethane

by Ahmed A. Taha[1a] and Sherril D. Christian[1b]

Department of Chemistry, The University of Oklahoma, Norman, Oklahoma 73069 *(Received February 20, 1970)*

The interaction of methanol (MeOH) with benzophenone [$(C_6H_5)_2CO$] in the nonvolatile solvent diphenylmethane (DPM) has been studied by a vapor pressure method described previously. Deviations from Henry's law in the condensed phase are attributed to the formation of the heteroaggregates $MeOH \cdot (C_6H_5)_2CO$ and $(MeOH)_2 \cdot (C_6H_5)_2CO$ which have formation constants of 0.87 ± 0.03 l. mol^{-1} and 1.96 ± 0.14 $l.^2$ mol^{-2}, respectively, at 30°. A dimerization constant for benzophenone in diphenylmethane, attributed to dipole–dipole interaction, is calculated to be 0.47 ± 0.10 l. mol^{-1}.

Introduction

Previously, we reported a study of the interaction of trifluoroacetic acid (TFA) with benzophenone [$(C_6H_5)_2CO$] in the nonvolatile solvent diphenylmethane (DPM).[2] Since TFA is the only appreciably volatile component in this system, it was possible to infer the extent of association of TFA with $(C_6H_5)_2CO$ from the decrease in vapor pressure which occurs when the ketone is added to TFA–DPM solutions.

We thought it would be worthwhile to extend this type of investigation to include proton donors less potent than TFA. Because the hydrogen bonding of methanol (MeOH) is currently of interest,[3-5] we decided to measure the vapor pressure of mixtures of MeOH and $(C_6H_5)_2CO$ in DPM in order to obtain information about the proton donor strength of methanol in a system where it is reasonably certain that the alcohol proton is the acidic group primarily responsible for heteroassociation. This report includes information about the formation of the complexes $MeOH \cdot (C_6H_5)_2CO$ and $(MeOH)_2 \cdot (C_6H_5)_2CO$ in DPM at 30°.

Experimental Section

Materials. All the reagents used were either analytical or CP grade except DPM, which was practical grade. DPM was purified by vacuum distillation, and methanol was purified by double distillation through a 30-plate Oldershaw column at a reflux ratio in excess of 10:1. Benzophenone was purified by double crystallization. After purification, all reagents were stored in vacuum desiccators over drying agent. The boiling point of the collected fraction of MeOH was 64.0–64.3°, corrected to 1 atm.

Apparatus and Technique. The apparatus and procedure were the same as those described previously,[2,6] except that MeOH was used in place of TFA. Increments of MeOH were added volumetrically to mixtures of $(C_6H_5)_2CO$ in DPM having molarities ranging from 0 to 0.800. From each measurement of the total vapor pressure, p, it was possible to infer the total concentration of MeOH bound to $(C_6H_5)_2CO$ species (Δf_A).

Method of Calculation. Attempts were made to fit the vapor pressure data for the ternary system by the method described earlier.[2] In this system, the concentration of $(C_6H_5)_2CO$ was varied over a wide range, and it became apparent from the discrepancies between calculated and experimental Δf_A values that the self-association of the ketone in DPM must be taken into account. The association is assumed to occur through a dipole–dipole interaction between the benzophenone molecules, the strength of which depends upon the dipole moment of the polar molecule and the type of solvent used.[7]

The formal concentration of $(C_6H_5)_2CO$ in DPM may be expressed as

$$f_B = c_B + 2K_{02}c_B^2 + K_{11}c_Ac_B + \ldots + K_{21}c_A^2c_B + \ldots \quad (1)$$

where K_{02} is the dimerization constant of $(C_6H_5)_2CO$; K_{11}, K_{21}, . . ., are heteroassociation constants, and c_A and c_B are the concentrations of monomeric alcohol and ketone, respectively. It is assumed that each solute species individually obeys Henry's law throughout the range of concentrations investigated.

Assuming the validity of Henry's law for each solute species, it is possible to obtain values of the total or for-

(1) (a) Chemistry Department, University College for Girls, Ain Sham, University, Heliopolis, Cairo, U.A.R. (b) To whom correspondence should be addressed.

(2) A. A. Taha and S. D. Christian, *J. Phys. Chem.*, **73**, 3430 (1969).

(3) E. E. Tucker, S. B. Farnham, and S. D. Christian, *ibid.*, **73**, 3820 (1969).

(4) R. M. Hammaker, R. M. Clegg, L. K. Patterson, P. E. Rider, and S. L. Rock, *ibid.*, **72**, 1837 (1968).

(5) A. N. Fletcher and C. A. Heller, *ibid.*, **72**, 1839 (1968); A. N. Fletcher, *ibid.*, **73**, 2217 (1969).

(6) A. A. Taha, R. D. Grigsby, J. R. Johnson, S. D. Christian, and H. E. Affsprung, *J. Chem. Educ.*, **43**, 432 (1966).

(7) T. F. Lin, S. D. Christian, and H. E. Affsprung, *J. Phys. Chem.*, **71**, 1133 (1967).

mal concentration of methanol bound to ketone molecules (Δf_A). This quantity is simply the measured difference between the formal concentration of MeOH in the ternary mixture at a given value of p and the formal concentration of MeOH in the binary system, MeOH–DPM, at the same p. In terms of equilibrium constants for heteroassociation, Δf_A may be expressed as

$$\Delta f_A = K_{11}c_Ac_B + 2K_{21}c_A^2c_B + \ldots \quad (2)$$

In both of eq 1 and 2, the monomer concentrations, c_A and c_B, appear explicitly. If Henry's law applies, $c_A = p/K_A^H$, where K_A^H is the limiting Henry's law constant for MeOH in DPM in the absence of added ketone. (At the levels of concentration employed here, methanol vapor may be treated as an ideal gas.[3]) Although there still appears to be considerable disagreement regarding the stoichiometry and magnitudes of formation constants of alcohol polymers in organic solvents,[3-5,8] it is relatively simple to determine K_A^H accurately from the limiting slope of p *vs.* f_A data for the binary system MeOH–DPM. The value $K_A^H = 453.2 \pm 12.1$ mm l. mol^{-1} at 30° has been calculated and used to infer values of c_A for all ternary solutions.[9]

Equations 1 and 2 relate the three measureable concentrations (f_B, Δf_A, and c_A) to the unknown equilibrium constants, K_{02}, K_{11}, K_{21}, . . . , and the ketone monomer concentration. A nonlinear least-squares method developed in this laboratory[10] was utilized to deduce values of the association constants from sets of f_B, Δf_A, and c_A measurements. First, a trial set of equilibrium constants was assumed and used in solving eq 1 for c_B for each point. These values of c_B were substituted into eq 2, and the root-mean-square deviation (RMSD) in Δf_A for all the data sets was computed for the chosen set of constants. A numerical optimum-seeking method[11] was used to vary the values of the equilibrium constants until an absolute minimum in RMSD was obtained for a given set of assumed species. The complete set of data was satisfactorily correlated by utilizing only the constants K_{02}, K_{11}, and K_{21}. The accuracy of the data did not appear to justify the inclusion of additional association constants.[12]

Results and Discussion

The least-squares fit of the pressure–concentration data yielded the following values of equilibrium constants (for formation of complexes from the monomers): $K_{02} = 0.47 \pm 0.10$ l. mol^{-1}, $K_{11} = 0.87 \pm 0.03$ l. mol^{-1}, and $K_{21} = 1.96 \pm 0.14$ l.^{2} mol^{-2}. The RMSD in Δf_A for the entire set of data was 0.00157 M. Table I lists values of pressure, formal concentrations of ketone (f_B) and alcohol (f_A), concentration of monomeric methanol (c_A), and the observed and calculated formal concentrations of alcohol present in complexes with ketone (Δf_A).

Previous investigators have proposed that both the 1:1 and the 2:1 complex are present when proton donors such as trifluoroacetic acid interact with benzophenone, water, and methanol.[2,13] Taha and Christian[2] postulated that in the ternary system trifluoroacetic acid–benzophenone in DPM the 1:1 complex is formed by a bridge between the trifluoroacetic acid hydrogen and the oxygen of the benzophenone and that the 2:1 complex has the structure

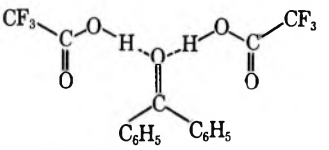

as inferred from the relative values of the constants for the formation of the self-associated species and those for the formation of the heteropolymers. Villepin, *et al.*,[13] proposed a similar structure for the 1:1 complex of trifluoroacetic acid with water and MeOH, but they suggested two possible structures for the 2:1 complex

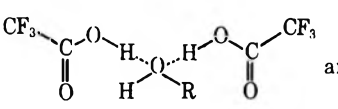

I

and

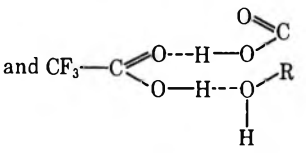

II

For the present system, MeOH + $(C_6H_5)_2CO$ in DPM, we tend to favor a structure similar to II

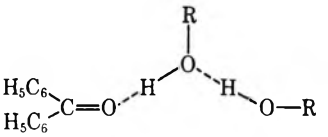

(8) U. Liddell and E. D. Becker, *Spectrochim. Acta*, **10**, 70 (1957).

(9) A. A. Taha, Ph.D. Dissertation, The University of Oklahoma, 1965.

(10) R. Van Duyne, S. A. Taylor, S. D. Christian, and H. E. Affsprung, *J. Phys. Chem.*, **71**, 3427 (1967).

(11) D. J. Wilde, "Optimum Seeking Methods," Prentice-Hall, Englewood Cliffs, N. J., 1964.

(12) A reviewer has questioned the assumption that the individual solute species (monomers and complexes) obey Henry's law throughout the range of concentrations investigated. The analysis presented here depends upon the validity of this assumption, which is in fact basic to virtually all procedures which have been used to infer association constants for interacting solute molecules from the departure of physical data (*e.g.*, vapor pressure, spectral intensity, dielectric constant) from the concentration dependence predicted by the ideal dilute solution laws. It is commonly conceded that individual solutes in nonelectrolyte solutions closely follow Henry's law at concentrations up to at least several mol %, and in the case of binary mixtures of $(C_6H_5)_2CO$ and DPM, at ketone concentrations up to 0.8 M, it seems to us reasonable to attribute deviations from ideality to the formation of discrete associated solute species. DPM and $(C_6H_5)_2CO$ are nearly equal in molecular size and polarizability; except for the specific interaction of the polar carbonyl groups of $(C_6H_5)_2CO$, there should be little tendency toward deviation from Henry's law. (See D. E. Martire and P. Riedl, *J. Phys. Chem.*, **72**, 3478 [1968] for partial justification of a similar assumption. These workers concluded that the molecular interaction of a given proton-donating solute with the solvents di-*n*-octyl ketone and *n*-heptadecane, respectively, is the same except for the formation of specific hydrogen bonds between the solute and polar solvent.) The addition of small concentrations of methanol (less than 0.22 M) should not introduce sizable nonspecific activity effects, and we attribute the large observed deviations of methanol from Henry's law entirely to complex formation.

(13) J. De Villepin, A. Lantie, and M. L. Josien, *Ann. Chim.* (*Paris*), 9–10, 365 (1966).

Table I: Dependence of Methanol Vapor Pressure on Concentration in the Ternary System Methanol–Benzophenone–Diphenylmethane at 30.0°

p, Torr	f_A, mol/l.	C_A, mol/l.	Δf_A^{obsd}, mol/l.	Δf_A^{calcd}, mol/l.
	f_B = 0.0803 mol/l.			
5.12	0.0118	0.0113	0.0003	0.0008
9.69	0.0236	0.0214	0.0015	0.0015
14.21	0.0355	0.0314	0.0025	0.0023
18.48	0.0474	0.0408	0.0037	0.0031
22.56	0.0591	0.0498	0.0051	0.0038
26.78	0.0712	0.0591	0.0058	0.0047
30.75	0.0831	0.0678	0.0068	0.0055
34.82	0.0950	0.0768	0.0070	0.0063
38.39	0.1069	0.0847	0.0084	0.0071
41.96	0.1188	0.0926	0.0094	0.0079
45.38	0.1308	0.1001	0.0104	0.0087
48.70	0.1428	0.1075	0.0114	0.0095
51.87	0.1548	0.1145	0.0124	0.0102
54.89	0.1668	0.1211	0.0136	0.0110
57.67	0.1788	0.1272	0.0153	0.0116
60.39	0.1908	0.1332	0.0169	0.0123
63.06	0.2029	0.1391	0.0183	0.0130
65.83	0.2149	0.1453	0.0188	0.0137
	f_B = 0.1898 mol/l.			
4.57	0.0118	0.0101	0.0016	0.0015
8.89	0.0237	0.0196	0.0035	0.0030
13.17	0.0356	0.0291	0.0051	0.0046
17.13	0.0475	0.0378	0.0072	0.0062
21.26	0.0594	0.0469	0.0086	0.0079
25.18	0.0713	0.0556	0.0103	0.0096
28.95	0.0832	0.0639	0.0120	0.0113
32.52	0.0952	0.0718	0.0139	0.0129
36.09	0.1071	0.0796	0.0156	0.0146
39.31	0.1191	0.0867	0.0178	0.0162
42.58	0.1311	0.0940	0.0197	0.0178
45.85	0.1431	0.1012	0.0211	0.0195
48.92	0.1551	0.1079	0.0229	0.0211
	f_B = 0.2992 mol/l.			
4.37	0.0119	0.0096	0.0021	0.0021
8.59	0.0238	0.0190	0.0042	0.0043
12.56	0.0357	0.0277	0.0066	0.0065
16.68	0.0476	0.0368	0.0084	0.0089
20.41	0.0595	0.0450	0.0109	0.0112
24.18	0.0714	0.0533	0.0130	0.0136
27.85	0.0834	0.0614	0.0151	0.0160
31.27	0.0953	0.0690	0.0176	0.0183
34.59	0.1073	0.0763	0.0201	0.0207
37.91	0.1193	0.0836	0.0222	0.0231
41.13	0.1313	0.0908	0.0244	0.0255
44.25	0.1433	0.0976	0.0265	0.0279
47.17	0.1553	0.1041	0.0293	0.0301
50.09	0.1673	0.1105	0.0311	0.0325
52.82	0.1794	0.1165	0.0337	0.0347
55.49	0.1914	0.1224	0.0361	0.0369
58.01	0.2035	0.1280	0.0387	0.0390
4.12	0.0119	0.0091	0.0027	0.0026
8.34	0.0238	0.0184	0.0048	0.0054
12.11	0.0357	0.0267	0.0078	0.0080
15.88	0.0476	0.0350	0.0104	0.0108
19.56	0.0596	0.0431	0.0132	0.0136
23.13	0.0715	0.0510	0.0159	0.0165
26.70	0.0835	0.0589	0.0183	0.0195
30.12	0.0954	0.0665	0.0209	0.0225
33.34	0.1074	0.0736	0.0238	0.0254
36.46	0.1194	0.0804	0.0267	0.0282
39.58	0.1314	0.0873	0.0293	0.0312
42.55	0.1434	0.0939	0.0321	0.0341
45.37	0.1555	0.1001	0.0351	0.0369
48.19	0.1675	0.1063	0.0378	0.0397
50.87	0.1796	0.1122	0.0407	0.0425
53.44	0.1916	0.1179	0.0437	0.0452
55.91	0.2037	0.1236	0.0467	0.0478
	f_B = 0.5999 mol/l.			
3.87	0.0119	0.0085	0.0033	0.0033
7.59	0.0239	0.0168	0.0066	0.0067
11.16	0.0358	0.0246	0.0102	0.0101
14.78	0.0478	0.0326	0.0133	0.0138
18.26	0.0597	0.0403	0.0166	0.0174
21.53	0.0717	0.0475	0.0202	0.0210
24.70	0.0837	0.0545	0.0239	0.0246
27.92	0.0957	0.0616	0.0272	0.0284
30.89	0.1077	0.0682	0.0310	0.0321
33.91	0.1197	0.0748	0.0344	0.0358
36.78	0.1317	0.0812	0.0380	0.0395
39.65	0.1437	0.0875	0.0414	0.0433
42.22	0.1558	0.0932	0.0455	0.0468
44.94	0.1678	0.0992	0.0488	0.0506
47.52	0.1799	0.1048	0.0525	0.0542
49.94	0.1920	0.1102	0.0563	0.0577
52.41	0.2040	0.1156	0.0598	0.0613
	f_B = 0.8001 mol/l.			
3.57	0.0120	0.0079	0.0040	0.0038
6.94	0.0239	0.0153	0.0082	0.0076
10.36	0.0359	0.0229	0.0121	0.0116
13.48	0.0479	0.0298	0.0166	0.0155
16.66	0.0599	0.0367	0.0201	0.0196
19.88	0.0719	0.0439	0.0247	0.0240
22.85	0.0839	0.0500	0.0290	0.0281
25.77	0.0959	0.0569	0.0333	0.0323
28.54	0.1079	0.0630	0.0378	0.0365
31.26	0.1200	0.0690	0.0423	0.0407
34.03	0.1320	0.0751	0.0464	0.0450
36.65	0.1441	0.0809	0.0508	0.0493
39.12	0.1561	0.0863	0.0554	0.0534
41.69	0.1682	0.0920	0.0595	0.0577
44.07	0.1803	0.0972	0.0641	0.0618
46.49	0.1923	0.1026	0.0683	0.0661
48.66	0.2044	0.1074	0.0731	0.0700

in view of the relative magnitudes of K_{11} and K_{21}. The ratio K_{21}/K_{11} = 2.3 l. mol^{-1} equals the equilibrium constant for the reaction $MeOH \cdot (C_6H_5)_2CO + MeOH = (MeOH)_2 \cdot (C_6H_5)_2CO$; the magnitude of the constant indicates that the 1:1 complex is a stronger base than monomeric $(C_6H_5)_2CO$. Since a combination

of statistical, steric, and inductive factors should act to decrease the basicity of the ketone carbonyl oxygen in the 1:1 complex relative to the basicity of monomeric $(C_6H_5)_2CO$, it does not appear that a structure analogous to I is tenable. On the other hand, induction should increase the basicity of the MeOH oxygen in $MeOH \cdot (C_6H_5)_2CO$, and a value of K of 2.3 l. mol for the addition of a second MeOH molecule to $MeOH \cdot (C_6H_5)_2CO$ seems reasonable, considering the values of formation constants reported for 2:1 MeOH–amine complexes.[14] Whetsel and Kagarise[15] have concluded that the 2:1 complex of *p*-cresol with acetone also has a structure similar to II, based on the observation that there is a relatively small shift in carbonyl frequency when the second cresol molecule bonds to the 1:1 complex.

Acknowledgment. This work was supported by the Office of Saline Water (Grants GS-14-01-0001-1315 and 14-01-0001-321). The authors wish to acknowledge the help of Dr. Sutton Farnham in fitting the data.

(14) E. E. Tucker, Ph.D. Dissertation, The University of Oklahoma Norman, Okla., 1969.

(15) K. D. Whetsel and R. G. Kagarise, *Spectrochim. Acta*, 18, 315 (1962).

The Fluorescence and Phosphorescence of 1,2;5,6-Dibenzacridine and 1,2;7,8-Dibenzacridine in Glassy and Liquid Solution[1a]

by John L. Kropp[1b] and J. J. Lou

Chemical Sciences Department, Systems Group of TRW, Inc., Redondo Beach, California 90278
(Received February 18, 1970)

The absorption and emission properties of 1,2;5,6-dibenzacridine (I) and 1,2;7,8-dibenzacridine (II) have been investigated at −196° and 23° in 3-methylpentane (MP) solutions as a function of propanol concentration between 0.01 and 40% propanol by volume. The singlet and triplet absorption spectra and fluorescence and phosphorescence spectra have been determined as well as the fluorescence and phosphorescence intensities and lifetimes. The addition of propanol to MP solutions of I does not change the absorption or emission properties of this compound significantly at either temperature studied. However, for II, the absorption and fluorescence spectra shift to the red as propanol is added, and at −196° small quantities (0.1%) of propanol cause a fourfold enhancement of phosphorescence. Corresponding to this, no T–T absorption of II is observed unless small quantities of propanol are added. Above 1% propanol by volume the fluorescence intensity sharply increases while the phosphorescence intensity and T–T absorption decrease.

I. Introduction

Aza-aromatic molecules have a greater variation in luminescence properties in a changing environment than do their hydrocarbon analogs. This is due to the presence of both (n,π^*) and (π,π^*) levels in the aza-aromatics. The fluorescence and phosphorescence properties of these molecules are affected by the positions of the (n,π^*) and (π,π^*) levels in the molecular energy scheme and particularly by the character of the lowest energy level in the excited singlet (S_1) and triplet (T_1) manifold. Changes in solvent that affect the (n,π^*) levels often result in changes in the spectral distribution and intensity of emission of these molecules.

There are many polycyclic monoazines whose lowest excited states, both singlet and triplet, appear to be (π,π^*) in character, yet whose absorption and emission properties show a marked variation as the solvent is varied from a hydrocarbon to one that is hydroxylic or polar.[2-9]

(1) (a) Prepared under Contract F33615-69-C-1052 for U. S. Air Force. (b) To whom correspondence should be addressed.

(2) (a) M. Kasha in "Light and Life," McElroy and Glass, Ed., Johns Hopkins Press, Baltimore, Md., 1961, p 58; (b) V. L. Ermolaev and I. P. Kotlyar, *Opt. Spektrosk.*, 9, 353 (1960).

(3) E. C. Lim and J. M. H. Yu, *J. Chem. Phys.*, 47, 3270 (1967).

(4) N. Mataga and S. Tsuno, *Bull. Chem. Soc. Jap.*, 30, 368 (1957).

(5) E. J. Bowen and J. Sahu, *J. Chem. Soc.*, 3716 (1958); E. J. Bowen, N. J. Holden, and G. B. Woodger, *J. Phys. Chem.*, 66, 2491 (1962).

(6) S. J. Ladner and R. S. Becker, *ibid.*, 67, 2481 (1963).

(7) G. Coppens, C. Gillet, J. Nasielski, and E. Vander Donct, *Spectrochim. Acta*, 18, 1441 (1962).

(8) M. Nakamizo and Y. Kanda, *ibid.*, 19, 1235 (1963).

(9) E. C. Lim and J. M. H. Yu, *J. Chem. Phys.*, 47, 3270 (1967).

We have made studies of 1,2;5,6-dibenzacridine (I) and 1,2;7,8-dibenzacridine (II) as potential photochromics. The spectral and intensity changes for fluorescence and absorption at room temperature and the fluorescence, phosphorescence singlet absorption spectra at −196° have been studied. In addition, we have studied the T–T absorption at −196° for comparison. In this paper we present the results of these studies which show the effect of solvent composition upon the properties of the excited singlet state.

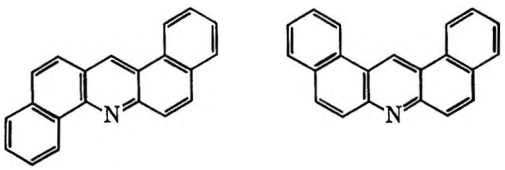

I II

II. Experimental Section

Materials. Both I and II were obtained from Aldrich Chemical. These samples were recrystallized from ethanol. The melting points were 213–219 and 222–223°, respectively. The absorption spectra in ethanol agreed with those published in the literature.[10] 3-Methylpentane (MP) was Phillips research grade passed over silica gel and stored over sodium. MP was prepared as needed, and fresh sodium was used each time. Propanol was Eastman Kodak White Label used without further purification. 1,1′,2,2′-Tetrafluoropropanol (TFP) was used as received from Aldrich Chemical. In preparing solutions the following technique was used. A stock solution of the compound (I or II) in MP was prepared. Aliquots were taken from this solution, the appropriate quantity of propanol was added, and the solution was diluted to mark. Samples were prepared so that the solute concentration was constant at room temperature for each run. All solutions were used the same day as prepared. Overnight storage gives significant changes in the spectral properties of a pure MP solution of II, which we have interpreted as the introduction of water into the solution to give "wet" 3-methylpentane. Changes that are most noticeable occur in the absorption spectrum of II at 77°K (*cf.* Figure 2b) and in the T–T absorption of II. Thus the criterion we use for "dryness" of MP is (1) strong absorption of II at 392 nm but little at 398 nm and (2) absence of T–T absorption at −196° (see Results section).

Measurements. Absorption spectra were taken on a Cary Model 14. In calculating values of ϵ_S at −196°, the room temperature concentration was increased by 20% to take into account the contraction of the glass between 23 and −196°. The reproducibility of extinction coefficients, ϵ_S, at −196° is about ±20% in propanol solution.

The T–T absorption spectra were measured by the apparatus described by Dawson,[11] or on an apparatus that was adapted for use on the Cary Model 14.[12] The latter arrangement was used for most T–T absorption spectra recorded in this paper. Values of $\epsilon_T\Phi_T$ have been determined for the MP solution of I and for an EPA solution for II.[12] The values of $\epsilon_T\Phi_T$ for propanol solutions are scaled from these values.

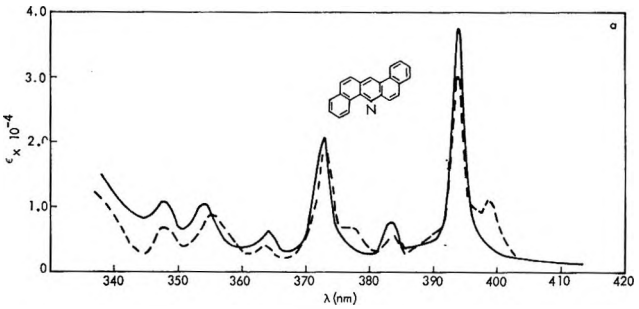

Figure 1. Singlet absorption spectrum for 1,2;5,6-dibenzacridine in 3-methylpentane–propanol solution at −196°. Concentration of propanol: —, 0%; - - -, 10%.

The fluorescence and phosphorescence were excited using 365-nm light at right angles using dilute (5×10^{-6} *M*) solutions. Intensities were computed by taking the total area under fluorescence and phosphorescence curves. These intensities of fluorescence *F* and phosphorescence *P* were corrected relative to each other for phototube response. Lifetimes were recorded using a TRW nanosecond light source.

III. Results

Absorption Spectra. The absorption spectrum of I at −196° is shown in Figure 1 for 0 and 10% propanol. The absorption spectrum at 23° is similar to that recorded at −196° except that it is broadened. The addition of 10% propanol to the MP solution does not affect the room temperature spectrum. At −196° a new peak is present at 399 nm (25,070 cm^{-1}) at propanol concentrations above 5%. This is shown in Figure 1 for the 10% propanol solution. Separate experiments were done with tetrafluoropropanol (TFP). This compound is a much stronger H-bonding compound than is propanol.[13] At room temperature a shoulder develops at 398 nm at less than 1% TFP which indicates that the band at 399 nm observed at low temperatures is due to H-bonding. The spectrum in ethanol and 100% propanol at room temperature shows a shift of the 0–0 band

(10) "UV Atlas of Organic Compounds," Plenum Press, New York, N. Y., 1966, spectrum H8/39 for I and spectrum H8/41 for II.

(11) W. R. Dawson, *J. Opt. Soc. Amer.*, **58**, 222 (1968).

(12) C. C. Stanley and J. L. Kropp, unpublished.

(13) E. M. Kowsower and G. S. Wu, *J. Amer. Chem. Soc.*, **83**, 3142 (1961). TFP is a more desirable compound to use in studying effects such as we are investigating since very small quantities need be used (less than 1%). This would not affect the bulk hydrocarbon properties of the solvent as do large quantities of propanol. However, the use of TFP at −196°, even at 0.01%, results in a hazy glass and the solute emission that is typical of the protonated form of the heterocyclic molecule. Thus TFP cannot be used in these studies at −196°. Other strong hydrogen-bonding species such as acetic acid and methanol were also considered but not used because they were either so strong as to form the protonated ion or did not give a clear glass.

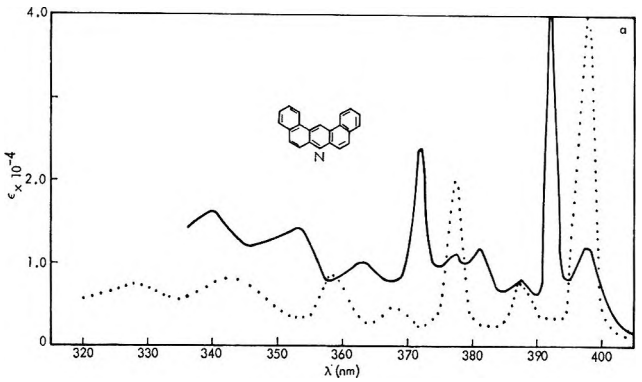

Figure 2. Singlet absorption spectrum of 1,2;7,8-dibenzacridine in 3-methylpentane–propanol solution at −196°. Concentation of propanol: —, 0%; · · ·, 0.1%.

to 394 nm and is in agreement with that published elsewhere.[10]

Absorption spectra for II were determined at 23 and −196° for various propanol concentrations. Representative spectra at −196° are shown in Figure 2. At 23° the spectrum shows resolvable changes at propanol concentrations above 1%. In those solutions the spectrum shifts to the red until at 20% propanol the spectrum is similar to the absorption spectrum observed in 100% propanol solution. When TFP is used in place of propanol as the H-bonding agent, the spectral shifts at 1% TFP, the spectrum corresponds to that of a 20% propanol solution. Thus TFP and propanol act in the same way upon the absorption, except that the spectral shifts are observed at much lower concentrations of TFP than of propanol.

At −196° the effect of propanol upon the absorption spectrum of II is much more pronounced than at 23°. In MP glass, the first intense band appears at 393 nm (25,450 cm^{-1}). We interpret this as the 0–0 band. The band at 397 nm (25,120 cm^{-1}) in Figure 2 is regarded as due to small amounts of hydroxylic impurities. This assignment is made because (1) the 0–0 band of fluorescence of II in dry MP is at 393 nm and (2) wet or old 3-methylpentane shows an enhancement of a band at 397 nm and a decrease of the 393-nm band. The absorption of a solution containing 0.01% propanol is already shifted to the red compared to that observed in MP glass, and the band at 393 nm characteristic of absorption in MP has disappeared. This red shift in the absorption spectrum is complete at a concentration of 0.1% propanol or lower. There are no further changes in the absorption spectrum at propanol concentrations above 0.1%. Thus we conclude that all molecules of II are in their H-bonded by the time 0.1% propanol has been added.

The extinction coefficients and areas under the absorption curves are equal at all propanol concentrations. In Figure 2 the extinction coefficients of the absorption spectrum of the MP glass are higher than the corresponding ones of the 0.01% sample. The background absorption of an MP glass rises at wavelengths less than 390 nm, while that of MP glass containing propanol does not. We did not correct for this difference since the base line is not exactly reproducible. However, differences in intensity of absorption of corresponding bands is probably due to inadequate correction for the baseline in the MP solution.

If we use 25,450 cm^{-1} as the 0–0 value for the absorption of II in MP and assume that the MP absorption consists of those peaks that are *not* coincident with an absorption peak in the propanol solution (*cf.* Figure 2), then the MP absorption of II has peaks at 25,450 cm^{-1}, 381 nm (26,180 cm^{-1}), 372 nm (26,920 cm^{-1}), and 363 nm (27,550 cm^{-1}) while in 10% propanol solution the absorption peaks are at 25,120, 25,770, 26,460, and 27,170 cm^{-1}. Thus the absorption spectra of II in MP and in propanol agree except for a shift of about 400 ± 50 cm^{-1} to the red when propanol is used.

Fluorescence Spectra. The room temperature fluorescence spectra of I as a function of propanol are all similar; however, above 5% a new band builds in at 398 nm (25,130 cm^{-1}), and the fluorescence shows considerable broadening. The 0–0 band for fluorescence occurs at 393 nm (25,450 cm^{-1}) for all propanol concentrations studied (up to 20%).

The room temperature fluorescence spectrum of II shows changes as propanol is added. There is a continuous red shift in wavelengths of emission as propanol concentration is varied. The main fluorescence bands at 0% are at 392, 402, 414, 426, and 440 nm (25,510, 24,880, 24,150, 23,420, and 22,730 cm^{-1}). At 10% propanol these bands have shifted to 398, 408, 419, and 444 nm (25,120, 24,510, 23,870, and 22,520 cm^{-1}). Above 10% propanol there are no further shifts. The fluorescence spectra in pure MP and with 10% propanol are similar with a shift of the latter to the red by 380 cm^{-1}.

The low-temperature fluorescence spectrum for I is given in Figure 3a as a function of added propanol. The band positions remain the same for all concentrations of propanol, and the 0–0 band is at 393 nm. However, at higher concentrations of propanol a new band builds in at 398 nm. The phosphorescence spectrum of I is given in Figure 3b. As can be seen from this figure, there is essentially no change in the shape of the phosphorescence spectrum with concentration of propanol. The 0–0 band is at 532 nm (18,780 cm^{-1}).

At −196° the fluorescence spectrum of II has three distinct changes of shape as propanol is added. These are illustrated in Figure 4a: the first in MP (no propanol), the second which is evident at the lowest concentration of propanol added (0.01%) and which continuously changes in shape from 0.01 to about 1% propanol to the final form shown in Figure 4a. This wavelength distribution of fluorescence does not change further up to 40% propanol. As in absorption we assume that the low-intensity bands which are observed in MP solution and which correspond closely in energy to those ob-

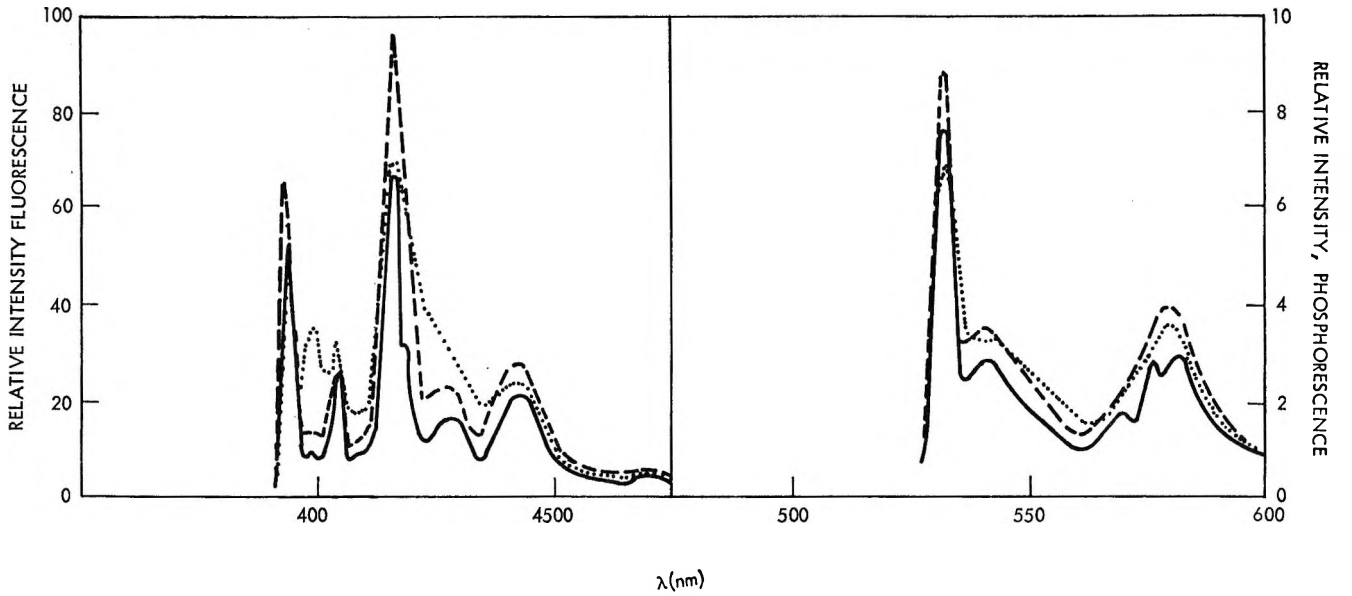

Figure 3. Fluorescence and phosphorescence spectra of 1,2;5,6-dibenzacridine in 3-methylpentane–propanol glass at −196°. Propanol concentrations are 0% (—), 0.1% (- - -), and 20% (. . . . .).

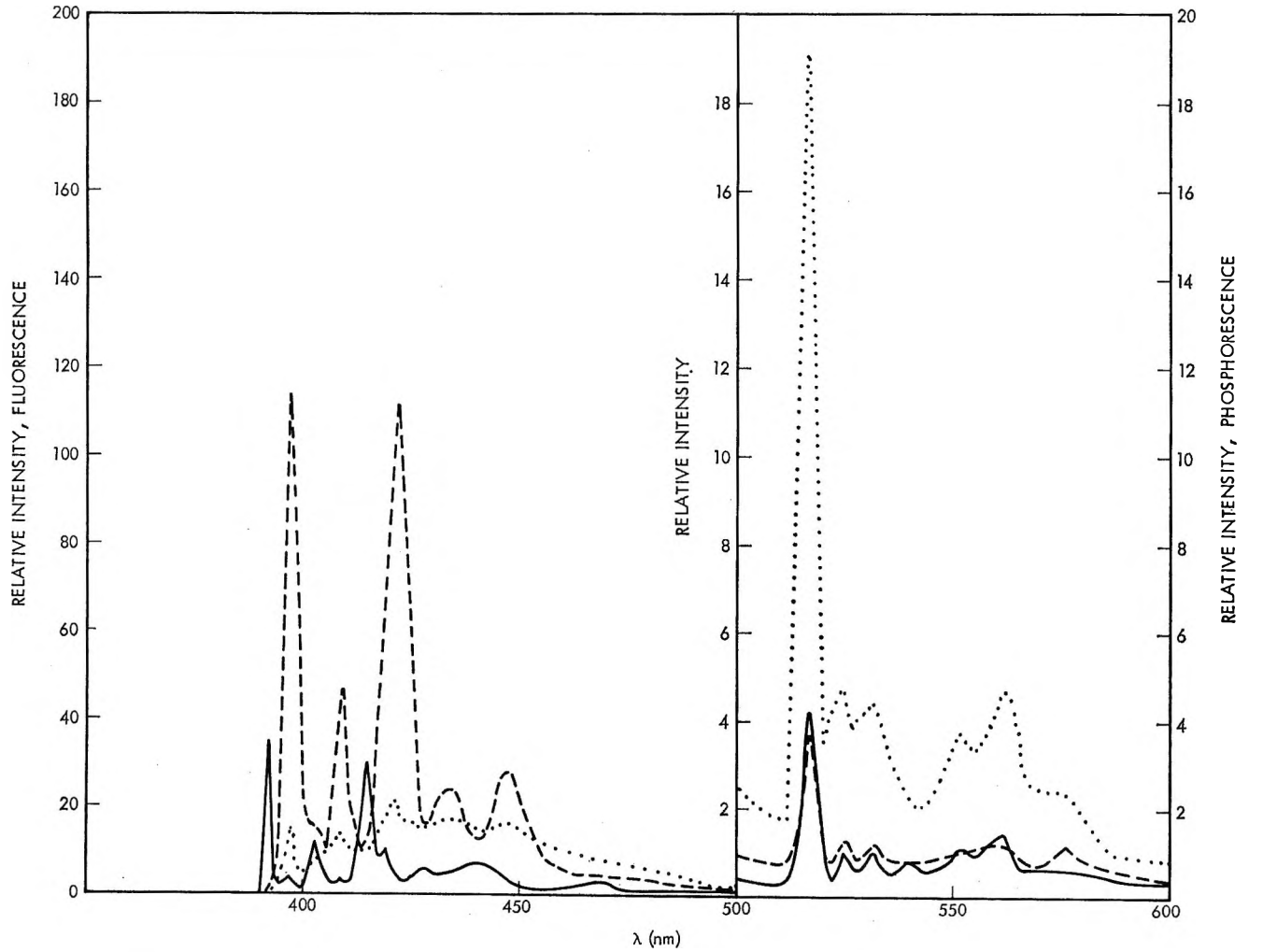

Figure 4. Fluorescence and phosphorescence spectra of 1,2;7,8-dibenzacridine in 3-methylpentane–propanol glass at −196°. Propanol concentrations: 0% (—); 0.1% (. . . . .); 10% (- - - - - -).

served in propanol solution are due to H-bonded II present in MP due to residual water. If we neglect these bands in MP, Figure 4a shows that there is a uniform shift of all bands in the fluorescence spectrum of about 400 cm^{-1} to the red when propanol is added. At 0.1% propanol the 0–0 band at 393 nm has already shifted to 398 nm, the same value observed for all higher propanol concentrations. The difference in the fluorescence spectrum between 0.1 and 20% propanol is only in the intensity distribution of the fluorescence. When the intensities of fluorescence are normalized to be 100 at the 0–0 band, the intensity distributions of the 0 and the 20% propanol solutions are roughly the same for corresponding bands. However, at 0.1% propanol the long wavelength portion of the fluorescence spectrum has a much higher intensity compared to the 0–0 band. This is seen in Figure 4 as a general broadening of the spectrum. This broadness in the spectrum is at a maximum at 0.01% propanol (the lowest concentration used), and the spectral distribution changes continuously from 0.01 to 1% propanol. Above 1% the spectral distribution is not further changed.

The phosphorescence spectrum of II is given in Figure 4 as a function of propanol concentration. The band positions do not shift with propanol concentration. However, the bands broaden with increasing propanol concentration and some of the fine structure disappears. The 0–0 band is 517 nm for all propanol concentrations.

Fluorescence Intensities. The fluorescence (F) and phosphorescence (P) intensities of I and II as a function of the propanol concentration have been determined by integrating the area under the appropriate curves. These results at −196° are plotted in Figure 5 as a function of propanol concentration. The values of P are multiplied by 10 in this figure. The values of F at −196 and +23° and values of P for I are all similar. The maximum change at −196° in fluorescence or phosphorescence is a 50% increase at about 10% propanol. At room temperature a maximum increase in fluorescence of about 30% is measured.

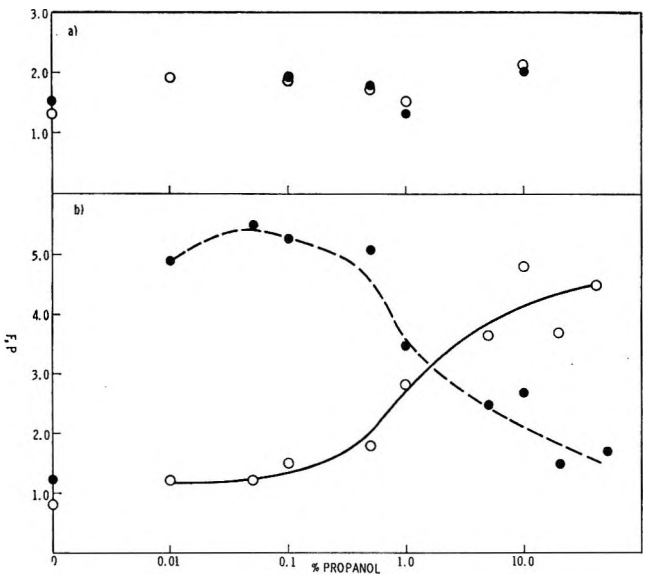

Figure 5. Fluorescence (○) and phosphorescence (●) intensities for 1,2;5,6-dibenzacridine (a) and 1,2;7,8-dibenzacridine (b) in 3-methylpentane glass at −196° as a function of propanol concentration.

For II the room temperature behavior of F is similar to that observed for I, and a maximum increase in fluorescence of 50% is observed. However, at −196° the changes are much more pronounced. The phosphorescence is enhanced by small quantities of propanol and at about 0.1% propanol has a maximum value of 4.65 that observed in MP alone (see Figures 4b and 5b). At higher concentrations of propanol, phosphorescence decreases until at 20–40% it is only 30% higher than at 0% propanol. On the other hand, F increases slowly until 1% and then increases sharply reaching a value 5.5 times that in MP at 40% propanol.

Values of the fluorescence yield (Φ_F) of 1,2;5,6-dibenzacridine and 1,2;5,6-dibenzacridine and 1,2;7,8-dibenzacridine have been measured in MP and EPA at 23°.[14,15] These values are 0.25 and 0.24 for I and 0.51 and 0.42 for II in EPA and 3-methylpentane, respectively. Since the EPA is 5:5:2 isopentane–ether–ethanol, the alcohol content is about 17%. These values agree within experimental error with the relative values from intensity comparisons.

The ratios of fluorescence to phosphorescence can be determined from data in Figure 5. For I the ratio F/P has a value of 9.8 ± 1.0 independent of the propanol concentration. The values of F/P for II, on the other hand, vary greatly depending on the propanol concentration and are about 4 at 1% propanol; beyond 1%, the values increase sharply reaching a maximum of 30 at 40%.

T–T Absorption Spectra. Figure 6 shows the T–T absorption spectra of I and II at various propanol concentrations. For I, T–T absorption is observed in pure MP solution and the intensity of T–T absorption is not enhanced by the addition of propanol. The value of $\epsilon_T\Phi_T$ in MP, where ϵ_T is the extinction coefficient and Φ_T is the triplet formation efficiency, has been determined relative to the value in EPA[16] and is 9500 ± 10%. There is no apparent shift in spectrum as propanol is added, and the main triplet absorption bands are at 520, 545, and 585 nm (19,230, 18,350, and 17,100 cm^{-1}). On the other hand, *for II no T–T absorption is observed in pure MP.* As propanol is added to a dry solution, the triplet absorption appears. The T–T absorption is essentially a broad single band peaking at 550 nm (18,200 cm^{-1}). At a propanol concentration

(14) These values were measured by W. R. Dawson using a technique described elsewhere.[15]

(15) W. R. Dawson and M. W. Windsor, *J. Phys. Chem.*, 72, 3251 (1968).

(16) J. L. Kropp, unpublished.

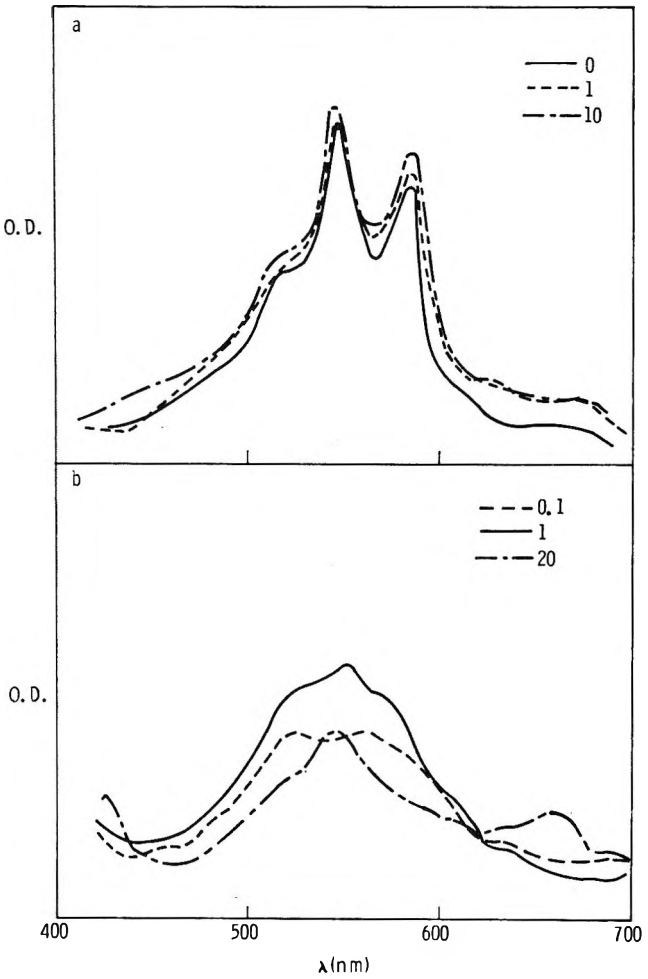

Figure 6. Triplet-triplet absorption for 1,2;5,6-dibenzacridine (a) and 1,2;7,8-dibenzacridine (b) in 3-methylpentane glass at various propanol concentrations. The percentage propanol present for each compound. No T–T absorption is observed at 0% propanol for 1,2;7,8-dibenzacridine.

above 20% a new band appears at 14,700 cm^{-1}. There is no permanent change in the sample as evidenced by the disappearance of all transient absorption upon removal of the excitation light. The concentration of propanol at which maximum T–T absorption occurs is between 0.5 and 1.0% propanol. The value of $\epsilon_T\Phi_T$ at 1% propanol is 3000 compared to EPA.[16] The appearance of new bands in the 20% propanol case is apparently real, and the bands are reproducible.

Lifetimes. Phosphorescence lifetimes (τ_P) of I are 0.84 sec in 3-methylpentane and 0.88 sec in all propanol concentrations. In II the lifetime at 0% propanol is 1.6 sec. The value of τ_P increases to a maximum of 2.1 sec at 0.1% and remains at this value up to 20% propanol. These lifetimes are first order over at least 1 decade of intensity. Fluorescence lifetimes were measured at −196° and are given in Table I. At 23° the values of τ_F are 8.8 nsec and 10.5 nsec in MP and MP + 20% propanol, respectively, for II.

Table I: Fluorescence Lifetimes of 1,2;7,8-Dibenzacridine and 1,2;5,6-Dibenzacridine in Methylpentane Solutions at −196°

1,2;7,8-Dibenzacridine

P, %	0	0.05	0.1	0.5	1.0	5.0	10.0	20.0
τ_F, nsec	15	22.5	22	20.9	16.0	13.0	11.0	11.0

1,2;5,6-Dibenzacridine

P, %	0	0.1	1.0	10
τ_F, nsec	7.0	7.0	6.2	6.1

IV. Discussion

The addition of small quantities of propanol markedly affects the spectral behavior of II at −196° and at room temperature. Significant changes occur in the absorption and emission spectra and in the fluorescence and phosphorescence intensities of this compound. In contrast, the behavior of I is almost independent of the solvent from pure 3-methylpentane up to mixtures containing 10% propanol in 3-methylpentane. The difference in behavior is attributable to the H bonding of II

$$(II) + H\text{–}OC_3H_7 \rightleftarrows (II)\ldots H\text{–}OC_3H_7$$

by propanol, while such H bonding occurs significantly for I only at propanol concentrations of 10% or higher. At room temperature propanol solutions of MP containing II show little evidence of H bonding below 1% propanol. However, when solutions are cooled to −196°, even 0.1% propanol in an MP glass is sufficient to cause a shift in absorption and emission properties (see Figures 2 and 4) and the energy of S_1 is lowered by about 400 cm^{-1}. This energy of S_1 is the same whether calculated from absorption or from emission spectra, thus indicating that the H bonding of II by propanol occurs to about the same extent in S_0 and in S_1.

The band structure observed in both fluorescence and phosphorescence spectra, together with the lifetimes observed (see Table I), indicate that both S_1 and T_1 are (π,π^*) states in all glasses studied. The model developed by Lim and Yu (LY)[9] can be used to explain the observations when small amounts of propanol are present in MP solutions of II compared to pure MP. The data observed are best explained by the mechanism

$$S_1{}^1(\pi,\pi^*) \xrightarrow{S.O.} {}^3(n,\pi^*) \xrightarrow{vib} T_1{}^3(\pi,\pi^*)$$

H bonding will raise the energy of the $^3(n,\pi^*)$ state and lower that of the S_1 state, thus lowering the energy gap and increasing the interaction between these two states. As El Sayed[17] has shown, the radiationless transition $^1(\pi,\pi^*) \rightarrow {}^3(n,\pi^*)$ is more allowed than is $^1(\pi,\pi^*) \rightarrow {}^3(\pi,\pi^*)$, and we expect an enhanced triplet population as the $^1(\pi,\pi^*) \rightarrow {}^3(n,\pi^*)$ energy is decreased.

(17) S. K. Lower and M. A. El Sayed, *Chem. Rev.*, **66**, 207 (1966).

This accounts for the increase in phosphorescence observed in II upon H bonding.

The intensity observed at −196° increases by about 50% at low propanol concentrations compared to that in MP and increases gradually up to about 1% propanol. The increase in F is accompanied by a corresponding increase in τ_F. Values of the radiative rate constant k_F are proportional to the product of F and τ_F^{-1}. At low propanol concentrations this product is constant indicating that k_F is independent of solvent for 3-methylpentane–propanol mixtures up to 1% propanol. However, beyond this the fluorescence increases sharply (Figure 5) while the value of τ_F decreases. This indicates that there is an increase in k_F above 1% propanol. An explanation consistent with these observations is that the glass structure changes at propanol concentrations above 1%. Such changes are observed for the system propanol–2-methylpentane system which is similar to ours.[18]

The phosphorescence spectrum shows no shift in wavelength at any concentration of propanol. However, above 1% propanol the increase in fluorescence intensity is accompanied by a decrease in phosphorescence intensity. One would expect the density of triplet–triplet absorption to mirror the phosphorescence intensity since both arise *via* the triplet state. However, the decrease in triplet absorption between 1 and 20% propanol is 30% while P decreases by a factor of 3 in the same region. The T–T absorption is proportional to $\epsilon_T\Phi_T\tau_P$ for a given light intensity where ϵ_T is the triplet extinction coefficient and Φ_T is the triplet formation efficiency. The phosphorescence intensity P is proportional to $\Phi_T k_P \tau_P$ where k_P is the rate constant for phosphorescence. Since τ_P is constant independent of propanol concentration, it is reasonable to assume k_P likewise does not change with propanol concentration. Thus, to account for the changes in P and T–T absorption we must assume that Φ_T is less at high propanol concentration and since T–T absorption decreases more slowly than P, ϵ_T also increases above 1% propanol.

When no propanol is present in MP glass at −196° containing II, both F and P are decreased relative to values observed when propanol is added and no T–T absorption is observed. Addition of only 0.1% propanol increases P fourfold while increasing F by 50%, with little change in radiative rate constant k_F. By contrast, in I there is no great change in F, P, or T–T absorption intensity from 0–10% propanol. Thus it seems that some process other than fluorescence or triplet formation must remove the energy of S_1 from II in pure MP. An obvious process that accounts for low yields of F, P, and T–T absorption in MP glasses containing II is a direct $S_1 \rightarrow S_0$ radiationless transition. Such S_1–S_0 internal conversions have been postulated to occur in other compounds.[19-21] In work with chlorophyll,[21] dimers were suggested to exist and exhibit fluorescence quenching. This explanation seems to fit our data also. In the absence of propanol, II may form dimers as the solution is cooled. Such dimers have a low bond energy and do not influence the absorption spectrum. In the excited state dimers form and the A_2^* complex crosses to a high vibrational level of the ground state. Just as there is no evidence for H bond formation in I, there is no evidence of dimer formation. Thus it is tempting to relate the ability to form H bonds and dimeric quenching, but further work is needed to substantiate this.

Acknowledgment. This work benefited from discussions with Dr. M. W. Windsor. This work was supported by Material Lab at Wright-Patterson Air Force Base, under Contract F33615-69-C-1052.

(18) D. J. Denny, H. Sutter, R. Wood, and A. Jones, *J. Chem. Phys.*, **45**, 402 (1966).

(19) A. Buettner, *ibid.*, **46**, 1398 (1967).

(20) J. R. Merrill and R. G. Bennett, *ibid.*, **43**, 1410 (1965).

(21) P. G. Bowers and G. Porter, *Proc. Roy. Soc., Ser. A*, **296**, 435 (1967).

from diphenylmethane.[20] All compounds were purified by preparative gas–liquid partition chromatography on a 12 ft × $^1/_4$ in. SE-30 column. All compounds had physical and spectral properties in agreement with literature values. The infrared spectra were determined in carbon tetrachloride solution on a Perkin–Elmer 457 grating infrared spectrometer. All nmr spectra were recorded on a Varian Associates HA-100. Spectra were recorded in the frequency sweep mode using an internal lock of chloroform or methylene chloride. Line positions were determined by measuring the sweep frequency at peak maximum using a Hewlett–Packard 5512A counter and were estimated to be accurate to ±0.1 Hz. Values for $J_{C_{13}-H}$ were obtained as the difference between the upfield and low-field ^{13}C natural abundance satellites and are estimated to be accurate to ±0.2 Hz.

Acknowledgments. This work was supported by a Biomedical Sciences Support Grant FR-07012-02 from the National Institutes of Health and by a grant from the Research Corporation.

(20) A. G. Brook, C. M. Warner, and M. E. McGriskin, *J. Amer. Chem. Soc.*, **81**, 981 (1959).

Electrical Conductivity of γ-Irradiated Solid Monomers at Low Temperature

by Hajime Kadoi, Yoneho Tabata,* and Keichi Oshima

Department of Nuclear Engineering, Faculty of Engineering, University of Tokyo, Tokyo, Japan
(Received January 20, 1970)

The electrical conductivity of solid monomers irradiated by γ rays at −196° was measured during temperature elevation and compared with that of nonirradiated systems. For the nonirradiated systems, peaks in the current–temperature curve were observed at the transition points which were determined by X-ray diffraction and thermal analysis. Activation energies for nonirradiated systems ranged from 0.3 to 1.2 eV in the higher temperature region. At low temperatures there are pronounced differences between the irradiated and nonirradiated systems, although a negative current is observed in both cases. In nonirradiated systems this negative current might be explained as rising from the depolarization of the oriented permanent dipoles, whereas in the case of irradiated systems it might result from the annihilation of charge pairs produced by the irradiation. In the latter case, the average migration distance of the electron was estimated to be about 100 Å.

I. Introduction

Since it was found that solid organic monomers can be polymerized by radiation at low temperature, many interesting phenomena have been reported on these systems.[1] For the polymer chains to grow in the rigid solid state, it is considered that ionic processes play an important role. For the polymer chains to propagate, the intermolecular distances between the propagating end and adjacent monomer must be reduced in the solid state and a large interaction should exist between them, which can be considered to be of Coulombic nature.

Measurement of the electrical conductivity as a means to follow, both directly and indirectly, the behavior of charges produced in the solid phase is useful for studying the solid state polymerization at low temperatures, as well as for studying ionic processes in general.

The measurement of electrical conductivity of irradiated monomers, at temperatures higher than −78°, was investigated by Okamura, *et al.*[2] The present paper deals with the conductivity of solid monomers as a function of temperature after irradiation at −196°.

* To whom correspondence should be addressed.

(1) (a) H. Sobue and Y. Tabata, *J. Polym. Sci.*, **43**, 459 (1960); (b) R. Bensasson and R. Marx, *ibid.*, **48**, 53 (1960); (c) Y. Tabata, E. Oda, and H. Sobue, *ibid.*, **45**, 469 (1960); (d) Y. Tsuda, *ibid.*, **49**, 369 (1961); (e) Y. Tabata, B. Saito, H. Shibano, H. Sobue, and K. Oshima, *Kogyo Kagaku Zasshi*, **64**, 3789 (1961) (Japanese); *Makromol. Chem.*, **76**, 89 (1964); (f) Y. Amagi, and A. Chapiro, *J. Chim. Phys.*, **59**, 539 (1962); *Compt. Rend.*, **255**, 299 (1962); (g) I. M. Barkalov, V. I. Goldanskii, N. S. Enikolopyan, S. F. Terekhova, and G. M. Trofimova, *Dokl. Akad. Nauk SSSR*, **147**, 395 (1962); *J. Polym. Sci.*, **C4**, 897, 909 (1964); (h) R. Bensasson, A. Bernas, M. Bodard, and R. Marx, *J. Chim. Phys.*, **60**, 950 (1963); (i) A. Chapiro and M. Inoue, *ibid.*, **62**, 835 (1965); (j) G. H. Gerasimov, M. A. Bruck, V. F. Gromov, A. D. Abkin, P. M. Khomikhovskii, A. B. Mateeva, and V. I. Tchernysk, *Vysokomol. Soedin.*, **8**, 961 (1966); *Dokl. Akad. Nauk SSSR*, **174**, 386 (1967); (k) I. M. Barkalov, D. A. Gareeva, V. I. Goldanskii, N. S. Enikolopyan, and Al. Al. Berlin, *Vysokomol. Soedin.*, **8**, 1140 (1966); (l) R. Marx and S. F. Fenistein, *J. Chim. Phys.*, **64**, 1424 (1967); (m) T. Suzuki, Y. Tabata, and K. Oshima, *J. Polym. Sci.*, **C16**, 1821 (1967); (n) Y. Tabata, H. Shibano, K. Oshima, and H. Sobue, *ibid.*, **C16**, 1821 (1967); (o) Y. Tabata, *J. Macromol. Sci. Chem.*, **A2**, 931 (1968); (p) K. Ishigure, Y. Tabata, and K. Oshima, *ibid.*, **A1**, 591 (1967).

(2) M. Sakamoto, K. Hayashi, and S. Okamura, *Ann. Rep. Jap. Ass. Radiat. Res. Polym.*, **4**, 167 (1964).

The conductivity of 3-methylpentane (3MP) irradiated at −196° was measured for a comparison with the results obtained by Willard, *et al.*,[3] and Somogyi, *et al.*[4] Willard, *et al.*,[5] also studied the conductivity of irradiated 2-methyltetrahydrofuran and methylcyclohexane, whereas Somogyi[6] reported on the conductivity of irradiated solid alcohols.

Furthermore, the present investigators also carried out conductivity measurements during irradiation, but without success because of the noise generated in the cables.

II. Experimental Section

1. The Irradiation Vessel and Measuring Cell. The cell used for measuring the current is shown in Figure 1a. The electrodes were a set of parallel aluminum plates with size of 1 cm² and thickness of 0.5 mm. The lead-wires were made by the silver coating of steel wire with subsequent Teflon covering. By using a steel wire, the distance between the electrodes could be kept constant and the heat conductance could be reduced to eliminate atmospheric water condensation on the lead-wires. The current between the electrodes of the cell was observed to be proportional to the applied voltage up to 700 V, and it can therefore be considered that the contact between the electrodes and the sample was ohmic in nature and that space charges had no effect on the system.

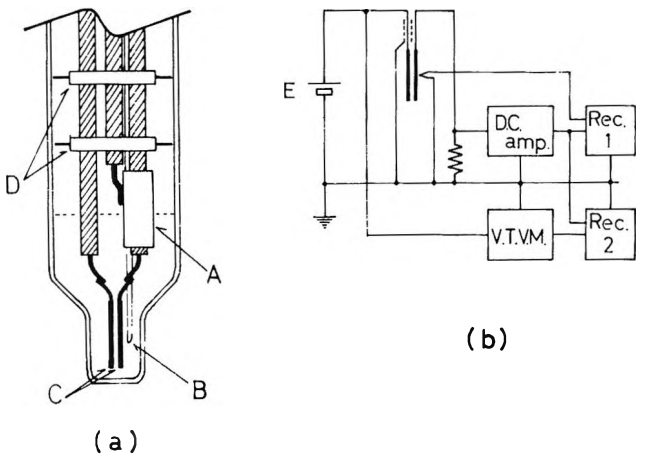

Figure 1. (a) Cell for the conductivity measurement: A, guard electrode (aluminum); B, thermocouple (copper–constantan); C, measuring electrodes (aluminum); D, stems for supporting the electrodes (Teflon).
(b) Electric circuit for the conductivity measurement.

A guard electrode was employed to exclude the effect of leakage current on the surface of the solid. Measurement of the temperature was carried out by means of a copper–constantan thermocouple which was sealed in a glass capillary tube and placed near the electrodes. The irradiation vessel was made from hard glass and had a stopcock for evacuating the system, and a tapered joint for the introduction of the samples. The terminals on the irradiation vessel were insulated by Teflon.

The purified samples were introduced into the irradiation vessel by means of vacuum distillation, cooled to liquid nitrogen temperature, and then irradiated. The current measurements were performed before and after irradiation of the sample.

2. Apparatus for Measuring Current. The circuit diagram for measuring current is shown in Figure 1b. An external field of 300 V was obtained from dry cells. Measurement of the current was achieved by means of a vibrating-reed type electrometer which can detect currents of the order of 10^{-13} A. The external field was checked with a vacuum-tube voltmeter.

The current, temperature of the sample, and the applied field were recorded simultaneously by a multi-input recorder. All the measuring systems were completely shielded from external electrostatic interferences.

3. Sample Preparation. The monomers, acrylonitrile (AN), methacrylonitrile (MAN), acetonitrile (AcN), vinyl acetate (VA), acrylamide (AA), and dimethyl itaconate (DMI), and 3-methylpentane (3MP) were obtained commercially.

AN, MAN, AcN, and 3MP were further purified by the subsequent washing with dilute sulfuric acid, dilute potassium hydroxide solutions, and then by distilled water before drying with calcium chloride and calcium hydride. These compounds were then given by a normal distillation before storing. AA was sublimed under vacuum, and DMI was twice recrystallized from methanol.

The irradiation source was a ^{60}Co source delivering a dose rate of 5.0×10^5 rads/hr as measured by the Fricke dosimeter.

The samples were irradiated *in vacuo* below 10^{-4} Torr at liquid nitrogen temperature, and the measurement of the current was started within 10 min after irradiation.

III. Results

The application of the external field initially gave rise to a transient current, due to polarization, in both the irradiated and the nonirradiated systems, although the currents were observed to be larger in the irradiated than in the nonirradiated systems. This difference in the initial current between the irradiated and the nonirradiated systems, in the case of 3MP, was quantitatively investigated by Willard, *et al.*[3]

Quite reproducible measurement could be made as to the temperature at which the peak appeared; however,

(3) B. Wiseall and J. E. Willard, *J. Chem. Phys.*, **46**, 4387 (1967).
(4) I. Kosa-Somogyi and J. Balog, "Radiation Chemistry II," Advances in Chemistry Series, No. 82, American Chemical Society, Washington, D. C., 1968, p 291.
(5) A. C. Ling and J. E. Willard, *J. Phys. Chem.*, **73**, 2408 (1969).
(6) I. Kosa-Somogyi, *Proc 9th Japan Conf. on Radioisotopes (Japan)*. 588 (1969).

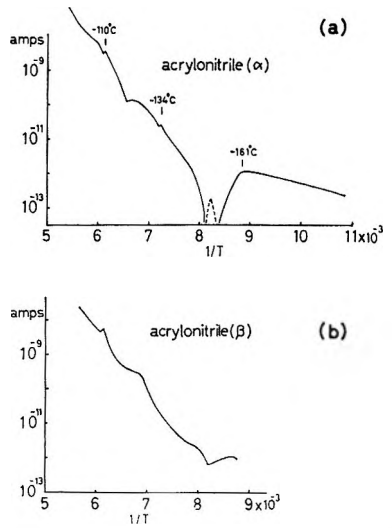

Figure 2. Current *vs.* $1/T$ for nonirradiated AN; applied voltage, 300 V. (a) α Phase (rapid cooling). Broken lines are absolute value of negative current. (b) β Phase (annealing).

the deviation of the current measurement was within 50%.

The current as a function of the temperature, in the case of the α phase of acrylonitrile, is shown in Figure 2a. The peaks at -161, -134, and $-110°$ correspond to the transitions in AN and are in good agreement with results obtained by X-ray studies[7] and from thermal analysis.[8-10] The negative peak is observed immediately after the positive peak at $-161°$. When the quenched AN was irradiated at $-196°$, the current as a function of temperature is as shown in Figures 3a, b, and c. In the case of low irradiation doses, several peaks in the irradiated and nonirradiated AN coincided with each other as shown in Figure 3a. Moreover, the shape of the current–temperature curve changed appreciably in the temperature regions at -120 and $-160°$. These differences became more pronounced at higher doses, to such an extent that negative currents were observed at very high doses as shown in Figures 3b and c. The AN annealed at $-130°$ showed only one peak at $-110°$ as shown in Figure 2b, supporting the results obtained from X-ray studies.[7] In this latter case, the monomer is in the β phase which is stable at low temperatures and therefore only the transition point from the β to the α phase appears. When AN in the β phase is irradiated to high doses, a negative current is also observed.

Although, in the case of MAN, a transition was not observed by X-ray studies[7] nor thermal analysis,[11] a peak was observed at $-98°$ if the monomer was cooled rapidly, as shown in Figure 4a(i). If the monomer is cooled again rapidly from -78 to $-196°$, no peaks are observed during temperature elevation as shown in Figure 4a(ii). This result is indicative of an unstable transition at $-98°$ which is undetectable by means of both X-ray and thermal analysis. In the case of ir-

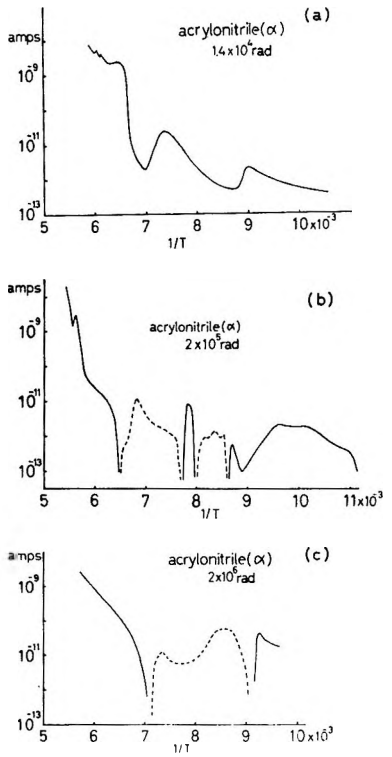

Figure 3. Current *vs.* $1/T$ for irradiated AN (α phase); applied voltage, 300 V. (a) Irradiation dose: 1.4×10^4 rads. (b) 2×10^5 rads. (c) 2×10^6 rads.

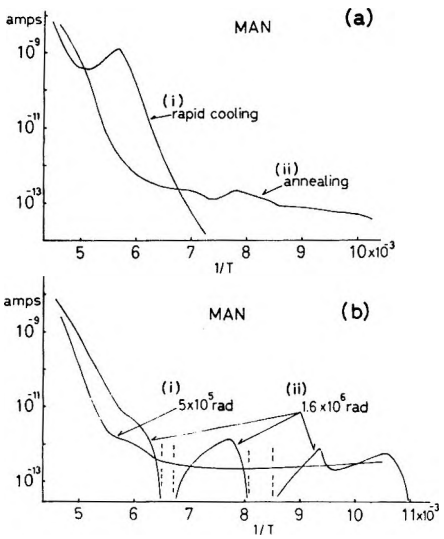

Figure 4. (a) Current *vs.* $1/T$ for nonirradiated MAN; applied voltage, 300 V; (i) rapid cooling, (ii) annealing. (b) Current *vs.* $1/T$ for irradiated MAN; applied voltage, 300 V: (i) irradiation dose: 5×10^5 rads; (ii) 1.6×10^6 rads.

(7) K. Ishigure, Thesis, University of Tokyo, 1966.

(8) R. Bensasson, A. Dwarkin, and R. Marx, *J. Polym. Sci.*, **C4**, 881 (1964).

(9) V. A. Kargin, V. A. Kabanov, I. M. Parisov, and B. P. Zubov, *Dokl. Akad. Nauk SSSR*, **141**, 389 (1961); *J. Polym. Sci.*, **C4**, 767 (1964).

(10) B. V. Lebedev, I. B. Rabinovich, and L. Ya. Martynenko, *Vysokomol. Soedin.*, **9**, 1640 (1967).

(11) Unpublished results.

radiated MAN, results are shown in Figure 4b for doses of 5×10^5 and 1.6×10^6 rads, two negative peaks being observed in the latter case.

AcN can be polymerized *via* nitrile groups with metal chloride catalyst,[12] with an electric discharge,[13] and with vacuum ultraviolet rays.[14] The current for the nonirradiated AcN was too small to detect at low temperatures. In the irradiated system a negative current was observed over a wide temperature range during temperature elevation as shown in Figure 5a.

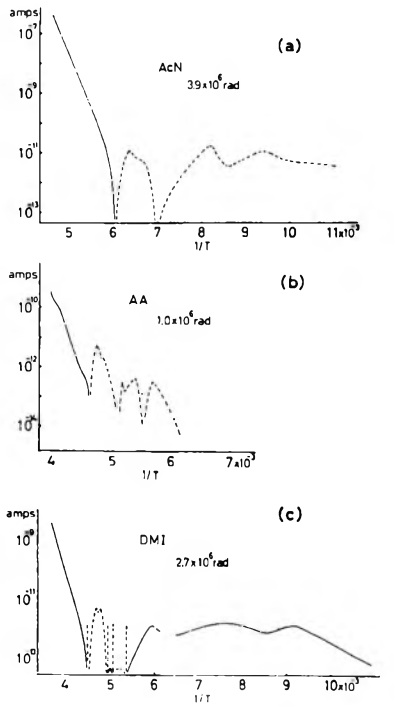

Figure 5. Current *vs.* $1/T$; applied voltage, 300 V. (a) For irradiated AcN; irradiation dose: 3.9×10^6 rads. (b) For irradiated AA, irradiation dose: 1×10^6 rads. (c) For irradiated DMI, irradiation dose: 2.7×10^6 rads.

No observable current could be detected at low temperatures for either AA or DMI in the nonirradiated state. In the irradiated systems, negative peaks were also observed for both the monomers, although these peaks appeared at higher temperatures than those of the above mentioned monomers, as shown in Figures 5b and c for AA and DMI, respectively.

In the case of VA, for the glassy state of the monomer, the nonirradiated monomer showed a negative peak at a temperature higher than −147°, following a pronounced positive peak as shown in Figure 6a. This phenomenon is similar to the negative current in the case of nonirradiated AN at −161°. The glass–crystalline transition of the nonirradiated VA obtained from these measurements does not agree well with the value obtained by thermal analysis.[15,16] In the case of the nonirradiated monomer in the crystalline state, the current could not be detected. Negative peaks were observed for the irradiated VA in the glassy state, although the temperature region where they occurred differs from that of the nonirradiated glassy state, as shown in Figure 6b. For the irradiated VA in the crystalline state, negative currents were observed in two regions, although it appeared at higher temperatures than in the case of the irradiated glassy state, as shown in Figure 6c.

In contrast to the glassy VA, 3MP glass is fairly stable at low temperatures, but even so, no current could be detected for 3MP in the nonirradiated glassy state. The results in the case of the irradiated 3MP are shown in Figure 6d where the upper curve indicates the results obtained with a guard electrode and the lower curve the results obtained without the guard electrode. The results were thus profoundly affected whether the guard electrode was used or not.

Activation energies for conductivity, ΔE, for nonirradiated systems at a higher temperature region obtained from the equation of $\sigma = \sigma_0 \exp(\Delta E/kT)$ are shown in Table I.

Table I: Activation Energies ΔE for Nonirradiated Systems at Higher Temperature Region

AN	α	0.37 eV
	β	0.44
MAN		0.85
AcN		0.35
AA		1.2
DMI		0.99
VA		0.35
MTHF		0.35[a]

[a] From Ling and Willard.[5]

IV. Discussion

When an external field is applied to nonirradiated organic systems at liquid nitrogen temperature, a transient current, due to the initial polarization, is generated which decreases within a few minutes. After this initial transient current fades away, no detectable current is observed at liquid nitrogen temperature.

When the temperature is elevated under an applied field of 300 V (6000 V/cm), the current increases with increasing temperature and reaches peak values at transition points. As temperatures at these peaks of the current correspond exactly to the transition points

(12) E. Oikawa, K. Mori and G. Saito, *Bull. Chem. Soc. Jap.*, **39**, 1182 (1966).

(13) W. G. Deichert and M. C. Tobin, *J. Polym. Sci.*, **54**, S-39 (1961).

(14) H. Kadoi, Y. Tabata, and K. Oshima, unpublished results.

(15) I. M. Barkalov, V. I. Goldanskii, N. S. Enikolopyan, S. F. Terekhova, and G. M. Trofimova, *Dokl. Akad. Nauk SSSR*, **147**, 395 (1962).

(16) I. M. Barkalov, V. I. Goldanskii, and V. B. Rapoport, *ibid.*, **161**, 1368 (1965).

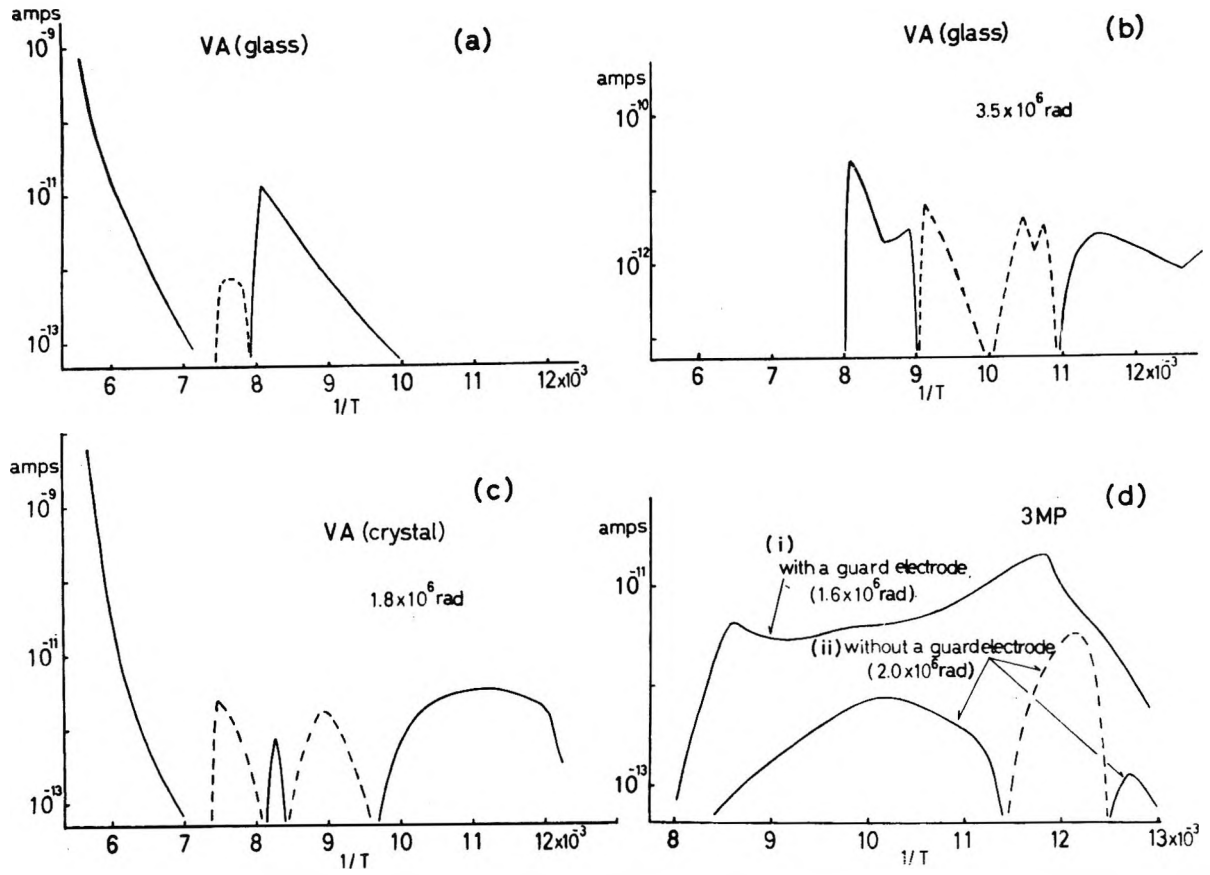

Figure 6. Current *vs.* $1/T$; applied voltage, 300 V. (a) For nonirradiated VA (glass). (b) For irradiated VA (glass): irradiation dose: 3.6×10^6 rads. (c) For irradiated VA (crystal); irradiation dose: 1.8×10^6 rads. (d) For irradiated 3MP: (i) with a guard electrode, irradiation dose: 1.6×10^6 rads; (ii) without a guard electrode, irradiation dose: 2.0×10^6 rads.

in most cases, it can be used as a method for detecting the transition points in organic solids.

When the monomers, AN, MAN, and VA, are rapidly frozen from the liquid phase to −196°, their current–temperature curves show irreversible peaks at −161, −147, and −98°, respectively, during temperature elevation from −196°. For both the monomers AN and VA negative peaks are observed immediately after the positive peaks appeared. If the monomer molecules, in an unstable state as a result of the rapid freezing are warmed up, they become rotatable by the external field, which results in a further orientation with the appearance of positive peaks. It is known from both X-ray[7] and thermal analyses[8,10] that AN has two crystal modifications, α above −110° and β below −110°. If the monomer is rapidly frozen from room temperature to −196°, the α form is quenched at this temperature. The unstable quenched α form transforms to the β form at −130° during the temperature elevation from −196°. When the temperature is further elevated, this β form again transforms to the α form at −110°. It was reported that AN has still another transition point at −160° which corresponds to the transition from the glassy to the crystalline state.[8,9] However, a glassy state of AN has not been confirmed by X-ray analysis,[7] and it is therefore difficult to clarify the nature of this transition from conductivity measurements. It is postulated that this transition is the temperature (−160°) at which postpolymerization starts. In the case of VA, the corresponding transition from the glassy to the crystalline state was observed at −129°[15,16] although the present investigation indicates the transition to be at −147°, based on the conductivity measurements. For both these monomers, the negative peaks which follow the positive peaks are believed to be due to a depolarization which results from an increase in the thermal energy of the monomer molecules during temperature elevations, as shown in Figures 7a and b.

In the case of 3MP, Willard, *et al.*,[3] observed a negative peak without using a guard electrode. When a guard electrode is not used, a negative peak can be observed in accordance with that of Willard; on the other hand, when the guard electrode is used no negative peak can be detected, in accordance with the results of Somogyi.[4] From these apparent discrepancies in the results, it is evident that the construction of the measuring cell plays an important role, and that special care should be taken to avoid the formation of surface currents. The cell used in the present investigation was of such a construction that a guard electrode had to be used to avoid surface conduction.

In the case of MAN, an irreversible positive peak was

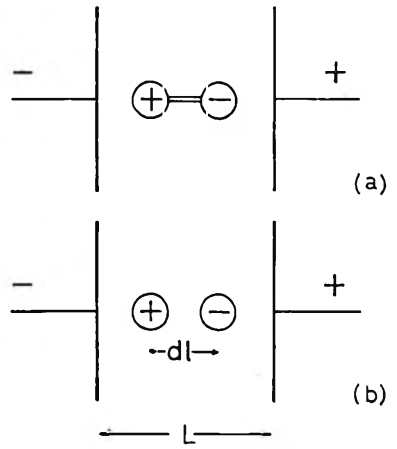

Figure 7. Schematic models of randomization of oriented dipoles and annihilation of ion pairs: (a) depolarization; (b) annihilation.

observed, suggesting an unstable transition, although no such a transition was detected by X-ray analysis.[7]

In irradiated systems an initial transient current, which is larger than that of nonirradiated systems, was observed. The differences between irradiated and nonirradiated systems are based on a charge separation due to the irradiation. Willard quantitatively investigated the conductivity of irradiated 3MP and concluded that this charge carrier is due to weakly trapped electrons and positive ions.[3]

During the temperature elevation of irradiated systems, the current initially increases rapidly in comparison with that of nonirradiated systems. The current then decreases and eventually becomes negative and then finally the current increases to positive values again. The peak of the current splits into two or more parts, depending on both the irradiation dose and the nature of the sample. The negative peak corresponds qualitatively to a phenomenon similar to that of the depolarization in nonirradiated systems as observed in both crystalline AN and glassy VA. Using a scavenger technique in the case of 3MP, Willard concluded that the first positive peak is due to strongly trapped electrons while the following negative peak is the result of depolarization and relaxation phenomena, dependent on radiation-induced charges.[3]

Let us consider these positive and negative peaks in more detail. It is certain that these peaks result from irradiation; moreover, the existence of a negative current suggests that a stronger electric field than the external applied field should act in a direction opposite to the applied field. The electrons produced by irradiation may be trapped under the influence of the strong Coulombic field of the parent ions. Figures 8a and b show a one-dimensional model for the potential curve of traps under the strong Coulombic field of a parent ion. An electron captured in such a trap is fated to recombine with the parent ion.

However, as these traps are randomly distributed

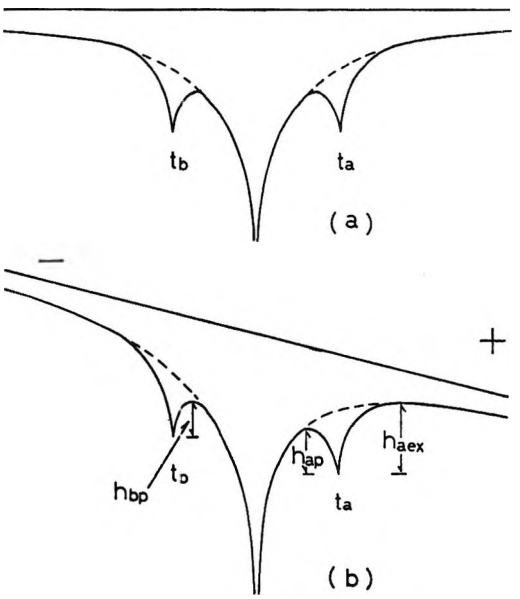

Figure 8. Potential curves for traps in the vicinity of parent ion: (a) without an applied field; (b) with an applied field.

around the corresponding parent ions, no current should be observed, even if the temperature is elevated. When an external field is applied to the irradiated solid, the potential of the system changes as indicated on the potential curve in Figure 8b. The trap between a parent ion and the positive electrode is represented by t_a, and the trap between the negative electrode and a parent ion is represented by t_b in Figure 8. The height of t_a and t_b is then altered by the external field. The height of each trap, h_{ap}, h_{aex}, h_{bp}, and h_{bex} is, respectively, defined as shown in Figure 8b, and it is clear that h_{ap} and h_{bp} are of equal depth when no external field is applied. However, if h_{ap} exceeds h_{bp} during the application of an external field, then firstly the condition prevails where $n_b > n_a$, and then, during the elevation of the temperature, the condition prevails where $n_a > n_b$, where n_b and n_a represent the number of electrons released from the traps t_b and t_a, respectively. The electron released from t_b will result in the formation of a positive current by being attracted to the positive electrode or by recombination with the parent ion. However, the electron released from t_a may recombine with the parent ion and produce a negative current if $h_{ap} < h_{ex}$, but, on the other hand, it may produce a positive current if $h_{ap} > h_{ex}$. The direction of flow of these latter electrons depends on the field strength of the parent ion relative to that of the external field. If this reasoning is applied to the negative peaks, an increase in the external field should result in a decrease of peak intensity in accordance with the experimental results of Willard.[3] The present model thus not only explains the formation of positive peaks but also the formation of the following negative peaks qualitatively fairly well.

In some monomers several negative peaks exist in the current–temperature curves of the irradiated system.

Table II: Mean Distances of Migration of Electrons for Annihilation[a]

	I, Mrad		dl, Å
3MP	1.4	+	157
with a guard	1.5	+	110
electrode	1.6	+	115
	3.9	+	58
3MP	1.4	+	64
without a		−	20
guard elec-	1.9	+	43
trode		−	14
AN	0.6	+	170
	2.0	+	150
		−	200
AcN	3.9	−	150
AA	1.0	+	69
DMI	2.7	−	30
		−	15
VA	1.5	+	14
(crystal)		−	17
	1.8	+	26
		−	36
VA	1.4	+	86
(glass)	1.5	+	120
	3.5	+	6
		−	9

[a] +, positive peak; −, negative peak.

These results suggest that there should be different types of traps associated with the parent ions in the same system. If the G values for the formation of electrons which are captured by the above mentioned different kind of traps are known, the average distance which such an electron migrates before annihilation can be estimated from both the separating distance of the electrodes of the cell and the total charges flowing in the electrometer. This relation is given by

$$dl = \frac{C_{ex}}{C_{in}} \times L; \quad C_{in} \propto GI$$

where dl is the mean traveling distance of an electron before annihilation, L the distance between the electrodes, C_{ex} is the total charge flowing in the electrometer, C_{in} is the total charge produced in the sample between the electrodes of the cell, and I is the radiation dose. Unfortunately, the G values for charge production under the present experimental conditions are not known exactly. In the case of 3MP, Willard assigned a value of 1 to the G value for the formation of charges. This value, however, seems to be overestimated, because this value takes into account all the electrons trapped in 3MP. Postulating a G value of about 0.1 for each trapping, the migration distance of the electron can be calculated to be about 100 Å, as shown in Table II.

Spectroscopic Properties of Solid Solutions of Erbium and Ytterbium Oxides

by Leonard Gruss[1a,b]

Pitman-Dunn Research Laboratories, Frankford Arsenal, Philadelphia, Pennsylvania

and Robert E. Salomon*

Department of Chemistry, Temple University of the Commonwealth System of Higher Education, Philadelphia, Pennsylvania 19122 *(Received April 9, 1970)*

Solid solutions of Er_2O_3 and Yb_2O_3 were prepared over the entire composition range. The visible and ultraviolet diffuse reflectance spectra, the magnetic susceptibility, and the lattice parameters of these solutions were determined. An unusual competition in the intensity stealing of an ultraviolet charge-transfer band was observed and analyzed.

Introduction

Paramagnetic ions in ionic lattices are subject to perturbations which may for convenience be classified into two categories. The first type are the crystal field perturbations together with possible covalent contributions from the neighboring ions. This is the full perturbation when the paramagnetic ions are dilute. The second type of perturbation, which comes into play at higher concentrations, involves the resonance interactions between pairs and higher groups of identical ions. These interactions, unlike the former, are difficult to observe directly because changes in concentration not only change the resonance interactions but, in general, also change the crystal field produced by the second coordination sphere.

The rare earth ions are unique in that they all produce nearly the same electrostatic field, since they differ only in their number of f electrons, and these are shielded by a closed shell of electrons with fairly similar radii. This similarity in outer electron configuration is of course the factor that makes it difficult to separate the rare earths from one another and conversely leads to isomorphous substitution. For many pairs this substitution occurs over the entire concentration range without change in structure.

In this work, the Er_2O_3–Yb_2O_3 system was chosen for study. The sesquioxides of Er_2O_3 and Yb_2O_3 are both cubic and belong to the Ia3 space group with 16 molecules per unit cell.[2] The crystal radii of trivalent Er and Yb are 0.87 and 0.85 Å, respectively. The oxygens are arranged as a slightly asymmetric tetrahedron about the rare earth ion with metal–oxygen distances of about 2.0 Å.[3] The electronic configurations of Er^{3+} and Yb^{3+} are $4f^{11}5s^25p^6$ and $4f^{13}5s^25p^6$ and the ground states are $^4I_{15/2}$ and $^2F_{7/2}$, respectively. The energy levels of Er^{3+} and Yb^{3+} in a number of different hosts are given by Dieke.[4] Er^{3+} exhibits a number of crystal field transitions in the visible and ultraviolet, while for Yb^{3+} the $^2F_{7/2} \rightarrow {}^2F_{5/2}$ manifold occurs in the region of 9700 Å.[5]

In the ultraviolet region below 2500 Å the optical transitions are described as either charge transfer from the oxygen 2p levels to empty 4f levels associated with the rare earth or transitions from oxygen 2p orbitals to oxygen 3s orbitals.[6] The former is characteristic of Yb_2O_3 while the latter is characteristic of Er_2O_3.

Changes in the positions and intensities of electronic absorption bands in solid solutions of Er_2O_3 with Yb_2O_3 can be attributed primarily to resonance interactions or possibly to small variations in the lattice parameters as the composition is varied.

Experimental Section

Erbium and ytterbium oxide powders, 99.9% pure, were purchased from the Michigan Chemical Corp., St. Louis, Mich. Solid solutions were prepared by first mechanically mixing appropriate proportions of the two oxides. The mechanical mix was then dissolved in hot 10% HCl, and the solution was filtered. Coprecipitation of the hydrous oxides was effected by addition of sufficient NH_4OH to ensure complete precipitation. The filtered precipitates were thoroughly

* To whom correspondence should be addressed.

(1) (a) This research is part of a dissertation submitted by L. Gruss to the Temple University Graduate Board in partial fulfillment of the requirements for the degree of Doctor of Philosophy. (b) This work was supported by U. S. Army Material Command under Project No. 1T061102B32A, Research in Materials.

(2) R. S. Roth and S. J. Schneider, *J. Res. Nat. Bur. Stand., Sect. A*, 64, 309 (1960).

(3) R. W. G. Wyckoff, "Crystal Structures," Vol. I, Interscience, New York, N. Y., 1948, pp 2–4.

(4) G. H. Dieke, "Spectra and Energy Levels of the Rare Earth Ions in Crystals," Wiley, New York, N. Y., 1968, Chapter 13.

(5) J. Hoagschagen, *Physica*, 11, 513 (1944).

(6) C. K. Jorgensen, R. Pappalardo, and E. Rittershaus, *Z. Naturforsch.*, 20A, 54 (1964).

washed with large volumes of hot distilled water until the washings were neutral to litmus. The precipitates were then dried, ground with a mortar and pestle, and passed through a 74-μ sieve. The fine powder was then heated in air in a quartz tube to 1000° and held at this temperature for over 100 hr. The long heating period ensured that the final samples were truly solid solutions and also eliminated any water, carbon dioxide, or nitrogen compounds. All samples, including pure Er_2O_3 and Yb_2O_3, were subject to the exact procedure described in the above to facilitate comparison of data.

X-Ray diffraction patterns were obtained on all samples using a Debye-Scherrer 114.59-mm camera (Norelco) and a Norelco Basic X-ray diffraction unit employing filtered copper Kα radiation. Lattice parameters were calculated from the Straumanis positioned film by averaging over the last ten hkl reflections.

Diffuse reflectance spectra between 220–700 mμ were obtained using a Cary Model 14 spectrophotometer equipped with a Model 1411 diffuse reflectance (ring collector) accessory. Most of the spectra were taken at approximately 297°K. For low-temperature measurements a specially designed cell[7] which permitted measurements down to 78°K was used.

Magnetic susceptibility measurements were made using the Guoy method at a temperature of 295°K.

Results

The X-ray patterns were indicative of solid solutions. The lattice parameters of pure Er_2O_3 and Yb_2O_3 agreed with literature values.[2,8] The lattice parameters, which varied linearly with composition, are given in Table I.

The magnetic susceptibility varied in a completely linear manner with composition within the experimental error of ±2%. The susceptibilities of pure Er_2O_3 and pure Yb_2O_3 were 9.2 and 4.2 BM, respectively, in agreement with reported values.[9-12]

Table I: Lattice Parameters and Concentrations of Er_2O_3–Yb_2O_3 Solid Solutions

Composition, mol %	Lattice parameter, Å
Er_2O_3	10.5481 ± 0.0011
99 Er_2O_3–1 Yb_2O_3	10.5475 ± 0.0008
95 Er_2O_3–5 Yb_2O_3	10.5415 ± 0.0013
90 Er_2O_3–10 Yb_2O_3	10.5380 ± 0.0014
75 Er_2O_3–25 Yb_2O_3	10.5194 ± 0.0011
65 Er_2O_3–35 Yb_2O_3	10.5096 ± 0.0011
50 Er_2O_3–50 Yb_2O_3	10.4914 ± 0.0011
35 Er_2O_3–65 Yb_2O_3	10.4740 ± 0.0016
25 Er_2O_3–75 Yb_2O_3	10.4621 ± 0.0008
10 Er_2O_3–90 Yb_2O_3	10.4451 ± 0.0013
5 Er_2O_3–95 Yb_2O_3	10.4389 ± 0.0009
1 Er_2O_3–99 Yb_2O_3	10.4349 ± 0.0008
Yb_2O_3	10.4336 ± 0.0008

In the visible region of the spectrum the sharp bands characteristic of Er^{3+} were observed. Table II lists the bands at several compositions. The observed shifts were less than the experimental accuracy of 10 cm^{-1} at 297 and 78°K. In the region between 39,600 and 42,500 cm^{-1} the strong absorption characteristic of $O_{2p} \rightarrow Yb_{4f}$ and $O_{2p} \rightarrow O_{3s}$ transitions were observed. The spectra of pure Er_2O_3, pure Yb_2O_3 and 25 Yb_2O_3–75 Er_2O_3 are shown in Figure 1. The shoulder in pure Yb_2O_3 was resolved into a band by assuming both a gaussian shape and that the absorbance in the region from 240 to 250 mμ is free from contributions from the $O_{2p} \rightarrow O_{3s}$ band. The latter is clearly suggested by the observed spectrum. When this was done, the entire spectrum in the region 250 to 220 mμ for all 11 compositions fit the following formula rather closely

$$A(X,\lambda) = A^{\circ}_{Er_2O_3}(\lambda) + A^{*}_{Yb_2O_3}(\lambda)[1 - (1 - X_{Yb})^4] \quad (1)$$

where $A^{\circ}_{Er_2O_3}$ is the apparent absorbance of pure Er_2O_3, $A^{*}_{Yb_2O_3}$ is the resolved $O_{2p} \rightarrow Yb_{4f}$ apparent absorbance of pure Yb_2O_3, and X_{Yb} is the mole fraction of Yb_2O_3.

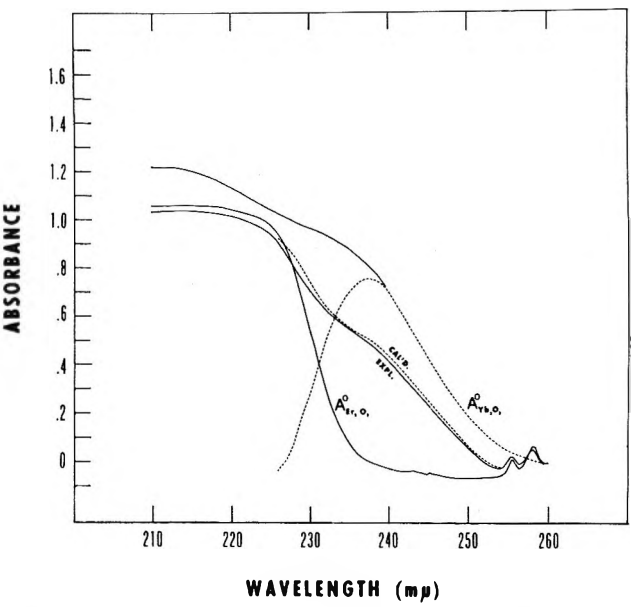

Figure 1. Comparison of experimental (—) and calculated (- - -) absorbance curves of the 75 Er_2O_3–25 Yb_2O_3 solid solution in the ultraviolet region at room temperature. The postulated $A^{\circ}_{Er_2O_3}$ and $A^{\circ}_{Yb_2O_3}$ curves are also shown.

(7) J. G. Bendoraitis, Ph.D. Thesis, Temple University, Philadelphia, Pa., 1968.

(8) National Bureau of Standards Circular 8, U. S. Government Printing Office, Washington, D. C., 1958, p 539.

(9) F. Hund, *Z. Phys.*, **33**, 855 (1925).

(10) J. H. Van Vleck and A. Frank, *Phys. Rev.*, **34**, 1494, 1625 (1929).

(11) W. Klem and A. Koczy, *Z. Anorg. Allg. Chem.*, **233**, 84 (1937).

(12) M. M. Pinaeva and E. I. Krylov, *Zh. Neorg. Khim.*, **11**(4), 728 (1966).

Table II: Comparison of the Absorption Peak Positions of Solid Solutions of Er_2O_3–Yb_2O_3 with Pure Er_2O_3 at Room Temperature

Er_2O_3 (10^4 cm^{-1}) $\bar{\nu}$	95 Er_2O_3–5 Yb_2O_3 (10^4 cm^{-1}) $\bar{\nu}$	90 Er_2O_3–10 Yb_2O_3 (10^4 cm^{-1}) $\bar{\nu}$	75 Er_2O_3–25 Yb_2O_3 (10^4 cm^{-1}) $\bar{\nu}$	65 Er_2O_3–35 Yb_2O_3 (10^4 cm^{-1}) $\bar{\nu}$	50 Er_2O_3–50 Yb_2O_3 (10^4 cm^{-1}) $\bar{\nu}$
1.5119	1.5121	1.5119	1.5118	1.5120	1.5121
1.5280	1.5279	1.5282	1.5284	1.5282	1.5272
1.9154	1.9150	1.9146	1.9154	1.9148	1.9154
1.9252	1.9252	1.9248	1.9252	1.9252	1.9247
2.0447	2.0440	2.0448	2.0438	2.0443	2.0445
2.6331	2.6344	2.6337	2.6332	2.6332	2.6328
2.6380	2.6398	2.6386	2.6398	2.6398	2.6393
2.7222	2.7229	2.7244	2.7235	2.7235	2.7243
3.8778	3.8796	3.8796	3.8796	3.8769	3.8782

Er_2O_3 (10^4 cm^{-1}) $\bar{\nu}$	35 Er_2O_3–65 Yb_2O_3 (10^4 cm^{-1}) $\bar{\nu}$	25 Er_2O_3–75 Yb_2O_3 (10^4 cm^{-1}) $\bar{\nu}$	10 Er_2O_3–90 Yb_2O_3 (10^4 cm^{-1}) $\bar{\nu}$	5 Er_2O_3–95 Yb_2O_3 (10^4 cm^{-1}) $\bar{\nu}$
1.5119	1.5122	1.5121	1.5117	1.5118
1.5280	1.5277	1.5280	1.5275	1.5280
1.9154	1.9154	1.9152	1.9159	1.9156
1.9252	1.9252	1.9252	1.9257	1.9258
2.0447	2.0453	2.0446	2.0445	2.0445
2.6331	2.6337	2.6332	2.6332	2.6328
2.6380	2.6394	2.6398	2.6376	2.6398
2.7222	2.7247	2.7225	2.7230	2.7249
3.8778	3.8776	3.8786	...	...

The apparent absorbance is the logarithm of the ratio of light diffusely reflected from a $MgCO_3$ white blank to the intensity of light diffusely reflected from the sample. Although the relation between the true absorbance and the apparent absorbance (*i.e.*, diffuse reflectance) is a complicated function of particle size and absorption coefficient, it is clear that if the particle size distribution of two samples is the same, and the apparent absorbances are the same, then the true absorbances are the same. The most important aspect of eq 1 and the observed data is the relative insensitivity of apparent absorbance to composition. It is recognized that although the diffuse reflectance may distort the spectrum the correlations at a given wavelength are quite good as long as the absorbance does not become too large. A further justification for the use of apparent absorbance data in this work was provided by a check on the diffuse reflectance on mechanical mixtures of Er_2O_3 and Yb_2O_3. The total apparent absorbances in this check were indeed sums of the separate absorbances.

Discussion

The linear dependence of magnetic susceptibility on concentration and the invariance of the crystal field peaks with composition are in accord with the view that the f orbitals on different atoms do not mix to any significant degree and that the crystal field about each metal ion is invariant with composition. The small but significant shift in lattice parameter (0.1 Å) would be expected to cause some shift in those peaks. The absence of any such shift is surprising if all the metal ion–oxygen distances vary as does the lattice parameters. It is conceivable that the individual metal–oxygen distances are preserved and that the lattice parameters reflect any average change in bond length.

Transitions involving f → d, f → g, f → p, etc., for Er^{3+} and Yb^{3+} occur in the vacuum ultraviolet[13–15] and, hence, do not overlap the charge-transfer band observed in this work. Loh[16] has shown that the lowest 4f → 5d band of Er^{3+} and Yb^{3+} in a CaF_2 crystal at room temperature occurs at 156 and 141 mμ, respectively. Hence, transitions involving 4f → 5g, 4f → 6p, etc., would absorb at a much higher energy so that these intraatomic transitions are well enough removed from the charge-transfer bands described here.

The most striking result of this work is eq 1. The term $[1 - (1 - X_{Yb})^4]$ is the fraction of oxygens adjacent to at least one ytterbium. Hence, the intensity of the charge-transfer band originating on a given oxygen would appear to be independent of the number of terminal states or independent of the degeneracy of the final level. From another point of view, eq 1 appears to violate Beer's law.

We propose the following explanation of this result. The transition $O_{2p} \rightarrow Yb_{4f}$ may be nominally forbidden

(13) G. H. Dieke and H. M. Crosswhite, *Appl. Opt.*, **2**, 675 (1963).

(14) S. R. Sinha, "Complexes of the Rare Earths," Pergamon Press, New York, N. Y., 1966, p 91.

(15) B. W. Bryant, *J. Opt. Soc. Amer.*, **55**, 771 (1965).

(16) E. Loh, *Phys. Rev.*, **147**, No. 1, 332 (1966).

or extremely weak since the overlap between these orbitals is negligible because of the shielding of the 4f orbitals by the $5s^25p^6$ orbitals. The oxygen 3s orbitals which have a larger radius may, on the other hand, overlap the 4f orbitals and mix with them. They are fairly close in energy. The $O_{2p} \rightarrow O_{3s}$ transition is strongly allowed. The mixing coefficients can be readily calculated using the method of linear variations. In this analysis, the approximations that f orbitals on different ytterbiums are orthogonal, that f orbitals are orthogonal to the O_{3s} orbitals, and that the matrix elements of the Hamiltonian connecting the O_{3s} orbital with each 4f orbital are identical, were made. These are essentially the Hückel MO approximations. The result which emerges from this analysis is that no matter how many Yb ligands surround an oxygen only one f level is perturbed and of course this is the only level which contains any 3s character. The square of the coefficient of the 3s function when there are jYb ligands, L_j, is found in eq 2 to be

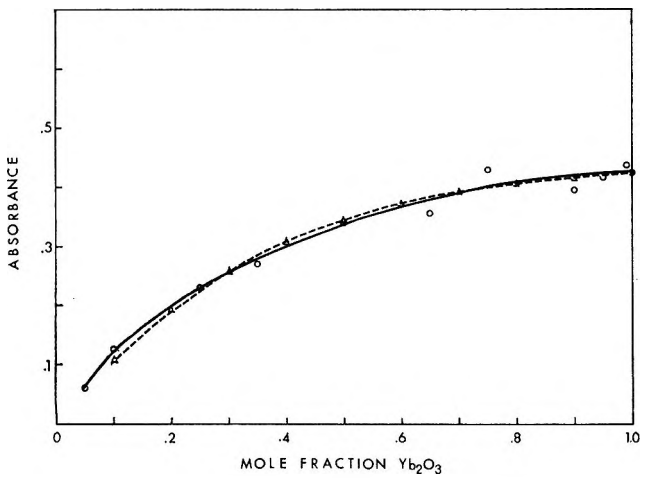

Figure 2. Comparison of the experimental (—) and calculated (- - -) absorbance as a function of mole fraction at a wavelength of 245 mμ.

$$L_j(\theta) = \frac{(\theta - \sqrt{\theta^2 + 4j})^2}{4j + (\theta - \sqrt{\theta^2 + 4j})^2} \quad (2)$$

where

$$\theta = \frac{\langle 3s|H|3s\rangle - \langle 4f|H|4f\rangle}{\langle 3s|H|4f\rangle} \quad (3)$$

$L_j(\theta)$ approaches 0.5 as θ approaches 0 and $L_j(\theta)$ becomes proportional to j as θ goes to infinity. $L_j(\theta)$ is proportional to the intensity of the transition. Hence for small θ ($\theta < 1$) the intensities as can be seen from eq 2 are nearly equal ($L_1(1) = L_2(1) = L_3(1) = L_4(1)$). Although the intensities for one, two, three, and four Yb ligand environments approach each other as $\theta \rightarrow 0$, the energy of the perturbed 4f level is expected to shift. The difference in energy between the perturbed f levels when there are n and n' ligands is found to be

$$En - En' = \frac{\langle 3s|H|3s\rangle - \langle 4f|H|4f\rangle}{2} \times \left[\sqrt{1 + \frac{4n}{\theta^2}} - \sqrt{1 - \frac{4n'}{\theta^2}}\right] \quad (4)$$

For $\theta = 1$, the calculated shift is less than 25 Å which is within experimental observation. Using the L values calculated from eq 2 at $\theta = 1$ and the statistical equation which follows, an almost perfect fit of the

$$A = A_{Er_2O_3} + \frac{A^\circ_{Yb_2O_3}}{L_4}(4X_{Yb}(1 - X_{Yb})^3L_1 + 6X^2_{Yb}(1 - X_{Yb})^2L_2 + 4X^3_{Yb}(1 - X_{Yb})L_3 + X^4_{Yb}L_4) \quad (5)$$

absorbance data was obtained. In this equation we have multiplied the fraction of oxygens surrounded by j ligands by L_j and summed the results. The remarkable fit of this equation to the experimental data is illustrated at a selected wavelength (245 mμ) by Figure 2.

Infrared Study of the Effect of Surface Hydration on the Nature of Acetylenes Adsorbed on γ-Alumina

by M. M. Bhasin,* C. Curran, and G. S. John

Department of Chemistry and the Radiation Laboratory,[1] University of Notre Dame, Notre Dame, Indiana 46556
(Received May 1, 1970)

The effect of alumina surface hydration on the nature of acetylenes absorbed on transparent plates of high surface area γ-alumina was studied by infrared spectroscopy and gravimetric measurements in the region of 4000–1100 cm^{-1}. An attempt has been made to identify the nature of the chemisorbed acetylenes and to explain the nature of active sites responsible for chemisorption of acetylenes. In case of acetylene and methylacetylene the chemisorbed complex is formed by eliminating an acetylenic proton which in turn (depending on the extent of surface hydration) migrates to an isolated oxide ion or an oxide ion adjacent to another hydroxyl group or a cluster of hydroxyl groups. The first process is favored at higher predrying temperatures (~800° and above) while the last two processes are favored at lower temperatures. The chemisorbed complex is probably formed by the donation of an electron from the carbanion of the acetylene to an aluminum ion on the surface, thus forming what be may called a "surface aluminum monoacetylide." Dimethylacetylene, on the other hand, is adsorbed as a surface complex where π electron of the C≡C bond forms a bond with either an aluminum ion or a hydrogen bond with the hydroxyl groups. Adsorbed acetylenes also underwent self-hydrogenation to form surface alkyl groups and carbon. There was also some evidence of polymerization of the acetylenes. Thus, it is concluded that the surface of dried γ-alumina contains electron poor and electron rich sites, *viz.*, aluminum ions, oxide ions, and hydroxyl groups, which can act as Lewis acid and base or a Brønsted acid and base. The concentration of these sites, termed ion-pair sites, was found to be ~10^{13} per square centimeter of surface.

Introduction

γ-Alumina and other active aluminas, used as catalysts and catalyst supports, have been studied intensively for many decades yet the nature of the sites responsible for their activity remains controversial.

Recent infrared studies of γ-alumina[2a,b] and of various adsorbates on activated aluminas[3–6] have advanced our understanding of chemisorbed complexes and of active surface sites. The present study was undertaken to determine the effect of surface hydration on the nature of active sites on dry γ-alumina and as to how this affects the structure of the chemisorbed complex. With this aim in mind, acetylene, methylacetylene, and dimethylacetylene adsorbed on transparent γ-alumina (dehydrated at different predrying temperature) aerogels were studied by infrared spectroscopy. A special cell was designed to facilitate the necessary heat treatment of γ-alumina as well as to permit measurement of gravimetric adsorption and infrared absorption in a single cell.

Experimental Section

A. Preparation and Purification of Materials. γ-Alumina aerogel of high transparency was prepared by procedures similar to those described in the literature.[2a,b] These aerogel plates of 2–5 mm thickness transmitted about 70–90% of the incident radiation in the region of 2000–4000 cm^{-1}. Below 2000 cm^{-1} the transparency of the aerogels decreased sharply; they became opaque beyond 1100 cm^{-1} due to the strong absorption of the Al–O vibrations.

Methylacetylene was obtained from the Matheson Co., Inc.; it had a stated purity of 98% minimum. As an infrared spectrum of the gas at a pressure of about 15 cm did not show evidence of impurities, the gas was not further purified.

Acetylene was also obtained from the Matheson Co., Inc. and was stated to have a minimum purity of 99.5%. The acetylene was stripped of any residual acetone by passing it through two traps kept at Dry Ice temperature (−78°). Purified acetylene did not show any impurity bands in the infrared spectrum at a pressure of 15 cm.

Dimethylacetylene (DMA) was obtained from Farchan Research Laboratories (28915 Anderson Road, Wickliffe, Ohio). A gas chromatographic analysis of the material showed that it contained some low boiling and some higher boiling impurities amounting in total to about 3%. Low boiling impurities were removed by freezing and degassing three times at a pressure of

* To whom correspondence should be addressed at Union Carbide Corporation, Chemicals and Plastics, Research and Development Department, P. O. Box 8361, South Charleston, W. Va. 25303.

(1) The Radiation Laboratory is operated by the University of Notre Dame under contract with the Atomic Energy Commission. This is A.E.C. Document No. COO-38-622.

(2) (a) J. B. Peri and R. B. Hannan, *J. Phys. Chem.*, **64**, 1526 (1960). (b) J. B. Peri, *ibid.*, **69**, 211 (1965).

(3) J. B. Peri, *Actes Congr. Int. Catal. 2nd, Paris*, **1**, 1353 (1961).

(4) D. J. C. Yates and P. J. Lucchesi, *J. Chem. Phys.*, **35**, 243 (1961).

(5) J. B. Peri, *J. Phys. Chem.*, **69**, 220 (1965).

(6) N. D. Parkyns, "Third Congress on Catalysis," Vol. II, North Holland Publishing Co., Amsterdam, 1965, p 914.

10^{-5} mm. High boiling impurities were removed by vacuum distillation from a trap at −45° (Dry Ice acetone mixture) to a trap at −196° (liquid nitrogen). Mass spectrometric and gas chromatographic analysis of the purified DMA indicated only a trace of a high boiling impurity (less than 0.02%). Total impurities in the purified product were less than 0.04%.

Reagent grade oxygen was obtained from the Matheson Company, Inc. The listed maximum limit of total impurities was 0.18 mol %, and the water content was less than 0.0002 mol %.

B. Vacuum System. A portable vacuum system was built on the sliding top of a rolling cart. The table top of the cart could be moved vertically or horizontally. The vacuum system consisted of a mercury diffusion and the usual combination of Pirani gauge, McLeod gauge, manometer, traps, and an automatic Toepler pump for collecting desorbed gases. Dynamic vacuum of the order of 10^{-5} to 10^{-6} mm was repeatedly obtained.

C. Adsorption and Infrared Spectral Measurements. Gravimetric adsorption and infrared spectral measurements were made in a single cell which has been described earlier.[7] All such measurements were made at room temperature. Weight changes of the order of 0.04 mg were measured using a cathetometer. Cells with KBr as well as CaF_2 windows were used during this investigation. Most of the spectra were obtained with Perkin-Elmer Model 421 spectrometer; in some of the earlier work a Perkin-Elmer Model 21 spectrometer was used. The aerogel plate was cleaned after each set of adsorption experiments by treating with oxygen for a few hours at 500–900°. The aerogel used to study the effect of drying temperature on the nature of chemisorption was always dried by evacuating it at a specified temperature between 400–900° for about 2–6 hr.

Results

A. Surface Hydroxyl Groups. The intensity of the three major OH stretching bands between 3800 and 3700 cm^{-1} (3798, 3738, 3700 cm^{-1}, and shoulders around 3780 and 3755) decreased as the predrying temperature was increased from 550 to 880° (Figure 1). These results are quite similar to those obtained in earlier investigations.[2a,b] The bands at 2340, 1560, and 1475 cm^{-1} are very likely due to an impurity or impurities associated with trapped or adsorbed CO_2. Similar bands have been reported in the literature.[8] The intensity of these impurity bands decreases only on calcination in oxygen at high temperature (~800–900°).

The γ-alumina is known to have a defect spinel structure with a unit cell of $Al_{21\frac{1}{3}}O_{32}$. The defect spinel structure[9] is of considerable significance in many catalytic systems as it possesses certain sites which are essentially unsaturated with respect to partial covalency. The γ-alumina surface is hydrophilic and when the water is removed by heating at high temperatures *in vacuo*, the surface of γ-alumina is terminated by different proportions of O^- ions, OH groups and Al^+ ions. An empirical model for the dehydration of the surface of γ-alumina has been presented[3] and infrared studies have been made by many workers. The infrared spectra of γ-alumina, at different levels of dehydration, obtained by the authors agreed very well with those obtained by Peri.[1,2] Three major types of hydroxyl groups (actually five or more types) exist on the surface of γ-alumina. These hydroxyl groups differ in that they have different electronic and structural environments and thus have different acidic character. The total number of such hydroxyl groups decreases sharply when γ-alumina is dried between 400 and 900°. Thus the greater the degree of dehydration, the greater the number of exposed aluminum ions, oxide ions, surface and lattice defects, and the lesser the number of OH groups. These changes in the surface of γ-alumina upon dehydration strongly influenced the mode of adsorption of acetylenes.

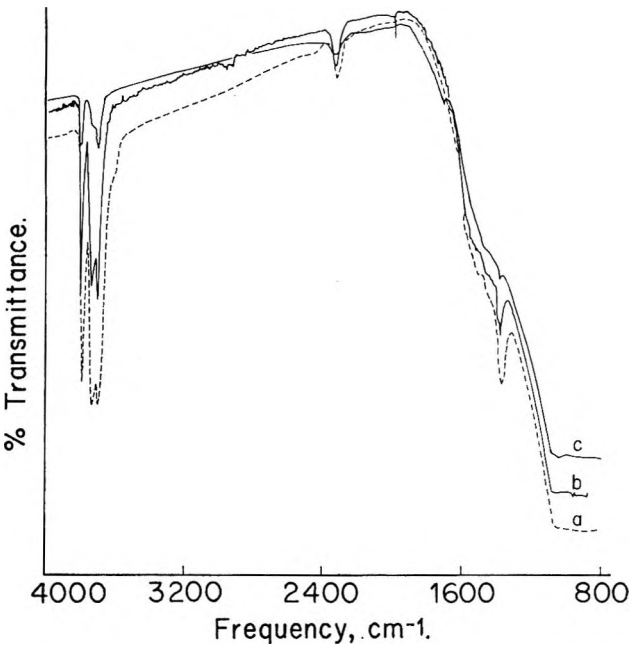

Figure 1. Infrared spectra of γ-alumina predried at different temperatures: (a) 550°; (b) 725°; and (c) 880°.

B. Ir Measurements of Adsorbed Acetylenes. Acetylene. Adsorption of acetylene was investigated on γ-alumina dehydrated at 500, 750, and 800°. On 550° predried γ-alumina, adsorption of acetylene at 1 mm and 12 mm pressure gave spectra (a) and (b) of Figure 2, respectively. Most of the adsorption bands due to physisorbed and some of the absorption bands due to

(7) M. M. Bhasin, C. Curran, and G. S. John, *Spectrochim. Acta*, **23A**, 455 (1967).

(8) L. H. Little, "Infrared Spectra of Adsorbed Species," Chapter 3, Academic Press, New York, N. Y., 1966.

(9) T. J. Gray, "The Defect Solid State," Interscience, New York, N. Y., 1957, pp 276–278.

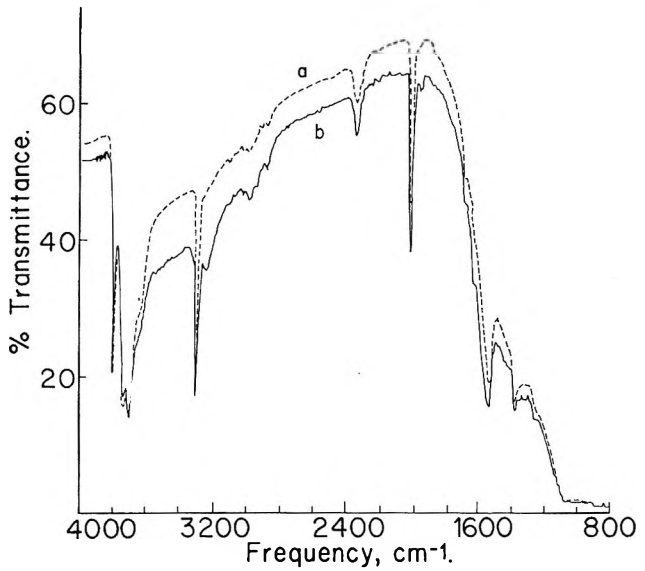

Figure 2. Infrared spectra of acetylene chemisorbed on γ-alumina predried at 550° (a) at a pressure of 1 mm, and (b) at a pressure of 1.2 cm.

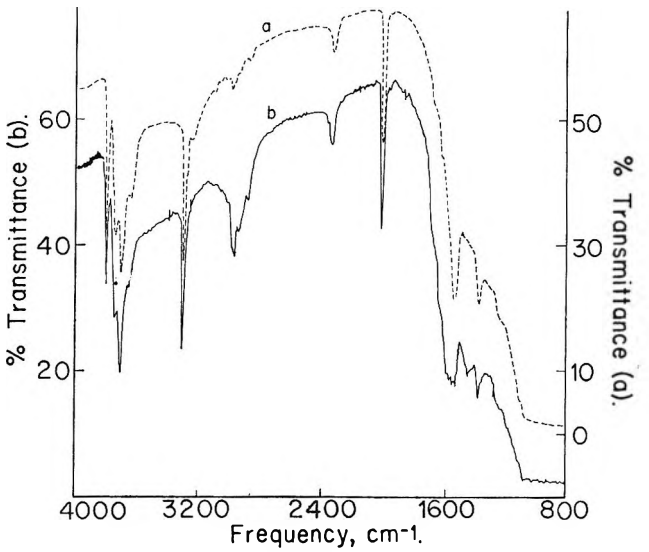

Figure 3. Infrared spectra of acetylene chemisorbed on γ-alumina predried at 750° (a) at a pressure of 5.5 mm, (b) at a pressure of 14.8 cm and subsequent removal of the gas by evacuation.

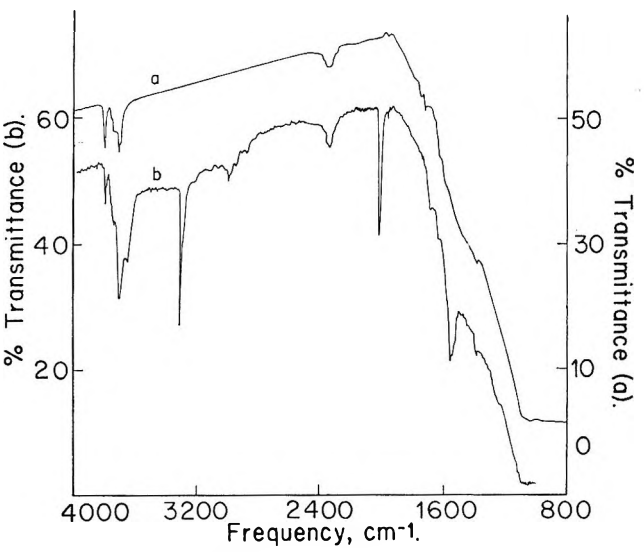

Figure 4. Infrared spectra of γ-alumina predried at 800° (a) and acetylene chemisorbed at a pressure of 14 cm and the back-ground gas evacuated to 1 mm (b).

Table I: New Vibration Frequencies (in the Region of 4000–1100 cm^{-1}) for Acetylenes Adsorbed on γ-Al_2O_3

Frequency, cm^{-1}	Assignment
	Acetylene
2970	CH_3 asymmetric stretch
2930	CH_2 asymmetric stretch
2875	CH_3 symmetric stretch
1680	Possibly C=C stretch
1630	Possibly C=C stretch
1540	Possibly CH_2 or CH_3 deformation
~3650	Hydrogen-bonded OH
	Methylacetylene
1625, 1600	Possibly C=C stretch
~3650	Hydrogen-bonded OH
~3600	Hydrogen-bonded OH
~3550	Hydrogen-bonded H_2O or OH
1550	Possibly CH_3 or CH_2 deformation
	Dimethylacetylene
3500–3300[a]	Weakly hydrogen-bonded DMA to surface OH
2950	Possibly CH_3 or CH_2 stretch
2890	Possibly CH_3 or CH_2 stretch
1635	Possibly C=C stretch
1487	Possibly CH_3 or CH_2 deformation
1315	Possibly CH_3 or CH_2 deformation

[a] The intensity of this band was greatly reduced by evacuation at room temperature. This band is attributed to OH groups hydrogen-bonded to adsorbed DMA.

chemisorbed acetylene were similar to those observed by the Yates and Lucchesi.[4] The spectra of acetylene adsorbed on 750 and 880° predried alumina are shown in Figures 3 and 4. The major absorption frequencies for adsorbed acetylene did not change significantly for alumina predried at different temperatures. The differences in these spectra were mainly in the OH stretching, hydrogen-bonding and CH_3/CH_2 stretching, and deformation regions of the spectrum (see Table I). Some of the significant differences between our work and that of Yates and Lucchesi[4] follow.

(1) The authors used a highly transparent γ-alumina aerogel (65–85% in the region of 4000–2000 cm^{-1}) while the alumina used by Yates and Lucchesi was of "η" type with a transparency of 2–30% in the region of 4000–2000 cm^{-1}.

(2) The γ-alumina predried at 550° showed only a slight perturbation of the strong OH stretching bands;

however, a broad band developed at 3650 cm^{-1} indicating the formation of hydrogen bonded OH groups. The 750° predried γ-alumina showed a small increase in the intensity of the OH groups on chemisorption followed by the appearance of a broad band at 3650 cm^{-1} (Figures 3a and 3b). The increase in the intensity of OH groups on chemisorption was clearly evident in the case of the 880° predried γ-alumina. The formation of a small, broad band at ~3650 cm^{-1} was also observed in this case (Figure 4). Thus the extent of surface dehydration strongly influenced the chemisorption of acetylene.

(3) Weak absorption bands in the CH_3 and CH_2 stretching region (2970–2875) cm^{-1} were observed on chemisorption of acetylene on γ-alumina. These bands grew in intensity on further exposures of acetylene to γ-alumina as well as with longer exposure time (Figures 2 and 3). The ratio of CH_2/CH_3 groups (based on 1.6 times the ratio of intensities at 2930 and 2970 cm^{-1}) indicated the presence of ethyl groups on the surface. The CH_3 and CH_2 stretching bands could not be removed by evacuation at room temperature.

(4) The γ-alumina aerogel turned yellow on chemisorption of acetylene. On standing in contact with acetylene, the γ-alumina aerogel slowly changed its color to dark brown. These color changes have not been reported by Yates and Lucchesi. A general lowering of transmission was also observed on prolonged exposure to acetylene.

(5) Absorption bands in the C=C stretching region were observed and weak bands in the CH_3/CH_2 deformation region were also present.

Methylacetylene. Adsorption of methylacetylene was studied on γ-alumina aerogel dehydrated at 450 and 800° (Figures 5 and 6, respectively). Most of the absorption bands due to the adsorbed methylacetylene were similar to those reported by Yates and Lucchesi.[4] Table I lists the new absorption bands observed on adsorption of methylacetylene and their possible assignment. The authors also observed the following. (1)

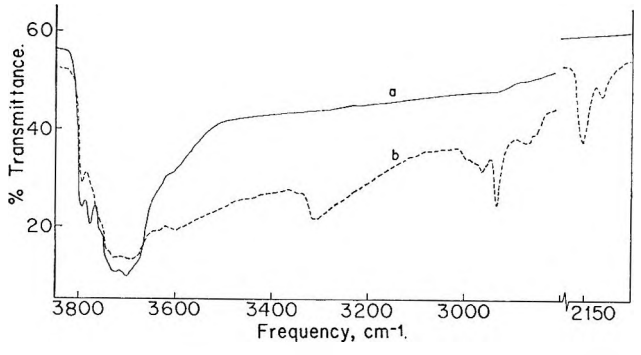

Figure 5. Infrared spectra of (a) γ-alumina predried at 450°, (b) methylacetylene chemisorbed on the γ-alumina at a pressure of 2 mm. The band associated with ≡CH stretching vibration (3305 cm^{-1}) was easily removed on evacuation at room temperature.

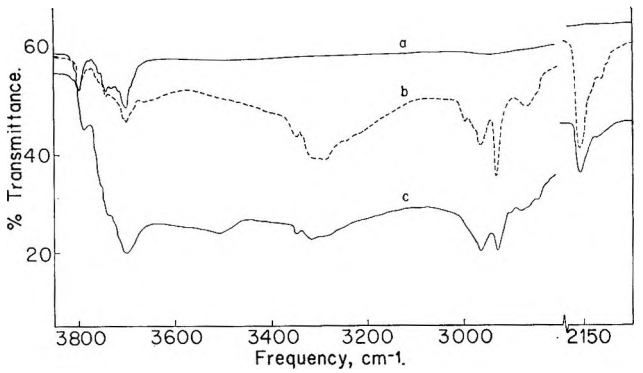

Figure 6. Infrared absorption of (a) γ-alumina predried at 800°, (b) methylacetylene chemisorbed on γ-alumina at a pressure of 5 mm and (c) 2 hr after the absorption in (b). The band associated ≡CH stretching vibration (3305 cm^{-1}) was easily removed on evacuation at room temperature.

Chemisorption of methylacetylene on 450° dried γ-Al_2O_3 resulted in disappearance of the 3775-cm^{-1} surface OH stretching band; however, on 800° dried γ-alumina, the intensity of all but the 3798-cm^{-1} OH stretching increased. While the 450° dried γ-alumina gave a broad band at 3600 cm^{-1}, the 800° dried γ-alumina gave a broad band initially at 3650 cm^{-1} and later on at 3550 cm^{-1}. (2) On longer exposure of methylacetylene to 800° dried γ-alumina, the intensity of all OH bands increased and the relative intensity of bands in the CH_3/CH_2 stretching region changed. (3) The color of γ-alumina aerogel changed slowly from its original milky-white to yellow and later to brown. (4) New absorption bands appeared at 1600 and 1625 cm^{-1}. These bands could be due to C=C stretching vibrations. (5) The ≡C–H stretching band could be removed easily by evacuation at room temperature while the bands due to chemisorbed methylacetylene could not be removed by heating under vacuum at 200–300°.

Dimethylacetylene. Adsorption of dimethylacetylene (on γ-alumina) dried at 550, 625, and 880° (Figures 7, 8, and 9, respectively) was studied. The γ-alumina predried at 550° showed clearly two bands at 3700 and 3798 cm^{-1} and a shoulder band at 3738 cm^{-1} (Figure 7, curve "a"). The new absorption bands, other than those observed by Yates and Lucchesi,[4] for the adsorbed dimethylacetylene are listed in Table I. On chemisorption, the intensity of the 3700 cm^{-1} (Figure 7, curve "b") band decreased and a broad general lowering of transmission occurred in the 3600–3000-cm^{-1} region. A weak absorption band at 2160 cm^{-1} (C≡C stretching) was also observed. The bands in the methyl stretching region were generally strong except for the bands at 2890 and 2950 cm^{-1}. The bands for methyl deformation frequency were observed as spikes on the strong cut-off absorption bands of Al–O vibrations from alumina. There were also absorption bands in the region of 1600 cm^{-1}, but their assignment is not certain.

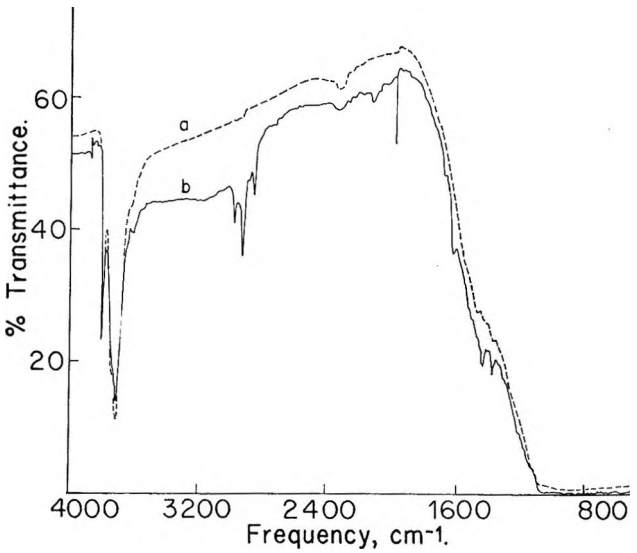

Figure 7. Infrared spectra of γ-alumina predried at 560° (a) and of dimethylacetylene chemisorbed at a pressure of 0.5 mm (b).

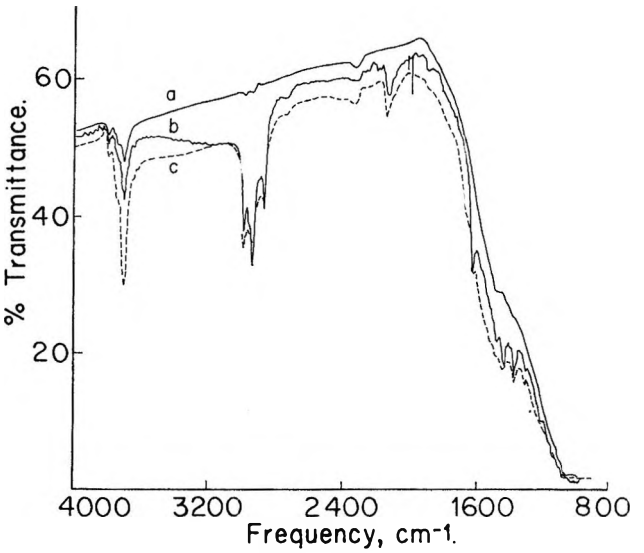

Figure 9. Infrared spectra of γ-alumina predried at 880° (a), chemisorbed dimethyl acetylene at a pressure of 0.5 mm (b), 10 hr later (c).

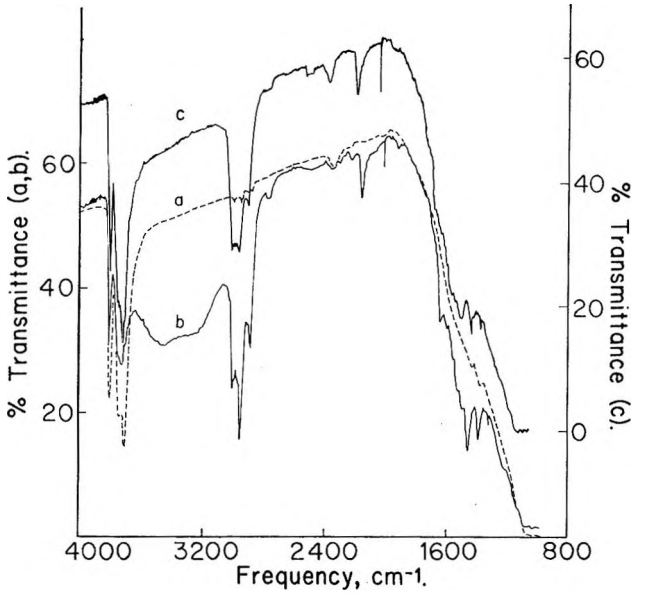

Figure 8. Infrared spectra of γ-alumina predried at 625° (a), of dimethylacetylene chemisorbed at a pressure of 4 mm (b), and following room temperature evacuation of chemisorbed dimethylacetylene (c).

Chemisorption of dimethylacetylene on γ-alumina predried at 625° (Figure 8, curve "b") resulted in a decrease in intensity of the bands at 3700 and 3738 cm^{-1} and in the appearance of a strong broad band in the 3500–3300-cm^{-1} region. On evacuation the broad band disappeared and the intensity of the 3700 and 3738-cm^{-1} bands was restored (Figure 8, curve "c"). However, the C≡C stretching absorption band at 2160 cm^{-1} was unaffected. In both cases the γ-alumina slowly changed color from reddish yellow to carmen red. The surface coverage measured in one experiment was ~5% of a monolayer.

Figure 9, curves "a," "b," and "c" show the spectra of the γ-alumina alone after predrying at 880°, after chemisorption of dimethylacetylene at a pressure of 0.5 mm and after contact with dimethylacetylene for about 10 hr, respectively. It is evident that the concentration of dimethylacetylene and of the isolated hydroxyl group at 3700 cm^{-1}, increased on standing. The band at 1635 cm^{-1} was relatively stronger here than in the other two previous cases. The color of the γ-alumina was found to change to dull red. The chemisorbed dimethylacetylene could not be removed by evacuation at room temperature.

C. Gravimetric Measurements on Acetylene Adsorption. The adsorption of acetylene on the γ-alumina predried at 750 and 550° was studied at several different surface coverages, Table II.

The figures in Table II show that although the amount of adsorbed gas increases about twofold, the intensity of the chemisorbed state changes very little (Figures 2 and 3, curves "a" and "b"), indicating that a rapid saturation of chemisorption sites occurs and that the gas adsorbed later on is essentially physically adsorbed. The number of ion-pair sites was found to be in the range of 2–5 × 10^{13} per cm^2 of the surface.

Discussion

Adsorption of acetylene and methylacetylene on γ-alumina gave absorption bands due to physically and chemically adsorbed species. The nature of the physically adsorbed or weakly chemisorbed species has been discussed by Yates and Lucchesi[4] and will not be discussed here as the authors only substantiate their findings. The nature of each of the chemisorbed acetylenes is discussed below.

Acetylene. The intensity of ν_2(C≡C stretch) band, infrared inactive in the free acetylene, was as strong as

Table II: Surface Coverages for Acetylene Chemisorbed on γ-Alumina Predried at 550 and 750°

Predrying Temperature							
550°C				750°C			
P(mm)	Weight, %	Monolayer %	No. of ion-pair sites per cm² × 10⁻¹³	P (mm)	Weight, %	Monolayer %	No. of ion-pair sites per cm² × 10⁻¹³
1	0.368	1.05	2	1	0.338	0.93	2
12	0.632	1.85	4	5.5	0.575	1.66	4
				12	0.795	2.32	5

that of the ν_3(C–H stretch) band in the adsorbed state. The striking intensity of the C≡C absorption band indicated a strong linear polar interaction with the acetylene molecule. Such an enhancement of the C≡C frequency could result from the formation of surface species of the type I, I′, and II.

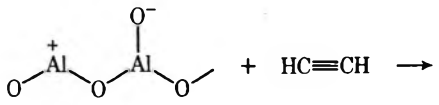

Highly dehydrated
γ-Al_2O_3 (~700–900°) under vacuum

I (Surface aluminum acetylide and proton transfer)

II (Surface aluminum oxyacetylide)

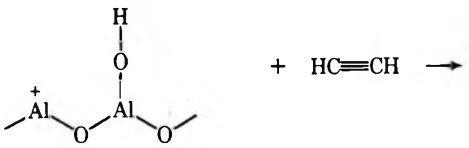

Mildly dehydrated γ-Al_2O_3
(~400–700° under vacuum)

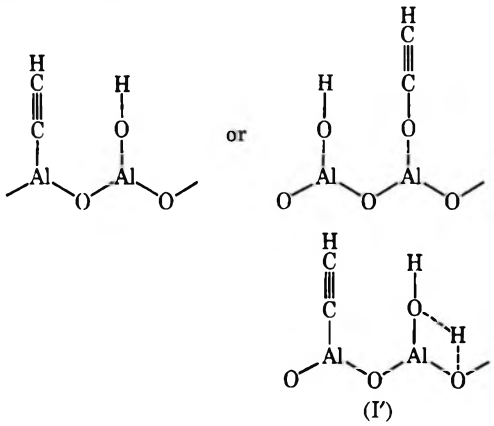

(I′)

Yates and Lucchesi[4,10] proposed structures of the type [HC≡C–H–Su] and [HC≡C–Su_1 + Su_2H], where Su, Su_1, and Su_2 are any surface atoms. The exact identity of these surface atoms was not disclosed. Moreover, the former structure seems inconsistent with a strongly held surface complex. The possibility of structure II was ruled out because the spectrum of adsorbed acetylene did not resemble that of ethoxy acetylene[11] (ν_2 of 2160 and ν_3 of 3330 cm^{-1}). The substitution of an alkyl group in ethoxy acetylene (R–O–C≡C–H) for a heavier group (as in the case of structure II) would not be expected to change the frequency of C≡C (ν_2) or ≡C–H (ν_3) frequencies very much since this would be a secondary effect. However, aluminum–carbon bonded structures (I and I′), involving a proton transfer, are favored as they can explain most of the observations. The formation of structure I involves the loss of a proton from each of several acetylene molecules. Some of these protons are picked up by an adjacent O^- ion on a highly dehydrated γ-alumina surface (after high temperature dehydration). Some of the resulting OH groups are hydrogen bonded. The formation of a broad band around 3600 cm^{-1} occurred on long standing on highly dehydrated alumina while the intensity of isolated OH groups increased immediately on adsorption. On mildly dehydrated alumina, protons are accepted in the vicinity of OH group forming hydrogen bonded O–H–OH groups, and to some extent by neighboring O^- ions to form isolated OH groups. This is evidenced by the rapid appearance of the broad band around 3600 cm^{-1} and the slight increase in intensity of OH groups. This mechanism for chemisorption of acetylene can very well explain the appearance of OD groups on adsorption of deuterated acetylene (C_2D_2) on a partially dehydroxylated γ-alumina as observed by Yates and Lucchesi.[4,10] The lowering in OH group intensity is probably associated with hydrogen bonding with weakly adsorbed acetylene. Thus, in general, the proton lost from acetylene does not have much mobility at room temperature and is accepted by an adjacent O^- ion or an OH group. Such types of sites may be called ion-pair or donor–acceptor or acid–base sites. Somewhat similar sites have also been proposed by Peri.[12] The formation of an aluminum acetylide type of species has been further supported by the works of Miller and Lemmon on acetylides of P, As, and Sb,[13] and of Coates and Parkin[14] on gold and mercury acetylides. The intensities and shifts of the C≡C frequency, of ≡C–H stretching frequency, and of other bands are analogous to those observed on the surface aluminum acetylides. The presence of

(10) D. J. C. Yates and P. J. Lucchesi, *J. Phys. Chem.*, **67**, 1197 (1963).

(11) "Brochure on Ethoxy Acetylene," Pfister Chemical Works, Ridgefield, N. J.

(12) J. B. Peri, *J. Phys. Chem.*, **70**, 3168 (1966).

(13) F. A. Miller and D. H. Lemmon, *Spectrochim. Acta*, **23A**, 1099 (1967).

(14) C. E. Coates and C. Parkin, *J. Chem. Soc.*, 3220 (1962).

Al–C bonds cannot be studied as their frequency (~700 cm^{-1}) falls under the strong absorption associated with the Al–O stretching vibrations.

Besides the weak and strong adsorption of acetylene on γ-alumina, it was found that γ-alumina changed its appearance during adsorption from milky translucent to light yellow. The light yellow color gradually became dark brown. At the same time bands in the region of CH_3, CH_2, and C=C stretching vibrations grew stronger. The ratio of CH_2/CH_3 was found to be approximately unity. These observations suggest the formation of CH_3CH_2 groups on γ-alumina as a result of the self-hydrogenation of acetylene. Also the color changes observed (and the general lowering of transmission) can be explained by the formation of a surface carbide species resulting from self-hydrogenation of acetylene. Such self-hydrogenations are very well known on surface of Ni, etc., but have not been observed on γ-alumina. From our data it is difficult to decide whether weakly or strongly held acetylene was involved in the self-hydrogenation reaction, although hydrogen lost during chemisorption could possibly hydrogenate the C≡C bond of the weakly held acetylene. The self-hydrogenation and the polymerization of acetylene (as evidenced by C=C stretching bands) observed with our γ-Al_2O_3 aerogel could possibly be due to its more active nature as compared to the η-Al_2O_3 used by Yates and Lucchesi.

The surface coverage for acetylene chemisorbed on γ-alumina (predried at 550 and 750°, Table II) ranged typically between 1–2.5% of a monolayer. These coverages indicate that the number of ion-pair sites per cm^2 of alumina surface responsible for acetylene chemisorption is of the order $2–5 \times 10^{13}$. This is in good agreement with the observations of Peri.[12]

Methylacetylene. The ≡C–H adsorption was assigned totally to the weakly adsorbed species as it disappeared on evacuation at room temperature along with other weak bands associated with weakly held acetylene. The strongly held methylacetylene was characterized by: (a) relatively unperturbed stretching and bending modes of CH_3 group; (b) a relatively strong absorption band in C≡C stretching frequency region indicating strong polar interaction with the C≡C bond. Also an increase of 25 cm^{-1} in the C≡C stretching frequency of strongly held methylacetylene from that in the dissolved state, suggesting the formation of a disubstituted acetylene; and (c) no absorption in the ≡C–H stretching region, indicating the loss of the acetylenic hydrogen.

These results indicate very strongly that the chemisorbed methylacetylene exists as an acetylide on the surface of γ-alumina. The acetylenic hydrogen lost during chemisorption is probably involved in the formation of hydrogen bonded O–H–OH groups (low temperature dehydrated alumina type I′ complex). The formation of isolated –OH groups is quite evident in the case of γ-alumina predried at 800°. (Type I chemisorbed complex).

Self-hydrogenation was once again evident in this case as the relative intensity of the 2980/2930 cm^{-1} bands increased on standing. The CH_2/CH_3 ratio could not be determined from the spectra. The formation of surface carbide was indicated by progressive deepening of the reddish color observed on chemisorption of methylacetylene. The general lowering of transmission on standing was also associated with the slow formation of surface carbide (or carbon like) species.

Thus, the formation of aluminum acetylide like species as shown in I and I′ for acetylene is strongly indicated for methylacetylene as well.

Dimethylacetylene. Dimethylacetylene (DMA) chemisorbed in a manner different from that of methylacetylene and acetylene. There are again two types of adsorption modes for dimethyl acetylene. In the weakly held mode, it is very likely hydrogen-bonded to OH groups on the surface, as for example, in structure III.

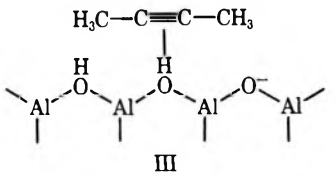

III

The weakly held DMA could be easily removed by evacuating at room temperature and the intensity of the OH groups returned to the level prior to adsorption. This suggested an interaction of the type shown in III. The weakly held DMA was formed easily on low-temperature dehydrated γ-alumina. The adsorbed species formed on high-temperature dried γ-alumina was probably identical with the strongly held DMA remaining after evacuation at room temperature. The structure of this species probably involves a much stronger interaction and species of type IV are postulated for such a chemisorbed complex.

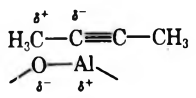

IV

Our data do not confirm such a structure (IV) but definitely suggest a stronger interaction of C≡C with the surface groups of γ-Al_2O_3. The presence of a C≡C stretching band after removal of weakly held DMA can be explained by weak polar interactions such as would be expected on an heterogeneous surface of γ-alumina (which consists of O^- ions, OH groups, and Al^+ ions). The presence of the C≡C bond could also be due to a methylacetylene impurity in DMA as suggested by Yates and Lucchesi,[4] and our work cannot rule out that possibility at present. Besides the two types of adsorbed DMA, there was also evidence of self-hydrogenation of DMA. Once again, γ-alumina gradually

changed its color from light yellow to dark carmen red (after several hours). Slow changes in the intensity of bands in alkyl stretching region were also observed. However, some of these changes could also be explained by polymerization of DMA. Adsorption of DMA on high-temperature (~800°) dehydrated γ-alumina resulted in some increase in the intensity of OH groups. This suggests self-hydrogenation of DMA on γ-alumina. The increase in intensity of OH groups, however, was appreciably smaller than that observed with acetylene and methylacetylene.

Nature of Active Adsorption Sites on γ-Alumina. There is a wide spectrum of opinions in the literature regarding the exact identity of active sites on γ-alumina.[5,15-20] However, our conclusions on the nature of active sites on γ-alumina are more in accord with those presented recently by Peri.[5,19,20]

For the chemisorption of methylacetylene and acetylene, exposed aluminum ions (Lewis acids) and neighboring oxide ion or OH groups (Brønsted acids) act as adsorption sites. These active sites may be called ion-pair sites or acid–base or acceptor–donor sites. The number of such sites is of the order of 10^{13} per cm^2 of the alumina surface. The number of ion-pair sites increases with an increase in the degree of dehydration of the surface. Thus the behavior of γ-alumina as an adsorbent is strongly dependent on the extent of dehydration. On the other hand, dimethylacetylene, which does not have an acidic hydrogen atom, is essentially nucleophilic at the C≡C bond. Thus in case of DMA a Lewis type acid (aluminum ion) constitutes the active site for the chemisorption. Physisorbed or weakly chemisorbed acetylene, methylacetylene, and DMA are probably hydrogen bonded parallel to the surface through OH groups.

Acknowledgments. The authors wish to thank Dr. J. B. Peri of American Oil Company for providing some of the γ-alumina aerogels used in this work.

(15) H. S. Taylor, *Z. Elektrochem.*, **35**, 545 (1929).
(16) D. W. Dowden, *J. Chem. Soc.*, 242 (1950).
(17) S. G. Hindin and S. W. Weller, *Advan. Catal.*, **10**, 70 (1957).
(18) E. B. Cornelius, T. H. Milliken, G. A. Mills, and A. G. Oblad, *J. Phys. Chem.*, **59**, 809 (1955).
(19) J. B. Peri, *ibid.*, **69**, 231 (1965).
(20) J. B. Peri, *ibid.*, **70**, 1482 (1966).

Solvent and Ligand Dependence of Electron Spin Relaxation of Manganese(II) in Solution

by L. Burlamacchi, G. Martini, and E. Tiezzi

Institute of Physical Chemistry, University of Florence, Florence, Italy *(Received March 26, 1970)*

Due to ionic association, solutions of Mn^{II} ions often contain several paramagnetic species which contribute simultaneously to the esr line shape. The analysis of the electron spin relaxation process is particularly difficult in the absence of a clear knowledge of the composition of the solution. Signal intensity and line width behavior as functions of temperature and ligand concentration allow determination of the conditions in which "pure" tetrahedral or octahedral complexes are present in different solvents. In the high-temperature region (above ~100°), the observed line broadening appears to be present in all complexes. It is shown that this broadening is not related to the rate of exchange of ligands in the coordination shells. Analysis of g factors and temperature dependence of the line width also excludes spin-rotation to be effective.

I. Introduction

Since McGarvey,[1] the electron spin relaxation mechanism for solutions of transition metal ions with $S \geq 1$ have been extensively studied.[2-5] Particular attention has been devoted to the manganous ion, which exhibits relatively narrow esr lines.[6-13] It is now generally accepted that modulation of the anisotropic zero-field splitting parameter is predominant in inducing spin transitions. In solution, the zero-field splitting of the electronic levels is related to the symmetry of the diamagnetic environment surrounding the central para-

(1) B. R. McGarvey, *J. Phys. Chem.*, **61**, 1232 (1957).
(2) S. A. Al'tshuler and K. A. Valiyev, *Soviet Phys. JETP*, **35**, 661 (1959).
(3) D. Kivelson, *J. Chem. Phys.*, **33**, 1094 (1960).
(4) A. D. McLachlan, *Proc. Roy. Soc. Ser. A*, **280**, 271 (1964).
(5) A. Carrington and G. R. Luckhurst, *Mol. Phys.*, **8**, 125 (1964).
(6) N. Bloembergen and L. O. Morgan, *J. Chem. Phys.*, **34**, 842 (1961).

magnetic ion. This establishes a dependence of the line width on the chemistry and kinetics of the system under study. In fact, it is well known that a number of complexes are formed between the solvated Mn^{2+} ion and the various anions which may be present in the solution. Different complexes will have different ligand field symmetry, with characteristic relaxation time and esr line shape, which may contribute to the overall spectrum.

In the room temperature region, the temperature dependence is governed by the correlation time for the fluctuating perturbation, which requires that the line width becomes sharper when the temperature is raised. However, in some cases, it was observed that above a certain temperature the line width increases again,[7,8] due to the overcoming of another relaxation mechanism. The nature of this process which exhibits a marked dependence on counterion concentration is still debated.

The purpose of the work described in this paper is to elucidate the nature of the various species which contribute to the esr line width. An analysis of the relaxation mechanism responsible for the high-temperature line broadening is also carried out.

II. Experimental Section

All salts used were carefully dried over P_2O_5 under reduced pressure at 110° for 24 hr. $Mn(ClO_4)_2 \cdot 6H_2O$ was analytical grade. All solvents employed were for spectroscopic use and were further purified by distillation over 5A Carlo Erba molecular sieves.

In all solutions Mn^{2+} concentration was 0.01 M. At this concentration dipolar and spin exchange effects on the esr line shapes are negligible.

Spectra were registered with a Varian V 4502 X-band 100-kc field modulation spectrometer, equipped with a dual sample cavity. Nitrosyldisulfonate ion (Fremy salt) was used as a reference standard for line width (ΔH) and signal intensity measurements. Sample temperatures were controlled with a Varian E4557 variable temperature assembly and measured with a copper–constantan thermocouple inserted in the heating nitrogen stream. Its accuracy was evaluated ±1°. The solutions were directly inserted in a quartz U-shaped capillary tube fixed in the microwave resonance cavity in order to obtain a sufficiently good reproducibility. For high-temperature measurements, samples were sealed in a quartz capillary tube.

Assuming Lorentzian line shape, the absorption intensity was evaluated by the known relation $\Delta H^2 \cdot h$, where h is the height of the signal. As long as the six hyperfine lines were completely resolved, the line width was directly measured as the peak–peak distance of the fourth line from the low-field side. When appreciable overlapping occurred, ΔH was derived by comparing experimental results with computer simulated spectra. This method is subject to some uncertainty, first because the lines are not expected to be strictly Lorentzian, and also because the calculated relative width and position of each esr transition are not in close agreement with the experimental line shape.[7,9] According to theory, when line broadening is sufficiently high, all lines should tend toward the same width. We followed this assumption in simulating the reference spectra.

Viscosity changes at various ionic concentration give little contribution to the line width. When necessary, corrections were made assuming linear dependence of ΔH upon η.

III. Theory of Electron Spin Relaxation

The shape of the esr spectrum of Mn^{II} in solution has been well known since the early stage of paramagnetic resonance. It contains six hyperfine components due to the interaction of the electronic spin with the $I = 5/2$ nuclear spin of ^{55}Mn. Experimentally the different lines have different widths. This seems to be due to the spread of the fine splitting components, rather than to inhomogeneous broadening. We are not concerned here with the M_I dependence of the line width. Although for most purposes this would be an over-simplification, we make the assumption that for the fourth hyperfine line, which is the narrowest, the splitting of the fine components is negligible.

The electron spin transition probability is theoretically evaluated by means of the density matrix formalism developed by Redfield.[14] If the time-dependent part of the Hamiltonian is expressed in terms of irreducible tensors operators, it takes the form[13,15,16]

$$\mathcal{H}(t) = \sum_{L,\mu,p} (-1)^p F_\mu^{(L,p)} T_\mu^{(L,-p)} \qquad (1)$$

where L is the rank of the tensor operators, p stands for the components, μ represents a particular perturbation, and $F_\mu^{(L,p)}$ operate on spatial variables and are time dependent. The $T_\mu^{(L,-p)}$ are time independent because they operate in a fixed axis system on the spin variables. The elements of the density matrix are given by

$$R_{\alpha\alpha'\beta\beta'} = \frac{1}{2\hbar^2}\left[J_{\alpha\alpha'\beta\beta'}(\alpha' - \beta') + J_{\alpha\beta\alpha'\beta'}(\alpha - \beta) - \sum_\gamma \delta_{\alpha'\beta'} J_{\gamma\beta\gamma\alpha}(\gamma - \beta) - \sum_\gamma \delta_{\alpha\beta} J_{\gamma\alpha'\gamma\beta'}(\gamma - \beta')\right] \qquad (2)$$

(7) B. B. Garrett and L. O. Morgan, *J. Chem. Phys.*, **44**, 890 (1966).
(8) R. G. Hayes and R. J. Myers, *ibid.*, **40**, 877 (1964).
(9) S. I. Chan, B. M. Fung, and H. Lütje, *ibid.*, **47**, 2121 (1967).
(10) H. Levanon and Z. Luz, *ibid.*, **49**, 2031 (1968).
(11) D. C. McCain and R. J. Myers, *J. Phys. Chem.*, **72**, 4115 (1968).
(12) G. P. Vishnevskaya and B. M. Kozyrev, *Zh. Strukt. Khim.*, **8**, 627 (1967).
(13) A. Hudson and G. R. Luckhurst, *Mol. Phys.*, **16**, 403 (1969).
(14) A. G. Redfield, *IBM J. Res. Develop.*, **1**, 19 (1957).
(15) A. Abragam, "The Principle of Nuclear Magnetism," Oxford, Clarendon Press, 1957 p 276.
(16) J. H. Freed and G. K. Fraenkel, *J. Chem. Phys.*, **39**, 326 (1963).

where the spectral densities for electronic spin transition $\alpha\beta$ and $\alpha'\beta'$ assume the form

$$J_{\alpha\beta\alpha'\beta'} = \sum_{L,L'\mu,\mu p,p'} (-1)^{p+p'} \langle\alpha|T_\mu^{(L,-p)}|\beta\rangle \times \langle\alpha'|T_\mu^{(L,-p')}|\beta'\rangle^* \frac{1}{2}\int_{-\infty}^{\infty} \langle F_\mu^{(L,p)}(t) F_{\mu'}^{(L',p')*} \times (t+\tau)\cos\omega\tau d\tau \quad (3)$$

The characteristic correlation time for the perturbation τ introduces the temperature dependence of the relaxation rate.

The line widths of the individual transitions are proportional to the eigenvalues of the density matrix R while the intensities are proportional to the eigenvectors.

Neglecting quartic terms, which give generally negligible contributions, the static zero-field splitting Hamiltonian which accounts for the spin relaxation of the manganous ion is given by

$$\mathcal{H} = D[S_z^2 - S(S+1)/3] + E(S_x^2 - S_y^2) \quad (4)$$

By applying the time-dependent perturbation to the eigenvalues of the static Hamiltonian, one finds[5] that the resonance line consists of three superimposed Lorentzians with different line widths and intensities attributed to

$$m_s = \pm 5/2 \rightleftharpoons \pm 3/2,\ \pm 3/2 \rightleftharpoons \pm 1/2, \text{ and } -1/2 \rightleftharpoons +1/2$$

transitions. In the limiting case $\omega_0\tau_c \ll 1$, (ω_0 being the Larmor frequency of the electronic spin), only one line is found. In this case, which is generally verified in the temperature region studied, the line width may be expressed as

$$1/T_2 = 1/T_1 \propto \langle D^2\rangle \tau_c \quad (5)$$

where $\langle D_2\rangle$ is the trace of the square of the zero-field splitting Hamiltonian $2/3D_2 + 2E^2$.

Equation 5, however, does not give any information about the perturbational correlation time.[13] In principle, two different situations are plausible: (a) the zero-field splitting is modulated by Brownian rotation of the complex (rotational modulation) with the characteristic correlation time τ_r given by the Debye theory; and (b) a finite mean zero-field splitting arises from rapid fluctuations of the geometry of the complex due to the collision with solvent molecules (solvent fluctuation). In this case, the correlation time, τ_v, represents the mean lifetime of the distorted form of the complex.

As long as no high-temperature broadening is present, the experiment simply shows that $1/T_2$ has a linear dependence on η/T which accounts for both perturbation models.

IV. Results

Octahedral Complexes. In water solution, as well as in other commonly used organic solvents, such as dimethylformamide (DMF), dimethyl sulfoxide (DMSO), methanol, acetonitrile etc., the manganous ions are solvated with a sixfold octahedral coordination shell. However, the presence of counterions or of added different electrolytes leads to association between ions of opposite charges. If association is weak, the anion may occupy a position outside the solvent coordination sphere. This will give rise to an "outer-sphere" complex or "ion-pair," characterized by low distortion of the cubic symmetry of the electric field around the cation. The next step, which occurs in solvents of lower dielectric constant or with stronger complexing agents, is interchange of one solvent molecule from the coordination sphere with the ligand ion coordinated in the outer sphere. The "inner-sphere" complex formed has symmetry lower than cubic. As a consequence, the electron spin relaxation time is almost always so short that the spectrum is no longer observed. All three species are in dynamical stepwise equilibrium represented by the equation

$$Mn^{2+} + L^{n-} \underset{k_{ba}}{\overset{k_{ab}}{\rightleftharpoons}} Mn^{2+} - \text{solvent} - L^{n-} \underset{k_{cb}}{\overset{k_{bc}}{\rightleftharpoons}} MnL^{(2-n)+} \quad (6)$$

hexasolvated ion — outer-sphere — inner-sphere

where L is the ligand.

Evaluation of the equilibrium constants K_{out} and K_{in} from the signal intensity and the line width as a function of ligand concentration is straightforward.[17] Since in solution the only two observable species are the free-ion and the outer-sphere complex, the decrease of the esr signal intensity is a measure of the inner-sphere complex formation. Only one set of two values of the equilibrium constants satisfies the experimental signal intensity *vs.* anion concentration curve. Therefore, the best set of values was easily obtained by a process of trial and error. Analysis of the line width behavior leads to the same results. According to Bijerrum's theory and to a number of experimental results,[8,18,19] it can be quite safely assumed that the interconversion rate between the free ion and the ion pair is $>10^{11}$ sec^{-1}. As the relaxation time for detectable manganese(II) complexes is of the order of 10^{-9} sec, the lifetime of the individual species is shorter than the respective relaxation times. This corresponds to the rapid exchange limit, where the line width is given by the well known modified Bloch equation[20]

$$1/T_{2\,obs} = (1 - X)/T_{2\,free\text{-}ion} + X/T_{2\,ion\text{-}pair} \quad (7)$$

where X is the mole fraction of the outer-sphere complex. This means that the spectrum is no longer the

(17) L. Burlamacchi and E. Tiezzi, *J. Mol. Struct.*, **2**, 261 (1968).
(18) G. Atkinson and S. K. Kor, *J. Phys. Chem.*, **71**, 673 (1967).
(19) L. Burlamacchi and E. Tiezzi, *ibid.*, **73**, 1588 (1969).
(20) H. M. McConnell, *J. Chem. Phys.*, **28**, 430 (1958).

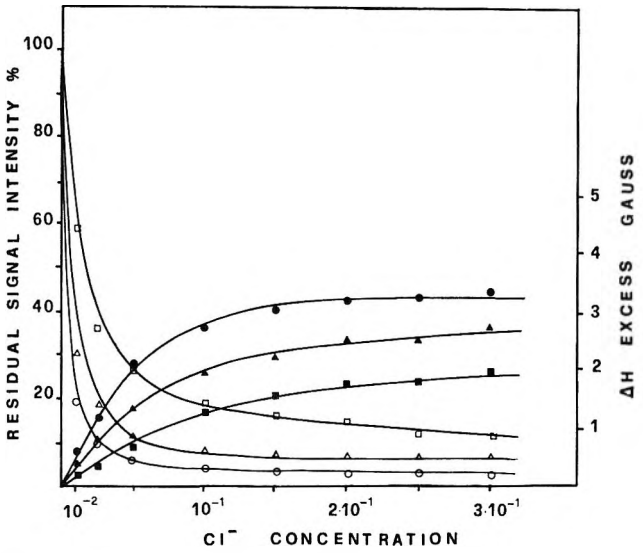

Figure 1. Residual signal intensity (open points) and excess line width (full points and right side scale) of 0.01 M $Mn(ClO_4)_2$ as function of added LiCl in methanol: ■, −20°; ▲, 20°; ●, 60°. The full lines are calculated from the values of equilibrium constants and $\Delta H_{ion\text{-}pair}$ given in Table I; $\Delta H_{free\text{-}ion}$ are 23.5, 16.4, and 12 G at −20°, 20°, and 60°, respectively.

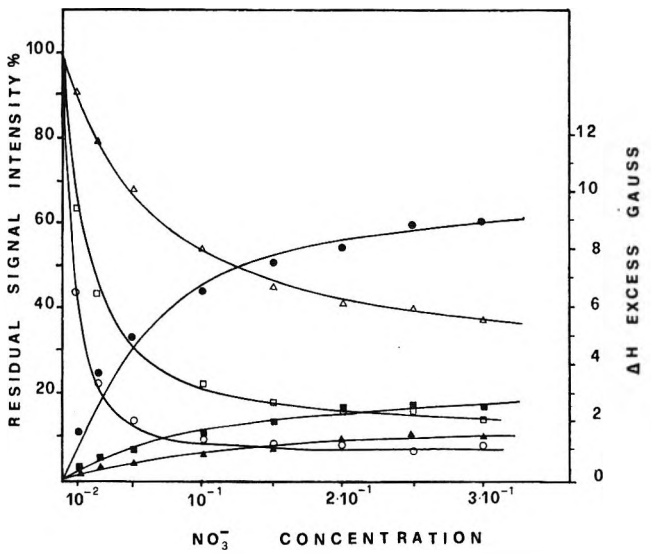

Figure 2. Residual signal intensity (open points) and excess line width (full points and right side scale) of 0.01 M $Mn(ClO_4)_2$ as function of $LiNO_3$ concentration in DMF: ▲, 20°; ■, 60°; ●, 100°. The full lines are calculated from the values of $K_{in} - K_{out}$, and $\Delta H_{ion\text{-}pair}$ in Table I; $\Delta H_{free\text{-}ion}$ are 17.6, 12.4, and 10.2 G at 20°, 60°, and 100°, respectively.

sum of the individual spectra but their weighted average. The excess line width is given by[17]

$$1/T_{2\,obs} - 1/T_{2\,free\text{-}ion} = \frac{K_{out}[L]}{K_{out}[L] + 1}(1/T_{2\,ion\text{-}pair} + 1/T_{2\,free\text{-}ion}) \quad (8)$$

$[L]$ is the effective concentration of ligand in solution which depends also on K_{in}. Derivation of equilibrium constants is again a problem of fitting, which can be solved with the aid of a small computer program. The $\Delta H_{free\text{-}ion}$ curve as function of temperature is generally obtained experimentally (see for instance Figure 7). In general, as the relaxation time is not known *a priori*, it is easier to use signal intensity results which may be verified in the fitting of $1/T_{2\,ion\text{-}pair}$. In some cases, *e.g.*, the Mn–ClO_4–DMF system of Figure 6, both $1/T_{2\,free\text{-}ion}$ and $1/T_{2\,ion\text{-}pair}$ are evaluated by fitting.

Actually, a number of Mn–electrolyte systems in different solvents can be investigated by this method. Figures 1 and 2 show two representative examples. The agreement between calculated values and the experimental points is reassuring. Equilibrium constants and the values of $\Delta H_{ion\text{-}pair}$ for the systems studied are given in Table I, together with the thermodynamic parameters. In the calculations, the activity coefficients for all species were assumed as unity, which we believe is a reasonable assumption in the range of concentration examined. In methanol, DMF, and DMSO, the ClO_4^- ion itself gives signal intensity decrease and line broadening from which equilibrium constants have been derived.

The temperature dependence of the equilibrium constants shown in Figure 3 agrees with the van't Hoff equation with the enthalpy changes given in Table I.

No evidence was found for the formation of bisubstituted complexes which, due to the symmetric structure, are presumed to contribute to the esr signal.

Tetrahedral Complexes. As long as no polysubstituted complexes are formed, addition of an appropriate electrolyte to a Mn^{2+} solution lowers the signal intensity toward a constant value which corresponds to the ion-pair concentration. However, in some cases, with further addition of the electrolyte, the signal intensity rises again, showing the formation of a new paramagnetic species with highly symmetrical structure. The nature of these complexes is well documented by optical spectra characteristic of tetrahedral structure.[21]

Esr evidence for tetrahalide complexes formation in acetonitrile and methanol has been reported by Chan, Fung, and Lütje[9] and by Levanon and Luz.[10] In DMF[22] and DMSO, tetracoordinated complexes are readily formed as soon as the ligand concentration has reached the stoichiometric amount. Generally, the esr spectra are characterized by an isotropic g factor somewhat higher than the octahedral complexes (g = 2.005–2.008) and hyperfine coupling constants of 75–80 G.

When excess halide is added to an Mn^{2+} solution after the tetracoordinated complex is formed, one observes an increase of line width. It is plausible that cationic complexation around the negative tetrahalide ion is the source of this broadening which can be under-

(21) S. Buffagni and T. M. Dunn, *Nature*, **188**, 937 (1960).

(22) J. R. Bard, J. T. Holman, and J. O. Wear, *Z. Naturforsch.*, **24b**, 989 (1969).

Table I: Equilibrium Constants, Enthalpy Changes, and Limiting Line Width of Mn^{II} Complexes

System	Temp, °C	K_{out}, l./mol	Enthalpy changes, kcal/mol	K_{in}	Enthalpy changes, kcal/mol	$\Delta H_{ion\text{-}pair}$, G
Mn^{2+}–Cl^-–CH_3OH	−20	9 ± 0.5	2.4 ± 0.1	10 ± 1	2.0 ± 0.1	27.0
	+20	18 ± 1.5		17.5 ± 2		19.4
	+60	30 ± 2		28 ± 3		15.8
Mn^{2+}–NO_3^-–DMF	+20	4.0 ± 0.2	4.2 ± 0.2	3.2 ± 0.3	4.4 ± 0.2	21.0
	+60	9.5 ± 0.5		8.5 ± 1		16.0
	+100	20 ± 2		17.5 ± 2		21.5
Mn^{2+}–ClO_4^-–DMF	+20	2.5 ± 1[a]	...	0.20 ± 0.05	3.1 ± 0.1	21.0
	+60			0.40 ± 0.05		16.0
	+100			0.7 ± 0.1		15.8
Mn^{2+}–ClO_4^-–CH_3OH	+20	0.5 ± 0.2[a]	...	0.4 ± 0.1	...	...
Mn^{2+}–ClO_4^-–DMSO	+35	0.5 ± 0.1[a]	...	0.3 ± 0.1	...	...
$[MnBr_4]^{2-}$–$(n\text{But})_4N^+$–CH_3CN	+20	8 ± 1	...	...	...	170
$[MnBr_4]^{2-}$–$(Me)_4N^+$–CH_3CN	+20	85 ± 5	...	...	...	130
$[MnBr_4]^{2-}$–Li^+–CH_3CN	+20	17 ± 2	...	...	...	120
$[MnBr_4]^{2-}$–$(Et)_4N^+$–CH_3CN	+20	20 ± 2	...	...	...	85
$[MnCl_4]^{2-}$–$(Et)_4N^+$–CH_3CN	+20	14 ± 2	...	...	...	13.5

[a] The temperature dependence is within the experimental error.

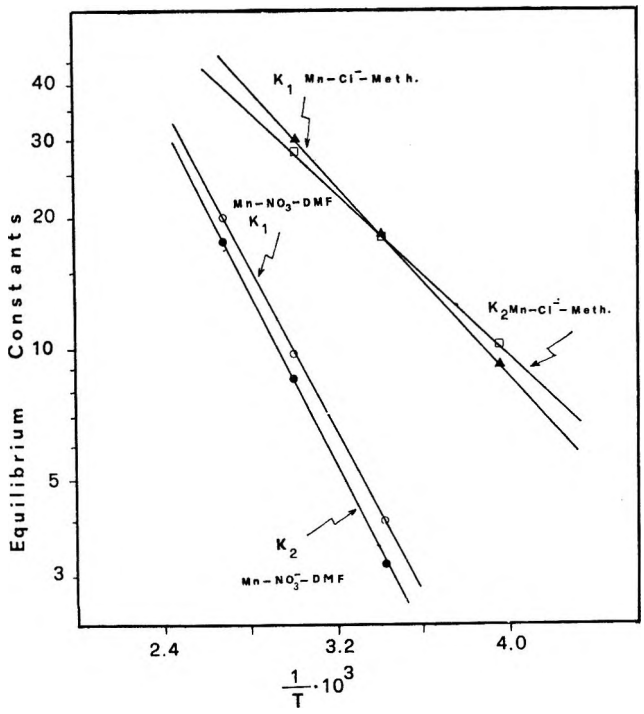

Figure 3. Equilibrium constants K_{in} and K_{out} *vs.* $1/T$ °K.

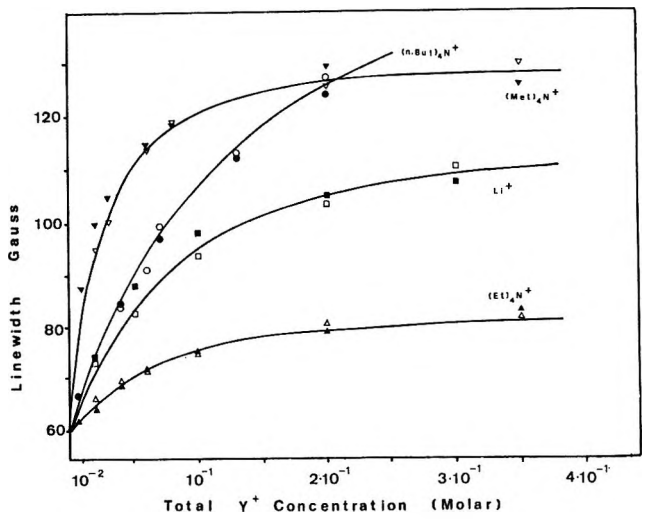

Figure 4. Esr line width of $[MnBr_4]^{-2}$ 5×10^{-3} M in acetonitrile *vs.* total counterion (Y^+) concentration. The counterion is added as bromide salt (full points) and as perchlorate salt (open points), with previous addition of the stoichiometric amount of Br^-. Full lines are calculated with equilibrium constants given in Table I. Line width over 3×10^{-1} M ligand concentration are corrected from viscosity contribution.

stood by essentially the same model as for hexasolvated complexes. If we assume ion-pair formation

$$[MnX_4]^{2-} + Y^+ \underset{k_{ba}}{\overset{k_{ab}}{\rightleftharpoons}} [MnX_4^{-2};\ Y^+] \qquad (9)$$

the equilibrium constants can be evaluated. Figure 4 shows the line width behavior as a function of total counterion concentration for $[MnBr_4]^{-2}$ with Li^+, tetramethylammonium $(Me)_4N^+$, tetraethylammonium $(Et)_4N^+$, and tetra-*n*-buthylammonium $(n\text{-But})_4N^+$ added as bromide or perchlorate salts. Calculated equilibrium constants and $\Delta H_{ion\text{-}pair}$ are given in Table I. The dependence on Br^- ion concentration seems clearly ruled out, while the dependence on Mn^{2+} concentration, in the range 5×10^{-3} to 2×10^{-2} M, is expected within the experimental error. Manganous tetraion chloride shows the same behavior (Figure 5) although the overall line width is much smaller.

High-Temperature Electron Spin Relaxation. From the above results, it appears that two different cases may occur in Mn^{2+} solutions: (1) tetrahedral or octa-

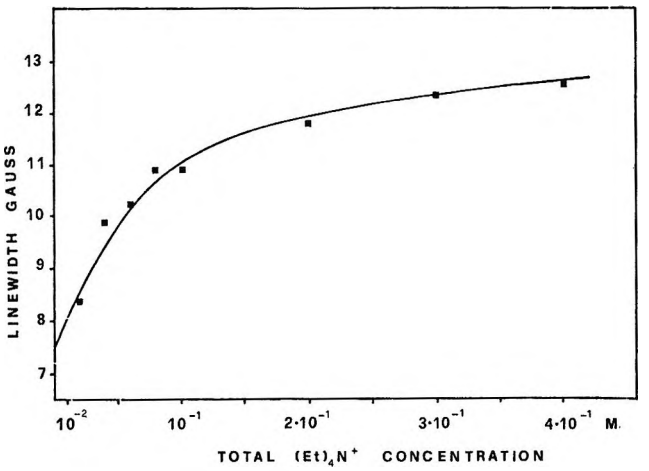

Figure 5. Esr line width of $[MnCl_4]^{-2}$ 5×10^{-3} M in acetonitrile *vs.* $(Et)_4N^+$ total concentration, added as chloride salt. Full line is calculated from equilibrium constant and $\Delta H_{ion\text{-}pair}$ given in Table I. Line widths over 3×10^{-1} M ligand concentration are corrected from viscosity contributions.

hedral complexes are formed which are practically the only species present in solution which exhibit detectable paramagnetic absorption. This occurs when small amounts of $Mn(ClO_4)_2$ are dissolved, so that inner- and outer-sphere complexation is negligible, or when the ligand/Mn^{2+} ratio is sufficiently high to account for the equilibrium being completely shifted toward ion-pair or tetracoordinated complexes; (2) intermediate situation, in which basicity of the solvent, charge, type, and concentration of the ion are favorable to appreciable amounts of inner- and outer-sphere complexation.

When a situation described in point 2 is reached, the typical anion concentration dependence found by Hayes and Myers[8] is observed. As an example, the temperature dependence of the line width for Mn–perchlorate systems in DMF is shown in Figure 6. The $\Delta H_{free\text{-}ion}$

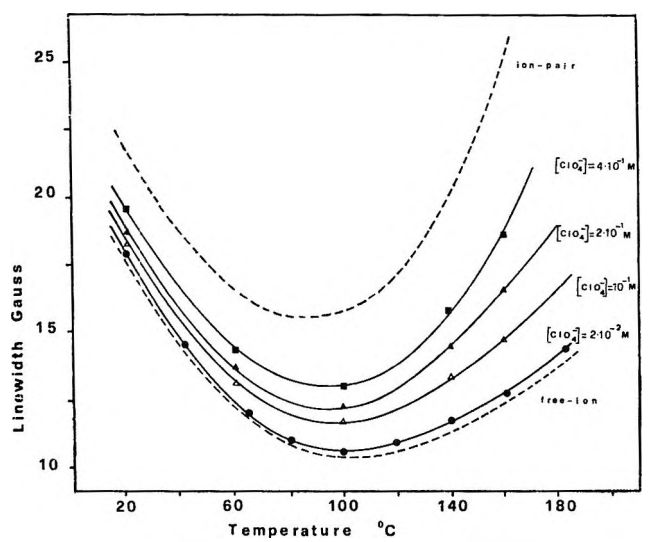

Figure 6. Esr line width of 0.01 M Mn^{2+} as function of temperature at different total ClO_4^- concentrations in DMF.

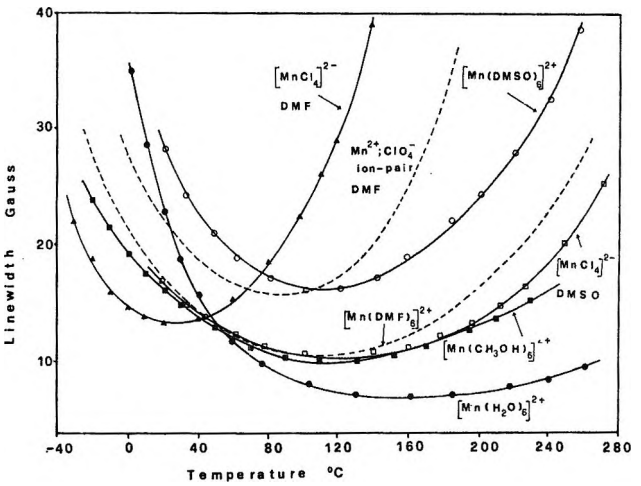

Figure 7. Esr line width of different Mn^{II} complexes as a function of temperature.

and $\Delta H_{ion\text{-}pair}$ lines in the graph represent the free-ion and outer-sphere complex behavior, which could be observed if they were the only species to exhibit paramagnetic absorption. In Figure 7 the line width of a number of pure complexes (point 1) as a function of temperature is reported. In water solution the resonance width was found to vary insignificantly by addition of ClO_4^- up to 0.5 M, at any temperature. The same is observed by addition of Cl^- 0.5 M to tetrahedral complexes, which shifts the entire curve toward higher ΔH values without changing the slope. From data of Table I, complexation by perchlorate in methanol and DMSO for 0.01 M $Mn(ClO_4)_2$ solutions is expected to be negligible.

V. Discussion

The experimental results show that free hexasolvated ions, ion-pair complexes, and the tetrahalide complexes always exhibit the high-temperature broadening even for the $Mn(H_2O)_6^{2+}$ complex. We feel quite confidently that this may be a general behavior intrinsic of the Mn^{II} complexes. Since the temperature dependence of the correlation time of the zero-field splitting relaxation mechanism cannot explain these results, an analysis should be made of those processes which account for the increase of relaxation rate with increasing temperature.

Ligand Exchange. In the above picture of anionic complexation, the ligand exchange mechanism may be rationalized as follows: (a) exchange of anionic ligands from the second coordination sphere to the bulk solution; (b) interconversion of anionic ligands between second and first coordination sphere; (c) exchange of solvent molecules in the solvent coordination sphere; (d) exchange between the coordinated anions and the bulk electrolyte when all solvent molecules are replaced by anionic ligands (tetracoordinated complexes). All processes may cause transient distortion of the cubic symmetry of the complex. When the distortion is strong,

transient mixing of the electronic spin states during the exchange induces spin transitions. In the limit of strong perturbation, this may limit the lifetime of the spin state to the lifetime of the complex.[8]

Process a, although very fast, is expected to cause only weak distortion during the exchange with negligible contribution to the relaxation, as shown by experimental results. Processes b, c, and d are known to occur at rates comparable to the spin relaxation and are potentially active in determining the temperature dependence of the line width. The excess line width due to process b was studied by Hayes and Myers.[8] In the rapid exchange limit, if $1/k_{bc} \ll T_{2\ \text{ion-pair}}$ and $1/k_{cb} \gg T_{2\ \text{inner-sphere}}$, eq 8 still applies with $1/k_{bc}$ replacing $T_{2\ \text{ion-pair}}$. This accounts for the line broadening over that of the free-ion; the high-temperature broadening of the free-ion itself is not justified. Furthermore, $k_{bc}/k_{cb} = K_{in}$ is very often ≤ 1. Since $k_{bc} \geq 10^9$ sec^{-1} and $T_{2\ \text{inner-sphere}} \simeq 10^{-10}$ sec, the above conditions of slow exchange between inner- and outer-sphere complexes are not completely fulfilled. A drastic increase of line width should then be observed at sufficiently high temperature, due to contribution of the broad inner-sphere spectrum to the observed resonance. Process c does not account for the broadening in tetracoordinated complexes. Finally, process d, when effective, would give $1/T_{2\ \text{obs}} = k[L]$, causing a linear increase of line width with ligand concentration. Crawford, Lynds, and Chan[23] attributed to this mechanism the abnormal breadth of $[MnBr_4]^{2-}$ spectrum in acetonitrile. However, the picture described above of cationic ion-pair formation seems much more plausible. Furthermore, the temperature dependence of $[MnCl_4]^{2-}$ line width even in the absence of excess ligands cannot be explained in these terms.

In general, it seems that ligand exchange does not have a strong effect on the spin relaxation rate, either because of weak perturbing effect on the symmetry of the complex or because of the too short lifetime of the intermediate activated complex to allow spin transition.

Spin Rotation. The theory of spin rotational interaction, as treated by Atkins and Kivelson[24] and by Nyberg,[25] predicts that the electron spin relaxation time is given by

$$1/T_2 = (1/12\ \pi r^3)(\Delta g(\Delta{:}\Delta g)kT/\eta \qquad (10)$$

where $\Delta g = g - 2.0023$ and $(\Delta g{:}\Delta g)$ is the inner product of the Δg tensors. The line width contribution from spin-rotational mechanism should therefore be linear in T/η. The principal values of the g tensor are not known. Assuming axial symmetry and $g_{||}$ close to g_e, we can assume that the deviation of the isotropic g from the free spin value is mainly due to $g_\perp$. However, no precise relation exists between isotropic g factor and the slope of the high-temperature broadening for the different complexes. Ion-pair formation, for instance, gives rise to enhanced high-temperature broadening, while no shift of g factor is observed. Furthermore, by assuming $r = 3$ Å for all complexes, contribution from spin rotation does not exceed 4.3×10^{-7} G P/°K even for tetrahedral complexes which have the highest deviation of the g factor from the free spin value ($\Delta g \simeq 0.005$), while experimental values range between 2.6×10^{-4} and 2.4×10^{-5} G P/°K.

Line broadening increase exceeding the Debye limit of eq 10 has been previously reported[26] for ClO_2 in nonpolar solvents, due to the effect of intermolecular forces on the correlation time for the angular momentum. However, in the present case, the disagreement between theory and experiments seems much too high.

VI. Conclusion

Spin rotation and ligand exchange seem improbable as effective mechanisms of electron spin relaxation. In addition to ligand exchange, internal motions such as restricted rotation of the methyl groups in the DMF might also be effective in relaxing the electronic spin. This mechanism has been examined by several authors[27,28] but it seems difficult to generalize this process to a wide range of solvents.

If collision with solvent molecules is effective in inducing fluctuations of the cubic symmetry, transient distortion of the complex may increase in magnitude with increasing kinetic energy of the colliding particles. This would lead to a temperature dependence of the D factor which may explain the high-temperature broadening. Al'tshuler and Valiyev[2] have treated a similar process which accounts for both low-temperature and high-temperature broadening. In their model the Brownian motion induces fluctuations on the normal modes of vibration of the complex which act on the zero-field splitting parameter. The transition probability is proportional to the mean values of the vibrational amplitude, which increase with temperature. While strongly effective in solids, mechanisms acting through vibrational fluctuations of the electric field at the ion when acting through the spin–orbit coupling are usually negligible in liquids.[29] However, we cannot exclude this process in the present case, although a complete reconsideration of the theory is necessary.

The hypothesis that high-temperature and low-temperature results are due to two different aspects of the same mechanism is also supported by the results from Fe^{3+} and Cr^{3+} which undergo the same mechanism as for Mn^{2+}. Some preliminary experiments performed in this laboratory have shown that a clear high-tempera-

(23) J. E. Crawford, L. Lynds, and S. I. Chan, *J. Amer. Chem. Soc.*, **90**, 7165 (1968).
(24) P. W. Atkins and D. Kivelson, *J. Chem. Phys.*, **44**, 169 (1966).
(25) G. Nyberg, *Mol. Phys.*, **12**, 69 (1967).
(26) R. E. D. McClung and D. Kivelson, *J. Chem. Phys.*, **49**, 3380 (1968).
(27) T. Chen, Thesis; *Diss. Abstr.*, **28B**, 4085 (1968).
(28) R. C. Phillips, Thesis; *ibid.*, **27B**, 3489 (1967).
(29) D. Kivelson, *J. Chem. Phys.*, **45**, 1324 (1966).

ture broadening is present in $[FeCl_4]^-$ in acetone and acetonitrile. Line broadening for Cr^{3+} above 250° is also reported by Al'tshuler and Kozyrev.[30]

At the present time, little can be said about the different behavior of the different complexes. In general, ion pairs display a larger temperature coefficient with respect to the corresponding free-ion which could be related, in the Al'tshuler model, to lower mean frequency of vibration of the complex coordinates.

Acknowledgment. The authors would like to acknowledge the benefit of discussions with Dr. A. Bambini. Thanks are also due to G. Tagliavini of IBM Italia for his help in performing the simulated spectra. Financial support was provided by National Council of Research (CNR).

(30) S. A. Al'tshuler and B. M. Kozyrev, "Electron Paramagnetic Resonnance," Academic Press, New York, N. Y., 1964, p 225.

Phase Equilibria, Electrical Conductance, and Density in the Glass-Forming System Zinc Chloride + Pyridinium Chloride. A Detailed Low-Temperature Analog of the Silicon Dioxide + Sodium Oxide System

by A. J. Easteal and C. A. Angell

Department of Chemistry, Purdue University, Lafayette, Indiana 47907 *(Received April 30, 1970)*

In a study of $ZnCl_2$-based binary chloride melts which may serve as analogs of the well known and technologically important glass-forming binary systems based on SiO_2 and BeF_2 as first component, a detailed phase-equilibrium, electrical conductance, and density study of the system zinc chloride + pyridinium chloride has been carried out. In contrast to the better known zinc chloride + alkali halide systems, this present system reproduces in great detail the phase relations and physicochemical behavior of the classic Na_2O + SiO_2 system, though at temperatures reduced by a factor of about $^1/_3$. Electrical conductance data have been analyzed in terms of the three parameter equation $\kappa = AT^{-1/2} \exp B/(T - T_0)$, and the "ideal" glass transition temperature T_0 found to closely parallel the experimentally measured glass transition temperature T_g. T_0 and T_g show complex composition dependences. A minimum at 33.3 mol % $ZnCl_2$ is interpreted in terms of formation of the orthochlorozincate ion $ZnCl_4^{2-}$, an approximately linear increase from 33.3 to 66 mol % is probably due to the formation of polymeric chains based on linked $ZnCl_4$ tetrahedra, and a plateau region at $ZnCl_2$-rich compositions (65–90 mol %) is associated with the tendency to, or occurrence of, subliquidus liquid–liquid phase separation. The classical concept of "network-breaking" satisfactorily explains dramatic changes in conductivity in the region 90–100 mol % $ZnCl_2$. There is some suggestion that the rapid decrease in "activation energy" for transport in this region may be associated primarily with changes in equilibrium thermodynamic properties (configurational heat capacity) rather than with changes in a purely kinetic energy barrier as is generally assumed.

There are a number of good reasons for studying the physicochemical behavior of binary systems containing $ZnCl_2$. Perhaps the clearest is that they provide low-melting, hazard-free, and noncorrosive analogs of the silica-based and beryllium fluoride-based systems of such importance to glass and nuclear reactor technology, respectively. It might, for instance, be hoped that the greater precision achievable in these experimentally more tractable systems will permit more detailed analyses of some of the more perplexing features of the behavior of such highly structured liquids.

A second reason is that $ZnCl_2$ is a strong Lewis acid, and its interaction with chloride ions donated by a solvent chloride melt of suitable characteristics provides some of the least ambiguous cases available of the formation of "complex ions" in molten salt chemistry. Since this has been an area of contention in the field for a long time, new methods of characterizing such interactions are needed.

A further reason of special interest to us is that although the most obvious $ZnCl_2$-based binary systems, *e.g.*, zinc chloride + alkali metal chlorides, crystallize readily at their liquidus temperatures, systems in which the second component is itself low-melting yield solutions of which bulk samples can be supercooled to the point of glass formation over a considerable range of compositions. Such noncrystallizing-composition regions provide "windows" through which we can observe the behavior of liquids of variable composition as they approach the thermodynamic bottom of the liquid state.

This low temperature limit is set by the vanishing of the difference between entropies of the liquid and crystalline states, the apparent inevitably of which can be argued, for the case of pure substances, from equilibrium thermodynamic data on liquid and crystalline states.[1,2]

Associated with the vanishing of the liquid excess entropy is a vanishing of the ionic (or molecular) mobility, a tendency which is reflected in the temperature dependence of liquid relaxation rates, Y, which are described to good precision over several orders of magnitude by the rate law

$$Y = A_Y T^{-1/2} \exp -B_Y/(T - T_0) \qquad (1)$$

where A_Y and B_Y are constants characteristic of the particular relaxation process and T_0 is an empirical parameter having the dimensions of temperature, often corresponding in the case of pure liquids to the temperature at which the extrapolated configurational entropy would vanish, and denoted earlier by the authors as the "ideal" glass transition temperature.[2] Behavior at T_0, however, cannot be observed because the system inevitably falls out of internal equilibrium at a higher temperature, denoted T_g, when the relaxation times become of the same order as the time scale of the particular experiment being performed. Except in very highly structured liquids, T_g and T_0 are separated by only a small temperature interval (~10–20°) and in ideal solutions both appear to change linearly with composition between values for the two components.[3] Theories for eq 1, among which the entropy theory of Adam and Gibbs currently seems the most plausible,[4] have been discussed elsewhere,[2a] and will not be treated in any detail here.

Easteal and Hodge[5] have given evidence from an eq 1 treatment of electrical conductance measurements that in binary solutions with covalent interactions (a tendency to complex ion formation) T_0 tends to a minimum at compositions of complex ion stoichiometry, but the certainty of these conclusions was limited by the fact that the liquidus temperatures in the system studied were high relative to T_0 and in consequence the departures from Arrhenius behavior from which T_0 is assessed were small. Since Angell and Moynihan[2a] have discussed such minima in terms of the loss of Coulomb cohesive energy implicit in the covalent interaction (provided complexes are of high symmetry), and since $ZnCl_2$-based systems combine strong covalent interactions with low liquidus temperatures and supercooling composition regions, it appeared that this interesting question could probably be clarified by the study of a $ZnCl_2$-based system.

In choosing a system for study, three possibilities were available: (1) a system containing only a simple inorganic ionic species. A possible system would be $ZnCl_2$ + KI[6,7] which has extensive glass-forming composition regions; (2) a system containing chloride anions and otherwise only inorganic constituents. A possible system would be the hydrate melt $ZnCl_2 + Mg(H_2O)_6Cl_2$ in which composition regions on the zinc chloride-rich side of the system are glass-forming; and (3) a system containing only chloride anions and a simple organic cation. Numerous possibilities are available, *e.g.*, (a) $ZnCl_2$ + $N(CH_3)_4$ Cl or other tetraalkyl cation chlorides, (b) zinc chloride + methylamine hydrochloride or higher homologs, (c) zinc chloride + pyridine hydrochloride, etc. Examples of each of a, b, and c were examined and shown to have glass-forming composition regions.

Of the above possibilities (1) was rejected on the basis of the desirability in initial investigations of dealing with a single ligand species and (2) was excluded on counts of restricted glass-forming composition regions and complications due to incomplete association of "hard base" water molecules with the "hard acid" Mg^{2+} cation (though a study of this system will be reported elsewhere).[8] Of the possibilities listed under (3) the zinc chloride + pyridine hydrochloride system was selected because of the previous usefulness of pyridine hydrochloride in molten salt studies,[9] ease of purification, and low melting point. Potentially simpler systems incorporating the quasispherical tetraalkylammonium cations were avoided because the pure salts decompose before melting precluding the 0–100% $ZnCl_2$ liquid range study considered very desirable for this project.

Glass-forming regions and characteristics of these various glass-forming chloride systems are discussed jointly elsewhere.[7] The structure and thermodynamics of the parent glass former, $ZnCl_2$, has been discussed in detail in a previous publication.[10]

Experimental Section

Pyridinium chloride, hereafter referred to as PyHCl, was obtained from two sources: (a) by fractional distillation at atmospheric pressure of the Eastman Organic Chemicals salt, the fraction distilling at 221–224° being collected, and (b) by the method of Audrieth and coworkers,[11] *viz.* addition of concentrated aqueous hy-

(1) J. H. Gibbs, "Modern Aspects of the Vitreous State," Vol. 1, J. D. McKenzie, Ed., Butterworth, London, 1960, Chapter 7.

(2) (a) C. A. Angell and C. T. Moynihan, "Molten Salts: Analysis and Characterization," G. Mamantov, Ed., Marcel Dekker, 1969; (b) C. A. Angell, *J. Chem. Educ.*, **47**, 583 (1970).

(3) C. T. Moynihan, C. R. Smalley, C. A. Angell, and E. J. Sare, *J. Phys. Chem.*, **73**, 2287 (1969).

(4) G. Adam and J. H. Gibbs, *J. Chem. Phys.*, **43**, 139 (1965). (However, see M. Goldstein, *ibid.*, **51**, 3728 (1969), and R. Weiler, S. Blaser, and P. B. Macedo, *J. Phys. Chem.*, **73**, 4147 (1969) and K. J. Rao and C. A. Angell, 3rd International Conference on Physics of Non-Crystalline Solids, Sheffield, Sept 1970.

(5) A. J. Easteal and I. M. Hodge, *J. Phys. Chem.*, **74**, 730 (1970).

(6) I. Schulz, *Naturwissenchaften*, **44**, 536 (1957).

(7) A. J. Easteal, D. Chin, J. Wong, I. Hodge, and C. A. Angell, submitted for publication to *Phys. Chem. Glasses.*

(8) C. A. Angell and D. Chin, unpublished work.

(9) V. C. Reinsborough, *Rev. Pure Appl. Chem.*, **18**, 281 (1968).

(10) C. A. Angell and J. Wong, *J. Chem. Phys.*, **52**, 2053 (1970).

(11) J. F. Audrieth, A. Long, and R. E. Edwards, *J. Amer. Chem. Soc.*, **58**, 428 (1936).

drochloric acid (Baker and Adamson, "Reagent ACS" grade) to a slight (about 5%) excess of a solution of pyridine (J. T. Baker, "Analyzed" Reagent) in ethanol, and fractional distillation (221–224°) of the mixture. The PyHCl prepared by both methods melted to a colorless liquid at 143.5°.

Zinc chloride was Fisher Certified ACS grade material. It was purified by passing hydrogen chloride through the molten salt at 450–500°, for 1–4 hr depending on the quantity of salt, followed by purging with dry nitrogen for several hours. The fused commercial salt contains flecks of a black carbonaceous impurity which are generally completely removed by the HCl–N_2 treatment.

Except for the highest $ZnCl_2$ content melts, solutions for study were prepared by addition of molten zinc chloride aliquots initially to pure PyHCl, and subsequently to $ZnCl_2$ + PyHCl solutions of known composition. Experiments were performed on several independently prepared sets of mixtures with overlapping composition ranges. At $ZnCl_2$ contents greater than 50 mol % solution was a slow process; temperatures in excess of 250° were avoided because of the tendency of PyHCl to undergo some decomposition and discolor the melt. At compositions >85 mol % $ZnCl_2$ high solution temperatures could not be avoided: such solutions prepared by addition of PyHCl to $ZnCl_2$ were dark brown in color, and gave less reproducible results than the other compositions.

In preparation of samples for phase diagram determination $ZnCl_2$ was used in the form of easily handled glass beads (produced by dropwise pouring of purified fused $ZnCl_2$ into liquid nitrogen). All preparations involving the use of solid $ZnCl_2$ (beads) and PyHCl were performed in a low (−75°) dew-point drybox[11a] (Kewaunee Scientific).

Glass transition temperatures were determined using a differential thermal analysis method essentially the same as previously described.[12] The glasses were produced by quenching fused mixtures (in 5-mm o.d. Pyrex tubes) either (a) in liquid nitrogen or (b) first in a trichloroethylene slush bath then in liquid nitrogen. Procedure b was used for mixtures in the composition regions 39–45 and 55–65 mol % $ZnCl_2$, for which the greater initial quenching rate obtainable with the trichloroethylene slush (~ 28° sec^{-1} compared with ~ 17° sec^{-1} for liquid nitrogen) was required to circumvent crystallization.

The phase diagram for the system was investigated using the method of cooling curves for initial work, and differential scanning calorimetry (Perkin-Elmer DSC IB) using small (~2–6 mg) samples encapsulated in aluminum pans to resolve uncertainties and establish the final diagram. Samples of mixtures in the composition region in which crystallization does not readily occur were caused to crystallize by fine grinding of the glassy samples.

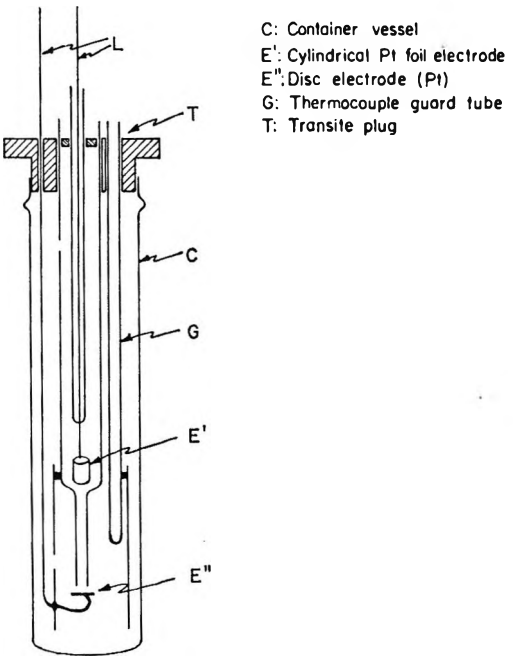

Figure 1. Conductance cell.

A dip-type cell constructed from Pyrex glass (Figure 1) in conjunction with a Wayne–Kerr Type B221 impedance bridge was utilized in measuring specific conductance. In addition to the cell components shown in Figure 1 the transite cap carried two further tubes to provide a slow flow of dry nitrogen through the cell, in order to prevent absorption of water vapor by the melts. Measurements of conductance were made at a single frequency, 1592 Hz.[13] The cell was calibrated using 1.0 and 0.1 Demal aqueous potassium chloride at 25.0°. The cell constant was 52.54 ± 0.04 cm^{-1} for one cell (A) and 25.77 ± 0.02 cm^{-1} for another cell (B) used for two melts. Cell A had overall length 15 cm, and the capillary was 2.5 mm i.d., 23 mm long. Cell B differed only in the length of the capillary. The electrodes were fixed relative to one another and to the capillary. The leads to the electrodes were immersed to different depths in different electrolytes, but it was found that the measured conductance of a given electrolyte was independent (within experimental precision) of the depth of immersion.

For the fused salt conductance measurements the cell was held in a cylindrical aluminum block furance (Figure 2), heated with two 250-W "Firerod" cartridge heaters (Watlow Electric Mfg. Co.). The aluminum block

(11a) It is found that $ZnCl_2$ glass beads provide an excellent dryness detector for dryboxes. The beads, which are crystal bright as prepared, frost over on the surface in the presence of very small traces of moisture.

(12) C. A. Angell, E. J. Sare, and R. D. Bressel, *J. Phys. Chem.*, 71, 2759 (1967). See also ref 27b.

(13) The frequency dispersion of conductance, which becomes very pronounced at temperatures approaching T_g as the liquid relaxation time and inverse bridge frequency match up, has been investigated in an all-metal cell and will be reported separately.

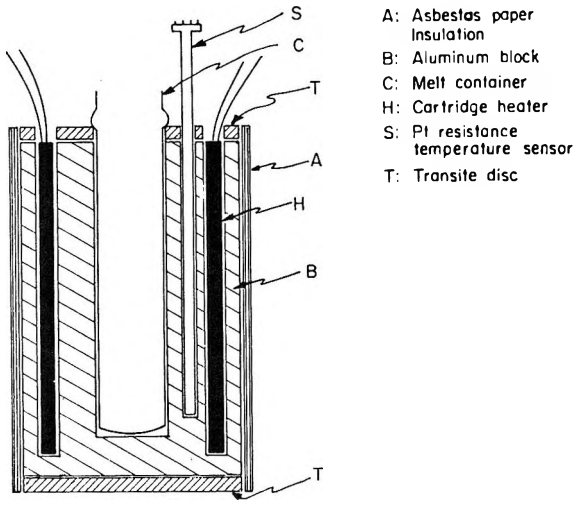

Figure 2. Furnace assembly used for conductance measurements.

was 7.5 cm in diameter and 16 cm long, the well in the center being 2.5 cm in diameter and 15.5 cm deep. The top of the cell was cooled with tap water, *via* a small copper coil.

Conductances were determined initially under both continuous cooling (up to 1° min^{-1}) and steady-state, *i.e.*, constant temperature conditions. When ln κ was plotted against $1/T$ for these mixtures, the steady-state and nonsteady-state points fell on the same curves within experimental precision. Subsequently conductances were determined only under continuous cooling conditions (except in the case of pure $ZnCl_2$, where both methods were used), with an approximately constant cooling rate. This was achieved by coupling the furnace heating elements to a Melabs Model CTC-1A proportional temperature controller in conjunction with a C1111 programmer and C1101 platinum resistance sensor. The sensor was located in the aluminum block adjacent to one of the heaters (3 mm separation). Using this arrangement cooling rates in the range 0.6–0.75° min^{-1} were achieved between 350 and 80°. For a given run the cooling rate was constant to within ±10%.

Conductances were measured at temperature intervals of 2° for the most part. At temperatures below 80° measurements were usually made at 1° intervals, provided crystallization did not intervene, in order to more precisely determine the temperature dependence of conductance. In this region the temperature coefficient becomes very large (up to 40% deg^{-1}).

Melt temperatures were determined with a chromel–alumel thermocouple, in association with a Leeds and Northrup Model K3 potentiometer. The thermocouple was calibrated at the boiling point of water and the melting point of lead and temperature measurement is believed accurate to ±0.2°. Precision of measurement was ±0.05°. Specific conductances should be accurate to within ±1%,[14] while mixture compositions have an uncertainty of ±0.5 mol % $ZnCl_2$.

Densities were measured dilatometrically, using dilatometers constructed by fusing 5-ml pipets, graduated in 0.1 ml (Kimax, No. 37020) to 10-ml volumetric flasks (Pyrex or Kimax). A 10/30 ground glass socket was fused to the upper end of each dilatometer to allow a drying tube filled with Drierite to be attached. Dilatometers were calibrated with water at 25.00 ± 0.02°, with precision 0.04%. They were loaded with premixed fused salt using an auxilary furnace and transferred to an oil bath (Dow Corning 200 Electronic fluid) for the measurements. The temperature of the bath was controlled (to ±0.2°) with a Melabs Proportional Controller. For two mixtures (82.3 and 92.8% $ZnCl_2$) the liquid temperature ranges were not accessible with the oil bath, and the dilatometer was heated in a conventional vertical tube furnace whose temperature was controlled with a Cole–Parmer Proportio Null (Series 1300) unit to within ±0.5°. The temperature range of measurement for mixtures was from approximately the liquidus temperature to about 210°, except for the 82.3 and 92.8% $ZnCl_2$ mixtures.

Results

The phase equilibrium study of the system indicates the existence of four congruently melting compounds: R_4ZnCl_6, R_2ZnCl_4, $RZnCl_3$, and RZn_2Cl_5 (R = pyridinium cation). An outline of the phase diagram is given in Figure 3.

$ZnCl_2$ + PyHCl fused mixtures can be quenched to the glassy state, in the composition ranges 39–45 and 55–100% $ZnCl_2$. On heating, many of the glasses spontaneously crystallize at temperatures not far above their glass transition temperatures. In a restricted composition range (*ca.* 60–90% $ZnCl_2$) liquid mixtures can be supercooled slowly to the glassy state and the glasses reheated, without crystallization.

The variation of glass transition temperature with composition is indicated by the subliquidus points in Figure 3. For each mixture T_g was determined at a number of different heating rates, generally in the range 5–20° min^{-1}. For all except two mixtures (96.5 and 97.7% $ZnCl_2$) the values of T_g are those appropriate to a heating rate of 8° min^{-1}. The heating rates for the two exceptional mixtures were 10.5° min^{-1} and 20° min^{-1} for 96.5 and 97.7% $ZnCl_2$ respectively. The uncer-

(14) We note here that reliable data could not be taken within ~60° of T_g using the present capillary cell. Measurements continued into this range showed an anomalous, frequency-dependent, minimum in conductance followed by a maximum several degrees lower in temperature, which are not reproduced if a parallel plate cell is substituted for the capillary cell. These effects arise from the fact that as the conductance reaches very low values the salt in effect becomes a dielectric medium which is the presence of a second dielectric (the glass of the cell) can give rise to a frequency dependent dispersion in capacitance [C. P. Smyth, Dielectric Behavior and Structure, McGraw Hill, New York, N. Y., 1955] which is read out on the bridge as an ac conductance contribution. Conductances in this regime must be measured in the absence of dielectric materials other than the substance of interest.

Table I: Transport Parameters for $ZnCl_2$ + PyHCl Mixtures

Mole fraction $ZnCl_2$	A	B	T_0	$\sigma \times 10^{3a}$	A'	B'	T_0'	T_g	Temp range, °C
0.0	3.989	668.3	212	0.9	0.4967	526.3	228	*b*	139–211
7.0	4.111	762.7	200	3.3	0.6088	611.7	215		116–217
12.6	4.230	831.3	197	1.3	0.7390	684.1	210		110–200
17.5	4.147	827.4	208	2.0	0.6506	681.8	221		120–214
21.5	4.304	953.0	196	1.8	0.7462	773.1	212		138–221
26.9	4.441	1039.2	185	0.6	0.9136	648.6	198		134–203
32.2	4.548	1215.9	159	0.8	0.9450	994.7	176		178–216
36.0	4.140	1005.6	189	0.9	0.5634	812.8	206	236	154–240
38.6	3.942	932.9	200	1.4	0.4237	774.6	213	241	112–236
40.5	3.843	882.1	209	2.6	0.3984	758.9	218	245	99–206
45.2	3.765	896.9	215	1.9	0.2986	754.2	225	255	113–215
53.6	3.697	895.4	229	2.5	0.2579	781.2	237	268	111–215
58.4	3.645	887.0	241	3.3	0.1781	766.4	250		124–244
								274	
58.4	3.129	733.6	255	3.5	−0.0474	702.3	256		72–122
63.2	3.717	930.6	248	1.4	0.2771	823.5	255		138–254
63.2	3.137	764.0	262	3.7	−0.0994	720.2	264	279	92–136
63.2	3.766	908.8	252	6.3	0.6038	877.0	253		66–90
68.3	3.742	956.0	256	1.8	0.2533	831.3	265		150–274
68.3	3.383	864.3	262	3.4	0.0801	804.1	265	281	100–148
68.3	3.358	877.7	260	5.3	0.1012	829.5	262		74–98
73.1	3.884	1046.7	257	2.1	0.3590	906.4	267		162–297
73.1	3.921	1060.3	256	2.5	0.5936	991.6	259	282	112–160
73.1	4.573	1207.3	249	5.1	1.2408	1133.0	252		82–110
84.6	4.237	1313.9	257	1.9	0.6725	1153.4	267		196–308
								288	
84.6	2.214	963.8	260	4.3	−0.0111	898.6	263		96–130
87.5	3.003	1137.8	247	2.0	0.4396	1027.7	253		130–202
								292	
87.5	2.164	909.1	262	5.6	−0.0109	860.8	264		92–128
91.3	5.101	1958.0	235	1.7	1.4342	1728.3	247	303	253–325
94.7	6.141	2707.2	210	2.1	2.4314	2437.3	221	320	266–338
100.0	8.490	3617.4	280	5.6	4.7024	3343.2	288	376	301–454

[a] σ is the rms deviation (in ln κ) of the experimental points from the calculated curves. [b] A T_g for PyHCl of 227°K has been estimated by I. M. Hodge[45] by a short extrapolation of pyridinium chloride + α-picolinium chloride solution T_g's.

tainty in T_g for mixtures containing up to 91.5% $ZnCl_2$ is of the order ±2°. For the two mixtures richest in $ZnCl_2$ and for pure $ZnCl_2$ the uncertainty is larger, of the order ±5°, due to the relatively small change of heat capacity occurring at T_g. The value for pure $ZnCl_2$ agrees within experimental uncertainty with the value of 102.5° determined dilatometrically[15] by Goldstein and Nakonecznyi.

The specific conductances of all the mixtures studied (7.0 to 94.7% $ZnCl_2$) and of the two pure components show non-Arrhenius temperature dependences. For the two pure salts and for mixtures containing up to 87.5% $ZnCl_2$ the temperature dependences are quite precisely (rms deviation 0.05–1 %) described by analytic functions both of the form of eq 1 in logarithmic form with $Y \equiv \kappa$, and of eq 2

$$\ln \kappa = A' - B'/(T - T_0') \qquad (2)$$

A', B', and T_0' being constants for a given mixture. The difference between eq 1 and 2 lies in the inclusion or otherwise of the preexponential $T^{-1/2}$ term. Since the most appropriate form is currently undecided, the "best-fit" parameters for both equations, evaluated by least-squares computer fit of experimental conductances, are presented in Table I.

Note that only in the composition region 0–50% $ZnCl_2$ does the form of the equation have any important effect on the T_0 and B values. Exercising a preference for eq 1, we show, in Figure 4, the composition variation of the best fit parameters: glass transition temperatures are included for purposes of comparison. For mixtures with compositions in the range 58.4–87.5% $ZnCl_2$ the experimental data were analyzed in separate temperature ranges corresponding to equal (~1 decade in κ) ranges of conductance (excluding conductances for temperatures within 60° of T_g). The values of the transport parameters corresponding to the separate temperature ranges are shown as unshaded symbols in Figure 4 and are tabulated in Table I. No systematic

(15) M. Goldstein and M. Nakonecznyi, *Phys. Chem. Glasses*, **6**, 126 (1965).

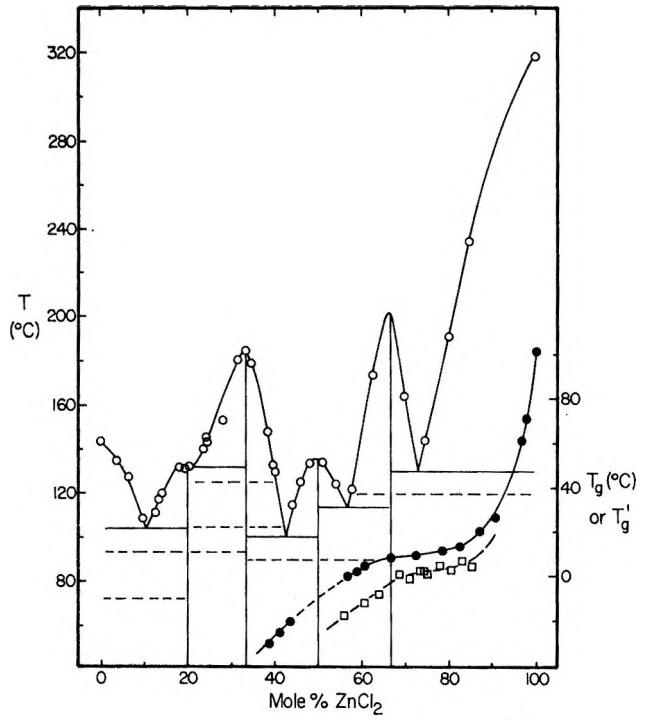

Figure 3. Phase diagram: $ZnCl_2$ + PyHCl. Open circles are experimental liquids temperatures and horizontal broken lines indicate solid-state transitions. Values of T_g for $ZnCl_2$ + PyHCl are shown as shaded circles: values of T_g' (see text for definition) for SiO_2 + Na_2O are indicated by open squares.

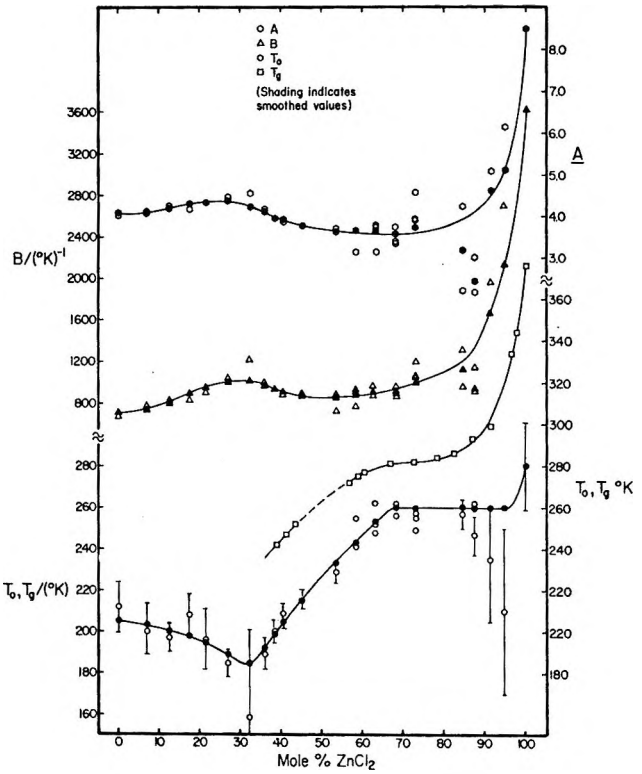

Figure 4. Composition variation of transport parameters and glass transition temperatures for $ZnCl_2$ + PyHCl solutions. Open circles are least-squares best fit values for eq 1. Filled circles are parameters corresponding to smoothed values of T_0. Where more than one open circle occurs at a given composition sufficient data were available for analysis in sections (see Table I). Error bars are drawn for 1.5 standard deviations.

variations in T_0 with temperature are apparent in the ~4 decade range of conductances examined in this study. Undoubtedly, at lower temperatures still, the tendency to return to Arrhenius behavior seen in other liquids near T_g (see ref 4b) would be observed in the present solutions.

The best-fit parameters show some random scatter, particularly for mixtures toward the two extremes of the composition range. The reason for the scatter is principally the relatively short liquid ranges accessible in these composition regions. On the basis of the composition variation of the best-fit parameters and of T_g, we have chosen a set of smoothed values of T_0 for which exist corresponding sets of smoothed values of A and B: the smoothed values of the parameters are represented with the shaded symbols of Figure 4.

Dilatometer volumes were measured to ±0.01 cm³. Densities were computer fitted (method of least squares) to linear equations of the form

$$\rho = a + bT \ (T \text{ in } °\text{K}) \qquad (3)$$

with precision (rms deviation) of the order (0.4–1.2) × 10^{-3}. Best-fit parameters of eq 3 are given in Table II. For the 92.8% $ZnCl_2$ mixture partial decomposition of the melt occurred, and the measured densities are less reliable for this mixture.

Figure 5 shows the composition dependence of density, in the form of isotherms for 150, 250, and 350° (the latter by extrapolation of measured values) in addition to the composition variations of molar volume (V_m) and thermal expansivity (α). The latter has been evaluated using eq 4

Table II: Density Parameters

$$\rho(\text{g cm}^{-3}) = a + bT \ (°\text{K})$$

Mole fraction $ZnCl_2$	a	$-(b \times 10^3)$	$(\sigma \times 10^3)^a$	Temp range, °K[b]
0.000	1.395	0.588	0.5	418–471
0.052	1.434	0.579	0.6	400–460
0.153	1.528	0.586	0.7	387–465
0.204	1.602	0.628	0.6	386–464
0.312	1.700	0.613	0.6	456–480
0.334	1.720	0.600	0.6	461–490
0.383	1.808	0.675	0.4	429–479
0.452	1.886	0.694	0.8	403–479
0.530	2.025	0.799	0.6	404–475
0.621	2.152	0.792	0.5	391–480
0.616	2.311	0.791	0.4	412–481
0.823	2.551	0.799	0.9	513–588
0.928	2.931	1.002	1.2	563–609

[a] σ is the rms deviation (in ρ) of the experimental points from the calculated straight line. [b] Temperature range of measurements.

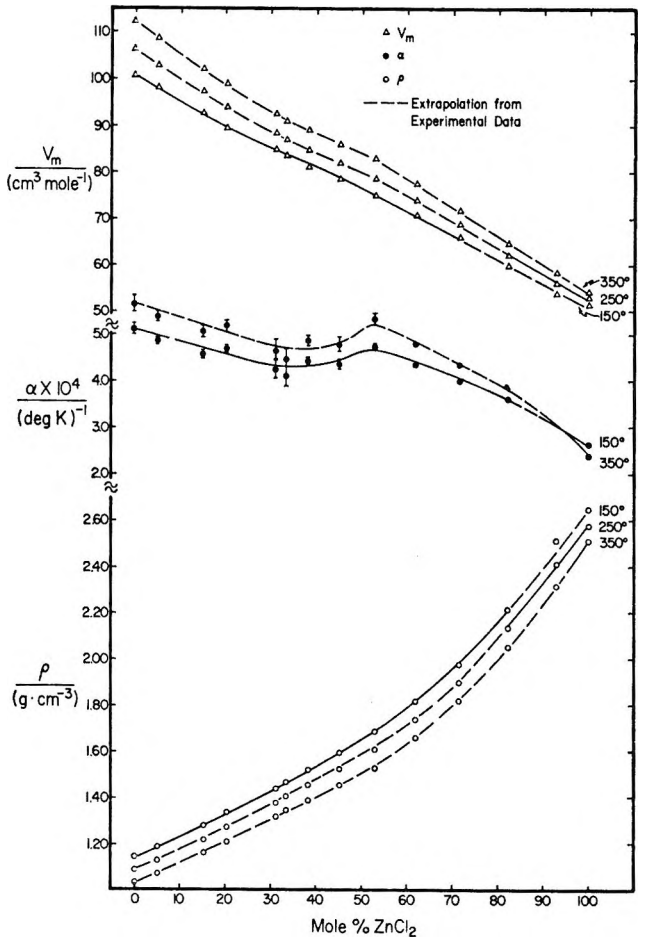

Figure 5. Composition dependence of density, thermal expansivity, and molar volume for $ZnCl_2$ + PyHCl solutions.

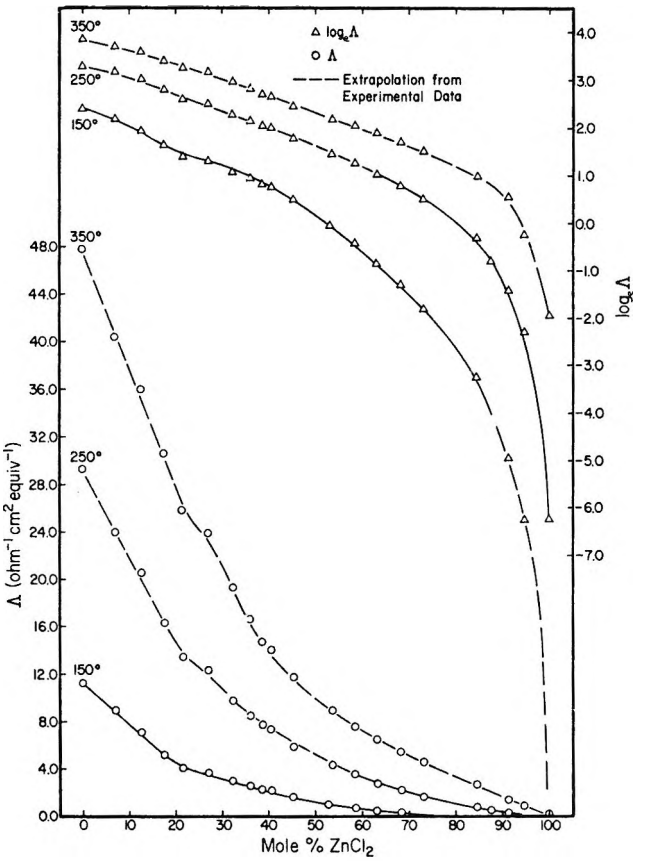

Figure 6. Isothermal composition dependence of equivalent conductance for $ZnCl_2$ + PyHCl solutions, shown on both linear and logarithmic (ln Λ) scales. As no temperature of measurement was common to all compositions, extrapolated values (based on eq 1) are utilized where necessary to complete the isotherms.

$$\alpha = -b/\rho \qquad (4)$$

b being the slope of the ρ *vs.* T graph. Estimated uncertainties in α are shown as error bars in Figure 5, and they vary from about 1 to 5%. The values of ρ, V_m, and α for pure $ZnCl_2$ at 150° were calculated from published data,[15] while the values for 350° are from the density data of Klemm.[16]

From a large-scale plot of density *vs.* composition, at 150, 250, and 350°, densities for those mixtures whose specific conductances were measured have been estimated by interpolation, and the equivalent conductances (Λ) of these mixtures evaluated using the relationships

$$V_E = (X_E \cdot E_{ZnCl_2} + (1 - X_E)E_{PyHCl})/\rho \qquad (5)$$

$$\Lambda = \kappa \cdot V_E \qquad (6)$$

where V_E is equivalent volume (cm³ equiv⁻¹), E is the equivalent weight, and X_E is the equivalent fraction of $ZnCl_2$ defined by

$$X_E = 2X_{ZnCl_2}/(1 + X_{ZnCl_2}) \qquad (7)$$

where X_{ZnCl_2} is the mole fraction of $ZnCl_2$.

Isotherms for 150, 250, and 350° of Λ *vs.* composition are given in Figure 6. On account of the very large change in Λ from pure pyridinium chloride to pure $ZnCl_2$, isotherms of ln Λ are also given to show more clearly the composition dependence for $ZnCl_2$-rich mixtures.

The Conductance of Pure $ZnCl_2$. There are at least six published reports [17-22] on the conductance of pure $ZnCl_2$ and its temperature dependence. No two sets of data agree closely over a wide temperature range (*e.g.*, 100°); in fact the variation in values for particular temperatures is very large. For example, at 336° the highest and lowest of the published specific conductances differ by almost 55% of the mean of the two values: at 400° the difference is 49%.

(16) W. Klemm, *Z. Anorg. Chem.*, **152**, 235 (1926).

(17) W. Biltz and W. Klemm, *Z. Physik. Chem. (Leipzig)*, **110**, 318 (1924).

(18) J. D. McKenzie and W. K. Murphy, *J. Chem. Phys.*, **33**, 366 (1960).

(19) F. R. Duke and R. A. Fleming, *J. Electrochem. Soc.*, **104**, 251 (1957).

(20) J. O'M. Bockris, E. H. Crook, H. Bloom, and N. E. Richards, *Proc. Roy. Soc. Ser. A*, **255**, 558 (1960).

(21) L. F. Grantham and S. J. Yosim, *J. Chem. Phys.*, **45**, 1192 (1966).

(22) H. Bloom and I. A. Weeks, *J. Chem. Soc., A*, 2028 (1969).

All sets of data show non-Arrhenius temperature dependence; however, the curvature of ln κ *vs.* $1/T$ plots varies widely from set to set. The literature data, together with the results of four of our experiments on pure $ZnCl_2$, have been analyzed using eq 1; the best-fit parameters are given in Table III.

Table III: Transport Parameters for Pure $ZnCl_2$

Ref	A	B	T_0, °K	$\sigma \times 10^3$	Temp range, °K
20	3.413	2345	339[a]	29.7	602–970
21	6.677	2602	327	34.6	586–1136
17	5.965	1978	384	41.1	597–923
19	6.370	2173	375	1.9[b]	748–923
18	0.503	255	521	4.6	593–673
22	7.384	2969	317	3.9	588–728[c]
This work[d]	8.490	3617	280	5.6	574–727

[a] Three of the published values appear to be significantly in error; they were excluded from the analysis. [b] This analysis was made on smoothed data rather than raw experimental data; hence the value of σ is not necessarily a reflection of the precision of the experimental data. [c] Bloom and Weeks' data extend to 851°K. Their data only for the range shown were analyzed in order to provide a more meaningful comparison with our own results. [d] Analysis made on the combined results of four experiments (numbers 2, 3, 5, and 6).

In the present study the conductance of $ZnCl_2$ has been measured in six separate experiments in an attempt to obtain reproducible data and to acertain the reliability of the purification procedure used. In each case the starting material was Fisher Certified ACS grade $ZnCl_2$ (maximum impurity listed as "substances not precipitated by $(NH_4)_2S$," 0.15%), which was dehydrated and purified using the procedure outlined above (Experimental Section). The results of these experiments are compared graphically with some of the literature data (for a limited temperature range) in Figure 7. The results of our first experiment (points denoted by ⊖ in Figure 7) are in doubt due to possible contamination: black flecks of material of unknown identity were dispersed in the melt. In subsequent experiments the melts were colorless and transparent, with no visual evidence of contamination. In the second experiment (●) a fresh sample of $ZnCl_2$ was purified by the HCl–N_2 purging sequence and its conductance measured at 403.0°. The salt was then treated for a further period and the conductance remeasured (at 399.5°, ■). The two values are in good agreement. The fourth experiment was done on a different batch of $ZnCl_2$ which yielded high results (⊕) due evidently to some prior contamination of the salt. For the last two experiments (△ and ○) a previously unopened batch of $ZnCl_2$ was used. In the final experiment the salt was heated with HCl for 7 hr followed by nitrogen for 16 hr. The results of the last two experiments agree well with the values obtained at 403.0 and 399.5° and are in reasonable accord at some temperatures with some of the published data. However, there is an approximately uniform discrepancy of about 28% with the most recently published data (Bloom and Weeks).[22]

It is noteworthy that the temperature dependence of κ found by us in the four experiments in which temperature was varied is very similar in that the values of T_0 (from eq 1) are all in the range 270–290°K. Also, these values of T_0 are consistent with that obtained from the temperature dependence of viscosity, which we have also determined. The best-fit value of T_0 from our viscosity data is 260 ± 20°K. Both values are somewhat lower than an estimate, T_0 = 325°K,[2a] made from the limited calorimetric data available.

It is apparent from Table III that several sets of published data show very poor precision: a notable exception is the data of Bloom and Weeks, who find T_0 = 317°K. The lack of precision is presumably due to instrumental factors and/or experimental technique. The large discrepancies in absolute values can probably be attributed to the highly developed network structure of $ZnCl_2$:[10] even very small amounts of contaminants can disrupt the network sufficiently to cause pronounced changes in ion mobilities. The discrepancies, in this interpretation, are attributable in large part to variations in the nature and concentration of impurities present in the various source materials which have been used.

In this respect a point in favor of the results of Bloom and Weeks is their distillation purification of the $ZnCl_2$, a procedure not adopted in the present work.

Although the conductance and transport parameters of pure $ZnCl_2$ are of considerable interest *per se*, it must be emphasized that in the present study we have been concerned primarily with the composition variation of transport and other parameters, of mixtures of $ZnCl_2$ with PyHCl. While there may be some uncertainty in the values of the conductance of $ZnCl_2$ itself, any trace contaminants which may be present in the pure salt will have a negligible influence on the conductances of the binary solutions, less still on their composition dependences.

Discussion

The general features of the behavior of the present system closely parallel those which have been previously found for SiO_2-based and BeF_2-based binary systems, and it is with an exploration of the details of this behavior that this discussion will be mainly concerned.

As in the analogous systems the most prominent feature, *viz.*, the enormous increase in particle mobility resulting from addition of PyHCl to pure $ZnCl_2$, is readily associated with the disruption of a highly structured three-dimensional network liquid by breaking up of chloride-bridge bonds in proportion to the number of added chloride ions. Such behavior was also observed

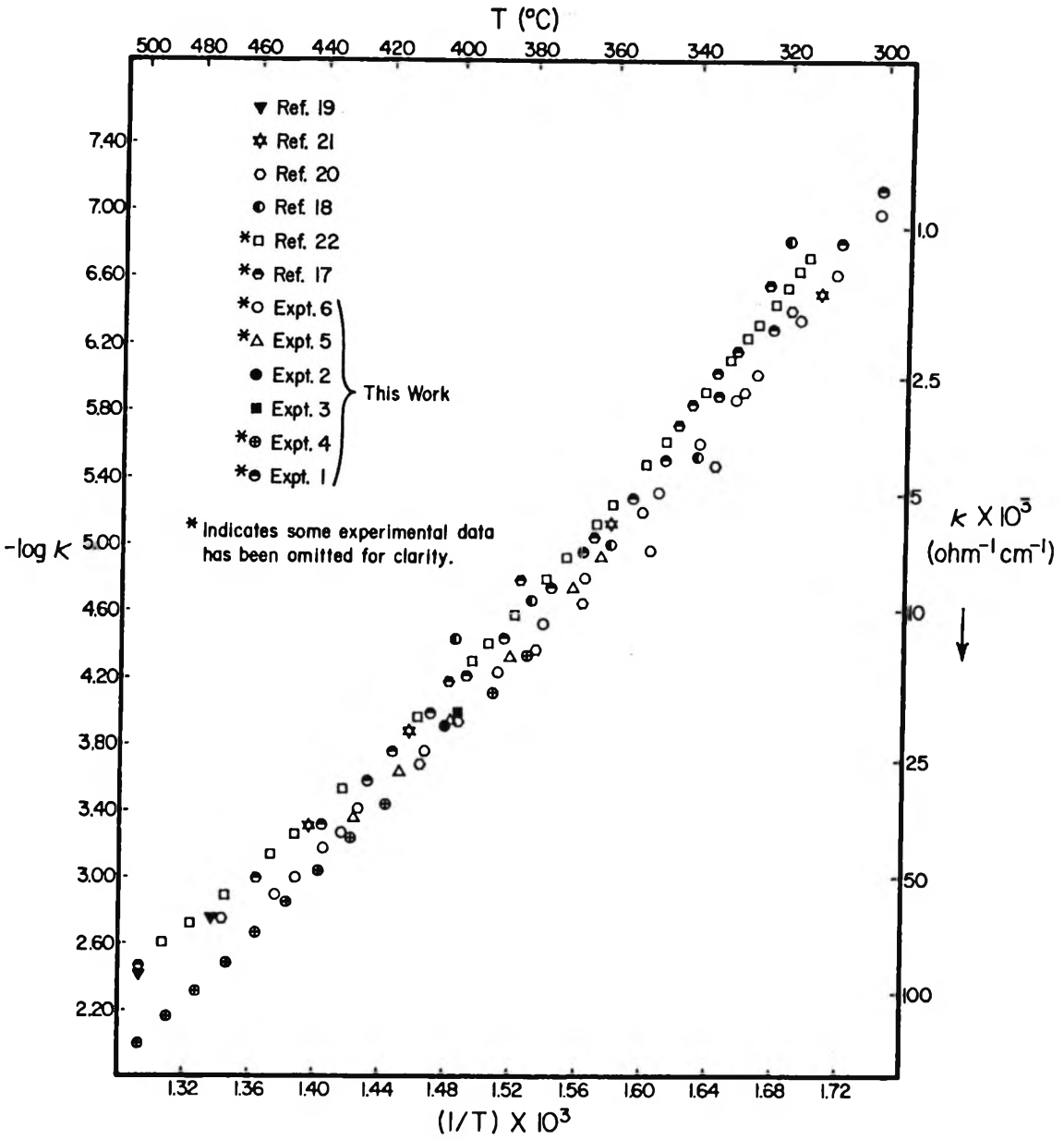

Figure 7. Comparison of published values with values found in this work for the specific conductance of pure $ZnCl_2$. Log κ is ln κ. Note inverted scale for κ.

and similarly interpreted by Duke and Fleming[23] in an earlier study of $ZnCl_2$ + KCl solutions.

Details of the phase diagram for $ZnCl_2$ + PyHCl will be discussed fully in a separate publication. However, some features are worthy of comment in the context of the present study. In particular this system has two congruently melting compounds (R_4ZnCl_6 and $RZnCl_3$) which are not known to form in zinc chloride + alkali metal chloride systems. The existence of these two compounds is probably evidence that the pyridinium ion acts in these mixtures as a very weak field cation *i.e.*, it has a small effective ionic potential.

The compound $RZnCl_3$ has analogies in beryllium fluoride + alkali fluoride mixtures. Thus NaF, KF, RbF, and CsF all form 1:1 compounds with BeF_2, while LiF + BeF_2 mixtures have been reported to form $LiBeF_3$ and $LiBe_2F_5$ as a subsolidus phase.[24] In binary silicate systems the analogous "metasilicates" Li_2SiO_3, Na_2SiO_3, K_2SiO_3, $BaSiO_3$, and $CaSiO_3$ are congruently melting compounds.[24]

It is significant that liquid mixtures in the composition region of the 1:1 compound (~45–55 mol % $ZnCl_2$) cannot be quenched to glasses without partial crystallization, even though the compound has a relatively low melting point (*ca.* 130°, T_m/T_g = 1.56). By contrast,

(23) F. R. Duke and R. A. Fleming, *J. Electrochem. Soc.*, 104, 251 (1957).

(24) E. M. Levin, C. R. Robbins, and H. F. McMurdie, "Phase Diagrams for Ceramists" American Ceramic Society, Columbus, 1964.

mixtures of composition close to that of the compound RZn_2Cl_5 may be supercooled very readily without crystallization, in spite of the much higher melting point (*ca.* 195°, $T_m/T_g = 1.67$) of this compound. It is likely, therefore, that crystalline $RZnCl_3$ has a structure which is closely related to that of liquid mixtures of similar composition, whereas in order for RZn_2Cl_5 to crystallize, rather severe changes in configuration of the liquid are necessary.

There is a close analogy here between the PyHCl + $ZnCl_2$ and $Na_2O + SiO_2$ systems. As in the case of the former melts, the sodium orthosilicate (Na_4SiO_4) melt does not form a glass, and glass formation does not readily take place at the metasilicate composition. Na_2SiO_3 (and Li_2SiO_3) has a crystal structure based on infinite chains of oxygen-bridged SiO_4 tetrahedra.[25] In a number of other crystalline metasilicates there exist closed rings of tetrahedra, and the structure of sodium metaphosphate ($NaPO_3$), whose melt forms a stable glass, is also based on closed rings of (PO_4) tetrahedra. However, fused $NaPO_3$ contains bridged PO_4 chains;[26] crystallization of the melt, therefore, requires fracture of a number of phosphorus–oxygen bonds, and supercooling to the vitreous state occurs readily. On the basis of these analogies, and the observation that $RZnCl_3$ forms acicular crystals, it seems likely that this compound has a crystal structure essentially similar to that of Na_2SiO_3 and that melts of composition close to the trichlorozincate stoichiometry contain principally long chains of chloride-bridged $ZnCl_4$ tetrahedra.

The principal distinction between this work and the published work on the related systems is the greater detail on departures from Arrhenius behavior in the present case, which have permitted the parameters of eq 1 to be determined with reasonable accuracy. The composition dependences of these parameters (Figure 4) are of unusual interest. In the first place the close relationship of the measured glass transition temperatures to the T_0 parameter is to be stressed. The two curves are approximately parallel, except in the region 85–100% $ZnCl_2$, and in this region T_0 and T_g change in the same direction. The paralleling of T_0 by T_g is also characteristic of concentrated aqueous electrolytes[27] and lends weight to the use[27b] of the readily measurable T_g as a structure-sensitive parameter or elucidation of the effects of composition variation on electrolyte constitution. T_0 is perhaps to be regarded as the thermodynamically more meaningful parameter, but its evaluation depends on extrapolation of high precision transport data to temperatures which are generally well below the lowest temperature at which measurements can be made. T_g by contrast is directly measured at temperatures which in general are not far above T_0. The parallel behavior observed for the two parameters therefore lends confidence to our interpretation of the variation of T_0, so that although T_g does not extend to compositions of less than 39% $ZnCl_2$, T_0 continues to provide a probe for interparticle interactions. Since the parameters A and B show little sensitivity to composition except near pure $ZnCl_2$ and $ZnCl_4^{2-}$ stoichiometries, most of the discussion of transport behavior in this system can be made in terms of the behavior of T_0.

The principal features are (a) an initial decrease, as $ZnCl_2$ is added to PyHCl, reaching a minimum at the stoichiometry of the tetrachlorozincate ion, (b) a rapid increase region extending from the minimum to *ca.* 65% $ZnCl_2$, (c) a "plateau" region from 65–85% $ZnCl_2$ in which the variation is slight, and (d) a terminal region of sharply rising T_g to the high value for pure $ZnCl_2$. These regions and their origin will be examined in the following discussion, but first it is appropriate to draw attention to a further example of the remarkable similarity in behavior of the present system and the classic Na_2O–SiO_2 system. Such data as exist for the glass transition temperature in the Na_2O–SiO_2 system[28] when scaled to the temperature of the present system [by multiplying all T_g by the factor $T_g(PyHCl–ZnCl_2)/T_g(Na_2O–SiO_2]$ determined at one mole ratio) closely reproduce not only the rapidly increasing T_g below 65% $ZnCl_2$ but also the "plateau" region above. These data, displaced for clarity 7° lower on the temperature axis, are compared with the data for the present system in Figure 3.

Composition Regions. A. The T_0 Minimum. The variation in T_0 and T_g is a manifestation of variation of the cohesive energy density of a liquid and hence reflects the effects of changing composition on the nature and strength of interparticle interactions. From this viewpoint the minimum in T_0 near the tetrachlorozincate composition seems significant. We interpret this minimum as a consequence of a decrease in Coulomb cohesive energy as the electrostatic charge density decreases. Assessing the volume of liquid containing 1 mol of (+ −) charge from the molar volume plot (Figure 5) we find this volume increases 24% (*i.e.*, charge density decreases 19%) on addition of 33 mol % $ZnCl_2$ to PyHCl, if the liquid at this composition is considered to contain only PyH^+ and $ZnCl_4^{2-}$ species. Some caution in accepting this interpretation in detail is, however, suggested by nmr studies of the acid proton chemical shift in this binary system[29] (which suggest a role for a hydrogen bonding contribution) and by direct T_g determinations in this composition range in a related system with glass-forming organic salt[30] (the T_g composition dependence differs from that of T_0 in Figure 4).

(25) A. Grund and M. M. Pizy, *Acta Crystallogr.*, 5, 837 (1952).

(26) G. W. Brady, *J. Chem. Phys.*, 28, 48 (1958).

(27) (a) C. A. Angell and R. D. Bressel, unpublished work; (b) E. J. Sare and C. A. Angell, *J. Chem. Phys.*, 52, 1058 (1970)

(28) These data are actually "incipient softening temperatures" by Turner and Winks, quoted in "Properties of Glass," 2nd ed, by G. W. Morey, Reinhold, New York, N. Y., 1954, p 277.

(29) J. W. Shuppert, private communication.

(30) I. M. Hodge, private communication.

The minimum in T_0 at the tetrachlorozincate composition indicates that a minimum in viscosity would also occur in this composition region. It is for this reason, we suggest, that melts such as $BeF_2 \cdot 2LiF$, which presumably are structurally similar to $ZnCl_2 \cdot 2PyHCl$, have the high-fluidity characteristics required of a nuclear reactor molten salt heat transfer and fuel-circulating medium.

Notwithstanding the doubts frequently expressed about the meaning of discreteness of complex ions in common molten salt solutions (*e.g.*, ref 2a), we feel $ZnCl_4^{2-}$ may be correctly regarded as a true anionic "species" in basic melts in the present system. The reason lies in the unusual "weakness" of the PyH^+ counter cation, which is responsible for the similarities, instanced several times in this discussion, between this system and Na_2O–SiO_2. SiO_4^{4-} is generally accepted as an anionic species in basic oxide melts, as is BeF_4^{2-} in basic fluoride melts.[31]

B. The 35–65% $ZnCl_2$ T_0, T_g Increase: Polymer Aspects. The increase of T_0 with addition of $ZnCl_2$ to the melt of $(ZnCl_4)$ stoichiometry is much more pronounced than that caused by addition of PyHCl. On the $ZnCl_2$-rich side the chloride ion content is insufficient to satisfy individually the tetra-coordination requirement of the Zn^{II} ions, forcing $ZnCl_4$ tetrahedra to share corners in order to preserve the favored coordination number. This leads first, at 40 mol % $ZnCl_2$, to the formation of (Zn_2Cl_7) structural groups for which evidence has been presented elsewhere[32–34] and then, as $ZnCl_2$ content increases beyond 40 mol %, to increasingly long, and/or complex associations.

The melt configurational restrictions associated with the buildup of these polymeric anions are no doubt responsible for the rapid increase in T_0 and T_g in this composition region. Such an increase is predicted qualitatively by the Gibbs–Dimarzio lattice theory of the glass transition for chain polymers,[35] although the theory is only quantitative for chain lengths of more than several monomer units. For noncrosslinking chain polymers T_g approaches a constant value as the chain length approaches infinity which, in the simplest view, would correspond to 50 mol % $ZnCl_2$ in the present system. Since the present polymeric species are not restricted to one-dimensional growth, however, such behavior is not to be expected in our case. In fact, the steady increase in T_g and T_0 through the 1:1 composition up to 65 mol % suggests that the polymerization proceeds simultaneously and probably haphazardly in two directions, if not three. The sharing of chloride ions between adjacent infinite

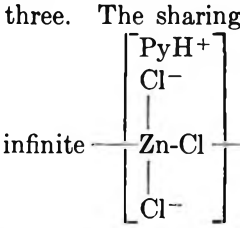

chains, for instance, is one way of generating the composition PyH-Zn_2Cl_5 (66.7 mol % $ZnCL_2$) near which (66 mol %) the increase of T_g and T_0 with increasing $ZnCl_2$ comes to a halt.

The 50 mol % composition is associated with distinct positive departures from molar volume additivity and maxima in expansion coefficient. This is of interest for two reasons: (a) in the related system CsCl + $ZnCl_2$ system positive departures from volume additivity are most pronounced at 33 mol % $ZnCl_2$[36] while in the KCl + $ZnCl_2$ system no deviations were observed outside the $ZnCl_2$-rich network-breaking region;[23,37] (b) molar volume deviations may often be correlated with glass temperature deviations, while in the present case T_g varies linearly with composition through the region.

The maximum in α might reasonably be associated with a predominance of extended one-dimensional polymeric chains with little cross-linking between chains. The decrease in this parameter beyond 50% $ZnCl_2$ is consistent with a rapid increase in cross-linking and resultant "tightening" of the polyelectrolyte structure.

Eisenberg and Sasada[38] have measured T_g in the 40–50% P_2O_5 region of the related Na_2O + P_2O_5 system. Evidence for polyphosphate chain structure in this region is strong,[39] yet T_g showed only a weak composition dependence in the phosphate system. This was attributed to a strong sodium ion cross-linking effect, which is surprising. Again the present system is found to resemble more closely the Na_2O + SiO_2 system, in which T_g increases rapidly with increasing SiO_2 content in the corresponding composition region.[38]

Other polymer-related aspects of the present system will be discussed in a separate publication.

C. The 65–85% $ZnCl_2$ T_g, T_0 Plateau. The origin of the plateau region is obscure. There is some empirical evidence from other systems[27b,28,40] that a levelling

(31) K. A. Romberger and J. Braunstein, private communication.

(32) C. A. Angell and D. M. Gruen, *J. Phys. Chem.*, **70**, 1601 (1966).

(33) W. E. Smith, J. Brynestad, and G. P. Smith, *J. Chem. Phys.*, **52**, 3890 (1970).

(34) We note that convincing Raman spectral evidence for a distinct $Al_2Cl_7^-$ species in alkali chloride melts has recently been presented (S. J. Cyvin, P. Klaboe, E. Rytter, and H. A. Oye, *J. Chem. Phys.* **52**, 2776, (1970)).

(35) J. H. Gibbs and E. A. Dimarzio, *ibid.*, **28**, 373 (1958).

(36) W. E. Smith and G. P. Smith, *J. Chem. Eng. Data*, **13**, 123 (1968).

(37) In the Na_2O + SiO_2 system measurements of ρ and α at 1400° have been reported by J. O'M. Bockris, J. W. Tomlinson, and J. L. White, *Trans. Faraday, Soc.* **52**, 299, (1956). These only cover the composition range 40–100% SiO_2 so comparisons are limited and are complicated by the peculiar temperature dependence of the SiO_2-rich solutions. However, it appears that while α shows positive deviations near 50 mol % SiO_2, as in the present system, V_m does not.

(38) A. Eisenberg and T. Sasada, "Physics of Non-Crystalline Solids," J. A. Prins, Ed., North-Holland, 1965, p 99.

(39) A detailed chromatographic study of distribution of chain lengths as a function of composition was performed by T. R. Meadowcroft and F. D. Richardson, *Trans. Faraday Soc.*, **61**, 54, (1965). There is a strong presumption that similar chains exist in Na_2O–SiO_2 liquid and glass in this composition region but the dissolution–chromatography technique cannot be successfully applied to prove this.

(40) R. L. Green, *J. Amer. Ceram. Soc.*, **25**, 83 (1942).

off in the T_g-composition relation is associated with a tendency of the supercooled liquid to separate into two immiscible liquid phases. It is known that in the Na_2O–SiO_2 system this subliquidus unmixing does actually occur[41] although the kinetics of the process are so slow that the growing particles only reach the dimensions of visible light wavelengths with special heat treatment: thus the unmixing phenomenon can usually only be observed in electron microscope studies. Drawing on the parallel with the Na_2O–SiO_2 behavior seen in Figure 3, we can suppose the present system microscopically phase separates in the same composition region. This being the case, the upswing in T_g occurs at or about the critical composition of the miscibility dome (90% SiO_2 in the Na_2O + SiO_2 system) and might be attributed to the matrix phase changeover, through this composition, from the PyHCl-rich to the more viscous $ZnCl_2$-rich fraction.

Above the critical temperature the structure of the liquid will be one in which large local fluctuations in composition occur, the different microregions probably tending to the compositions and structures of pure $ZnCl_2$ and some $ZnCl_2$-poor liquid, possibly ~66% $ZnCl_2$ in the present case.[42] Even though these fluctuations rapidly decrease in magnitude as temperature rises above the consolute temperature, it would seem from the parallel composition dependence to T_0 (determined from measurements made well above the immiscibility dome) and T_g that their effect on the average mass transport properties remains strong and qualitatively unchanged, the matrix "cryptophase" having the dominant influence.

D. The 85–100% $ZnCl_2$ Region. This region, as mentioned at the start of this discussion, closely parallels the behavior of the silicon oxide + basic oxide systems and is interpreted in the classical network-breaking terms. Most striking is the rapid increase in A_κ and B_κ parameters (in both smoothed and unsmoothed forms). It is not clear whether the erratic behavior of T_0 and large standard deviation of best fit reflects a real failure of eq 1 or the small temperature range which could be studied before crystallization occurs (Table I) and the increasing difficulty of preparing decomposition-free solutions in this composition region. Our inclination has been to attribute the rapid rise in the B_κ parameter to the increase in some energy barrier term as the network perfection increases and more bonds need to be broken to permit the local structure rearrangement to occur. However, in our T_g studies we have observed, in this region, a rapidly decreasing *dta* signal, suggesting the change of heat capacity at T_g decreases rapidly as pure $ZnCl_2$ is approached. According to the Adam–Gibbs[4] theory, the parameter B_y (eq 1) contains, besides invariant terms, the ratio of a free energy barrier ($\Delta\mu_y$) and the change in heat capacity at T_g (ΔC_p)

$$B_y = \text{constants} \times \frac{\Delta\mu_y}{\Delta C_p}$$

It would, of course, be of great interest if the thermodynamic term, ΔC_p, should prove of greater importance than the kinetic term $\Delta\mu$; it would also render invalid an important assumption made by one of us[43] in a discussion of residual entropies of network and nonnetwork glasses based on the Adam–Gibbs theory. It is hoped to perform the necessary heat capacity measurements in the near future. Discussion of the molecular basis of ΔC_p[10] will be deferred until such measurements are at hand.

The Role of the Organic Cation. Finally, some comments on the nature of the organic cation are necessary to relate the present system to the more commonly studied alkali chloride + zinc chloride systems. The first point of interest is whether the pyridinium cation is really a cation, *i.e.*, whether the full +1 charge can be associated with pyridinium ion. Nmr studies[29] designed to answer this question (a suggestion of C. T. Moynihan) are affirmative only for compositions in which "free" chloride ion is absent. Also it is evident that the charge, when fully transferred, remains localized on the nitrogen atom.

The second point of interest is that in chloride-free regions the pyridinium cation functions as a much "weaker" cation than an alkali metal cation such as K^+. T_0 estimates for KCl–$ZnCl_2$ solutions,[44] for instance, fall 69° above those of corresponding pyridinium solutions, and measured T_g in solutions of composition $K_xPyH_{1-x}Cl$ + $ZnCl_2$ increases sharply with increasing x at a rate which confirms the estimated T_0 difference.[44] Since the size of the pyridinium cation (ring radius ~2.1 Å) is not so much greater than that of the larger univalent inorganic cations, it seems likely that the charge asymmetry of the organic cation leads to orientation toward a near neighbor negative charge center and consequent appearance, to more distant neighbors, of an apparent cation radius (distance from positive charge center) greater than actual.

Clearly there is great opportunity for manipulation of melt properties through choice of cation,[45] and it is hoped to develop this aspect of these studies in the future.

Concluding Remarks

Concluding Remarks. Comparison of the plot of the

(41) R. J. Charles, *J. Amer. Ceram. Soc.*, 49, 55 (1966).

(42) This type of structure was first suggested for Na_2O + SiO_2 melts by Bockris, *et al.*, (see footnote 37) as an alternative to their own "discrete ion" model. Structures of this type can explain the otherwise puzzling persistence of $ZnCl_2$ "polymer" bands in the Raman spectra of $ZnCl_2$ + alkali chloride solutions (see, *e.g.*, J. R. Moyer, J. C. Evans, and G. Y.-S. Lo, *J. Electrochem. Soc.*, 113, 158 (1966); R. B. Ellis, *ibid.*, 113, 485 (1966).

(43) C. A. Angell, *J. Amer. Ceram. Soc.*, 51, 117 (1968).

(44) C. A. Angell, unpublished work, in part discussed in ref 43.

(45) It has already been found (I. M. Hodge, private communication) that addition of a methyl group to the pyridinium ring can completely eliminate the T_g plateau region characteristic of the present system (Figure 3), giving substantially reduced T_g values in this composition range.

eq 1 parameters, Figure 4, with the comparatively featureless conductance isotherms plotted in Figure 6 emphasizes the advantages of this type of analysis for extracting information on variations in particle interactions in molten salt systems. It is notable, however, that many of the useful observations could have been made on the basis of the much simpler T_g measurements taken alone. It is hoped that parallel studies of viscosity in this system will permit more to be said about the kinetic, as opposed to the system thermodynamics, aspects of the mass transport process in these solutions.

The parallel with SiO_2-based systems can no doubt be developed. Behavior found in alkaline earth oxide + silica systems should, for instance, be sought in alkali metal chloride + zinc chloride systems; indeed it has already been noted above that substitution of KCl for PyHCl raises T_g just as substitution of CaO for Na_2O in silicate melts raises T_g. This being the case, the region over which phase separation is incipient (and accordingly T_g (or T_0) almost composition independent) should be broader for KCl + $ZnCl_2$ melts than in the present system. Although limited data are available, the finding that T_0 in the KCl + $ZnCl_2$ system is the same at 60% $ZnCl_2$ as at 73% $ZnCl_2$[44] tends to confirm this extension of the analogy. Decisions on the useful limits of these comparisons must await further study. Current studies on beryllium fluoride + alkali fluoride melts[46] will presumably provide further opportunity for useful intersystem comparisons.

Acknowledgment. The authors are indebted to the Atomic Energy Commission for support of this research under Contract AT(11-1)-2008. We acknowledge also many useful discussions with Professor C. T. Moynihan.

(46) G. D. Robbins and J. Braunstein, private communication.

NOTES

Use of the Nitrogen Dioxide Titration Technique for Oxygen Atom Determination at Pressures above 2 Torr

by A. M. Mearns* and A. J. Morris

Department of Chemical Engineering, University of Newcastle upon Tyne, Newcastle upon Tyne, NE1 7RU, England *(Received June 1, 1970)*

The determination of oxygen atom flow rates by titration with NO_2 is a widely used technique but most often employed at pressures below 2 Torr.[1] In the course of a study of the efficiency of oxygen atom production in a microwave discharge, oxygen pressures of up to 10 Torr were used, the oxygen atom concentrations being measured by NO_2 titration. The conditions under which the titration may be employed at these pressures and the accuracy of the technique are assessed in this note.

The viability of the method depends on the fact that reaction 1

$$O + NO_2 \longrightarrow NO + O_2 \qquad (1)$$

is very fast compared with the chemiluminescent reaction 2

$$O + NO \longrightarrow NO_2 + h\nu \qquad (2)$$

At low pressures, when the flow rate of added NO_2 is increased until it is equivalent to that of oxygen atoms any luminescence arising through reaction 2 is sharply extinguished since virtually all oxygen atoms are removed by reaction 1. At higher pressures however, the sharpness of the end point decreases rapidly because of a pronounced gradient in the afterglow intensity along the tube arising from the occurrence of reaction 3

$$O + NO + O_2 \longrightarrow NO_2 + O_2 \qquad (3)$$

followed by the rapid regeneration reaction 1.

The decline in atomic oxygen concentration along a flow tube, when NO_2 is added to discharged oxygen, can be calculated by solving the following simultaneous differential equations

$$-\frac{d(O)}{dt} = k_1 (O)(NO_2) + k_3 (O)(NO)(O_2) \qquad (4)$$

$$-\frac{d(NO_2)}{dt} = k_1 (O)(NO_2) - k_3 (O)(NO)(O_2) \qquad (5)$$

$$\frac{d(NO)}{dt} = -\frac{d(NO_2)}{dt} \qquad (6)$$

$$\frac{d(O_2)}{dt} = k_1 (O)(NO_2) \qquad (7)$$

For a given set of initial conditions of pressure, temper-

* To whom correspondence should be addressed.

(1) F. Kaufman, *Proc. Roy. Soc., Ser. A*, **247**, 123 (1958).

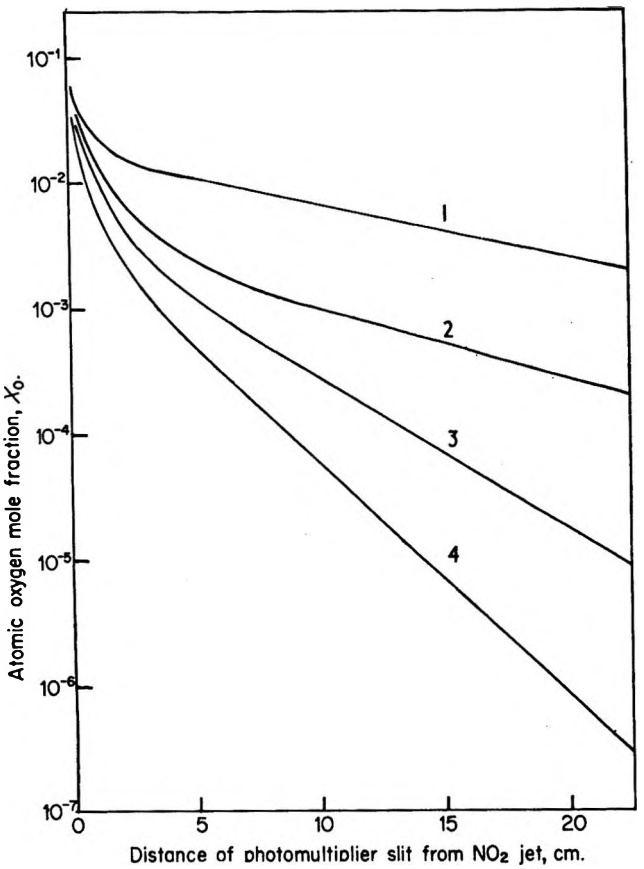

Figure 1. Oxygen atom decay curves (theoretical).

Curve	Pressure, Torr	Oxygen flow rate, μg mol/sec	Initial O atom mole fraction	Initial NO_2 mole fraction	O atom detection limit, mole fraction
1	1	20	0.3	0.28	3×10^{-6}
2	4	1000	0.15	0.145	2×10^{-6}
3	4	200	0.05	0.045	6×10^{-6}
4	8	1000	0.05	0.045	5×10^{-7}

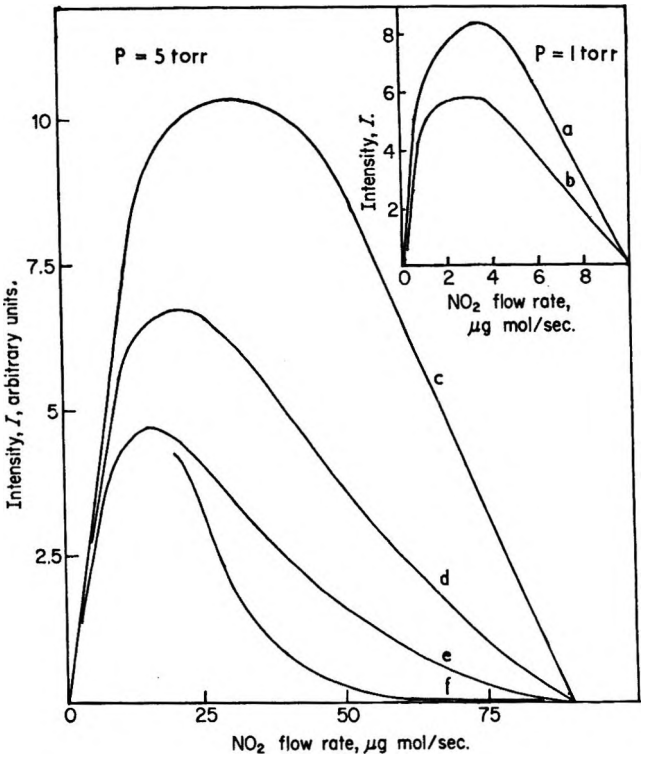

Figure 2. NO_2 titration curves.

Curve	Oxygen flow rate, μg mol/sec	Initial oxygen atom flow rate, μg atom/sec	Distance between NO_2 addition point and photomultiplier slit, cm
a	50	10	12
b	50	10	18
c	1200	90	6
d	1200	90	12
e	1200	90	18
f	600	90	12

ature, oxygen flow rate, per cent dissociation, and amount of NO_2 added and using literature values for k_1[2] and k_3,[3] eq 4–7 were solved numerically, using the Kutta–Merson method,[4] for (O) at various distances along a reaction volume equivalent to that between the NO_2 addition jet and the slit of the photomultiplier used to detect the luminescence intensity. Representative results are illustrated in Figure 1. No term for wall recombination of oxygen atoms is included in the above reaction scheme since such a process would only be significant, relative to 3, at pressures <1 Torr when the end point is sharp anyway. Similarly, reaction 8

$$O + O_2 + O_2 \longrightarrow O_3 + O_2 \qquad (8)$$

is neglected because $k_8 \approx k_3/100$ at 25°[5] and the ozone producing reaction would be important only when (NO) $\ll$ (O_2).

Titration curves for various conditions showing luminescence intensity, which for a given pressure is proportional to (O)(NO),[6] plotted against NO_2 flow rate are shown in Figure 2. These curves indicate that the error in end point determination is greater at higher pressures and may be reduced by moving the photomultiplier slit nearer to the point of NO_2 addition, or, in cases where this is not convenient, by operating at high oxygen flow rates. Using the intensity data shown in Figure 2 at various positions of the photomultiplier slit relative to the NO_2 injection point, a value for k_3 of about 1.8×10^{16} cm^6 mol^{-2} sec^{-1} may be calculated, the diameter of the flow tube employed being 29 mm. This figure is of the same order as values quoted in ref 3.

Because of the falloff in the sharpness of the end point

(2) A. A. Westenberg and N. de Haas, *J. Chem. Phys.*, **50**, 707 (1969).
(3) F. S. Klein and J. T. Herron, *ibid.*, **41**, 1285 (1964).
(4) L. Fox and D. F. Mayers, "Computing Methods for Scientists and Engineers," Clarendon Press, Oxford, 1968, p 205.
(5) F. Kaufman and J. R. Kelso, *J. Chem. Phys.*, **46**, 4541 (1967).
(6) H. P. Broida, H. I. Schiff, and T. M. Sugden, *Trans. Faraday Soc.*, **57**, 259 (1961).

for pressures >1 Torr, the accuracy of measurement of the end point is a function of the photomultiplier sensitivity. The "extinction-point" of the afterglow may be defined as the minimum value of (O)(NO) which will produce a detectable photocurrent. For the detection system used this product may be estimated to be of the order of 5×10^{-21} g mol^2 cm^{-6} for pressures of about 5 Torr. Therefore the minimum atomic oxygen concentration required to produce a detectable photocurrent is given by (O) = $5 \times 10^{-21}/(\mathrm{NO})$ g mol cm^{-3}, and (O) calculated in this manner may be called the O-atom detection limit. The detection limits for conditions simulated in Figure 1 are shown on the diagram.

The detection limits for the cases illustrated by curves 3 and 4 in Figure 1 are 6×10^{-6} and 5×10^{-7}, respectively. Now the indicated atom mole fractions at the photomultiplier slit, 22 cm downstream from the NO_2 addition point, are 10^{-5} and 5×10^{-7}, respectively, both close to the detection limit. In these cases NO_2 addition equivalent to 90% of atomic oxygen produced bring about extinction of the glow at the photomultiplier position, and the degree of undertitration due to removal of O atoms by reaction 3 is 10%. Hence, in general, if the detection limit is accurately known and with a knowledge of the decay reactions involved, the minimum flow of added NO_2 which would extinguish the glow at the photomultiplier can be calculated and the degree of undertitration, and hence the real titration value, assessed. In the case of curves 1 and 2 in Figure 1, the undertitration errors would have been negligible since the O atom concentration at the detection point are well above the limit in each case and the flow rate of NO_2 would have been increased until luminescence ceased.

The rapid onset of exponential oxygen atom decay a short distance from the point of NO_2 admixture with the gas stream is explained by the very fast nature of reaction 1, which is substantially complete a short distance from the jet. For such a rapid reaction the efficiency of mixing of the gaseous reactants is important and in experiments in this laboratory NO_2 was introduced into the oxygen stream through a "pepper-pot" nozzle in which the titrating gas was fed through a network of fine holes located on the rounded tip of the feed tube. The photomultiplier slit must be positioned at a point downstream from the region where this fast reaction is taking place, where the rate of O atom decay is controlled by reaction 3.

It may be concluded that the NO_2 titration is reasonably accurate for determining atomic oxygen flow rates for pressures of up to 10 Torr if precautions are taken to ensure good mixing at the point of NO_2 admixture and to position the photomultiplier close to the NO_2 injection jet, bearing in mind the volume required for the completion of reaction 1. In addition, if low O atom flow rates are to be measured the accuracy will increase still further because the importance of reaction 3 is then much reduced.

Lifetime of a Soluble Sphere of Arbitrary Density[1]

by Daniel E. Rosner[2] and Michael Epstein

Department of Engineering and Applied Science, Yale University, New Haven, Connecticut 06520 and AeroChem Research Laboratories Incorporated, Division of Sybron Corporation, Princeton, New Jersey 08540 *(Received April 9, 1970)*

Despite the importance of transport-controlled dissolution of spheres (particles, or bubbles) in industrial and research applications, previous theoretical work has not yielded sufficiently extensive or general results for the total lifetime of a soluble sphere of arbitrary density (compared to the surrounding solvent density).[3] However, Rosner[4] has recently shown that, in the dense sphere limit, a simple closed-form result can be obtained for the total particle lifetime which simultaneously accounts for the effects of appreciable solubility and interface kinetic limitations. In the present note we (i) present the first quantitative results for the diffusion-controlled lifetime of spheres of arbitrary density and solubility in a universal form suitable for correlating future "exact" computer solutions and relevant experimental data; (ii) define the accuracy of the "mixed control" lifetime correlation developed in ref 4 and suggest the form of its extension to arbitrary solvent/sphere density ratio; and (iii) illustrate one way in which the versatile integral (profile) method[5] may be applied to this important class of nonlinear moving boundary problems.

Physicochemical Model

With the exception that we here confine our attention to the frequently encountered limiting case of diffusion-controlled dissolution,[6,7] our continuum model and nomenclature are identical with that of ref 4, *viz.*

(1) Supported by the Propulsion and Energy Conversion Division of the U. S. Air Force Office of Scientific Research under Contracts AF 49(638)-1654 and F 44620-70-C-0026.

(2) Associate Professor, Chemical Engineering Group; to whom inquiries concerning this paper should be addressed.

(3) Numerical (finite difference) calculations for specific cases have been reported (see, *e.g.*, D. E. Readey and A. R. Cooper, *Chem. Eng. Sci.*, **21**, 917 (1966) and M. Cable and D. J. Evans, *J. Appl. Phys.*, **38**, 2899 (1967)); however, we have found several such lifetime results to be higher than an expected upper bound ($\tau_{\mathrm{life}} = 1$) discussed in footnote 14. Similar discrepancies have been independently noticed by J. L. Duda and J. S. Vrentas (*A.I.Ch.E. J.*, 15, 351 (1969)) in a mathematically interesting paper devoted to the radius–time relation for dissolving bubbles.

(4) D. E. Rosner, *J. Phys. Chem.*, **73**, 382 (1969). [Author's note: The reader should correct an obvious printing error in the location of the subscript zero in the denominator of eq 13 of this reference.]

(5) T. R. Goodman in "Advances in Heat Transfer," Vol. I, T. F. Irvine and J. P. Hartnett, Ed., Academic Press, New York, N. Y., 1964, pp 51–122.

(6) Thus, departures from solute concentration equilibrium at the phase boundary are neglected compared to concentration differences across the outer "long-range" diffusion "boundary layer." In ref 4 it is shown that this limit ($c_w \approx c_{sat}$) is attained provided $(kR_0/D) \cdot (1 - c_{sat}) \gg 1$, where k is the first-order rate constant for dissolution.

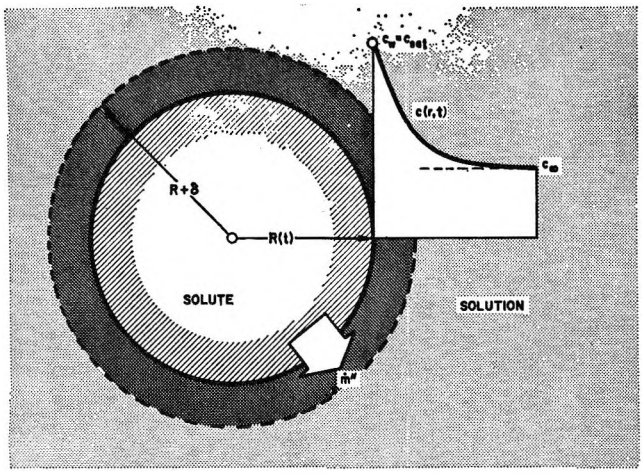

Figure 1. Dissolution of an isolated sphere controlled by long-range solute diffusion; configuration and notation.

we consider an isolated sphere of initial radius R_0 dissolving into an isothermal, constant property, otherwise quiescent solvent (see Figure 1 and the Nomenclature). As before,[4] the assumption of spherical symmetry implies that the Reynolds number (based on terminal settling or rising velocity) and Grashof number (based on solute concentration-induced density differences) must both be small.[7] Our results will therefore be immediately relevant to "captive" spheres (constrained to be motionless) but can also provide useful (upper) limit values for the dissolution lifetime of isolated spheres free to move under the influence of gravity and/or other forces. Clearly, this "stagnant" limit will be approached for a sphere of any size or density provided the solvent (continuous phase) is sufficiently viscous.[7]

Analysis

To obtain quantitative expressions and numerical predictions for the time, t_{life}, necessary to completely dissolve the sphere, applicable for arbitrary solvent/sphere density ratio and solubility, we reduce the nonlinear partial differential equation–boundary-value problem to a computationally simpler one involving an ordinary differential equation for $R(t)$ using a variant of the integral method.[5] We thereby obtain an expression for the sphere lifetime in the form of a readily calculated quadrature. Experience with this method in other nonlinear transient transport processes with spherical symmetry[8] suggests that its accuracy should be sufficient for design purposes. Moreover, in addition to guiding future numerical calculations and gaining experience with such approximate methods, the procedures outlined below could be readily generalized to compute the simultaneous effects of finite interfacial kinetics.

Consider first the normalized concentration variable $\Theta(r,t)$, [defined by $(c - c_\infty)/(c_{sat} - c_\infty)$] which must satisfy the *local* solute conservation relation.[9]

$$\frac{\partial\Theta}{\partial t} + \frac{R^2}{r^2}\left(1 - \frac{\rho_S}{\rho}\right)\dot{R}\frac{\partial\Theta}{\partial r} = \frac{D}{r^2}\frac{\partial}{\partial r}\left(r^2\frac{\partial\Theta}{\partial r}\right) \quad (1)$$

together with the obvious conditions

$$\Theta(R,t) = 1 \quad (2)$$

$$\Theta(\infty,t) = 0 \quad (3)$$

$$\Theta(r,0) = 0 \quad (4)$$

The convective (second) term in eq 1, evaluated here for the case of an external solution of constant density, is seen to depend on the pure solute/solution density ratio, ρ_S/ρ, and the instantaneous dissolution rate $-\dot{R}$. The latter quantity is, however, related to the instantaneous value of $(\partial\Theta/\partial r)_{r=R}$ through a solute balance at the solute/solution interface; *viz.*

$$\rho_S\dot{R} = D\rho B(\partial\Theta/\partial r)_{r=R(t)} \quad (5)$$

These equations, and the "initial" condition $R(0) = R_0$, are in principle sufficient to simultaneously determine $\Theta(r,t)$ and $R(t)$, from which the lifetime would follow from the definition $R(t_{life}) = 0$.

Rather than numerically dealing with this nonlinear boundary value problem in its present form, we adopt the following method.

1. A reasonable functional form for $\Theta(r,t)$ is postulated, involving two undetermined, time-dependent functions, *viz.*, a "shape" function ϕ and a boundary layer thickness δ.

2. These latter functions (ϕ, δ) are evaluated by imposing the conditions that $\Theta(r,t)$ satisfy (i) an *integrated* conservation relation and (ii) a "curvature" condition at $r = R$ (derived from eq 1).

3. The lifetime is then calculated from an integrated dimensionless form of eq 5, *viz.*

$$\tau_{life} = 2\frac{\ln(1+B)}{B}\int_0^1 \frac{d(R/R_0)}{R_0(\partial\Theta/\partial r)_{r=R}} \quad (6)$$

(7) For relevant correlation formulas see, *e.g.*, R. B. Bird, W. E. Stewart, and E. N. Lightfoot, "Transport Phenomena," Wiley, New York, N. Y., 1960. If the terminal Reynolds number (based on sphere diameter) is in the Stokes range ($\leq$0.3) and the corresponding Peclet group $Re\cdot(\nu/D)$ is also small (say $\leq$0.3), then the relative change in instantaneous mass transfer coefficient (for a solid or viscous sphere of fixed radius) can be shown to be $|(\rho_s/\rho) - 1|\cdot(gR^3)/(9D\nu)$. For a dense sphere, the initial value of this grouping should provide an upper bound to the effect of gravitational settling on τ_{life} since τ_{life} depends upon some time-average of the effective mass transfer coefficient.

(8) See, for example, G. Poots, *Int. J. Heat Mass Transfer*, **5**, 525 (1962).

(9) See for example, L. E. Scriven, *Chem. Eng. Sci.*, **10**, 1 (1959),[7] who first demonstrated a class of self-similar solutions to eq 1 for the special case of sphere *growth* from zero initial radius. While similarity solutions do not exist for the dissolution of finite radius spheres, we have used Scriven's exact solutions to show that the integral method exploited below, when combined with the assumption of a thin concentration boundary layer, adequately predicts the transport limited growth of bubbles in the parameter range: $10 < (\rho/\rho_S)\cdot|B| < 10^3$, $4 \times 10^1 < \rho/\rho_S < \infty$ [D. E. Rosner and M. Epstein, in preparation]. However, we expect the integral method to be put to a more severe test in the case of the present *dissolution* predictions, the accuracy of which will remain to be systematically studied as more reliable finite difference results become available.

For Θ we choose the transcendental profile[10]

$$\Theta = \frac{\exp\left\{-\phi\frac{R}{r}\left[1 - \left(\frac{r-R}{\delta}\right)\right]^2\right\} - 1}{\exp(-\phi) - 1} \qquad (R \leqslant r \leqslant R + \delta) \quad (7a)$$

$$\Theta = 0 \qquad (R + \delta \leqslant r \leqslant \infty) \quad (7b)$$

which not only satisfies conditions 2 and 3, but also has the properties

$$\Theta = 0 \qquad \text{for } r = R + \delta \quad (8)$$

$$\partial\Theta/\partial r = 0 \qquad \text{for } r = R + \delta \quad (9)$$

Together with the initial condition $\delta(0) = 0$, these equations serve to define the boundary layer thickness δ. An *integral* condition on Θ follows directly from the consideration that the total amount of solute associated with a given reduction in sphere radius must be present in the boundary layer surrounding the sphere. This leads to the following convenient condition, obtained from a radial integration of eq 1

$$4\pi\rho\int_R^{R+\delta} r^2\Theta dr = \frac{4\pi}{3}\left(\frac{1 - c_\infty}{c_{sat} - c_\infty}\right)\rho_S(R_0^3 - R^3) \quad (10)$$

Finally, we impose a relation between $(\partial\Theta/\partial r)_{r=R}$ and $(\partial^2\Theta/\partial r^2)_{r=R}$ which is explicitly independent of $\dot{R}$ and derivable from eq 1 evaluated at $r = R(t)$, *viz.*[11]

$$R^2B\left(\frac{\partial\Theta}{\partial r}\right)^2_{r=R} = -\left[\frac{\partial}{\partial r}\left(r^2\frac{\partial\Theta}{\partial r}\right)\right]_{r=R} \quad (11)$$

Equations 5, 7, 10, and 11 suffice to determine ϕ, δ, R, and Θ, from which τ_{life} is obtained in accord with eq 6[12] by simple numerical quadratures.

Results and Discussion

The predicted behavior of the sphere lifetime as a function of density ratio (from dense particles to bubbles)[13] is shown in Figure 2 for values of the solubility parameter B between 10^{-2} ("sparing" solubility) to 10 (extensive solubility, with $c_\infty \ll c_{sat}$). One notes

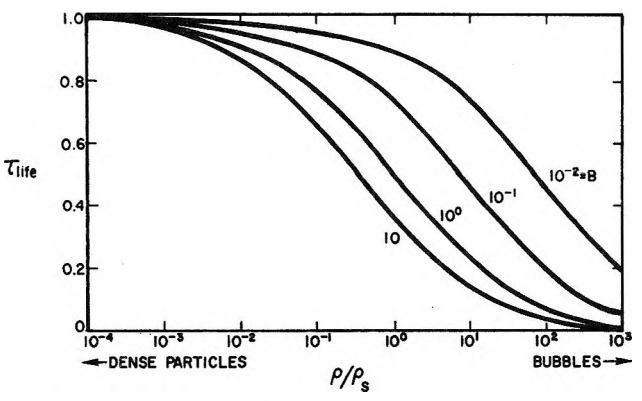

Figure 2. Predicted correlation of diffusion-controlled sphere lifetimes for arbitrary solute-solvent density ratio and solubility (integral method).

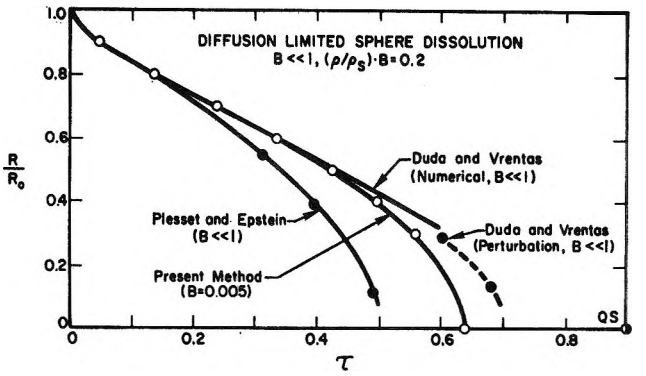

Figure 3. Comparison of predicted radius-time curves for the dissolution of an isolated, sparingly soluble sphere [$B << 1$, $(\rho/\rho_S)\cdot B = 0.2$].

that, *regardless of the value of* B, $\tau_{life} \to 1$ for sufficiently small ρ/ρ_S—a feature which, of course, motivated the choice of τ_{life} as a convenient lifetime variable[14] in ref 4. Indeed, Figure 2 is immediately useful in revealing how small the product $(\rho/\rho_S)\cdot B$ must be to ensure the validity of the closed-form dense particle limit results of ref 4 (since the diffusion-controlled extreme provides the most stringent requirement on the smallness of $(\rho/\rho_S)\cdot B$). Some indication of the expected accuracy of the present extension can be gained from Figure 3, which compares sphere radius-time relations as predicted by several distinct methods[15] for the case of sparing solubility ($B \ll 1$) with $(\rho/\rho_S)\cdot B = 0.2$. Assuming the recent finite difference solutions of Duda and Vrentas[3] to be free of the inaccuracies appearing in

(10) While other functional forms may be computationally more convenient, eq 7 is expected to lead to accurate results for this problem, at least for the case of dense spheres, since it is functionally similar to that obtained by neglecting the explicit transient term in eq 1 (as in the well known quasi-steady (QS) approximate method[4]).

(11) It should be noted that since R is time-dependent, one cannot simply set $\partial\Theta/\partial t = 0$ at $r = \dot{R}(t)$. Instead, one has $\partial\Theta/\partial t + \dot{R}\partial\Theta/\partial r = 0$ at $r = R(t)$.

(12) For the results reported here it proved convenient to transform this τ_{life} integral to a definite integral over the variable ϕ, part of the integrand of which was itself calculable from a second quadrature (obtainable from eq 7, 10, and 11) in which ϕ appears as a parameter.

(13) For $\rho/\rho_S \to 1$ our results should also be applicable to the case of solid-state dissolution of a spherical precipitate particle (see, *e.g.*, F. V. Nolfi, Jr., P. G. Shewmon, and J. S. Foster, *Trans. Met. Soc. AIME*, **245**, 1427 (1969)).

(14) The asymptotic validity of this τ_{life} limit can be rigorously demonstrated for arbitrary B (W. S. Chang and D. E. Rosner, in preparation). This result, when taken together with predictions of the effects of nonvanishing $(\rho/\rho_S)\cdot B$ on τ_{life} [*cf.* our present results (Figure 2), results of the extended quasistationary method (ref 4, footnote 20), or results of the perturbation method of Duda and Vrentas[3] in the bubble limit] support our conjecture that the dimensionless lifetime τ_{life} cannot exceed unity for any combination of ρ/ρ_S and B (when the dissolution reaction is diffusion controlled[6]).

(15) The $R(t)$ relation due to P. S. Epstein and M. S. Plesset [*J. Chem. Phys.*, **18**, 1505 (1950)] follows from an approximate analytical theory in which radial convection and boundary motion are neglected in solving the transient diffusion equation, with the resulting values of $\partial c/\partial r$ at $r = R$ *then* used to predict the boundary motion, $\dot{R}$, based on mass conservation. The predicted lifetime marked QS on the abscissa of Figure 3 follows from neglecting the transient term in eq 1 and then using the resulting value of $\partial c/\partial r$ at $r = R$ to predict $R(t)$.

previous numerical work on this problem, we would tentatively conclude that the present integral method underestimates τ_{life} by less than 10% for $(\rho/\rho_S)\cdot B < 0.2$ even in the bubble limit. Undoubtedly, the present results reveal the proper τ_{life} *trends* for any combination of ρ/ρ_S and B.

These solutions, and the work of ref 4, also suggest the following convenient correlation for the effects of finite dissolution kinetics on τ_{life} when the density ratio and solubility are arbitrary. In the dense particle limit it was shown that $1/\tau_{life}$ could be obtained as a simple function of a kinetic-diffusion parameter[4] varying between 0 and 1 depending upon the magnitude of $(kR_0/D)(1 - c_{sat}) \equiv \kappa$. The present diffusion-controlled solutions [*i.e.*, $\tau_{life} < 1$, depending upon (ρ/ρ_S) and B] suggest that, in the most general "mixed-control" case, one should display the dependence of $\tau_{life,diff}/\tau_{life}$ *vs.* $^1/_2\kappa/(1 + {}^1/_2\kappa)$ for assigned values of B. Here $\tau_{life,diff}$ the "diffusion-controlled" sphere lifetime (estimated, *e.g.*, from Figure 2) should account for the dominant density ratio effect in this correlation. Thus, when combined, the present results and those of ref 4 provide a useful and comprehensive picture of the dissolution of spheres for all combinations of density ratio, solubility, and interface kinetic limitations. It is suggested that future numerical or experimental work be cast in terms of this framework and also used to provide a valuable feedback on the accuracy of integral methods[16] for this class of nonlinear transport problems.

Acknowledgments. It is a pleasure to acknowledge the assistance of Mrs. L. Paul in programming and obtaining the numerical lifetime predictions shown in Figure 2.

Appendix

Glossary of Symbols

B	Solubility parameter[4] $\equiv (c_{sat} - c_\infty)/(1 - c_{sat})$
c	Mass fraction of solute in solution
D	Effective Fick diffusion coefficient (solute/solution)
g	Gravitational acceleration
k	First-order dissolution rate constant[4]
$\dot{m}''$	Mass flux across solute–solution interface $(-\rho_S\dot{R})$
R	Particle radius
$\dot{R}$	dR/dt
Re	Reynolds number based on sphere diameter
r	Radial coordinate
t	Time

Greek Symbols

ν	Kinematic viscosity of solution
ρ	Density
τ_{life}	Dimensionless sphere lifetime, $2(\rho/\rho_S)(Dt_{life}/R_0^2)\cdot\ln(1 + B)$
κ	Interfacial chemical kinetic parameter, $\equiv (kR_0/D)(1 - c_{sat})$

Subscripts

diff	Diffusion controlled
S	Pertaining to pure solute
sat	Saturated (equilibrium at solute/solution interface)
0	Evaluated at $t = 0$
∞	Far from sphere surface

Note: While the details of the formulation and choices of concentration variables in the works cited in ref 3 differ from ours, the mathematical boundary value problems ultimately solved become identical if one makes the following identifications: our $(\rho/\rho_S)\cdot B$ with N_a (Duda and Vrentas) or β (Readey and Cooper); our B with N_b (Duda and Vrentas) and our ρ/ρ_S with $1/\alpha$ (Readey and Cooper).

(16) T. G. Theofanous, H. S. Isbin, and H. K. Fauske have just reported an integral method treatment of bubble dissolution for $B \ll 1$ [*A.I.Ch.E. J.*, **16**, 687 (1970)]. While their results are similar to ours in this parameter extreme [large ρ/ρ_S, small B, small $(\rho/\rho_S)\cdot B$], we had previously found that the simple profile $\Theta = \{1 - [(r - R)/\delta(t)]\}^2\cdot(R/r)$ utilized by these authors leads to unreasonable results for cases of arbitrary density ratio and solubility of major interest here.

A Dielectric Relaxation Study of Some *N,N*-Disubstituted Amides

by V. L. Brownsell and A. H. Price*

Edward Davies Chemical Laboratories, University College of Wales, Aberystwyth, Cards., Great Britain (*Received June 25, 1970*)

We wish to report some dielectric properties of *N,N*-dimethylacetamide and of *N,N*-diphenylacetamide. If the $-NR_2$ group is nonplanar then both inversion at the nitrogen atom and rotation of the $-NR_2$ group about the C–NR_2 bond involve a change in the dipole moment direction with respect to the applied field. Dielectric relaxation studies are appropriate to the investigation of such internal motions. The presence of such internal motions would be detected by a broadening of the absorption arising from the relaxation of the whole molecule or by the appearance of a new absorption characteristic of the internal process involved.

Experimental Section

All materials used were purified by recrystallization (or distillation) until the melting (or boiling) point agreed with the literature value.

Dielectric measurements over the frequency range 250 MHz to 36 GHz were made using apparatus described in previous publications from this laboratory.[1]

* To whom correspondence should be addressed.

(1) G. Williams, *J. Phys. Chem.*, **63**, 534 (1959); V. L. Brownsell, Ph.D. Thesis, University of Wales, 1960 [see also H. Kramer, *Z. Phys.*, **157**, 134 (1959)].

Table I: Dielectric Properties of Some Substituted Amides

Amide	Solvent	Concn, mol l.$^{-1}$	T, °K	ϵ' (150 MHz)	$10^{12}\tau$, sec	β	$(\epsilon_0 - \epsilon_\infty)$	μ, D	ΔH, kJ mol^{-1}
N,N-Dimethyl acetamide	Pure liquid		313	37.9 ± 0.2	10.0 ± 0.5	0.80	34.9 ± 0.5	4.1 ± 0.1	
			293	39.8 ± 0.2	15.5 ± 0.5	0.90	37.7 ± 0.5	4.1 ± 0.1	11.9
			273	46.6 ± 0.5	20.0 ± 0.5	0.80	45.8 ± 0.5	4.3 ± 0.1	
			253	52.1 ± 0.2	28.9 ± 0.5	0.85	49.3 ± 0.5	4.3 ± 0.1	
	Benzene	0.010	293	2.51 ± 0.05	6.0 ± 0.1	0.89	0.191 ± 0.005	3.78	
		0.996	293	4.37 ± 0.05	8.4 ± 0.1	0.89	2.04 ± 0.01	3.85	
	Decalin	0.998	343	3.67 ± 0.05	6.9 ± 0.1	0.84	1.56 ± 0.01	3.50	
N,N-Diphenyl acetamide	Benzene	0.498	298	3.14 ± 0.05	65.5 ± 0.5	1.0	0.84 ± 0.01	3.61	

The dielectric loss (ϵ'') data were analyzed using the Fuoss–Kirkwood equation

$$\epsilon''/\epsilon_m'' = \text{sech } [\beta \ln (f_m/f)]$$

where β is the distribution parameter ($0 < \beta < 1$) and f the frequency of the measurement. The subscript m refers to the properties at maximum absorption. This equation was solved by choosing ϵ_m'' so that a plot of $\cosh^{-1}(\epsilon_m''/\epsilon)$ against $\log f$ is linear. The slope of the linear plot is 2.30β and the intercept on the $\log f$ axis is $\log f_m$. Dipole moments were calculated using the Onsager equation with $(\epsilon_0 - \epsilon_\infty) = 2\epsilon_m''/\beta$. Activation energies ($\Delta H$) were evaluated from the Arrhenius equation

$$(\tau^{-1}) = A \exp(-\Delta H/RT)$$

Experimental Results and Discussion

The experimental results are listed in Table I. The absorption curves are only slightly broader than the Debye absorption. Comparison of the observed relaxation times with those observed for rigid molecules (after correcting for viscosity and molecular volume differences) show that the reported relaxation times are reasonable for the rotation of the amide molecule effectively as a rigid entity. The activation energy for the relaxation process in the *N,N*-dimethylacetamide is 11.9 kJ mol^{-1}. The relaxation times and activation energy found for the *N,N*-dimethylacetamide compare well with the relaxation time (13×10^{-12} sec at 310.5° K) and activation energy (11.4 kJ mol^{-1}) reported for *N,N*-dimethylformamide.[2] Dielectric relaxation measurements over the frequency range studied here do not provide evidence for molecular flexibility. Nuclear magnetic resonance studies[3] have shown that the internal rotation of the $-NR_2$ group about the $C-NR_2$ bond occurs at much lower frequencies than used in the present work. The activation energy involved in this internal rotation process is about 40 kJ mol^{-1}. Any deviations from the Debye behavior found in the high-frequency dielectric properties of these amides would probably arise from the inversion process. No such anomalies were found in the liquid state. In the solid state the overall molecular motion is frequently "frozen," but internal molecular motions may persist. Electrode polarization effects prevented a satisfactory study of these molecules in the solid state.

(2) S. J. Bass, W. I. Nathan, R. M. Meighan, R. H. Cole, *J. Phys. Chem.*, **68**, 509 (1964).
(3) H. S. Gutowsky and C. H. Holm, *J. Chem. Phys.*, **25**, 1228 (1956).

COMMUNICATIONS TO THE EDITOR

The Near-Infrared Spectra of Water and Heavy Water at Temperatures between 25 and 390°

Sir: We have recently examined the near-infrared region of the H_2O and D_2O spectra at temperatures between 25 and 390°. We have observed two new absorption bands at 6000 and 6600 Å for H_2O and three new bands at 7200, 8000, and 8500 Å for D_2O having molar absorptivities of $\sim 10^{-5}$. The transition energies and the intensities of the five water bands between 5900 and 10,500 Å increase as the temperature of the liquid water increases, but these parameters cease to change for water above the critical point where the single-phase sample is restricted by the constant cell volume; *i.e.*, the sample is at constant molar concentration. The same changes were observed for the vapor phase above the liquid phase, and again the changes ceased when only one phase was attained.

We found the changes in the transition energies and intensities of the water absorption bands to be linear functions of the molar concentration of water over the range of 55 to 4 *M* whether the state of the water is liquid or vapor. (Lower concentrations were not investigated because the observed band intensities would have been too low for accurate determination.) This indicates that the association of H_2O molecules is continuously dependent upon the molar concentration regardless of the physical state, and essentially independent of temperature. The extrapolation of the band parameters to zero molar concentration gives values for the absorption band parameters of completely dissociated water molecules (Table I). These results disagree with some conclusions based upon spectral changes of liquid water through the 25 to 375° range that water molecules are dissociated near the critical point,[1] where the molar concentration is 17.5.

Table I: The Parameters of Some Near-Ir Bands of Water at 55 and 0 *M*

Concn, *M*	Transition energy, cm^{-1}	Molar absorptivity (10^6), $l.\ mol^{-1}\ cm^{-1}$
55	16540	1
	15060	0.5
	13520	20
	11940	30
0	16900	7
	15380	10
	13800	100
	12170	135

At 4 *M* and 330° the near ir bands of H_2O vapor separate into fine structure, and this resolution of fine structure further indicates significant association of the water molecules at the critical point and at even lower concentrations.

The changes in the near ir bands of D_2O over the 55 to 4 *M* range are very similar to those changes for the water spectra with comparable changes in the transition energies, the band intensities, and the resolution of fine band structure at the low concentrations.

(1) W. A. P. Luck, *Ber. Bunsenges. Phys. Chem.*, **69**, 626 (1965).

* To whom correspondence should be addressed.

Chemical Development Section A — J. T. Bell*
Chemical Technology Division — N. A. Krohn
Oak Ridge National Laboratory
Oak Ridge, Tennessee 37830

Received December 8, 1969

Comments on "Near-Infrared Spectra of Water and Heavy Water," by Bell and Krohn

Sir: The observations of Bell and Krohn that the spectra of water above the critical temperature T_c are density dependent are in accord with earlier work.[1-5] In addition, the heat content of water vapor shows that the interaction energy between the water molecules under saturation conditions at T_c is 3.6 kcal/mol.[6] This induces a large disturbance of the rotation structure of the ir bands.

I think we have to differ between the H-bond interaction (~8 kcal/mol) and the normal intermolecular interaction (~3.6 kcal/mol).[6] Both disturb the ir band—the H bonds strongly, the normal intermolecular forces less.[7] An exception is the disappearance of the rotation structure of the vapor spectra owing to dispersion forces, but a quantitative analysis of this disappearance of the rotation structure is complicated,[8] although in the case of HF we could show that H bonds

(1) E. U. Frank and K. Roth, *Discuss. Faraday Soc.*, **43**, 108 (1967).
(2) W. A. P. Luck, *ibid.*, **43**, 135, 141 (1967).
(3) W. A. P. Luck in "Physico-Chemical Processes in Mixed Aqueous Solvents," Heinemanns, London 1967, p 28 and Figure 2.28.
(4) W. A. P. Luck and W. Ditter, *Ber. Bunsenges.*, **72**, 371 (1968).
(5) W. A. P. Luck and W. Ditter, *Z. Naturforsch.*, **24b**, 487 (1969).
(6) W. A. P. Luck, *Discuss. Faraday Soc.*, **43**, 115 (1967).
(7) W. A. P. Luck, *J. Phys. Chem.*, in press.
(8) W. A. P. Luck, *Z. Naturforsch.*, **6a**, 191 (1951).

induce a new H-bond band in the ir in the case of vapor state too.[9]

We have tried and stressed to give only an *approximation* method to determine the H-bond state in liquid water, assuming the spectra under critical conditions as a standard state of the liquid state without any H bonds.[5] The goal of this method has been to show that there are fewer H bonds in liquid water than all theories claimed at this time. Our values can only give the upper limit of the percentage of non-H-bonded OH groups; this can only be an approximation. We are sorry that the short paper of Bell and Krohn gives no definite improvement over our method; therefore our method has to persist until a better one is known. The agreement with the calorimetric data[6] and the comparison with the spectra of alcohols[10] show that our approximation cannot be too bad.

(9) W. A. P. Luck, *J. Mol. Struct.*, 1, 261 (1967).
(10) W. A. P. Luck and W. Ditter, *Ber. Bunsenges.*, 72, 365 (1968).

BADISCHE ANILIN- & SODA-FABRIK AG W. A. P. LUCK
LUDWIGSHEFEN AM RHEIN, GERMANY

RECEIVED JANUARY 5, 1970

Reversibility between the Electron-Excess Center, $e^-(CH_3CN)_2$, and Methyl Radicals in γ-Irradiated Acetonitrile-h_3[1]

Sir: The electron-excess center formed by γ irradiation of the high-temperature phase of crystalline acetonitrile[2] at 77°K is characterized by a broad optical absorption with λ_{max} at 510 nm.[3] Spectra for CH_3CN and CD_3CN are almost indistinguishable in terms of the absorption envelope and differ only in the vibrational fine structure.[3] Electron spin resonance (esr) studies on single crystals of $CD_3C^{14}N$, $CD_3C^{15}N$, $CD_3{}^{13}C^{14}N$, and $^{13}CD_3C^{14}N$ have shown[4,5] that the hyperfine structure of this center arises from interaction of the unpaired electron with the above-labeled nuclei in two equivalent acetonitrile molecules. Only the $M_I = 0$ component of the electron-excess center is revealed in the esr spectrum of γ-irradiated $CH_3C^{14}N$,[2] but this result is understandable[6] if unresolved hyperfine interaction with the six ^1H nuclei broadens the outer lines to the extent that they become obscured by the broad overlapping spectrum of the $\cdot CH_2CN$ radical which is also produced in the radiolysis.[7] In fact, conclusive evidence for such line broadening comes from parallel studies[8] on this electron-excess center in $CHD_2C^{14}N$. Therefore, to summarize, the spectroscopic results provide every assurance that essentially the same center is produced in CH_3CN as in CD_3CN. Recognition of this point is important to the contribution reported below.

From the outset, an awkward problem was posed by what appeared to be a most abnormal isotope effect resulting from the different chemistry of this center in CH_3CN and CD_3CN. Photobleaching by red light produced the appropriate methyl radicals[9] cleanly in each case, but on subsequent standing in the dark at 77°K, the $CH_3\cdot$ radicals disappeared irreversibly (as denoted by the absence of any renewed methyl production on photobleaching) whereas the much slower thermal decay of $CD_3\cdot$ radicals led to the regeneration of the original center with hardly any loss of intensity.[2] These observations have been confirmed on numerous occasions. This communication now presents some new results which provide the solution to the problem and demonstrate that reversibility of the center in CH_3CN can be also achieved under certain conditions.

In the course of warming a sample of γ-irradiated CH_3CN considerably above 77°K after it had been photobleached just below 77°K, visual examination indicated that a trace of purple color had returned to the previously bleached portion of the sample tube. That partial recovery of the electron-excess center had indeed occurred was confirmed by the formation of $CH_3\cdot$ radicals on subsequent exposure to light. In previous work,[10,11] it has been found that $CH_3\cdot$ radicals decay irreversibly at 77°K with measured half-times of 21.4 min (ref 10) and 26.6 min (ref 11). Thermal decay of $CH_3\cdot$ radicals below 77°K is even slower and in the prior experiment which led to the recovery, about 50% of the $CH_3\cdot$ radicals initially produced on photobleaching had survived to the point at which the sample tube was warmed up past 77°K. Now if $CH_3\cdot$ radicals undergo two competing reactions, and the activation energy for

(1) This work was supported by the U. S. Atomic Energy Commission under Contract No. AT-(40-1)-2968. This is AEC Document No. ORO-2968-52.

(2) (a) M. A. Bonin, K. Tsuji, and F. Williams, *Nature*, 218, 946 (1968); (b) K. Takeda and F. Williams, *Mol. Phys.*, 17, 677 (1969).

(3) L. Holloman, E. D. Sprague, and F. Williams, *J. Amer. Chem. Soc.*, 92, 429 (1970).

(4) M. A. Bonin, K. Takeda, and F. Williams, *J. Chem. Phys.*, 50, 5423 (1969).

(5) K. Takeda and F. Williams, unpublished work.

(6) R. J. Egland and M. C. R. Symons, *J. Chem. Soc. A*, 1326 (1970).

(7) P. B. Ayscough, R. G. Collins, and T. J. Kemp, *J. Phys. Chem.*, 70, 2220 (1966).

(8) E. D. Sprague and F. Williams, unpublished work.

(9) Originally[2a] there was an element of doubt about the assignment to $CD_3\cdot$ of the septet spectrum produced on photobleaching the electron-excess dimer center in CD_3CN. This assignment has since been confirmed by examination of the radical spectra derived from $^{13}CD_3CN$ and $CD_3{}^{13}CN$. The ^{13}C splitting in the former case agrees with expectations for $^{13}CD_3\cdot$, whereas no ^{13}C splitting was observed in the spectrum of the radical formed from $CD_3{}^{13}CN$. Moreover, the possibility of confusion[2a,10] between the spectra of $CD_3\cdot$ and the anion radical, $CD_3CN\cdot^-$, has been removed[5] by the identification of the anion radical as the monomeric form of the electron-excess center[2b] produced by the γ irradiation of the low-temperature phase of acetonitrile. This latter assignment is firmly based on the observation[5] of an isotropic ^{13}C splitting of 60 G in the spectrum of the monomer species derived from a single crystal of $CD_3{}^{13}C^{14}N$.

(10) F. P. Sargent, *Can. J. Chem.*, 48, 1780 (1970).

(11) M. A. Bonin, Ph.D. Thesis, The University of Tennessee, 1969.

recovery of the electron-excess center is greater than that for the irreversible decay, this would explain why a significant amount of recovery takes place in the region above 77°K although the irreversible decay predominates almost exclusively at 77°K. Experiments were then designed to test these suggestions as described below.

In the first set of experiments, a sample of CH_3CN was γ irradiated at 77°K and then photobleached at 84°K in the esr cavity. Immediately after monitoring the methyl radical signal, the light was turned off and the sample temperature quickly raised to 113°K. The spectrum recorded a few minutes later showed no trace of methyl radicals whereupon the sample temperature was returned to 84°K and the spectrum recorded again to verify the absence of methyl radicals. Photobleaching at this temperature as before regenerated methyl radicals with an intensity corresponding to about 70% of the original signal. In several subsequent cycles of thermal recovery and photobleaching carried out in like manner, the methyl radical signal was observed to drop uniformly by about 30 to 40% per cycle.

The reversibility of the electron-excess center in CH_3CN was also confirmed by an isothermal experiment at 113°K. As a preliminary step, the γ-irradiated sample was partially bleached at 85°K to obtain a weak signal from methyl radicals so that the magnetic field could be adjusted to the peak position for one of the innermost lines of the methyl quartet. Then the sample was photobleached at 113°K for a few seconds and the recorder traced out a continuous curve showing the growth of the methyl signal to a maximum during illumination followed by thermal decay in the dark. Repetition of this photobleaching procedure showed that the maximum signal amplitude decreased about 20% in consecutive illumination periods. Evidently most of the methyl radicals undergo the recovery reaction at 113°K, and the net decrease is accounted for by what is essentially the uncompetitive operation of the irreversible process during the short period of illumination.

It has been observed[7,10,11] that the largely irreversible decay of methyl radicals at 77°K is accompanied by the formation of the $\cdot CH_2CN$ radical, and Sargent has recently suggested[10] that the corresponding abstraction reaction in CD_3CN is likely to have a higher activation energy rendering it much less able to compete with the recovery process in CD_3CN at 77°K. This proposal is also consistent with previous observations made in this laboratory[11,12] on mixtures of CH_3CN and CD_3CN. For example, recovery of $CH_3\cdot$ radicals to the electron-excess center occurs without significant loss for 10% CH_3CN in CD_3CN where, on the average, the $CH_3\cdot$ radical would be mainly surrounded by CD_3CN molecules and consequently protected from irreversible decay.

The activation energy for the recovery process in pure CD_3CN is 4.5 ± 0.5 kcal,[11] and a similar value applies to the recovery from $CH_3\cdot$ in the CH_3CN–CD_3CN mixtures. Therefore it seems reasonable to assume that the activation energy of this recovery reaction is not subject to a deuterium isotope effect, and this is further supported by our findings for the recovery of this dimeric form of the electron-excess center in succinonitrile-h_4 and succinonitrile-d_4. By contrast, the activation energy for the largely irreversible decay of $CH_3\cdot$ radicals in CH_3CN between 77 and 87°K is calculated[10] to be only 1.3 kcal.

From the above considerations it is clear that a simple kinetic competition can explain the findings in CH_3CN and our preliminary data on this compound indicate that the Arrhenius plots for the two reactions cross at about 100°K with a first-order rate constant of 2×10^{-1} min^{-1}.

A smaller extent of reversibility between the monomeric form of the electron-excess center,[2b] now definitely known to be the acetonitrile radical anion, and methyl radicals has been demonstrated in the low-temperature phase of acetonitrile-h_3; these results will be reported in due course.

(12) M. A. Bonin, K. Takeda, K. Tsuji, and F. Williams, *Chem. Phys. Letters*, 2, 363 (1968).

* To whom correspondence should be addressed.

DEPARTMENT OF CHEMISTRY
UNIVERSITY OF TENNESSEE
KNOXVILLE, TENNESSEE 37916

KEIJI TAKEDA
FFRANCON WILLIAMS*

RECEIVED JULY 13, 1970